Design of High Permittivity Polysiloxane Elastomers for Dielectric Elastomer Transducers

Thèse N° 9505

Présentée le 24 mai 2019

à la Faculté des sciences et techniques de l'ingénieur
Unité de rattachement pour scientifiques IMX
Programme doctoral en science et génie des matériaux

pour l'obtention du grade de Docteur ès Sciences

par

Philip Horst CASPARI

Acceptée sur proposition du jury

Prof. D. Damjanovic, président du jury
Prof. F. Nüesch, Dr. D. M. Opris, directeurs de thèse
Prof. M. Sangermano, rapporteur
Prof. P. Walde, rapporteur
Prof. H. Frauenrath, rapporteur

2019

ÉCOLE POLYTECHNIQUE
FÉDÉRALE DE LAUSANNE

Gewidmet meiner Familie und den Schweizer Steuerzahlern.
In Dankbarkeit.

Meine Definition von Glück? Keine Termine und leicht einen sitzen.
Harald Juhnke

Acknowledgements

My gratitude goes first to my supervisors Dr. Dorina M. Opris and Prof. Dr. Frank A. Nüesch for their support and guidance during the last four years. I thank them for their inspiration, enthusiasm and patience.

In particular, I would like to thank Beatrice Fischer, Daniel Rentsch, Lukas Düring, Christian Walder and Tina Küninger for all their help in various measurements and all their knowledge, they were so kind to share with me.

Furthermore, I thank all members of the Functional Polymers group in Dübendorf for encouragement and assistance in the last years. Especially the help of Yee Song Ko, Simon Dünki, Jose Enrico Quinsaat, Elena Perju and Yauhen Sheima deserves all my gratitude and admiration.

Sincere thanks are given to Yun Jae Lee, Yeon Ju Lee, Hong Hee Kim and Won Kook Choi from the Korea Institute of Science and Technology for their hospitality and sociability during my visit in Seoul.

The Swiss Federal Laboratories of Materials Science and Technology (Empa) and the Swiss National Science Foundation are acknowledged for their financial contribution which made this work possible.

Finally, I wish to express my deepest gratitude to my family and friends in and outside Switzerland.

Abstract

Electroactive polymers are a new class of materials that are capable of converting electric energy into mechanical work or *vice versa*. Dielectric elastomer transducers consist of a dielectric elastomer between two compliant electrodes. When the elastic capacitor is electrically charged, the dielectric elastomer elongates until a balance of elastic and electrostatic force is reached (actuator mode). Electrical energy is converted into mechanical work. Contrary, in the generator mode, the capacitor is stretched by an outside mechanical force. The mechanical work is converted into electrical energy due to the change of capacitance. In sensors, the mechanical stress deforms the elastic capacitors and the change in capacitance can be used for sensing.

The need of a high voltage power supply is the main obstacle for the elastomer transducer technology in various applications. Siloxane elastomers are the most frequently tested elastomers with excellent mechanical stability, processability and electrically insulating properties. It is well-known that an increase in permittivity of the silicone elastomer would allow a reduction of the driving voltage of the elastic transducer. Hence, manifold research activities have been initiated to enhance the permittivity of siloxane elastomers. Several high permittivity silicone elastomers and silicone composites were reported. However, those materials could not prove the same mechanical stability or processability like well-stablished silicone elastomers.

In the present work, siloxane elastomers were developed that combined increased permittivity with high mechanical stability and cost-efficient processability of the siloxane materials. The synthesis of polar thiols as the first step of siloxane functionalization was studied. Serious challenges in the synthesis of polar groups that can be integrated by thiol-ene addition as side group of polysiloxanes were found. Therefore, commercially available alkylthiols were selected for the functionalization of siloxane due to their chemical stability.

The alkylthiols were grafted onto the polysiloxane by thiol-ene addition and subsequently cross-linked in the well-established organotin-catalyzed condensation reaction. The impact of different types of cross-linker on the electromechanical properties of the polar siloxane elastomers was analyzed. A significant improvement in the performance of actuator test devices was demonstrated. In addition, the electromechanical stability of the polar siloxane elastomer was illustrated by 50.000 actuation cycles. However, solvent had to be used in the production process of the siloxane elastomers and the cross-linking reaction time was about two days.

Apart from their application in thin film actuators, these polar siloxane elastomers were studied with respect to their performance in dielectric elastomer generators together with siloxane composites. Nanospring carbon nanotubes were blended as high permittivity fillers in siloxanes subsequent to cross-linking. Indeed, improved performances of the high permittivity silicone elastomers were found and a deeper understanding for the design of dielectric elastomers for generator applications was gained.

The most significant result of this work was the development of polar siloxane elastomers that could be processed into thin film elastomers without any solvent within a few minutes. Two different synthetic approaches were developed based on low viscosity mixtures of cross-linkable oligo(ethylthioethyl)(methyl)siloxanes and multifunctional thiol cross-linkers. The cross-linking reaction was selectively initiated by UV-induced radical formation. These siloxane elastomers possessed an increased permittivity and showed a high electromechanical stability in actuator tests illustrated by 180.000 actuation cycles. This novel synthetic approach to polar silicone elastomers might be applied to other interesting polar siloxanes.

Keywords: dielectric elastomers, dielectric elastomer transducer, siloxanes, polar silicone elastomers, permittivity, thiol-ene addition, cross-linking reactions.

Zusammenfassung

Elektroaktive Polymere sind eine neue Materialklasse, die elektrische Energie in mechanische Arbeit umwandeln und umgekehrt. Ein dielektrisch-elastischer Wandler ist ein Kondensator bestehend aus einem elastischen Dielektrikum fixiert zwischen zwei flexiblen Elektroden. Wenn dieser elastische Kondensator aufgeladen wird, verformt sich das Elastomer bis ein Gleichgewicht aus elastischem und elektrostatischem Druck erreicht ist. Elektrische Energie wird dabei in mechanische Arbeit umgewandelt. Ein solches Bauteil wird als dielektrisch-elastischer Aktor bezeichnet. Umgekehrt wird ein aufgeladener dielektrisch-elastischer Generator durch einen äusseren mechanischen Druck gedehnt und dadurch elektrische Energie gewonnen. In Sensoren deformiert der äussere mechanische Druck den elastischen Kondensator, was zu einer entsprechenden Änderung der Kapazität führt, die gemessen werden kann.

Die hohen Betriebsspannungen sind das Haupthindernis der dielektrischen Elastomer-Technologie in vielen Anwendungsgebieten. Silikon-elastomere gehören zu den oftmals verwendeten Elastomeren aufgrund ihrer exzellenten mechanischen Stabilität, Verarbeitungsmöglichkeiten und elektrisch-isolierenden Eigenschaften. Bekanntermaßen würde eine Erhöhung der Permittivität des Silikonelastomers eine Erniedrigung der Betriebsspannung ermöglichen. Deshalb wurden einige Forschungsanstrengungen unternommen, die Permittivität des dielektrischen Elastomers zu erhöhen. Unzählige Silikonelastomere und Silikonkomposite mit erhöhter Permittivität sind bekannt aus der Literatur. Jedoch konnten diese Materialien bisher nicht die gleiche mechanische Stabilität und Verarbeitbarkeit von industriellen Silikonelastomeren nachweisen.

In der hier vorgelegten Arbeit wurden Silikonelastomere entwickelt, die eine erhöhte Permittivität mit hoher mechanischer Stabilität und kostengünstiger Verarbeitung der Siloxane kombinieren. Zunächst wurden die Möglichkeiten der Synthese polarer Thiole erforscht. Dies war der erste Schritt der Funktionalisierung des Siloxans. Ernsthafte Schwierigkeiten bezüglich der Synthesemöglichkeiten polarer Gruppen, die mittels Thiol-En Addition als Nebengruppe des Siloxans integriert werden können, wurden entdeckt. Dementsprechend wurden kommerziell erhältliche und chemisch unreaktive Alkylthiole für die Funktionalisierung des Siloxans ausgewählt.

Die Alkylthiole wurden mittels Thiol-En Addition an das Siloxan gebunden und anschliessend durch die wohlbekannte Siloxankondensationsreaktion unter Organozinnkatalyse vernetzt. Der Einfluss unterschiedlicher Typen des Vernetzermoleküls auf die elektromechanischen Eigenschaften wurde untersucht. Eine signifikante Verbesserung der Leistungsfähigkeit des Aktors wurde festgestellt. Zusätzlich zeigte sich die mechanische Stabilität des polaren Silikonelastomers anhand von 50.000 Lebenszyklen des Aktor-Bauteils. Allerdings muss erwähnt werden, dass die Herstellung des Silikonelastomers unter Einsatz von Lösungsmitteln erfolgte und die Vernetzungsreaktion ungefähr zwei Tage in Anspruch nahm.

Zudem wurde die Leistungsfähigkeit des polaren Silikonelastomers, zusammen mit Silikonkompositen, auch in Bezug auf dielektrisch-elastische Generatoren getestet. Zyklische Kohlenstoffnanoröhren wurden als Füllstoffe mit hoher Permittivität mit Siloxanen vermischt und anschliessend vernetzt. Tatsächlich konnte eine verbesserte Leistung des maßangefertigten Generatorbauteils festgestellt werden. Zudem wurde das Verständnis für die Konstruktion dieser dielektrisch-elastischen Generatoren vertieft.

Das bedeutendste Ergebnis dieser Arbeit war die Entwicklung von polaren Silikonelastomeren, die lösungsmittelfrei in wenigen Minuten durch Vernetzungsreaktion in dünnen Filmen hergestellt werden konnten. Zwei unterschiedliche Synthesewege wurden erprobt, basierend auf dem Konzept der niedrig-viskosen Mischungen aus Oligosiloxanen und multivalenten Thiol-Vernetzungsmolekülen. Die Vernetzungsreaktion wurde durch UV-induzierte Radikalbildung gesteuert. Die Silikonelastomere zeigten eine erhöhte Permittivität gepaart mit hoher elektromechanischer Stabilität in elektromechanischen Aktoren-Tests. Die dielectrisch-elastischen Aktoren erreichten bis zu 180.000 Lebenszyklen. Diese neu entwickelte Synthesestrategie für polar Silikonelastomere wird sich in Zukunft womöglich auf weitere polare Siloxane übertragen lassen.

Stichworte: Dielektrische Elastomere, DE Aktoren, DE Generatoren, Siloxane, Silikonelastomere, Permittivität, Thiol-En Addition, Vernetzungsreaktionen.

Content

List of Figures

List of Schemes

List of Tables

List of Abbreviations

A	*Area*
AC	Alternating current
AIBN	Azobisisobutryronitrile
ATRP	Atom transfer radical polymerization
C	Capacitance
$CDCl_3$	Deuterated chloroform
C_p	Heat capacity
c	Damping constant
CNT	Carbon nanotube
d	Thickness
DC	Direct current
DE	Dielectric elastomer
DEA	Dielectric elastomer actuator
DEG	Dielectric elastomer generator
DET	Dielectric elastomer transducer
DMA	Dynamic mechanical analysis
DMF	Dimethylformamide
DMPA	2,2-Dimethoxy-2-phenylacetophenone
DSC	Differential scanning calorimetry
ε_0	Vacuum permittivity
ε'	Relative permittivity
ε''	Dielectric losses
E	Electric field
E'	Storage modulus
E''	Loss modulus
EA	Elemental analysis
E_c	Capacitor energy
E_{max}	Dielectric breakdown field
EAP	Electroactive polymer
EMI	Electromechanical instability
eq.	Stoichiometric equivalent
Eq.	Equation
F	Mechanical force
FT-IR	Fourier-transform infrared spectroscopy
G	Shear modulus
GPC	Gel permeation chromatography
η	Viscosity
η^x	Hapticity of a ligand

HRMS	High resolution mass spectrometry
I	Electric current
I_{leak}	Leakage current
MS	Mass spectrometry
M_n	Number-average molar mass
M_w	Weight-average molar mass
NMR	Nuclear magenetic resonance
v	Frequency
p	Pressure
P	Polarization
PDI	Dispersity index
PDMS	Polydimethylsiloxane
PET	Polyethylene terephtalate
PVA	Polyvinylalcohol
[Pt]	Platinum(0)-1,3-divinyl-1,1,3,3-tetramethyldisiloxane
Q	Electric charge
ROP	Ring-opening polymerization
rt	Room temperature
σ	Conductivity
σ_s	Stress
s	Strain
[Sn]	Dibutyltin dilaurate
t	Time
T	Temperature
$tan(\delta)$	Mechanical loss factor
$tan(\delta)_{el}$	Dielectric loss factor
T_g	Glass transition temperature
TGA	Thermogravimetric analysis
TLC	Thin layer chromatography
THF	Tetrahydrofuran
T_m	Melting temperature
TMAH	Tetramethylammonium hydroxide
TMS-Cl	Trimethylsilyl chloride
UV	Ultraviolet
U_e	Electrical energy
V	Voltage
V_4	1,3,5,7-Tetravinyl-1,3,5,7-tetramethylcyclotetrasiloxane
Y	Young's modulus
XL	Cross-linker
$Z(v)$	Impedance

Chapter 1 Introduction

1.1 Electroactive polymers

The term *electroactive polymers* (EAPs) describes a broad range of polymeric materials that respond mechanically to an external electric pulse.[1] These polymeric materials are categorized in two main branches *i.e*. *ionic* EAPs and *electronic* EAPs. Figure 1.1 gives an overview of various polymeric materials that are classified as EAPs.[2] The working principle of ionic EAPs is based on the diffusion of ions in an applied electric field which results in mechanical deformation of the material. Promising materials are carbon nanotubes (CNTs) composites,[3] polymer gels,[4] conjugated polymers,[5] and polymer-metal-composites[6]. Due to the low driving voltages of about 1-2 Volts, these materials are particularly in the focus of biological applications.[7–10] Electronic EAPs are electrically insulating materials. The mechanical deformation of the electronic EAP is related to the electric field created by the electronic charges on its surface. Polymer classes associated with electronic EAPs are ferroelectric polymers,[11] piezoelectric polymers,[12] electrostrictive polymers,[13] liquid crystal elastomers,[14] and dielectric elastomers. Dielectric elastomers are of particular interest in this work as their need of high driving voltages has prevented broader applicability so far.[15]

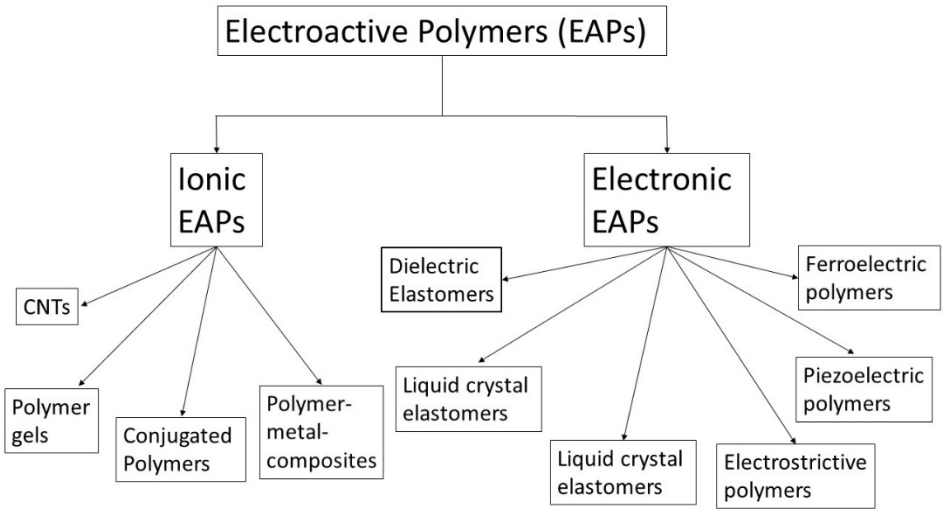

Figure 1.1 Classification of electroactive polymers (EAPs).

Dielectric elastomer thin films placed between two compliant electrodes to form an elastic capacitor are referred to as dielectric elastomer transducers (DETs). Due to the charging of the capacitor, electrostatic forces are created between the charges on the surface of the compliant electrodes. The overall electrostatic force results in a mechanical pressure on the incompressible dielectric elastomer (DE) that leads to a lateral strain until a balance of elastic and electrostatic pressure is reached. After discharging of the compliant electrodes by the external voltage source the dielectric elastomer relaxes back to its original shape.[16] In dielectric elastomer actuators (DEAs), electrical energy is converted into mechanical work. In dielectric elastomer generators (DEGs), external mechanical work is applied on the flexible capacitor before charging by an external voltage source. The stored elastic energy of the dielectric elastomer is the driving force in regaining its original shape after the external voltage source is switched off. The increase in thickness and the reduction of the electrode area of the flexible capacitor result in a decrease of capacitance and an elevated voltage. The potential difference of the electric charges on the relaxed DEG can be harvested.[17] In dielectric elastomer sensors (DESs), the variation of capacitance caused by the external pressure is utilized for sensing.[18]

1.1.1 Dielectric elastomer actuators

Already in 1880 C.W. Roentgen described the reversible actuation of a thin film of natural rubber after charging the opposite surfaces by corona discharge.[16] More than a century later, since the late 1990s the actuation of dielectric elastomers and its technological relevance have gained attraction by many scientists and engineers until today.[19–22]

Illustrated in Figure 1.2, the dielectric elastomer actuator (DEA) consists of two compliant electrodes separated by the dielectric elastomer. Various materials[23] *e.g.* carbon black powder,[24] carbon black rubber composites,[25] carbon nanotubes,[26] patterned gold,[27,28] and patterned gold/chromium alloys,[29] can be used as compliant electrodes. As dielectric elastomers polyacrylates, polyurethanes, polysiloxanes and natural rubber are the most prominent candidates.[2,30–34] Typically, the thickness of the DE ranges from 20-200 µm.

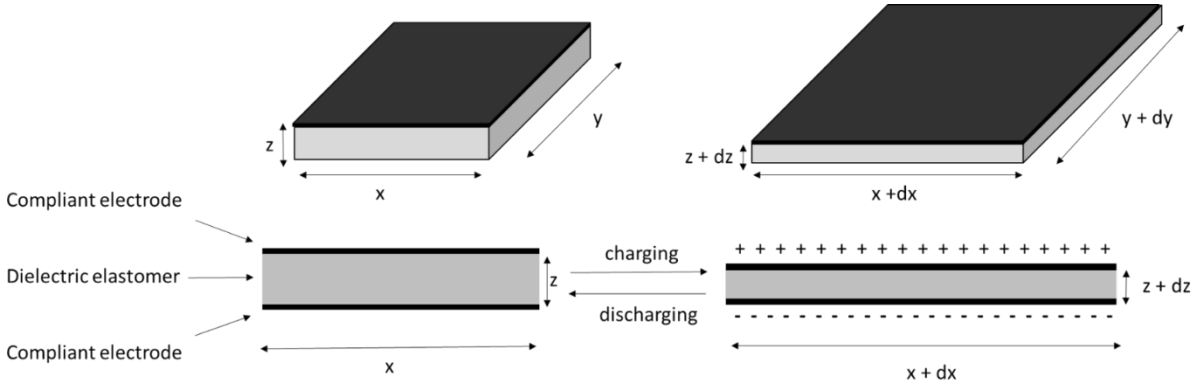

Figure 1.2 The working principle of DEAs. Left: The dielectric elastomer (DE) film is coated on the top and bottom side with compliant electrodes. The surface area *A* is defined by the length *x* and the width *y*. Right: Electrical charging leads to a lateral strain *dx and dy* of the DE accompanied by a decrease in thickness *dz*. The repulsive Coulombic forces of the likewise charges and attractive Coulumbic forces of the unlike charges are at equilibrium with the elastic force of the DE. In the linear elastic regime, the elastic forces are directly proportional to the strain according to Hooke's law. Electrical discharging allows the DE to regain its original shape driven by the elastic forces of the DE.

DEAs prove to show a quick response upon applying an electric field (< 1ms) with an actuation force of up to 2 MPa[22] and a noise-free actuation strain of more than 100%.[35] Also, the ability to remain in the strained state after charging without additional energy consumption is advantageous.[31] In addition, to increase the overall mechanical work output the stacking of multiple layers of DEAs can be technically realized.[36–40] A number of novel devices including DEAs has emerged over the last years in various application fields[41] *i.e.* robotics,[42,43] haptic displays,[44] brailles,[45] micro-pumps,[46,47] gas valves,[48] optics,[49–52] and loud speakers[53]. DEA products *e.g.* microfluidic-pumps, laser speckle reducers[54,55] and multi-layer actuators[56,57] are already commercialized. The main obstacle in the commercialization of DEAs is their need of a high voltage power supply (kV regime) which raises questions regarding product safety[58] and cost efficiency.[59]

Pelrine *et al.*[60] introduced a mathematical approximation that allows the correlation of the intrinsic material properties of the DE and the macroscopic behavior of the DEA. Focusing on the plate capacitor arrangement the stored electrical energy U_e is given in Equation 1.1 where the capacitance *C* is only depending on the vacuum permittivity ε_0 (8.85 10^{-12} F·m^{-1}), the relative permittivity ε', the area *A* and the thickness *z* of the dielectric.

$$U_e = \frac{1}{2} C\, V^2 = \frac{1}{2}\frac{\varepsilon_0 \varepsilon' A}{z}\, V^2 \qquad \text{Eq. 1.1}$$

Assuming constant volume ($(xy)dz + (zy)dx + (xz)dy = 0$) of the DE the actuation pressure p (mechanical force *F* per unit strain *dz* and unit area *A*: $\frac{F}{dz\, A}$) on the DE can be described by Equation 1.2.[21,22]

$$p = \varepsilon_0 \varepsilon' \left(\frac{V}{z}\right)^2 = \varepsilon_0 \varepsilon' E^2 \qquad \text{Eq. 1.2}$$

V is the applied voltage on the DE, and *z* the thickness of the DE. $(\frac{V}{z})$ describes the electric field *E* applied on the DE. The actuation pressure *p* in *z* direction can be interpreted as the maximum mechanical output work of the DEA. Assuming the DE is operated in the linear elastic regime, Hooke's law can be applied to obtain an expression for the thickness strain *dz/z* of the DE (Eq. 1.3).

$$\frac{dz}{z} = \frac{p}{Y} = \varepsilon_0 \varepsilon' \left(\frac{V}{z}\right)^2 = \frac{\varepsilon_0 \varepsilon'}{Y}\left(\frac{V}{z}\right)^2 \qquad \text{Eq. 1.3}$$

In Equation 1.2 only two variables that can be considered as intrinsic material properties of the DE *i.e.* the relative permittivity ε' and the dielectric strength $(\frac{V}{z})_{max} = E_{max}$ can be found. The mechanical output stress for a given electric field *E* applied on the DEA is determined by the relative permittivity of the DE. The dielectric strength E_{max} restricts the maximum output work for a given permittivity. In Equation 1.3 an additional material parameter, the elastic modulus *Y* gains relevance. *Y* is defined by the ratio of stress (force per area) to strain of an elastomer. Therefore, the strain of a DEA will be determined by the permittivity ε', the elastic modulus *Y*, and the electric field *E* applied on the DEA. Finally, the thickness *z* of the DE plays a significant role for the applied external voltage. Since the electric field output stress and strain are inversely proportional to the square of the thickness. The achievable strain depends on the elastic modulus *Y*, the thickness *z*, and the permittivity ε' of the DE. In Section 1.4 it is discussed what the implications of Equations 1.2/1.3 are on the future design of dielectric elastomers.

1.1.2 Dielectric elastomer generators

In addition to the electrostatic pressure due to the electrical charging of the compliant electrodes, the DE in the dielectric elastomer generator (DEG) is also exposed to mechanical pressure.[61] Figure 1.3 illustrates the fundamental working principle of the DEG.

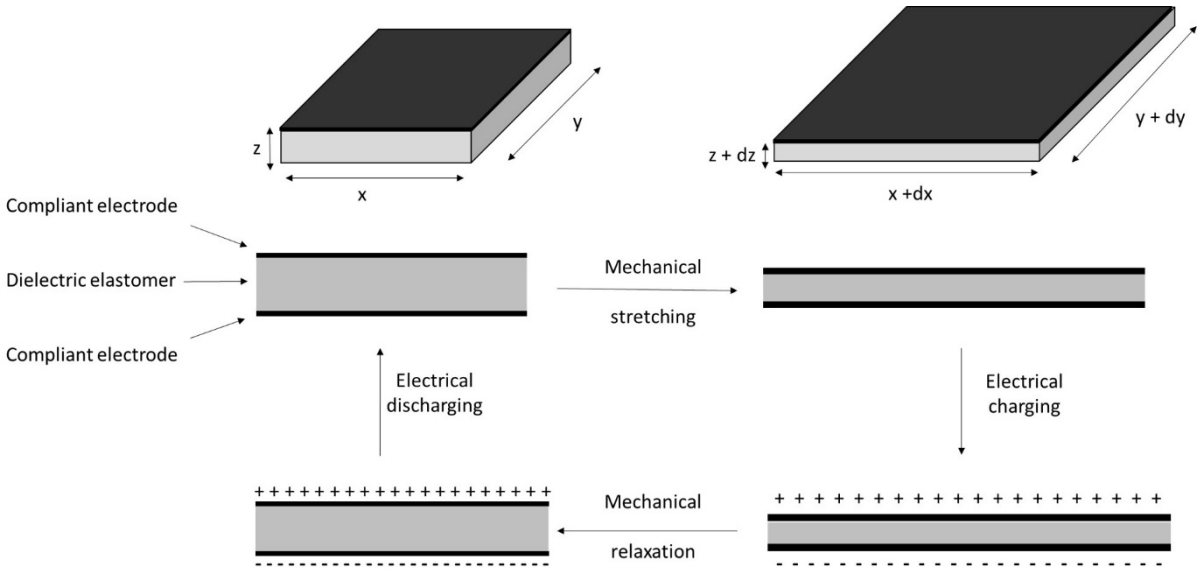

Figure 1.3 The fundamental working principle of the DEG.

First, the DE is laterally strained by an outside mechanical force. Assuming incompressibility of the DE, the lateral strain induces an increase in area and a reduction in thickness of the DE. The second step is identical to the first step of the DEA. The DEG is electrically charged to a maximum voltage level. This leads to an additional increase in area and an additional decrease in thickness. The outside mechanical force and the electrostatic forces are at equilibrium with the elastic forces of

the DE. In the third step the mechanical energy is converted into electrical energy by the DE. The mechanical force is removed. The elastic force contracts the DE until the Coulombic forces of the charges compensate. Thereby, likewise charges on the top and bottom electrodes are squeezed together, whereas the distance between unlike charges increases. Assuming that the overall amount of charge stays constant, *i.e.* no leakage current, the relaxation results in an elevated voltage level of the electrical charges on the DE. Eventually, electrical energy is harvested by discharging the DEG to an external voltage source. This leads to full relaxation of the DE back to its original shape. The amount of converted energy per cycle depends on the design of the device *i.e.* area and thickness of the DE and the efficiency of the electronics and on the dielectric and mechanical properties of the DE as well.[17,62] Starting with the well-known description of capacitor energy E_C and assuming ideal plate capacitor arrangement (see Eq. 1.1), Equation 1.4 shows the dependence of E_c on its relative permittivity ε', its area A, the thickness z, the vacuum permittivity ε_0 (8.85 10^{-12} F·m^{-1}), the applied voltage V, and the electric charge Q.

$$E_C = \frac{1}{2} C\, V^2 = \frac{1}{2} \frac{\varepsilon_0 \varepsilon' A}{z} V^2 = \frac{1}{2} \frac{Q^2 z}{\varepsilon_0 \varepsilon' A} \qquad \text{Eq. 1.4}$$

The difference in energy of the strained and unstrained state of the capacitor dE_c represents the maximum amount of energy that can be harvested. The DE is assumed to be incompressible and thus no volume change occurs $(A_1 z_1) = (A_2 z_2)$. In the ideal case of constant charge Q *i.e.* no leakage current is observed ($Q = V_1 C_1 = V_2 C_2$), the description for dE_c can be simplified to Equation 1.5 where $E_2 = \frac{V_2}{z_2}$ is the electric field in the relaxed state and $E_{12} = \frac{V_1}{z_1}$ in the mechanically strained state, respectively.[63] The electric field in the relaxed state is lower than in the strained state ($E_1 < E_2$). A_2 is the area in the unstrained state and thus smaller than A_1. The thickness of the DE increases in the relaxation process ($z_2 > z_1$).

$$dE_C = \frac{1}{2} d(CV^2) = \frac{1}{2} C_2 V_2^2 - \frac{1}{2} C_1 V_1^2 = \frac{1}{2} \varepsilon_0 \varepsilon' \left(\frac{A_2}{z_2} (E_2\, z_2)^2 - \frac{A_1}{z_1} (E_1\, z_1)^2 \right) = \frac{1}{2} \varepsilon_0 \varepsilon' (A_2\, E_2^2 z_2 - A_1 E_1^2\, z_1) =$$
$$\frac{1}{2} \varepsilon_0 \varepsilon' A_1 z_1 (E_2^2 - E_1^2) \qquad \text{Eq. 1.5}$$

Most obviously, the maximum output energy dE_c is linearly dependent on the relative permittivity ε' of the DE. The area A and thickness z, *i.e.* the volume of the DE determines the maximum output energy but A and z are not intrinsic material parameters. Moreover, the dielectric strength E_{max} of the DE limits the maximum electric field *i.e.* the total amount of charge on the DE. The DE's mechanical strain at break s_{max} is the limiting factor for the difference of E_2 and E_1 *i.e.* the difference of z_2 and z_1.

There are also alternative operation modes of DEGs that work under constant voltage or constant electric field.[64] Also, Koh *et al.*[65] highlighted that there are additional various failure modes *e.g.* the loss of tension of the elastomer, out-of-plane deformation, and electro-mechanical instability of the DE that might further reduce the amount of convertible energy per cycle.

The scope of application of DEGs ranges from wave energy converters[66–70] to wearable textiles[71–73] and shoe soles[17,74] to harvest the energy of human motion. The advantages of DEGs are their simple and lightweight construction and their wide frequency response.[17] The first wave energy converter will emerge on the market soon.[75] Nonetheless, the need for an external voltage source and the requirement of complex electronics in the operation mode of the device are reviewed critically.[76–79] In Chapter 4, a novel DEG design in cooperation with specially tailored DEs will be discussed.

1.1.3 Dielectric elastomer sensors

In dielectric elastomer sensors (DES)s the change of the electric capacitance due to outside mechanical pressure is utilized for sensing. Figure 1.4 shows the fundamental working principle of the DES.

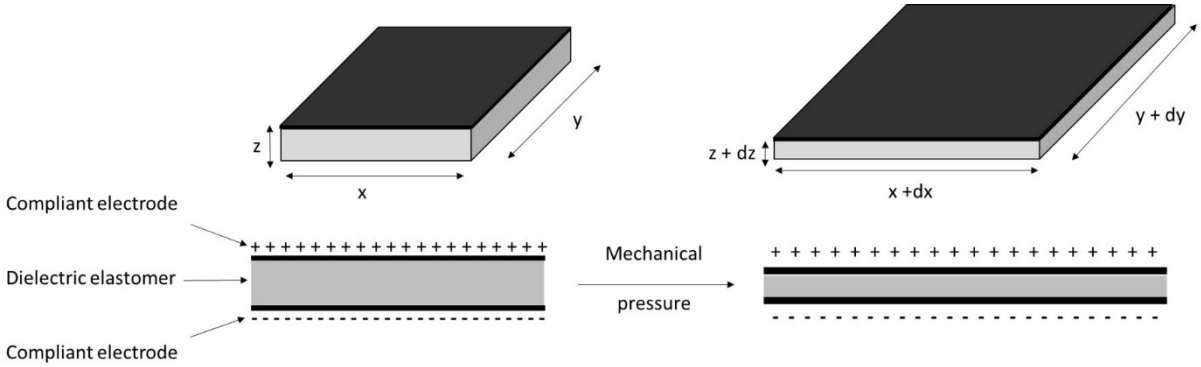

Figure 1.4 The fundamental working principle of the DES. The change in area and thickness due to the outside mechanical pressure results in a change in capacitance that is utilized for detection. The amount of charges remains constant. However, the distance between unlike charges reduces, whereas the density of likewise charges on the electrode areas decreases.

The potential difference ΔV due to the change in capacitance can be easily detected (Eq. 1.6).

$$\Delta V = \frac{Q}{(C_2 - C_1)} = \frac{1}{\varepsilon' \varepsilon_0}\left(\frac{d_2}{A_2} - \frac{d_1}{A_1}\right) Q \qquad \text{Eq. 1.6}$$

DESs can be operated in low voltage regime for the measurement of the capacitance which is considered as a great advantage for their commercialization compared to the DEA and DEG technology.[80] The first devices for pressure measurements are already commercially available.[81,82] An interesting field for novel applications is the sensing of human body motions in wearable textiles.[83–85] The change in capacitance of the DES is linearly dependent on the relative permittivity ε' of the DE. DESs might be improved by the use of a high permittivity elastomers. However, reliability, life time, and minimum leakage current are the more dominant aspects in the research for DES materials.[80,86,87]

1.2 Relevant mechanical properties of dielectric elastomers

Most obviously, the dielectric elastomer must fulfill the definition of elasticity. This means the material must be able to change its shape upon an external force reversibly.[88] This also implies shape-persistence of the elastomer in the strained and unstrained state. On a microscopic level, the material must be a cross-linked polymer chain above its glass transition temperature. Below the glass transition temperature the activation energy for reorientation of polymer chains by rotation under outside mechanical stress exceeds the thermal energy available. The material becomes brittle regardless of the nature of cross-linking. Thus, the glass transition temperature determines the lower temperature limit for the operation range of DETs. As illustrated in Figure 1.5, the nature of cross-linking can be physical by entanglements of polymer chains or by high modulus domains of a block-copolymer or mixture of polymers (thermoplastic elastomer) and chemical by covalently connected polymer chains (thermoset).[63] High modulus domains are formed due to strong intermolecular forces *e.g.* hydrogen-bonding, van der Waals forces. Up to now, most DEs published for DETs are chemically cross-linked polymers (Section 1.4).[30]

Elasticity results from conformational changes of the polymer backbone in the reaction to external mechanical stress and its release. In the unstrained state the chains form random coils in order to maximize the entropy of the elastomer.[89,90] Higher energy levels of chain conformation are occupied according to Boltzmann distribution. In the strained state, the external mechanical stress increases the energy difference of polymer conformations. The polymer chains react accordingly. The chains are more likely in the conformational ground state which results in a loss of entropy. This corresponds to the maximum strained state s_{max} before rupture. When the outside mechanical force is removed the polymer chains will regain their conformational orientation as it is accompanied by an increase in entropy of the elastomer.

Already in 1859, decades before the concept of macromolecular polymer chains was established,[91] the contraction of strained elastomers upon heating and elongation upon cooling were observed.[92] This can only be explained by an increase in occupation of high energy conformational levels of chain segments *i.e.* an increase in entropy which leads to random polymer coils and to the macroscopic observation of shrinking upon heating and *vice versa*.

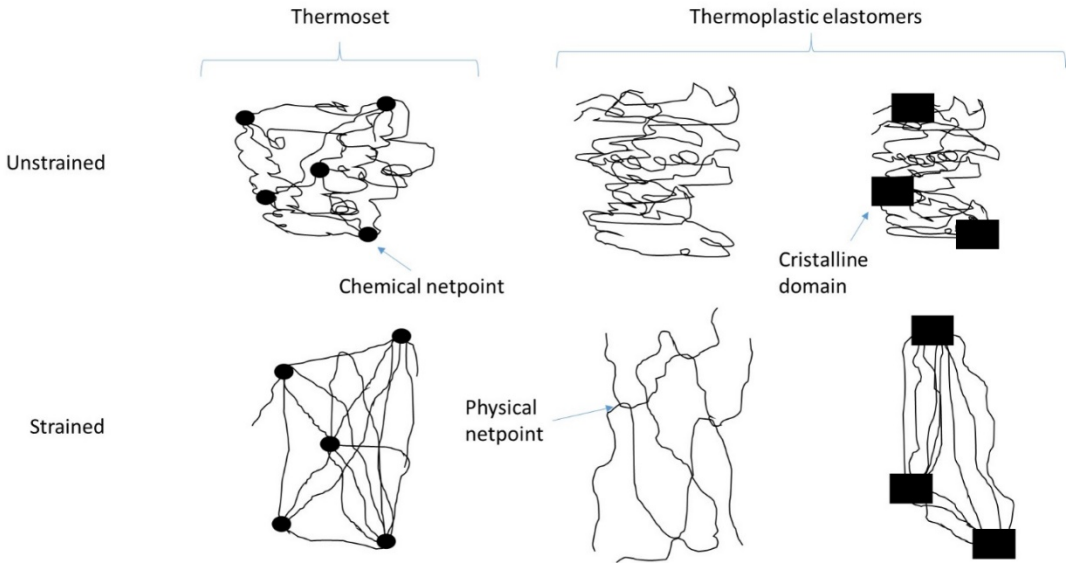

Figure 1.5 Left: Covalently connected polymer network in the unstrained (top) and strained (bottom) state. In the ideal case a perfectly cross-linked elastomer consists of only one single molecule. Middle: The polymers are only intermolecularly connected by chain entanglements. The material is thermoplastic *i.e.* it can be molten and processed. Right: The material contains high modulus domains (*e.g.* crystalline domains) that connect the polymer chains.[93]

The maximum reversible strain relies on the flexibility of the polymer chains *i.e*. number of achievable conformational changes between the cross-links of the network. This requires a certain chain length between the netpoints.[63] The smaller the chain length, the higher is the density of cross-links. Macroscopically, this is described as elastic modulus or Young's modulus *Y* of an elastomer (Section 1.2.1). Unconnected polymer chains do not contribute to the elasticity but to the viscous losses of the material (Section 1.2.2).

Finally, also the thickness of DE as an extrinsic material parameter must be taken into account in the design of DEs. The actuation strain of the DEA is inversely dependent on the thickness to the power of 2 (Eq. 1.3). Furthermore, the impact of thickness on intrinsic material parameters *e.g.* dielectric strength of the DE is under discussion.[24,94–96] This might be explained by variations in the reaction control of thin films.[97] Typically, DEs reported in literature have a thickness range of 20 µm up to 150 µm.[30] Dielectric silicone thin films are available on the market with a thickness of 20 µm to 400 µm.[98]

1.2.1 Tensile behavior

In the linear-elastic regime the strain of an elastomer is proportional to the applied stress which can be accurately described by Hooke's law (Eq. 1.7).[99] Conventionally, the elastic modulus is also named as Young's modulus *Y* given in Pascal [Pa] which describes the ratio of applied stress σ_s [Pa] and strain *s*. Typical DEs show *Y* values ranging from 0.05 to several MPa for small strains (*e.g.* 10% lateral strain).[33]

$$\sigma_s = Y\, s \qquad Y = \frac{\sigma_s}{s} \qquad \text{Eq. 1.7}$$

Equation 1.7 is only valid for small strains. Figure 1.6 illustrates the typical unilateral stress-strain curve of a silicone elastomer highlighting its non-linear behavior in a tensile test.

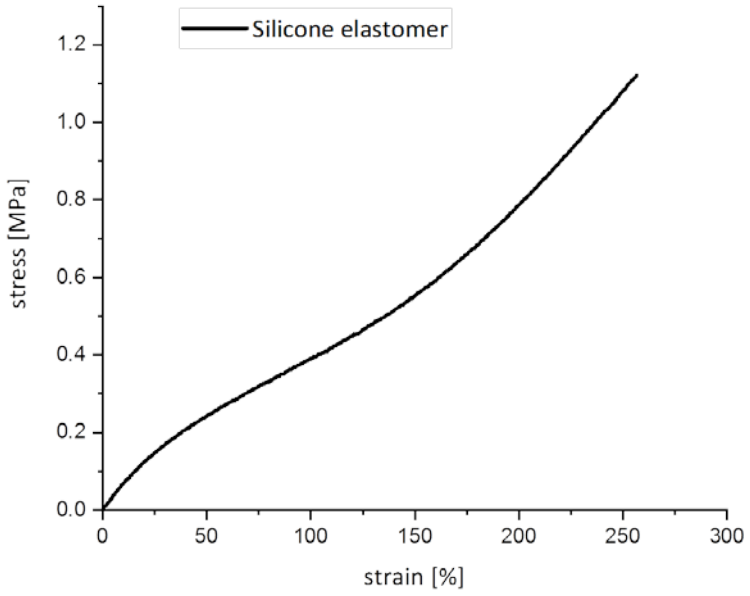

Figure 1.6 Stress-strain curve of a silicone elastomer in a unilateral tensile test. The elastic modulus *Y* is defined as the slope of the curve. For small strains below 25% the curve is linear. The elastic modulus *Y* is constant. At around 50% strain, the slope decreases (strain-softening behavior) until the deflection point at 100% when the strain-stiffening behavior sets in until mechanical rupture occurs.

For DEAs laterally strained up to 5%, the linear elasticity model fits into the electromechanical behavior of the DEA very accurately.[100] However, in DETs lateral strains above 100% have been realized already.[35] This means that the mathematical description by Equation 1.3 fails as the elastic modulus is not constant.[101,102] A detailed description for the mechanical behavior of the dielectric elastomer upon stress requires hyperelastic models including hyperelastic parameters.[103–106] These models consider the time-dependent response, the strain energy as a function of deformation (hyperelasticity), and the viscous behavior of elastomers.[101,107–109] They accurately describe the strain-softening trend followed by drastic strain-stiffening behavior observed in the stress-strain-curve before rapture of the DE. Mechanical rapture of the DEA is rather unlikely to occur due to electromechanical pressure as the dielectric strength of DE materials is too low. However, for DEGs and DESs the strain at break defines the upper operation limit.

The elastic modulus is one key parameter in the development of DEs. It determines the elongation of the DEA upon electrostatic stress and the elongation of the DEG and DES upon outside mechanical stress. Thus, DEAs with a low elastic modulus show a higher mechanical strain response to a certain driving voltage. For DEGs and DESs the elastic modulus determines the change in area expansion and thickness reduction caused by a certain mechanical pressure. This defines the sensitivity of DESs towards mechanical pressure and the energy efficiency in the DEG mode. Therefore, control over the elastic modulus is relevant.

For DEAs one prominent failure mode is the electromechanical instability (EMI) also known as pull-in or snap-through instability of the elastomer. Firstly reported in 1955,[110] EMI is observed for an area actuation strain of approximately 40% for DEAs.[90][111] During the operation mode of the DEA the applied voltage increases. The elastomer responds accordingly by lateral strain and reduction in thickness. This positive feedback results in a sudden increase of the electric field *E*. If the elastomer is operated in the strain-softening regime, the actuation strain will accelerate drastically. The elastomer has no time to compensate the increasing electromechanical pressure and decreasing elastic forces.[28,112,113] Typically, this effect provokes the electrical breakdown of the dielectric elastomer.[114,115] Even though, in 2012 a targeted strategy based on external mechanical pressure in combination with EMI led to area actuation deformations of 1600% without immediate electrical breakdown of the DE.[116] Therefore, the tensile behavior of the DE is highly important for its reliability in DEAs. In 2010, Zhao *et al.* have already proposed molecular strategies capable of suppressing EMI. Figure 1.7 illustrates the strategies that lead to unfolding of the polymer chain coils and thus shift the DEA operation range into the strain-stiffening elastic regime.[117]

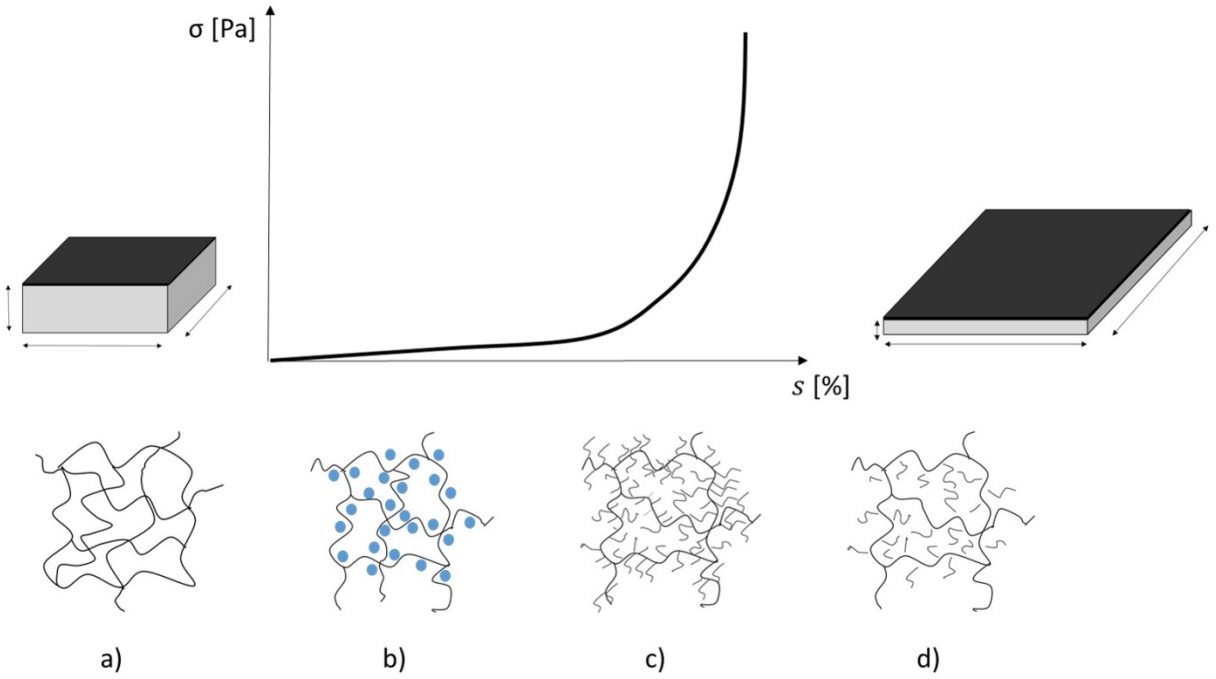

Figure 1.7 Stress-strain curve of an idealized DE under biaxial stress, adapted from literature.[117] The curve shows linear elastic behavior followed by a rapid rise in elastic modulus at higher strains. a) Mechanically prestrained polymer network. b) Polymer network containing particles. c) Polymer network with side chains *e.g.* bottle-brush polymers. d) Swollen polymer network containing plasticizer.

The first reported DETs were constructed from mechanically prestrained commercially available DE thin films *e.g.* the acrylate *VHB 4910*™.[35] This led to a shift of the starting point of electromechanical actuation around the deflection point of strain-softening and strain-stiffening behavior of the DE. Thus, the elastic modulus of the DE was softer, which enabled higher linear strains of the DEAs of up to 200%.[22] The DEs were operated in the strain-stiffening regime of the elastomers which protected them from EMI. Mathematical models explaining the impact of prestrain on the DE have already been published.[118]

The first chemical approach of tuning *Y* by modifying the polymer network of the DE was the addition of small molecules such as solvent to the commercial thin film.[119] The addition of small molecules leads to an increase in flexibility of the polymer chains in the network as the interaction between different polymer chains is less pronounced. It is observed macroscopically by a decrease in glass transition temperature. Also, the incorporation of small molecules leads to an expansion of the elastomeric network comparable to outside mechanical prestrain.[120] Swollen polysiloxane networks showed reduced elastic moduli of 0.05 kPa only. This was accompanied by an enhanced electromechanical performance in actuation strain of the corresponding DEAs.[121,122] Moreover, an understoichiometric amount of cross-linker in the cross-linking reaction led to a reduced elastic moduli of the silicone elastomer.[123,124] Interestingly, the addition of small molecules opens the possibility of tuning the dielectric properties of the DE simultaneously.[125] This will be discussed in detail in Section 1.6. The major disadvantage of additives is their effect on viscoelasticity, the reduction of life time and the reduction of tensile strength *i.e.* the reduction of maximum mechanical work that can be performed by the DEA.[122]

There are several reports on the design of polymeric networks that allow fine-tuning of the elastic modulus adapted for the specific necessities of DETs. This can be realized by precise control over the molecular weight of the polymer chains,[126] polymer chains with different molecular weight (interpenetrating networks),[127–131] the amount,[130,132] and chemical composition[133,134] of cross-linker. In Chapter 3, the effect of different side groups and cross-linker molecules on the shape of the stress-strain curve will be discussed as critical parameter in the performance of functional silicone elastomers in DEAs.

1.2.2 Viscoelastic properties

In the previous section it has already been stated that modern models vary from Hooke's law describing tensile behavior more precisely. In reality, the behavior of DEs upon mechanical stress shows not only (hyper)elastic characteristics but also viscous behavior.[135] The actuation strain of the DE becomes time-dependent. Unlike Hooke's law the behavior of the DE cannot be described by the reaction of a spring upon elongation. The mechanical behavior of ideal liquids is described by Newton's law. Stress is proportional to the velocity of change in strain. Based on this classic descriptions, viscoelasticity models were developed that combine the mechanical reaction of the elastomer by a spring coupled with a damper as shown in Figure 1.8.[136]

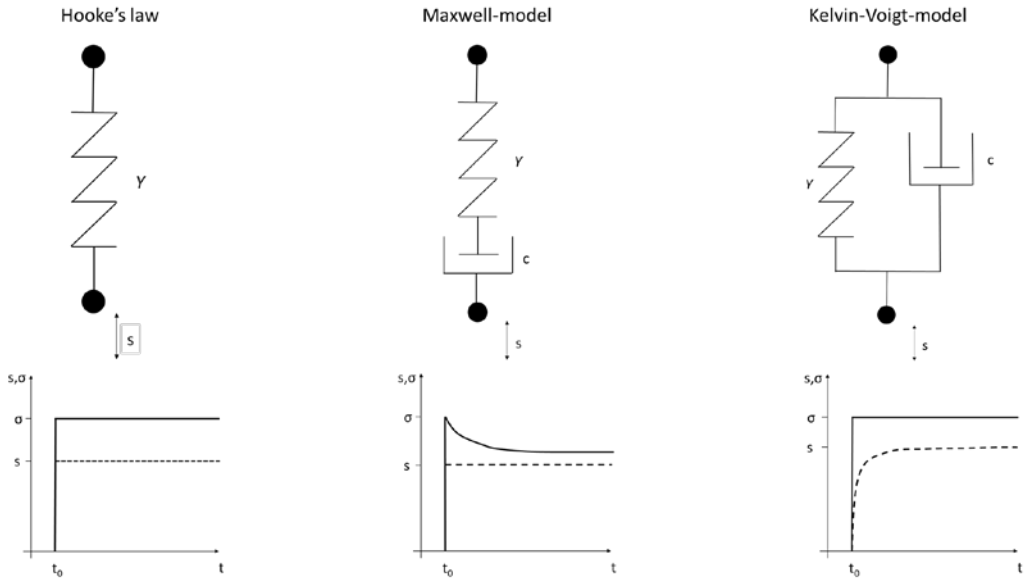

Figure 1.8 Left: Mechanical equivalent circuit of an ideal elastomer described by Hooke's law. No time-dependence can be observed. Strain *s* and stress *σ* are in phase. Middle: Mechanical equivalent circuit of a viscoelastic material described by Maxwell's model. The spring with the elastic modulus *Y* is in-line coupled with the dashpot having the damping constant *c*. The stress on the elastomer decreases with time. Right: Mechanical equivalent circuit of a viscoelastic material described by the Kelvin-Voigt model. Spring and dashpot are connected in parallel. The material reacts on the mechanical stress with a time delay.

The Maxwell-model defines the relaxation of the elastomer upon stress (Eq. 1.8). The polymer chains rearrange with time and thus release the mechanical stress until the initial stress level σ_0. The strain remains constant. The Kelvin-Voigt-model describes the creeping of the elastomer upon stress. The polymer network reacts with a time delay on the outside mechanical stress (Eq. 1.9).

$$\sigma_s(t) = \sigma_0 \, e^{-\frac{Y}{c}t} \qquad \frac{ds}{dt} = 0 \qquad \text{Eq. 1.8}$$

$$s = \frac{\sigma_0}{Y}\left(1 - e^{-\frac{Y}{c}t}\right) \qquad \frac{d\sigma_s}{dt} = 0 \qquad \text{Eq. 1.9}$$

In particular, polyacrylate DEs show viscoelastic behavior which leads to a very slow electromechanical response in the DEA and permanent deformation of the elastomer upon mechanical stress.[137–140] Viscoelastic behavior is clearly identified as a crucial parameter in the reliability of DETs.[138,141–144] This can be rationalized by the microscopic reasons of viscoelasticity. Perfectly cross-linked polymer networks do not show viscous behaviour.[122] Only components that are not covalently bond to the network such as dangling polymer bonds, particles, solvent and additives contribute to the viscous behavior.[145–148] These components can freely diffuse through the elastomer and change concentration with time. In case of elastomeric composites, viscoelasticity particularly occurs during the first operation cycles and is referred to as Mullins and Payne effect.[149–153] In case no additives are incorporated into the elastomer, viscoelasticity is a clear sign of poor cross-linking. In this case unreacted polymer chains cannot participate in the elastomeric network. Instead, the polymer chains will react to an outside stress by permanent flow (plastic deformation). This hinders the DE to regain its initial shape during the operation cycles of DETs. It will show hysteresis.[139]

Therefore, in recent years the viscoelasticity of DEs has been thoroughly characterized.[139,140,145] Dynamic mechanical analysis (DMA) is the most frequently used method to characterize the time-dependent response of the DE on mechanical strain. The sinusoidal deformation of the specimen is measured with respect to frequency.[136] The stress is recorded simultaneously (Figure 1.9).

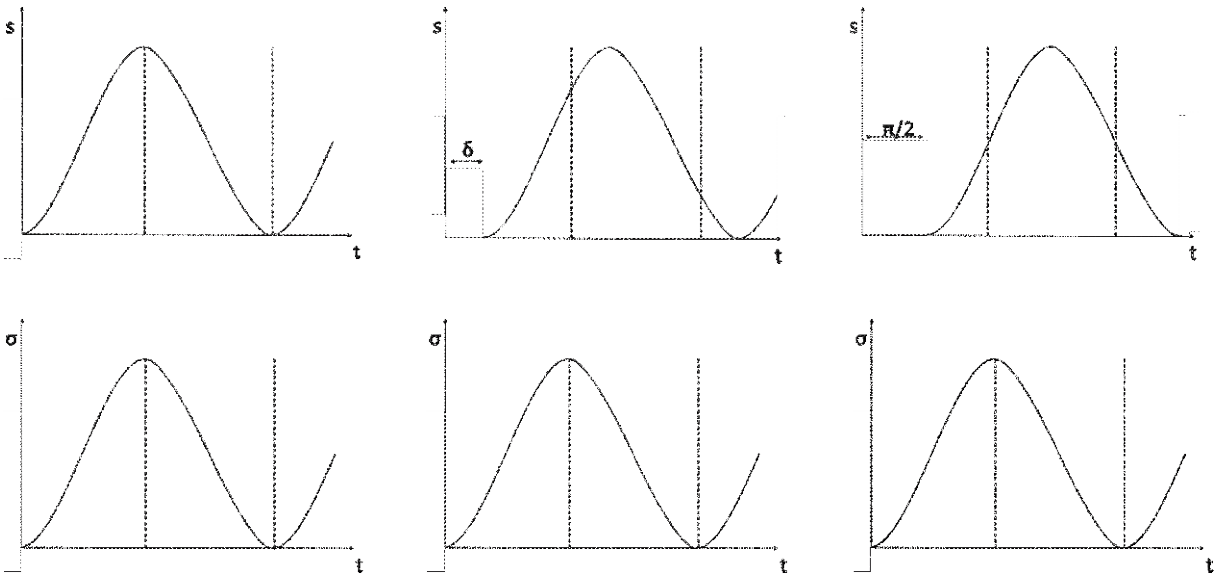

Figure 1.9 Time-dependent stress-strain behavior. Left: An ideal elastomer without phase lag (δ=0) between stress and strain. Middle: Viscoelastic material with a phase lag δ between stress and strain. Right: Ideal viscous liquid with a phase lag δ of π/2 radians (90°).

In an ideal elastomer there is no phase shift of strain and stress according to Hooke's law. The viscosity is zero. In an ideal liquid there is a phase angle of strain and stress of π/2 = 90°. Viscoelastic material shows a phase lag between the ideal elastomer and the ideal liquid. There are two types of time-dependent elastic modulus defined by the phase lag of stress and strain. The storage modulus E' defines the in-phase ratio of stress and strain whereas the loss modulus E'' the stress-strain-

ratio with a π/2-phase lag (Eq.1.11 and 1.12). The ratio of E'' and E' is a measure for viscoelasticity given as mechanical loss factor *tan(δ)* (Eq. 1.13). It depends strongly on the applied frequency ω of the DMA (Eq. 1.10).

$s(t) = s_0 \sin(\omega t)$ $\sigma(t) = \sigma_0 \sin(\omega t + \delta)$ σ_0/s_0 at t=0 Eq. 1.10

$$E' = \frac{\sigma_o}{s_o}\cos(\delta)$$ Eq. 1.11

$$E'' = \frac{\sigma_o}{s_o}\sin(\delta)$$ Eq. 1.12

$$\tan(\delta) = \frac{E''}{E'}$$ Eq. 1.13

In an ideal elastomer *tan(δ)* approaches zero. The ideal liquid shows values heading infinity. Typical DEs achieve values of 0.01 up to 0.1.[140] In Chapter 3, the mechanical loss factor tan(δ) and its significance for the DEA performance will be discussed in detail. In Chapter 4, the correlation of tan(δ) and the stability of dielectric elastomers in a DEG application will be highlighted.

1.3 Relevant dielectric material properties

All DETs are elastic capacitors that are electrically charged during operation. Most obviously, any material used as dielectric between the electrodes should be insulating in order to separate the unlike charges on the electrode of the capacitor. No material should be considered as perfectly insulating though. Due to electronic or ionic conductivity a loss of charge on the electrode's surface can be observed as leakage current. As it is one unique feature of DETs not to consume electrical energy in the charged state, the conductivity of the DEs must be as low as possible. This is also relevant with respect to lifetime and applicability of DETs as the DEs warm up significantly due to heat formed by the leakage current. The dissipation of heat is particularly difficult for multi-layer devices. Typical DEs show conductivity values around 10^{-15} S/cm.

Associated with conductivity is the dielectric breakdown strength E_{max} of the DE. It is defined as the highest electric field that the dielectric can withstand before it suffers a drastic rise in conductivity. The dielectric strength defines the operation voltage range of the DET. For DESs, the dielectric strength is less considerable as the device is not operated in the high voltage regime. However, for DEGs the dielectric strength is the most significant parameter as the energy conversion is directly proportional to the maximum electric field applied. Dielectric strength values of typical DEs range from 50 to 200 V μm^{-1}.[31] For DEAs the dielectric strength also limits the maximum achievable actuation strain, albeit high electric fields *i.e.* applied voltages are not considered as safe or economic for many technological applications.

The permittivity of the DE is certainly a crucial factor as it determines the capacitance of the DETs *i.e.* the ability of an electric field to store electric charges on it. Typical permittivity values of DEs vary from 3 for silicones up to 7 for polyurethanes.[33] The sensitivity of DESs and the energy conversion of DEGs is linearly dependent on the permittivity of the DE. For DEAs an increased permittivity is highly attractive as it allows the DEA operation at reduced electric fields *i.e.* lower driving voltages.

1.3.1 Permittivity

Whenever unlike charges are separated by an insulator they form an electric field in between them.[154] The capability of the capacitor to store unlike charges on its opposite surfaces per unit voltage is defined as capacitance *C* (Eq. 1.14). For simplicity the focus is laid on the plate capacitor arrangement. Between the plates of the capacitor the electric field strength *E* can be considered as homogeneous (Eq. 1.15). It only depends on the voltage applied between the electrodes *V* and the distance between the unlike charges. This results in the well-known description of the plate capacitance, which is only dependent on the area *A*, the thickness *d* of the capacitor, the vacuum permittivity ε_0 and relative permittivity ε' of the dielec-

tric. Rearrangement of this description gives the mathematical definition of the relative permittivity shown in Equation 1.16. The vacuum permittivity ε_0 is a natural constant of 8.856 10^{-12} F m^{-1}. The relative permittivity is a material parameter of the dielectric. Traditionally, it is also referred to as dielectric constant of the dielectric material.

$$C = \frac{Q}{V} \qquad \text{Eq. 1.14}$$

$$C = \epsilon' \epsilon_0 \frac{A}{d} \qquad \text{Eq. 1.15}$$

$$\epsilon' = \frac{Q}{E\ A\ \epsilon_0} \qquad \text{Eq. 1.16}$$

In Equation 1.16 the relative permittivity ε' is defined by the amount of charge per unit area and unit electric field *E* of the capacitor times the vacuum permittivity. It is the proportionality factor for the ability of the dielectric material to store charge on the capacitor at given electric fields related to vacuum. Typical values of the relative permittivity ε' are given in Table 1.1.[155] The relative permittivity can be simply determined by capacity measurements of the plate capacitor in comparison to the plate capacitor using vacuum as dielectric (Eq.1.17).[156]

$$\epsilon' = \frac{C}{C_0} \qquad \text{Eq. 1.17}$$

This means that a capacitor charged to a certain electric potential *V* will reduce its voltage level by a factor of 4000 if the dielectric material air is replaced by barium titanate.

Table 1.1 Overview of relative permittivity values of various material classes.

Material	Relative permittvity ε'
Air	1.006
Paper	4-60
Glas	5-70
Water	81
Non-polar organic solvents	1-10
Elastomers	3-7
Barium titanate	1000-4000

The physical reason behind this observation is the capability of dielectric materials to respond to the outside electric field by the separation of electric charge inside the dielectric material itself. This phenomenon is named as polarization *P* of the material (Eq. 1.18). The general mathematical description can be highly complex. However, Equation 1.18 is a good approximation for most materials and electric fields as the polarization of the material is linear to the electric field and the relative permittivity ε' of the material.[156] In literature another proportionality constant is introduced to denominate (ε' -1) as the electric susceptibility ξ_e. It indicates the ability of a material to be polarized by an applied electric field.

$$P = (\epsilon' - 1)\epsilon_0 E \qquad \text{Eq. 1.18}$$

Polarization itself leads to the formation of an electric field inside the dielectric material that weakens the outside electric field induced by the charges on the capacitor electrodes.[157] On the molecular level, the polarization of the dielectric can be attributed to microscopic effects inside the material such as electronic polarization, dipole polarization, ionic polarization, and interfacial polarization (Figure 1.10).

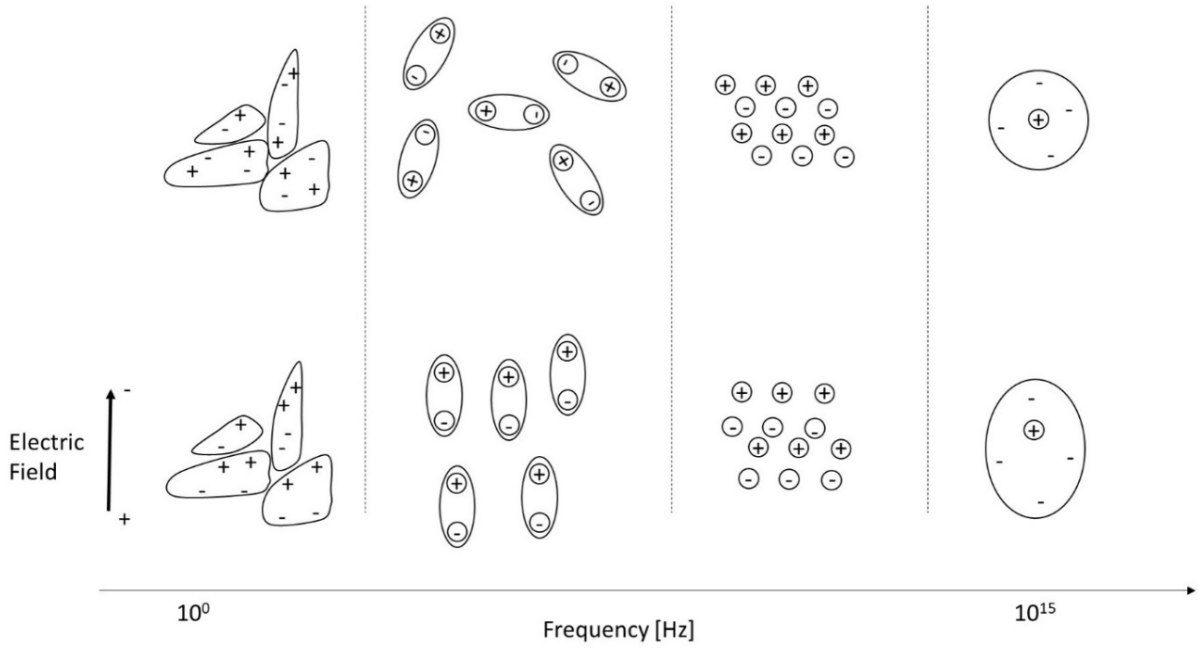

Figure 1.10 Polarization phenomena of dielectric materials depending on the frequency of the electric field applied. From left to right: Interfacial polarization. Dipole polarization. Atomic polarization. Electronic polarization.

Electronic polarization occurs in all dielectric materials until high frequencies. The electron clouds of the atoms and molecules orientates parallel to the electric field. A dipole moment is induced as the atom core does not move. Depending on the volume of the electron orbitals this effect can be more pronounced. Atomic polarization describes the shift of atoms and ions in particular in response to the electric field. Dipole polarization results from the orientation of permanent dipoles in parallel to the outside electric field. This requires steric flexibility of the dipoles. Furthermore, depending on the thermal energy of the dielectric material the dipoles will also occupy high energy levels *i.e*. align perpendicular according to Boltzmann distribution. In DEs the effect of dipoles has been intensely studied in recent years.[30] Interfacial polarization is related to mobile charges that migrate over short distances inside domains of the dielectric leading to charge accumulation at the domain interfaces as well as on the electrode surface.

Figure 1.10 refers to an alternating electric field applied on the plate capacitor. At different frequencies polarization effects cannot be observed any more. Atomic polarization occurs at frequencies of 10^{12} Hz and electronic polarization until 10^{15} Hz. Dipole polarization relies on the flexibility of dipoles to adapt their spatial orientation on the fluctuating electric field. The size of the dipole and the steric environment influences the flexibility.[158] Hence, the dipole polarization and the corresponding relative permittivity is found to be strain-dependent in DEs *e.g.* the acrylate VHB.[159,160] Typical dipole polarization in polymers can be observed up to a frequency of 10^6 Hz. Interfacial polarization can only be observed at low frequencies as it depends on the diffusion of charges through the material. Interfacial polarization at low frequencies leads to the formation of an interface on the electrode surface. This results in the macroscopic observation of a drastic increase in capacitance and relative permittivity ε' at low frequencies. This increase cannot be considered as an intrinsic property of the dielectric material. Therefore, permittivity measurements of DEs are conducted by broadband impedance spectroscopy.[97,161,162] The dielectric material is characterized over a typical frequency range of 10^6-10^{-1} Hz. The frequency-dependent impedance *Z(ν)* is given by the ratio of frequency-dependent voltage *V*(ν) and frequency-dependent current *I*(ν). Eq. 1.19 gives the relation of time-dependent relative permittivity $\varepsilon^*(\nu)$ and impedance *Z(ν).* I(ν) is measured with respect to the sinusoidal alternating voltage applied. Thus, the intensity and the phase lag of *I(ν)* is recorded.

$$\varepsilon^* = \frac{1}{i\,2\pi\nu\,C_0 Z(\nu)} = \frac{I(\nu)}{i2\pi\nu\,C_0 U(\nu)} \qquad \text{Eq. 1.19}$$

However, energy losses occur during the polarization *i.e.* the alignment of dipoles. The movement of dipoles inside the polymer matrix is not completely energy reversible. This can be analyzed by the variation of phase lag *(ν*). Without polarization effects of the dielectric the voltage lags the current by π/2 or 90° behind, respectively. The complex time-dependent relative permittivity $\varepsilon^*(\nu)$ is described as real part ε' and imaginary part ε''. The real part describes the reversible polarization

effect of the outside electric field whereas the imaginary part defines the residual polarization effect. Similar to the mechanical loss factor, Eq. 1.20 describes the dielectric loss factor $\tan(\delta)_{el}$ given as the ratio of imaginary and real part permittivity. It is a measure for the energy efficiency of polarization effects in the dielectric. For DEs the loss factor $\tan(\delta)$ might gain importance depending on the operation frequency of DETs.

$$\tan(\delta)_{el} = \frac{\varepsilon''}{\varepsilon'} \qquad \text{Eq. 1.20}$$

1.3.2 Conductivity and dielectric breakdown strength

The applied electric field might cause the migration of ions or electrons through the material. As this leads to leakage current of the charged DET the DE used should neither contain ions nor allow electron transport. Typically, elastomers are not electron-conductive due the absence of π-bonds in the polymer backbone. However, ionic impurities or ions formed inside the material due to heterolytic dissociation might contribute to the conductivity of the DE. Particularly, water molecules and their dissociated ions have to be mentioned with respect to DET applications in a humid environment. Typical conductivity values of DEs range around 10^{-15} S/cm in laboratory environments.

Conductivity of the DE is not only an issue regarding energy efficiency but also its life time. Even small leakage current I_{leak} (µA) will result in a considerable amount of energy loss given the high electric fields that are typically applied on DEGs and DEAs. The electric power is converted into heat. Eq. 1.21 illustrates this aspect that is even more significant for multi-layer DETs as the amount of heat that must be dissipated multiplies. P_{el} is the electric heat power delivered to the DE which is linearly dependent on the applied electric field E, the leakage current I_{leak}, the thickness d and the number of layers n.

$$P_{el} = E\ d\ I_{leak}\ n \qquad \text{Eq. 1.21}$$

This is a serious concern for the scale-up of DET devices. In a multi-layer DET of 100 layers with a film thickness of 100 µm driven by an electric field of 50 V/µm,[24] a hypothetical leakage current I_{leak} of 10 µA would lead to a heat power of 5 W to be dissipated to the outside environment.

The dielectric breakdown strength E_{max} is closely related to the leakage current. It defines the utter limit of electric field applicable on the DE before a sharp increase in electric current through the DE accompanied by a drop of the applied voltage is observed. Usually, electrical breakdown leads to the destruction of the DE. However, there are also examples of self-healing DEs.[126] Apart from external factors *e.g.* temperature,[163] humidity, electrode shape and area as well as operation frequency there are also intrinsic parameter of the DE that influence E_{max}. The elastic modulus of the DE *i.e.* the density of cross-links of the elastomer affects the E_{max} which is also related to EMI of the elastomer in case of large deformations.[160,164,165] The applied mechanical prestrain also influences E_{max} which can also be related to the non-linear behavior of the elastic modulus of the elastomer used.[166–168]

Therefore, for the evaluation of E_{max} as an intrinsic material property, the sample size *i.e.* area and thickness, the properties of the compliant electrode, the environmental conditions *i.e.* temperature and humidity as well as the outside mechanical manipulation must be taken into consideration.[68]

1.4 Materials for dielectric elastomer transducers

Starting from Roentgen in 1890 who used a strip of natural rubber *via* Pelrine in 2000 who used commercially available silicone rubber and adhesive band *VHB*, scientists have used various DE materials either commercially available or specially designed elastomers for DETs.[1] One possible performance assessment of various DE materials reported in recent years is the simple description as figure of merit (FOM) for DEAs or DEGs as shown in Eq. 1.22[169] and Eq. 1.23[170]. In Eq. 1.24 the FOM of DEGs is related not only to the dielectric properties *i.e.* relative permittivity and dielectric strength but also to the mechanical strain energy function φ *i.e.* the strain-dependent elastic modulus of the elastomer. In Eq. 1.30 the figure of merit for DEAs is determined by the dielectric properties *i.e.* relative permittivity ε' and dielectric strength E_{max} and by the elastic modulus *Y*.

$$FOM_{DEA} = \frac{3\,\varepsilon\prime\varepsilon_0 E_{max}^2}{Y} \qquad \text{Eq. 1.22}$$

$$FOM_{DEG} = \frac{\varepsilon\prime\varepsilon_0 E_{max}^2}{2\varphi} \qquad \text{Eq. 1.23}$$

Certainly, FOM values should be considered with caution as the focus is on the maximum performance of the device exclusively. Reported values of the dielectric strength E_{max} can be misleading as the electromechanical strain is suppressed, the elastomer is heavily mechanically prestrained or the electrode area is unclear. In addition, also values of the electromechanical sensitivity ε'/Y are given in literature in comparison to reference materials.[125,126]

Reliability, durability, temperature-independence, processibility in thin films, cost-efficiency and toxicity of the DE can be equally important depending on the field of application of the DET. However, standardized tests and thus simple FOM values for reliability or processibility do not exist. As an example, mechanical prestrain of thin film elastomers might be considered as an additional working step in the manufacturing of DET devices. It increases costs and is not applicable in the manufacturing of multi-layer-actuators.[36] However, mechanical prestrain reduces the thickness of the elastomeric membrane. This might be attractive whenever direct film processing does not yield thin films in high quality at reasonable costs.[31]

This complicates comparison studies on various dielectric elastomer materials. Moreover, the intrinsic material parameters are not equally important for all DET applications. High voltages *i.e.* high electric fields are not applicable in wearable textiles or medical implants. Soft materials result in a high FOM. The output work of the DEA will be rather low though.

There is a multitude of data regarding the electromechanical performance of DEA test devices. A direct comparison is rather complex though. Many tests were based on mechanical manipulation of the DEA such as mechanical prestrain, a bias air pressure during the measurement,[171] and mechanical influence of the passive area of the DE. Moreover, the size of the DET *i.e.* the area and thickness is a crucial aspect for the dielectric strength, and thus performance of the DET. Over the last years, four polymer classes were intensely studied for DET application *i.e*. PDMS, polyacrylates, natural rubber and polyurethanes. Table 1.2 gives an overview on the most prominent material parameters for the different material classes.

Table 1.2 Properties and molecular structure of typical dielectric elastomer materials, adapted from literature.[1,2,31]

Material class	Relative permittivity ε'	Elastic modulus *Y* [MPa]	Dielectric strength E_{max} [V/µm]
PDMS	3	0.05-1.3	60-100
Polyacrylates	3-6	0.05-3	200
Polyurethanes	6-7	1-17	130-220
Natural rubber	3	0.1-1	20-120

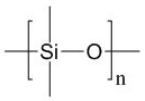

Polydimethylsiloxane

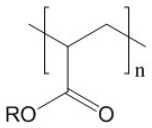

Polyacrylate

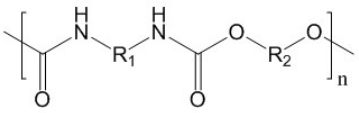

Polyurethane

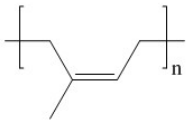

Polyisoprene/Natural rubber

It should be emphasized that the DE materials might not have been selected necessarily based on their properties but due to their commercial availability. The most-frequently used *VHB* acrylate was initially designed as adhesive tape and the natural rubber elastomer 'OPPO BAND 8003' was developed for the commercial market of physiotherapy equipment.[139] The exact chemical composition is unknown. This severely hinders the analysis of structure-property relationships. In the following sections scientific reports are highlighted based on the performance of DETs and on relevant information of the chemical structure of the DEs in particular. In addition to the electromechanical performance assessment, the lifetime and the processibility of thin films must always be taken into consideration in the design of novel dielectric elastomers.

1.4.1 Polyacrylates

Polyacrylate dielectric elastomer thin films were among the first commercially available materials studied for DET applications. The *VHB* adhesive films can be obtained with a thickness of 50 µm (*VHB F9460PC*), 500 µm (*VHB 4905*) and 1000 µm (*VHB 4910*). The exact chemical composition of *the VHB* adhesive films is unknown. *VHB* films were employed without any chemical modification and met many requirements of DET applications. In DEAs, the *VHB* film showed area strains of 380%, and linear strains of 220% were reported at electric fields of more than 400 V/µm strongly depended on the mechanical prestrain applied.[35] The mechanical stability of the *VHB* film allowed high prestrains up to 600% biaxial strain that also allowed the reduction in film thickness in order to operate at lower driving voltages. *VHB* films showed a mechanical strain at break of more than 800%. Interestingly, ε' and E_{max} strength tended to be dependent on the elastic regime.[173] Without prestrain E_{max} was 20 V/µm, whereas for 500% laterally prestrained *VHB* film E_{max} of over 200 V/µm was reported.[168] Without mechanical prestrain the maximum area actuation strain of the DEA drops correspondingly to 8% only.[174] ε' decreased from 4.7 to 4.5 with an area strain of 20%. As there are different types of *VHB* adhesive films a general elastic modulus *Y* cannot be given. In literature various elastic modulus values from 0.05 MPa (*VHB 4905*),[140] 0.2 MPa [126], 1-2MPa[31] up to 3 MPa (*VHB 4910*)[35] were published. It is important to highlight the tensile behavior of *VHB* as it shows a typical strain-softening trend at low strains. In case of *VHB 4905* the elastic modulus decreased from $Y_{10\%}$= 0.15 MPa to $Y_{100\%}$= 0.03 MPa.[126] Thus, the material was very prone to EMI without mechanical prestrain.[90,166] In addition, *Y* increased drastically below 0°C due to the relatively high glass transition temperature of -40°C.[175,176] The adverse effect of humidity on the lifetime of acrylic DEAs was also perceived critically.[31]

Despite the strong performance in reaching extraordinarily high actuation strains in mechanically prestrained DEAs, the viscoelastic behavior of *VHB* adhesive films was a serious concern for the reliability and life time of DET devices.[112,142] Viscoelasticity led to a very slow electromechanical response of approximately a second in a DEA test device.[31] Stress-relaxation appeared to be very pronounced. After 10 seconds less than 50% of applied stress was preserved in the elastomeric film.[140,177] DMA revealed mechanical losses *tan(δ)* of 0.05-0.1 in the frequency range of 1-10 Hz.[35] Also for DEG applications, VHB thin films were extensively tested.[17,61,178] The viscous losses were reported as serious challenge in the realization of efficient and reliable electric power generation.[178]

To overcome the necessity of mechanical prestrained *VHB*, the latter was chemically manipulated in order to obtain an interpenetrating elastomeric network.[36,127,177,179] For this purpose the *VHB* thin film was 400% mechanically stretched and treated with 1,6-hexanediol diacrylate which polymerized inside the *VHB* polymer network. 35-55 wt% were sufficient to conserve the complete mechanical prestrain applied on the pristine *VHB* polymer network. Even at 5 wt% of 1,6-hexanediol diacrylate 100% of mechanical prestrain was preserved.[127] DEA test devices showed area actuation strains of up to 300% at 400 V/µm.[180]

This strategy was also combined with the addition of plasticizers in order to soften the elastic modulus simultaneously. Trimethylolpropane trimethacrylate formed an interpenetrating network leading to higher mechanical stability but also a rise in the elastic modulus. This was compensated by the addition of plasticizer molecules *e.g.* bis(2-ethylhexyl) phthalate.[179] Area actuation strains of 40% at 50 V/µm were achieved. Again, pronounced viscoelasticity of the interpenetrating networks was observed at higher DEA operation frequencies *i.e.* 2-15 Hz by a decrease in area expansion to only 30% of its

maximum value. Interestingly, the temperature dependence of area actuation strain was less significant. The DEAs could be operated until -40 °C. The positive effect of plasticizers on the glass transition temperature of *VHB* had been reported already in 2004.[181] The general downside of these strategies is their dependence on the commercial *VHB* thin film with unknown chemical composition.

There are recent examples of chemically-tailored polyacrylate DEs. The designs focus primarily on the mechanical properties of the acrylic elastomer and less on enhancing the relative permittivity. The first example by W. Hu *et al.* is a thermoreversibly cross-linked acrylate due to the reversible character of the Diels-Alder reaction of furan and maleiminde moieties.[182] The radical polymerization is UV induced. DEA area actuation strain of approximately 35% at 65 V/µm were reported for an area of 6 mm in diameter and a thickness of 100 µm using 5% biaxial prestrain only. The mechanical loss tangent *tan(δ)* varied from 0.05-0.1 depending on the elastic modulus which could be controlled by the thermoreversible Diels-Alder cross-linking reaction. The preparation of thin films with a thickness of about 100 µm was solvent-free. However, the polymerization and cross-linking process are time-consuming (> 24h) and labour-intensive as the thin film thermoplastic had to be removed from a top and bottom-substrate before thermally induced Diels-Alder cross-linking.

Another approach utilizes atom-transfer-radical-polymerization (ATRP) of monoacrylic terminated PDMS of low molecular weight cross-linked by the telechelic diacrylic terminated PDMS.[171] The polymerization and cross-linking is simultaneously UV induced (Scheme 1.1). Thin films of 250 µm were prepared protected from air by a top and bottom substrate with a monomer conversion of about 90%. This necessitated tedious work-up steps *e.g.* extraction of monomers, deswelling with a non-solvent and removal of volatiles *in vacuo*. The obtained bottlebrush elastomer showed favourable strain-stiffening tensile behavior. Thus, it did not suffer EMI and achieved area actuation strains of approximately 300%. However, the sample was mechanically manipulated by a bias air pressure during the electromechanical charaterization. The elastic modulus could be tuned by the concentration of cross-linker and was below 0.1 kPa. The relative permittivity ε' was below 3 due the high amount of PDMS side chains. Viscoelastic properties were not tested.

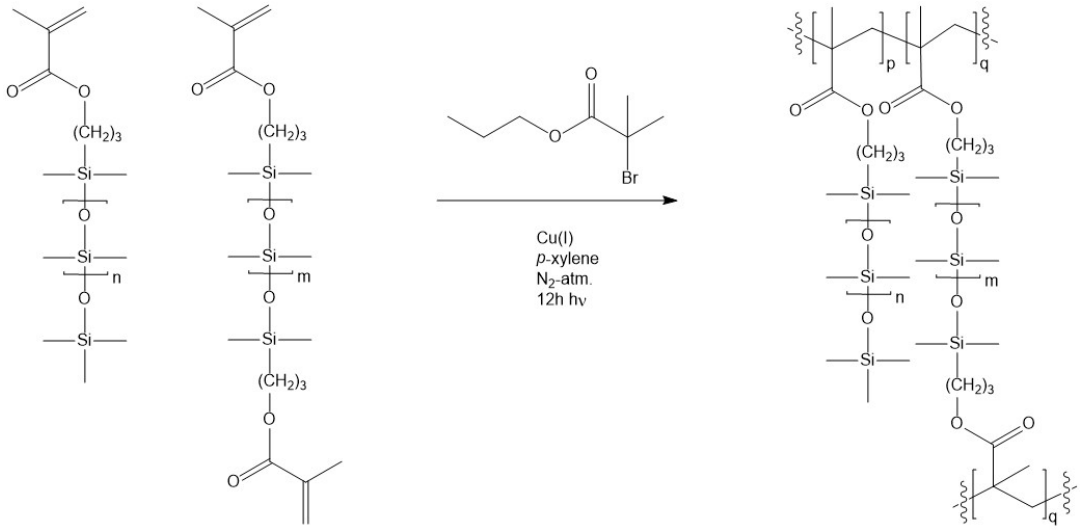

Scheme 1.1 ATRP of monoacrylic terminated PDMS cross-linked simultaneously by the diacrylic terminated PDMS.

Most recently, Zhao *et al.* presented the cross-linking of via epoxy-opening reaction of the side groups of the polyacrylate.[183] The polymer was synthesized by ATRP of *n*-butyl acrylate and 2,3-epoxypropyl methacrylate. The polymerization under inert atmosphere showed a monomer conversion of about 90%. The preparation of thin films (280 µm) took about 12h at 80 °C. The elastic modulus of the elastomers obtained ranged from 0.1 to 0.41 MPa with a relative permittivity ε' of almost 6. An area actuation strain of 50% at 20 V/µm was reported. The viscoelasticity was characterized by DMA. At ambient temperature mechanical losses *tan(δ)* of more than 0.5 was found. In cyclic stress-strain curves strong hysteresis was observed. Permanent deformation of 10% after the first cycle might raise doubts on the durability of these acrylate elastomers in any DET application.

Until today, polyacrylate elastomers miss the mechanical stability for technological exploitation in DETs. Slow and laborious production methods are an additional obstacle. This is in sharp contrast to their unprecentented high actuation strains in DEAs facilitated by their high dielectric strength.

1.4.2 Polyurethanes

Polyurethanes are prepared in a step-growth polymerization of diisocyanates and dialcohols. Polyurethane elastomers can be physically cross-linked thermoplastic elastomers or chemically cross-linked thermosets. The urethane group has a strong impact on the relative permittivity ε' of the elastomer. Values between 7 and 12 are reported for ε' depending linearly on the concentration of the urethane moiety.[31] Chemical cross-linking is realized by the incorporation of tri- or tetra-functional monomers. Physical cross-linking of polyurethanes can be observed *via* intermolecular forces such as hydrogen bonding between the urethane group or crystallization of polyurethane segements. This might be an advantage in the production of DEs as the thermoplastic polyurethanes can be easily processed in the molten state. This might explain why polyurethanes gain attention not only from academia[184–186] but also from industry. This advantage in processibility was exploited in the fast and low-cost film casting process giving access to thin films of 50 µm only.[31] The industrially developed polyurethane thin film *Bayfol EA 102* showed an elastic modulus of 1.44 MPa at 50% strain, a relative permittivity ε' of 7.1 and a dielectric strength of 130 V/µm. The viscoelastic losses were reported to be 20 times lower than for the acrylic VHB films. However, the high polarity of polyurethanes led to an increased sensitivity against humidity. Also, the elevated conductivity of polyurethanes is considered as a remaining challenge for DET operations as it leads to significant leakage current.[28]

Leakage current and heat formation in DEAs was already observed by Pelrine *et al.* in 2000.[28] The commercial elastomer *Deerfield PT6100S* showed an area actuation of 11% which corresponded to an output pressure of 1.6 MPa as the elastic modulus was 17 MPa. The applied electric field was 160 V/µm with a relative permittivity of ε' of 7. The elastic modulus of polyurethane might be considered as a severe issue for DEA and DES applications. For DEGs the elastic modulus of the elastomer can be higher and must be adapted to the outside mechanical stress in any case.

In 2008 Petit *et al.* characterized the electromechanical performance of a carbon nanopowder polyurethane composite based on the commercially available polyurethane *TPU5888*.[184] In a solvent-based process elastomeric films with a thickness of around 70 µm were obtained. Apart from the actuation strain of 8% at 8 V/µm, no additional information were given on the mechanical behavior. The chemical composition of polyurethane *TPU5888* was not revealed.

More recently, Liu *et al.* presented a graphene oxide polyurethane composite.[185] The elastic modulus was in the order of 3 to 7 MPa. Nonetheless, the rise in conductivity was significant from 10^{-12} S/cm of particle-free polyurethane to 10^{-7} S/cm of the composite. Again, the chemical structure of the polyurethane was not elucidated. In 2017 the graphene oxide polyurethane was modified by the addition of polyethylene glycol.[187] This led to material with reduced elastic moduli below 1 MPa accompanied by an increased conductivity of 10^{-8} S/cm. The dielectric strength of the DEAs was of less than 10 V/µm. The values of relative permittivity ε' could be enhanced up to 70 at 10^{-3} Hz. However, the values were significantly lower at higher frequencies and the strong increase was accompanied by an increase in dielectric losses which was a clear sign for ionic conductivity and interfacial polarization of the electrodes even at 10^{3} Hz.

There are no reports on the targeted design of polyureathane elastomers for DEGs until 2017 when Wang *et al.* published the synthesis of a barium titanate polyurethane composite and also tested it electromechanically.[186] The polyurethane thermoplastic of unknown chemical composition was commercially available (*Elastollan 1185A10*). In order to compensate the stiffening effect of the barium titanate, dibutyl phthalate was used as plasticizer. The tensile strain at break ranged between 280% and 800% with tensile strengths over 6 MPa which can be relevant for DEG applications. The rise in elastic modulus could be attenuated by the addition of plasticizer to values around 10 MPa. Containing 50 wt% barium titanate, the composite achieved a value of relative permittivity ε' of about 13. As a result, the harvest energy density in a DEG test device was 8 times higher compared to *VHB* thin film.

In summary, the evaluation of the potential of polyurethane elastomers for DET applications is restricted by the insufficient amount of data. This might be explained by the interest of industry which commonly does not publish all relevant data. However, until today custom-tailored DE materials based on polyurethanes have not appeared on the commercial markets. Based on the provided data from academia there is still a lack of clarity on the conductivity level and elastic modulus of pol-

yurethane DEs. Both seem to be too high for DET applications. In Section 1.5.1, the impact on conductivity of polyurethanes blended in PDMS elastomers will be discussed in greater detail.

1.4.3 Natural rubber/polybutadiene elastomers

Starting with the experiment of Roentgen in 1880, natural rubber elastomers have been attractive materials for DETs.[28] The simplified structure of natural rubber is 1,4-polyisoprene. The fundamental challenge that Roentgen was confronted with in 1880 remained considerable today. The exact chemical structure of natural rubber or related polybutadiene elastomers that were tested for DET applications was unknown in most studies. Hence, a direct correlation of chemical structure to elastic and dielectric properties is difficult. No detailed chemical information were given neither for *Isoprene Natural Rubber Latex* tested by Pelrine et al.[28], nor for *Dr.Scholls™ gelactive tubing* presented by Carpi *et al.*,[188] nor for ZruElast™ studied by Tröls *et al.*,[160] nor for the *TheraBand™ Latex Free Resistance Band Yellow* and the *OPPO Band Red 8012* reported by Vertechy *et al.*[139]. Particularly, the nature of cross-linking remained unclear. A common feature of the reported polybutadiene elastomers was their relative permittivity ε' of about 3 and the low elastic moduli below 1 MPa. Values of dielectric strength E_{max} varied from 67 V/µm,[28] 80-90 V/µm[139,189] to 120 V/µm[160]. The deviation might not only be related to intrinsic material properties but also to variations of the measurement condition.[160] The *OPPO Band 8003* and *ZruElast™* were also intensely studied with respect to their application in DEGs.[190] The authors observed significant hysteresis *i.e.* permanent mechanical deformation in the first operation cycles which they attributed to the Mullins effect of the elastomers.

Most notably, polybutadiene elastomers were already used in the targeted design of high permittivity DEs. In 2012 nitrile-butadiene DEs were published with a relative permittivity ε' of 23.[191] The DEs were synthesized by peroxide-induced cross-linking of hydrogenated nitrile–butadiene copolymer. The copolymer was commercially available with different nitrile concentration. A direct correlation of nitrile content to relative permittivity and elastic modulus was reported. Actuation strains of 12-16% were observed at electric fields of 30-50 V/µm without mechanical manipulation of the specimen. By using dioctyl phthalate as plasticizer the elastic modulus could be reduced from 2.7 MPa to 1.4 MPa. The impact of the plasticizer was demonstrated by the electromechanical strain of more than 20% below 30 V/µm. However, the influence of the plasticizer on the viscoelastic behavior of the DE and its DEA lifetime was not discussed.

Polybutadiene and natural rubber contain the carbon double bond as part of the polymer backbone, in contrast to polyurethane, polyacrylate, and PDMS. It can be used for post-polymerization modifications. The traditional cross-linking reaction of raw natural rubber is based on the addition of sulfur on the carbon double bond generally known as vulcanization.[192] More recently, the reactivity of the carbon double bond was utilized by Ning *et al.* in the UV induced thiol-ene addition of methyl thioglycolate[193] or thioglycolic acid[194] on the poly(styrene)-block-poly(butadiene)-block-poly(styrene) thermoplastic (Scheme 1.2). Elastomeric films were obtained by solution casting followed by drying at 50°C under vacuum. An increase in T_G was observed due to thiol-ene functionalization. In case of thioglycolic acid the T_G reached ambient temperature already. For methyl thioglycolate functionalization values of relative permittvitiy ε' of 12 with an elastic modulus above 3 MPa were reported. This corresponded to an actuation strain of about 6% at 30 V/µm. Data regarding viscoelastic behavior, conductivity and actuator lifetime were not provided, so far.

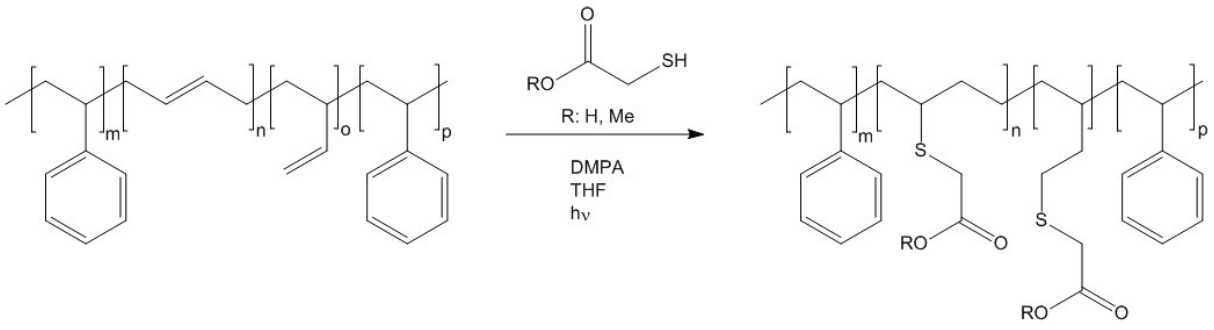

Scheme 1.2 UV-induced thiol-ene addition on poly(styrene)-block-poly(butadiene)-block-poly(styrene).

1.4.4 PDMS elastomers

The terms *silicone elastomer, silicone rubber* or *siloxane elastomer* are mostly devoted to chemically cross-linked polydimethylsiloxane. The backbone of this polymer is the silicon oxygen single bond. In contrast to all other promising DE candidates, PDMS is the only polymer with an inorganic backbone. The silicon oxygen single bond is much longer *e.g. 1.63* Å in $(SiH_3)_2O$[195] than the carbon oxygen single bond *e.g.* 1.41 Å in $(CH_3)_2O$[196] and the bond angles are much larger *e.g.* Si-O-Si 144.1° in $(SiH_3)_2O$; C-O-C 111.5° in $(CH_3)_2O$.[197] Macroscopically, this leads to a greater polymer chain flexibility of PDMS and thus its low glass transition temperature and low viscosity.[198] It also explains the temperature operation range of PDMS elastomers which is an important requirement for DETs operated in fluctuating weather conditions.[35] Properties of PDMS are summarized in Table 1.3.

Table 1.3 Important chemical properties of siloxane.[198]

Property	Value
σ-Si-O-bond length[195]	1.63 Å
σ-Si-O-bond energy[199]	445 kJ/mol
σ-O-Si-O-bond angle[197]	144°
Siloxane rotation energy [200]	≤ 1 kJ/mol
Glass transition temperature[201]	≤ -120 °C

In addition the polysiloxanes show an outstanding chemical stability *e.g.* against UV irradiation, ozone, air and heat.[122] PDMS elastomers are always chemically cross-linked. Polymerization and cross-linking reactions of PDMS are well-established and will be discussed in detail in the following sections. The elastic modulus and the mechanical strength depend on the cross-linking density. It can also be tuned by addition of filler or plasticizer. The non-polar character of the dimethyl side group gives PDMS elastomers a hydrophobic character that enables constant functionality of the DE even at high levels of humidity. Hence, it is a particularly attractive material for DEGs in ocean wave energy harvesters.[68] However, the missing polarity of the side groups and the polysiloxane backbone results in the low relative permittivity ε' of 3 only. Nonetheless, PDMS elastomers are the only DE products that reached maturity for commercial markets.[54,56] Elastosil®Film is produced in DIN A4 film sheets available in various layer thicknesses with a minimum of 20 µm.[98] Relevant dielectric and mechanical properties are given in Table 1.4. The thin films are used as reference material in this work.

PDMS elastomers have already been extensively studied since the beginning of 2000.[22] Firstly, many commercially available PDMS formulations were tested e.g. *NuSil CF19-2186*, *HS3* of Dow Corning,[22] and *Sylgard 186.*[28,35] For *NuSil CF19-2186* the DEA lifetime in the order of million cycles was reported.[35] In comparison to the *VHB* acrylate the overall actuation strain was smaller in case of mechanically prestrained DEs.

Table 1.4 Dielectric, mechanical and electromechanical properties of Elastosil®Film.

	ε	$Y_{10\%}$	*Emax*	s_{act}	σ	$tan(\delta)_{DMA}$
Elastosil®Film	2.9	1.2 MPa	95 V/µm	4.5%	2 10^{-14} S/cm	0.03

This could be rationalized by the lower dielectric strength of PDMS elastomers. However, in measurements without high mechanical prestrain, PDMS elastomers showed higher actuation strains or higher mechanical output pressure depending on the elastic moduli (Y = 0.1-1 MPa) of the PDMS elastomers compared to *VHB*. The superior DEA performance of *NuSil CF19-2186* was also demonstrated by its ultra-fast time response which allows DEA operations in the order of 10^3 Hz.[202] Another silicone of Dow Corning, *DC3481* cross-linked with *81-R* was tested in comparison the acrylic elastomers.[140] The low viscous losses resulting in faster response speed and high mechanical stability were considered as the main advantage of the silicone. However, the achievable actuation strains of the DEAs based on acrylic elastomers were higher. *DC3481* was converted with various cross-linkers *81-R*, *81-F* and *81-VF* in various concentrations. The elastic properties were tuned accordingly. A clear correlation between maximum actuation strain and the dielectric strength was found. The rise in dielec-

tric strength was accompanied by an increasing elastic modulus.[124] In addition, the polar cross-linkers *81-F* and *81-VF* led to a small increase of relative permittivity of 3.7. Already in 2005 the commercial silicone *TC-5005 A/B-C* was selected in the construction of complex multi-layer DEAs due to its simple tuning of mechanical properties and its reliable actuation strain in the absence of mechanical prestrain.[203] The time-dependent DEA performance of the silicone *Neukasil RTV-23* was analyzed in detail.[204] In contrast to *VHB 4910* and the natural rubber based elastomer, the silicone could be operated at frequencies above 0.1 Hz with a constant actuation strain. Again, rheology tests revealed the very low viscoelastic losses of *Neukasil RTV-23* compared to the acrylate and natural rubber materials. Commercially available silicone thin films *i.e. Elastosil RT 625* with a thickness of 40-100 µm have been used in the engineering of DEAs[177] and DEGs,[68,72] already. A long-term stability of over 1 million cycles was reported for silicone DEAs.[205]

In addition, engineering efforts in the development of thin film formation processes should not be ignored.[206–208] The reduction of silicone film thickness has the strongest effect on the operation voltage of DETs. Even though, an industrial implementation of academic developments *e.g*. molecular-beam-deposition, ink-jet 3D printing at reasonable cost might be challenging. Commercial PDMS formulations casted and bladed for a thickness of 20 µm still require driving voltages of the DE thin film in the order of hundreds of volts which limits the scope of application of DETs considerably.[30,37]

Based on the manifold research activities over the last 20 years and in comparison to alternative DE materials the relative permittivity ε' and elastic modulus Y must be considered as the only intrinsic material parameters of silicone elastomers that leave significant room for improvement. However, the reduction of elastic modulus corresponds to a reduction of output pressure of the DEA. Thus, for a given output pressure generated from the DEA the only intrinsic material parameter is the relative permittivity ε'. However, every modification of the siloxane might affect the cross-linking reaction of silicone elastomers. The clean and fast cross-linking reactions of PDMS elastomers give them a great technological advantage in the preparation of elastomeric thin films. PDMS multi-layer DETs are produced at a production speed of 5 minutes per layer.[209]

In Section 1.6, recent research activities on high permittivity silicones will be reviewed in detail.

1.5 Synthesis of PDMS elastomers

Due to the dominant role of PDMS elastomers in DETs the various well-established reaction techniques should be discussed in detail. Polysiloxanes can be synthesized by hydrolysis of chlorosilanes followed by polycondensation reaction of silanols under acidic conditions with a tertiary silanol as end-blocker. High monomer conversion is realized by the removal of water. In the synthesis of high molecular weight polysiloxanes ring-opening polymerization (ROP) is considered as the best option.[210] The initiator must be an ion exchange catalyst. ROP can be executed by anionic *e.g.* tetramethylammonium hydroxide[211] or cationic initiators *e.g.* sulfuric acid, bis(trifluoromethane)sulfonamide, trifluoromethanesulfonic acid.[212–214] It is either thermodynamically (thermodynamic equilibrium) or kinetically (irreversible end-capping) controlled. The molecular mass of the polysiloxane is tuned by the addition of tertiary siloxanes or by the monomer/initiator ratio in case of thermodynamic reaction control.[215] The reaction pathways of polycondensation and anionic ROP are outlined in Scheme 1.3. The removal of water during the polycondensation of silanols is the main driving force. The polysiloxane can be end-capped to stop the polymerization. End-blocking also hinders the formation of cyclic oligosiloxanes. The ROP of cyclosiloxanes relies on the gain of entropy due to the siloxane ring-opening. The polymerization kinetics is directly related to the size of the counterion. Polar additives such as DMSO and DMF further reduce ion-ion interaction of the living chain-ends and lower the tendency of anionic chain-end aggregation. Cyclotrisiloxanes show the highest reactivity in the ring-opening polymerization due to their ring strain. In contrast to carbon, 6-membered trisiloxane rings cannot form thermodynamically preferred conformations. The Si-O-Si bond angle in hexamethyltrisiloxane is 136°.[216] Finally in ROP, the active chain end can be either quenched chemically or by thermal decomposition of the ion pair which prevents tedious work-up procedures.[217]

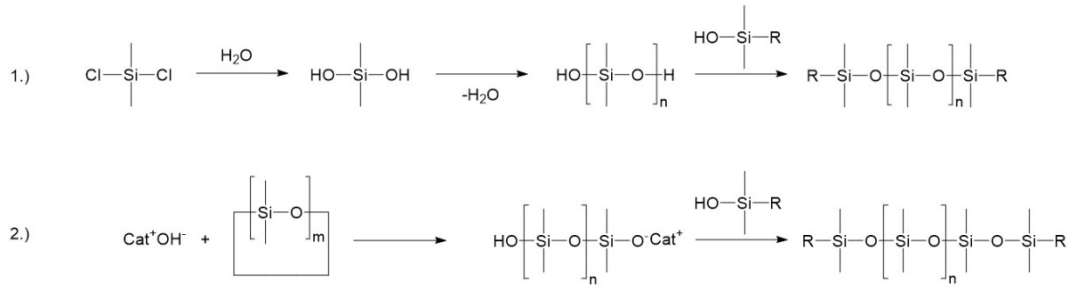

Scheme 1.3 Hydrolysis of secondary chlorosilane followed by the polycondensation of the corresponding secondary silanol. The polymerization process can be controlled by the addition of end-capping molecules *i.e.* tertiary silanols. 2.) Anionic ring-opening polymerization of cyclosiloxane followed by end-capping of the polysiloxane.

The end-capping reaction is irreversible and allows kinetic reaction control of anionic ROP. End-capping can also be realized by using tertiary silanolates as initiators in anionic ROP. Thus, possible side reactions *e.g*. *back-biting* and chain-transfer reactions can be eliminated (Scheme 1.4). The *back-biting* reaction of the reactive chain end of the polysiloxane is the back reaction of the chain prolongation step. Due to *back-biting* siloxane cycles are formed from the polysiloxane. The ring size varies from 3 up to about 20 siloxane units.[218] This can lead to a considerable amount of side products that need to be removed from the polysiloxane. Chain-transfer reaction occurs between an active polysiloxane chain end and another polysiloxane chain or any other molecule *e.g.* solvent and water impurities. The chain propagation reaction of the original chain is terminated, the reactive center is transferred and a new polymer chain starts propagating. This limits the control over the weight distribution of the polysiloxane.[218]

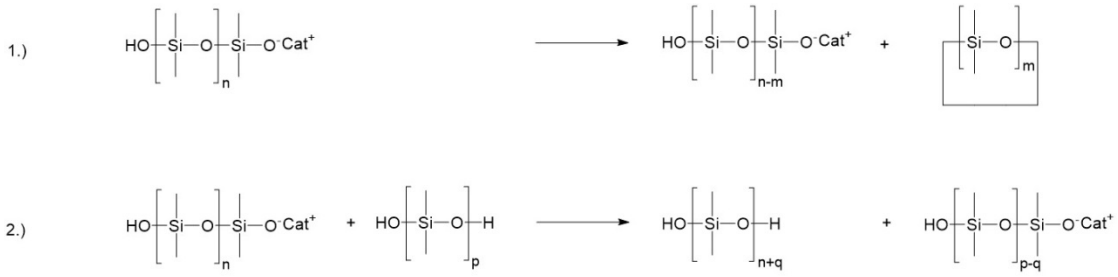

Scheme 1.4 *Back-biting* of the active polymer chain is the back reaction of the chain propagation reaction of ROP. It leads to a lower molecular weight of the polysiloxane and cyclosiloxanes as side products. 2.) *Chain-transfer* of the active polymer chain end due to intermolecular reaction with another polysiloxane chain.

The most important reaction pathway for PDMS elastomers is the cross-linking by the hydrosilylation reaction of silanes on vinyl-terminated PDMS.[219,220] Platinum catalyzed hydrosilylation reactions have been well-established since the early 1950s.[221,222] As catalyst hexachloroplatinum(IV) acid can be used as precursor directly (H_2PtCl_6 x $6H_2O$; *Speier's catalyst*) or in form of platinum(0)-1,3-divinyl-1,1,3,3-tetramethyldisiloxane in solution (*Karstedt's catalyst*).[223] The catalytically active platinum form is Pt(0). Pt(0) is formed *via* reduction with silane. The catalytic cycle is outlined in Scheme 1.5.

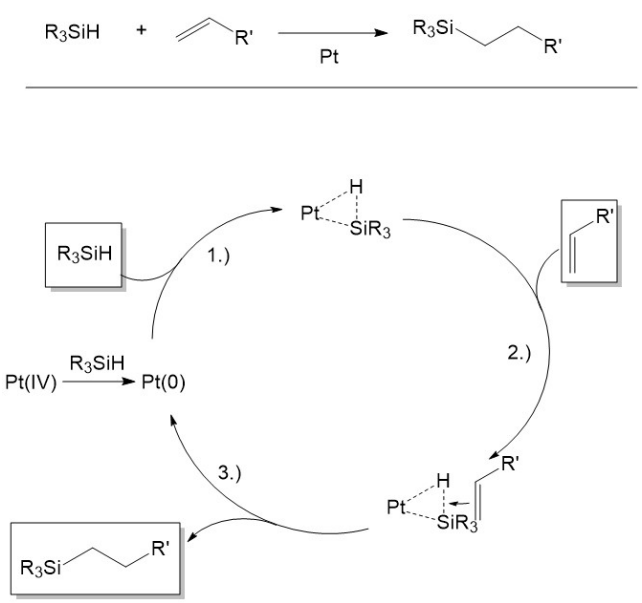

Scheme 1.5 General reaction scheme and catalytic cycle of the platinum-mediated hydrosilylation of alkenes, adapted from literature.[219] 1.) η^2- Si-H-Pt complex formation. 2.) Coordination of the alkene on the η^2- Si-H-Pt complex. 3.) Insertion of the alkene into the Si-H-σ-bond accompanied by simultaneous release of Pt(0).

A critical aspect in this process is the Pt-induced Si–H-σ-bond activation. An earlier concept proposed the oxidative addition of Pt(0) on the Si-H-σ-bond.[224] Recent studies on η^2-SiH_4 complexes suggest the formation of an η^2-complex as the reactive intermediate in the catalytic cycle.[225] This aspect might deserve some attention as the dehydrogenative silane coupling may occur as side reaction leading to unreacted vinyl groups. Further side reactions may result from the reactivity of the vinyl group used, *e.g.* isomerization of carbon double bonds, polymerization, and hydrogenation of the vinyl.[226] These side reactions play a key role. Side products or unreacted starting materials might not be easily removed from the elastomeric PDMS thin film. Even though *Karstedt's catalyst* is perfectly soluble in PDMS, the platinum-catalyzed hydrosilylation reactions cannot be considered as purely homogenous catalysis. Colloidal Pt(0) particles can be formed.[227] The surface of the Pt(0) particles is catalytically active as well.[228] However, there are no reports on the formation of particles and its effect on the dielectric and elastic properties of PDMS DE thin films. Novel *N*-heterocyclic carbene (NHC) platinum complexes proved to have a greater stability and a lesser tendency towards agglomeration. NHC platinum complexes cannot compete with the well-established catalysts in terms of catalytic activity *i.e.* turnover frequency though.[229] The PDMS cross-linking reaction proceeds in less than one minute at elevated temperatures of about 100°C with *Karstedt's catalyst*.[122] The amount of platinum that is consumed worldwide in this single reaction is estimated with 5.6 tons per year. Even though catalyst loadings could be optimized by modern reaction conditions to only 25-35 ppm, the platinum cannot be regained from the elastomeric PDMS.[230]

A considerable issue in the platinum catalyzed cross-linking reaction of PDMS is the sensitivity of the catalyst against functional groups or impurities *e.g.* sulfur poisoning.[231] This hinders its utilization in the cross-linking of functionalized polysiloxanes and polysiloxane composites.[229,232] Developments in the design of platinum complexes focus on the stabilization of the complex by electron-rich ligands *e.g.* phosphines[231] and NHCs[233–235]. Phosphines and *N*-heterocyclic carbenes as σ-donor ligands increase the electron density of the platinum and thus regulate its reactivity. Therefore, the selectivity is increased. They show a greater tolerance against a wide range of functionalities *e.g.* hydroxyl and epoxide moieties.[236] Recent reports of platinum-catalyzed hydrosilylation reactions compatible with sulfur compounds might also be highly attractive.[232,237] Up to now, none of these concepts could be utilized for a platinum-based cross-linking reaction of functional polysiloxanes. In the following Section 1.5.2 the consequences on the mechanical properties of high permittivity polysiloxanes due to sluggish cross-linking reactions will be discussed in detail.

An alternative to Pt-hydrosilylation cross-linking is the Sn-catalyzed condensation reaction (Scheme 1.6).[238–242] Very conveniently, one-package moisture-curable silicone solutions are commercially available *i.e.* self-condensating hydrosilanes.

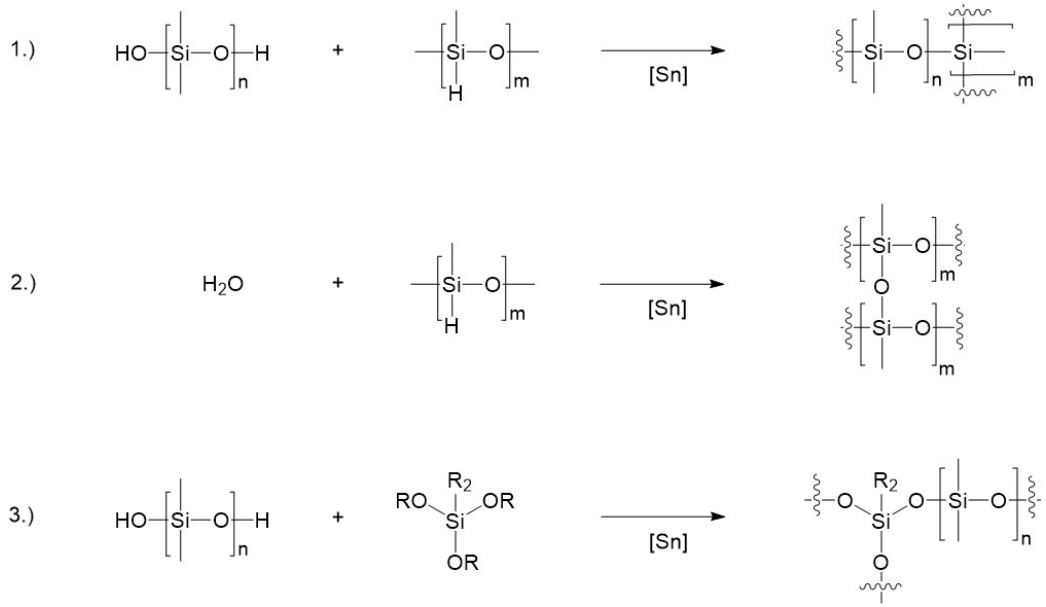

Scheme 1.6 Tin-catalyzed dehydrogenative silane-siloxane-coupling. 2.) Tin-catalyzed dehydrogenative silane-water-coupling. 3.) Tin-catalyzed siloxane-alkoxysilane-coupling.

It should be mentioned that organotin catalysts are toxic which narrows the scope of application. Its use and content in commercial products is regulated by law *e.g.* 0.1 wt% dibutyltin compounds are permitted in commercial products in the EU.[243,244] Dibutyltin dilaurate is a frequently used reagent showing high catalytic activity. It facilitates PDMS cross-linking at room temperature, commonly described as room temperature vulcanizing (RTV) silicones. The condensation of the hydroxyl-end-groups in the cross-linking makes the necessity of end-capping of the PDMS obsolete. Hydrosilanes (dehydrogenative coupling reaction), water or alkoxy/hydroxysilanes can be used as cross-linking agents. The catalytic cycle of the coupling of hydroxy-terminated PDMS and alkoxysilane is described in Scheme 1.7.[245] In case of cross-linking by the dehydrogenative coupling reaction the only byproduct is gaseous hydrogen. Due to the nature of the cross-linking condensation reaction with an alkoxysilane the corresponding alcohol is generated. In addition, the activation of the organotin-catalyst leads to acid formation. Thus, the concentration of organotin should as low as possible in order to avoid negative effects on the dielectric and mechanical properties of the PDMS elastomer.

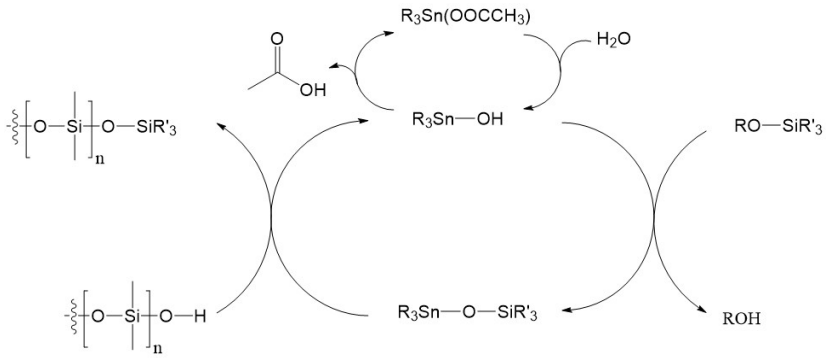

Scheme 1.7 Catalytic cycle of the organotin-catalyzed condensation reaction of hydroxyl-terminated PDMS and alkoxysilane.

In the presence of alcohol the cross-linking reaction of PDMS at 90 °C is reported to result in the formation of a viscous gel. The silanol end-groups are blocked by alcohol (Scheme 1.8). However, the tin-catalyzed PDMS condensation suffers from this side reaction only at elevated temperatures.[245] At ambient temperature a large excess of alkoxysilane is observed not to affect the cross-linking reaction adversely. It is the major advantage of organotin catalysts not to accelerate the coupling reaction of silanol and alcohol in comparison to other acidic catalyst *i.e.* sulfuric acid.

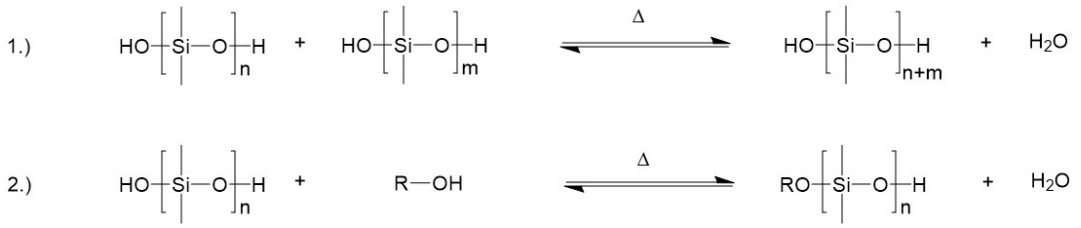

Scheme 1.8 Condensation of hydroxy-terminated PDMS chains at elevated temperature accompanied by H_2O formation. 2.) Condensation of hydroxy-terminated PDMS and alcohol at elevated temperature accompanied by H_2O formation.

The tin-catalyst condensation cross-linking reaction and its tolerance against functional groups will be further discussed in Section 1.5.2. In future, novel catalyst designs such as acrylic acids,[243] bismuth,[246] and carboxyamide[247] might substitute the toxic organotin catalysts in the condensation reaction of polysiloxanes. Organotitanium catalysts have already been well-established in the condensation cross-linking of silanes.[248–250] The sensitivity against functional groups, short shelf life and the release of acetic acid in case of acetoxytitanium catalysts is reviewed critically though.[251]

In contrast to tin and platinum catalyzed cross-linking reactions, metal-free cross-linking reactions have already been developed in 1948.[252] The reaction is illustrated in Scheme 1.9.[253,254] The cross-linking proceeds *via* radical intermediates generated by thermal radical initiators *i.e.* peroxides,[252] or homolytic bond cleavage due to high energy irradiation *e.g.* γ-irradiation [255–257]. The decomposition of the thermal radical initiator requires accelerated temperatures of up to 200°C (high temperature vulcanizing silicones). As the radical formation is not regioselective, there is only limited control on the cross-linking density of the elastomer and its mechanical properties. Approximately, the elastic properties depend on the concentration of radical initiator in case of highly reactive peroxides *e.g.* di-benzoyl peroxides. The use of less reactive radial initiators *e.g.* di-tertiary butyl peroxide allows the regioselective radical cross-linking of vinyl-substituted polysiloxane.[258] Due to the high reactivity of free radicals the cross-linking reaction is very sensitive towards functional groups. In siloxane composites *e.g.* carbon nanotubes in PDMS[259] were reported to suppress the radical cross-linking reaction. Moreover, the cross-linking process needs to be performed under inert atmosphere as oxygen reacts with radicals.

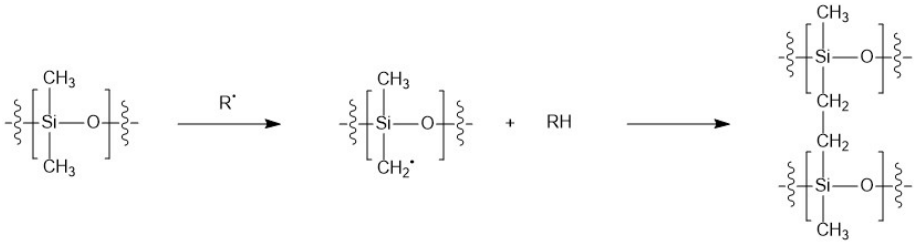

Scheme 1.9 High temperature free radical cross-linking of PDMS.

In recent years, the radical cross-linking of PDMS gained attraction due to the possibility of UV-induced cross-linking of telechelic acrylic siloxanes.[260,261] This allows regioselective cross-linking of the end groups and better control over the physical properties of the siloxane resins. PDMS-diacrylates were successfully cross-linked by acrylic cross-linkers in UV-induced radical cross-linking tested for various coating applications.[253] Radical formation due to the decomposition of photoinitiators under UV light is fast and the process is executed at ambient temperature. Interestingly, it is reported that the use of hydrosilanes facilitates radical cross-linking at air.[262]

An alternative metal-free radical cross-linking reaction is the thiol-ene addition of vinyl-substituted PDMS.[263–266] In general, the thiol-ene addition is characterized by the addition of the thiyl radical across a carbon double bond (Scheme 1.10).[267] The vinyl-functionality of PDMS is either introduced by copolymerization of vinylsiloxanes[211] or by vinyl-carrying end-blocker molecules[268]. As cross-linker either dithiols *e.g.* diethylene glycol di(ethanethiol) or thiol-functionalized PDMS[266] can be employed. The addition is regioselective yielding the anti-Markovnikov product. The thiol-ene addition is most frequently initiated by photoinitiators and UV light. Thermal radical initiators *e.g.* AIBN can also mediate the radical addition at the expense of prolonged reaction times and elevated reaction temperatures of at least 60 °C.[269–271] Photoinitiators such as 2,2-dimethoxy-2-phenylacetophenone (DMPA) facilitate full conversion within minutes.[272] However, the degradation products are not volatile.

The major advantage of radical thiol-ene addition over free radical cross-linking reactions is the insensitivity towards oxygen. Oxygen reacts with carbon radicals by forming peroxide radicals. The peroxy radical cannot activate the carbon double bond. Thus, the radical chain reaction based on carbon radical chain propagation is quenched by oxygen. In the presence of thiols, the peroxide radicals can react with the thiol though. New thiyls are formed that undergo radical addition on the carbon double rapidly. The conversion rate is faster for electron rich carbon double bonds. Full conversion of vinyl-terminated PDMS can be detected in less than one minute.[266]

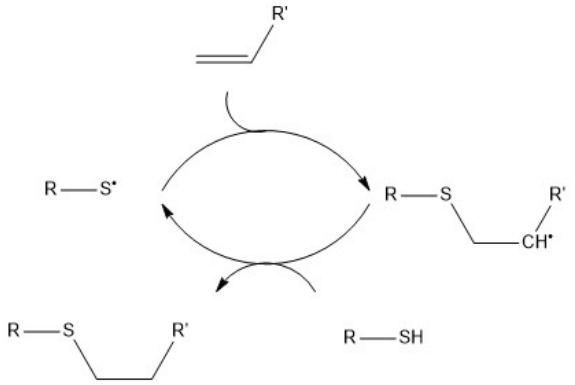

Scheme 1.10 Schematic description of the reaction mechanism of the thiol-ene addition.

Due to its high reaction rate at ambient temperature, high yields and versatility, and its tolerance against environmental influences *i.e.* moisture and air, thiol-ene reactions are commonly referred to as 'thiol click chemistry'.[273,274] The step-growth polyaddition of dithiols on divinyls is also extensively studied.[275,276] However, the formation of side products is not entirely suppressed. In particular, carbon radicals can add directly on adjacent carbon double bonds at low thiol concentration.[272,274] In case of an intermolecular addition of vinyl-substituted PDMS this leads to cross-linked PDMS elastomers as well. Interestingly, the thiyl radicals react very selectively with the vinyl group. This allows the mild chemical connection of various functional groups *e.g.* nitriles,[161] amines,[277] carboxylic acids and organo chlorides,[278] as well as sulfones[279] with vinyl-substituted polysiloxane.

In summary, most PDMS elastomers synthesized for DET applications were cross-linked *via* platinum-catalyzed hydrosilylation reaction. Apart from the very user-friendly commercial siloxane mixtures, this process is characterized by its high reaction speed, low toxicity, high conversion and selectivity. The cross-link density is controlled by the molecular weight of the vinyl-terminated PDMS. A serious disadvantage is the use of precious platinum as catalyst which cannot be regained. However, the catalyst loadings are very low and adverse effects on the dielectric properties due to the platinum catalyst have not been reported yet.

In free-radical cross-linking reactions the vinyl-groups also preferably react in the cross-linking of vinyl-substituted PDMS. However, the radical cross-linking reaction is less selective and requires either elevated temperatures when thermal radical initiators are used or UV-irradiation. In addition, the free-radical cross-linking reaction is inhibited by oxygen.

The organotin-catalyst cross-linking of PDMS is a rather slow condensation reaction. However, the cross-linking reaction proceeds at ambient temperature and humidity. So far, there are only reports from academia on the synthesis of PDMS elastomers for DET applications. The toxicity of organotin compounds might be a severe issue for the commercialization of PDMS dielectric elastomers cross-linked by this technique.

The thiol-ene cross-linking of PDMS is a relatively novel strategy. So far, none of the reported PDMS elastomers cross-linked by thiol-ene addition have been studied sufficiently with respect to its mechanical and dielectric properties. There is only one report that presents merely viscoelastic data.[268] In Section 1.6.2 and in Chapter 5 the thiol-ene cross-linking of functionalized polysiloxane and its corresponding mechanical and dielectric properties will be discussed in greater detail.

1.6 High permittivity siloxane elastomer materials

High permittivity siloxane elastomers can be categorized into two main classes of materials: Heterogeneous siloxane composites and chemically modified polar siloxanes. Composites consist of siloxane mixtures containing high permittivity solid additives. Silicone blends are mixtures of liquids and siloxane. This approach is well known from the addition of plasticizer to PDMS elastomers. So far, PDMS was exclusively chosen as siloxane matrix. Chemically modified polar siloxanes might also contain filler material contributing to the reinforcement of mechanical stability. However, the increase in permittivity is attributed to the chemical bonding of dipolar groups either into the polysiloxane side chain, the siloxane backbone or as part of the cross-linker. The assessment of the potential of novel PDMS materials for the DET technology is not trivial though. In many studies neither all relevant properties are reported nor is the exact chemical composition given. Nonetheless, several structure-property-relationships can be observed that are of general relevance for the chemical design of dielectric elastomers.

1.6.1. High permittivity silicone composites and blends

One of the advantages of mixtures is the simplicity of their preparation. The cross-linking reactions of PDMS are well-established. In the ideal case, filler and PDMS are homogeneously dispersible and the filler material does not interfere with the PDMS cross-linking reaction. This concept strongly relies on the compatibility of the high permittivity filler and PDMS. Aggregation of filler material inside the elastomeric composite must be excluded. Therefore, surface functionalization of several promising filler materials had to be done prior use. Homogeneous dispersibility is not only important for the insulating properties of the composite as aggregation might lead to conductive percolation pathways. It is also relevant for the mechanical stability of the elastomer during operation in the DET. Permanent deformation due to mechanical stretching limits the lifetime of DETs. The strain-softening effect (Mullin's effect) in the operation of dielectric elastomers is predominantly observed in elastomeric composites.[122]

The first report on DE siloxane composites can be dated back in 2003.[280] As filler material titanium dioxide, barium titanate, lead magnesium niobate-lead titanate and poly(copper phthalocyanine) were used. The properties of the resulting composites were not comprehensively investigated though.

In 2005, Carpi *et al*. presented the design of titanium dioxide siloxane composites for DEAs.[281] Rutile-type TiO_2 with an average grain size of 10 µm was suspended in a commercial three-component siloxane mixture. The mixture contained softener. Indeed, an increase in permittivity ε' of 6 was achieved at 30 wt% TiO_2, whereas the elastic modulus remained in the low kPa regime. The actuation strain of the composite was considerably higher at lower electric fields compared to the PDMS reference material. The transverse strain was given with 11% at 9 V/µm which was the maximum electric field of the DEA.

In addition, PDMS-surface functionalized TiO_2 nanoparticles (20 nm) were tested in a PDMS matrix.[282] The relative permittivity of the TiO_2 nanoparticles was ε' = 128 and the highest permittivity measured for the corresponding siloxane composite was up to 2.7 times higher compared to the pristine PDMS elastomer. However, a drastic increase in the elastic modulus *Y* was observed directly related to the weight amount of TiO_2. This resulted in a decrease of actuation strain but in an increase of output pressure of the DEA device. Lifetime experiments were not published but the mechanical loss factor tan(δ) was with 0.15 higher than in common PDMS elastomers. The mechanical losses were not related to the amount of TiO_2 filler. Thus, it is more likely that the understoichiometric amount of cross-linker in the commercial two-component siloxane mixture showed its detrimental effect on the viscoelasticity of the siloxane composite. The effect of titanium dioxide filler on the dielectric strength of siloxane elastomers was also tested. No adverse effect was found up to 12 wt% TiO_2.[283]

The commercial lead magnesium niobate-lead titanate powder $Pb(Mg_{1/3}Nb_{2/3})O_3$ /$PbTiO_3$ (ε'= 17.600 at 1kHz)[284] was reported to enhance the permittivity of siloxane elastomers.[285] The commercial three-component formulation *TC-5005 A/B–C* was used as siloxane matrix. 1 mm thick composite films with 30% volume fraction of filler showed a relative permittivity of about 15. The elastic modulus was around 100 kPa as *TC-5005 A/B–C* contained significant amount of silicone oil as softening agent. Electromechanical tests were not presented.

The impact of barium titanate particles on the dielectric and mechanical properties of siloxane elastomer was intensely studied by Böse *et al.* in 2011. The mean particle size was below 3 µm. As siloxane matrix the commercial Pt-catalyzed two-component mixture *RT 625* from Wacker was chosen. An increase in permittivity up to 11 was reached by the addition of 30 vol% of particles. The authors had expected higher values given the high permittivity of above 1000 for pure barium titanate. The processing in thin films failed due to the high viscosity of the 30 vol% barium titanate siloxane suspension. At maximum, only 20 vol% composite thin films could be manufactured. The elastic modulus Y was around 0.16 MPa due to the addition of silicone oil as plasticizer. The mechanical loss factor tan(δ) with 20 vol% barium titanate was around 0.1 at 1 Hz. The dielectric strength dropped from above 40 V/µm for the pristine PDMS elastomer to 20 V/µm with 10 vol% barium titanate. Remarkably, the actuation strain was measured in a multi-layer DEA test device. 20 layers were prepared by spin-coating with an average film thickness of 250 µm. At 20 V/µm, a maximum actuation strain of 6-7% compared to 1-2% of the pristine PDMS elastomer was realized by the incorporation of 20 vol% of barium titanate. Moreover, the impact of mechanical prestrain on the performance of DEAs made of barium titanate siloxane composites was studied.[286] Very recently, barium titanate siloxane composite elastomers with nanoparticles of an average size of 100 nm were prepared by high-temperature free radical cross-linking reaction.[287] The highest relative permittivity value reported was 3.9.

Calcium copper titanate ($CaCu_3Ti_4O_{12}$) prepared in a custom-made sintering process was evaluated for high permittivity siloxane composites.[288] The elastomeric composite was formed by peroxide mediated free radical cross-linking. Interestingly, up to an addition of 8 wt% filler material, only a moderate increase in the elastic modulus *Y* of around 500 MPa was reported. The relative permittivity could be enhanced to a value of $\varepsilon' = 5.5$. An improvement in electromechanical response (2% → 4% at 20 V/µm) was experimentally proven using pristine PDMS elastomer as reference material. Only 2 wt% of magnesium-doped calcium copper titanate powder were reported to enhance ε' in a siloxane composite by a factor of 0.4 (ε': 9.8 → 13.4 at 10^2 Hz) accompanied by a moderate increase in elastic modulus *Y* of about 10% (0.2 MPa → 0.23 MPa).[289] Accordingly, the actuation strain of a 500 µm thin film could be increased by a factor of 0.4 in a DEA test device.

Custom-made iron oxide nanoparticles in PDMS proved to enhance the relative permittivity in a PDMS composite up to 5.[290] The conductivity of the composite remained at a low level even at 20 wt%. However, the elastic modulus was about 1.9 MPa. Organic clay was also considered as high permittivity filler material in siloxane elastomers.[291] In 2018, montmorillonite clay ($(Na,Ca)_{1/3}(Al,Mg)_2(Si_4O_{10})(OH)_2$ x n H_2O) was reported to improve the relative permittivity of siloxane elastomers by a factor of 0.3 at a low weight amount of 4 wt% while keeping the elastic modulus *Y* below 500 kPa.[292]

Silicone oil and various liquid compounds were known for a long time to reduce the elastic modulus of PDMS elastomers. This is a fundamental contrast between liquids and solid filler material. Additionally, liquid additives can eliminate the need of solvent in the siloxane formulations. Therefore, mixtures of PDMS and high permittivity polymers and liquids were studied for DE applications.

Carpi *et al.* reported the positive effect on permittivity of undoped polythiophene as a highly polarizable conjugated polymer inside PDMS.[293] The commercial three-component PDMS formulation contained additional softening agent. The maximum weight amount was 6 wt% of polythiophene. The elastic modulus remained well below 100 kPa. The viscoelastic behavior was not studied. The enhancement of permittivity ε' of up to 9 (10^3 Hz) was accompanied by an increase in dielectric losses ε'' and conductivity at low frequencies. This was attributed to the diffusion of mobile charges through the PDMS blend. Nonetheless, the maximum actuation strain could be enhanced. At electric fields below 10 V/µm, the actuation strain of 6 wt% polythiophene-PDMS composite was 4 times higher compared to the pristine PDMS.

Furthermore, polyurethane-PDMS blends were studied.[294] The chemical composition of the polyurethane was unknown as the step-growth polymerization was performed directly in the PDMS formulation. 40 vol% polyurethane blended in PDMS resulted in a relative permittivity ε' of about 5.5 at high frequency. At low frequency (< 10^3 Hz) drastic electrode polarization was observed. This was attributed to the diffusion of free charges. Interestingly, in the polyurethane-PDMS mixture the diffusion of charges was more pronounced than in the pure polyurethane thermoplastic. This might be rationalized by the lower elastic modulus of the blend. The electric breakdown in the DEA measurement occurred below 10 V/µm already.

About 8 wt% of polyethylene glycol (M_n: 600 g/mol) in PDMS led to a reduction in elastic modulus *Y* from 0.4 MPa to 0.2 MPa.[295] The relative permittivity could be improved to a value of 5. However, the conductivity increased by a factor of 10 compared to the two-component PDMS elastomer.

A custom-made cyanopropyl-substituted silicone oil was blended in a custom-made PDMS formulation.[125] The vinyl-terminated PDMS (M_n: 67 000) was Pt-catalyzed cross-linked by a methylhydrosiloxane–dimethylsiloxane copolymer (*HMS-301*). The elastic modulus dropped from 1 MPa to about 0.2 MPa in case of 39 wt% of cyanofunctionalized oil. The relative

permittivity rose to a value of about 6. The DEA characterization revealed a drastic drop in dielectric strength from 80 V/µm to 20 V/µm clearly related to the addition of cyano-functionalized oil.

Fluoropropyl-substituted silicone oil was mixed with a two-component PDMS elastomer (*RT 625*).[296] The relative permittivity was between 5-6 with a maximum weight amount of 45% of fluorinated oil. The conductivity was below 10^{-12} S/cm. The elastic modulus of 45 wt% blend was below 0.1 MPa. The actuation strain improved by a factor of 5 until 10 V/µm when dielectric breakdown occurred. As the fluoropropyl-substituted silicone oil was vinyl-terminated it could have been incorporated into the elastomeric PDMS network as well. An increase in mechanical instability due to the addition of fluorinated oil was measured though. The mechanical loss factor tan(δ) ranged from 0.06 to 0.09 at 1 Hz.

Chloropropyl-substituted silicone oil was added to PDMS.[297] *LR3043/50*, a two-component PDMS formulation, was used. The elastic modulus declined below 0.1 MPa and the relative permittivity exhibited a maximum of 5.5 in case of 50 wt% polar silicone oil. However, the mechanical loss factor tan(δ) was about 0.45 at 1 Hz illustrating the negative effect of the silicone oil on the mechanical stability.

More recently, Glycerol-PDMS blends were reported as promising high permittivity dielectric elastomers.[298,299] 50 vol% of glycerol in PDMS resulted in a relative permittivity of about 12 while the conductivity remained below 10^{-13} S/cm. The elastic modulus was reduced to 0.3 MPa but the effect on the mechanical stability remained unclear as electromechanical and dynamic-mechanical measurements were not presented.

Conductive particles were tested for high permittivity siloxane composites. The enhancement in permittivity was accompanied by an increase in conductivity as well. Thus, the amount of filler was limited by the electric percolation threshold of the siloxane composite. Ag-siloxane composites showed conductivities above 1 S/cm with Ag filler (2-3.5 µm) loadings of about 13 vol%.[300] Custom-made graphene oxide sheets showed a smaller tendency to form conductive pathways in the siloxane composite. The conductivity of a 2 wt% siloxane composite was about 10^{-10} S/cm with a relative permittivity of about 8-9. The dispersibility of CNTs in PDMS could be improved by chemical bonding of siloxanes on the CNT surface.[301] Only 0.1 wt% of functionalized CNTs in a PDMS composite gave a relative permittivity of 3.7 with a dielectric strength of about 25 V/µm in DEA testing.

A percolation threshold of 1.6 wt% was reported for custom-made graphene nanoplates in PDMS.[302] The relative permittivity of the composite was about 12 with an elastic modulus *Y* of 1.2 MPa. A strong correlation of elastic modulus and filler content was observed. The Young's modulus increased from 0.5 MPa to 1.8 MPa with 2 wt% filler content. The dielectric strength of the composite was around 35 V/µm compared to 45 V/µm of the pristine PDMS elastomer. Commercially available expanded graphite was tested with a maximum amount of 4 wt% in PDMS.[303] The authors observed a dependence of dielectric strength on the mixing techniques. The permittivity of the graphite siloxane composite increased linearly in the range of 1-4 wt% filler content with a maximum permittivity of 8 for 4 wt% expanded graphite.[303] The dielectric strength declined from about 80 V/µm of the pristine PDMS to 20-50 V/µm of 4 wt% graphite content.

The formation of conductive pathways in siloxane composites due to conductive filler materials was a serious concern with respect to DET applications. An electrically insulating coating of conductive particles was considered as a possible solution.

In 2010, conductive polyaniline particles with a shell of poly(divinyl benzene) were dispersed in PDMS and cross-linked in a titanium-catalyzed condensation reaction. Interestingly, the Pt-based hydrosilylation cross-linking of the polyaniline PDMS dispersion failed.[304] The dielectric breakdown strength ranged between 50-60 V/µm even at 13-30 vol% filler content leading to elastic moduli between 400 kPa and 4 MPa in case of 30 vol%. The relative permittivity increased correspondingly from 4.2 (14 vol%) to 7.2 (30 vol%). Electromechanical tests proved the long-term stability of the composite for 1000 actuation cycles.[305]

Custom-made Ag/SiO_2 core-shell nanoparticles were tested in a PDMS as high permittivity siloxane elastomer.[306,307] The silica shell was less than 4 nm. The Ag/SiO_2 mean particle size was 60 nm. The composite was cross-linked by a tin-catalyzed dehydrogenative coupling reaction of the hydroxyl-terminated PDMS and hydrosilane. 18 vol% of Ag/SiO_2 core-shell nanoparticles could be added to PDMS without reaching the percolation threshold. The relative permittivity could be enhanced to a maximum value of 7.8. The elastic modulus *Y* increased from 0.2 MPa of the pristine PDMS to 7.5 MPa of the 18 vol% of Ag/SiO_2-PDMS composite. The use of a high molecular PDMS and thus the reduction of cross-linking density allowed a modulation of elastic modulus towards softer composites. A PDMS composite with 20 vol% Ag/SiO_2 was tested with a modulus Y of 1.4 MPa possessing a permittivity of 5.9. The electric breakdown ranged between 10 and 14 V/µm.

Very recently, Cu_xO-encapsulated Cu nanoparticles were used for PDMS composites and tested with respect to DET applicability.[308] Up to 30 wt% of Cu/Cu_xO particles could be added to PDMS without reaching the percolation threshold. Even though, the dielectric strength in the DEA measurements was considerably reduced to an electric field of about 12 V/µm.

Core-shell multi-walled CNTs were tested as high permittivity filler material in PDMS.[309] The hydroxylated surface of the carbon nanotube served as electric encapsulation. Indeed, the rise in conductivity was less pronounced compared to unfunctionalized CNTs. Nonetheless, the conductivity increased from 10^{-11} to 10^{-6} S/cm for 1 to 10 wt% core-shell CNTs in the siloxane composite. Therefore, the interpretation of relative permittivity values was complicated by the strong effect of interfacial polarization. In Chapter 4, functionalized nanospring-single-walled CNTs[310] in siloxane composites and their electromechanical performance in DEGs will be discussed in greater detail.

Table 1.5 Permittivity ε' and elastic modulus *Y* of novel silicone elastomers containing additives.

Additive	ε'	*Y* [MPa]	Additive	ε'	*Y* [MPa]
TiO_2	6	< 0.1	Fluoroalkyl silicone oil	5-6	0.1
$Pb(Mg_{1/3}Nb_{2/3})O_3/PbTiO_3$	15	0.1	Chloroalkyl silicone oil	5.5	0.1
$BaTiO_3$	11	0.2	Glycerol	12	0.3
$CaCu_3Ti_4O_{12}$	5.5	0.5	Multi-walled CNT	3.7	0.4
Fe_2O_3	5	1.9	Graphene nanoplates	12	1.2
Clay	3.6	0.5	Functionalized graphite	8	0.2
Polythiophene	9	0.1	Core-shell polyaniline	7.2	4.0
Polyurethane	5.5	-----	Ag/SiO_2	7.8	7.5
Polyethylene glycol	5	0.2	Cu/Cu_xO	8	> 1
Cyanoalkyl silicone oil	6	0.2			

Table 1.5 summarizes the properties of silicone composites and blends designed in recent years. Indeed, the addition of high permittivity additives allowed the preparation of high permittivity silicone blends and composites. However, the relative permittivity of many siloxane composites was much lower than initially expected.[282,285,311] The permittivity values were not additive based on the values of the single components.[312] It was proposed that polarization effects at the grain boundaries due to free diffusion of charges in the bulk material might be suppressed at the low filler concentration in siloxane elastomers.[313–315]

A general trend is the decline of dielectric strength E_{max} of all high permittivity silicone composites and blends. It remains ambiguous to what extent this can be exclusively related to the high permittivity filler. The elastic modulus also differed from the pristine PDMS elastomer used as reference material. In addition, the testing conditions *i.e.* electrode area, electromechanical strain, mechanical prestrain of E_{max} measurements varied considerably.

Until today, there was no silicone blend or composite film tested with a thickness below 75 µm.[305] The processing of siloxane composites in thin films is limited to the particle size. This requires precise control over the particle synthesis process, particle agglomeration and dispersion in PDMS. So far, the mechanical properties of most siloxane composites and blends have not been comprehensively studied. In particular, when additional plasticizers were used in order to compensate the stiffening effect of the solid filler material. Future investigations with respect to DET applications are necessary. So far, the provided DMA data indicated an increasing viscoelastic behavior of PDMS composites and blends. It might be arguable whether the additives might interfere with the Pt-catalyzed PDMS cross-linking reaction.[304] Nonetheless, mechanical strains of about 800%[306] are reported in tensile tests which could be of interest for DEG applications.

Ultimately, the use of solvent in most siloxane composite formulations poses an additional challenge to the development of fast and cost-efficient thin film processing methods. Future research activities should combine the design of novel silicone elastomers with thin film processing techniques subsequent to its integration in DET devices.

1.6.2 High permittivity silicone elastomers

Chemical modification of polysiloxane is an approach to increase the permittivity intrinsically by covalent bonding of dipolar molecules to the polysiloxane backbone. The most obvious advantage is the absence of compatibility issues of heterogeneous phases in the siloxane blend or composite. In addition, the introduction and dispersion of polar groups is permanent. The polar groups cannot diffuse and agglomerate inside the siloxane matrix. Therefore, neither negative effects on the viscoelasticity nor the long-term durability should be expected.

However, the chemical modification requires deeper insight into the chemical composition of the polysiloxane. In addition, the chemical modification of the polysiloxane must not interfere with the subsequent cross-linking reaction. This necessitates a critical analysis of the chemically modified polysiloxane and possible residues of the modification reaction *e.g.* by-products, side products, solvents and catalysts. Therefore, many scientific reports of recent years provided detailed information on the electromechanical properties of the polar siloxane elastomer, the synthetic pathway and on its chemical structure.

In 2011 Kussmaul *et al.*published the film casting of a high permittivity polysiloxane.[316–318] It is a one-step film formation process. Scheme 1.11 illustrates the simultaneous side group functionalization and cross-linking of a trimethylsiloxane-terminated (30%-methylhydrosilane)-PDMS-copolymer (M_n: 2000 g/mol). In a Pt-catalyzed hydrosilylation reaction the copolymer was covalently bonded to *N*-allyl-*N*-methyl-*p*-nitroaniline and cross-linked by vinyl-terminated PDMS (M_n: 28000 g/mol). The sterically demanding aromatic groups with electron-withdrawing and electron-donating substituents were introduced into literature as *push-pull-dipoles*. At a maximum dipole content of 13.4 wt% a relative permittivity of 6 was achieved. A strong effect on the elastic modulus was observed. The incorporation led to a decrease from 1.9 MPa (0 wt%) to 0.5 MPa (13.4 wt%). The actuation strain could be enhanced by a factor of 7 due to the high permittivity and low elastic modulus. The dielectric strength declined from 130 V/µm to 39 V/µm though. Swelling-extraction experiments revealed the strong interference of the dipole addition with the cross-linking reaction. The extractable fraction increased almost linearly with the amount of dipole incorporated into the PDMS network to a maximum of about 40 wt%. The film preparation process resulted in thin films of about 80 µm. The process was solvent based *i.e.* 90 wt% chloroform as the dipole precursor and PDMS were not compatible. The formation of homogeneous thin films required more than two hours due to the slow evaporation of the solvent at ambient temperature prior to high-temperature-vulcanization.

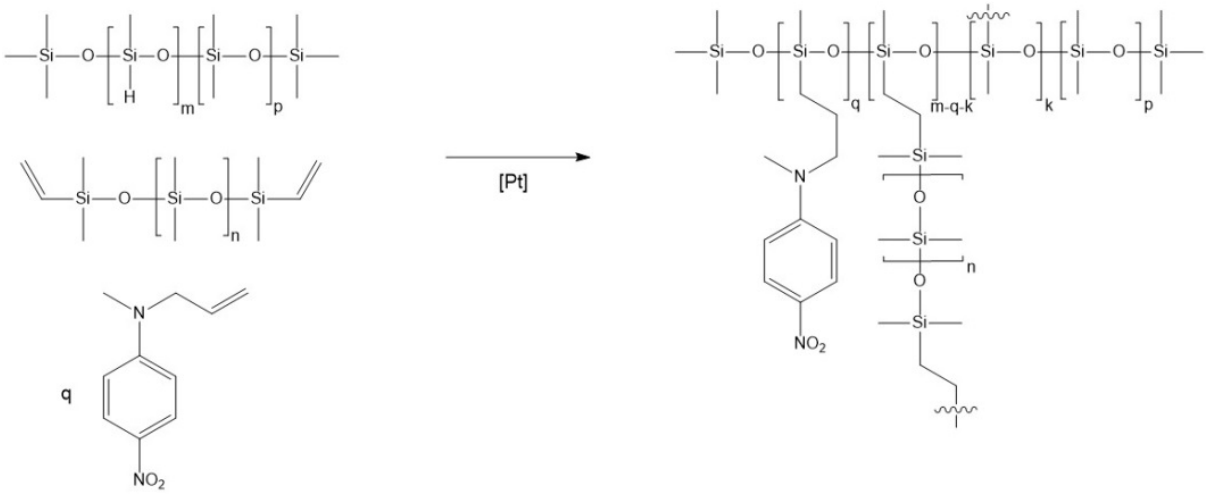

Scheme 1.11 Pt-catalyzed hydrosilylation PDMS cross-linking reaction accompanied by simultaneous addition of p-nitroaniline to the PDMS network.

A further development in the synthesis of dipolar silicone elastomers was presented in 2013 by Madsen *et al.*[134,319] by the separation of dipole functionalization and cross-linking reaction illustrated in Scheme 1.12. The dipoles were grafted on the cross-linker by a copper-catalyzed azide-alkyne cycloaddition reaction. A vinyl-substituted PDMS copolymer was added as secondary cross-linking agent.

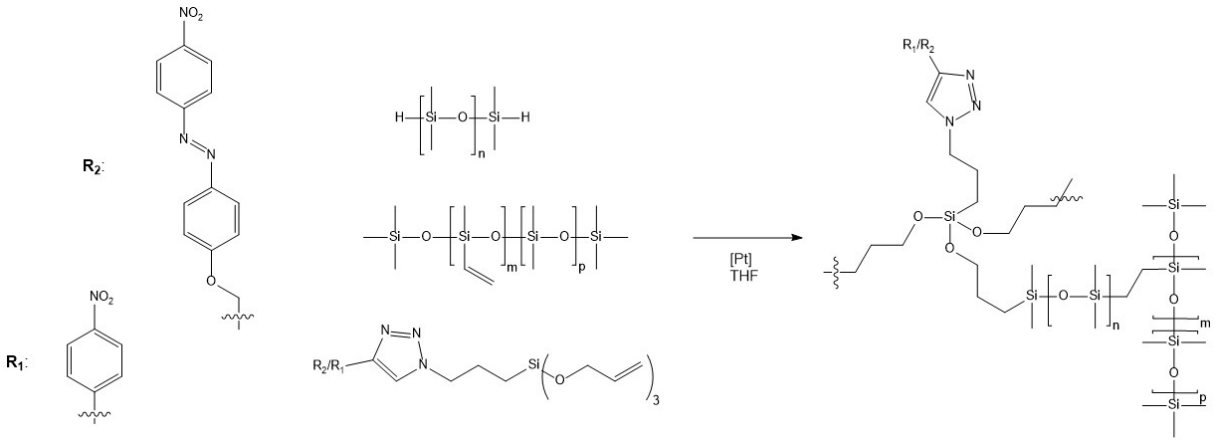

Scheme 1.12 Pt-catalyzed hydrosilylation cross-linking of a hydro-terminated PDMS with a dipolar cross-linker and additional vinyl-substituted PDMS. **R_1**: 4-(4-nitrophenylazo) phenyl. **R_2**: 4-nitrophenyl.

The polar silicone elastomers were casted as 150 µm thin films in a solvent-based process. The increase in permittivity was rather moderate as the concentration of the dipolar group inside the PDMS elastomer was limited to the cross-linking density. Interestingly, permittivity and dipole content did not show linear correlation. Instead, a peak in permittivity at 1.35 wt% (ε' = 3.3) was observed whereas the permittivity at 3.6 wt% was 3.0. The values were given at an electric field frequency of 100 Hz. Thus, the dipole orientation to the applied electric field was restricted inside the PDMS network. The integration of the organic dipole severely affected the dielectric strength E_{max} of the DE. In case of 0.7 wt% 4-nitrophenyl-content E_{max} declined from 92 V/µm to 39 V/µm. It remained unclear whether this originated from an increased conductivity caused by the organic dipoles or the decrease in elastic modulus accompanied by higher mechanical losses.

Calculated from the given shear modulus *G* (*Y* = 2(1+*v*)*G*; *v*: Poisson ratio of silicones ~ 0.5) values of *Y* ranged between 0.05 and 0.4 MPa. A clear softening effect due to the grafting of dipoles was reported. This was unexpected as the dipole was part of the cross-linker. Most remarkably, there are different trends in E_{max} as well as mechanical losses and gel fraction for the two types of organic dipole. The sterically more demanding **R_1** affected the mechanical properties less than **R_2**. The content of extractables increased to about 36 wt% in case of **R_2** compared to 11 wt% in case of the **R_1**.

In summary, this is a strong indication for an interference of the platinum-catalyzed cross-linking reaction by the organic dipole.[320] So far, the electromechanical performance of the thin films remains to be tested in DETs.

In 2015, Zhang *et al.*[321] reported on an alternative to the platinum-catalyzed hydrosilylation cross-linking of polar siloxanes. PDMS was cross-linked by tetraalkoxysilane in an organotin-catalyzed condensation reaction. Scheme 1.13 shows the push-pull-dipole *Disperse Red 19* that was integrated into the PDMS network. *Disperse Red 19* was dissolved in tetraethoxysilane and THF subsequent to further addition of PDMS and dibutyltin dilaurate.

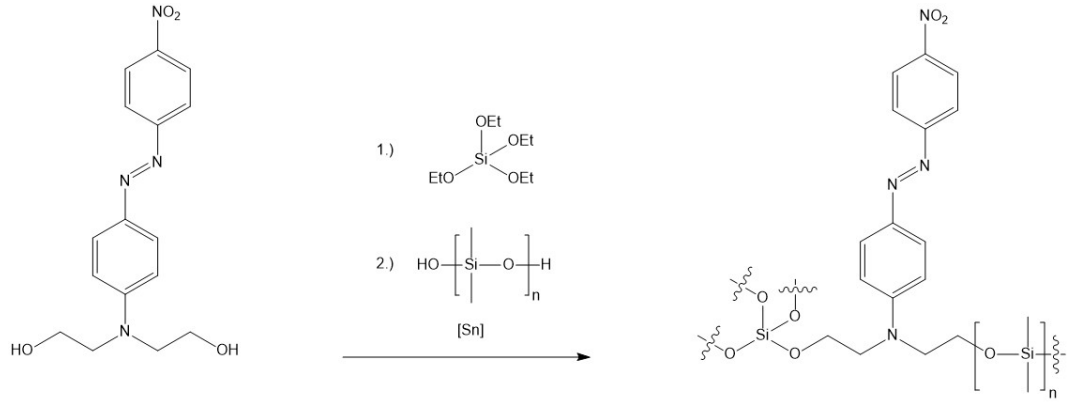

Scheme 1.13 The synthetic approach of the *Disperse Red 19* functionalized PDMS network.

Thin films of about 170 µm were prepared. The relative permittivity showed a linear trend with the dipole content to a maximum value of 4.9 at 13 wt% *Disperse Red 19.* The elastic modulus *Y* increased moderately up to 10 wt% dipole content to

about 0.4 MPa and reached a maximum of 0.7 MPa at 13 wt%. Correspondingly, 10 wt% dipole resulted in the highest actuation strain of 9% in the DEA below 50 V/µm. The maximum DEA area strain was tested for 7 wt% dipole content at an electric field of about 65 V/µm. An adverse effect of the dipole incorporation on E_{max} was not found.

Interestingly, the viscoelastic behavior was characterized by the DEA measurement. The authors found a time delay of about 0.4 seconds between applied voltage and actuation response of the polar silicone containing 7 wt% of dipole. This is consistent with the swelling-extraction tests that showed a linear rise in the extractable amount from 5 wt% of the pristine PDMS to 18 wt% of the polar silicone with 13 wt% dipole content.

Bele *et al.* reported on the tin-catalyzed PDMS condensation cross-linking by an excess of polar cross-linker.[132,133] Scheme 1.14 describes the cross-linking reaction and the different types of dipole used. The polar cross-linkers were commercially available. Polar silicone elastomers were obtained with a film thickness ranging from 400 to 800 µm in a solvent-based process. The synthesis benefits from the self-condensation of the polar cross-linker at ambient humidity. It allows overstoichiometric use of cross-linker in order to facilitate quantitative conversion of the PDMS cross-linking and *in situ* formation of silsesquioxane segments of the polar silicone. The material might be considered as a hybrid form of polar silicone and silicone composite.

The rate of cross-linking was not precisely studied. However, film formation took about one day. The permittivity did not exceed values over 3.7 at dipole contents between 6 and 9 wt%. Interestingly, the cyanopropyl-substituted cross-linker led to the high permittivity and elastic modulus *Y* of about 1 MPa as well. Unfortunately, neither DMA measurements nor swelling-extraction experiments were reported.

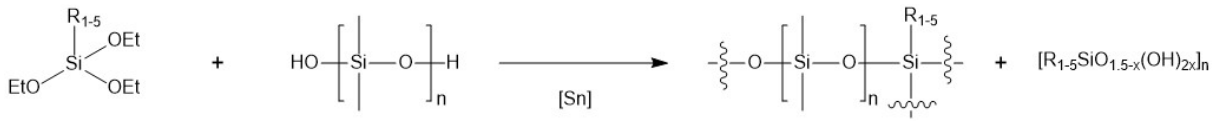

Scheme 1.14 Organotin-catalyzed condensation cross-linking reaction of PDMS and the *in situ* formation of silsesquioxanes. $R_{1\text{-}5}$: -H, $-(CH_2)_3Cl$, $-(CH_2)_3NH_2$, $-(CH_2)_3CN$, $-C_6H_5$.

The effect of the 3-chloroproply moiety was thoroughly investigated.[132] 50 wt% of cross-linker gave an elastomer with an elastic modulus of 2.5 MPa and a remarkably high mechanical strength of over 5 MPa in the tensile test. At 15 wt% of polar cross-linker, the elastic modulus was about 0.6 MPa with a relative permittivity of about 3.7 (10^2 Hz). The material was electromechanically characterized in a DEA. A lateral actuation strain of about 7% was observed compared to 6% of the PDMS reference material. Due to the elevated elastic modulus *Y* this corresponds to a doubling of output pressure. Interestingly, the time response and the mechanical durability were comparable as well. Both materials were strained to about 6% at a frequency of 6.7 Hz which corresponds to a time response of 0.15 seconds. Mechanical durability was demonstrated by 100 actuation cycles at constant strain in 15 seconds.

Even though this approach led to a drastic rise in elastic modulus *Y* of the polar silicone elastomers, it is particularly interesting due to its functional group tolerance. Therefore, it will be of further interest in Chapter 3 and Chapter 4 when the organotin-catalyzed condensation reaction of ethoxysilanes is combined with novel polar silicones and CNT-PDMS composites.

The use of polar cross-linkers allow well-dispersed dipoles inside the PDMS elastomer. However, this synthetic approach is constraint by the cross-link density of the elastomer *i.e.* its elastic modulus. This limits the gain in permittivity of the polar silicone elastomers. Thus, the design of soft polar silicone elastomers based on silicone copolymers has gained importance in recent years. Already in 2013, Racles *et al.* have proposed a synthetic route towards cyanopropyl functionalized polysiloxane based on post-polymerization modification of vinyl-substituted polysiloxane or copolymerization of polar cyclosiloxane.[322] The functionalization was performed by a Pt-catalyzed hydrosilylation reaction whereas the hydroxy endgroups were subsequently cross-linked by a titanium-catalyzed condensation reaction with ethyltriacetoxysilane (Scheme 1.15).

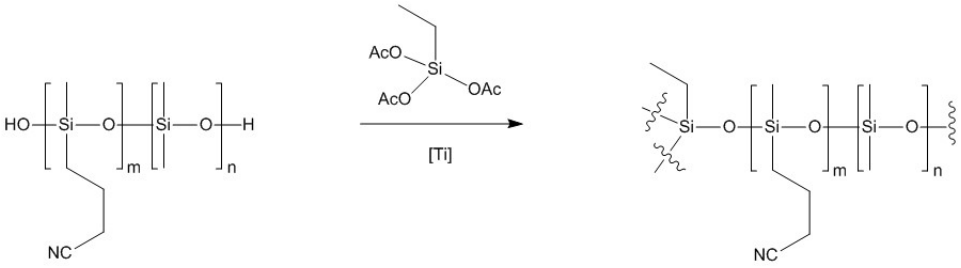

Scheme 1.15 Preperation of cyanopropyl functionalized siloxane elastomers by titanium-catalyzed condensation cross-linking. [Ti]: titanium tetra(2-ethylhexoxide).

However, the addition of the hydrosilane group on allyl cyanide by Pt-catalyzed hydrosilylation did not reach quantitative conversion. The unreacted hydrosilane groups hydrolyzed and a secondary cross-linking reaction was observed in the presence of *Karstedt's catalyst.* Nonetheless, elastomers with up to 23 mol% cyanoproyl modified polysiloxane units were prepared with a thickness of about 100 µm. An enhanced permittivity of up to 6.5 was measured. In case of trimethylsilyl-end blocked polysiloxane 89 mol% of cyano side groups were grafted on the siloxane chain which gave a relative permittivity of about 16.[323] However, only cross-linked polar silicones with 4 mol% polar side groups were mechanically stable enough to be tested. The tensile tests revealed no significant increase in elastic modulus due to the incorporation of the cyanopropyl side group. This led to a considerable increase in lateral actuation strain of the DEA. At 40 V/µm a lateral strain of 10% was observed for the polar silicone with respect to 3% lateral strain of the pristine PDMS elastomer. The long-term mechanical stability was studied by cyclic DEA measurements. A sinusoidal electric field of 30 V/µm with a frequency of 2.5 Hz was applied. A permanent deformation of about 1% was observed after 100 cycles.

A more comprehensive study on the effect of dipoles incorporated as side groups of polysiloxane was recently published.[278] Even though the polysiloxanes were end-capped and thus not cross-linkable, the effect of the incorporation of various dipoles on permittivity and conductivity was presented. The molecular structures of the polar side groups are depicted in Figure 1.10. About 8 mol% of the side groups were modified in a PDMS-copolymer. The highest ε' value was measured for **D_6** with 7.4. However, the increase was accompanied by a rise in conductivity over 10^{-8} S/cm. Both trends could be rationalized by the strong absorption of H_2O at ambient humidity. **D_1-D_5** and **D_7** led to enhanced permittivity values ranging between 3.8 and 5.4 of the siloxane copolymer with conductivities in the order of 10^{-9} to 10^{-12}. The post-polymerization modification was catalyzed either by platinum in a hydrosilylation of a hydrosiloxane copolymer or by UV light with DMPA as photoinitiator in the thio-ene addition on a vinylsiloxane copolymer.

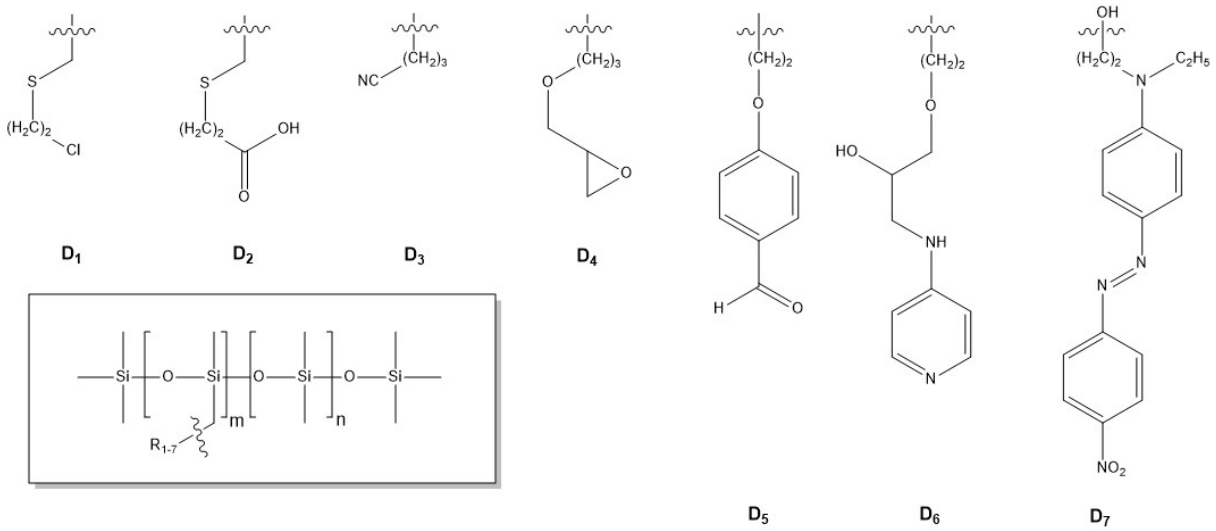

Figure 1.11 End-capped polar siloxane copolymers. m/n : 1/12.

Already in 2013, the functionalization of polysiloxanes by thiol-ene addition of various commercially available polar thiols on poly(methylvinylsiloxane) was reported.[324] Isolated yields higher than 90% using stoichiometric amount of polar thiol and the thermal stability of the obtained polysiloxanes were emphasized. The dielectric properties were not investigated though.

In 2015 and 2016, Dünki *et al.*[126,325] presented the quantitatively functionalized polar silicone simultaneously cross-linked in a thiol-ene addition of a dithiol. In a solvent-based one-step process, thin film elastomers were formed with a thickness of about 120 µm (Scheme 1.16). Swelling-extraction tests showed an extractable content of about 10 wt%.

Scheme 1.16 Simultaneous thiol-ene addition of 2-cyanoethanethiol and 2,2′-(Ethylenedioxy)diethanethiol on poly(methylvinylsiloxane).

At 100 mol% of cyano-functionalized siloxane units a maximum permittivity of 17.4 was achieved. The addition of the less polar 1-butanethiol has already led to an increased permittivity of the silicone elastomer of about 4.3. Even though the material was mechanically strengthened by the addition of 5 wt% silica particles, the elastic modulus *Y* of all polar elastomers was kept constant around 0.1 MPa. This was explained by the use of high molecular weight polysiloxanes and thus low cross-link density. The mechanical strain at break ranged from 200% to 300% which could be of particular relevance in DEG operations. In DEA operations the polar silicone outperformed the unpolar silicone by a factor of 4 in actuation strain at 10 V/µm. In cyclic DEA tests the polar silicone suffered dielectric breakdown at 8 V/µm. Interestingly, the DE recovered by itself very shortly afterwards from electric breakdown. The reason for the rather low dielectric strengths E_{max} of the cyano-functionalized silicone elastomers remained blurry. The increase in conductivity to a maximum of about 10^{-9} S/cm was accompanied by an increase in viscoelasticity at very low elastic moduli *Y*. In Chapter 2, novel molecular designs of mercaptonitriles will be discussed with respect to their dielectric properties and possible applications as precursor in polar silicone elastomers.

Most recently, Dünki *et al.* published the functionalization of siloxanes by sulfonyl side groups. Due to complete thiol-ene addition on poly(methylvinylsiloxane) the permittivity increased to 23.[279] It remains to be seen whether the cross-linked sulfonyl-functionalized polysiloxane will show superior electromechanical behavior in a DET. The cross-linking of sulfonyl-functionalized polysiloxane has already been presented in 2001 based on free radical cross-linking reaction at elevated temperature but no mechanical properties were studied.[326]

As an alternative to post-polymerization modification by thiol-ene addition or Pt-catalyzed hydrosilylation reaction the co-polymerization of polar cyclosiloxanes with trifluoropropyl[327] or chloropropyl[328] side groups was reported.

In case of the trifluoropropyl-functionalized siloxane copolymer a maximum permittivity of 6.4 was realized (Scheme 1.17). The vinyl-terminated siloxane copolymers were cross-linked in a Pt-catalyzed hydrosilylation. The elastic moduli *Y* were remarkably low (< 0.05 MPa) but the mechanical losses *tan(δ)* increased considerably above 28%. The best DEA performance was demonstrated by a siloxane copolymer with 47% trifluoropropyl side groups. It could be reversibly strained to 4% by 8 V/µm with a frequency of 0.4 Hz for 100 cycles.

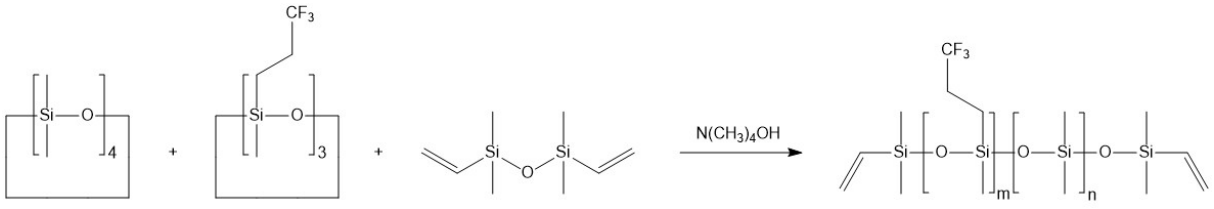

Scheme 1.17 Synthesis of vinyl end-functionalized siloxane copolymers. As starting material octamethylcyclotetrasiloxane, trifluoropropyl-methyl-cyclotrisiloxane, and divinyl siloxane end-blocker were used.

In contrast, the synthesis of chloropropyl-substituted siloxane elastomers was rather complex (Scheme 1.18).[329] Under inert atmosphere the hydride-terminated PMDS reacted in a *Piers-Rubinsztajn* condensation reaction[330,331] with 3-(chloropropyl)-methyldimethoxysilane catalyzed by tris(pentafluorophenyl)borane. Subsequently, the methoxy-terminated polar polysiloxane reacts *in situ* with allyldimethylsilane to give a vinyl-terminated chloropropyl-substituted PDMS copolymer.

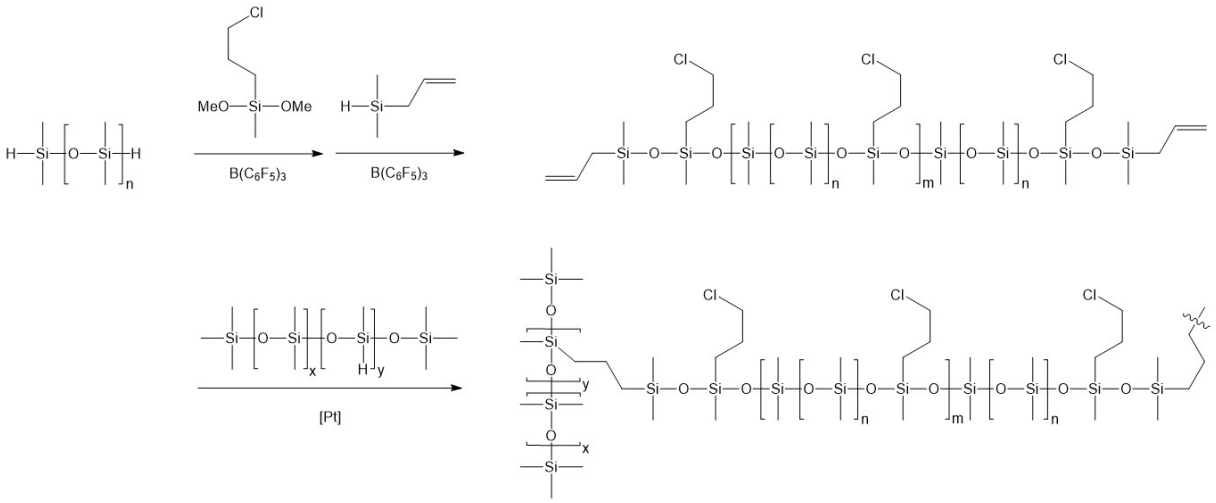

Scheme 1.18 Two-step one-pot synthesis of vinyl-terminated 3-(chloropropyl)methylsiloxane-PDMS-copolymers followed by solvent-free Pt-catalyzed cross-linking.

The dipole concentration could be adjusted by the molecular weight of the hydride-terminated PDMS. The copolymers were cross-linked in a Pt-catalyzed hydrosilylation reaction with a hydrosilane-PDMS-copolymer. 150 µm thin films were obtained after 2 hours in a solvent-free process. A maximum permittivity of about 4.7 with an elastic modulus of 1.0 MPa was achieved. Mechanical losses *tan(δ)* of 0.09 at 1 Hz were rather high whereas the extractable content was with 8 wt% low which can be rationalized by the amount of 25 wt% of silica filler material. Correspondingly, the tensile strength was above 2 MPa at 130% strain. Up to date, electromechanical characterizations await to be reported.

A similar approach of α-functionalized high permittivity silicones was patent-registered by Stepp *et al.* in 2015.[332] Both, the vinyl-terminated siloxane (M_n: 3600 g/mol) and the hydrosilane-copolymer cross-linker carried a polar moiety in α-position. A silica filler was added to the mixture which was cross-linked by *Karstedt's catalyst* in a solvent-free process at 160 °C. The cross-linking reaction was controlled by the addition of 5 wt% 1-ethinyl-cyclohexanol as volatile catalytic inhibitor. Detailed information were given on the preparation of 100 µm thin films of poly(chloromethylmethylsiloxane)-PDMS-copolymer summarized in Scheme 1.19. Even though the mixture possessed a high viscosity (1000 Pa s at 0.1 Hz), the mixing and film formation process was finalized within 30 minutes. A maximum permittivity of 6.8 was reported for 60 mol% of chloromethyl side groups. The elastic moduli were not reported but the tensile strength was 2 MPa at 200%. The electrical breakdown strength was at 50 V/µm. Electromechanical tests have not been published so far.

In summary, polar silicone elastomers are very promising candidates as future replacements of PDMS elastomers in DETs. The greatest advantage of chloro-and fluoro-functionalized polysiloxanes is their compatibility with the well-established hydrosilylation cross-linking reaction catalyzed by *Karstedt's catalyst.* This allows solvent-free preparation of thin films at elevated temperatures within 30 minutes. The highest permittivity of Pt-catalyst cross-linked silicone elastomers reported up to date was 6.8.

Significantly higher permittivities of cyano- and sulfonyl-functionalized polysiloxanes were reported. An extraordinary increase in permittivity of over 700% compared to PDMS was achieved. However, well-established platinum- and tin catalyzed cross-linking reactions were reported to fail in cases of highly dipolar functionalities. Future design of suitable cross-linking reactions will determine the network integrity of the polar polysiloxane and thus the mechanical lifetime of any DET device. Therefore, the cross-linking process will define the technological relevance of high permittivity silicones for DET applications.

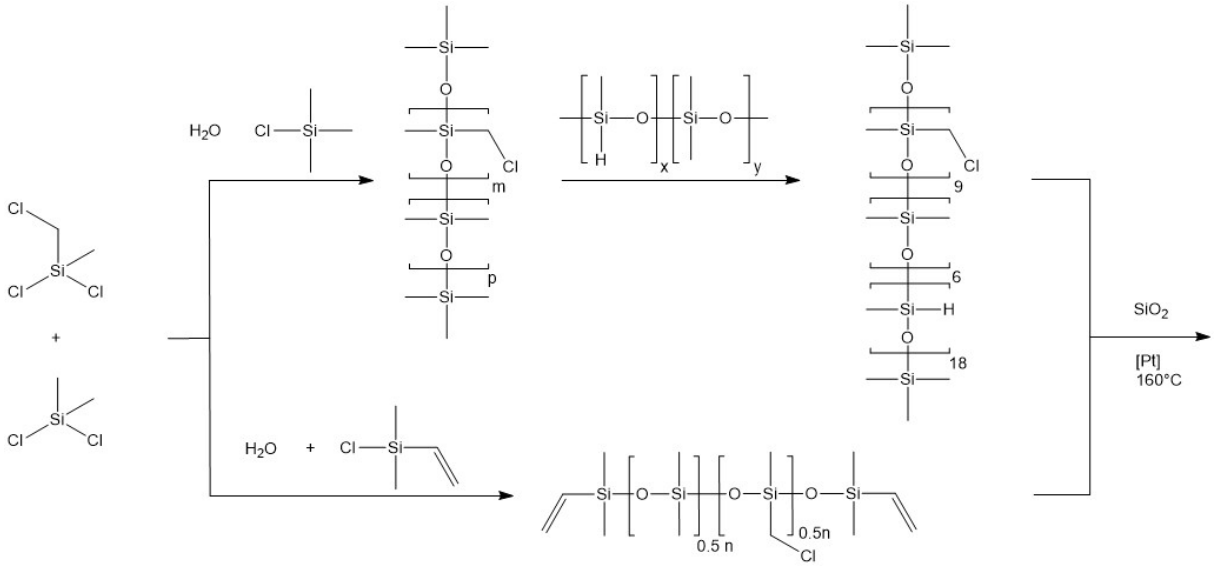

Scheme 1.19 Synthetic route for poly(chloromethylmethyl)(dimethyl)siloxane copolymer elastomers. [Pt] represents *Karstedt's catalyst* with 5 wt% of 1-ethinyl-cyclohexanol. The silica filler material SiO_2 used was surface passivated by trimethylsilyl moieties.

1.7 Goal and scope of the thesis

It is the overall goal of this thesis to develop a high permittivity siloxane elastomer that is of technological relevance with respect to DET applications.

This involves the preparation of high permittivity polysiloxane composites for dielectric elastomer generators as well as the design of chemically modified siloxane elastomers for dielectric elastomer actuators. The development of cross-linking reactions suitable for polysiloxane composites and chemically modified polysiloxane elastomers is of prime importance. The synthetic strategy depends on the thiol-ene addition of various thiols on vinyl-substituted polysiloxanes. Therefore, cross-linking reactions compatible with the thioether side group must be utilized. The dielectric properties and the mechanical properties must be tailored to meet the demands for dielectric elastomer actuators and generators. This includes permittivity ε' and conductivity σ as well as elastic modulus Y, viscoelastic behavior ($tan(\delta)_{DMA}$) and mechanical strain at break s_{max} of the dielectric elastomer. Advantages and disadvantages of high permittivity polysiloxanes in comparison to PDMS elastomers are shown in electromechanical test devices and discussed in detail. A particular focus of this work will be on the mechanical long-term stability of high permittivity polysiloxanes and the development of technologically relevant thin film processing methods.

In Chapter 2, the synthetic approaches of various mercaptonitriles as precursors for thiol-ene addition on polysiloxanes are studied. The challenges in the reaction control due to the high nucleophilicity of thiols towards the nitrile group are nicely illustrated by the X-ray diffraction analysis on the single crystals of the corresponding cyclization products. Therefore, in the course of this thesis the focus is limited on high permittivity polysiloxanes synthesized by thiol-ene addition of alkylthiols exclusively.

In Chapter 3, the dielectric and mechanical properties of thioether-substituted polysiloxane elastomers are characterized by impedance spectroscopy, tensile testing and dynamic mechanical analysis. The performance in an actuator test device is demonstrated in comparison to PDMS elastomers. The effect of thioether-substituted polysiloxane on the tin-catalyzed cross-linking reaction and the resulting electromechanical behavior is discussed in detail. Additionally, the electromechanical long-term stability is analyzed.

In Chapter 4, the effect of single-walled nanospring carbon nanotubes as filler material in PDMS and thioether functionalized polysiloxanes is presented as a dielectric elastomer material for dielectric elastomer generators. The impact of the filler material on the dielectric and mechanical properties of polysiloxane elastomers is of interest with respect to dielectric elastomer generators. The potential of the functionalized polysiloxane and the PDMS carbon nanotube composites is highlighted by their performance in dielectric elastomer generator test devices.

Finally, the cross-linking process of thioether functionalized oligosiloxanes is addressed in Chapter 5. This implies the development of a solvent-free, fast, on-demand and reproducible cross-linking process. The characterization of the dielectric and mechanical properties is presented. Eventually, the prepared polysiloxane elastomers are evaluated in dielectric elastomer actuator tests.

1.8 References

[1] C. Ellingford, C. Bowen, T. McNally, C. Wan, *Macromol. Rapid Commun.* **2018**, *39*, 1800340.

[2] P. Brochu, Q. Pei, *Macromol. Rapid Commun.* **2010**, *31*, 10.

[3] T. Sugino, Y. Shibata, K. Kiyohara, K. Asaka, *Proc. SPIE* **2012**, *8340*, 83400T.

[4] L. Yao, S. Krause, *Proc. SPIE* **2002**, *4695*, 478.

[5] M. Urdaneta, Y. K. Liu, M. Christophersen, S. Prakash, P. Abshire, E. Smela, *Proc. SPIE* **2005**, *5759*, 232.

[6] C. Y. Yu, Y. W. Zhang, G. D. J. Su, *Sens. Actuators, A* **2015**, *232*, 183.

[7] C. Saltó, E. Saindon, M. Bolin, A. Kanciurzewska, M. Fahlman, E. W. H. Jager, P. Tengvall, E. Arenas, M. Berggren, *Langmuir* **2008**, *24*, 14133.

[8] A. Richter-Dahlfors, R. M. Berggren, E. Jager, K. Persson, K. Abdul, *(OBOE IPR AB)*, **2010**, WO 2010/072257 A1.

[9] E. Jager, D. Carlsson, M. Krogh, M. Skoglund, *(Micromuscle AB)*, **2008**, WO 2008/113372 A2.

[10] S. A. Wilson, R. P. J. Jourdain, Q. Zhang, R. A. Dorey, C. R. Bowen, M. Willander, Q. U. Wahab, M. Willander, S. M. Al-hilli, O. Nur, E. Quandt, C. Johansson, E. Pagounis, M. Kohl, J. Matovic, B. Samel, W. van der Wijngaart, E. W. H. Jager, D. Carlsson, Z. Djinovic, M. Wegener, C. Moldovan, E. Abad, M. Wendlandt, C. Rusu, K. Persson, *Mat. Sci. Eng. R.* **2007**, *56*, 1.

[11] J. F. Capsal, J. Galineau, M. Lallart, P. J. Cottinet, D. Guyomar, *Sens. Actuators, A* **2014**, *207*, 25.

[12] S. Zhukov, D. Eder-goy, C. Biethan, S. Fedosov, *Smart Mater. Struct.* **2018**, *27*, 015010.

[13] K. Ren, S. Liu, M. Lin, Y. Wang, Q. M. Zhang, *Sens. Actuators, A* **2008**, *143*, 335.

[14] H. Shahsavan, S. M. Salili, A. Jákli, B. Zhao, *Adv. Mater.* **2015**, *27*, 6828.

[15] S. M. Mirvakili, I. W. Hunter, *Adv. Mater.* **2018**, *30*, 1.

[16] W. C. Röntgen, *Ann. Phys.* **1880**, *247*, 771.

[17] R. Pelrine, R. D. Kornbluh, J. Eckerle, P. Jeuck, S. Oh, Q. Pei, S. Stanford, *Proc. SPIE* **2001**, *4329*, 148.

[18] M. Rosenthal, N. Bonwit, C. Duncheon, J. Heim, *Proc. SPIE* **2007**, *6524*, 65241F.

[19] Y. Bar-Cohen, T. Xue, B. Joffe, S.-S. Lih, M. Shahinpoor, J. S. Harrison, J. G. Smith, P. Willis, *Proc. SPIE* **1997**, *3041*, 697.

[20] R. D. Kornbluh, R. Pelrine, Q. Pei, R. Heydt, S. Stanford, S. Oh, J. Eckerle, *Proc. SPIE* **2002**, *4698*, 254.

[21] R. E. Pelrine, R. D. Kornbluh, J. P. Joseph, *Sens. Actuators, A* **1998**, *64*, 77.

[22] R. Pelrine, R. Kornbluh, Q. Pei, J. Joseph, *Science (80-.).* **2000**, *287*, 836.

[23] S. Rosset, H. R. Shea, *Appl. Phys. A Mater. Sci. Process.* **2013**, *110*, 281.

[24] M. Matysek, P. Lotz, K. Flittner, H. F. Schlaak, *Proc. SPIE* **2008**, *6927*, 692722.

[25] J.-C. Huang, *Adv. Polym. Technol.* **2002**, *21*, 299.

[26] W. Yuan, L. Hu, Z. Yu, T. Lam, J. Biggs, S. M. Ha, D. Xi, B. Chen, M. K. Senesky, G. Grüner, Q. Pei, *Adv. Mater.* **2008**, *20*, 621.

[27] L. Bay, K. West, P. Sommer-Larsen, S. Skaarup, M. Benslimane, *Adv. Mater.* **2003**, *15*, 310.

[28] R. Pelrine, R. Kornbluh, J. Joseph, R. Heydt, Q. Pei, S. Chiba, *Mater. Sci. Eng. C* **2000**, *11*, 89.

[29] N. K. A. Pimpin, Y. Suzuki, *J. Microelectromech. Syst.* **2007**, *16*, 753.

[30] D. M. Opris, *Adv. Mater.* **2018**, *30*, 1703678.

[31] J. Biggs, K. Danielmeier, J. Hitzbleck, J. Krause, T. Kridl, S. Nowak, E. Orselli, X. Quan, D. Schapeler, W. Sutherland, J. Wagner, *Angew. Chem. Int. Ed.* **2013**, *52*, 9409.

[32] R. Shankar, T. K. Ghosh, R. J. Spontak, *Soft Matter* **2007**, *3*, 1116.

[33] L. J. Romasanta, M. A. Lopez-Manchado, R. Verdejo, *Prog. Polym. Sci.* **2015**, *51*, 188.

[34] C. Graf, J. Hitzbleck, T. Feller, K. Clauberg, J. Wagner, J. Krause, J. Maas, *Proc. SPIE* **2013**, *8687*, 86870N.

[35] R. D. Kornbluh, R. Pelrine, Q. Pei, S. Oh, J. Joseph, *Proc. SPIE* **2000**, 51.

[36] G. Kovacs, L. Duering, S. Michel, G. Terrasi, *Sens. Actuators, A* **2009**, *155*, 299.

[37] S. Rosset, H. R. Shea, *Appl. Phys. Rev.* **2016**, *3*, 031105.

[38] D. Tepel, T. Hoffstadt, J. Maas, *Proc. SPIE* **2014**, *9056*, 905627.

[39] H. Bochmann, B. von Heckel, J. Maas, *Proc. SPIE* **2017**, *10163*, 101632P.

[40] T. Hoffstadt, J. Maas, *Proc. SPIE* **2017**, *10594*, 105940Y.

[41] A. O'Halloran, F. O'Malley, P. McHugh, *J. Appl. Phys.* **2008**, *104*, 071101.

[42] Q. Pei, M. Rosenthal, S. Stanford, H. Prahlad, *Smart Mater. Struct.* **2004**, *13*, N86.

[43] G. Kovacs, P. Lochmatter, M. Wissler, *Smart Mater. Struct.* **2007**, *16*, S306.

[44] H. Boys, G. Frediani, S. Poslad, J. Busfield, F. Carpi, *Proc. SPIE* **2017**, *10163*, 101632D.

[45] P. Chakraborti, H. A. K. Toprakci, P. Yang, N. Di Spigna, P. Franzon, T. Ghosh, *Sens Actuators A* **2012**, *179*, 151.

[46] A. K. Price, C. T. Culbertson, *Anal. Chem.* **2009**, *81*, 8942.

[47] D. McCoul, C. Murray, D. Di Carlo, Q. Pei, *Proc. SPIE* **2013**, *8687*, 86872G.

[48] K. Flittner, M. Schlosser, H. F. Schlaak, *Proc. SPIE* **2011**, *7976*, 79761K.

[49] M. Aschwanden, A. Stemmer, *Proc. SPIE* **2007**, *6524*, 65241N.

[50] M. Aschwanden, D. Niederer, A. Stemmer, *Proc. SPIE* **2008**, *6927*, 69271R.

[51] Q. Wang, Z. Y. Wang, D. W. Zhang, Y. S. Huang, Z. J. Ni, S. L. Zhuang, *Optik (Stuttg).* **2014**, *125*, 1990.

[52] S. Casutt, M. Bueeler, M. Blum, M. Aschwanden, *Proc. SPIE* **2014**, *8982*, 89820Y.

[53] R. Heydt, R. Kornbluh, J. Eckerle, R. Pelrine, *Proc. SPIE* **2006**, *6168*, 61681M.

[54] Optotune, "https://www.optotune.com/products/laser-speckle-reducers/eap-lsr," **2019**.

[55] C. Graetzel, M. Suter, M. Aschwanden, *Proc. SPIE* **2015**, *943004*, 943004.

[56] Compliant Transducer Systems GmbH, "http://www.ct-systems.ch/index.php/products," **2019**.

[57] L. Düring, G. Kovacs, *(EMPA)*, **2009**, WO 2009/135328 A2.

[58] T. Hoffstadt, J. Maas, *Proc. SPIE* **2015**, *943007*, 943007.

[59] F. Carpi, S. Bauer, D. De Rossi, *Science* **2010**, *330*, 1759.

[60] R. Pelrine, R. Kornbluh, *Electromechanical Transduction Effects in Dielectric Elastomers: Actuation, Sensing, Stiffness Modulation and Electric Energy Generation*, Elsevier Ltd., Boston, **2008**.

[61] R. Pelrine, H. Prahlad, *Dielectric Elastomers as Electromechanical Transducers*, Elsevier Ltd., Oxford, **2008**.

[62] S. J. A. Koh, C. Keplinger, T. Li, S. Bauer, Z. Suo, *IEEE/ASME Trans. Mechatronics* **2011**, *16*, 33.

[63] A. Ladegaard Skov, P. Sommer-larsen, *Physical and Chemical Properties of Dielectric Elastomers*, Elsevier Ltd., Oxford, **2008**.

[64] C. Graf, J. Maas, D. Schapeler, *Proc. SPIE* **2010**, *7642*, 764217.

[65] S. J. A. Koh, X. Zhao, Z. Suo, *Appl. Phys. Lett.* **2009**, *94*, 262902.

[66] G. Neidlein, C. Hentschel, N. Scharmann, C. Langenstein, M. Voss, B. Hagemann, *(Robert Bosch GmbH)*, **2009**, DE 10 2009 053 393 A1.

[67] S. Chiba, M. Waki, R. Kornbluh, R. Pelrine, *Proc. SPIE* **2008**, *6927*, 692715.

[68] P. Jean, A. Wattez, G. Ardoise, C. Melis, R. Van Kessel, A. Fourmon, E. Barrabino, J. Heemskerk, J. P. Queau, *Proc. SPIE* **2012**, *8340*, 83400C.

[69] R. Vertechy, M. Fontana, G. P. Rosati Papini, M. Bergamasco, *Proc. SPIE* **2013**, 86870I.

[70] T. Hoffstadt, R. Heinze, T. Wahl, F. Kameier, J. Maas, *Proc. SPIE* **2014**, 90561E.

[71] C. Jean-Mistral, S. Basrour, J. Chaillout, *Proc. SPIE* **2008**, *6927*, 692716.

[72] T. Vu-Cong, C. Jean-Mistral, A. Sylvestre, *Smart Mater. Struct.* **2013**, *22*, 025012.

[73] I. A. Anderson, S. Rosset, T. McKay, I. A. Anderson, S. Rosset, T. Mckay, H. Shea, *Proc. SPIE* **2014**, *9056*, 90560Q.

[74] W. H. McKnight, W. C. McGinnis, *(The U.S.A. by the Secr. of Navy)*, **2002**, US 6,433,465 B1.

[75] SBM Offshore, "https://www.sbmoffshore.com/wp-content/uploads/2016/06/Technology-Wave-Energy-Converter-FINAL-LOW-RESOLUTION.pdf," **2019**.

[76] C. Jean-Mistral, T. Porter, T. Vu-Cong, S. Chesné, A. Sylvestre, *IEEE/ASME* **2014**, 1430.

[77] C. Jean-Mistral, T. Vu Cong, A. Sylvestre, *Appl. Phys. Lett.* **2012**, *101*, 162901.

[78] C. Jean-Mistral, T. Vu-Cong, A. Sylvestre, *Smart Mater. Struct.* **2013**, *22*, 104017.

[79] T. Vu-Cong, C. Jean-Mistral, A. Sylvestre, *Proc. SPIE* **2013**, *8687*, 86870H.

[80] H. Böse, E. Fuß, P. Lux, *Proc. SPIE* **2015**, *9430*, 943029.

[81] Parker-Hannifin Corp., "http://ph.parker.com/us/en/electroactive-polymer-technology-monitors-movement-and-stretch-eap-sensor-evaluation-kits," **2019**.

[82] Strechsense, "http://stretchsense.com/," **2019**.

[83] B. O'Brien, T. Gisby, I. A. Anderson, *Proc. SPIE* **2014**, *9056*, 905618.

[84] D. Xu, T. G. McKay, S. Michel, I. A. Anderson, *Proc. SPIE* **2014**, *9056*, 90561A.

[85] H. Böse, M. Thuy, S. Stier, *Proc. SPIE* **2018**, *10594*, 105940X.

[86] K. Jung, K. J. Kim, H. R. Choi, *Sens. Actuators, A* **2008**, *143*, 343.

[87] T. Hoffstadt, M. Griese, J. Maas, *Proc. SPIE* **2014**, *9056*, 90561B.

[88] G. de Witt, *Structure, Deformation, and Integrity of Materials, Volume I: Fundamentals and Elasticity.*, Wiley, Weinheim, **2006**.

[89] W. Hu, *Polymer Physics*, Springer, Wien, **2013**.

[90] S. J. A. Koh, T. Li, J. Zhou, X. Zhao, W. Hong, J. Zhu, Z. Suo, *J. Polym. Sci. Part B Polym. Phys.* **2011**, *49*, 504.

[91] H. Staudinger, *Ber. Dtsch. Chem. Ges.* **1920**, *53*, 1073.

[92] J. P. Joule, *Phil. Trans. R. Soc. Lond.* **1859**, *149*, 91.

[93] S. Fakirov, *Handbook of Condensation Thermoplastic Elastomer*, Wiley-VCH, Weinheim, **2005**.

[94] F. Förster-Zuegel, T. Grotepaß, H. F. Schlaak, *SPIE Proc.* **2015**, *9430*, 94300D.

[95] A. P. Gerratt, S. Bergbreiter, *J. Micromech. Microeng.* **2013**, *23*, 067001.

[96] K. Larson, *Proc. SPIE* **2015**, *943013*, 943013.

[97] F. Carpi, I. Anderson, S. Bauer, G. Frediani, G. Gallone, M. Gei, C. Graaf, C. Jean-Mistral, W. Kaal, G. Kofod, M. Kollosche, R. Kornbluh, B. Lassen, M. Matysek, S. Michel, S. Nowak, B. O'Brien, Q. Pei, R. Pelrine, B. Rechenbach, S. Rosset, H. Shea, *Smart Mater. Struct.* **2015**, *24*, 105025.

[98] Wacker Chemie, "https://www.wacker.com/cms/media/publications/downloads/7091_EN.pdf," **2019**.

[99] R. Hooke, *De Potentia Restitutiva, or of Spring. Explaining the Power of Springing Bodies*, London, **1678**.

[100] F. Carpi, D. De Rossi, *Mater. Sci. Eng. C* **2004**, *24*, 555.

[101] M. Wissler, E. Mazza, *Smart Mater. Struct.* **2005**, *14*, 1396.

[102] M. Wissler, E. Mazza, *Sens. Actuators, A* **2007**, *138*, 384.

[103] O. H. Yeoh, *Rubber Chem. Technol.* **1990**, *63*, 792.

[104] M. Mooney, *J. Appl. Phys.* **1940**, *11*, 582.

[105] R. W. Ogden, *Proc. R. Soc. A Math. Phys. Eng. Sci.* **1972**, *328*, 567.

[106] S. Rosset, L. Maffli, S. Houis, H. R. Shea, *Proc. SPIE* **2014**, *9056*, 90560M.

[107] Y. Wang, H. Xue, H. Chen, J. Qiang, *Appl. Phys. A Mater. Sci. Process.* **2013**, *112*, 339.

[108] R. S. Rivlin, *Philos. Trans. R. Soc.* **1948**, 379.

[109] F. Carpi, M. Gei, *Smart Mater. Struct.* **2013**, *22*, 104011.

[110] G. H. Stark, C. G. Carton, *Nature* **1955**, *176*, 1955.

[111] X. Zhao, Q. Wang, *Appl. Phys. Rev.* **2014**, *1*, 021304.

[112] J. S. Plante, S. Dubowsky, *Sens. Actuators, A* **2007**, *137*, 96.

[113] X. Zhao, W. Hong, Z. Suo, *Phys. Rev. B - Condens. Matter Mater. Phys.* **2007**, *76*, 134113.

[114] X. Zhao, Z. Suo, *J. Appl. Phys.* **2008**, *104*, 123530.

[115] X. Zhao, Z. Suo, *Appl. Phys. Lett.* **2007**, *91*, 061921.

[116] C. Keplinger, T. Li, R. Baumgartner, Z. Suo, S. Bauer, *Soft Matter* **2012**, *8*, 285.

[117] X. Zhao, Z. Suo, *Phys. Rev. Lett.* **2010**, *104*, 1.

[118] H. Kim, S. Oh, K. Hwang, H. Choi, J. Jeon, J. Nam, *Proc. SPIE* **2001**, *4329*, 482.

[119] A. L. Larsen, P. Sommer-Larsen, O. Hassager, *Proc. SPIE* **2004**, *5385*, 108.

[120] J. Murphy, *Additives for Plastics Handbook*, Elsevier, Oxford, **2001**.

[121] F. Galantini, F. Carpi, G. Gallone, *Smart Mater. Struct.* **2013**, *22*, 104020.

[122] F. B. Madsen, A. E. Daugaard, S. Hvilsted, A. L. Skov, *Macromol. Rapid Commun.* **2016**, *37*, 378.

[123] A. L. Larsen, K. Hansen, P. Sommer-Larsen, O. Hassager, A. Bach, S. Ndoni, M. Jørgensen, *Macromolecules* **2003**, *36*, 10063.

[124] X. Zhang, C. Löwe, M. Wissler, B. Jähne, G. Kovacs, *Adv. Eng. Mater.* **2005**, *7*, 361.

[125] S. Risse, B. Kussmaul, H. Krüger, G. Kofod, *Adv. Funct. Mater.* **2012**, *22*, 3958.

[126] S. J. Duenki, Y. S. Ko, F. A. Nueesch, D. M. Opris, *Adv. Funct. Mater.* **2015**, *25*, 2467.

[127] S. M. Ha, W. Yuan, Q. Pei, R. Pelrine, S. Stanford, *Adv. Mater.* **2006**, *18*, 887.

[128] P. Brochu, H. Stoyanov, X. Niu, Q. Pei, *Smart Mater. Struct.* **2013**, *22*, 055022.

[129] P. Brochu, X. Niu, Q. Pei, *Proc. SPIE* **2011**, *7976*, 797606.

[130] X. Niu, H. Stoyanov, W. Hu, R. Leo, P. Brochu, Q. Pei, *J. Polym. Sci. Part B Polym. Phys.* **2013**, *51*, 197.

[131] K. Goswami, F. B. Madsen, A. E. Daugaard, A. L. Skov, *Proc. SPIE* **2013**, *86871Z*, 86871Z.

[132] A. Bele, M. Dascalu, C. Tugui, M. Iacob, C. Racles, L. Sacarescu, M. Cazacu, *Mater. Des.* **2016**, *106*, 454.

[133] A. Bele, M. Cazacu, C. Racles, G. Stiubianu, D. Ovezea, M. Ignat, *Adv. Eng. Mater.* **2015**, *17*, 1302.

[134] F. B. Madsen, I. Dimitrov, A. E. Daugaard, S. Hvilsted, A. L. Skov, *Polym. Chem.* **2013**, *4*, 1700.

[135] H. F. Schlaak, M. Gei, E. Bortot, H. Haus, H. Mößinger, *Electromechanically Active Polymers*, Springer, Cham, **2016**.

[136] A. N. Gent, K. Scott, Hanser Verlag, Munich, **2012**, pp. 96–101.

[137] M. Pharr, J. Y. Sun, Z. Suo, *J. Appl. Phys.* **2012**, *111*, 104114.

[138] H. Wang, M. Lei, S. Cai, *J. Appl. Phys.* **2013**, *113*, 213508.

[139] R. Vertechy, M. Fontana, *Proc. SPIE* **2015**, *9430*, 94300K.

[140] S. Michel, X. Q. Zhang, M. Wissler, C. Löwe, G. Kovacs, *Polym. Int.* **2010**, *59*, 391.

[141] H. S. Park, T. D. Nguyen, *Soft Matter* **2013**, *9*, 1031.

[142] J. Zhang, J. Ru, H. Chen, D. Li, J. Lu, *Appl. Phys. Lett.* **2017**, *110*, 5.

[143] J. Sheng, H. Chen, L. Liu, J. Zhang, Y. Wang, S. Jia, *J. Appl. Phys.* **2013**, *114*, 134101.

[144] X. Lv, L. Liu, Y. Liu, J. Leng, *Smart Mater. Struct.* **2015**, *24*, 115036.

[145] S. Zakaria, P. H. F. Morshuis, M. Y. Benslimane, K. V. Gernaey, A. L. Skov, *Proc. SPIE* **2014**, *9056*, 90562V.

[146] J. Fröhlich, W. Niedermeier, H. D. Luginsland, *Compos. Part A* **2005**, *36*, 449.

[147] A. L. Skov, A. Bejenariu, J. Bøgelund, M. Benslimane, A. D. Egede, *Proc. SPIE* **2012**, *8340*, 83400M.

[148] C. Miehe, J. Keck, *J. Mech. Phys. Solids* **2000**, *48*, 323.

[149] T. Bhave, M. Tehrani, M. Ali, A. Sarvestani, *Compos. Commun.* **2018**, *9*, 92.

[150] G. MacHado, G. Chagnon, D. Favier, *Mech. Mater.* **2010**, *42*, 841.

[151] L. Mullins, *Rubber Chem. Technol.* **1969**, *42*, 339.

[152] R. Payne, R. E. Whittaker, *Rubber Chem. Technol.* **1971**, *44*, 440.

[153] J. Diani, B. Fayolle, P. Gilormini, *Eur. Polym. J.* **2009**, *45*, 601.

[154] R. P. Deshpande, *Capacitors*, McGraw-Hill Education, New York, **2015**.

[155] R. Pitka, S. Bohrmann, H. Stöcker, G. Terlecki, H. Zetsche, Verlag Harri Deutsch, Frankfurt Am Main, **2005**, pp. 280–291.

[156] F. Kremer, A. Schönhals, *Broadband Dielectric Spectroscopy*, Springer, Heidelberg, **2003**.

[157] C. J. F. Böttcher, *Polarization and Energy*, Elsevier, Oxford, **1973**.

[158] A. M. North, *Chem. Soc. Rev.* **1972**, *1*, 49.

[159] T. Schlögl, S. Leyendecker, *Sens. Actuators, A* **2017**, *267*, 156.

[160] A. Tröls, A. Kogler, R. Baumgartner, R. Kaltseis, C. Keplinger, R. Schwödiauer, I. Graz, S. Bauer, *Smart Mater. Struct.* **2013**, *22*, 104012.

[161] S. J. Dünki, M. Tress, F. Kremer, S. Y. Ko, F. A. Nüesch, C.-D. Varganici, C. Racles, D. M. Opris, *RSC Adv.* **2015**, *5*, 50054.

[162] F. Kremer, A. Schönhals, Springer, Heidelberg, **2017**, pp. 35–57.

[163] L. Liu, H. Chen, B. Li, Y. Wang, D. Li, *Appl. Phys. Lett* **2015**, 062906.

[164] D. M. Opris, J. E. Q. Quinsaat, S. Dünki, Y. S. Ko, M. Alexandru, C. Racles, F. A. Nüesch, *Proc. SPIE* **2015**, *9430*, 94300A.

[165] M. Kollosche, G. Kofod, *Appl. Phys. Lett.* **2010**, *96*, 2008.

[166] J. Huang, S. Shian, R. M. Diebold, Z. Suo, D. R. Clarke, *Appl. Phys. Lett.* **2012**, *101*, 122905.

[167] D. Gatti, H. Haus, M. Matysek, B. Frohnapfel, C. Tropea, H. F. Schlaak, *Appl. Phys. Lett.* **2014**, *104*, 052905.

[168] G. Kofod, P. Sommer-Larsen, R. Kornbluh, R. Pelrine, *Proc. SPIE* **2001**, *4329*, 141.

[169] P. Sommer-Larsen, A. L. Larsen, *Proc. SPIE* **2004**, *5385*, 68.

[170] T. G. McKay, E. Calius, I. A. Anderson, *Proc. SPIE* **2009**, *7287*, 72870P.

[171] M. Vatankhah-Varnoosfaderani, W. F. M. Daniel, A. P. Zhushma, Q. Li, B. J. Morgan, K. Matyjaszewski, D. P. Armstrong, R. J. Spontak, A. V. Dobrynin, S. S. Sheiko, *Adv. Mater.* **2017**, *29*, 1604209.

[172] F. Carpi, P. Chiarelli, A. Mazzoldi, D. De Rossi, *Sens. Actuators, A* **2003**, *107*, 85.

[173] B. Li, H. Chen, J. Qiang, S. Hu, Z. Zhu, Y. Wang, *J. Phys. D. Appl. Phys.* **2011**, *44*, 155301.

[174] P. H. Vargantwar, A. E. Özçam, T. K. Ghosh, R. J. Spontak, *Adv. Funct. Mater.* **2012**, *22*, 2100.

[175] R. Palakodeti, M. R. Kessler, *Mater. Lett.* **2006**, *60*, 3437.

[176] X. Zhang, M. Wissler, B. Jaehne, R. Breonnimann, G. Kovacs, *Proc. SPIE* **2004**, *5385*, 78.

[177] C. Jordi, A. Schmidt, G. Kovacs, S. Michel, P. Ermanni, *Smart Mater. Struct.* **2011**, *20*, 075003.

[178] T. McKay, B. O'Brien, E. Calius, I. Anderson, *Smart Mater. Struct.* **2010**, *19*, 055025.

[179] H. Zhang, L. Düring, G. Kovacs, W. Yuan, X. Niu, Q. Pei, *Polym. Int.* **2010**, *59*, 384.

[180] S. M. Ha, W. Yuan, Q. Pei, R. Pelrine, S. Stanford, *Smart Mater. Struct.* **2007**, *16*, S280.

[181] Q. Pei, R. Pelrine, M. A. Rosenthal, S. Stanford, H. Prahlad, R. D. Kornbluh, *Proc. SPIE* **2004**, *5385*, 41.

[182] W. Hu, Z. Ren, J. Li, E. Askounis, Z. Xie, Q. Pei, *Adv. Funct. Mater.* **2015**, *25*, 4827.

[183] Y. Zhao, J. W. Zha, L. J. Yin, Z. S. Gao, Y. Q. Wen, Z. M. Dang, *Polymer.* **2018**, *137*, 269.

[184] L. Petit, B. Guiffard, L. Seveyrat, D. Guyomar, *Sens. Actuators A* **2008**, *148*, 105.

[185] S. Liu, M. Tian, B. Yan, Y. Yao, L. Zhang, T. Nishi, N. Ning, *Polymer.* **2015**, *56*, 375.

[186] G. Yin, Y. Yang, F. Song, C. Renard, Z. M. Dang, C. Y. Shi, D. Wang, *ACS Appl. Mater. Interfaces* **2017**, *9*, 5237.

[187] N. Ning, S. Li, H. Sun, Y. Wang, S. Liu, Y. Yao, B. Yan, L. Zhang, M. Tian, *Compos. Sci. Technol.* **2017**, *142*, 311.

[188] F. Carpi, A. Mazzoldi, D. De Rossi, *Proc. SPIE* **2003**, *5051*, 419.

[189] R. Vertechy, M. Fontana, G. Stiubianu, M. Cazacu, *Proc. SPIE* **2014**, *9056*, 90561R.

[190] R. Kaltseis, C. Keplinger, S. J. Adrian Koh, R. Baumgartner, Y. F. Goh, W. H. Ng, A. Kogler, A. Tröls, C. C. Foo, Z. Suo, S. Bauer, *RSC Adv.* **2014**, *4*, 27905.

[191] D. Yang, M. Tian, Y. Dong, H. Liu, Y. Yu, L. Zhang, *Smart Mater. Struct.* **2012**, *21*, 035017.

[192] A. Y. Coran, in *Sci. Technol. Rubber*, Elsevier, **2013**, pp. 337–381.

[193] H. Sun, C. Jiang, N. Ning, L. Zhang, M. Tian, S. Yuan, *Polym. Chem.* **2016**, *7*, 4072.

[194] M. Tian, H. Yan, H. Sun, L. Zhang, N. Ning, *RSC Adv.* **2016**, *6*, 96190.

[195] A. Almenningen, O. Bastiansen, V. Ewing, K. Hedberg, M. Traetterberg, *Acta Chem. Scand.* **1963**, *17*, 2455.

[196] U. Blukis, P. H. Kasai, R. J. Myers, *J. Chem. Phys* **1963**, *38*, 2753.

[197] N. Wiberg, *Lehrbuch Der Anorganischen Chemie*, Walter De Gruyter&Co., Berlin, **2007**.

[198] M. J. Owen, *Advances in Silicones and Silicone-Modified Materials*, American Chemical Society, Washington DC, **2010**.

[199] A. E. Beezer, C. T. Mortimer, *J. Chem. Soc. A* **1966**, 514.

[200] A. V. Tobolsky, *Properties and Structures of Polymers*, John Wiley And Sons, New York, **1960**.

[201] S. J. Clarson, K. Dodgson, J. A. Semlyen, *Polymer.* **1985**, *26*, 930.

[202] L. Maffli, S. Rosset, M. Ghilardi, F. Carpi, H. Shea, *Adv. Funct. Mater.* **2015**, *25*, 1656.

[203] F. Carpi, A. Migliore, G. Serra, D. De Rossi, *Smart Mater. Struct.* **2005**, *14*, 1210.

[204] M. Molberg, C. Walder, D. Opris, C. Löwe, F. Nüesch, Y. Leterrier, C. Plummer, J. A. E. Månson, S. Bauer, *J. Appl.*

Phys. **2009**, *106*, 054112.

[205] S. Rosset, A. de Saint-Aubin, Christine Poulin, H. R. Shea, *Rev. Sci. Instrum.* **2017**, *88*, 105002.

[206] F. M. Weiss, F. B. Madsen, T. Töpper, B. Osmani, V. Leung, B. Müller, *Mater. Des.* **2016**, *105*, 106.

[207] A. Poulin, S. Rosset, H. R. Shea, *Appl. Phys. Lett.* **2015**, *107*, 244104.

[208] D. McCoul, S. Rosset, S. Schlatter, H. Shea, *Smart Mater. Struct.* **2017**, *26*, 125022.

[209] P. Lotz, M. Matysek, H. F. Schlaak, *IEEE/ASME Trans. Mechatronics* **2011**, *16*, 58.

[210] P. Dubois, O. Coulembier, J.-M. Raquez, *Handbook of Ring-Opening Polymerization*, Wiley, Weinheim, **2009**.

[211] Y. Zuo, H. Lu, L. Xue, X. Wang, L. Ning, S. Feng, *J. Mater. Chem. C* **2014**, *2*, 2724.

[212] D. Yang, M. Tian, W. Wang, D. Li, R. Li, H. Liu, L. Zhang, *Electrochim. Acta* **2013**, *87*, 9.

[213] J. R. Desmurs, L. Ghosez, J. Martins, T. Deforth, G. Mignani, *J. Organometalic Chem.* **2002**, *646*, 171.

[214] G. Toskas, G. Besztercey, M. Moreau, M. Masure, P. Sigwalt, *Macromol. Chem. Phys.* **1995**, *196*, 2715.

[215] M. Cazacu, *Recent Developments in Silicone-Based Materials*, Nova Science Publishers, Inc., New York, **2010**.

[216] T. Alvik, J. Dale, *Acta Chem. Scand.* **1971**, *25*, 2131.

[217] M. Cazacu, M. Marcu, A. Vlad, D. Caraiman, C. Racles, *Eur. Polym. J.* **1999**, *35*, 1629.

[218] P. V. Wright, J. A. Semlyen, *Polymer.* **1970**, *11*, 462.

[219] C. Elschenbroich, *Organometalics*, Wiley, Weinheim, **2006**.

[220] J. K. Fink, *Reactive Polymers Fundamentals and Applications - A Concise Guide to Industrial Polymers*, Elsevier Inc., Oxford, **2013**.

[221] J. L. Speier, J. A. Webster, G. H. Barnes, *J. Am. Chem. Soc.* **1957**, *79*, 974.

[222] B. D. Karstedt, *(General Electric Co.)*, **1973**, US 3,775,452.

[223] J. W. Sprengers, M. J. Mars, M. A. Duin, K. J. Cavell, C. J. Elsevier, *J. Organomet. Chem.* **2003**, *679*, 149.

[224] A. J. Chalk, J. F. Harrod, *J. Am. Chem. Soc.* **1965**, *87*, 16.

[225] X. L. Luo, G. J. Kubas, C. J. Burns, J. C. Bryan, C. J. Unkefer, *J. Am. Chem. Soc.* **1995**, *117*, 1159.

[226] D. Troegel, J. Stohrer, *Coord. Chem. Rev.* **2011**, *255*, 1440.

[227] L. N. Lewis, R. J. Uriarte, N. Lewis, *J. Catal.* **1991**, *74*, 67.

[228] L. N. Lewis, N. Lewis, *J. Am. Chem. Soc.* **1986**, *108*, 7228.

[229] Y. Nakajima, S. Shimada, *RSC Adv.* **2015**, *5*, 20603.

[230] A. J. Holwell, *Platin. Met. Rev.* **2008**, *52*, 243.

[231] A. Fehn, F. Achenbach, S. Dietl, *(Wacker-Chemie GmbH)*, **2000**, DE 19837855 A1.

[232] J. Li, C. Niu, J. Peng, Y. Deng, G. Zhang, Y. Bai, C. Ma, W. Xiao, G. Lai, *Appl. Organomet. Chem.* **2014**, *28*, 454.

[233] S. S. O. Buisine, I. Markó, *(Rhodia Chimie)*, **2006**, EP1392708 B1.

[234] I. Markó, S. Stérin, *(Rhodia Chimie)*, **2004**, EP1235836 B1.

[235] G. L. Larson, B. C. Arkles, R. A. Cameron, *(Gelest Technologies Inc.)*, **2010**, US20100280266 A1.

[236] G. H. Peslherbe, J. T. Hynes, F. M. Tao, D. C. Clary, R. Bianco, M. J. Rosker, A. H. Zewail, *Science (80-.).* **2002**, *298*, 204.

[237] C. M. Downing, H. H. Kung, *Catal. Commun.* **2011**, *12*, 1166.

[238] T. Yokoyama, N. Kinjo, Y. Wakashima, *Polym. Eng. Sci.* **1986**, *26*, 940.

[239] F. Guebbels, S. Texeira, *(Dow Corning Corp.)*, **2016**, WO 2016/120270 A1.

[240] T. Kuroda, Yasuyoshi; Kobayashi, Yuta; Yamamoto, Kenji; Nakajima, *(Jpn. Kokai Tokkyo Koho)*, **2013**, JP 2013112686 A 20130610.

[241] F. Chen, J. Li, W. Deng, H. Zhang, Z. Wang, *(Dongguan Zhaoshun Silicone New Material Technology Co.)*, **2011**, CN102181264A.

[242] J. Stein, T. Brydon, J. A. Cella, *(General Electric Company)*, **2000**, US 6107381.

[243] M. M. Patel, A. B. Mohammad, S. Dinkar, A. Dhanabalan, *(Momentive Performance Materials Inc.)*, **2013**, WO 2013/165552 A2.

[244] European Commision, *Commission Regulation (EU) No 276/2010*, **2010**.

[245] F. Willern Van Der Weij, *Makromol. Chem* **1980**, *181*, 2541.

[246] C. Byrne, *(Momentive Performance Materials Inc.)*, **2013**, WO 2013/101755 A1.

[247] C. Maliverney, *(Bluestar Silicones France)*, **2010**, WO 2010/146250 A1.

[248] J. M. Pujol, C. Prébet, *J. Adhes. Sci. Technol.* **2003**, *17*, 261.

[249] F. De Buyl, P. Leempoel, *(Dow Corning S.A.)*, **1999**, US 5,908,909.

[250] D. R. Weyenberg, *(Dow Corning Corp.)*, **1965**, US 3175993.

[251] A. Gutacker, E. Mejia, U. Kragl, J. Klein, M. Höhne, *(Henkel AG & CO.)*, **2017**, WO 2017/102510 A1.

[252] J. G. E. Wright, S. G. Oliver, *US Patent*, **1948**, 2.448.565.

[253] M. L. Dunham, D. L. Bailey, R. Y. Mixer, *Ind. Eng. Chem.* **1957**, *49*, 1373.

[254] G. Baquey, L. Moine, M. Degueil-Castaing, J. C. Lartigue, B. Maillard, *Macromolecules* **2005**, *38*, 9571.

[255] A. Charlesby, *Proc. R. Soc. A Math. Phys. Eng. Sci.* **1955**, *230*, 120.

[256] R. K. Jenkins, N. S. Laboratories, *J. Polym. Sci. Part A-2* **1966**, *4*, 41.

[257] R. K. Traeger, T. T. Castonguay, *J. Appl. Polym. Sci.* **1966**, *10*, 535.

[258] J. C. Caprino, R. F. Macander, in *Rubber Technol.*, Springer, Boston, **1987**, pp. 375–409.

[259] Z. Li, K. S. Moon, Z. Lin, Y. Yao, S. Wilkins, C. P. Wong, *J. Appl. Polym. Sci.* **2014**, *131*, 40355.

[260] H. K. Kim, H. T. Ju, J. W. Hong, *Eur. Polym. J.* **2003**, *39*, 2235.

[261] C. E. Corcione, A. Previderio, M. Frigione, *Thermochim. Acta* **2010**, *509*, 56.

[262] U. Müller, H. J. Timpe, J. Neuenfeld, *Eur. Polym. J.* **1991**, *27*, 621.

[263] L. M. Campos, I. Meinel, R. G. Guino, M. Schierhorn, N. Gupta, G. D. Stucky, C. J. Hawker, *Adv. Mater.* **2008**, *20*, 3728.

[264] C. Zhou, Y. H. Li, Z. H. Jiang, K. D. Ahn, T. J. Hu, Q. H. Wang, C. H. Wang, *Chinese Chem. Lett.* **2016**, *27*, 685.

[265] L. Xue, Y. Zhang, Y. Zuo, S. Diao, J. Zhang, S. Feng, *Mater. Lett.* **2013**, *106*, 425.

[266] U. Müller, A. Kunze, C. Herzig, J. Weis, *J. Macromol. Sci. - Pure Appl. Chem.* **1996**, *33*, 439.

[267] C. E. Hoyle, T. Y. Lee, T. Roper, *J. Polym. Sci. Part A Polym. Chem.* **2004**, *42*, 5301.

[268] K. Goswami, A. L. Skov, A. E. Daugaard, *Chem. Eur. J.* **2014**, *20*, 9230.

[269] Y. Suzuki, T. Higashihara, S. Ando, M. Ueda, *Macromolecules* **2012**, *45*, 3402.

[270] C. Cohen, D. Damiron, S. Ben Dkhil, E. Drockenmuller, F. Restagno, L. Léger, *J. Polym. Sci. Part A Polym. Chem.* **2012**, *50*, 1827.

[271] J. Zhang, Y. Chen, M. A. Brook, *Langmuir* **2013**, *29*, 12432.

[272] D. J. Lunn, C. E. Boott, K. E. Bass, T. A. Shuttleworth, N. G. McCreanor, S. Papadouli, I. Manners, *Macromol. Chem. Phys.* **2013**, *214*, 2813.

[273] H. C. Kolb, M. G. Finn, K. B. Sharpless, C. Chemistry, *Angew. Chem. Int. Ed.* **2001**, *40*, 2004.

[274] C. E. Hoyle, C. N. Bowman, *Angew. Chem. Int. Ed.* **2010**, *49*, 1540.

[275] C. Decker, *Prog. Polym. Sci.* **1996**, *21*, 593.

[276] C. R. Morgan, F. Magnotta, A. D. Ketley, *J Polym Sci Polym Chem Ed* **1977**, *15*, 627.

[277] L. Herczynska, L. Lestel, S. Boileau, J. Chojnowski, S. Polowinski, *Eur. Polym. J.* **1999**, *35*, 1115.

[278] C. Racles, V. Cozan, A. Bele, M. Dascalu, *Des. Monomers Polym.* **2016**, *5551*, 1.

[279] S. J. Dünki, E. Cuervo-Reyes, D. M. Opris, *Polym. Chem.* **2017**, *8*, 715.

[280] J. P. Szabo, J. A. Hiltz, C. G. Cameron, R. S. Underhill, J. Massey, B. White, J. Leidner, *Proc. SPIE* **2003**, *5051*, 180.

[281] F. Carpi, D. De Rossi, *IEEE Trans. Dielectr. Electr. Insul.* **2005**, *12*, 835.

[282] H. Stoyanov, P. Brochu, X. Niu, E. Della Gaspera, Q. Pei, *Appl. Phys. Lett.* **2012**, *100*, 262902.

[283] A. L. Skov, S. Vudayagiri, M. Benslimane, *Proc. SPIE* **2013**, *8687*, 86871I.

[284] W. Ren, A. J. Masys, G. Yang, B. K. Mukherjee, *J. Phys. D. Appl. Phys.* **2002**, *35*, 316.

[285] G. Gallone, F. Carpi, D. De Rossi, G. Levita, A. Marchetti, *Mater. Sci. Eng. C* **2007**, *27*, 110.

[286] L. Jiang, A. Betts, D. Kennedy, S. Jerrams, *J. Mater. Sci.* **2015**, *50*, 7930.

[287] D. Yang, S. Huang, M. Ruan, S. Li, Y. Wu, W. Guo, L. Zhang, *Compos. Sci. Technol.* **2018**, *155*, 160.

[288] L. J. Romasanta, P. Leret, L. Casaban, M. Hernández, M. A. De La Rubia, J. F. Fernández, J. M. Kenny, M. A. Lopez-Manchado, R. Verdejo, *J. Mater. Chem.* **2012**, *22*, 24705.

[289] L. Duan, G. L. Wang, Y. Y. Zhang, Y. N. Zhang, Y. Y. Wei, Z. F. Wang, M. Zhang, *Polym. Compos.* **2018**, *39*, 691.

[290] M. Iacob, C. Tugui, V. Tiron, A. Bele, S. Vlad, T. Vasiliu, M. Cazacu, A. L. Vasiliu, C. Racles, *Smart Mater. Struct.* **2017**, *26*.

[291] M. Razzaghi-Kashani, N. Gharavi, S. Javadi, *Smart Mater. Struct.* **2008**, *17*, 065035.

[292] G. Boccalero, C. Jean-Mistral, M. Castellano, C. Boragno, *Compos. Part B Eng.* **2018**, *146*, 13.

[293] F. Carpi, G. Gallone, F. Galantini, D. De Rossi, *Adv. Funct. Mater.* **2008**, *18*, 235.

[294] G. Gallone, F. Galantini, F. Carpi, *Polym. Int.* **2010**, *59*, 400.

[295] H. Liu, L. Zhang, D. Yang, N. Ning, Y. Yu, L. Yao, B. Yan, M. Tian, *J. Phys. D. Appl. Phys.* **2012**, *45*.

[296] H. Böse, D. Uhl, R. Rabindranath, *Proc. SPIE* **2012**, *8340*, 83402E.

[297] F. B. Madsen, L. Yu, S. Hvilsted, A. L. Skov, *Proc. SPIE* **2015**, *9430*, 94301D.

[298] P. Mazurek, S. Hvilsted, A. L. Skov, *Polymer.* **2016**, *87*, 1.

[299] P. Mazurek, L. Yu, R. Gerhard, W. Wirges, A. L. Skov, *J. Appl. Polym. Sci.* **2016**, *133*, 1.

[300] A. Larmagnac, S. Eggenberger, H. Janossy, J. Vörös, *Sci. Rep.* **2014**, *4*, 1.

[301] S. K. Yadav, I. J. Kim, H. J. Kim, J. Kim, S. M. Hong, C. M. Koo, *J. Mater. Chem. C* **2013**, *1*, 5463.

[302] M. Tian, Z. Wei, X. Zan, L. Zhang, J. Zhang, Q. Ma, N. Ning, T. Nishi, *Compos. Sci. Technol.* **2014**, *99*, 37.

[303] A. Egede Daugaard, S. S. Hassouneh, M. Kostrzewska, A. G. Bejenariu, A. L. Skov, *Proc. SPIE* **2013**, *8687*, 868729.

[304] M. Molberg, D. Crespy, P. Rupper, F. Nüesch, J. A. E. Manson, C. Löwe, D. M. Opris, *Adv. Funct. Mater.* **2010**, *20*, 3280.

[305] D. M. Opris, M. Molberg, C. Walder, Y. S. Ko, B. Fischer, F. A. Nüesch, *Adv. Funct. Mater.* **2011**, *21*, 3531.

[306] J. E. Q. Quinsaat, M. Alexandru, F. a. Nüesch, H. Hofmann, A. Borgschulte, D. M. Opris, *J. Mater. Chem. A* **2015**, *3*, 14675.

[307] J. E. Q. Quinsaat, F. a. Nüesch, H. Hofmann, D. M. Opris, *RSC Adv.* **2013**, *3*, 6964.

[308] L. Duan, J. Zhang, M. Zhang, C.-H. Li, J.-L. Zuo, *J. Mater. Chem. C* **2018**, *6*, 12175.

[309] R. R. Kohlmeyer, A. Javadi, B. Pradhan, S. Pilla, K. Setyowatt, J. Chen, S. Gong, *J. Phys. Chem. C* **2009**, *113*, 17626.

[310] Y. J. Lee, S. R. Ham, J. H. Kim, T. H. Yoo, S. R. Kim, Y. T. Lee, D. K. Hwang, B. Angadi, W. S. Seo, B. K. Ju, W. K. Choi, *Sci. Rep.* **2018**, *8*, 4851.

[311] H. Böse, D. Uhl, K. Flittner, H. Schlaak, *Proc. SPIE* **2011**, *7976*, 79762J.

[312] V. I. Kushch, R. Springhetti, S. V. Shmegera, *Int. J. Eng. Sci.* **2018**, *123*, 51.

[313] C. Pecharromán, J. S. Moya, *Adv. Mater.* **2000**, *12*, 294.

[314] G. M. Tsangaris, G. C. Psarras, N. Kouloumbi, *J. Mater. Sci.* **1998**, *33*, 2027.

[315] H. Sun, H. Zhang, S. Liu, N. Ning, L. Zhang, M. Tian, Y. Wang, *Compos. Sci. Technol.* **2018**, *154*, 145.

[316] B. Kussmaul, S. Risse, G. Kofod, R. Waché, M. Wegener, D. N. McCarthy, H. Krüger, R. Gerhard, *Adv. Funct. Mater.* **2011**, *21*, 4589.

[317] H. Krüger, B. Kussmaul, G. Kofod, S. Risse, *(Fraunhofer-Gesellschaft E. V.)*, **2012**, WO 2012/038093 A1.

[318] S. Risse, B. Kussmaul, H. Krüger, G. Kofod, *RSC Adv.* **2012**, *2*, 9029.

[319] F. B. Madsen, A. E. Daugaard, S. Hvilsted, M. Y. Benslimane, A. L. Skov, *Smart Mater. Struct.* **2013**, *22*, 11.

[320] S. M. G. Frankær, M. K. Jensen, A. G. Bejenariu, A. L. Skov, *Rheol. Acta* **2012**, *51*, 559.

[321] L. Zhang, D. Wang, P. Hu, J.-W. Zha, F. You, S.-T. Li, Z.-M. Dang, *J. Mater. Chem. C* **2015**, *3*, 4883.

[322] C. Racles, M. Cazacu, B. Fischer, D. M. Opris, *Smart Mater. Struct.* **2013**, *22*, 10.

[323] C. Racles, M. Alexandru, A. Bele, V. E. Musteata, M. Cazacu, D. M. Opris, *RSC Adv.* **2014**, *4*, 37620.

[324] L. Xue, D. Wang, Z. Yang, Y. Liang, J. Zhang, S. Feng, *Eur. Polym. J.* **2013**, *49*, 1050.

[325] S. Dünki, F. Nueesch, D. M. Opris, *J. Mater. Chem. C* **2016**, 10545.

[326] A. P. Purdy, A. Hwang, *Polym. Mater. Sci. Eng.* **2001**, *84*, 641.

[327] D. Opris, M. Dascalu, S. Dünki, J. E. Quinsaat, Y. S. Ko, *RSC Adv.* **2015**, *5*, 104516.

[328] F. B. Madsen, L. Yu, A. E. Daugaard, S. Hvilsted, A. L. Skov, *RSC Adv.* **2015**, *5*, 10254.

[329] F. B. Madsen, I. Javakhishvili, R. E. Jensen, a. E. Daugaard, S. Hvilsted, A. L. Skov, *Polym. Chem.* **2014**, *5*, 7054.

[330] D. J. Parks, J. M. Blackwell, W. E. Piers, *J. Org. Chem.* **2000**, *65*, 3090.

[331] S. Rubinsztajn, J. A. Cella, *Macromolecules* **2005**, *38*, 1061.

[332] M. Stepp, F. Achenbach, A. Koellenbacher, *(Wacker Chemie AG)*, **2015**, WO 2015/121261 A1.

Chapter 2 Mild Synthesis of Mercaptonitriles from Vinyl Nitriles and their Cyclization Reactions

This chapter is based on the publication

Mild synthesis of mercaptonitriles from vinyl nitriles and their cyclization reactions

by

Philip Caspari,[1,2] Frank A. Nüesch,[1,2] Antonia Neels,[3] Dorina M. Opris[2]

[1]Ecole Polytechnique Fédérale de Lausanne (EPFL), Institut des matériaux, Station 12, CH 1015, Lausanne, Switzerland.

[2]Empa, Swiss Federal Laboratories for Materials Science and Technology, Laboratory for Functional Polymers, Ueberlandstr. 129, CH-8600, Dübendorf, Switzerland

[3]Empa, Swiss Federal Laboratories for Materials Science and Technology, Center for X-ray Analytics, Ueberlandstr. 129, CH-8600, Dübendorf, Switzerland.

Adapted from

RSC Adv. **2016**, *6*, 98059.

DOI: 10.1039/c6ra21948a

https://pubs.rsc.org/en/Content/ArticleLanding/2016/RA/C6RA21948A#!divAbstract

with permission from the Royal Society of Chemistry

Author Contributions:

P. Caspari performed the synthesis of all compounds and their characterization except for the X-ray analysis, mass spectrometry and elemental analysis as well as contributed to the manuscript.

2.1 Abstract

Thiol-ene addition of thioacetic acid **A** is widely used in the synthesis of thiols from vinyl precursor, but so far was not conducted on non-conjugated vinyl nitriles. The challenge when vinyl nitriles are used is to selectively conduct the thiol-ene addition, while avoiding the nucleophilic addition of **A** to the nitrile group. We have found that vinyl nitriles give selective UV-induced thiol-ene addition in presence of photoinitiators as long as stoichiometric amount of **A** to the vinyl group and sterically unhindered vinyls are used. On the contrary, when a sterically hindered vinyl is used, the nucleophilic addition of the nitrile is favoured. The prepared mercaptonitriles can easily undergo cyclization reactions in basic and acidic conditions as well as in presence of silica gel. This illustrates the high reactivity of nitriles towards thiol addition. 1,2-ethanedithiol **B** is presented as an alternative reagent to **A** as it allows conversion of vinyl nitriles directly into mercaptonitriles under mild and non-acidic reaction conditions.

2.2 Introduction

The radical addition of thiols to carbon-carbon double bonds is widely known as thiol-ene reaction. This reaction is regioselective and gives the anti-Markovnikov adduct as major product.[1] Due to high conversion, small amount of by-products and fast reaction time, the thiol-ene reaction is often referred to as "thiol click chemistry" in the literature.[2–5] The addition is mediated by either thermal[6] or by UV radical initiators. Thiol-ene reaction is a versatile tool in biochemistry[7–10] and polymer science. In polymer science, the thiol-ene reaction is a well-established process for the preparation of dithiol monomers[6] and in the synthesis of polythioethers[11–13] and polythioesters.[14] Due to its high conversion it was often used in post-polymerization modifications.[15–21] When photoinitiators are used, the reaction proceeds to completion within few minutes.[7] In their absence thiols can be activated by UV irradiation but the reaction rate is considerably lower.[8] The addition of thioacetic acid **A** to alkenes followed by acetyl cleavage is one of the most frequently used synthetic routes to thiols. Cleavage of the acetyl moiety can be conducted under acidic[6] and basic conditions[22] or by reduction with lithium aluminium hydride.[23] Hydrogen sulfide addition to alkenes leads to formation of significant amount of dialkylsulfides side-products. Already in 1941 Schjanberg *et al.* published the selective thiol-ene addition of **A** to non-conjugated pentenoic acids.[24] Later, Brown et al. reported the selective thiol-ene addition of **A** to allyl alcohol, allyl acetate, and maleic anhydride mediated by peroxides.[25] More recently thiol-ene addition of non-conjugated vinyl amides using BEt_3 and O_2 as initiator was reported.[26] Thiol-ene addition of aliphatic thiols to allyl cyanide is known,[27,28] however, the formed sulfides cannot be converted into mercaptonitriles. While selective 1,4-addition of **A** to acrylonitrile under basic conditions is known,[29] the thiol-ene addition of **A** and 1,2-ethanedithiol **B** to non-conjugated vinyl nitrile compounds *i.e.* allyl cyanide was not explored so far. The addition of A to aliphatic nitriles was reported to occur under acidic or basic conditions with formation of thioamides.[30,31] It is also known that mercaptonitriles can undergo intramolecular reactions under acidic conditions.[32] Given the reactivity of **A** to nitriles it was unclear whether a selective thiol-ene addition of **A** to various vinyl nitriles followed by the deprotection of the thioester to thiol can be realized.

In polymer science, mercaptonitriles are attractive precursor for the functionalization of polyvinylsiloxanes via thiol-ene reaction.[17] We have recently shown that the dielectric permittivity (ε') of polysiloxanes modified with polar nitrile groups increases linearly with the content of the nitrile groups. By increasing the content of nitrile groups on the polysiloxane, it is to be expected that the permittivity can be further increased. To be attractive precursors for post-polymerization reactions, mercaptonitriles must be synthesized cost-efficiently on g-scale and have to be stable during thiol-ene addition to the polyvinylsiloxane.

This work describes the thiol-ene reaction of **A** and 1,2-ethanedithiol **B** to allyl cyanide, allyl malononitrile, and 3-vinyl-1,3,5-tricarbopentanitrile which should allow formation of thiols with different content of nitrile groups in two steps or directly, respectively.

2.3 Experimental section

General Remarks: All reactions were carried out in dried glassware under argon atmosphere. Unless otherwise stated, all chemicals were reagent grade and used as received. Methanol, dichloromethane (DCM), heptane, ethyl acetate, petroleum ether and tetrahydrofurane (THF) were purchased from VWR. Anhydrous methanol was purchased from Sigma Aldrich. Silica gel was purchased from VWR ('Normasil 60' 40-63 μm). Analytical TLC was carried out on 'TLC Silica gel 60 F_{254}' from Merck. TLC plates were visualized with UV light or aqueous $KMnO_4$ solution. THF was dried over sodium and distilled prior use. All other chemicals were purchased from Sigma-Aldrich. A mercury vapour UV-light source UVAHAND 250 GSH1 from Dr. Hönle AG without additional filters providing an irradiation intensity of 15 mW cm^{-2} in the frequency range between 320 and 600 nm was used. ^{1}H and ^{13}C NMR spectra were recorded on a Bruker Avance III 400 NMR spectrometer using a 5 mm BBO Prodigy^{TM} CryoProbe at 400.18 and 100.63 MHz, respectively. Chemical shifts (δ) in ppm are calibrated to residual solvent peaks according to literature.[33] Mass spectrometry was conducted by the laboratory of organic chemistry of ETH Zurich. EI-MS was measured with Waters' AutoSpec Ultima (EI-triSector-MS), ESI-MS with Bruker's maXis (ESI/NanoSpray-Qq-TOF-MS). Elemental analysis was determined with LECO TruSpec Micro, LECO RO-478 and LECO CHNS-932 by the laboratory of organic chemistry of ETH Zurich. For the broadband dielectric spectroscopy (BDS) measurements a high impedance Alpha Analyzer combined with a Quatro temperature controller (both from Novocontrol) has been employed to cover a broad frequency from 0.1 Hz to 1 MHz. Two stainless steel discs with a diameter of 20 mm served as electrodes which were separated by three glass fibers with a diameter of 100 μm.

S-3-cyanopropyl thioacetate **1**: Allyl cyanide (20.0 ml, 0.25 mol), thioacetic acid (26.6 ml, 0.38 mol), and 2,2-dimethoxy-2-phenylacetophenone (DMPA) (0.64 g, 0.0025 mol) were dissolved in THF. The solution was degassed and irradiated for 5 min with a UV light. All volatiles were removed *in vacuo* at 60 °C to obtain 36 g crude product mixture. The residue was fractionally distilled at 117 °C and 1 x 10^{-3} mbar to give **1** (25.4 g, 73%) as pale yellowish liquid. ^{1}H NMR (400 MHz, $CDCl_3$) δ, ppm: 2.97 (t, ^3J=6.9 Hz, 2H, -S-C$\underline{H_2}$-CH_2-), 2.42 (t, ^3J=8.0 Hz, 2H, -CH_2-C$\underline{H_2}$-CN,), 2.35 (s, 3H, C$\underline{H_3}$-CO-S-), 1.94 (q, ^3J=7.1 Hz, 2H, -CH_2-C$\underline{H_2}$-CH_2-CN).^{13}C NMR (100 MHz, $CDCl_3$) δ, ppm: 195.33 (CH_3-$\underline{C}$O-S-), 119.09 (-CH_2-CH_2-$\underline{C}$N), 30.77 ($\underline{C}H_3$-CO-S-), 28.00 (-S-$\underline{C}H_2$-CH_2-), 25.93 (-S-CH_2-$\underline{C}H_2$-), 16.42 (-CH_2-$\underline{C}H_2$-CN). MS (EI) *m/z* (%): 43.02 (100), 128.02 (10.97), 143.04 (4.38). EA: calculated: [C] 50.32% [H] 6.33% [N] 9.78% [O] 11.17 [S] 22.39 found: [C] 50.27% [H] 6.54% [N] 9.54% [O] 11.40 [S] 22.22%.

4-Mercaptobutanenitrile **2**: 4-thioacetic butanenitrile **1** (10 g, 0.07 mol), trimethylsilyl chloride (1.8 ml, 0.014 mol), and methanol (150 ml, 52 mol) were stirred at 65 °C for 18 h. The reaction mixture was allowed to cool down to ambient temperature and all volatiles were removed *in vacuo*. The residue was dissolved in chloroform and filtered. After removing all volatiles *in vacuo*, 4.3 g of crude product was obtained. The residue was fractionally distilled at 77 °C and 10 mbar to give **2** (3 g, 43%) as colourless liquid.^{1}H NMR (400 MHz, $CDCl_3$) δ, ppm: 2.68 (dt, ^3J=7.0 Hz, 8.3 Hz, 2H, HS-C$\underline{H_2}$-CH_2-), 2.54 (t, ^3J=7.0 Hz, 2H, -CH_2-C$\underline{H_2}$-CN,), 1.96 (q, ^3J=7.0 Hz, 2H, -CH_2-C$\underline{H_2}$-CH_2-), 1.38 (t, ^3J=8.3 Hz, 2H, $\underline{H}$S-CH_2-).^{13}C NMR (100 MHz, $CDCl_3$) δ, ppm: 119.10 (-CH_2-CH_2-$\underline{C}$N), 29.39 (-S-$\underline{C}H_2$-CH_2-), 23.34 (-S-CH_2-$\underline{C}H_2$-), 15.90 (-CH_2-$\underline{C}H_2$-CN). MS (EI) *m/z* (%): 54.03 (100), 68.05 (23.84), 101.03 (97.52).

2-Iminothiolane hydrochloride **3: 1** (1.4 g, 0.01 mol), trimethylsilyl chloride (1.3 ml, 0.01 mol), and methanol (20.2 ml, 52 mol) were stirred at 65 °C for 18 h. The reaction mixture was allowed to cool down to ambient temperature and all volatiles were removed *in vacuo*. The residue was washed with chloroform to give **3** (0.6 g, 45%) as fine powder. ^{1}H NMR (400 MHz, DMSO-d_6) δ, ppm: 12.37 (s, 2H, -CH_2=N$\underline{H_2}$), 3.51 (t, ^3J=6.6 Hz, 2H, -CH_2-C$\underline{H_2}$-S-), 3.18 (t, ^3J=7.1 Hz, 2H, -C(=NH_2)-C$\underline{H_2}$-CH_2-), 2.56 (q, ^3J=6.8 Hz, 2H, -CH_2-C$\underline{H_2}$-CH_2-). ^{13}C NMR (100 MHz, DMSO-d_6) δ, ppm: 203.78 (-S-$\underline{C}$=NH_2), 39.38 (-S-$\underline{C}H_2$-CH_2-), 37.61 (-C(=NH_2)-$\underline{C}H_2$-CH_2-), 27.55 (-CH_2-$\underline{C}H_2$-CH_2-).

Allylmalononitrile **5:** To a solution of malononitrile (66 g, 1 mol) in DCM (300 ml), allyl bromide (86 ml, 1 mol) and subsequently diisopropylethylamine (165 ml, 0.95 mol) were dropped slowly at 0 °C. The solution was allowed to warm up and stirred overnight. The reaction mixture was washed several times with H_2O. The organic phase was separated and dried over $MgSO_4$, filtered and concentrated *in vacuo* to give 83 g crude product mixture. It was purified by column chromatography (petroleum ether (40-60 °C)/ ethyl acetate 9:1) to give **5** (35 g, 35%) as colourless viscous liquid. R_F= 0.4 (heptane/ethyl acetate 2:1). ^{1}H NMR (400 MHz, $CDCl_3$) δ, ppm: 5.91-5.80 (m, 1H, -CH_2-C$\underline{H}$=CH_2), 5.43-5.38 (m, 2H, -CH_2-CH=C$\underline{H_2}$), 3.78 (t, ^3J=6 Hz, 1H, $(NC)_2$-C$\underline{H}$-CH_2-,), 2.75 (dt,^4J=1 Hz, ^3J=6.6 Hz 2H, CH-C$\underline{H_2}$-CH=). ^{13}C NMR (100 MHz, $CDCl_3$) δ, ppm: 129.29 (-$\underline{C}$H=CH_2), 122.55 (-CH=$\underline{C}H_2$), 112.35 (-*C*N), 34.74 (-CH-$\underline{C}H_2$-), 23.16 (-$\underline{C}$H-CH_2-).

S-(4,4-dicyanobutyl) thioacetate **6:** A solution of allyl malononitrile (1.06 g, 0.01 mol), thioacetic acid (1.2 ml, 0.012 mol) and DMPA (0.025 g, 0.0002 mol) in THF (15 ml) was carefully degassed and then irradiated for 5 min with UV light. The volatiles were removed *in vacuo* and the crude product mixture (2.6 g) was purified by column chromatography (Heptane/Ethyl acetate 2:1, R_F= 0.3). **6** was obtained as colourless viscous liquid (1.35 g, 74%). ^{1}H NMR (400 MHz, $CDCl_3$) δ, ppm: 3.87 (t, ^3J=6.8 Hz, 1H, $(NC)_2$-C$\underline{H}$-CH_2-), 2.95 (t, ^3J=6.8 Hz, 2H, CH_2-C$\underline{H_2}$-SAc), 2.36 (s, 3H, CH_2-S-C$\underline{H_3}$), 2.13-2.06 (m, 2H, CH-C$\underline{H_2}$-CH_2-), 1.95-

1.84 (m, 2H, CH-CH_2-C$\underline{H_2}$-). ^{13}C NMR (100 MHz, $CDCl_3$) δ, ppm: 195.65 (-S-$\underline{C}$=O-CH_3), 112.53 (-$\underline{C}$N), 30.76 (-S-C(=O)-$\underline{C}H_3$), 29.55 (CH_2-$\underline{C}H_2$-CH_2), 27.22 ($\underline{C}H_2$-SAc), 26.84 (CH-$\underline{C}H_2$-), 22.30 (-$\underline{C}$H-CH_2-). MS (EI+) *m/z* (%): 182.05 (5.53), 43.02 (100). EA: calculated: [C] 52.73% [H] 5.53% [N] 15.37% [O] 8.78% [S] 17.59% found: [C] 52.53% [H] 5.75% [N] 15.31% [O] 9.05 [S] 17.53%.

4,4-dicyanobutyl thiol **7**: To a degassed solution of **6** (4.7 g, 0.025 mol) in anhydrous MeOH (43 ml, 1.07 mol) trimethylsilyl chloride was added (0.54 ml, 0.0043 mol). The reaction was refluxed for 18 h. The reaction was allowed to cool down to ambient temperature. All volatiles were removed *in vacuo*. The residue was redissolved in $CHCl_3$ and filtered through a syringe filter. After removing all volatiles *in vacuo* 3.5 g yellowish viscous liquid was obtained. The residue was fractionally distilled to give 2.5 g pale yellowish liquid (71%; purity ~ 85%). Further attempts to purify this compound by column chromatography were not successful. **7** gives a cyclization reaction to **8** during this purification step. ^{1}H NMR (400 MHz, $CDCl_3$) δ, ppm: 3.80 (t, ^3J=6.8 Hz, 1H, $(NC)_2$-C$\underline{H}$-CH_2-), 2.61-2.67 (m, 2H, CH_2-C$\underline{H_2}$-SH), 2.23-2.17 (m, 2H, CH-C$\underline{H_2}$-CH_2-), 1.98-1.90 (m, 2H, CH-CH_2-C$\underline{H_2}$-), 1.43 (t, ^3J=8.1 Hz, 1H, -CH_2-S$\underline{H}$). ^{13}C NMR (100 MHz, $CDCl_3$) δ, ppm: 195.60 (-S-$\underline{C}$=O-CH_3), 112.54 (-$\underline{C}$N), 29.47 (CH_2-$\underline{C}H_2$-CH_2), 30.39 ($\underline{C}H_2$-SH), 23.39 (CH-CH_2-), 22.46 (-CH-$\underline{C}H_2$-). HRMS (ESI): calc. $C_6H_9N_2S$ *m/z*: 141.0481 [M+H]; found 141.0481 [M+H].

6-Amino-3,4-dihydro-2H-thiopyran-5-carbonitrile **8:** To a degassed solution of **6** (2.6 g, 0.014 mol) in anhydrous MeOH (24 ml, 0.593 mol) trimethylsilyl chloride was added (0.03 ml, 0.0024 mol). The reaction was refluxed for 17 h. Then, additional trimethylsilyl chloride (0.03 ml) was added and the reaction mixture stirred for another 72 h at r.t. All volatiles were removed *in vacuo*. The residue was redissolved in $CHCl_3$ and filtered through a syringe filter. After removing all volatiles *in vacuo* 1.63 g yellow viscous liquid was obtained. An aliquot of 0.5 g of crude product mixture was purified by column chromatography and recrystallized from *n*-heptane/ ethyl acetate to give **8** (0.3 g, 49%) as colourless solid. R_F= 0.2 (DCM/ heptane 3:1). ^{1}H NMR (400 MHz, $CDCl_3$) δ, ppm: 4.33 (br s, 2H, -NH_2), 2.94 (t, ^3J=5.6 Hz, 2H, -CH_2-C$\underline{H_2}$-S), 2.35 (t, ^3J=6.4 Hz, 2H, -C$\underline{H_2}$-CH_2-CH_2-), 2.03-1.96 (m, 2H, -CH_2-C$\underline{H_2}$-CH_2).^{13}C NMR (100 MHz, $CDCl_3$) δ, ppm: 154.19 (C=$\underline{C}$(-NH_2)-S), 120.13 (-$\underline{C}$N), 72.94 ((NC)-$\underline{C}$=C-S), 28.17 (S-$\underline{C}H_2$-CH_2-CH_2-), 24.37 (S-CH_2-CH_2-$\underline{C}H_2$-), 22.47 (-CH_2-$\underline{C}H_2$-CH_2-). HRMS (ESI) calcd. for $C_6H_9N_2S$ [M+H] 141.0481, found 141.0481. EA: calculated: [C] 51.40% [H] 5.74% [N] 19.98% found: [C] 51.44% [H] 5.83% [N] 19.73%.

3-Vinylpentane-1,3,5-trinitrile **9:** Allyl cyanide (12.1 ml, 0.15 mol) and vinyl cyanide (21 ml, 0.32 mol) were added dropwise to a mixture of trimethylbenzylammonium hydroxide (1.2 ml of 40 wt% aqueous solution, 0.003 mol) in *tert*-butanol (25 ml) at 25°C. The temperature was kept constant by use of an ice bath. After complete addition, the reaction mixture was stirred overnight at ambient temperature. The mixture was acidified with diluted aqueous HCl and washed several times with DCM. The organic phase was dried over $MgSO_4$ and the volatiles were removed *in vacuo.* The residue was purified by column chromatography (*n*-heptane/ethyl acetate 2:1) to give a pale yellowish solid (9.0 g). The solid was dissolved in ethyl acetate and precipitated by slow addition *n*-heptane to obtain **9** (8.2 g, 31%) as colourless solid. R_F= 0.5 (heptane/ ethyl acetate 1:1). ^{1}H NMR (400 MHz, $CDCl_3$) δ, ppm: 5.67 (d, ^3J=16 Hz, 1H, C$\underline{H}$H=CH-), 5.58 (d, ^3J=11 Hz, 1H, CH$\underline{H}$=CH-), 5.44 (dd, ^3J=10.2 Hz, ^3J=16.8 Hz , 1H, CH_2=C$\underline{H}$-), 2.57-2.39 (m, 4H, CH_2-C$\underline{H_2}$-CN), 2.24-2.17 (m, 2H, CH$\underline{H}$-CH_2-CN), 2.00-1.92 (m, 2H, CH$\underline{H}$-CH_2-CN). ^{13}C NMR (100 MHz, $CDCl_3$) δ, ppm: 132.76 (CH_2=$\underline{C}$H-), 122.17 ($\underline{C}H_2$=CH-), 117.98 (C_{quart}-$\underline{C}$N), 117.85 (CH_2-$\underline{C}$N), 45.81 (C_{quart}), 34.22 ($\underline{C}H_2$-CH_2CN), 13.66 (CH_2-$\underline{C}H_2$-CN). MS (EI) *m/z* (%): 55.05 (49.53), 80.05 (34.74), 92.05 (70.69), 119.06 (100). EA: calculated: [C] 69.34% [H] 6.40% [N] 24.26% found: [C] 69.21% [H] 6.33% [N] 24.16%.

4-Cyano-4-vinylheptane bis(thioamide) **12**: A solution of 3-vinylpentane-1,3,5-tricarbonitrile (0.5 g, 0.0029 mol), thioacetic acid (4.8 ml, 0.024 mol), and AIBN (0.015 g, 0. 09 mmol) dissolved in toluene (30 ml) was carefully degassed. The reaction mixture was stirred for 18 h at 70 °C. After removing all volatiles *in vacuo*, the mixture was purified by column chromatography (*n*-heptane/ethyl acetate 1:1) to give (0.4 g, 58%) of **12**. R_F= 0.2 (heptane/ethyl acetate 1:1). ^{1}H NMR (400 MHz, acetone-d_6) δ, ppm: 8.68 (br s, 4H, -CS-N$\underline{H_2}$), 5.71 (dd, ^3J=10Hz, ^3J=17 Hz, 1H, CH_2=CH-), 5.42 (d, ^3J=17 Hz, 1H, CH$\underline{H}$=CH-), 5.35 (d, ^3J=10 Hz, 1H, C$\underline{H}$H=CH-), 2.77-2.63 (m, 4H, CH_2-C$\underline{H_2}$-C(S)NH_2), 2.28-2.11 (m, 4H, C$\underline{H_2}$-CH_2-CN).^{13}C NMR (100 MHz, acetone-d6) δ, ppm: 208.12 (-$\underline{C}$(S)NH_2), 136.79 (CH_2=$\underline{C}$H-), 120.21 ($\underline{C}H_2$=CH-), 117.37 (C_{quart}-$\underline{C}$N), 45.60 (C_{quart}), 40.14 ($\underline{C}H_2$-$\underline{C}H_2$C(S)NH_2), 37.31 (CH_2-$\underline{C}H_2$-C(S)NH_2); MS (ESI): calc. for $C_{10}H_{16}N_3S_2$ [M+H] 242.0780; found 242.0779.

4-((2-Mercaptoethyl)thio)butanenitrile **13**: Allyl cyanide (20 ml, 0.25 mol), 1,2-ethanedithiol (freshly distilled) (168 ml, 2 mol), and DMPA (1.3 g, 0.005 mol) were solved in THF. The solution was degassed and irradiated for 5 min. All volatiles were removed *in vacuo* at 60 °C to obtain 46 g crude product mixture. The residue was fractionally distilled at 105 °C and 1 x 10^{-3} mbar to give **13** (26.2 g, 67%) as colourless liquid (95% Anti-Markovnikov product). ^{1}H NMR (400 MHz, $CDCl_3$) δ, ppm: 2.76-2.71 (m, 4H, -S-C$\underline{H_2}$-C$\underline{H_2}$-SH), 2.68 (t, ^3J=7.2 Hz, 2H, -S-C$\underline{H_2}$-CH_2-), 2.51 (t, 2H, -CH_2-C$\underline{H_2}$-CN, *J*= 6.8 Hz), 1.94 (dt, ^4J=7.44 Hz, 2H, -CH_2-C$\underline{H_2}$-CH_2-CN), 1.71 (t, ^3J=8.1 Hz, 1H, -CH_2-S$\underline{H}$).^{13}C NMR (100 MHz, $CDCl_3$) δ, ppm: 119.27 (CH_2-$\underline{C}$N), 36.20 (HS-CH_2-$\underline{C}H_2$-S-), 30.66 (–S-$\underline{C}H_2$-CH_2-), 25.36 (-CH_2-$\underline{C}H_2$-CH_2-), 24.77 (HS-$\underline{C}H_2$-CH_2-), 16.14 (-CH_2-$\underline{C}H_2$-CN). MS [EI+] *m/z* (%): 114.03 (94.2), 161.03 (60.5). EA: calculated: [C] 44.68% [H] 6.87% [N] 8.68% [S] 39.76 found: [C] 44.51% [H] 7.12% [N] 8.58% [S] 39.78.

2-(3-((2-Mercaptoethyl)thio)propyl)malononitrile **14**: To a solution of allyl malononitrile (15 g, 0.14 mol) dissolved in freshly distilled THF (500 ml), freshly distilled 1,2-ethanedithiol (52 ml, 0.70 mol) and DMPA (0.7 g, 0.003 mol) was added under ar-

gon atmosphere. The reaction mixture was irradiated for 5 minutes. All volatiles were removed *in vacuo* (10 mbar). The residue was fractionally distilled at 145 °C and 9 x 10^{-3} mbar to give **14** as colourless liquid (9 g, 31%).^{1}H NMR (400 MHz, $CDCl_3$) δ, ppm: 3.83 (t, ^{3}J=6.8 Hz, 1H, (CN)C*H*-CH_2-), 2.79-2.69 (m, 4H, -S-(CH_2)$_2$-SH), 2.64 (t, ^{3}J=7.1 Hz, 2H, CH_2-CH_2-S-,), 2.21-2.15 (m, 2H, CH-CH_2-CH_2), 1.96-1.88 (m, 2H, CH_2-CH_2-CH_2), 1.72 (t, ^{3}J= 8.0 Hz, 1H, CH_2-S-*H*,).^{13}C NMR (100 MHz, $CDCl_3$) δ, ppm: 112.47 ((CN)$_2$-CH-), 36.11 (-CH_2-CH_2-SH), 30.62 (-CH_2-CH_2-S-), 29.64 (CH-CH_2-CH_2), 26.11 (CH_2-CH_2-CH_2), 24.72 (CH_2-CH_2-SH), 22.48 ((CN)$_2$-CH-). MS (ESI) m/z (%): 167 (100), 359.24 (22.5), 423 (23.8). EA: calculated: [C] 47.97% [H] 6.04% [N] 13.98% [S] 32.01%/ found: [C] 47.90% [H] 6.24% [N] 13.74% [S] 31.86%.

3-(2-((2-Mercaptoethyl)thio)ethyl)pentane-1,3,5-tricarbonitrile **15**: A solution of **9** (0.173 g, 0.001 mol), freshly distilled 1,2-ethanedithiol (0.84 ml, 0.01 mol), and DMPA (0.77 g, 0.003 mol) in THF (20 ml) was carefully degassed and then irradiated for 5 min with a UV lamp. To the reaction mixture additional 1,2-ethanedithiol (0.42 ml, 0.004 mol) and DMPA (0.77 g, 0.003 mol) were added followed by 10 min irradiation. All volatiles were removed *in vacuo* and the product was purified by column chromatography (Heptane/ Ethyl acetate 1:1) to give (0.09 g, 34%) **15** as yellowish liquid. ^{1}H NMR (400 MHz, $CDCl_3$) δ, ppm: 2.83-2.72 (m, 4H, HS-CH_2-CH_2-S), 2.67 (t, 2H,-S-CH_2-CH_2-C_{quart}, ^{3}J=8 Hz), 2.57 (t, ^{3}J=8Hz, 4H, -CH_2-CH_2-CN), 2.07 (t, ^{3}J=8 Hz, 4H, -CH_2-CH_2-CN,), 1.96 (t, ^{3}J=8 Hz, 2H, -CH_2-C_{quart}), 1.73 (t, 1H, -S*H*). ^{13}C NMR (100 MHz, $CDCl_3$) δ, ppm: 119.96 (C_{quart}-CN), 117.89 (-CH_2-CN), 40.62 (C_{quart}), 36.65 (-CH_2-SH) 35.78 (S-CH_2-CH_2-C_{quart}-), 31.63 (CH_2-CH_2-CN), 26.79 (S-CH_2-CH_2-C_{quart}-), 24.89 (HS-CH_2-CH_2-S), 13.48 (CH_2-CN). MS (EI+) *m/z* (%): 61.01 (100), 69.05 (15.55), 207.08 (17.18), 267.08 (13.02). EA: calculated: [C] 53.90% [H] 6.41% [N] 15.71% [S] 23.98 found: [C] 53.78% [H] 6.60% [N] 15.43% [S] 23.82%.

Compounds**16**&**17:** To a solution of allyl malononitrile (53 g, 0.5 mol) dissolved in freshly distilled THF (500 ml), 1,2-ethanedithiol (235 ml, 2.5 mol) and DMPA (2.5 g, 0.002 mol) was added under argon atmosphere. The reaction mixture was irradiated for 5 minutes. All volatiles were removed at 80 °C *in vacuo* (10 mbar). The residue was purified by SiO_2 column chromatography (heptane/ ethyl acetate → methanol→ DMF) to give **17** (2 g, 2%) as colourless crystals and **16** (40 g, 40%) as pale brownish, viscous liquid.

16: ^{1}H NMR (400 MHz, *N,N*-dimethylformamide-d_7) δ, ppm: 3.83 (t, ^{3}J=6.8 Hz, 1H, (CN)C*H*-CH_2-), 2.79-2.69 (m, 4H, -S-(CH_2)$_2$-SH), 2.64 (t, ^{3}J=7.1 Hz, 2H, CH_2-CH_2-S-,), 2.21-2.15 (m, 2H, CH-CH_2-CH_2), 1.96-1.88 (m, 2H, CH_2-CH_2-CH_2), 1.72 (t, ^{3}J=8.0 Hz, 1H, CH_2-S-*H*,).^{13}C NMR (100 MHz, $CDCl_3$) δ, ppm: 112.47 ((CN)$_2$-CH-), 36.11 (-CH_2-CH_2-SH), 30.62 (-CH_2-CH_2-S-), 29.64 (CH-CH_2-CH_2), 26.11 (CH_2-CH_2-CH_2), 24.72 (CH_2-CH_2-SH), 22.48 ((CN)$_2$-CH-).

17: ^{1}H NMR (400 MHz, *N,N*-dimethylformamide-d_7) δ, ppm: 6.63 (br s, -N*H*$_2$), 6.37 (br s, -N*H*$_2$), 3.20-3.30 (m, 2H, -CH_2-CH_2-S-C), 2.74-2.79 (m, 2H, CH_2-S-CH_2-CH_2), 2.61-2.68 (m, 2H, CH_2-CH_2-CH_2-S), 1.69-1.81 (m, 2H, CH_2-CH_2-CH_2), 2.27-2.40 (m, 2H, C-CH_2-CH_2). ^{13}C NMR (100 MHz, *N,N*-dimethyformamide-d_7) δ, ppm: 152.17 ((C=*C*(NH_2)-S), 122.13 (C-CN), 80.72 (C=*C*(CN)-), 31.97 (CH_2-CH_2-S-C), 31.21 (CH_2-CH_2-S-C), 30.53 (CH_2-CH_2-CH_2-S), 28.55 (CH_2-CH_2-CH_2-S), 27.16 (CH_2-CH_2-CH_2-S). HRMS (ESI): calc. for $C_{16}H_{25}N_4S_4$ [M+H] 401.0957; found: 401.0957.

Poly(3-cyanopropyl-2-thioethyl-2-thioethyl)methylsiloxane **P13**: To a solution of polyvinylmethylsiloxane (0.9 g, 0.01 mol) dissolved in freshly distilled THF (500 ml), 1,2-ethanedithiol (235 ml, 2.5 mol) and DMPA (2.5 g, 0.002 mol) was added under argon atmosphere. The reaction mixture was irradiated for 5 minutes. All volatiles were removed at 80 °C *in vacuo* (10 mbar). ^{1}H NMR (400 MHz, THF-d_8) δ, ppm: 2.8257 (br s, 4H, S-CH_2-CH_2-S-), 2.77-2.60 (m, 4H, Si-CH_2-CH_2-S, S-(CH_2)$_3$-), 2.58 (t, 2H, -CH_2-CH_2-CN, *J*= 7.2 Hz),1.99-1.93 (m, 2H, -CH_2-CH_2-CH_2-CN), 1.06-1.02 (m, 2H, Si-CH_2-CH_2-, 0.2871 (br s, 3H, Si-CH_3). ^{13}C NMR (100 MHz, *THF*-d_8) δ, ppm: 118.9377, 32.005, 31.8706, 30.4372, 26.4282, 25.6443, 25.4203, 18.3654, 15.4538, -0.4031.

2.4 Results and discussion

Allyl cyanide is the simplest aliphatic non-conjugated vinyl nitrile. The thiol-ene addition of **A** to allyl cyanide initiated by 1 mol% DMPA gave S-3-cyanopropyl thioacetate **1** in 73% isolated yield within 5 min (Scheme 2.1). Compound **1** is known in the literature and was prepared starting from potassium salt of **A** and 4-bromobutyronitrile. Unfortunately, no reaction yield is given for this reaction.[34,35] Cleavage of the acetyl moiety of **1** under acidic conditions (20 mol% trimethylsilyl chloride (TMSCl) in methanol) proceded at low reaction rate and gave 4-mercaptobutanenitrile **2** in moderate yields (43%). When a stoichiometric amount of TMSCl was used, 2-iminothiolane hydrochloride **3** formed in 60% yield. Compound **2** is known and was prepared starting from 4-isothioureidobutyronitrile hydrochloride but the reaction yield was very low (15%).[36] Compound **3** is also known in the literature and was prepared by nucleophilic substitution starting from 4-halogenobutanenitrile and **A** or thiourea, respectively.[37–39] It is widely used as thiolation reagent in biochemistry and is referred to as 'Traut's reagent'.[40-43]

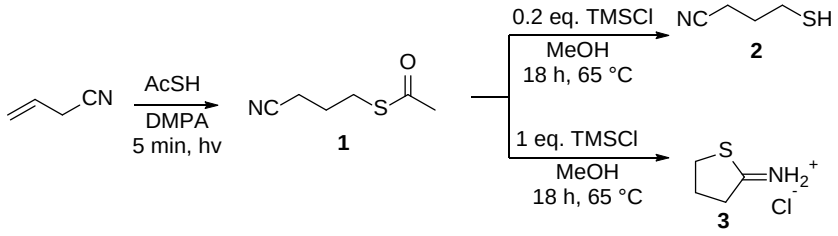

Scheme 2.1 Thiol-ene addition of A to allyl cyanide followed by the cleavage of the acetyl group to give **2** and **3**.

Allyl malononitrile **5** was synthesized according to the literature starting from malononitrile and allyl bromide in one step (Scheme 2.2).[41]

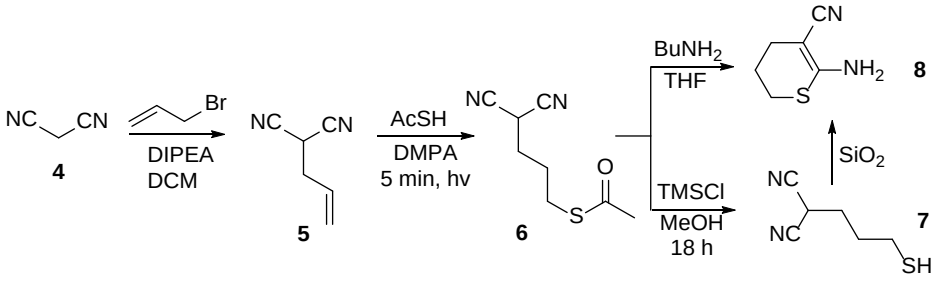

Scheme 2.2 Synthetic route to 4,4-dicyanobutyl thiol **7**.

The thiol-ene addition of a slight excess of **A** to **5** in presence of DMPA gave S-(4,4-dicyanobutyl) thioacetate **6** in 74% yield within 5 min (Scheme 2). When a large excess of **A** was used, addition to the nitrile groups was observed. Acetate cleavage under basic conditions in presence of butyl amine resulted in quantitative cyclization of **6** to 6-amino-3,4-dihydro-2H-thiopyran-5-carbonitrile **8**. The quantitative conversion of **6** to **8** is supported by the ^{1}H NMR spectra where the characteristic signals of **6** disappeared and new signals appeared which can be easily assigned to **8** (Figure 2.1).

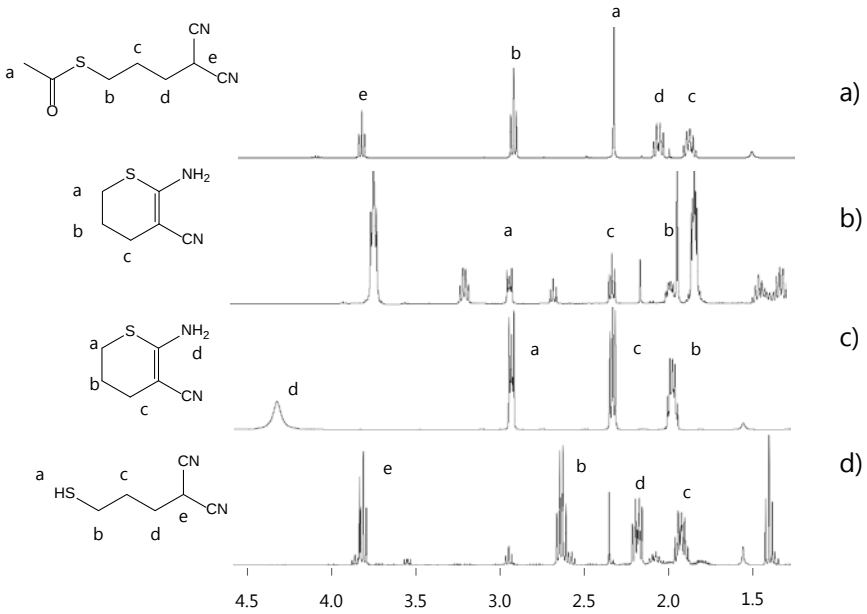

Figure 2.1 ^{1}H NMR spectra of: a) **6**, b) of the crude reaction mixture obtained by reacting **6** with butyl amine, c) of **8**, and d) of **7**.

Single crystals of **8** suitable for x-ray analysis were grown from ethyl acetate/heptane. The proposed six-membered ring was confirmed by x-ray structure (Figure 2.2). The transesterification reaction with methanol under acidic conditions allowed formation of 4,4-dicyanobutyl thiol **7**, but the reaction did not proceed to completion. Attempts to purify this compound by vacuum distillation were only partially successful. The compound still contained about 15% impurities (Figure 1d). Further attempts to increase the purity of **7** by column chromatography purification on silica gel were unsuccessful. The intramolecular cyclization of **7** occurred quantitatively with formation of **8** (Figure 1). The synthesis of the analog five-membered cycle starting from malononitrile and ethylene sulfide was already described in the literature, but an over-stoichiometric amount of a strong base such as sodium hydride had to be used and the reaction yield was only moderate (57%).[45]

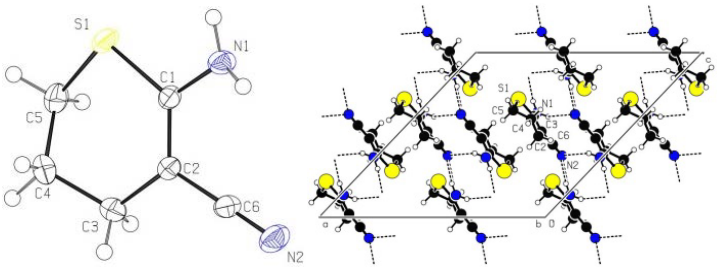

Figure 2.2 ORTEP of **8**, view perpendicular to the cycle (left) and the molecular packing down the crystallographic b axis showing the stacking of the cycles and the hydrogen bonding network (right).

3-vinylpentane-1,3,5-trinitrile **9** was synthesized according to literature starting from allyl cyanide (Scheme 2.3).[46] The vinyl group of **9** is sterically hindered due to the bulky $-(CH_2)_2CN$ moieties in alpha position to the vinyl group. This is nicely illustrated by the ^{1}H NMR spectrum of **9** where the two protons of the $-CH_2$-CH_2-CN group next to the quaternary carbon are not equivalent, as one would expect (see ESI). This indicates a lack of free rotation of the $-(CH_2)_2CN$ moiety. The thiol-ene addition of **A** to **9** initiated by DMPA did not occur even after 60 min UV irradiation. Instead, instability of the nitriles was observed. When AIBN as thermal radical initiator and excess of **A** was used, the addition of **A** to the nitrile group was observed. NMR analysis of the crude product mixture showed the formation of **11** which hydrolysed to 4-cyano-4-vinylheptane bis(thioamide) **12** during work-up (60% yield). Formation of 3-(2-thioacetic)ethylpentane-1,3,5-carbonitrile **10** was not observed. The conversion of aliphatic nitriles to thioamides is known, however this occurrs either under acidic or basic catalysis.[30,31] At 70 °C the acidity of **A** was sufficient to catalyse its addition to the nitrile of **9**.

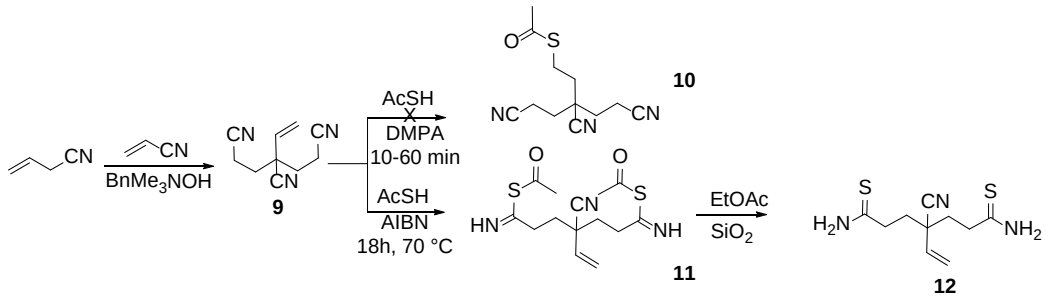

Scheme 2.3 Synthesis of **9** by cyanoethylation of allyl cyanide and its reaction with AcSH.

As an alternative to **A** in the transformation of vinyl nitriles to mercaptonitriles, 1,2-ethanedithiol **B** was tested (Scheme 2.4). The advantage of **B** is that it allows formation of mercaptonitriles directly *via* thiol-ene reaction of vinyl nitriles, even though an excess of **B** has to be used and the spacer between the thiol and the nitrile group is prolonged. Intramolecular cyclization reactions of the formed mercaptonitriles are less favored as five or six-membered rings cannot form.

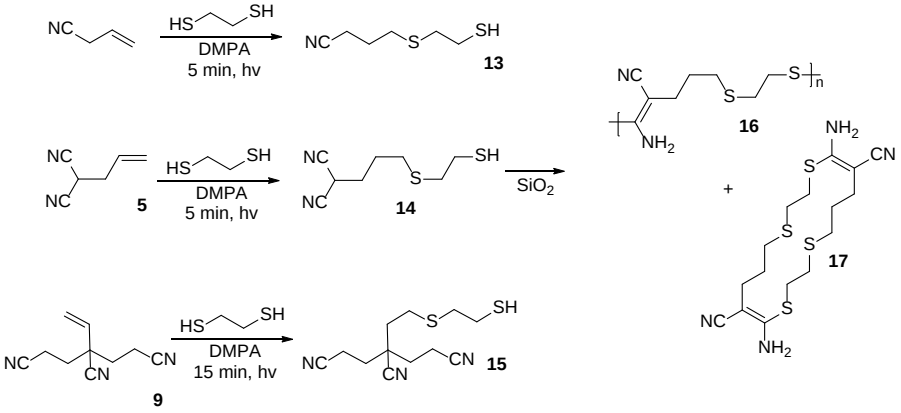

Scheme 2.4 Thiol-ene addition of 1,2-ethanedithiol to vinyl nitriles.

Addition of **B** to allyl cyanide gave 4-((2-mercaptoethyl)thio)butanenitrile **13**, which did not show any susceptibility to cyclization. The purification of **13** was done by distillation and the compound could be easily prepared on 30 g scale. The reaction of **5** with **B** gave 2-(3-((2-mercaptoethyl)thio)propyl)malononitrile **14**. The isolation of **14** by distillation was possible, but challenging given **14**'s high boiling point. Again, silica gel during chromatography purification catalyzed the intramolecular cyclization with formation of cyclic dimer **17** in small amounts. The structure of **17** was confirmed by x-ray diffraction analysis on a single crystal (Figure 2.3). The main product after chromatography was oligomer **16** which was obtained *via* silica gel extraction with DMF and methanol as can be seen in the ^{1}H NMR spectrum in the supporting information. No further characterizations were conducted on **16** due to its poor solubility.

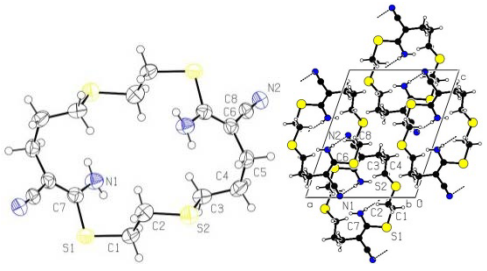

Figure 2.3 ORTEP of **17**, view perpendicular to the cycle (left) and the molecular packing down the crystallographic a axis showing the hydrogen bonding network (right).

In contrast to **A**, selective thiol-ene addition of **B** to the vinyl group of **9** was achieved by using **B** in excess, an over-stoichiometric amount of photoinitiator, and prolonged reaction times. The difference in the reactivity of **A** and **B** can be explained by the acidity of the two reagents used.[47] Due to the presence of electron-withdrawing group, **A** is more acidic as compared to 1,2-ethanedithiol and therefore chemically more reactive towards nitrile. NMR analysis of the reaction mixture showed product conversion of approximately 50%. The nitrile groups were unaffected during reaction and chromatography purification process. The mercaptonitriles **13-15** did not crystallize. Traces of Markovnikov addition product were detected in all cases.

Thiols **13** and **14** were identified as being promising candidates for the post polymerization modification of polyvinylsiloxanes *via* thiol-ene addition. **13** and **14** can be prepared easily on a 20 g scale and can be purified by distillation. Although the high boiling points of these thiols may be considered disadvantageous since high vacuum and high temperatures have to be used for their distillation, they have the advantage that they are less volatile and therefore do not have the typical pungent odor characteristic for thiols. The thiols show a dielectric permittivity at high frequencies of $\varepsilon' = 15.4$ and $\varepsilon' = 17$ for **13** and **14**, respectively. **13** was successfully used in the selective thiol-ene addition to polyvinylsiloxane and no side reactions were observed. Poly(3-cyanopropyl-2-thioethyl-2-thioethyl)methylsiloxane **P13** possessed a dielectric permittivity at high frequencies of $\varepsilon' = 10.5$ (Fig 2.52).

2.5 Conclusions

In conclusion, the thiol-ene addition of **A** and **B** to allyl cyanide, allyl malononitrile, and 3-vinylpentane-1,3,5-carbonitrile was investigated. All vinyl nitriles reacted with **A** and **B** as expected except 3-vinylpentane-1,3,5-carbonitrile. This compound with its sterically hindered vinyl group did not give the thiol-ene addition product **A** but the addition product to the nitriles. The cleavage of the acetyl groups to generate the respective mercaptonitriles must be conducted under mild acidic conditions due to the high tendency of the generated thiols to undergo addition to the nitriles under acidic and basic conditions. Purification of the mercaptonitriles by column chromatography over silica gel should be avoided. Thiol-ene addition of **B** to non-conjugated vinyl nitrile compounds proved to be a fast and efficient alternative for **A** in the synthesis of mercaptonitriles in one step and mild reaction conditions.

2.6 References

[1] V. N. Ipatieff and B. S. Friedman, *J. Am. Chem. Soc.* **1939**, *61*, 71.

[2] C. E. Hoyle and C. N. Bowman, *Angew. Chem. Int. Ed.* **2010**, *49*, 1540.

[3] L. Gu, Q. Xue, S. Peng, G. Wang, J. Han and X. Wu, *Polymer* **2016**, *7*, 625.

[4] C. Ligeour, L. Dupin, A. Marra, G. Vergoten, A. Meyer, Y. Dondoni, A. Souteyrand, E. Vasseur, J.-J. Chevolot and F. Morvan, *Eur. J. Org. Chem.* **2014**, *34*, 7621.

[5] Z. Liu, T. Liu, Q. Lin, C. Bao and L. Zhu, *Angew. Chem. Int. Ed.* **2015**, *54*, 174.

[6] Y. Suzuki, T. Higashihara, S. Ando and M. Ueda, *Macromolecules* **2012**, *45*, 3402.

[7] N. K. Singha, M. I. Gibson, B. P. Koiry, M. Danial and H.-A. Klok, *Biomacromolecules* **2011**, *12*, 2908.

[8] M. H. Stenzel, *ACS Macro Lett.,* **2013**, *2*, 14.

[9] Y. Chen, G. Chen and M. H. Stenzel, *Macromolecules* **2010**, *43*, 8109.

[10] J. Z. Du, X. J. Du, C. Q. Mao and J. Wang, *J. Am. Chem. Soc.* **2011**, *133*, 17560.

[11] M. Podgorski, E. Becka, M. Claudino, A. Flores, P. K. Shah, J. W. Stansbury and C. N. Bowman, *Dent. Mater.* **2015**, *31*, 1255.

[12] E. Klemm and S. Sensfuss, *Makromol. Chem.* **1991**, *64*, 159.

[13] A. S. Quick, J. Fischer, B. Richter, T. Pauloehrl, V. Trouillet, M. Wegener and C. Barner-Kowollik, *Macromol. Rapid Commun.*, **2013**, *34*, 335.

[14] C. S. Marvel and A. Kotch, *J. Am. Chem. Soc.* **1951**, *73*, 1100.

[15] S. J. Duenki, Y. S. Ko, F. A. Nueesch and D. M. Opris, *Adv. Funct. Mater.* **2015**, *25*, 2467.

[16] S. J. Dünki, M. Tress, F. Kremer, S. Y. Ko, F. A. Nüesch, C.-D. Varganici, C. Racles and D. M. Opris, *RSC Adv.* **2015**, *5*, 50054.

[17] C. Decker and T. Nguyen Thi Viet, *Polymer* **2000**, *41*, 3905.

[18] A. Gress, A. Vo and H. Schlaad, *Macromolecules* **2007**, *40*, 7928.

[19] J. C. Persson, K. Josefsson and P. Jannasch, *Polymer* **2006**, *47*, 991.

[20] M. Li, P. De, H. Li and B. S. Sumerlin, *Polym. Chem.* **2010**, *1*, 854.

[21] D. M. Opris, E. Perju and S. J. Duenki, *J. Polym. Sci. Part A: Polym. Chem.* **2016**, *56*, 2940.

[22] M. Le Neindre, B. Magny and R. Nicolaÿ, *Polym. Chem.* **2013**, *4*, 5577.

[23] J. Polster and P. Schieberle, *J. Agric. Food Chem.* **2015**, *63*, 1419.

[24] E. Schjanberg, *Ber. Dtsch. Chem. Ges.*, **1941** *74*, 1751.

[25] R. Brown, W. E. Jones and A. R. Pinder, *J. Chem. Soc* **1951**, 2123.

[26] J. Gorges and U. Kazmaier, *Eur. J. Org. Chem.* **2015**, *36*, 8011.

[27] J. W. Lynn, R. L. Roberts and J. R. Kilsheimer, *J. Org. Chem.* **1961**, *26*, 4300.

[28] A. Kjaer and J. Conti, *Acta Chem. Scand.* **1954***, 8*, 295.

[29] M. Yunhai and X. Jiaxi, *Synthesis* **2012**, *44*, 2225.

[30] J. Y. Gauthier and H. Lebel, *Phosphorus, Sulfur Silicon Relat. Elem.* **1994**, *95*, 325.

[31] K. A. Mahammed, V. P. Jayashankara, N. Rai, K. Raju, K. Mohana and P. N. Arunachalam, *Synlett* **2009**, *14*, 2338.

[32] R. Jue, J. M. Lambert, L. R. Pierce and R. R. Traut, *Biochemistry* **1978**, *17*, 5399.

[33] G. R. Fulmer, A. J. M. Miller, N. H. Sherden, H. E. Gottlieb, A. Nudelman, B. M. Stoltz, J. E. Bercaw and K. I. Goldberg, *Organometallics* **2010**, *29*, 2176.

[34] N. Park, K. Park, M. Jang and S. Lee, *J. Org. Chem*. **2011**, *76*, 4371–4378.

[35] Los, M. (American Cyanamid Co.) Eur. Pat. Appl. EP 133310, **1985**.

[36] R. R. Traut, A. Bollen, T. T. Sun, J. W. B. Hershey, J. Sundberg and L. R. Pierce, *Biochemistry* **1973**, *12*, 3266.

[37] M. Wallace, A. J. Allentoff, J. Brailsford, S. Gong, S. Bonacorsi and F. Rinaldi, *J. Label. Compd. Radiopharm.* **2015**, *58*, 429.

[38] S. F. Carroll and D. A. Goff, WO 90/06774, **1990**.

[39] T. P. King, Y. Li and L. Kochoumian, *Biochemistry* **1978**, ***17***, 1499.

[40] T. P. King, Y. Li and L. Kochoumian, *Biochemistry* **1986**, *25*, 5774.

[41] A. Braden, M. Roner, J. Ganter and K. Nelson, *J. Nanosci. Nanotechnol.* **2007**, *7*, 925.

[42] T. Tada, K. Mano, E. Yoshide, N. Tanaka and S. Kunugi, *Bull. Chem. Soc. Jpn.*, **2002**, *75*, 2247.

[43] T. T. Ngo, *Appl. Biochem. Biotechnol.*, **1986**, *13*, 213.

[44] M. K. Ghorai, R. Talukdar and D. P. Tiwari, *Org. Lett.*, **2014,** *16*, 2204.

[45] K. Yamagata, T. Yukihiko, M. Yamazaki, T. Matsuda and K. Noda, *Chem. Pharm. Bull.* **1982**, *30*, 4396.

[46] H. A. Bruson and T. W. Riener, *J. Am. Chem. Soc.* **1943**, *65*, 18.

[47] B. Dmuchovsky, F. B. Zienty and W. A. Vredenbur, *J. Org. Chem.* **1966**, *31*, 865.

2.7 Supporting information

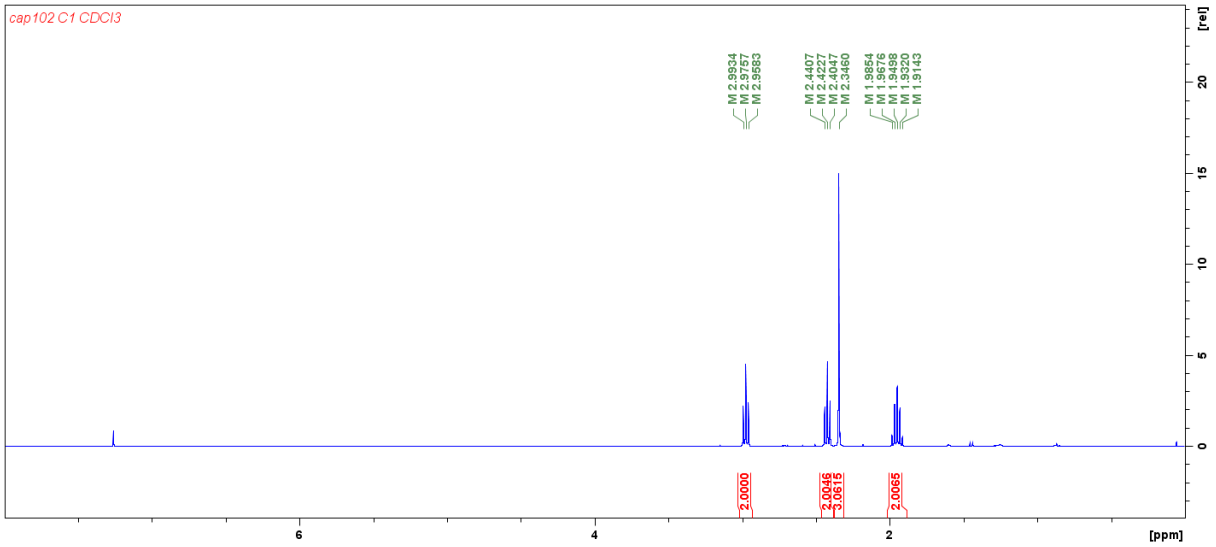

Figure 2.4 ^{1}H NMR spectrum of **1** in $CDCl_3$.

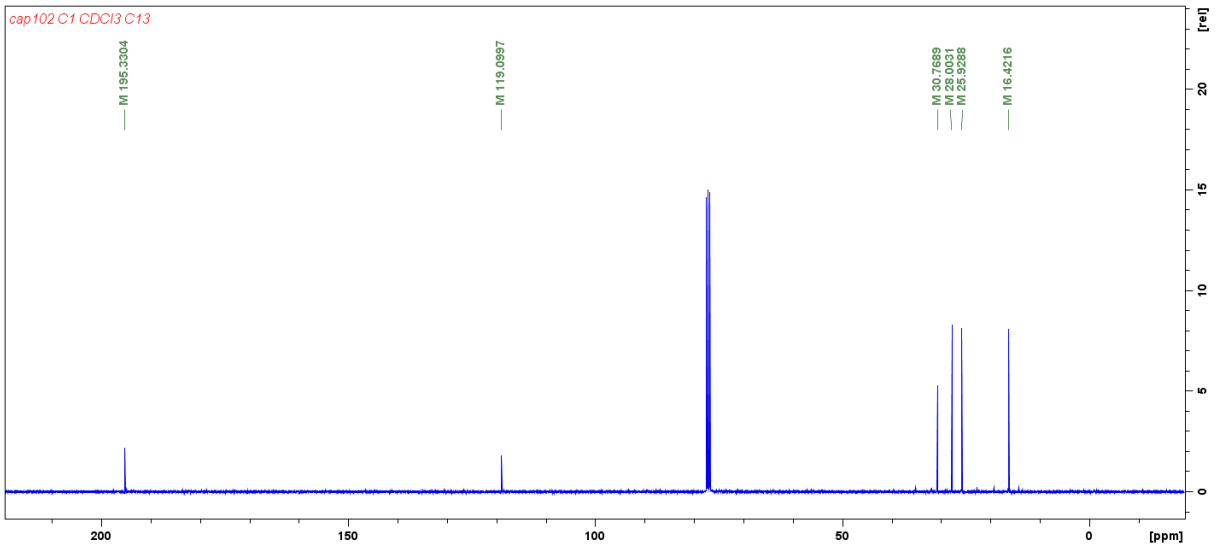

Figure 2.5 ^{13}C NMR spectrum of **1** in $CDCl_3$.

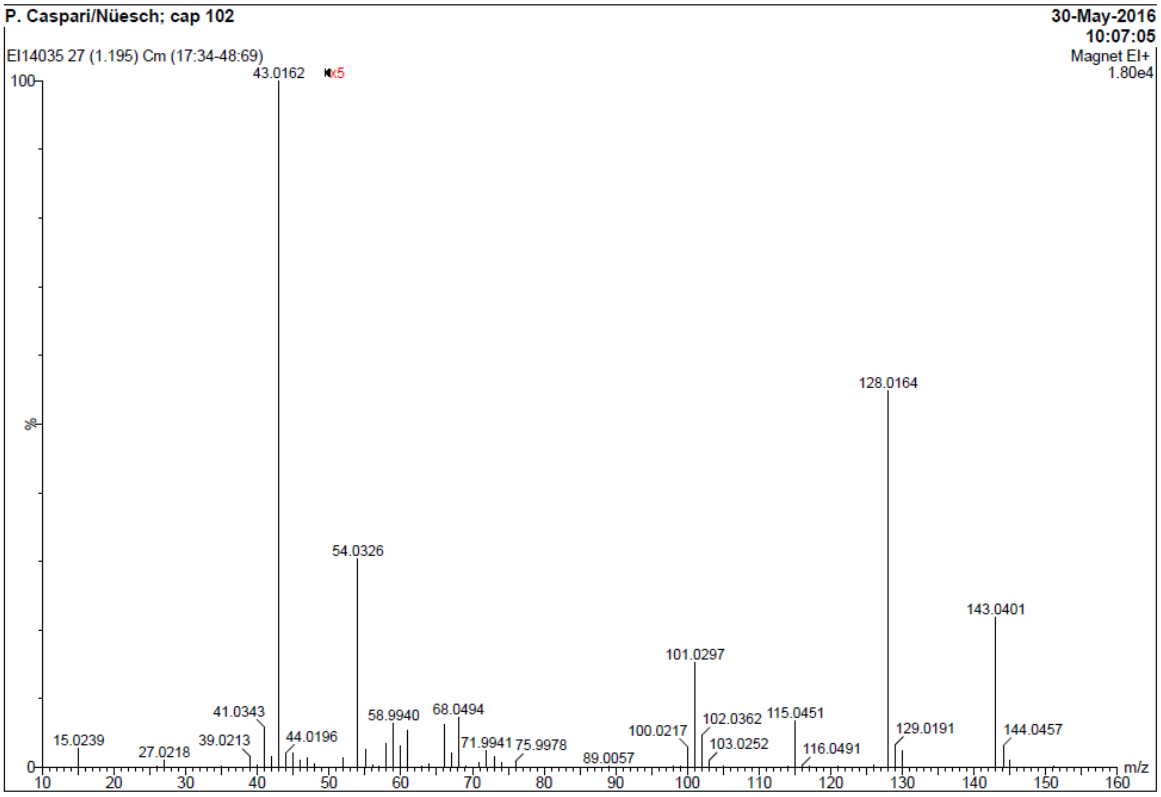

Figure 2.6 MS of **1**.

Substanz: cap102
Molekularformel: C6 H9 N O S Mr = 143.21g/mol

Siedepunkt: 117°C/0.01mbar
gereinigt: Dest. getrocknet: ????

Bestimmungen: C H N O S

Eingang: 11.04.16 Ausgang: 22.04.16

M-161980 Operator: SM

Berechnete Gewichtsanteile:

[C] 50.32% [H] 6.33% [N] 9.78% [O] 11.17% [S] 22.39%

Gefundene Gewichtsanteile:

Einwaage: 2.358mg LECO TruSpec Micro
[C] 50.27% [H] 6.54% [N] 9.54% 12.04.16

Einwaage: 2.889mg LECO RO-478
[O] 11.40% 22.04.16

Einwaage: 1.640mg LECO CHNS-932
[S] 22.22% 20.04.16

Figure 2.7 EA of **1**.

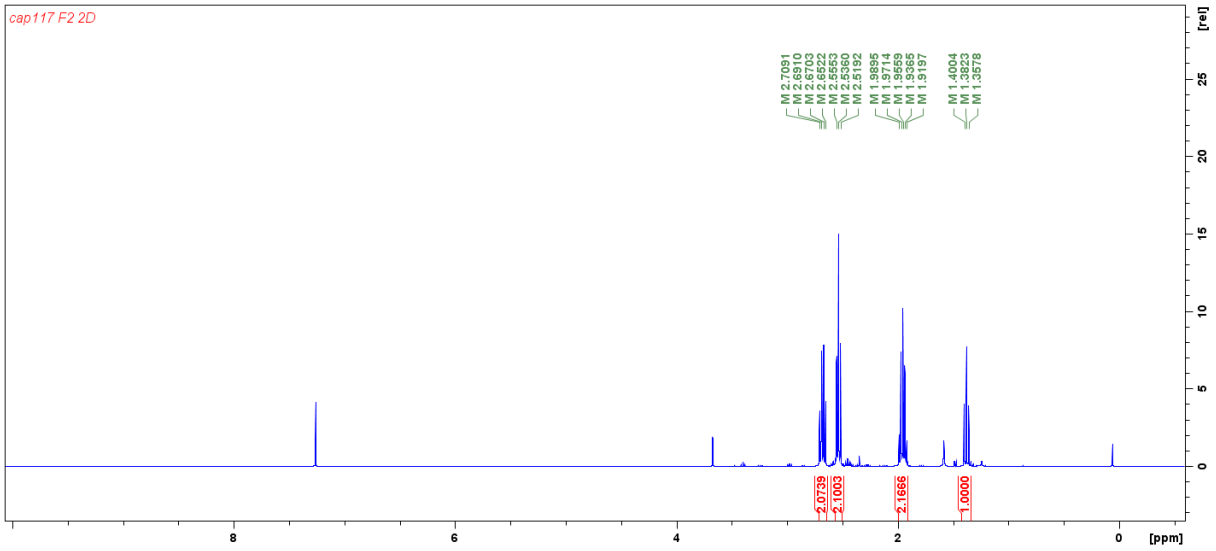

Figure 2.8 ^{1}H NMR spectrum of **2** in $CDCl_3$.

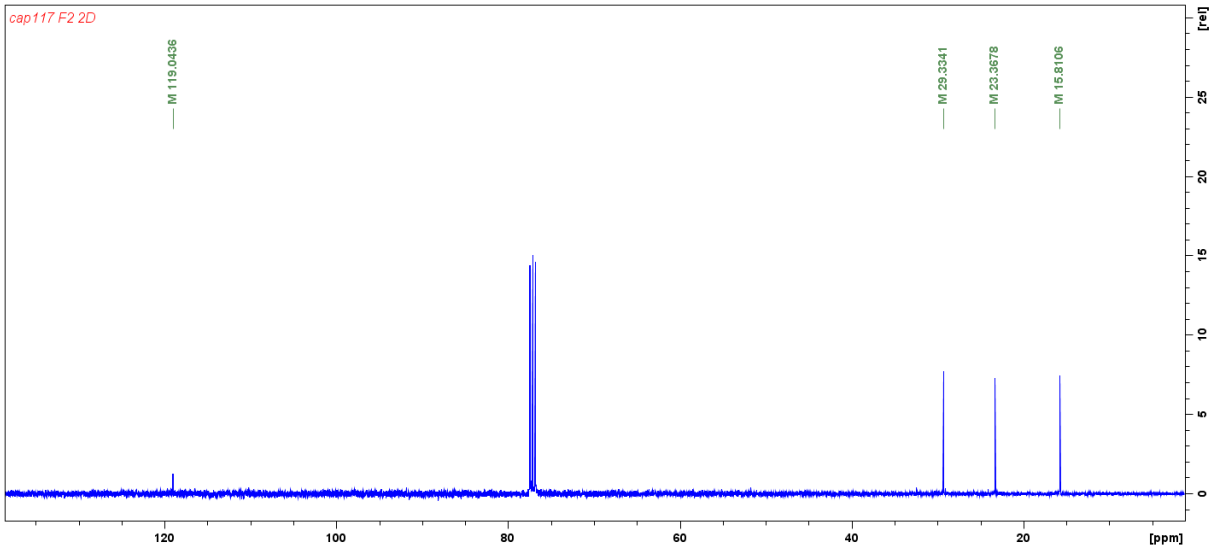

Figure 2.9 ^{13}C NMR spectrum of **2** in $CDCl_3$.

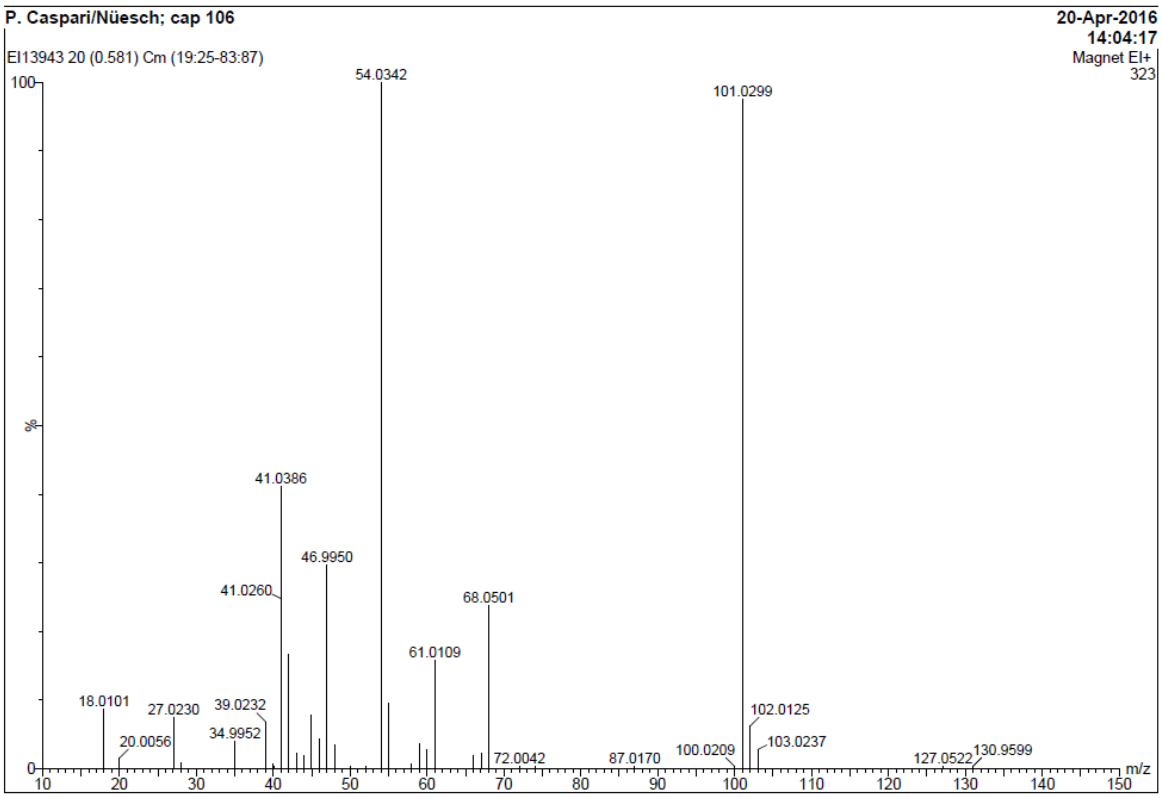

Figure 2.10 MS of **2**.

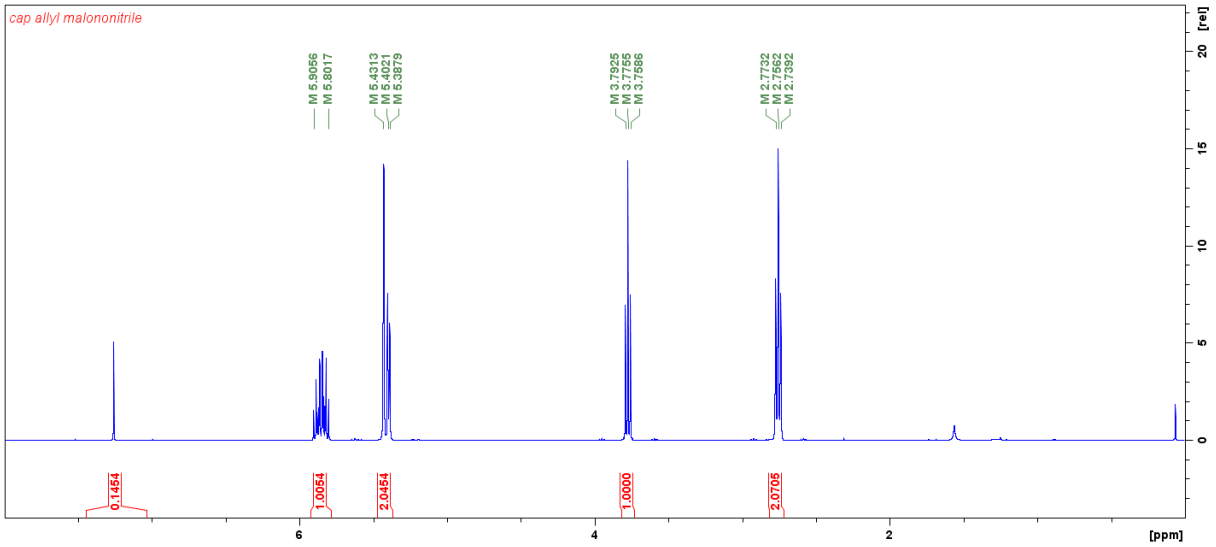

Figure 2.11: ^{1}H NMR spectrum of **5** in $CDCl_3$.

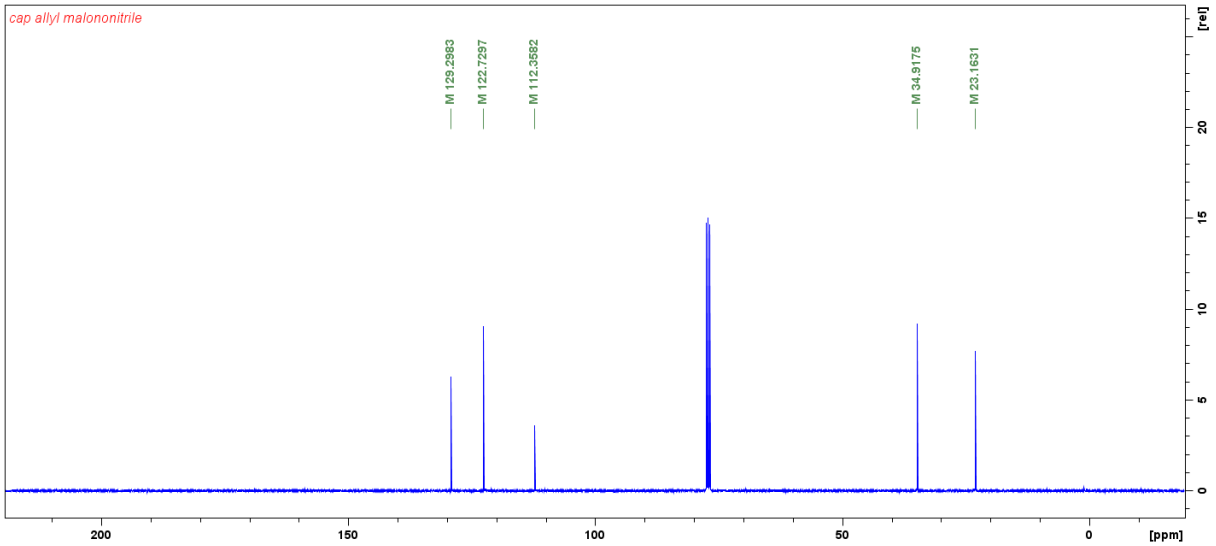

Figure 2.12 ^{13}C NMR spectrum of **5** in $CDCl_3$.

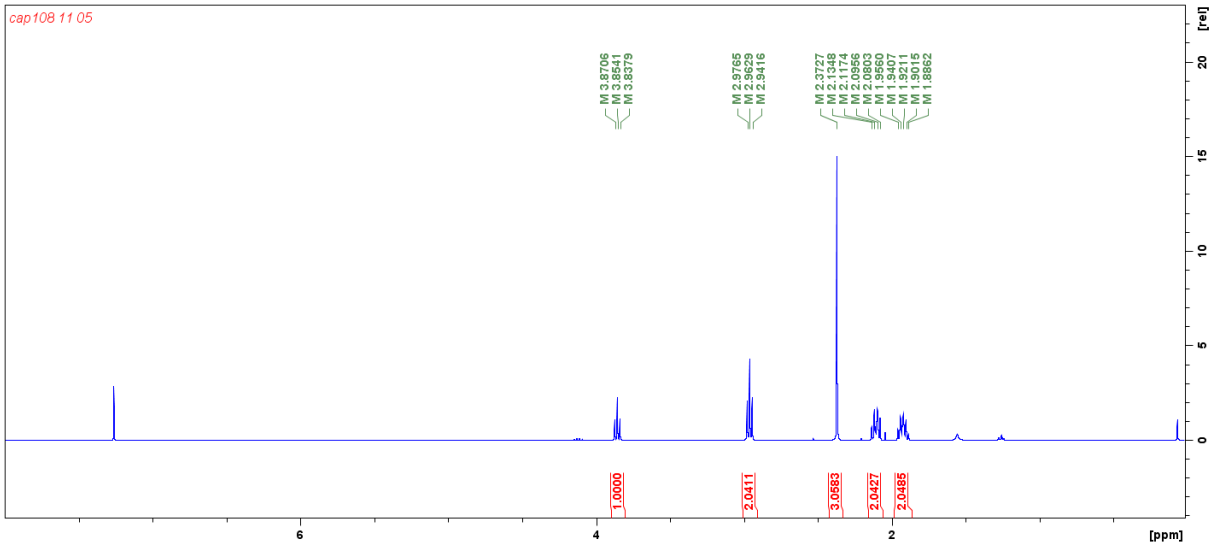

Figure 2.13 ^{1}H NMR spectrum of **6** in $CDCl_3$.

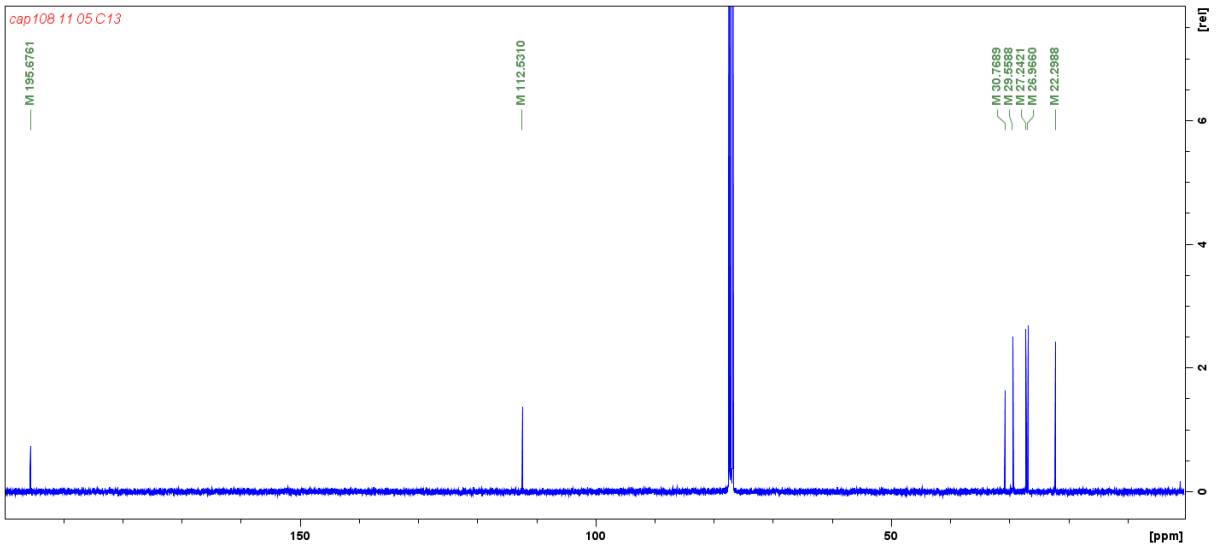

Figure 2.14 ^{13}C NMR spectrum of **6** in $CDCl_3$.

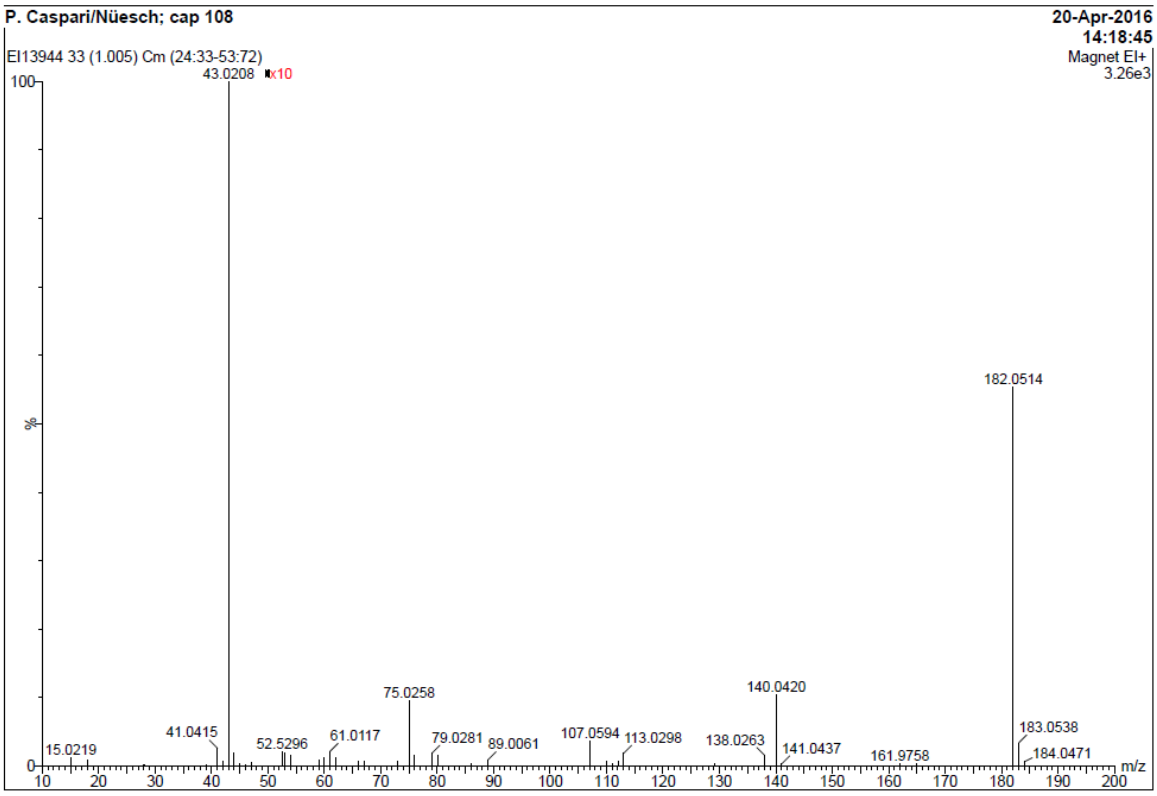

Figure 2.15 MS of **6**.

Bestimmungen: C H N O S

Eingang: 19.05.16 Ausgang: 03.06.16

M-162242 Operator: SM

Berechnete Gewichtsanteile:

[C] 52.72% [H] 5.53% [N] 15.37% [O] 8.78% [S] 17.59%

Gefundene Gewichtsanteile:

Einwaage: 1.968mg LECO CHNS-932
[C] 52.53% [H] 5.75% [N] 15.31% 19.05.16

Einwaage: 1.308mg LECO RO-478
[O] 9.05% 03.06.16

Einwaage: 1.189mg LECO CHNS-932
[S] 17.53% 24.05.16

Figure 2.16 EA of **6**.

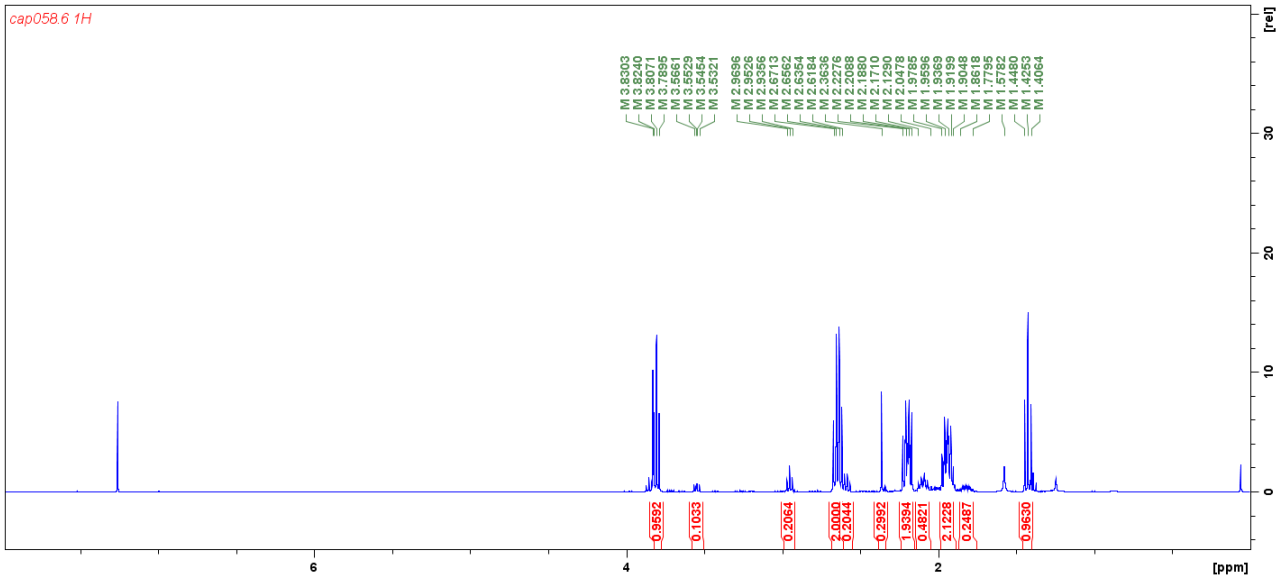

Figure 2.17 ^{1}H NMR spectrum of **7** in $CDCl_3$ which contains about 15% impurities. Our attempts to increase the purity of this compound by column chromatography were not successful since intramolecular cyclization of **7** occurred with formation of **8**.

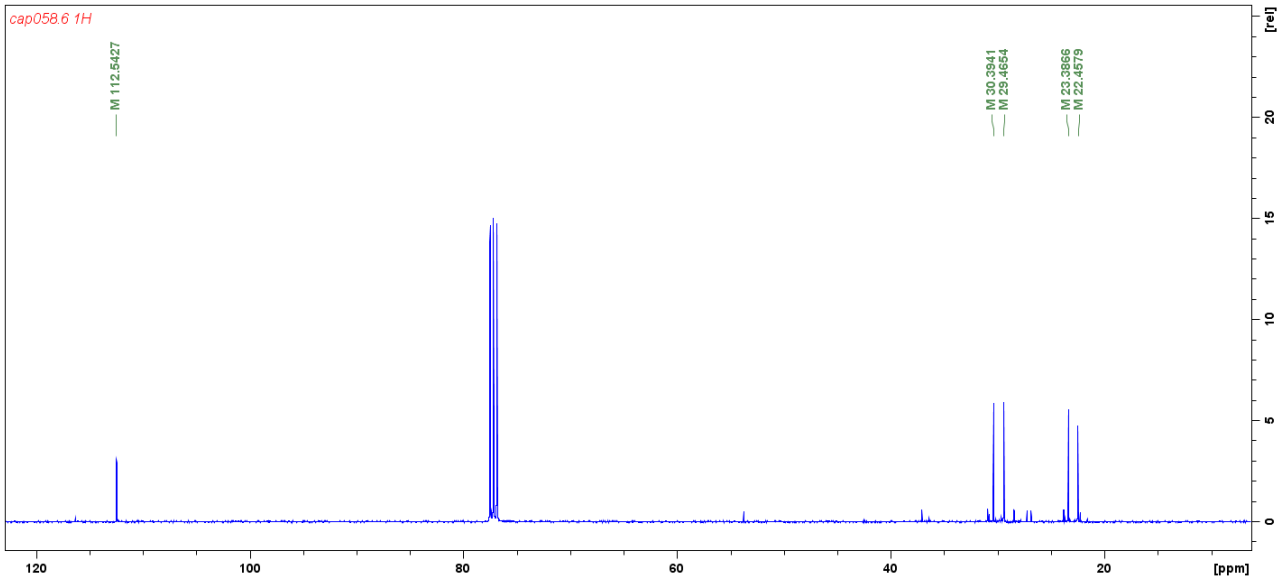

Figure 2.18 ^{13}C NMR spectrum of **7** in $CDCl_3$.

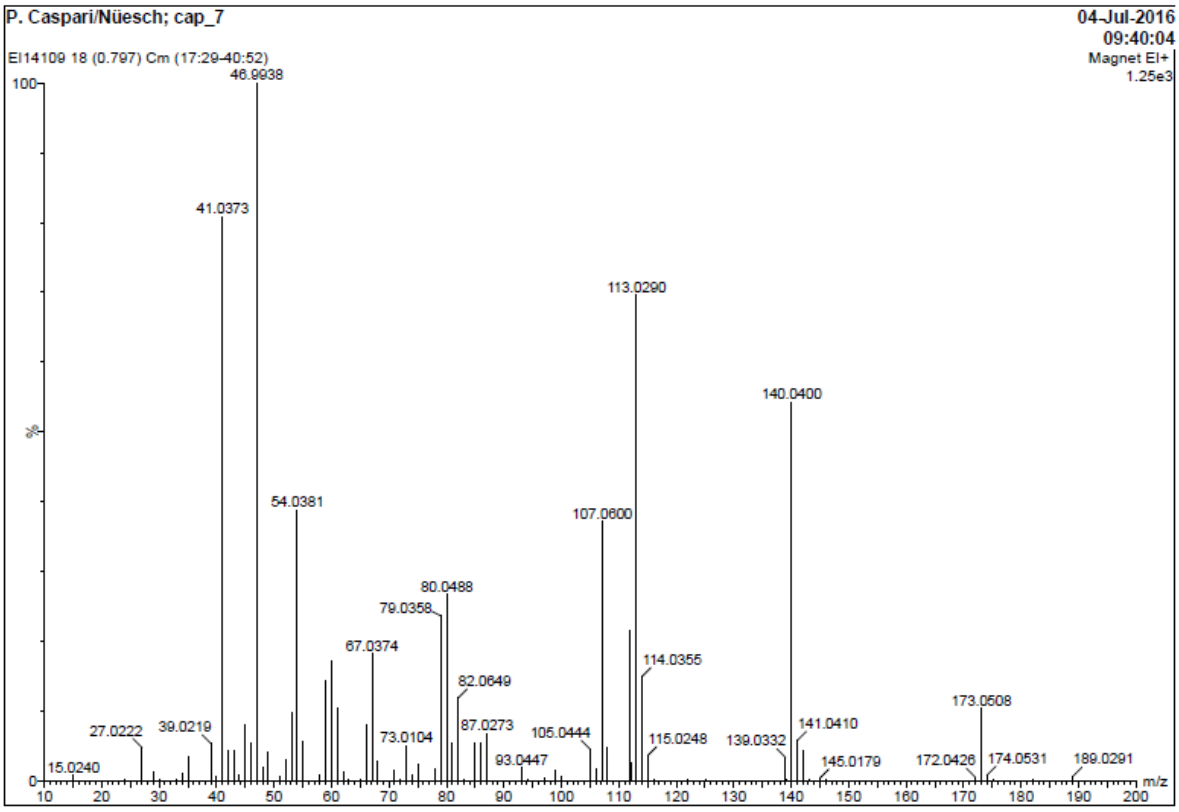

Figure 2.19 MS of **7.**

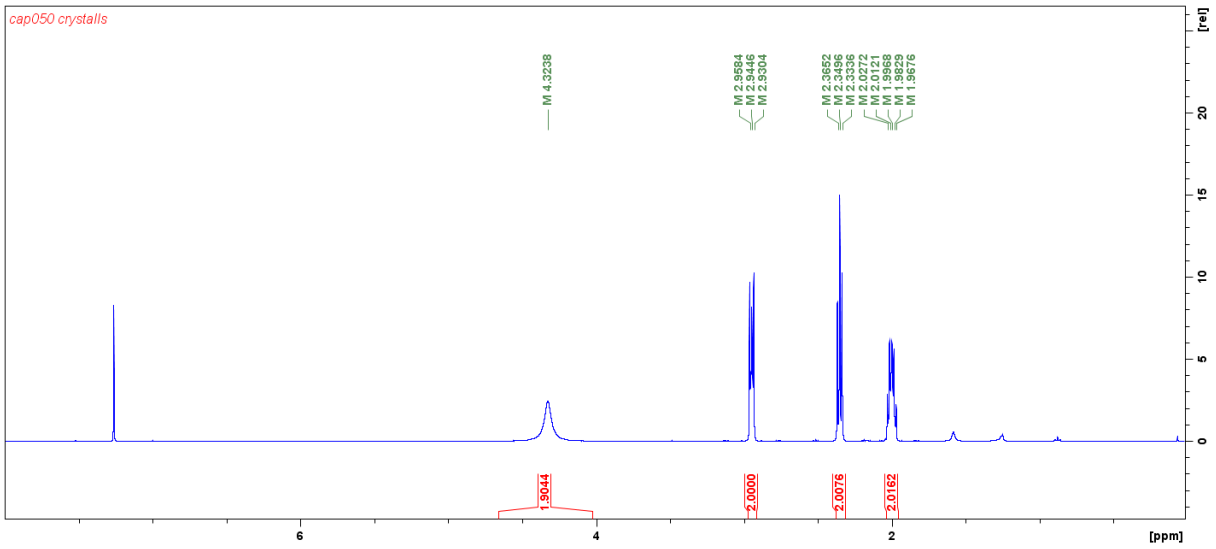

Figure 2.20 ^{1}H NMR spectrum of **8** in $CDCl_3$.

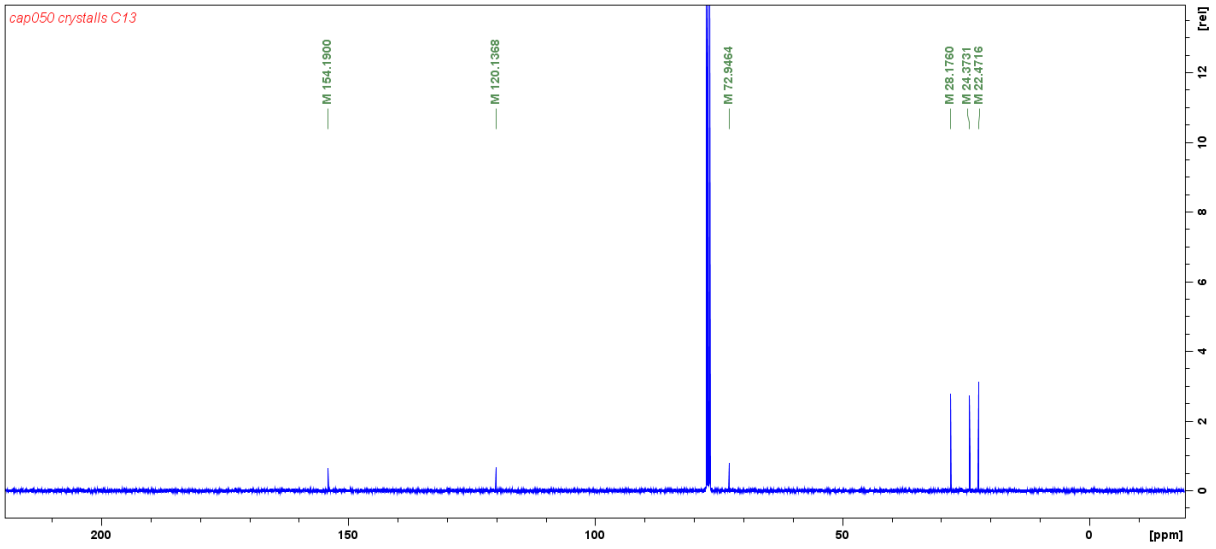

Figure 2.21 ^{13}H NMR spectrum of **8** in $CDCl_3$.

MAX27275 Philip Caspari/Nuesch - cap050 - DCM/MeOH

ETH Eidgenössische Technische Hochschule Zürich Swiss Federal Institute of Technology Zurich

Acquisition Parameter

Method:	ETH_HyStar_HPLC_QTOF_POS_LowMass_Loop-AS.m			Acquisition Date:	08.03.2016 15:36:37
File Name:	D:\Data\max272xx\MAX27275.d			Operator:	Louis Bertschi
Source Type	ESI	Ion Polarity	Positive	Set Nebulizer	1.6 Bar
Focus	Not active	Set Capillary	4500 V	Set Dry Heater	200 °C
Scan Begin	50 m/z	Set End Plate Offset	-500 V	Set Dry Gas	8.0 l/min
Scan End	1300 m/z	Set Collision Cell RF	200.0 Vpp	Set Divert Valve	Source

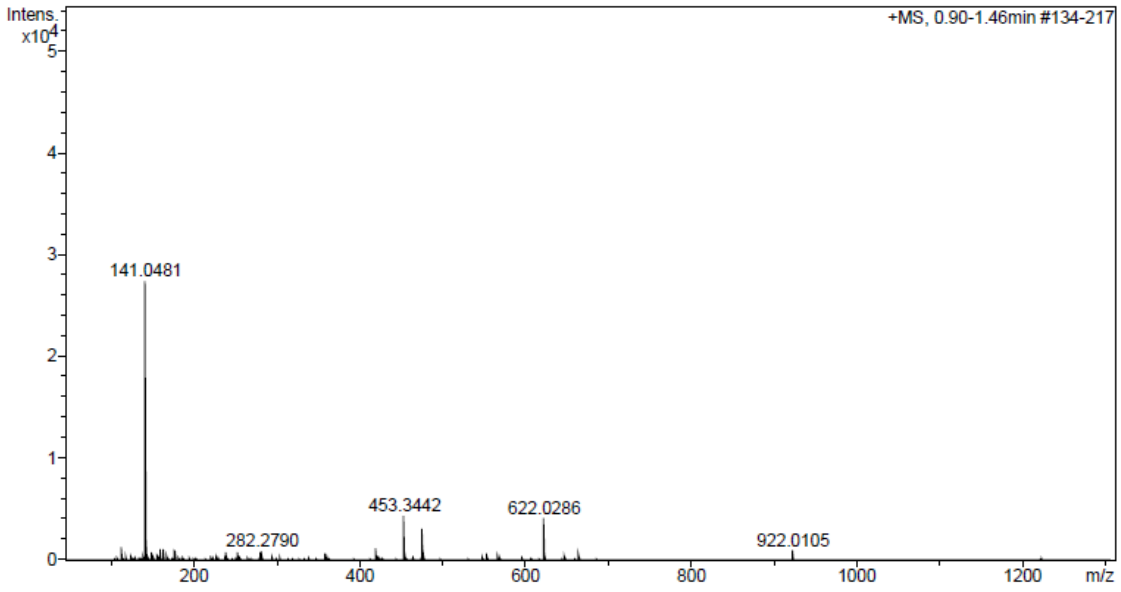

Figure 2.22 MS of **8**.

Substanz: cap503
Molekularformel: C6 H8 N2 S Mr = 140.21g/mol

Schmelzpunkt: bitte messen
gereinigt: UK getrocknet: 48h Vac

Bestimmungen: C H N

Eingang: 11.04.16 Ausgang: 12.04.16

M-161981 Operator: PK

Berechnete Gewichtsanteile:

[C] 51.40% [H] 5.75% [N] 19.98% [S] 22.87%

Gefundene Gewichtsanteile:

Einwaage: 1.241mg LECO TruSpec Micro
[C] 51.44% [H] 5.83% [N] 19.73% 12.04.16

Figure 2.23 EA of **8**.

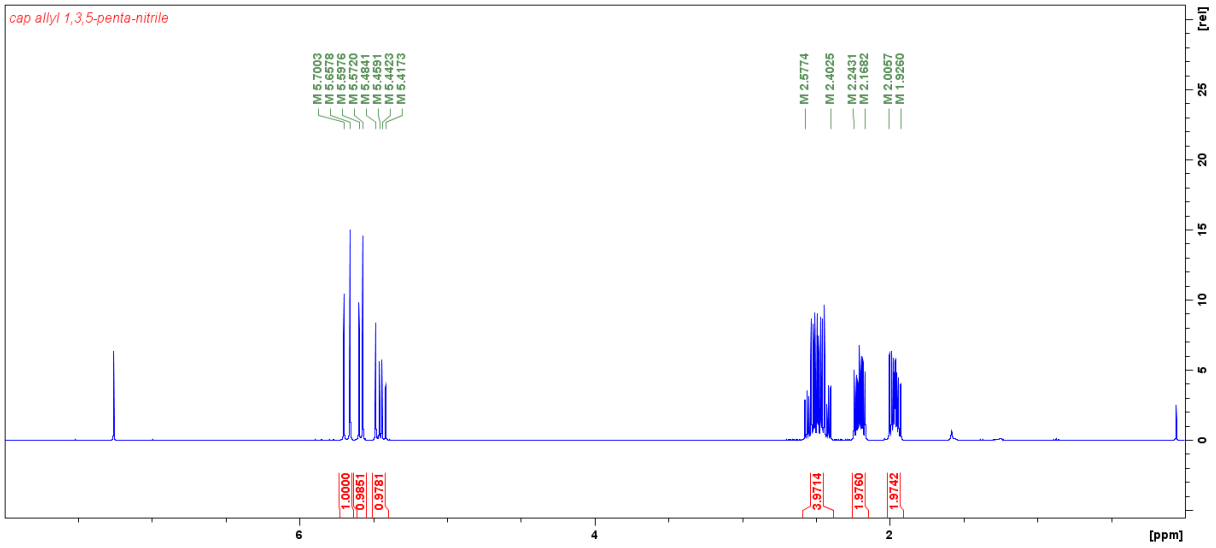

Figure 2.24 ^{1}H NMR spectrum of **9** in $CDCl_3$.

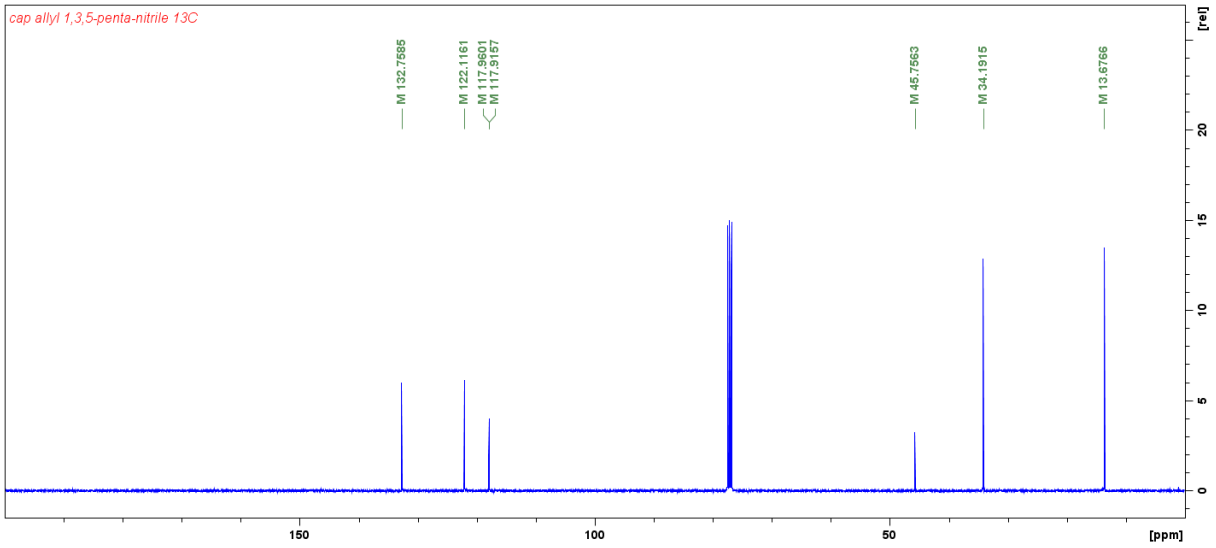

Figure 2.25 ^{13}C NMR spectrum of **9** in $CDCl_3$.

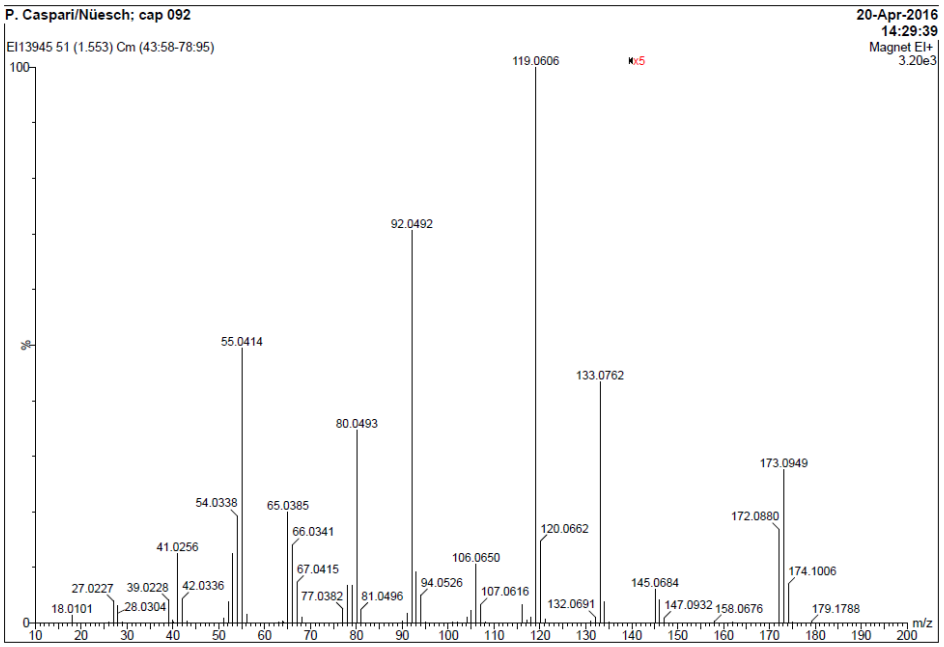

Figure 2.26 MS of **9**.

Substanz: cap092
Molekularformel: C10 H11 N3 Mr = 173.22g/mol

Schmelzpunkt: 61°C
gereinigt: UK getrocknet: 48h Vac

Bestimmungen: C H N

Eingang: 11.04.16 Ausgang: 12.04.16

M-161979 Operator: PK

Berechnete Gewichtsanteile:

[C] 69.34% [H] 6.40% [N] 24.26%

Gefundene Gewichtsanteile:

Einwaage: 0.932mg LECO TruSpec Micro
[C] 69.21% [H] 6.33% [N] 24.16% 12.04.16

Figure 2.27 EA of **9**.

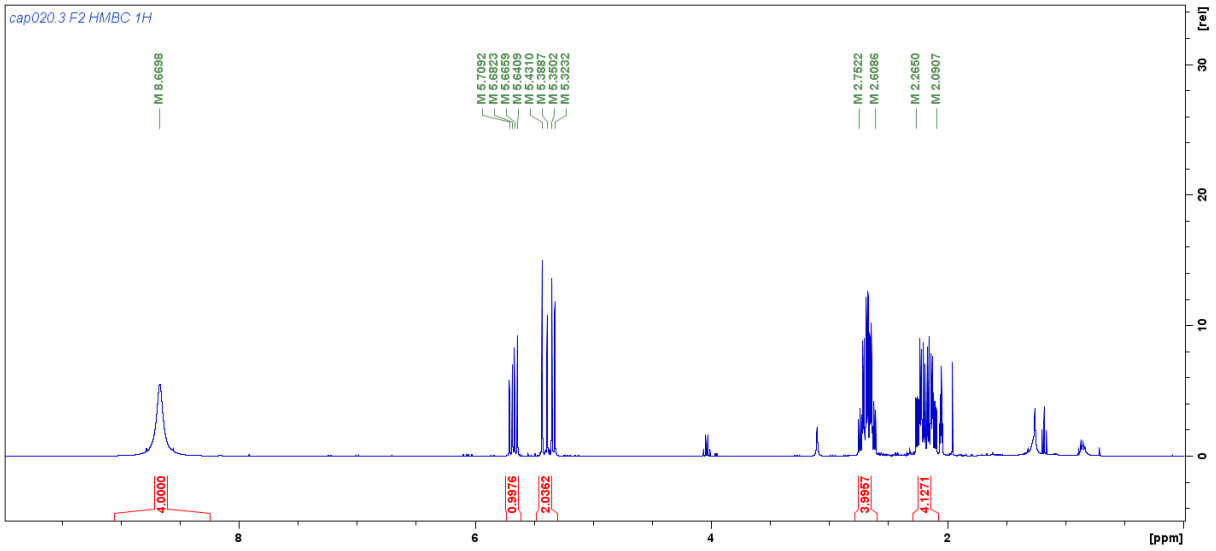

Figure 2.28 ^{1}H NMR spectrum of **12** in acetone-d_6.

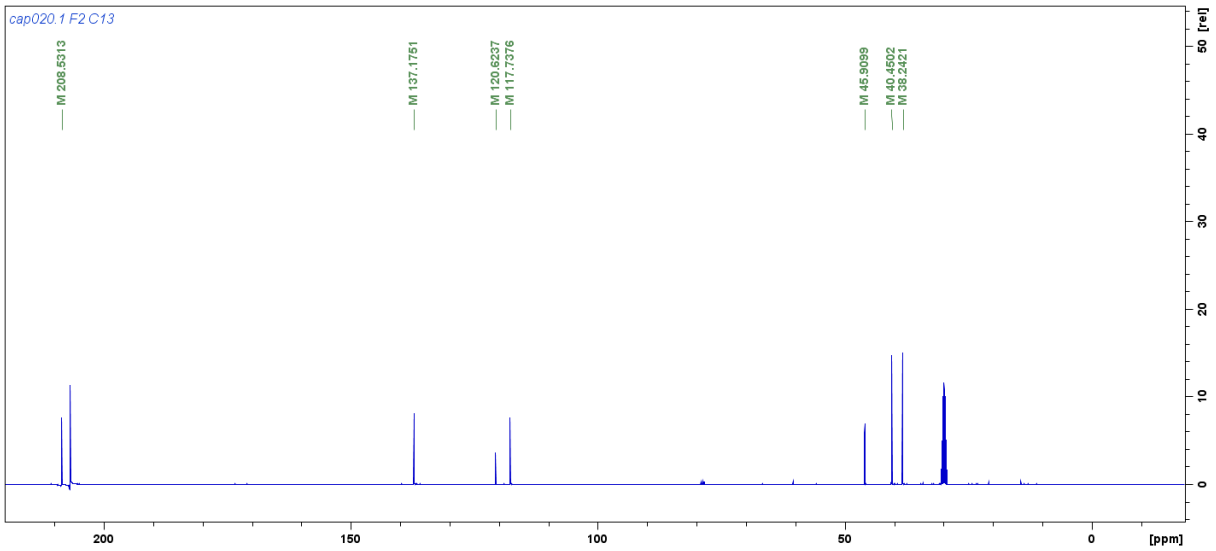

Figure 2.29 ^{13}C NMR spectrum of **12** in acetone-d_6.

Acquisition Parameter

Method:	ETH_HyStar_HPLC_QTOF_Pos_LowMass_Loop-AS.m			Acquisition Date:	30.09.2016 09:48:29
File Name:	D:\Data\max297xx\MAX29715.d			Operator:	Oswald Greter
Source Type	ESI	Ion Polarity	Positive	Set Nebulizer	1.6 Bar
Focus	Not active	Set Capillary	4500 V	Set Dry Heater	200 °C
Scan Begin	50 m/z	Set End Plate Offset	-500 V	Set Dry Gas	8.0 l/min
Scan End	1300 m/z	Set Collision Cell RF	200.0 Vpp	Set Divert Valve	Source

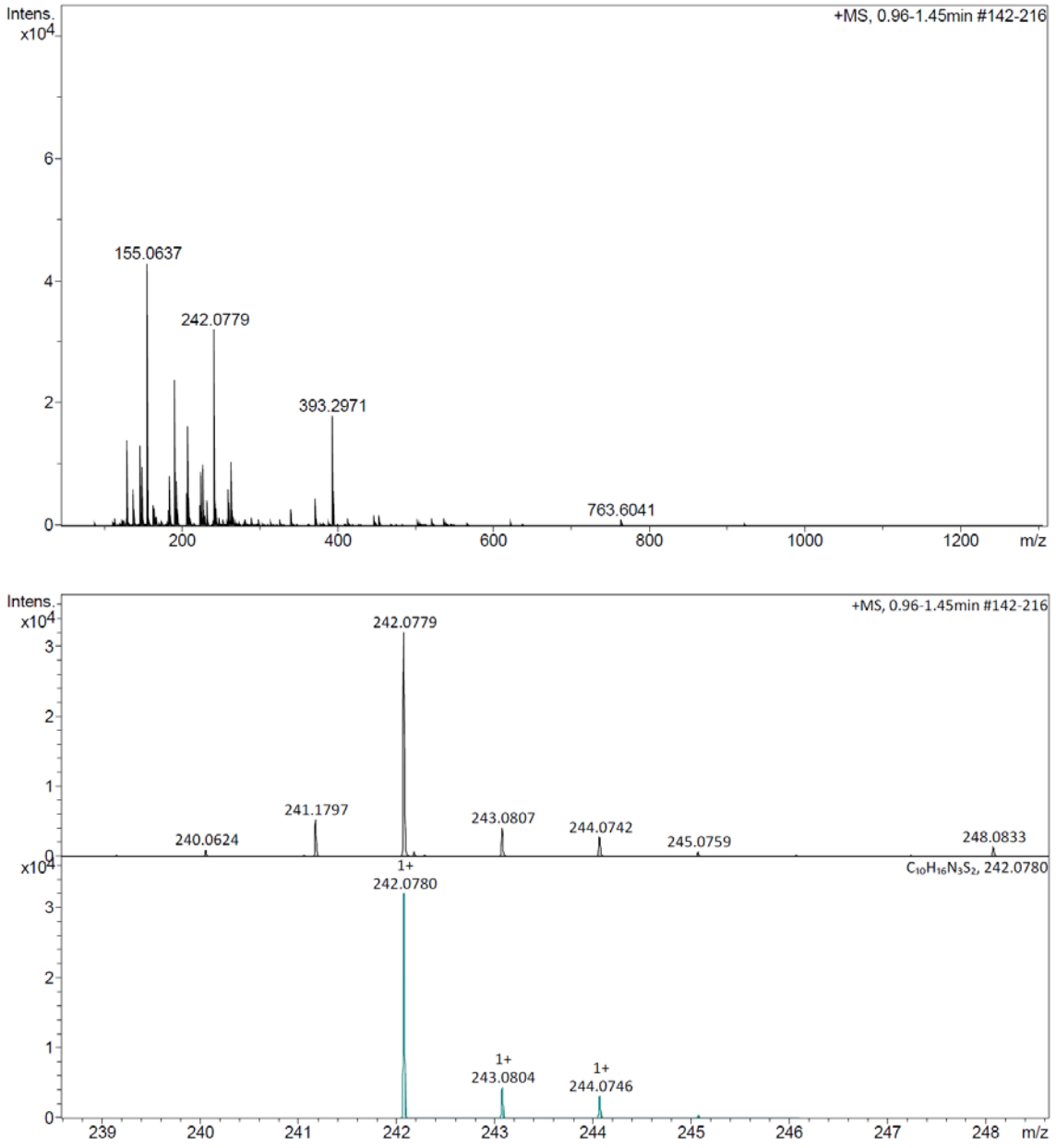

Figure 2.30 MS spectrum of **12**.

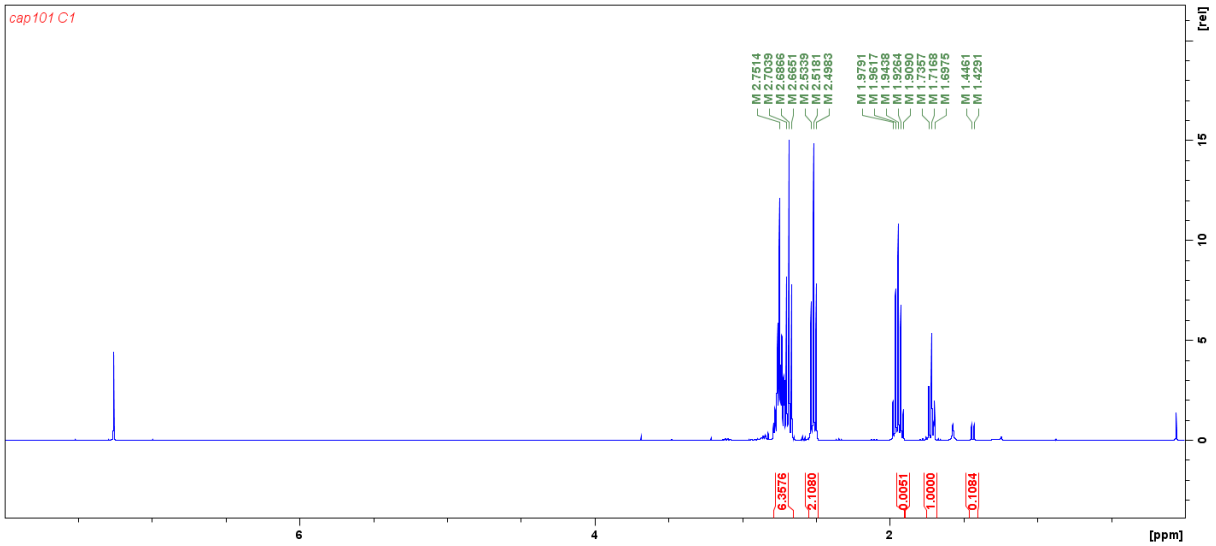

Figure 2.31 ^{1}H NMR spectrum of **13** in $CDCl_3$.

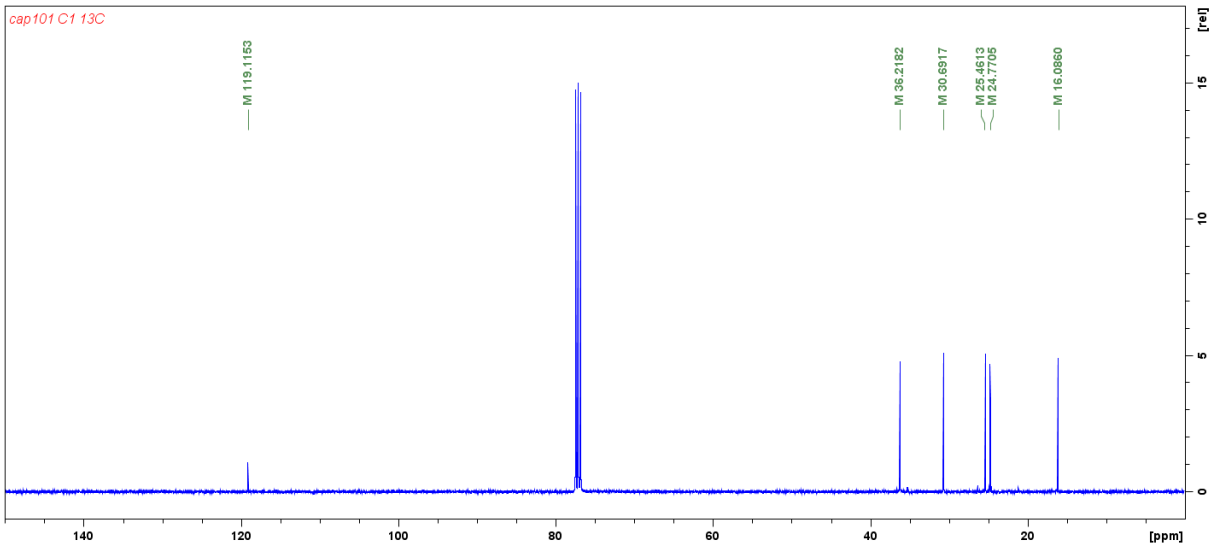

Figure 2.32 ^{13}C NMR spectrum of **13** in $CDCl_3$.

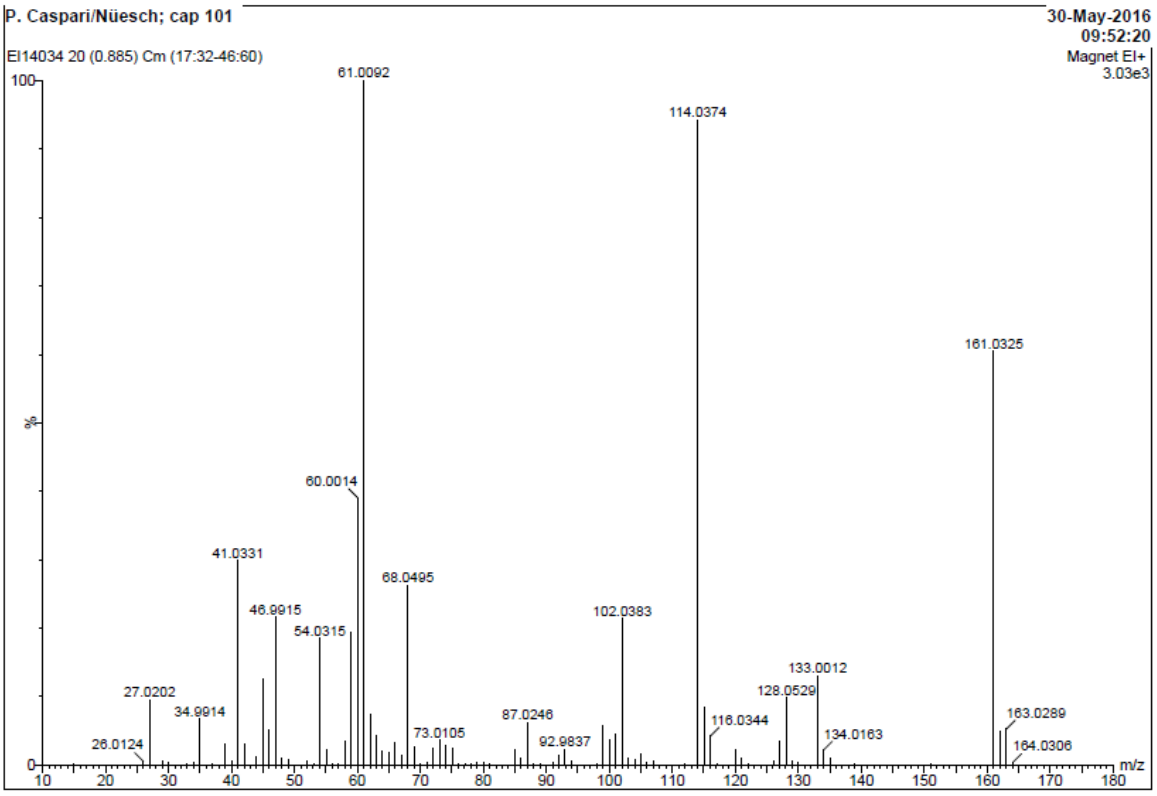

Figure 2.33 MS of **13**.

Bestimmungen: C H N S

Eingang: 19.05.16 Ausgang: 24.05.16

M-162241 Operator: SM

Berechnete Gewichtsanteile:

[C] 44.68% [H] 6.87% [N] 8.68% [S] 39.76%

Gefundene Gewichtsanteile:

Einwaage: 2.563mg LECO CHNS-932
[C] 44.51% [H] 7.12% [N] 8.58% 19.05.16

Einwaage: 1.064mg LECO CHNS-932
[S] 39.78% 24.05.16

Figure 2.34 EA of **13**.

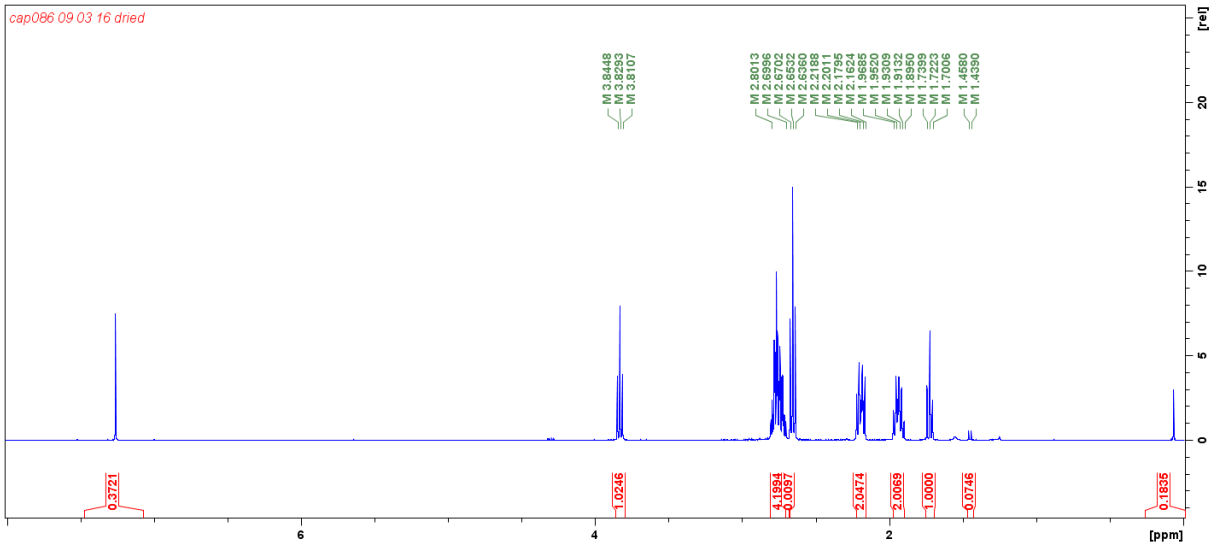

Figure 2.35. ^{1}H NMR spectrum of **14** in $CDCl_3$.

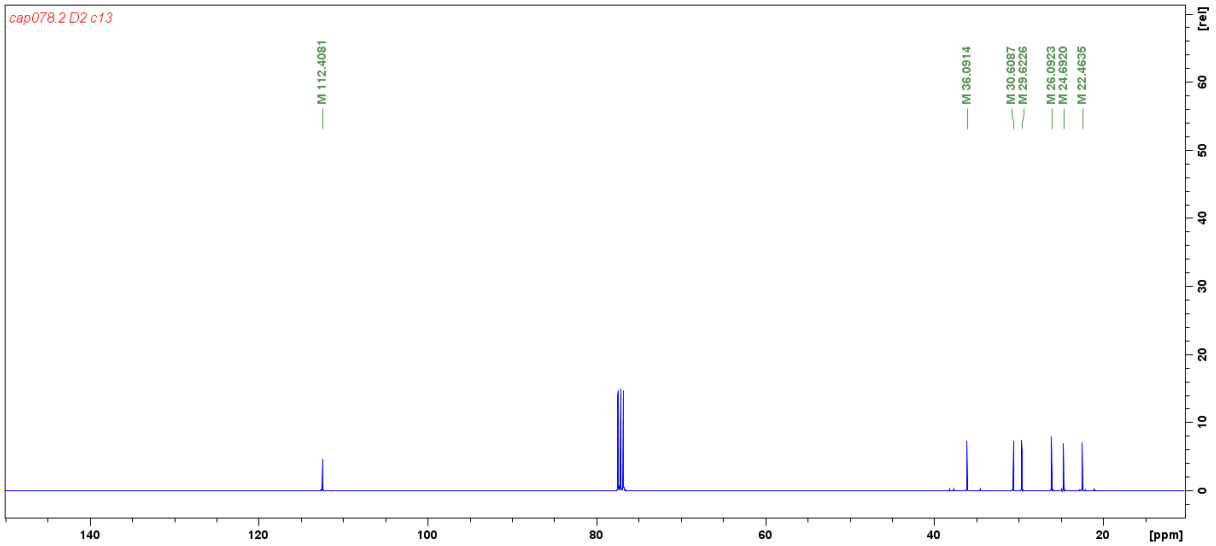

Figure 2.36 ^{13}C NMR spectrum of **14** in $CDCl_3$.

MAX27273 Philip Caspari/Nuesch - cap086 - DCM/MeOH

ETH Eidgenössische Technische Hochschule Zürich Swiss Federal Institute of Technology Zurich

Acquisition Parameter

Method:	ETH_HyStar_HPLC_QTOF_POS_LowMass_Loop-AS.m			Acquisition Date:	08.03.2016 15:30:40
File Name:	D:\Data\max272xx\MAX27273.d			Operator:	Louis Bertschi
Source Type	ESI	Ion Polarity	Positive	Set Nebulizer	1.6 Bar
Focus	Not active	Set Capillary	4500 V	Set Dry Heater	200 °C
Scan Begin	50 m/z	Set End Plate Offset	-500 V	Set Dry Gas	8.0 l/min
Scan End	1300 m/z	Set Collision Cell RF	200.0 Vpp	Set Divert Valve	Source

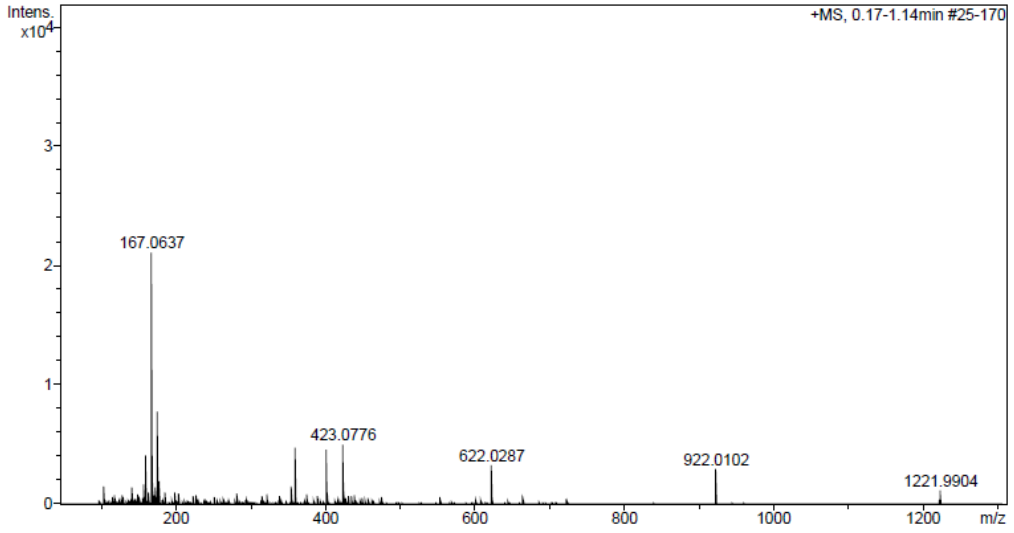

Figure 2.37 MS of **14**. M: 167 fragment (-H2S) 401 dimer, 423 dimer+Na can be seen.

Bestimmungen: C H N S

Eingang: 11.04.16 Ausgang: 20.04.16

M-161978 Operator: SM

Berechnete Gewichtsanteile:

[C] 47.97% [H] 6.04% [N] 13.98% [S] 32.01%

Gefundene Gewichtsanteile:

Einwaage: 1.981mg LECO CHNS-932
[C] 47.90% [H] 6.24% [N] 13.74% 12.04.16

Einwaage: 1.570mg LECO CHNS-932
[S] 31.86% 20.04.16

Figure 2.38 EA of **14**.

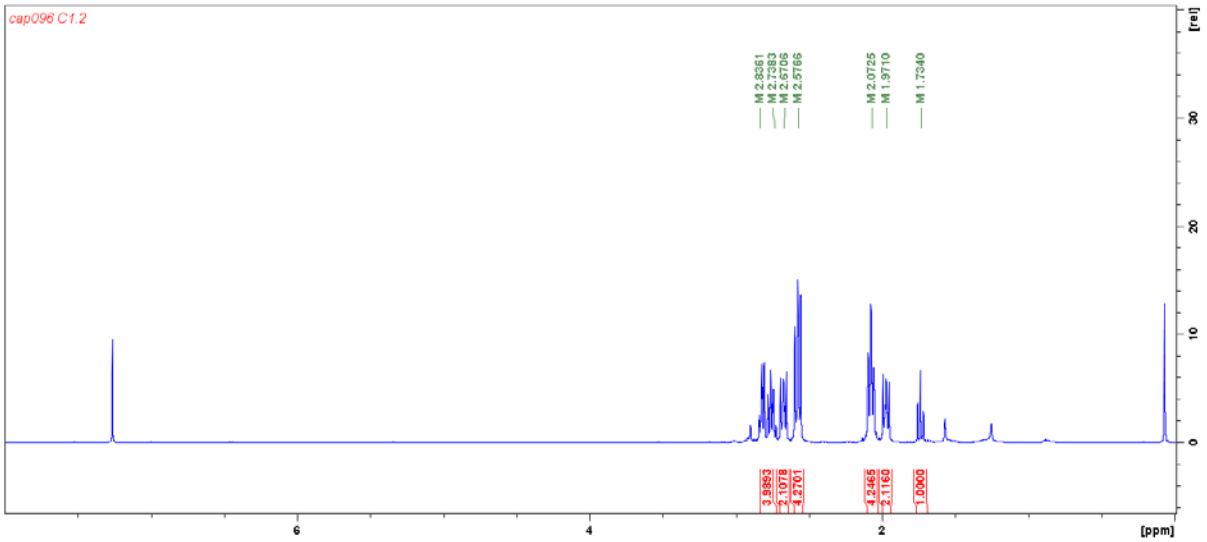

Figure 2.39 ^{1}H NMR spectrum of **15** in $CDCl_3$.

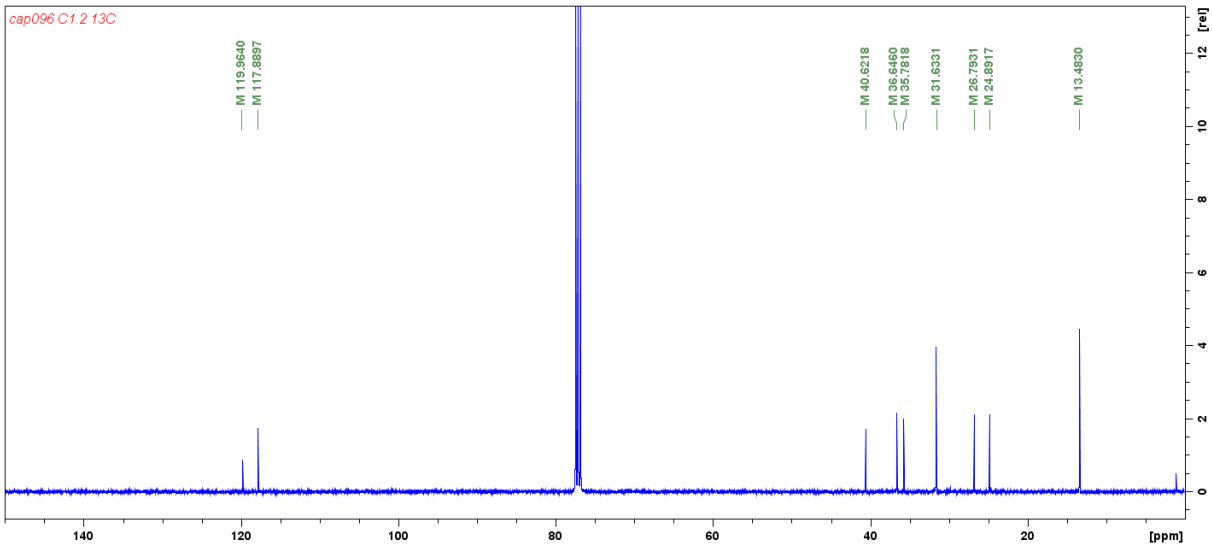

Figure 2.40 ^{13}C NMR spectrum of **15** in $CDCl_3$.

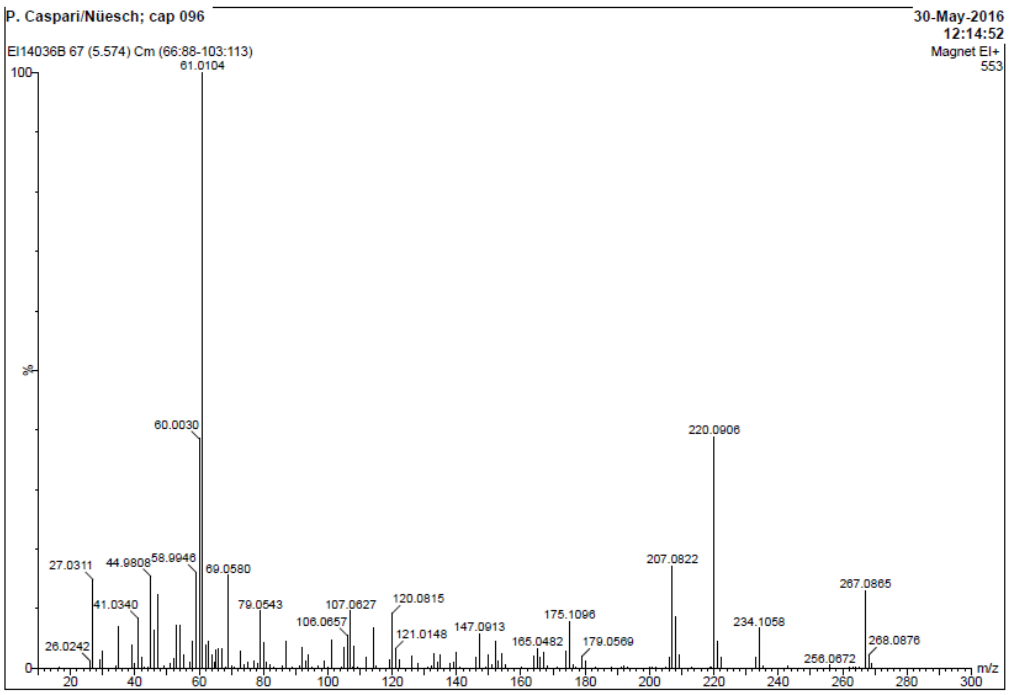

Figure 2.41 MS of **15**.

Bestimmungen: C H N S

Eingang: 19.05.16 Ausgang: 24.05.16

M-162240 Operator: SM

Berechnete Gewichtsanteile:

[C] 53.90% [H] 6.41% [N] 15.71% [S] 23.98%

Gefundene Gewichtsanteile:

Einwaage: 2.104mg LECO CHNS-932
[C] 53.78% [H] 6.60% [N] 15.43% 19.05.16

Einwaage: 1.049mg LECO CHNS-932
[S] 23.82% 24.05.16

Figure 2.42 EA of **15**.

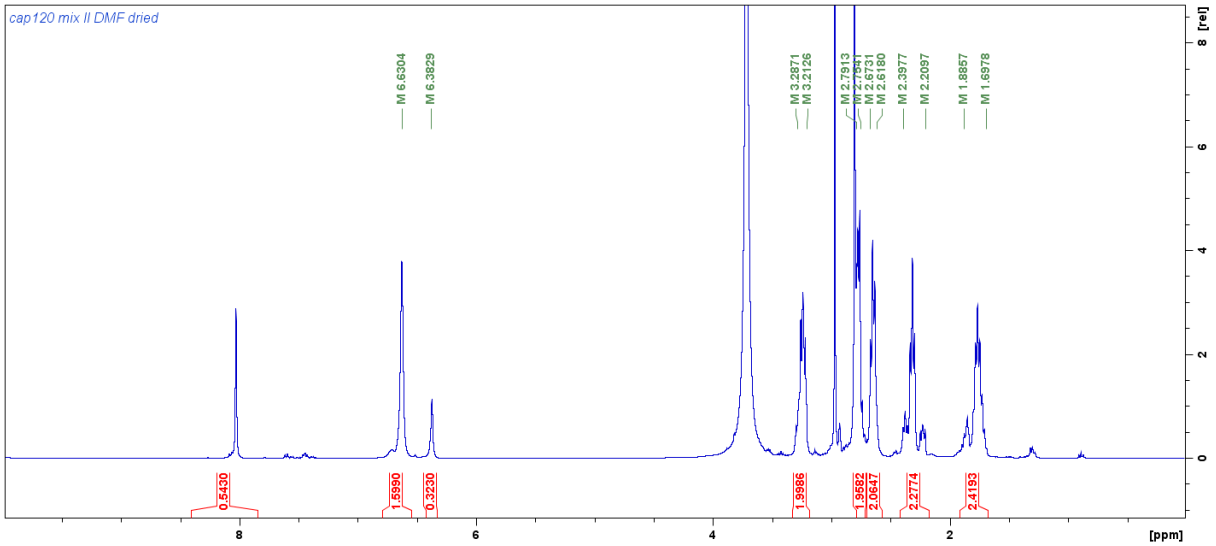

Figure 2.43 ^{1}H NMR spectrum of **16**.

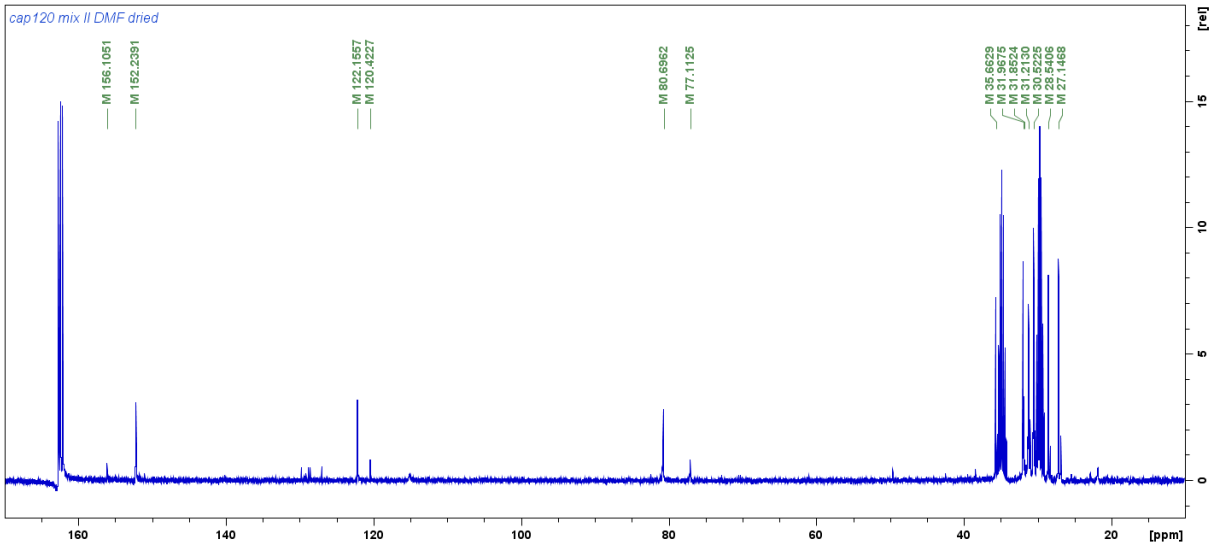

Figure 2.44 ^{13}C NMR spectrum of **16**.

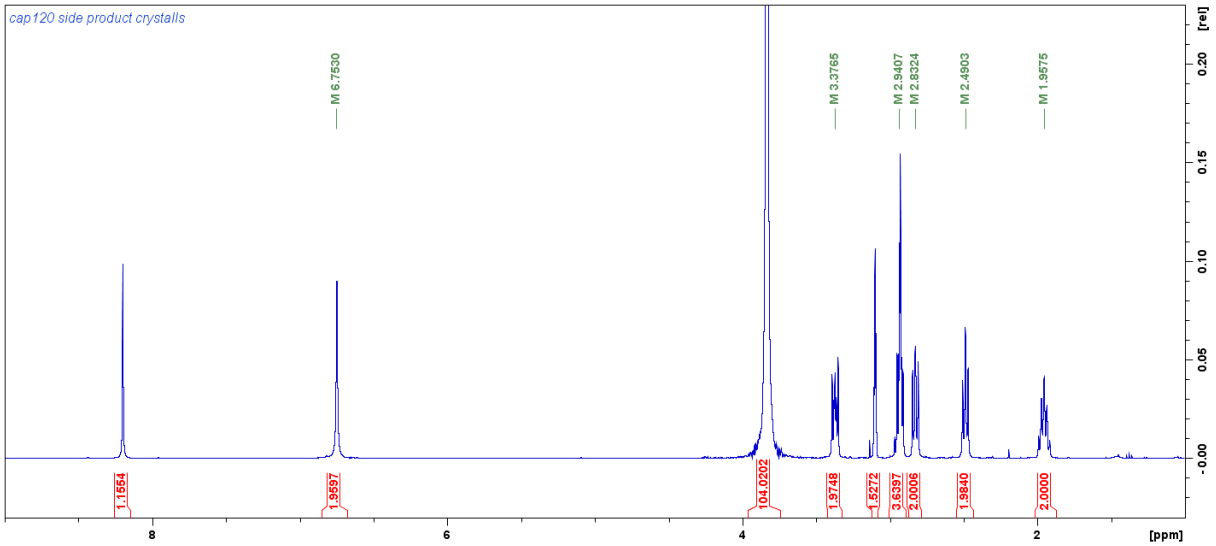

Figure 2.45 ^{1}H NMR spectrum of **17**.

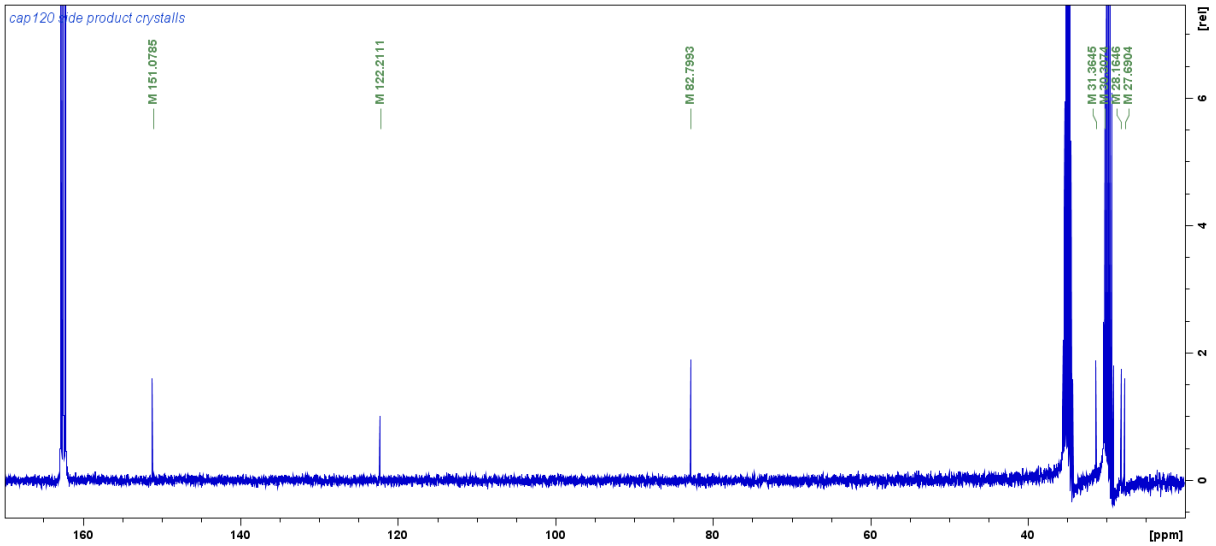

Figure 2.46 ^{13}C NMR spectrum of **17**.

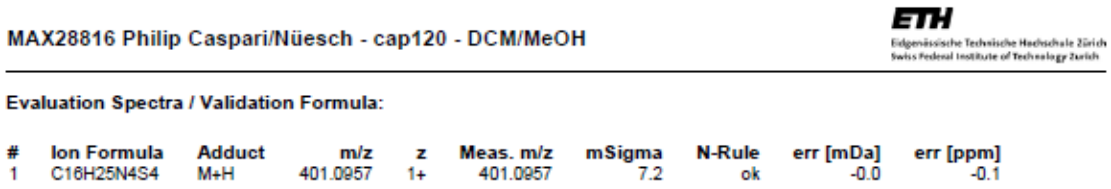

MAX28816 Philip Caspari/Nüesch - cap120 - DCM/MeOH

ETH Eidgenössische Technische Hochschule Zürich Swiss Federal Institute of Technology Zurich

Evaluation Spectra / Validation Formula:

#	Ion Formula	Adduct	m/z	z	Meas. m/z	mSigma	N-Rule	err [mDa]	err [ppm]
1	C16H25N4S4	M+H	401.0957	1+	401.0957	7.2	ok	-0.0	-0.1

Figure 2.47 MS of **17**.

Crystallography of 9

A transparent colourless block like shaped crystal of compound **9** was mounted on a Stoe Mark II-Imaging Plate Diffractometer System (Stoe & Cie, 2015) equipped with a graphite-monochromator. Data collection was performed at –100˚C using Mo-Kα radiation (λ = 0.71073 Å). 120 exposures (0.5 min per exposure) were obtained at an image plate distance of 100 mm, ϕ= 0˚ and 0 < ω < 180˚ with the crystal oscillating through 1.5˚ in ω. The resolution was D_{min} - D_{max} 24.00 - 0.72 Å. The compound crystallises in a centrosymmetric monoclinic cell, space group C2/c. The molecular formula is $[C_{10}H_{11}N_3]$. The structure was solved by direct methods using the program SHELXS[4] and refined by full matrix least squares on F^2[5] with SHELXL[4]. The hydrogen atoms were included in calculated positions and treated as riding atoms using SHELXL-97 default parameters. All non-hydrogen atoms were refined anisotropically. No absorption correction was applied. The drawings carried out with PLATON.

Table 2.1 Crystal data table for **9**.

Identification code	Cap092
Crystal shape	block
Crystal colour	colourless
Crystal size	0.500 x 0.400 x 0.350 mm
Empirical formula	C10 H11 N3
Formula weight	173.22

Crystal system	Monoclinic
Space group	C2/c
Unit cell dimensions	a = 17.3808(10) A alpha = 90 deg. b = 9.7356(5) A beta = 131.088(3) deg. c = 16.4358(9) A gamma = 90 deg.
Volume	2096.1(2) A^3
Cell refinement parameters	
Reflections	7806
Angle range	2.38 < theta < 29.51
Z	8
Density (calculated)	1.098 g/cm^3
Radiation used	MoK\a
Wavelength	0.71073 81A
Linear absorption coefficient	0.069 mm^-1
Temperature	173(2) K

Table 2.2 Data Collection Details for **9**.

Diffractometer	STOE IPDS 2
Scan method	rotation method
Number of Reflections measured	8890
Number of Independent reflections	2833
Number of observed reflections	2252
Criterion for recognizing	I > 2\s(I)
R(int) =	0.0947
Theta range for data collection	2.477 to 29.221 deg.
Index ranges	-23<=h<=23, -13<=k<=13, -22<=l<=22
F(000)	736

Table 2.3 Refinement Details for **9**.

Refinement method Full-matrix least-squares on F^2

Final R indices [I>2sigma(I)] R1 = 0.0489, wR2 = 0.1298

R indices (all data) R1 = 0.0607, wR2 = 0.1413

R1 [=SUM(||Fo|-|Fc||)/SUM|Fo|]

wR^2 {=[SUM(w(Fo^2-Fc^2)^2)/SUM(wFo^4)]^1/2}

H-locating and refining Method refall

Number of reflections used 2833

Number of L.S. restraints 0

Number of refined Parameters 162

Goodness-of-fit on F^2 1.061
S {=[SUM w(Fo^2-Fc^2)^2]/(n-p)^1/2}, n= number of reflections,
p= Parameters used.
w=1/[\s^2^(Fo^2^)+(0.0728P)^2^+0.2260P] where
P=(Fo^2^+2Fc^2^)/3

Maximum delta/sigma 0.000

Maximum e-density 0.362 e.A^-3

Minimun e-density -0.224 e.A^-3

Table 2.4 Computer Programs used for **9**.

Data collection program	STOE X-AREA
Cell refinement program	STOE X-AREA
Data reduction program	STOE X-RED
Structure Solving Program	SHELXS
Structure Refinement Program	SHELXL-2014/7 (Sheldrick, 2014)
Pictures drawn with	PLATON
Tables made with	CIFTAB
Extinction coefficient	n/a

Table 2.5 Atomic coordinates (x 10^4) and equivalent isotropic displacement parameters (A^2 x 10^3) for **9**. U(eq) is defined as one third of the trace of the orthogonalized Uij tensor.

	x	y	z	U(eq)
C(1)	5048(1)	4659(1)	6497(1)	36(1)
C(2)	3956(1)	4928(1)	5650(1)	36(1)
C(3)	3539(1)	4303(1)	4576(1)	31(1)
C(4)	2389(1)	4584(1)	3652(1)	28(1)
C(5)	2054(1)	3856(1)	2627(1)	33(1)
C(6)	925(1)	4062(1)	1656(1)	41(1)
C(7)	632(1)	3429(1)	681(1)	42(1)
C(8)	2188(1)	6110(1)	3447(1)	38(1)
C(9)	1579(1)	6854(2)	3475(1)	60(1)
C(10)	1816(1)	3997(1)	3943(1)	35(1)
N(1)	5902(1)	4449(1)	7148(1)	46(1)
N(2)	409(1)	2926(1)	-76(1)	56(1)
N(3)	1371(1)	3534(1)	4165(1)	53(1)

Table 2.6 Bond lengths [A] and angles [deg] for **9**.

C(1)-N(1)	1.1408(15)
C(1)-C(2)	1.4614(15)
C(2)-C(3)	1.5263(14)
C(2)-H(1A)	0.962(18)
C(2)-H(1B)	0.997(15)
C(3)-C(4)	1.5456(13)
C(3)-H(3A)	0.982(15)
C(3)-H(3B)	0.991(14)
C(4)-C(10)	1.4731(13)
C(4)-C(8)	1.5129(14)
C(4)-C(5)	1.5460(14)
C(5)-C(6)	1.5242(14)
C(5)-H(5A)	0.969(14)
C(5)-H(5B)	0.985(15)
C(6)-C(7)	1.4611(16)
C(6)-H(6A)	1.01(2)
C(6)-H(6B)	0.976(17)
C(7)-N(2)	1.1414(17)
C(8)-C(9)	1.3075(19)
C(8)-H(8A)	0.981(16)
C(9)-H(9A)	1.02(2)
C(9)-H(9B)	0.98(2)
C(10)-N(3)	1.1435(14)
N(1)-C(1)-C(2)	179.06(11)
C(1)-C(2)-C(3)	111.28(9)
C(1)-C(2)-H(1A)	108.4(9)
C(3)-C(2)-H(1A)	111.1(9)
C(1)-C(2)-H(1B)	110.5(8)
C(3)-C(2)-H(1B)	109.4(8)
H(1A)-C(2)-H(1B)	106.0(13)
C(2)-C(3)-C(4)	112.93(8)
C(2)-C(3)-H(3A)	110.1(8)
C(4)-C(3)-H(3A)	108.2(7)
C(2)-C(3)-H(3B)	108.8(8)
C(4)-C(3)-H(3B)	107.8(8)
H(3A)-C(3)-H(3B)	109.0(11)
C(10)-C(4)-C(8)	110.30(9)
C(10)-C(4)-C(3)	109.06(8)
C(8)-C(4)-C(3)	110.67(8)
C(10)-C(4)-C(5)	108.99(8)
C(8)-C(4)-C(5)	109.93(8)
C(3)-C(4)-C(5)	107.83(8)
C(6)-C(5)-C(4)	112.60(8)
C(6)-C(5)-H(5A)	111.4(8)
C(4)-C(5)-H(5A)	106.1(8)
C(6)-C(5)-H(5B)	109.1(8)
C(4)-C(5)-H(5B)	108.4(8)
H(5A)-C(5)-H(5B)	109.0(11)
C(7)-C(6)-C(5)	111.97(9)
C(7)-C(6)-H(6A)	106.9(11)
C(5)-C(6)-H(6A)	111.5(10)

C(7)-C(6)-H(6B)	107.2(9)
C(5)-C(6)-H(6B)	111.5(9)
H(6A)-C(6)-H(6B)	107.5(14)
N(2)-C(7)-C(6)	179.45(14)
C(9)-C(8)-C(4)	127.57(12)
C(9)-C(8)-H(8A)	119.1(9)
C(4)-C(8)-H(8A)	113.3(9)
C(8)-C(9)-H(9A)	122.2(12)
C(8)-C(9)-H(9B)	119.7(12)
H(9A)-C(9)-H(9B)	117.9(17)
N(3)-C(10)-C(4)	179.51(13)

Table 2.7 Torsion-angles for **9**.

C(1)-C(2)-C(3)-C(4)	-179.07(8)
C(2)-C(3)-C(4)-C(10)	-59.68(11)
C(2)-C(3)-C(4)-C(8)	61.84(11)
C(2)-C(3)-C(4)-C(5)	-177.89(8)
C(10)-C(4)-C(5)-C(6)	61.73(11)
C(8)-C(4)-C(5)-C(6)	-59.28(12)
C(3)-C(4)-C(5)-C(6)	179.99(9)
C(4)-C(5)-C(6)-C(7)	177.03(9)
C(10)-C(4)-C(8)-C(9)	-2.11(17)
C(3)-C(4)-C(8)-C(9)	-122.89(14)
C(5)-C(4)-C(8)-C(9)	118.10(14)

Table 2.8 Anisotropic displacement parameters ($A^2 \times 10^3$) for **9**.

The anisotropic displacement factor exponent takes the form:
-2 pi^2 [h^2 a*^2 U11 + ... + 2 h k a* b* U12]

	U11	U22	U33	U23	U13	U12
C(1)	42(1)	41(1)	28(1)	-3(1)	25(1)	-7(1)
C(2)	40(1)	40(1)	30(1)	-1(1)	24(1)	0(1)
C(3)	31(1)	36(1)	28(1)	-1(1)	21(1)	-1(1)
C(4)	32(1)	27(1)	30(1)	2(1)	22(1)	0(1)
C(5)	30(1)	34(1)	31(1)	-2(1)	18(1)	1(1)
C(6)	33(1)	44(1)	35(1)	-3(1)	17(1)	6(1)
C(7)	34(1)	40(1)	33(1)	1(1)	15(1)	4(1)
C(8)	50(1)	29(1)	35(1)	2(1)	28(1)	-1(1)
C(9)	82(1)	36(1)	67(1)	7(1)	52(1)	17(1)
C(10)	32(1)	34(1)	39(1)	8(1)	25(1)	5(1)
N(1)	43(1)	60(1)	33(1)	-3(1)	24(1)	-6(1)
N(2)	52(1)	57(1)	38(1)	-4(1)	21(1)	5(1)
N(3)	43(1)	64(1)	63(1)	24(1)	39(1)	9(1)

Table 2.9 Hydrogen coordinates (x 10^2) and isotropic displacement parameters (A^2 x 10^2) for **9**.

	x	y	z	U(eq)
H(1A)	3851(12)	5906(18)	5588(12)	58(4)
H(1B)	3572(11)	4552(14)	5856(12)	45(4)
H(3A)	3644(9)	3304(15)	4649(10)	38(3)
H(3B)	3910(10)	4707(14)	4365(11)	39(3)
H(5A)	2482(10)	4226(14)	2496(11)	37(3)
H(5B)	2193(10)	2866(15)	2781(11)	42(3)
H(6A)	747(13)	5060(20)	1491(15)	67(5)
H(6B)	493(12)	3661(17)	1777(12)	54(4)
H(8A)	2593(11)	6561(16)	3303(12)	50(4)
H(9A)	1146(15)	6440(20)	3627(15)	77(5)
H(9B)	1500(16)	7840(30)	3306(17)	96(7)

Table 2.10 Hydrogen-bonds for **9** [A and deg.].

D-H...A	d(D-H)	d(H...A)	d(D...A)	<(DHA)
C(6)-H(6A)...N(2)#1	1.01(2)	2.670(19)	3.5781(17)	150.2(14)
C(6)-H(6B)...N(3)#2	0.976(17)	2.512(16)	3.3059(16)	138.3(12)

Symmetry transformations used to generate equivalent atoms:
#1 -x,-y+1,-z #2 -x,y,-z+1/2

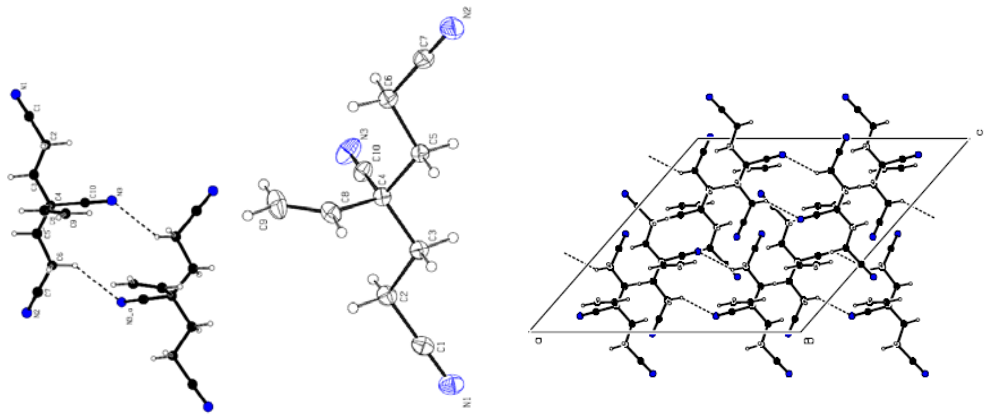

Figure 2.48 ORTEP plot of **9**.

Crystallography of **17**

A colourless rod like shaped crystal of compound **17** was mounted on a Stoe Mark II-Imaging Plate Diffractometer System (Stoe & Cie, 2015) equipped with a graphite-monochromator. Data collection was performed at –100˚C using Mo-Kα radiation (λ = 0.71073 Å). 180 exposures (3 min per exposure) were obtained at an image plate distance of 100 mm, ϕ= 0˚ and 0 < ω < 180˚ with the crystal oscillating through 1˚ in ω. The resolution was D_{min} - D_{max} 24.00 - 0.84 Å. The compound crystal-

lises in a centrosymmetric orthorhombic cell, space group P21/n; the molecule lies on a symmetry center. The molecular formula is [($C_{16}H_{24}N_4S_4$)]. The structure was solved by direct methods using the program SHELXS and refined by full matrix least squares on F^5 with SHELXL[4]. The NH2 hydrogen atoms have been derived through Fourier difference maps while the remaining hydrogen atoms were included in calculated positions and treated as riding atoms using SHELXL-97 default parameters. All non-hydrogen atoms were refined anisotropically. Intra-molecular hydrogen bonds have been found. No absorption correction has been applied.

Crystallographic details are given in the supplementary data file. The drawings carried out with PLATON.

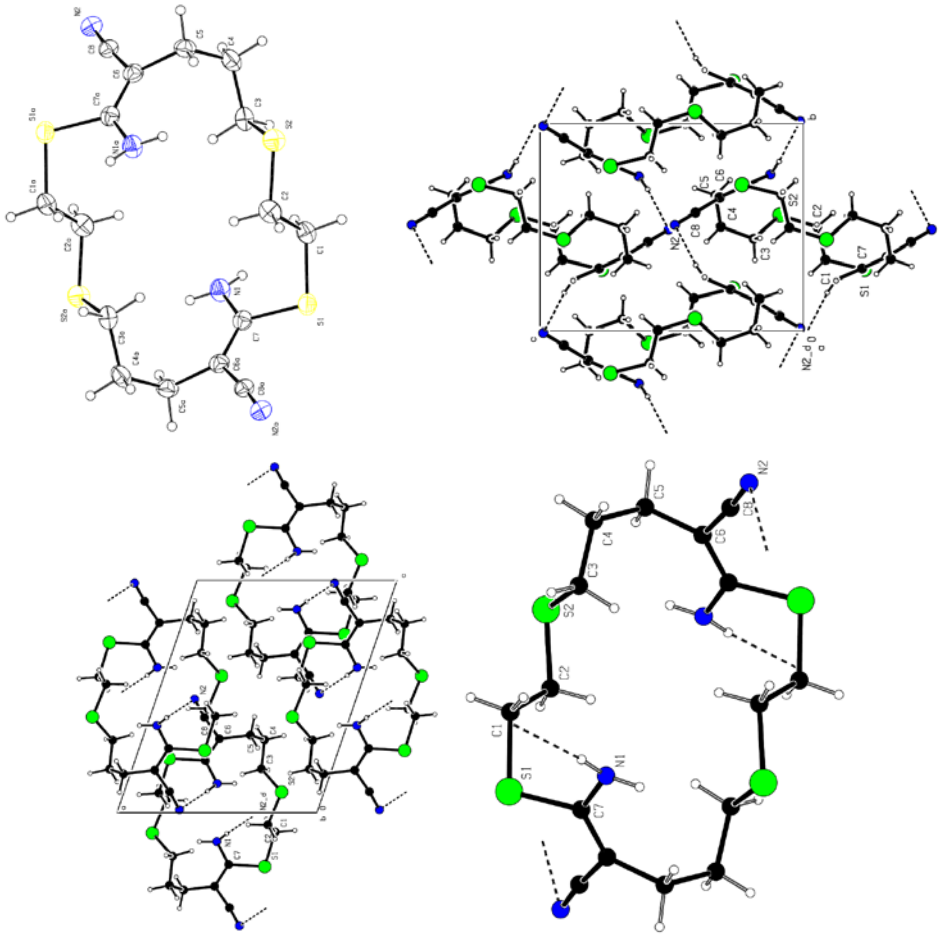

Figure 2.49 ORTEP plot of **17**.

Table 2.11 Crystal data table for **17**.

Table 1. Crystal data table for Cap120.

Identification code	Cap120
Crystal shape	block
Crystal colour	colourless
Crystal size	0.400 x 0.350 x 0.200 mm
Empirical formula	C16 H24 N4 S4
Formula weight	400.63
Crystal system	Monoclinic
Space group	P2(1)/n
Unit cell dimensions	a = 9.7678(7) A alpha = 90 deg. b = 8.9291(5) A beta = 109.007(5) deg. c = 12.0069(8) A gamma = 90 deg.
Volume	990.12(12) A^3
Cell refinement parameters	
Reflections	18427
Angle range	1.79 < theta < 29.56
Z	2
Density (calculated)	1.344 g/cm^3
Radiation used	MoK\a
Wavelength	0.71073 A
Linear absorption coefficient	0.486 mm^-1
Temperature	293(2) K

Table 2. Data Collection Details for Cap120.

Diffractometer	STOE IPDS 2
Scan method	rotation method
Number of Reflections measured	13148
Number of Independent reflections	2679
Number of observed reflections	2334
Criterion for recognizing	I > 2\s(I)
R(int) =	0.1111
Theta range for data collection	2.346 to 29.191 deg.
Index ranges	-13<=h<=13, -12<=k<=11, -16<=l<=16
F(000)	424

Table 2.12 Refinement Details for **17**.

Table 3. Refinement Details for Cap120.

Refinement method	Full-matrix least-squares on F^2
Final R indices [I>2sigma(I)]	R1 = 0.0525, wR2 = 0.1510
R indices (all data)	R1 = 0.0579, wR2 = 0.1653
R1 [=SUM(||Fo|-|Fc||)/SUM|Fo|]	
wR^2 {=[SUM(w(Fo^2-Fc^2)^2)/SUM(wFo^4)]^1/2}	
H-locating and refining Method	mixed
Number of reflections used	2679
Number of L.S. restraints	0
Number of refined Parameters	117
Goodness-of-fit on F^2 S {=[SUM w(Fo^2-Fc^2)^2]/(n-p)^1/2}, n= number of reflections, p= Parameters used.	1.060 w=1/[\s^2^(Fo^2^)+(0.0953P)^2^+0.2587P] where P=(Fo^2^+2Fc^2^)/3
Maximum delta/sigma	0.000
Maximum e-density	0.395 e.A^-3
Minimun e-density	-0.587 e.A^-3

Table 4. Computer Programs used for Cap120.

Data collection program	STOE X-AREA
Cell refinement program	STOE X-AREA
Data reduction program	STOE X-RED
Structure Solving Program	?
Structure Refinement Program	SHELXL-2014/7 (Sheldrick, 2014)
Pictures drawn with	?
Tables made with	?
Extinction coefficient	n/a

Table 5. Atomic coordinates (x 10^4) and equivalent isotropic displacement parameters (A^2 x 10^3) for Cap120.
U(eq) is defined as one third of the trace of the orthogonalized Uij tensor.

	x	y	z	U(eq)
C(1)	8248(2)	6571(2)	841(2)	46(1)
C(2)	7759(3)	4979(2)	529(2)	51(1)
C(3)	6473(2)	5559(2)	-1879(2)	46(1)
C(4)	6124(2)	4973(3)	-3133(2)	54(1)
C(5)	4661(2)	6539(3)	3334(2)	48(1)
C(6)	6152(2)	6437(2)	3176(2)	42(1)
C(7)	6477(2)	6992(2)	2238(2)	41(1)
C(8)	7262(2)	5710(2)	4098(2)	42(1)
N(1)	5492(2)	7548(2)	1250(2)	49(1)
N(2)	8074(2)	5108(2)	4879(2)	49(1)
S(1)	8315(1)	7050(1)	2327(1)	48(1)
S(2)	7874(1)	4408(1)	-885(1)	51(1)

Table 2.13 Bond lengths and angles for **17**.

Table 6. Bond lengths [A] and angles [deg] for Cap120.

C(1)-C(2)	1.508(3)
C(1)-S(1)	1.814(2)
C(1)-H(1A)	0.9700
C(1)-H(1B)	0.9700
C(2)-S(2)	1.810(2)
C(2)-H(2A)	0.9700
C(2)-H(2B)	0.9700
C(3)-C(4)	1.525(3)
C(3)-S(2)	1.8141(19)
C(3)-H(3A)	0.9700
C(3)-H(3B)	0.9700
C(4)-C(5)#1	1.533(3)
C(4)-H(4A)	0.9700
C(4)-H(4B)	0.9700
C(5)-C(6)	1.532(3)
C(5)-C(4)#1	1.533(3)
C(5)-H(5B)	0.9700
C(5)-H(5A)	0.9700
C(6)-C(7)	1.359(3)
C(6)-C(8)	1.429(3)
C(7)-N(1)	1.355(3)
C(7)-S(1)	1.764(2)
C(8)-N(2)	1.146(3)
N(1)-H(1N)	0.85(3)
N(1)-H(2N)	0.82(3)
C(2)-C(1)-S(1)	111.96(14)
C(2)-C(1)-H(1A)	109.2
S(1)-C(1)-H(1A)	109.2
C(2)-C(1)-H(1B)	109.2
S(1)-C(1)-H(1B)	109.2
H(1A)-C(1)-H(1B)	107.9
C(1)-C(2)-S(2)	112.80(15)
C(1)-C(2)-H(2A)	109.0
S(2)-C(2)-H(2A)	109.0
C(1)-C(2)-H(2B)	109.0
S(2)-C(2)-H(2B)	109.0
H(2A)-C(2)-H(2B)	107.8
C(4)-C(3)-S(2)	109.49(15)
C(4)-C(3)-H(3A)	109.8
S(2)-C(3)-H(3A)	109.8
C(4)-C(3)-H(3B)	109.8
S(2)-C(3)-H(3B)	109.8
H(3A)-C(3)-H(3B)	108.2
C(3)-C(4)-C(5)#1	113.41(17)
C(3)-C(4)-H(4A)	108.9
C(5)#1-C(4)-H(4A)	108.9
C(3)-C(4)-H(4B)	108.9
C(5)#1-C(4)-H(4B)	108.9
H(4A)-C(4)-H(4B)	107.7
C(6)-C(5)-C(4)#1	112.04(17)
C(6)-C(5)-H(5B)	109.2
C(4)#1-C(5)-H(5B)	109.2
C(6)-C(5)-H(5A)	109.2
C(4)#1-C(5)-H(5A)	109.2
H(5B)-C(5)-H(5A)	107.9
C(7)-C(6)-C(8)	119.02(18)
C(7)-C(6)-C(5)	124.66(17)
C(8)-C(6)-C(5)	116.32(17)
N(1)-C(7)-C(6)	124.65(19)
N(1)-C(7)-S(1)	117.42(16)
C(6)-C(7)-S(1)	117.89(15)
N(2)-C(8)-C(6)	174.7(2)
C(7)-N(1)-H(1N)	116(2)
C(7)-N(1)-H(2N)	113(2)
H(1N)-N(1)-H(2N)	124(3)
C(7)-S(1)-C(1)	102.90(9)
C(2)-S(2)-C(3)	101.14(10)

Symmetry transformations used to generate equivalent atoms:
#1 -x+1,-y+1,-z

Table 2.14 Top: Torsion-angles for **17**. Middle: Anisotropic displacement parameters for **17**. Bottom: Hydrogen coordinates and isotropic displacement parameters for **17**.

Table 7. Torsion-angles for Cap120.

S(1)-C(1)-C(2)-S(2)	-173.58(11)
S(2)-C(3)-C(4)-C(5)#1	70.0(2)
C(4)#1-C(5)-C(6)-C(7)	106.5(2)
C(4)#1-C(5)-C(6)-C(8)	-73.9(2)
C(8)-C(6)-C(7)-N(1)	172.08(18)
C(5)-C(6)-C(7)-N(1)	-8.3(3)
C(8)-C(6)-C(7)-S(1)	-10.1(2)
C(5)-C(6)-C(7)-S(1)	169.47(14)
N(1)-C(7)-S(1)-C(1)	-39.80(17)
C(6)-C(7)-S(1)-C(1)	142.22(15)
C(2)-C(1)-S(1)-C(7)	-66.54(17)
C(1)-C(2)-S(2)-C(3)	-68.23(18)
C(4)-C(3)-S(2)-C(2)	-165.68(14)

#1 -x+1,-y+1,-z

Table 8. Anisotropic displacement parameters (A^2 x 10^3) for Cap120.
The anisotropic displacement factor exponent takes the form:
-2 pi^2 [h^2 a*^2 U11 + ... + 2 h k a* b* U12]

	U11	U22	U33	U23	U13	U12
C(1)	43(1)	46(1)	52(1)	7(1)	19(1)	1(1)
C(2)	58(1)	40(1)	57(1)	10(1)	22(1)	4(1)
C(3)	38(1)	41(1)	58(1)	8(1)	15(1)	1(1)
C(4)	46(1)	69(1)	52(1)	14(1)	24(1)	2(1)
C(5)	52(1)	53(1)	41(1)	-6(1)	19(1)	4(1)
C(6)	45(1)	38(1)	41(1)	-7(1)	14(1)	-1(1)
C(7)	41(1)	35(1)	45(1)	-3(1)	13(1)	-1(1)
C(8)	47(1)	40(1)	39(1)	-9(1)	15(1)	-6(1)
N(1)	42(1)	51(1)	52(1)	10(1)	12(1)	2(1)
N(2)	50(1)	54(1)	40(1)	-4(1)	10(1)	-2(1)
S(1)	39(1)	54(1)	49(1)	3(1)	12(1)	-6(1)
S(2)	46(1)	53(1)	54(1)	2(1)	15(1)	14(1)

Table 9. Hydrogen coordinates (x 10^4) and isotropic displacement parameters (A^2 x 10^3) for Cap120.

	x	y	z	U(eq)
H(1A)	7587	7246	289	55
H(1B)	9201	6704	770	55
H(2A)	6765	4877	516	61
H(2B)	8352	4315	1134	61
H(3A)	5609	5532	-1648	55
H(3B)	6801	6589	-1839	55
H(4A)	7018	4872	-3312	64
H(4B)	5524	5702	-3674	64
H(5B)	4075	7267	2783	57
H(5A)	4776	6888	4125	57
H(1N)	4620(30)	7580(30)	1250(30)	61(8)
H(2N)	5840(30)	8170(40)	920(30)	67(8)

Table 2.15 Hydrogen-bonds for **17**.

Table 10. Hydrogen-bonds for Cap120 [A and deg.].

D-H...A	d(D-H)	d(H...A)	d(D...A)	<(DHA)
C(1)-H(1A)...N(2)#2	0.97	2.63	3.415(3)	138.5
C(1)-H(1B)...S(2)#3	0.97	2.99	3.872(2)	152.5
C(4)-H(4A)...N(2)#4	0.97	2.70	3.508(3)	141.2
N(1)-H(1N)...S(2)#1	0.85(3)	2.93(3)	3.621(2)	140(2)
N(1)-H(2N)...N(2)#2	0.82(3)	2.38(4)	3.204(3)	174(3)

Symmetry transformations used to generate equivalent atoms:
#1 -x+1,-y+1,-z #2 -x+3/2,y+1/2,-z+1/2 #3 -x+2,-y+1,-z
#4 x,y,z-1

Crystallography of **8**

A transparent colourless rod like shaped crystal of compound **8** was mounted on a Stoe Mark II-Imaging Plate Diffractometer System (Stoe & Cie, 2015) equipped with a graphite-monochromator. Data collection was performed at –100˚C using Mo-Kα radiation (λ = 0.71073 Å). 120 exposures (1 min per exposure) were obtained at an image plate distance of 100 mm, ϕ= 0˚ and 0 < ω < 180˚ with the crystal oscillating through 1.5˚ in ω. The resolution was D_{min} - D_{max} 24.00 - 0.72 Å.The compound crystallises in a centrosymmetric monoclinic cell, space group C2/c. The molecular formula is [$C_6H_8N_2S$]. The structure was solved by direct methods using the program SHELXS[4] and refined by full matrix least squares on F^2[5] with SHELXL.The hydrogen atoms were included in calculated positions and treated as riding atoms using SHELXL-97 default parameters. All non-hydrogen atoms were refined anisotropically. No absorption correction was applied. Crystallographic details are given in the supplementary data file. The drawings carried out with PLATON.

Table 2.16 Crystal data table for **8**.

Identification code	Cap503
Crystal shape	rod
Crystal colour	colourless
Crystal size	0.500 x 0.300 x 0.200 mm
Empirical formula	C6 H8 N2 S
Formula weight	140.20
Crystal system	Monoclinic
Space group	C2/c
Unit cell dimensions	a = 15.7040(8) A alpha = 90 deg. b = 7.7645(4) A beta = 133.640(3) deg. c = 15.7661(9) A gamma = 90 deg.
Volume	1391.23(14) A^3
Cell refinement parameters	
Reflections	10685

Angle range	2.82 < theta < 29.47
Z	8
Density (calculated)	1.339 g/cm^3
Radiation used	MoK\a
Wavelength	0.71073 93A
Linear absorption coefficient	0.371 mm^-1
Temperature	173(2) K

Table 2.17 Data Collection Details for **8**.

Diffractometer	STOE IPDS 2
Scan method	rotation method
Number of Reflections measured	10854
Number of Independent reflections	1867
Number of observed reflections	1656
Criterion for recognizing	I > 2\s(I)
R(int) =	0.0574
Theta range for data collection	2.816 to 29.189 deg.
Index ranges	-21<=h<=21, -10<=k<=10, -21<=l<=21
F(000)	592

Table 2.18 Refinement Details for **8**.

Refinement method	Full-matrix least-squares on F^2
Final R indices [I>2sigma(I)]	R1 = 0.0301, wR2 = 0.0876
R indices (all data)	R1 = 0.0357, wR2 = 0.0969
R1 [=SUM(||Fo|-|Fc||)/SUM|Fo|]	
wR^2 {=[SUM(w(Fo^2-Fc^2)^2)/SUM(wFo^4)]^1/2}	

H-locating and refining Method refall

Number of reflections used 1867

Number of L.S. restraints 0

Number of refined Parameters 114

Goodness-of-fit on F^2 1.149
S {=[SUM w(Fo^2-Fc^2)^2]/(n-p)^1/2}, n= number of reflections,
p= Parameters used.
w=1/[\s^2^(Fo^2^)+(0.0548P)^2^+0.3965P] where P=(Fo^2^+2Fc^2^)/3

Maximum delta/sigma 0.000

Maximun e-density 0.272 e.A^-3

Minimun e-density -0.400 e.A^-3

Table 2.19 Computer Programs used for **8**.

Data collection program	STOE X-AREA
Cell refinement program	STOE X-AREA
Data reduction program	STOE X-RED
Structure Solving Program	SHELXS
Structure Refinement Program	SHELXL-2014/7 (Sheldrick, 2014)
Pictures drawn with	PLATON
Tables made with	CIFTAB
Extinction coefficient	n/a

Table 2.20 Atomic coordinates (x 10^4) and equivalent isotropic displacement parameters (A^2 x 10^3) for **8**.
U(eq) is defined as one third of the trace of the orthogonalized
Uij tensor.

---

x	y	z	U(eq)

C(1)	-155(1)	5254(2)	1141(1)	21(1)
C(2)	-1142(1)	4399(2)	209(1)	22(1)
C(3)	-1218(1)	2508(2)	-69(1)	28(1)
C(4)	-180(1)	1462(2)	972(1)	32(1)
C(5)	979(1)	2244(2)	1497(1)	31(1)
C(6)	-2188(1)	5375(2)	-588(1)	25(1)
N(1)	-136(1)	6971(1)	1355(1)	27(1)
N(2)	-3049(1)	6150(2)	-1254(1)	35(1)
S(1)	1231(1)	4303(1)	2177(1)	28(1)

Table 2.21 Bond lengths [A] and angles [deg] for **8**.

C(1)-C(2)	1.3632(16)
C(1)-N(1)	1.3703(15)
C(1)-S(1)	1.7451(12)
C(2)-C(6)	1.4151(16)
C(2)-C(3)	1.5137(17)
C(3)-C(4)	1.5229(19)
C(3)-H(3A)	0.983(17)
C(3)-H(3B)	0.96(2)
C(4)-C(5)	1.513(2)
C(4)-H(4A)	0.933(17)
C(4)-H(4B)	0.995(19)
C(5)-S(1)	1.8095(14)
C(5)-H(5A)	0.994(18)
C(5)-H(5B)	0.94(2)
C(6)-N(2)	1.1542(18)
N(1)-H(1N)	0.893(18)
N(1)-H(2N)	0.875(19)
C(2)-C(1)-N(1)	123.69(11)
C(2)-C(1)-S(1)	123.95(9)
N(1)-C(1)-S(1)	112.35(9)
C(1)-C(2)-C(6)	117.12(10)
C(1)-C(2)-C(3)	126.05(11)
C(6)-C(2)-C(3)	116.82(11)
C(2)-C(3)-C(4)	113.17(11)
C(2)-C(3)-H(3A)	109.7(10)
C(4)-C(3)-H(3A)	109.7(10)
C(2)-C(3)-H(3B)	108.0(11)
C(4)-C(3)-H(3B)	109.0(11)
H(3A)-C(3)-H(3B)	107.1(15)
C(5)-C(4)-C(3)	111.33(11)
C(5)-C(4)-H(4A)	110.4(11)
C(3)-C(4)-H(4A)	110.5(11)
C(5)-C(4)-H(4B)	110.3(11)
C(3)-C(4)-H(4B)	107.9(10)
H(4A)-C(4)-H(4B)	106.3(14)
C(4)-C(5)-S(1)	111.54(10)
C(4)-C(5)-H(5A)	112.0(11)
S(1)-C(5)-H(5A)	108.2(10)

C(4)-C(5)-H(5B)	112.1(12)
S(1)-C(5)-H(5B)	104.5(12)
H(5A)-C(5)-H(5B)	108.2(15)
N(2)-C(6)-C(2)	178.70(14)
C(1)-N(1)-H(1N)	115.9(11)
C(1)-N(1)-H(2N)	115.6(12)
H(1N)-N(1)-H(2N)	115.9(16)
C(1)-S(1)-C(5)	101.43(6)

Symmetry transformations used to generate equivalent atoms:

Table 2.22 Torsion-angles for **8**.

N(1)-C(1)-C(2)-C(6)	1.64(18)
S(1)-C(1)-C(2)-C(6)	-176.73(9)
N(1)-C(1)-C(2)-C(3)	-179.81(12)
S(1)-C(1)-C(2)-C(3)	1.81(19)
C(1)-C(2)-C(3)-C(4)	17.57(19)
C(6)-C(2)-C(3)-C(4)	-163.88(12)
C(2)-C(3)-C(4)-C(5)	-52.98(16)
C(3)-C(4)-C(5)-S(1)	67.45(14)
C(2)-C(1)-S(1)-C(5)	10.10(12)
N(1)-C(1)-S(1)-C(5)	-168.44(9)
C(4)-C(5)-S(1)-C(1)	-42.91(11)

Table 2.23 Anisotropic displacement parameters (A^2 x 10^3) for **8**.

The anisotropic displacement factor exponent takes the form:
-2 pi^2 [h^2 a*^2 U11 + ... + 2 h k a* b* U12]

	U11	U22	U33	U23	U13	U12
C(1)	20(1)	22(1)	19(1)	2(1)	12(1)	2(1)
C(2)	19(1)	22(1)	21(1)	1(1)	12(1)	1(1)
C(3)	26(1)	23(1)	29(1)	-3(1)	16(1)	-4(1)
C(4)	35(1)	21(1)	36(1)	5(1)	24(1)	1(1)
C(5)	28(1)	26(1)	32(1)	6(1)	18(1)	8(1)
C(6)	19(1)	27(1)	22(1)	-3(1)	12(1)	-2(1)
N(1)	22(1)	24(1)	26(1)	-5(1)	13(1)	1(1)
N(2)	22(1)	37(1)	31(1)	1(1)	13(1)	6(1)
S(1)	17(1)	30(1)	22(1)	2(1)	8(1)	4(1)

Table 2.24 Hydrogen coordinates (x 10^4) and isotropic displacement parameters (A^4 x 10^3) for **8**.

	x	y	z	U(eq)
H(3A)	-1279(15)	2380(20)	-729(15)	32(4)
H(3B)	-1933(17)	2060(20)	-320(16)	42(5)
H(4A)	-213(15)	1370(20)	1539(15)	32(4)
H(4B)	-255(16)	270(20)	694(15)	39(4)
H(5A)	1019(16)	2410(20)	900(16)	38(4)
H(5B)	1627(18)	1560(30)	2108(17)	46(5)
H(1N)	526(16)	7360(20)	2049(15)	32(4)
H(2N)	-792(17)	7390(20)	1110(15)	36(4)

Table 2.25 Hydrogen-bonds for **8** [A and deg.].

D-H...A	d(D-H)	d(H...A)	d(D...A)	<(DHA)
N(1)-H(1N)...N(2)#1	0.893(18)	2.290(18)	3.1668(16)	166.8(15)
N(1)-H(2N)...N(2)#2	0.875(19)	2.286(19)	3.1069(16)	156.3(15)

Symmetry transformations used to generate equivalent atoms:
#1 x+1/2,-y+3/2,z+1/2 #2 -x-1/2,-y+3/2,-z

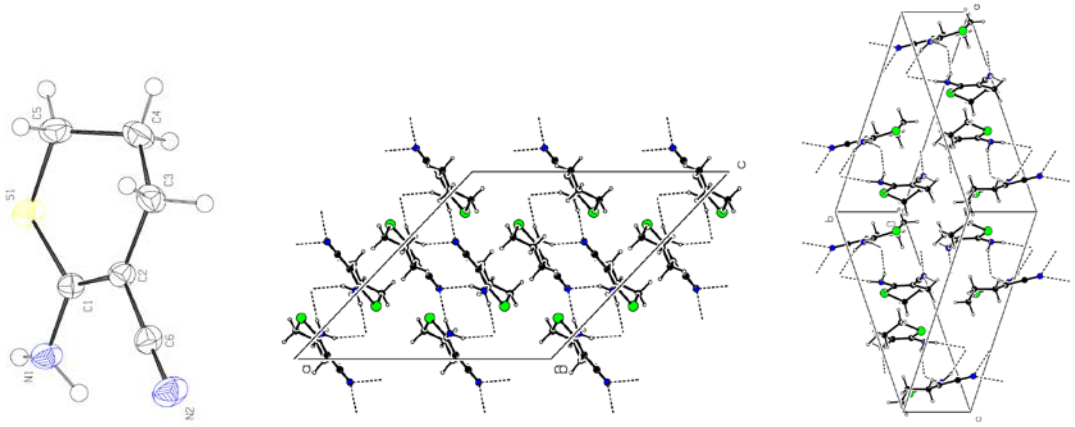

Figure 2.50 ORTEP plot of **8**.

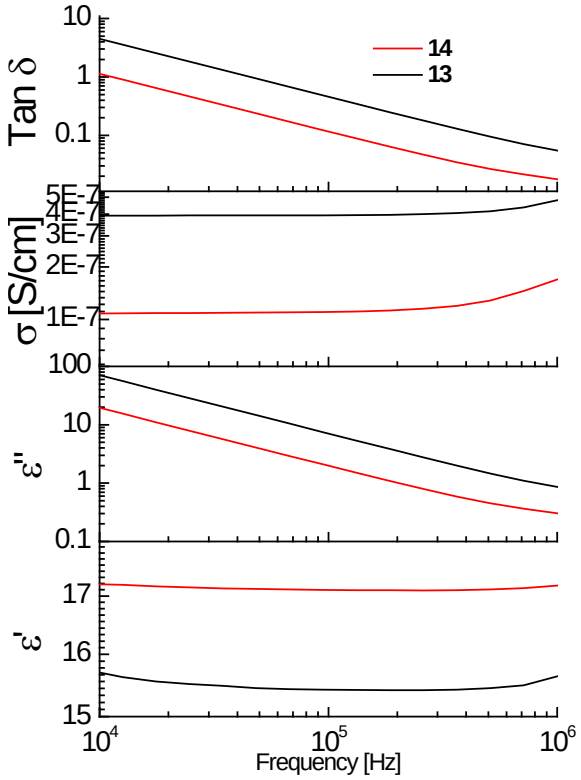

Figure 2.51 Dielectric properties (permittivity, dielectric loss, conductivity, and loss factor) as function of frequency for **13** and **14**.

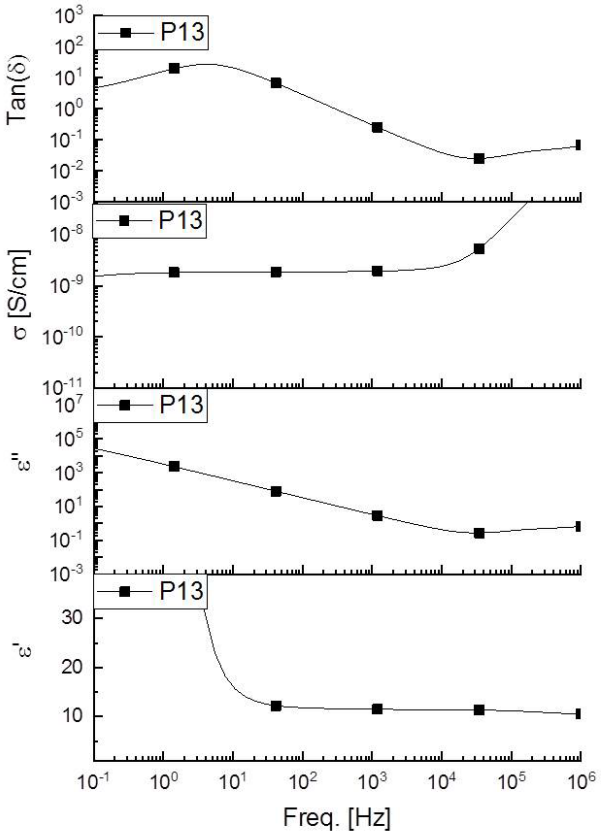

Figure 2.52 Dielectric properties (permittivity, dielectric loss, conductivity, and dielectric loss factor) as function of frequency for poly(3-cyanopropyl-2-thioethyl-2-thioethyl)methylsiloxane **P13**.

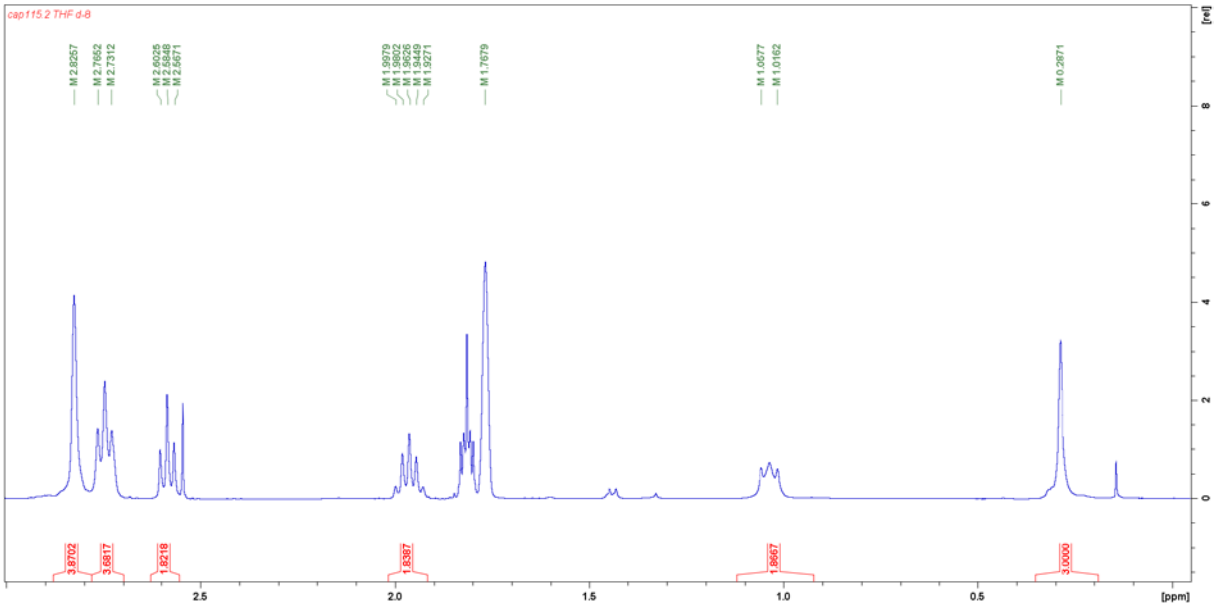

Figure 2.53 ^{1}H NMR spectrum of **P13**.

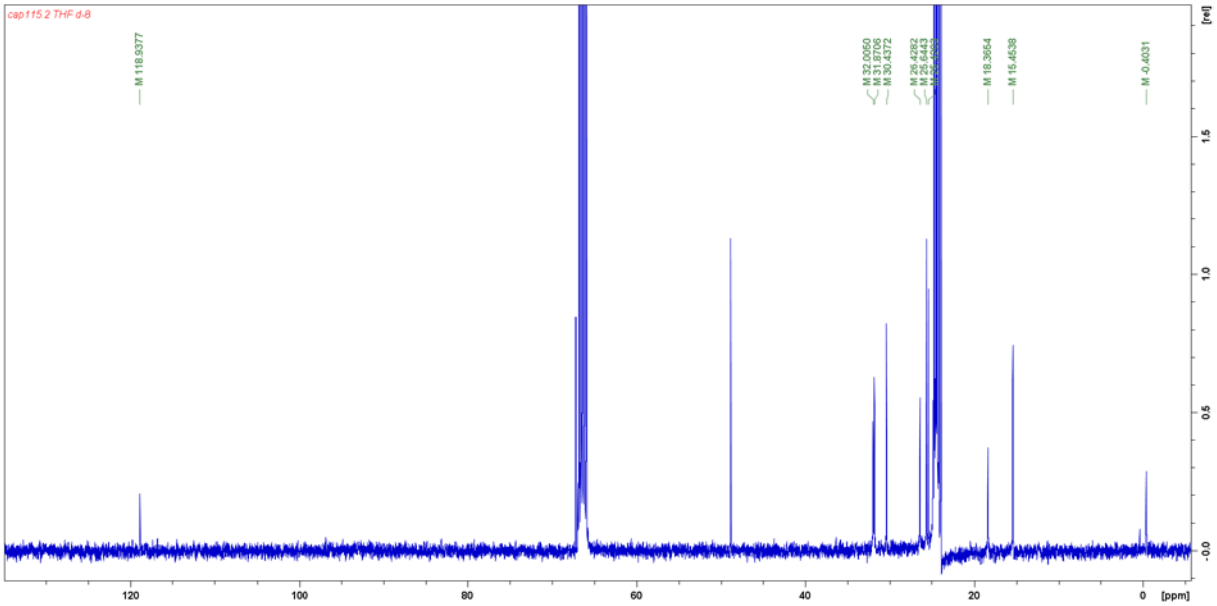

Figure 2.54 ^{13}C NMR spectrum of **P13**.

Chapter 3 Dielectric Elastomer Actuators with Increased Dielectric Permittivity and Low Leakage Current

This chapter is based on the publication

Dielectric elastomer actuators with increased dielectric permittivity and low leakage current capable of suppressing electromechanical instability

by

Philip Caspari,[1,2] Simon J. Dünki,[1,2] Frank A. Nüesch,[1,2] Dorina M. Opris[2]

[1]Ecole Polytechnique Fédérale de Lausanne (EPFL), Institut des matériaux, Station 12, CH 1015, Lausanne, Switzerland.

[2]Empa, Swiss Federal Laboratories for Materials Science and Technology, Laboratory for Functional Polymers, Ueberlandstr. 129, CH-8600, Dübendorf, Switzerland

Adapted from

J. Mater. Chem. C **2018**, *6,* 2043.

DOI: 10.1039/c7tc05562e

https://pubs.rsc.org/en/Content/ArticleLanding/2016/RA/C6RA21948A#!divAbstract

with permission from the Royal Society of Chemistry

Author Contributions:

P. Caspari performed the preparation of compounds and devices as well as their characterization and contributed to the manuscript.

3.1 Abstract

Dielectric elastomers with increased dielectric permittivity (*ε'*), excellent insulating and mechanical properties have a broad application potential ranging from flexible electronics to dielectric elastomer transducers. Up to date, several reports exist on elastomers with increased permittivity, but unfortunately in most cases this increase in permittivity is associated with an increase in conductivity, which detrimentally affects the insulating properties, such as leakage current and dielectric breakdown. Here, novel polysiloxane based elastomers were prepared in three steps starting from a silanol end-terminated poly(methylvinyl)siloxane, whose vinyl groups were reacted with alkyl thiols *via* thiol-ene reaction. The resulting polymers were cross-linked using condensation reactions and the dielectric, mechanical and electromechanical properties were evaluated. Eventually, an optimized material with a relative permittivity of $\varepsilon' = 5.4$, a conductivity of 4×10^{-11} S cm^{-1}, a storage modulus of 300 kPa, and a mechanical loss factor below 0.05 was achieved. Actuators constructed from this optimized material showed no electromechanical instability in the absence of prestrain. An area actuation strain of about 200% at an electric field of 53 V µm^{-1} was achieved. This excellent electromechanical behavior can be rationalized by the increased permittivity due to the thioether side chain and its favorable strain-stiffening effect on the material when crosslinked with polar alkoxysilanes. The actuators gave a stable lateral actuation strain of 10% for more than 50000 cycles when subjected to an electric field of 27 V µm^{-1} at a modulation frequency of 8 Hz. Due to the combined properties of this material such as a low leakage current density of 0.5 µA cm^{-2} at 27 V µm^{-1}, an attractively low glass transition temperature, a very fast electromechanical response and an increased permittivity, the dielectric elastomers developed in this work may be considered as future replacement for polydimethylsiloxane elastomers in dielectric elastomer transducers.

3.2 Introduction

Dielectric elastomers (DEs) with increased dielectric permittivity and high dielectric breakdown field are important materials for future electromechanical transducers (DETs).[1-7] Such devices can convert electrical into mechanical energy (actuator mode)[1-5] or *vice versa* (generator mode)[6] and can sense changes in pressure due to capacitance changes with strain.[7] While for the last application, the dielectric breakdown is not a critical parameter, for the first two applications, elastomers with high breakdown field are advantageous.[8] Unfortunately, dielectric elastomer actuators (DEAs) are prone to electromechanical instability (EMI), which sets in at an area actuation strain of about 40%.[9-12] As the voltage *U* increases and the thickness of the dielectric elastomer *d* decreases, the electric field *U*/*d* increases rapidly, which leads to a positive feedback of the dielectric elastomer, also known as *pull-in* or *snap-through* instability. This effect may cause electrical breakdown of the dielectric elastomer.[10] According to Stark and Garton, dielectric breakdown is proportional to the square root of the elastic modulus.[8] It has been shown that the stress-strain characteristics of an elastomer can be tuned such as to suppress EMI in actuators.[13,14] This can be achieved with materials that show a strain-stiffening effect, *e.g.* a sharp increase in the elastic modulus above a certain strain.[11] This concept was nicely confirmed experimentally using prestrained VHB foil for which giant area expansions as high as 1600% were reported.[15-17] While prestraining the films can increase the actuation strain, the energy density and allows for actuation in a predetermined direction, several disadvantages can be noted.[1] Firstly, prestraining the elastomer implies an additional processing step and is therefore time consuming. Secondly, it requires rigid frames to maintain the tension in the films, which increases the volume and the mass of the device.[18,19] Thirdly, actuator life time is significantly reduced due to creep and fatigue of the elastomer. Therefore, it would be advantageous to have elastomers capable of suppressing EMI while unprestrained. Unfortunately, most available elastomers such as polydimethylsiloxanes and acrylates show strain-stiffening only at very high strains and thus actuation is hampered by EMI.

It was proposed that interpenetrated polymer networks, swelled networks, or cross-linked bottle-brush polymers may be able to overcome the EMI.[11] Meanwhile, novel DE materials and composites have been developed showing high actuation in the absence of prestrain. For example, block copolymers swollen with an aliphatic oil, an interpenetrated network based on prestrained VHB and a poly(1,6-hexanediol diacrylate) network formed inside[20] as well as interpenetrating networks composed of long and short polymer chains were shown to be capable of overcoming EMI.[20-23] Most recently, cross-linked bottlebrush polymers were introduced as DE materials for actuators.[24] Bottlebrush elastomers are inherently prestrained due to the steric demand of the side chains. By varying side chain length, grafting density, and cross-link density, elastomers with elastic moduli that vary from 1 MPa to 100 Pa with a relative permittivity of $\varepsilon' = 2.95$ were prepared.

Despite the substantial amount of research on high permittivity elastomers, none of the reported materials combines a high permittivity with low glass transition temperature (T_g) and favorable mechanical properties that suppress EMI.[25-28] To increase the permittivity, composites containing polarizable fillers such as conductive particles and high permittivity ceramics as well as low T_g polar polymers have been used.[28] The increase in permittivity ε' is usually accompanied by an increase in conductivity.[29,30] Actuators constructed with such materials have usually a low breakdown field and thus suffer premature breakdown. Madsen *et al.* reported that silicones modified with chloropropyl groups have $\varepsilon' = 4.7$ and an increased dielectric breakdown field, which according to the authors is due to the presence of chlorine in the materials.[31] By replacing the chloropropyl groups with chloromethyl groups, elastomers with even higher dielectric permittivity of $\varepsilon' = 6$ and a breakdown strength of 60 V µm^{-1} were achieved.[32] While none of these materials was evaluated in electromechanical tests, it seems that the presence of chlorine increases the dielectric strength of silicone elastomers.

We have recently introduced a novel elastomer for actuators, a polysiloxane modified with butylthioether side groups. Its dielectric permittivity is $\varepsilon' = 4.3$, higher as compared to regular polydimethylsiloxane (PDMS) elastomers ($\varepsilon' \sim 3$) and it actuates at lower electric field. However, the dielectric breakdown occurred at 23 V µm^{-1}. [29,33,34]

Encouraged by the theoretical predictions and the outstanding performance of bottle brush polyacrylate actuators,[24] we developed a high permittivity silicone elastomer which is capable of suppressing EMI while unprestrained. It also has a fast response time which is comparable to PDMS elastomers.[35] To achieve this material, we first investigated the influence of alkyl-thioether side groups of different lengths grafted on the polysiloxane on T_g, mechanical, dielectric, and electromechanical properties. Our approach consisted of optimizing the length of the alkyl chain allowing the formation of materials with good mechanical properties and maximum increase in permittivity while suppressing electromechanical instability. This allowed us to develop a silicone elastomer that showed unprecedentedly high actuation strain, fast electromechanical response and high reliability. Because of its low leakage current and low glass transition temperature, this material can be considered as a serious alternative to regular PDMS elastomers for DE applications.

3.3 Experimental section

3.3.1 Materials and methods

Unless otherwise stated, all chemicals were reagent grade and used without purification. 1,3,5,7-Tetramethyl-1,3,5,7-tetravinyl cyclotetrasiloxane (**V4**), (25-35% methylhydrosiloxane)-dimethylsiloxane (AB109380) **A** and polydimethylsiloxane (AB116665, $M_n = 90.000$ g mol^{-1}, $M_w = 130.000$ g mol^{-1}) were purchased from ABCR. 2,2-Dimethoxy-2-phenylacetophenone (DMPA), ethanethiol, 1-propanethiol, 1-butanethiol, 1-hexanethiol, 1-octanethiol, tetramethylammonium hydroxide 25% in MeOH (TMAH), 3-chlorpropyltriethoxysilane, 2-cyaonoethyltriethoxysilane, and dibutyltin dilaurate were purchased from Aldrich. Methanol and tetrahydrofuran were purchased from VWR. The synthesis of polymethylvinylsiloxane **P0** was done according to the literature ($M_n = 91.000$ g mol^{-1}, $M_w = 176.000$ g mol^{-1}, PDI = 1.93). Films of Elastosil®Film (200 µm, 100 µm, 50 µm, 20 µm) were provided by DRAWIN Vertriebs-GmbH, Riemerling. PVA was purchased from Swiss Composite. Photoreactions were conducted with a UVAHAND 250 GS H1 mercury vapor UV lamp from Dr. Hoenle AG.

^{1}H and ^{13}C NMR spectra were recorded at 298 K on a Bruker Avance 400NMR spectrometer using a 5 mm broadband inverse probe at 400.13 and 100.61 MHz, respectively. Chemical shifts (δ) in ppm were calibrated to residual solvent peaks ($CDCl_3$: δ = 7.26 and 77.16 ppm).

Gel permeation chromatograms were recorded using an Agilent 1100 Series HPLC (Columns: serial coupled PSS SDV 5 m, 100A and PSS SDV 5 m, 1000A, detector: DAD, 235 nm and 360 nm; refractive index), with THF as mobile phase. PDMS standards were used for calibration and toluene as an internal standard.

Differential scanning calorimetry (DSC) investigations were undertaken on a Pyris Diamond DSC (Perkin Elmer USA) instrument under a nitrogen flow (50 ml × min^{-1}), in aluminum crucibles shut with pierced lids and using a 10 mg sample mass.

The tensile tests were performed on a Zwick Z010 tensile test machine with a crosshead speed of 50 mm min^{-1} (278% min^{-1}). Tensile test specimens with a gauge width of 2 mm and a gauge length of 18 mm were prepared by die cutting. The strain was determined using a longitudinal strain extensometer. The curves were averaged from 3 different samples. The elastic

modulus *Y* was determined from the slope of the stress–strain curves using a linear fit to the data points within ±5% strain. Dynamic mechanical analysis was carried out on a RSA 3 DMA from TA Instruments. Stripes of 10 mm × 20 mm were measured under a dynamic load of 2 g, at 2% strain in the frequency range of 0.05–10 Hz at 25 °C. $Tan(\delta)_{DMA}$ is given as the fraction of imaginary and real elastic modulus at 2% strain.

Permittivity measurements were performed in the frequency range from 10^{-1} Hz to 10^{6} Hz using a Novocontrol Alpha-A frequency analyzer. The VRMS (root mean square voltage) of the probing AC electric signal applied to the samples was 1 V. Au electrodes with a thickness of 20 nm were sputtered on both sides of the film. The permittivity ε' was determined from the capacitance $C= \varepsilon'\varepsilon_0 A/d$, where A is the electrode area, d is the thickness of the film, and ε_0 is the vacuum permittivity. The thickness of the film was measured by a micrometer gauge with an uncertainty of ±5 µm. For temperature variable dielectric spectroscopy (BDS) measurements a high impedance Alpha Analyzer combined with a Quatro temperature controller (both from Novocontrol) has been employed to cover a broad frequency and temperature range from 10^{-1} Hz to 10^{6} Hz and from -150 to 60 °C, respectively. Two stainless steel discs with a diameter of 20 mm served as electrodes which were separated by three glass fibers with a diameter of 100 µm± 5 µm. The samples were annealed at 80 °C for 18 h at 10 mbar to remove any residual solvents before isothermal measurements were performed. During measurement the samples were kept in dry nitrogen atmosphere.

Electromechanical tests were performed using circular membrane actuators, for which the films were fixed between two circular frames. Circular electrodes (8 mm diameter) of carbon black powder were applied to each side of the film. A custom-made radial stretching device was used to prestrain the samples. Samples **E2**, **E3**, **Er**, **En-X-Y**, were prestrain biaxially by 7.5%, while sample **E3-Cl-20** different biaxial prestrains were used: 0%, 22.5, and 30%. A FUG HCL- 35-12500 high voltage source served as power supply for actuator tests. The voltage was increased by 50 V steps every 2 s up to maximum 5.6 kV. The actuation strain was measured optically as the extension of the diameter of the electrode area *via* a digital camera, using an edge detection tool of a LabView program to detect the boundary between the black electrode area and the transparent silicone film. The maximum resolution of LabView was 30 measurements per second. Leakage current was measured up to a voltage of 5 kV.

3.3.2 Synthesis of Pn

To a solution of **P0** (20.01 g, 232.2 mmol of vinyl groups, 1 eq) in dry THF (200 ml), alkylthiol (464.5 mmol, 2.0 eq thiol, 28.80 g of ethanethiol for **P2**, 35.30 g of 1-propanethiol for **P3**, 41.81 g of 1-butanethiol for **P4**, 54.81 g of 1-hexanethiol for **P6**, 67.82 g 1-octanethiol for **P8**, 80.98 g 1-decanethiol for **P10,** 93.83 g 1-dodecanethiol for **P12,** respectively) and DMPA (560 mg, 2.18 mmol, 0.009 eq) were added. The solution was degassed by three freeze-pump-thaw cycles and irradiated with UV light for 5 min. It was then concentrated *in vacuo* to about 50 ml. To this concentrated solution, methanol was added whereupon the polymer precipitated. The polymer was redissolved in THF and again precipitated with methanol. The dissolution/precipitation process was repeated three times. The highly viscous liquids were then dried at 10^{-2} mbar at 60 °C to obtain **P2**-**P8** in 90-95% yield.

P2: ^{1}H NMR (400 MHz, $CDCl_3$, δ): 2.58 – 2.50 (m, 4H, -C*H*$_2$-S-C*H*$_2$-), 1.24 (t, ^3J= 7.4 Hz, 3H, -CH_2-C*H*$_3$), 0.92 – 0.86 (m, 2H, Si-C*H*$_2$-CH_2-), 0.13 (s, 3H, Si-C*H*$_3$); ^{13}C NMR (100 MHz, $CDCl_3$, δ): 25.9, 25.8, 18.4, 14.8, 0.0.

P3: ^{1}H NMR (400 MHz, $CDCl_3$, δ): 2.57 – 2.48 (m, 4H, -C*H*$_2$-S-C*H*$_2$-), 1.60 (tq, ^3J= 7.3 Hz, ^3J= 7.3 Hz, 2H, -C*H*$_2$-CH_3), 0.99 (t, ^3J= 7.3 Hz, 3H, -CH_2-C*H*$_3$), 0.92 – 0.87 (m, 2H, Si-C*H*$_2$-CH_2-), 0.14 (s, 3H, Si-C*H*$_3$); ^{13}C NMR (100 MHz, $CDCl_3$, δ): 34.2, 26.5, 23.0, 18.6, 13.8, 0.1.

P4: ^{1}H NMR (400 MHz, $CDCl_3$, δ): 2.60 – 2.48 (m, 4H, -C*H*$_2$-S-C*H*$_2$-), 1.60 – 1.52 (m, 2H, C*H*$_2$-CH_2-CH_3), 1.46 – 1.37 (m, 2H, C*H*$_2$-CH_3), 0.94 – 0.87 (m, 5H, Si-C*H*$_2$-, CH_2-C*H*$_3$), 0.14 (s, 3H, Si-C*H*$_3$); ^{13}C NMR (100 MHz, $CDCl_3$, δ): 31.9, 31.8, 22.2, 18.5, 13.9, 0.1.

P6: ^{1}H NMR (400 MHz, $CDCl_3$, δ): 2.57-2.49 (m, 4H, -C*H*$_2$-S-C*H*$_2$-), 1.60-1.53 (m, 2H, C*H*$_2$-CH_2-CH_3), 1.42 – 1.35 (m, 2H, C*H*$_2$-CH_3), 1.33 – 1.25 (m, 4H, -C*H*$_2$-C*H*$_2$-CH_2-CH_2-CH_3), 0.90 – 0.87 (m, 5H, Si-C*H*$_2$-, CH_2-C*H*$_3$), 0.14 (s, 3H, Si–C*H*$_3$); ^{13}C NMR (100 MHz, $CDCl_3$, δ): 32.3, 31.7, 29.8, 28.9, 26.6, 22.8, 18.5, 14.3, 0.2.

P8: ^{1}H NMR (400 MHz, $CDCl_3$, δ): 2.57-2.49 (m, 4H, -C*H*$_2$-S-C*H*$_2$-), 1.60-1.53 (m, 2H, C*H*$_2$-CH_2-CH_3), 1.42 – 1.33 (m, 2H, C*H*$_2$-CH_3), 1.27 (br s, 8H, -S-CH_2-(C*H*$_2$)$_4$-CH_2-CH_2-CH_3), 0.92 – 0.85 (m, 5H, Si-C*H*$_2$-, CH_2-C*H*$_3$), 0.13 (s, 3H, Si–C*H*$_3$); ^{13}C NMR (100 MHz, $CDCl_3$, δ): 32.3, 32.0, 29.8, 29.5, 29.4, 29.3, 26.6, 22.9, 18.5, 14.3, 0.1.

P10: ^{1}H NMR (400 MHz, $CDCl_3$, δ): 2.58-2.48 (m, 4H, -C*H*$_2$-S-C*H*$_2$-), 1.60-1.52(m, 2H, C*H*$_2$-CH_2-CH_3), 1.44 – 1.33 (m, 2H, C*H*$_2$-CH_3), 1.29 (br s, 12H, -S-CH_2-(C*H*$_2$)$_6$-CH_2-CH_2-CH_3), 0.92 – 0.85 (m, 5H, Si-C*H*$_2$-, CH_2-C*H*$_3$), 0.13 (s, 3H, Si–C*H*$_3$); ^{13}C NMR (100 MHz, $CDCl_3$,δ): 32.31, 32.07, 29.80, 29.55, 29.51, 29.27, 26.60, 22.80, 18.49, 14.24, 0.08.

P12: ^{1}H NMR (400 MHz, $CDCl_3$, δ): 2.56-2.48 (m, 4H, -C*H*$_2$-S-C*H*$_2$-), 1.60-1.53 (m, 2H, C*H*$_2$-CH_2-CH_3), 1.43 – 1.34 (m, 2H, C*H*$_2$-CH_3), 1.25 (br s, 16H, -S-CH_2-(C*H*$_2$)$_4$-CH_2-CH_2-CH_3), 0.92 – 0.85 (m, 5H, Si-C*H*$_2$-, CH_2-C*H*$_3$), 0.13 (s, 3H, Si–C*H*$_3$); ^{13}C NMR (100 MHz, $CDCl_3$, δ): 32.33, 32.08, 29.90, 29.88, 29.85, 29.81, 29.56, 29.55, 29.32, 26.62, 22.86, 18.52, 14.28, 0.09.

3.3.3 General synthesis of the elastomers

A solution of **Pn** (4 g), cross-linker **A**, **Cl-CL**, or **CN-CL** (for the amount used, see Table 3.1), and dibutyltin dilaurate (80 µl, 0.056 g, 0.1 mmol) in THF (4 ml) was casted on a PTFE or PVA/glass substrate by doctor blade technique. The films were stored in a closed chamber at ambient temperature of 25 °C and humidity 30% for 48 h. The films were dried at 70 °C *in vacuo* for 12 h before further testing.

Table 3.1 The amount of reagents used for the synthesis of **En** and **En-X-Y**.

Entry	Polymer	Polymer [g]	**A** [ml]	**Cl-CL** [g]	**CN-CL** [g]
Er	PDMS	4	0.21	-	-
E2	**P2**	4	0.13	-	-
E3	**P3**	4	0.13	-	-
E4	**P4**	4	0.12	-	-
E6	**P6**	4	0.11	-	-
E8	**P8**	4	0.09	-	-
E10	**P10**	4	0.08	-	-
E12	**P12**	4	0.07	-	-
Er-Cl-33	PDMS	4	-	2 g	-
Er-Cl-20	PDMS	4	-	1 g	-
E2-Cl-33	**P2**	4	-	2 g	-
E2-Cl-20	**P2**	4	-	1 g	-
E3-Cl-33	**P2**	4	-	2 g	-
E3-CL-20	**P3**	4	-	1 g	-
E2-CN-33	**P2**	4	-	-	2 g
E2-CN-20	**P2**	4	-	-	1 g
E3-CN-33	**P3**	4	-	-	2 g
E3-CN-20	**P3**	4	-	-	1 g

3.4 Results and discussion

A series of polysiloxanes, $\mathbf{P_n}$, modified with alkyl-thioethers of different length, where 'n' refers to the number of C-atoms in the alkyl chains, was synthesized starting from a silanol-terminated poly(methylvinyl)siloxane $\mathbf{P_0}$ (M_n = 91.000 g mol^{-1}) *via* photoinduced thiol-ene addition with various alkyl thiols (Scheme 3.1; Figure 3.9 and 3.10 (see Section 3.7)). All reactions were carried out with the same batch of $\mathbf{P_0}$. The disappearance of the vinyl groups in the ^{1}H NMR spectra of the final products was used as a clear indication for the success of the post-polymerization modification (Figure 3.11-3.24, Section 3.7). Differential scanning calorimetry (DSC) was conducted to investigate the influence of the alkyl-thioether length on both T_g and melting temperature (T_m) (Figures 3.25-3.31, Section 3.7). The results are compiled in Table 3.2. While polymers **P2**, **P3**, **P4**, and **P6** show a glass transition, they do not exhibit a melt transition. In contrast, polymers **P8**, **P10**, and **P12** do not undergo a glass transition, however, they do melt.

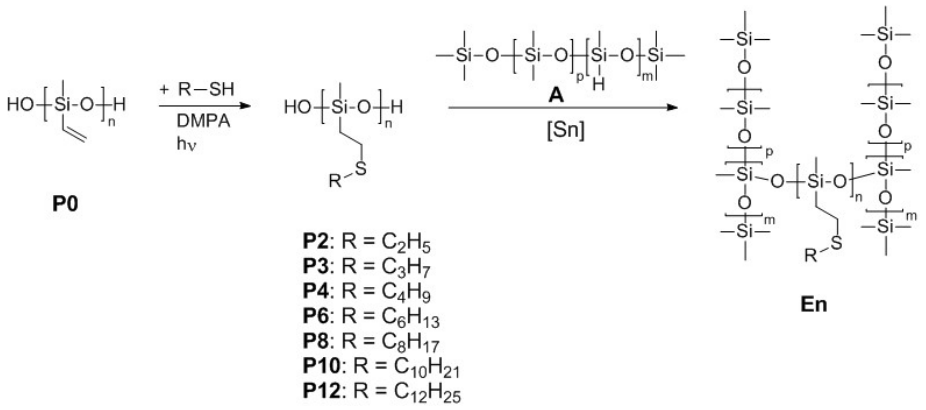

Scheme 3.1 Synthesis of polysiloxanes **Pn** modified with alkyl thioether groups and their cross-linking with (methylhydrosiloxane)-dimethylsiloxane-copolymer A (m: 25-30%; p: 75-70%) *via* tin-catalyzed dehydrogenative coupling reaction.

All polymers of Table 3.2 were cross-linked using (methylhydrosiloxane)-dimethylsiloxane-copolymer **A** cross-linker (m: 25-30%; p: 75-70%) to give materials **En**, whereby 'E' indicates that these products are elastomers and 'n' refers to the number of C-atoms in the lateral substituents. This was achieved with a tin-catalyzed dehydrogenative coupling reaction between the silanol end groups of the polymers and the hydrosilyl groups of **A** (Scheme 3.1). As reference material, **Er** was used which was obtained by cross-linking a silanol end-terminated polydimethylsiloxane (PDMS, M_n = 90.000 g mol^{-1}) with **A** under exact same conditions. The amount of cross-linker **A** was in all cases very low (5-2 wt-%) so that its influence on permittivity could be neglected. It was noted that the condensation reaction was slowed down for the polymers that carry a shorter thioalkyl group and thus a higher content of sulfur.

Table 3.2 Transition temperatures observed for **Pn**, the ΔC_p of the transitions, M_w, M_n, and PDI.

Pn	T [°C]			ΔC_p [J g^{-1} °C^{-1}]		M_w [g mol^{-1}]	M_n [g mol^{-1}]	PDI
	Tg[a)]	T_m[a)]	cooling[b)]	2nd heating	cooling[b)]			
P2	-93.3	-	-102.1	0.365	0.503	340.000	75.000	4.5
P3	-96.9	-	-103.1	0.387	0.499	225.000	90.000	2.5
P4	-97.5	-	-	0.395	-	220.000	100.000	2.2
P6	-92.9	-	-99.6	0.452	0.658	100.000	40.000	2.5
P8	-	-48.5	-63.1 (T_c)	-	-	640.000	55.000	11.6
P10	-	-9.3	-23.1 (T_c)	-	-	150.000	40.000	3.8
P12	-	16.2	1.4 (T_c)	-	-	350.000	60.000	5.8

a)Data from second heating cycle. b) Data from first coolingΔC_p is heat capacity.

First, it was checked whether the elastomers **En** form free standing films. As this was the case only for the networks **E2-E8**, only those materials were further investigated. The dielectric properties of **En** and **Er** were analyzed by impedance spectroscopy. As expected, an increase in the dielectric permittivity with increasing sulfur content in materials **En** was observed (Figure 3.1). Materials **E2** and **E3** had ε' = 5.4 and 5.2, respectively, whereas **Er** had ε'= 2.8. When the alkyl chain length in polymers **En** was further increased, the permittivity decreased. An increase in conductivity with increasing the sulfur content was observed from 2×10^{-14} S cm^{-1} for **Er** to 9.8×10^{-12} S cm^{-1} for **E3** and 3.56×10^{-11} S cm^{-1} for **E2**. The dielectric losses at high frequencies were also low, but increased with decreasing frequency due to electrode polarization.

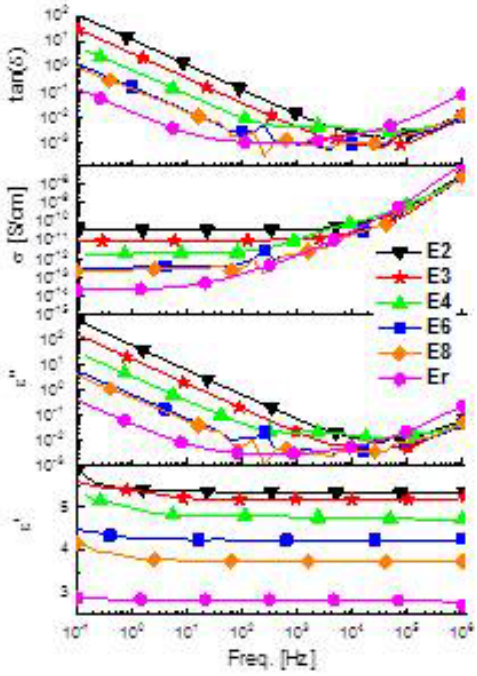

Figure 3.1 Dielectric properties of **E2**-**E8** and **Er**.

The mechanical properties of **En** were evaluated in tensile tests. The strain at break for all materials was below 200% and decreased with increasing alkyl chain length (Figure 3.2, Table 3.3). The elastic moduli of **En** slightly decreased at small strains and remained unchanged above a certain strain level, whereas the elastic moduli of the reference **Er** decreased for strains between 0% and 65%, remained almost unchanged up to 120%, and increased at strains above 120% (Figure 3.2 middle). **En** were further evaluated as dielectric in actuators for which 7.5% biaxial prestrain was used. Attempts to construct actuators from materials **E4**-**E8** were not successful as these materials were rather fragile and ruptured during manipulation. The mechanical properties of materials **E2** and **E3** allowed to construct circular actuator devices. Material **E2** gave 12% lateral strain at 15 V µm^{-1}, whereas **E3** gave 9.5% strain at 19 V µm^{-1} (Figure 3.2 right).

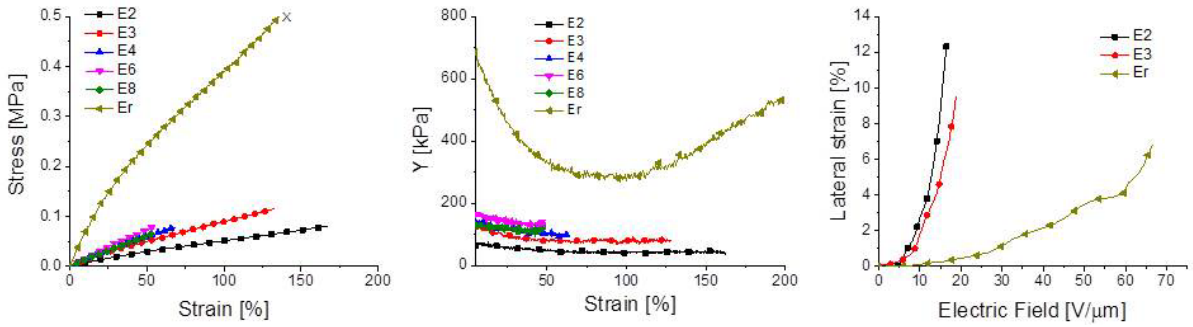

Figure 3.2 Stress-strain curves (left) and elastic moduli at different strains (middle) of **En** at a stretch rate of 50 mm min^{-1} as well as lateral actuation strain of **E2**, **E3** and **Er** as function of applied electric field (right). The stress-strain curves were averaged from 3 different samples.

Despite the low dielectric breakdown of the actuators constructed from **E2** and **E3**, their maximum actuation was higher as compared to **Er** which gave only 7% lateral actuation at much higher electric field of 66 V µm^{-1}. These results show the positive effect of the thioether side group on the electromechanical sensitivity ε/Y which enables high actuation strains of **E2** and **E3** at relatively low electric fields. However, the actuators' dielectric breakdown of 15 V µm^{-1} and 19 V µm^{-1} for E2 and E3, respectively, is too low.

Table 3.3 Dielectric, mechanical, and electromechanical properties of **E2**-**E8** and **Er**.

Entry	ε' @ 10^6 Hz	σ @ 10^{-1} Hz	tan(δ) @ 10^6 Hz	$Y_{10\%}$ [kPa]	s_{max} [%]	$s_{act,max}$ [%]	$E_{b,act}$ [V µm^{-1}]
Er	2.8	2 10^{-14}	0.08	600	300	7%	66
E2	5.4	3.56 10^{-11}	0.013	70	190	12%	15
E3	5.2	9.8 10^{-12}	0.010	120	150	10%	19
E4	4.7	1.9 10^{-12}	0.008	135	71	-	-
E6	4.2	3 10^{-13}	0.010	160	58	-	-
E8	3.7	2 10^{-13}	0.013	130	54	-	-

To evaluate whether **P2** and **P3** can be cross-linked to elastomers with improved properties, other cross-linking reactions were explored. It is known that the mechanical properties of polysiloxanes can be enhanced by fillers which are either *ex situ* or are generated *in situ*.[36-38] Homogenous materials with uniformly dispersed silica particles generated in-situ *via* hydrolysis and condensation of tetraethoxysilane were reported. More recently trialkoxy(alkyl)silanes with different polar groups were used to cross-link PDMS.[33,39] Trialkoxy(alkyl)silanes undergo condensation reactions with the silanol end-groups of the polysiloxane and also self-condensation reactions with formation of silsesquioxane structures. From all trialkoxy(alkyl)silanes used, 3-chloropropyl(triethoxy)silane (**Cl-CL**) and 2-cyanoethyl(triethoxy)silane (**CN-CL**) were found to allow formation of materials with improved dielectric and mechanical properties.[33,40] These cross-linkers have also attractive dielectric permittivity, *e.g.* $\varepsilon' = 5.8$ for **Cl-CL** and $\varepsilon' = 12.3$ for **CN-CL** (Figure 3.32, Section 3.7). Therefore, we used these two cross-linkers in two different concentrations, 33 wt-% and 20 wt-%, respectively to cross-link **P2** and **P3**. This allowed formation of materials **En-X-Y**, where 'E' indicates that these products are elastomers, 'n' refers to the number of C-atoms of the thiol used for the functionalization of **Pn**, X refers to the type and Y refers to the wt-% of cross-linker used, respectively. For example, the cross-linking of **P2** with 33 wt-% **Cl-CL** allowed formation of material **E2-Cl-33** and with 20 wt-% **Cl-CL** the formation of material **E2-Cl-20**. Materials with attractive mechanical properties formed after cross-linking for about 48 h at ambient temperature (Table 3.4).

Thermal stability of **En-X-Y** was investigated by TGA (Figure 3.33-3.43, Section 3.7) which showed that all elastomers are stable up to 370 °C where a small amount of volatiles is removed. Above 450 °C the elastomers lose more than half of their weight. DSC investigations show that these materials have no transition at temperatures above -80 °C which is an attractive feature (Figure 3.44-3.53, Section 3.7).

As expected, because **E2-X-Y** has a higher content of sulfur as compared to **E3-X-Y**, its dielectric permittivity is slightly higher as compared to **E3-X-Y** (Table 3.4). Furthermore, the permittivity increases with increasing the content of cross-linker. The dielectric permittivity of materials **En-CN-Y** was higher as compared to materials **En-Cl-Y**, but they also showed higher conductivity at low frequencies. Table 3.4 summarizes several dielectric characteristics of the new materials. The highest relative permittivity of $\varepsilon' = 7.0$ (10^6 Hz) was measured for **E2-CN-33**. This material has the highest content of both sulfur and polar nitrile groups (Figure 3.3). Unfortunately, also the conductivity was the highest $\sigma = 10^{-11}$ S cm^{-1} at 10^{-1} Hz. When **Cl-CL** was used, the highest achieved relative permittivity was $\varepsilon' = 6.4$ for material **E2-Cl-33** which has the highest content of sulfur and chlorine. A sharp increase in permittivity at low frequencies for all materials was observed. This increase is due to electrode polarization, due to ions accumulated at the electrodes.[41] This effect is stronger for elastomers containing the nitrile functionality.

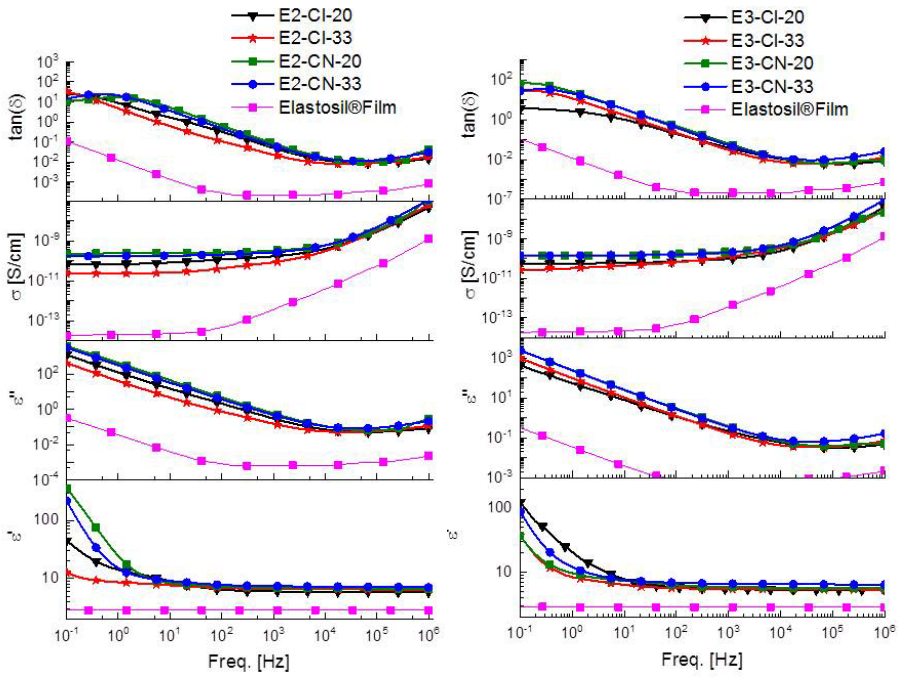

Figure 3.3 Dielectric properties of materials **E2-X-Y** (left) and **E3-X-Y** (right) as well as the one of the reference Elastosil®Film.

Dynamic mechanical analysis (DMA) was used to further characterize the elastic behaviour of our materials (Figure 3.4). The reference material **Elastosil®Film** had the highest storage modulus and has a low loss factor *tan(δ)* which did not change in the investigated frequency range. Materials **E2-X-Y** were softer as compared to **E3-X-Y** and showed larger loss factors which increased with frequency. Particularly, **E2-CN-Y** elastomers had a *tan(δ)* higher than 0.15 at frequencies above 2 Hz, which may be an indication of poor cross-linking. Swelling extraction tests conducted on **En-X-Y** are in agreement with the DMA results (Table 3.4). The highest amount of extractable was found for **E2-CN-Y**.

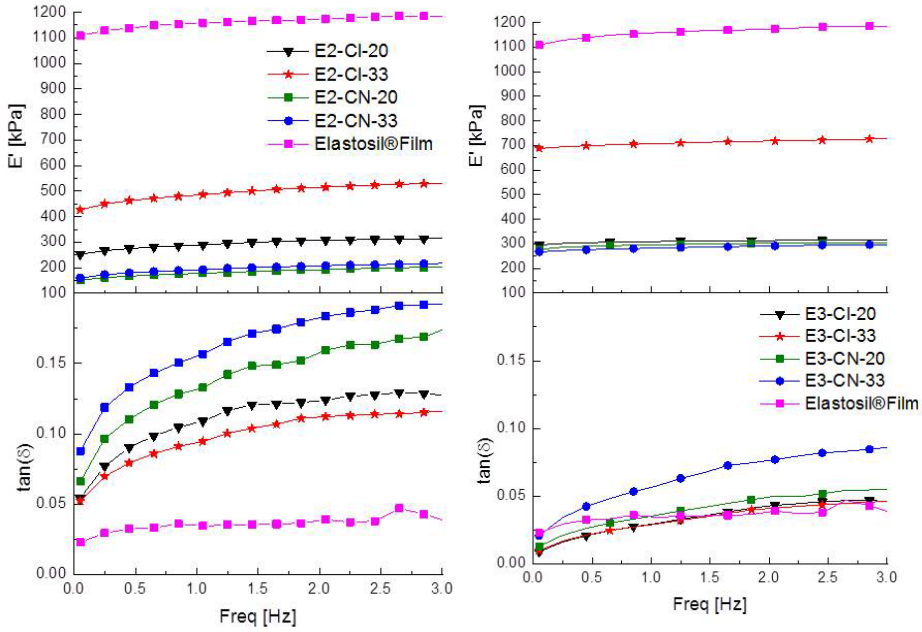

Figure 3.4 Dynamic mechanical analysis of **En-X-Y** and **Er** ranging from 0.05 Hz to 3 Hz at a strain of 2%.

Materials **E3-X-Y** showed very good mechanical properties with *tan(δ)* below 0.1 at all frequencies, with **E3-Cl-Y** showing the best performance. Material **E3-Cl-33** had a storage modulus of about 700 kPa while **E3-Cl-20** had a storage modulus of 300 kPa. Both materials showed a mechanical loss factor below 0.05 which only slightly increased with frequency (Figure 3.4).

Table 3.4 Dielectric and mechanical properties of **En-X-Y** and **Er**.

Entry	ε' @ 10^6 Hz	σ @ 10^{-1} Hz	$tan(\delta)$ @ 10^6 Hz	$Y_{(10\%)}$ [a)] [kPa]	$Y_{50\%}$ [a)] [kPa]	$Y_{100\%}$ [a)] [kPa]	s_{max} [%]	$tan(\delta)$ [b)] [2 Hz]	Extractable [%]
E2-Cl-20	5.8	$3\ 10^{-11}$	$5\ 10^{-2}$	330	640	1380	125	$1.2\ 10^{-1}$	17.2
E2-Cl-33	6.4	$1\ 10^{-11}$	$2\ 10^{-2}$	700	2600	-	65	$1.1\ 10^{-1}$	14.5
E2-CN-20	6.7	$1\ 10^{-10}$	$2\ 10^{-2}$	200	150	220	175	$1.6\ 10^{-1}$	27.6
E2-CN-33	7.0	$4\ 10^{-9}$	$4\ 10^{-2}$	250	220	470	190	$1.8\ 10^{-1}$	32.6
E3-Cl-20	5.4	$4\ 10^{-11}$	$2\ 10^{-2}$	370	500	1230	100	$4\ 10^{-2}$	13.4
E3-Cl-33	5.5	$4\ 10^{-11}$	$2\ 10^{-2}$	580	1380	-	60	$4\ 10^{-2}$	11.8
E3-CN-20	5.8	$1\ 10^{-10}$	$7\ 10^{-2}$	370	330	830	100	$5\ 10^{-2}$	17.8
E3-CN-33	6.3	$2\ 10^{-9}$	$3\ 10^{-2}$	250	370	-	80	$8\ 10^{-2}$	22.7
Er-Cl-20	2.9	$10\ 10^{-12}$	$2\ 10^{-3}$	500	260	190	350	$2\ 10^{-2}$	8.9
Er-Cl-33	3.4	$7\ 10^{-12}$	$2\ 10^{-3}$	530	260	170	390	$2\ 10^{-2}$	9.7
Er	2.8	$2\ 10^{-14}$	$8\ 10^{-2}$	600	320	280	300	$1\ 10^{-2}$	8.6
Elastosil® Film	2.9	$2\ 10^{-14}$	$1\ 10^{-3}$	1200	730	1040	486	$3\ 10^{-2}$	1.6

[a)]The elastic moduli were determined from the slope of the stress–strain curves using a linear fit to the data points within ±5% strain. These data were averaged from 3 different samples. [b)]Taken from DMA.

Figure 3.5 shows the unilateral stress-strain curves of **En-X-Y**. The strain at break of all materials was rather low, *e. g.* only two samples **E2-CN-20** and **E2-CN-33** showed a strain at break above 150% (Figures 3.54-3.69, Section 3.7). While this property is important for DETs operated in the generator mode, in actuator devices, the strain at break is not a limiting factor. Irrespective of the type of cross-linker used, the materials got stiffer with increasing the cross-linker content with the strongest effect observed for materials **En-Cl-Y**. The elastic moduli of materials **E2-CN-Y** were almost constant with strain. Materials **E2-Cl-Y** and **E3-X-Y** showed a strong increase in the elastic moduli at strains above 50%. For example **E3-Cl-33** showed a doubling in elastic modulus from *Y*= 580 kPa at 10% strain to *Y*= 1380 kPa at 50% strain. Two reference materials **Er-Cl-20** and **Er-Cl-33** were also prepared by cross-linking a silanol terminated PDMS with 20 wt-% and 33 wt-% **Cl-CL**, respectively. During cross-linking in thin films silsesquioxane structures are *in situ* generated. While, the reference materials **Er-X-Y** were becoming softer with the strain,[33] materials **E3-X-Y** and **E2-Cl-Y** showed a synergetic effect between the thioether side groups and the *in situ* generated silsesquioxane reflected by a rapid stiffening of the materials above a certain strain (Figure 3.5 d,e).

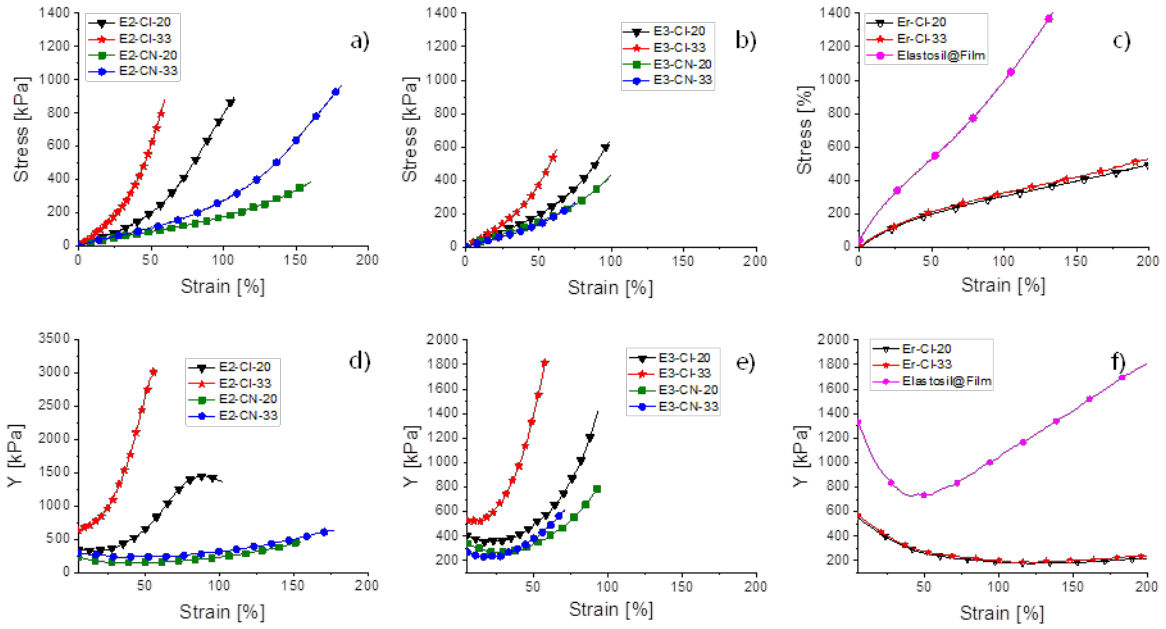

Figure 3.5 Stress-strain curves for materials **E2-X-Y** (a), **E3-X-Y** (b) and **Er-Cl-Y** and **Elastosil®Film** (c) and the elastic moduli at different strains for **E2-X-Y** (d), **E3-X-Y** (e) and **Er-Cl-Y** and **Elastosil®Film** (f). The stress-strain curves were averaged from three independent samples. The strain at break is the minimum value obtained from the three tests.

All materials **En-X-Y** were investigated in electromechanical tests using circular electrodes. As reference the commercially available PDMS elastomer Elastosil®Film was used. The films were bilaterally prestrained by 7.5% and fixed between two rigid plastic frames (Φ = 25 mm). Electrodes consisting of carbon black powder were smeared on both sides (Φ = 8 mm). Figure 3.6 gives the lateral actuation strain as function of applied electric field, while Table 3.5 summarizes the actuation sensitivity ($\varepsilon'/Y_{10\%}$) as well as the maximum actuation s_{max}, actuator breakdown E_b, lateral actuation at 10 V µm^{-1}, and thickness. It should be mentioned that due to out-of-plane deformation, *i.e.* buckling which typically set in at actuations above 10%, the lateral actuation cannot be accurately measured. Thus, the measured lateral actuation above 10% is underestimated (Figure 3.6).

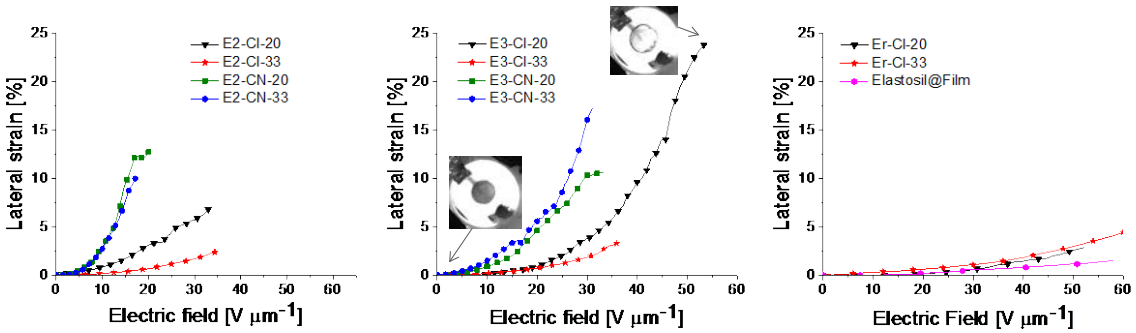

Figure 3.6 Lateral actuation as a function of the applied electric field of materials **E2-X-Y** (left), of **E3-X-Y** (middle) with photos of the actuator constructed from **E3-Cl-20** in the relaxed state and actuated at an electric field of 53 V µm^{-1} whereby out of plane deformation dome shape was observed (middle), and **Er-Cl-Y** and **Elastosil®Film** (right). The elastomeric films were prestrained by 7.5%.

Because materials **E2-CN-Y** were softer and had a slightly higher permittivity as compared to **E3-CN-Y**, they actuated at lower electric field. The highest lateral actuation strain of 12% at the lowest electric field of 17 V µm^{-1} was achieved for material **E2-CN-20**. It should be noted that the elastic moduli of **E2-CN-Y** only slightly changed with strain, while for materials **E3-CN-Y** an increase of the elastic moduli at strains higher than 25% was observed. Because materials **E3-CN-Y** were stiffer as compared to **E2-CN-Y**, they actuated at higher electric fields (Figure 3.6). The rather low dielectric breakdown field of the

actuators constructed from **En-CN-Y** is likely due to the increased conductivity of these materials. All materials **En-Cl-Y** showed rapid stiffening above a certain strain which may allow suppressing EMI. As we were limited by the maximum voltage of 5600 V of our voltage source, the dielectric breakdown of actuators constructed from **En-Cl-Y** was not reached. Materials **En-Cl-20** were softer as compared to **En-Cl-33** and actuated at lower electric field. For example, material **E2-Cl-20** gave a maximum lateral actuation strain of 6.5% at 33 V μm^{-1}, while material **E3-Cl-20** gave only 3.5% lateral actuation at an electric field of 36 V μm^{-1}. Material **E3-Cl-20** allowed construction of actuators that were capable of suppressing EMI and for which ultra-large actuations were measured. An accurate measurement of the lateral actuation strain was not possible, as out of plane deformation occurred (Figure 3.6 middle). This material could be repeatedly actuated at 53 V μm^{-1} without degradation. Considering the actuation shape a half sphere, the areal actuation strain was estimated using the measured lateral actuation strain of 24% at 53 V μm^{-1}. With this assumption, an area actuation strain of about 200% was calculated.

Table 3.5 Maximum actuation strain s_{max}, dielectric breakdown of actuator $E_{b,act}$, lateral actuation strain at 10 V μm^{-1}, the electromechanical sensitivity $\varepsilon'/Y_{10\%}$, and the film thickness d.

Sample	$\varepsilon'/Y_{10\%}$ [MPa^{-1}]	$s_{(max)}$ [%]	$E_{b,act}$ [a)] [V/μm]	s @ 10V/μm [%]	d [μm]
E3-Cl-20	15	24	53 [b)]	0.2	105
E3-CN-33	25	17.5	31	1.5	180
E2-CN-20	34	12	19	3	130
E3-CN-20	19	10	33	1	150
E2-CN-33	28	10	17	3	140
E2-Cl-20	18	6.5	33 [b)]	0.2	170
E3-Cl-33	10	3.5	36 [b)]	0.2	155
E2-Cl-33	9	2.5	35 [b)]	0.2	160
Er-Cl-33	6	5.5	64	0.3	50
Er-Cl-20	6	3	50	0	65
Elastosil®Film	3	2.5	59 [b)]	0	95

[a]7.5% bilateral prestrain was applied. [b]No electric breakdown occurred.

The processability of **E3-Cl-20** in thin films was further optimized. To achieve more uniform films, a sacrificial layer of polyvinyl alcohol deposited on a glass plate was used, on which the new material was cross-linked. The formed material **E3-Cl-20*** had very similar dielectric properties to the previous one, but was slightly softer, *e.g.* **E3-Cl-20*** had a $Y_{10\%}$ = 260 kPa, while **E3-Cl-20** had a $Y_{10\%}$ = 370 kPa, respectively. In an attempt of getting accurate actuation measurements, **E3-Cl-20*** was tested at different biaxial prestains (0%, 22.5%, and 30%). Also here an accurate measurement of actuation was not possible. For actuators constructed from films that were biaxially prestrained by 22.5% and 30%, out of plane deformation occurred when the lateral actuation was above 10% (Figure 3.7). When no mechanical prestrain was used, out-of-plane actuation occurred from the very beginning. No dielectric breakdown was observed in all actuators constructed from **E3-Cl-20***, irrespective of the applied prestrain. High lateral actuation of 21% (more than 150% area actuation) at an electric field of 40 V μm^{-1} of actuators constructed from un-prestrained **E3-Cl-20*** were measured. This result indicates that **E3-Cl-20*** is capable of achieving high actuation strain without prestrain while completely suppressing EMI. Photos and a movie of an actuator constructed from an un-prestrained **E3-Cl-20*** film (Figure 3.7 middle, right) clearly show the huge out of plane deformation at 42 V μm^{-1} (see Figure 3.71, Section 3.7).

Figure 3.7 Lateral actuation strain **E3-Cl-20*** as function of the applied electric field (left) and photos of the actuator prepared from unprestrained films at 0 V µm^{-1} (middle) and at 42 V µm^{-1} (right). No dielectric breakdown occurred in actuators.

The leakage current during actuation is a very important material parameter as this current is converted into heat and thus may influence the reliability and life time of DEA.[23] While for single membrane actuator, efficient dissipation of heat may occur, this process is slowed down in stacked actuators and therefore the impact of leakage current is expected to be even more important. The leakage current of the new material was found to be low, comparable to the one measured for **Elastosil®Film**. An actuator constructed from **E3-Cl-20*** 22.5% prestrained showed a leakage current of 1 µA at an electric field of 27 V µm^{-1}. At this field a lateral actuation strain of 10% was measured. When increasing the electric field to 42 V µm^{-1} an increase in the leakage current to 4 µA was observed.

The electromechanical response speed was demonstrated by cyclic actuation tests at frequencies ranging from 0.5 Hz to 8 Hz performed using a 30% prestrained film. This prestrain was selected to minimize the measurement error due to buckling (Figure 3.8, left).

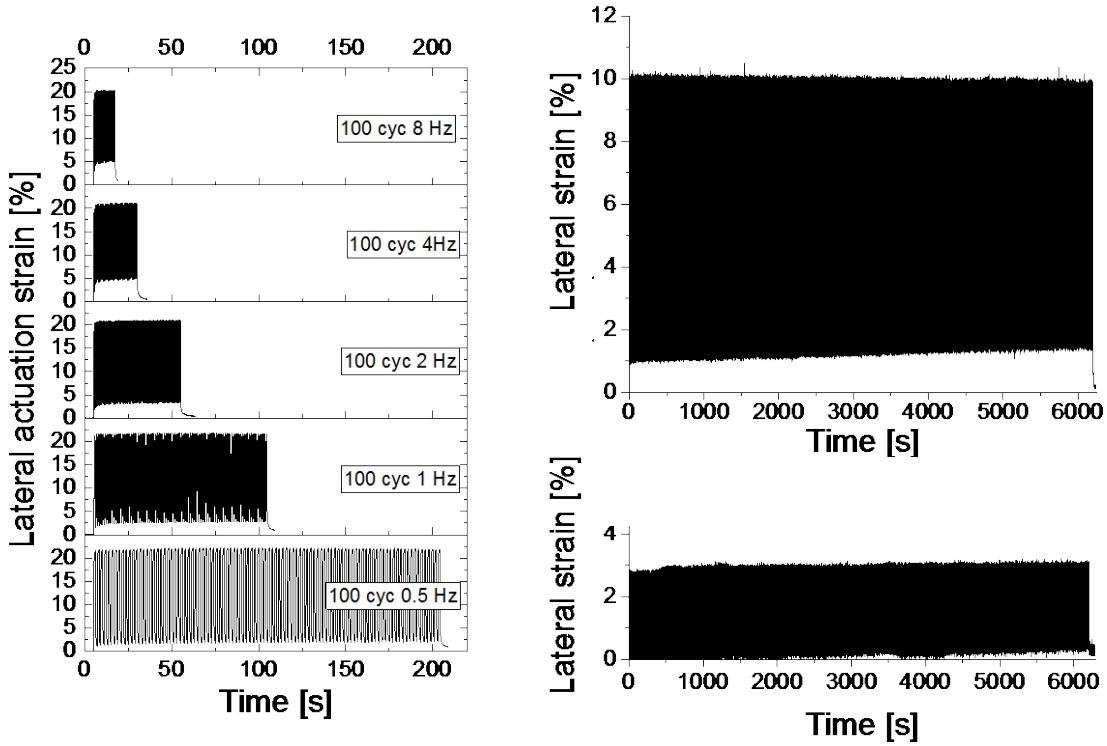

Figure 3.8 100 actuation cycles at 0.5-8 Hz and an electric field of 42 V µm^{-1} of **E3-Cl-20*** prestrained by 30% (left), 50.000 actuation cycles at 8 Hz and an electric field of 27 V µm^{-1} of **E3-Cl-20*** (top right), and 50.000 actuation cycles at 8 Hz and 67 V µm^{-1} of **Elastosil®Film** prestrained by 22.5% (bottom right).

For each frequency, 100 cycles were conducted. A slight decrease of the actuation with increasing actuation frequency was observed, *e.g.* at 0.5 Hz an actuation strain of 22% was measured, while at 8 Hz the actuation decreased to 20%. It should be noted that at higher frequencies (4 and 8 Hz), the actuator constructed from our new material did not completely recover the initial shape after discharging, about 5% remnant strain was observed, but the actuation strain was the same for consecutive cycles. Thus, a lateral actuation strain of 15% was measured. Elastosil®Film showed no limit of response speed.

Due to the low dielectric permittivity, Elastosil®Film showed a maximum actuation strain of only 8% at an electric field as high as 90 V µm^{-1} (Figure 3.70, Section 3.7). Cyclic actuation measurement of **E3-Cl-20*** over 50.000 cycles at 8 Hz showed a constant actuation of about 10% at 27 V µm^{-1} and a leakage current density of 0.5 µA cm^{-2} (Figure 3.8 right). Cyclic actuation of Elastosil®Film over 50.000 cycles at 8 Hz showed a lateral actuation strain of 3% at 67 V µm^{-1} and a leakage current density of 0.5 µA cm^{-2}. Due to the increased permittivity, good mechanical properties with low mechanical losses, excellent, fast, and reliable actuation at electric fields where leakage current is very low, this material can be considered as a promising replacement for regular PDMS.

3.5 Conclusions

Grafting of alkyl thiols to polymethylvinylsiloxane has been shown to be an effective approach to polymers with increased permittivity. Appropriate cross-linking allowed formation of elastomers with excellent insulating properties and high actuation strain. A synergetic effect between the thioether side groups of the polymer and the *in situ* generated silsesquioxane reflected by a rapid stiffening of the materials above a certain strain is desirable to suppress electromechanical instability and to achieve large actuation strains. A novel dielectric elastomer material was achieved starting from a silanol end-terminated polysiloxane modified with propyl-thioether side groups and 3-chloropropyl(triethoxy)silane. The material showed relative permittivity of $\varepsilon' = 5.4$ which was attributed to the presence of sulfur and chlorine in our material. The material shows a conductivity of $\sigma = 4\times10^{-11}$ S cm^{-1} and good mechanical properties with a storage modulus of 300 kPa and a loss factor below 0.1, but a uniaxial strain at break of 100%. The stiffening of the material at rather low strains completely suppressed electromechanical instability and prevented the dielectric from premature breakdown. Area actuation strain of about 200% was calculated at an electric field of 53 V µm^{-1}. This large actuation was possible due to the sharp stiffening of the elastomer above a certain strain. Additionally, the material could be actuated for more than 50.000 times at 8 Hz and gave a stable lateral actuation strain of 10% at an electric field of 27 V µm^{-1} with a leakage current density of 0.5 µA cm^{-2}.

Because of the attractive dielectric characteristics and actuation behavior, this material recommends itself as a future replacement for regular PDMS elastomers. The increased permittivity allows for a reduction of driving voltage of actuators, an increased energy density in generators, and an increased sensitivity of sensors. Further work is devoted in implementing this class of materials in printable stacked devices.

3.6 References

[1] R. Pelrine, R. Kornbluh, Q. Pei and J. Joseph, *Science* **2000**, *287*, 836.

[2] Q. Pei, M. A. Rosenthal, R. Pelrine, S. Stanford and R. Kornbluh, *Proc. SPIE* **2003**, *5051*, 281.

[3] C. Jordi, S. Michel, G. Kovacs and P. Ermanni, *Sens. Actuators A* **2010**, *161*, 182.

[4] O. A. Araromi and S. C. Burgess, *Smart Mater. Struct.* **2012**, *21*, 032001.

[5] F. M. Weiss, H. Deyhle, G. Kovacs and B. Mueller, *Proc. SPIE* **2012**, *8340*, 83400A.

[6] R. D. Kornbluh, R. E. Pelrine, H. Prahlad, S. Chiba, J. S. Eckerle, B. Chavez, S. E. Stanford and T. Low, *US 7557456*, **2007**.

[7] F. Carpi, *Electromechanically active polymers*, Springer, Cham, Switzerland **2016**.

[8] A. Tröls, A. Kogler, R. Baumgartner, R. Kaltseis, C. Keplinger, R. Schwödiauer, I. Graz and S. Bauer, *Smart. Mater. Struct.* **2013**, *22*, 104012.

[9] J. S. Plante and S. Dubowsky, *Int. J. Solids Struct.* **2006**, *43*, 7727.

[10] X. Zhao and Z. Suo, *Appl. Phys. Lett.* **2007**, *91*, 061921.

[11] X. Zhao and Z. Suo, *Phys. Rev. Lett.* **2010**, *104*, 1.

[12] M. Moscardo, X. Zhao, Z. Suo and Y. Lapusta, J. Appl. Phys. **2008**, *104*, 093503

[13] T. Lu, J. Huang, C. Jordi, G. Kovacs, R. Huang, D. R. Clarke and Z. Suo, *Soft Matter* **2012**, *6*, 6167.

[14] R. Pelrine, R. Kornbluh, J. Joseph, R. Heydt, Q. Pei and S. Chiba, *Mater. Sci. Eng. C* **2000**, *11*, 89.

[15] J. Huang, T. Li, C. C. Foo, J. Zhu, D. R. Clarke and Z. Suo, *Appl. Phys. Lett.* **2012**, *100*, 041911.

[16] C. Keplinger, T. Li, R. Baumgartner, Z. Suo and S. Bauer, *Soft Matter* **2012**, *8*, 285.

[17] T. Li, C. Keplinger, R. Baumgartner, S. Bauer, W. Yang and Z. Suo, *J. Mech. Phys. Solids* **2013**, *61*, 611.

[18] S. M. Ha, M. Wissler, R. Pelrine, S. Stanford, G. Kovacs and Q. Pei, *Proc. SPIE* **2007**, *6524*, 652408.

[19] C. Jordi, A. Schmidt, G. Kovacs, S. Michel and P Ermanni, *Smart Mater. Struct.* **2011**, *20*, 075003.

[20] X. Niu, H. Stoyanov, W. Hu, R. Leo, P. Brochu and Q. Pei, *J. Polym. Sci., Part B: Polym. Phys.* **2013**, *51*, 197.

[21] P. Brochu, H. Stoyanov, X. Niu and Q. Pei, *Smart Mater. Struct.* **2013**, *22*, 0550227.

[22] R. Shankar, T. K. Ghosh and R. J. Spontak, *Adv. Mater.* **2007**, *19*, 2218.

[23] R. Shankar, T. K. Ghosh and R. J. Spontak, *Macromol. Rapid Commun.* **2007**, *28*, 1142.

[24] M. Vatankhah-Varnoosfaderani, W. F. M. Daniel, A. P. Zhushma, Q. Li, B. J. Morgan, K. Matyjaszewski, D. P. Armstrong, R. J. Spontak, A. V. Dobrynin and S. S. Sheiko, *Adv. Mater.* **2017**, *29*, 1604209.

[25] D. M. Opris, *Adv. Mater.* **2018**, *30*, 17036778.

[26] P. Brochu and Q. Pei, *Macromol. Rapid Commun.* **2010**, *31*, 10.

[27] L.J. Romasanta, M.A. Lopez-Manchado and R. Verdejo, *Prog. Polym. Sci.* **2015**, *51*, 188.

[28] F. B. Madsen, A. E. Daugaard, S. Hvilsted and A. L. Skov, *Macromol. Rapid Commun.* **2016**, *37*, 378.

[29] D. Opris, S. Dünki and F. Nüesch, *J. Mater. Chem. C*, **2016**, *4*, 10545.

[30] L. Zhang, D. Wang, P. Hu, J.-W. Zha, F. You, S.-T. Li and Z.-M. Dang, *J. Mater. Chem. C*, **2015**, *3*, 4883.

[31] F. B. Madsen, L. Yu, A. E. Daugaard, S. Hvilsted and A. L. Skov, *RSC Adv.* **2015**, *5*, 10254.

[32] M. Stepp, F. Achenbach and A. Koellnberger*, PCT Int. Appl., WO 2015/121261 A1 20150820*, **2015**.

[33] S. J. Dünki, M. Dascalu, F. A. Nüesch and D. M. Opris, *Proc. SPIE*, **2016**, *9798,* 97982K.

[34] S. J. Dünki, M. Tress, F. Kremer, S. Y. Ko, F. A. Nüesch, C.-D. Varganici, C. Racles and D. M. Opris, *RSC Adv.* **2015**, *5*, 50054.

[35] L. Maffli, S. Rosset, M. Ghilardi, F. Carpi and H. Shea, *Adv. Funct. Mater.* **2015**, *25*, 1656.

[36] J. E. Q. Quinsaat, M. Alexandru, F. A. Nüesch, H. Hofmann, A. Borgschulte and D. M. Opris, *J. Mater. Chem. A*, **2015**, *3*, 14675**.**

[37] M. Cazacu, M. Ignat, C. Racles, M. Cristea, V. Musteata, D. Ovezea and D. Lipcinski, *J. Compos. Mater.* **2014**, *48*, 1533.

[38] M. Alexandru, M. Cazacu, A. Nistor, V. E. Musteata, I. Stoica, C. Grigoras and B. C. Simionescu, *J. Sol-Gel Sci. Techol.* **2010**, *56*, 310.

[39] A. Bele, M. Cazacu, C. Racles, G. Stiubianu, D. Ovezea and M. Ignat, *Adv. Eng. Mater.* **2015**, *17*, 1302.

[40] A. Bele, M. Dascalu, C. Tugui, M. Iacob, C. Racles, L. Sacarescu and M. Cazacu, *Mater. Des.* **2016**, *106*, 454.

[41] S. J. Dünki, E. Cuervo-Reyes and D. M. Opris, *Polym. Chem.* **2017**, *8*, 715.

3.7 Supporting information

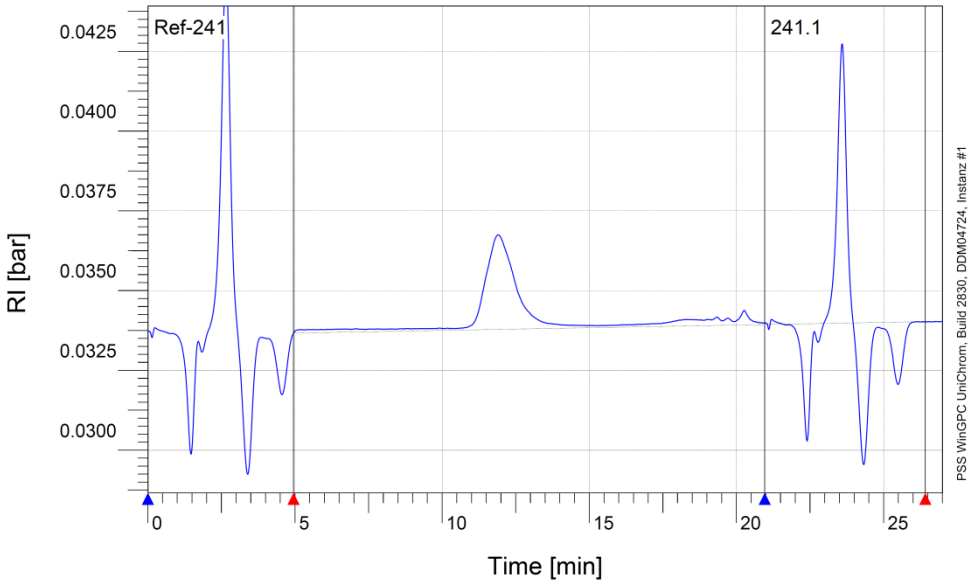

Probe :	Ref-241	**Methode :**	C:\EmpaDaten\Methoden\TFE_Fischer_01_2014.
Basislinie von :	4.950 ml	**bis :**	26.417 ml
Integration von :	4.917 ml	**bis :**	26.242 ml
Kalibration :	PDMS_THF_alteSäule_31012014.cal	**Eluent :**	THF
MHK - A (Kal.):	0.000E+0	**MHK - K (Kal.):**	1.000E+0 ml/g
Int.Stand.-K :	23.429 ml	**Int.Stand.-M :**	23.585 ml
Pumpe :	PSS SECcurity	**Flußrate :**	1.000 ml/min
Konzentration :	2.000 g/l	**Injektvolumen :**	20.000 ul
Säule 1 :	PSS SDV 5µm	**Temperatur :**	30.000 °C
Säule 2 :	PSS SDV 5µm	**Temperatur :**	30.000 °C
Detektor 1 :	PSS SECcurity UV	**Versatz :**	0.000 ml
Detektor 2 :	PSS SECcurity UV	**Versatz :**	0.160 ml
Detektor 3 :	PSS SECcurity RI	**Versatz :**	0.000 ml
Operateur :	Beatrice Fischer	**Messintervall :**	1.000 sec

Figure 3.9 GPC elution curve of **P0**.

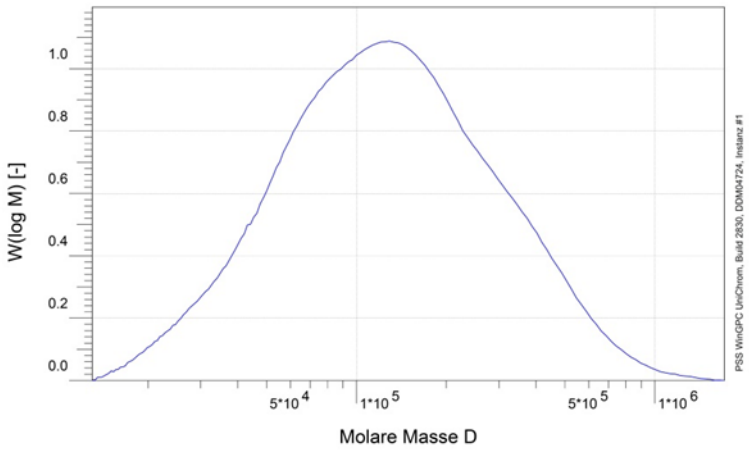

Probe :	Ref-241		
Integration von :	Mittwoch 29.03.17 12:29:05		10.748 ml
Integration bis :	Mittwoch 29.03.17 12:31:53		13.519 ml
Kalibration :	PDMS_THF_alteSäule_31012014.cal	**Eluent :**	THF
MHK - A (Kal.):	0.000E+0	**MHK - K (Kal.):**	1.000E+0 ml/g
Int.Stand.-K :	23.429 ml	**Int.Stand.-M :**	23.585 ml
Pumpe :	PSS SECcurity	**Flußrate :**	1.000 ml/min
Konzentration :	2.000 g/l	**Injektvolumen :**	20.000 ul
Säule 1 :	PSS SDV 5µm	**Temperatur :**	30.000 °C
Säule 2 :	PSS SDV 5µm	**Temperatur :**	30.000 °C
Detektor 1 :	PSS SECcurity UV	**Versatz :**	0.000 ml
Detektor 2 :	PSS SECcurity UV	**Versatz :**	0.160 ml
Detektor 3 :	PSS SECcurity RI	**Versatz :**	0.000 ml
Operateur :	Beatrice Fischer	**Messintervall :**	1.000 sec

PSS SECcurity RI

Mn :	9.1277e4	g/mol
Mw :	1.7597e5	g/mol
Mz :	3.1971e5	g/mol
Mv :	0.000000	g/mol
D :	1.9278e0	
[n]:	0.000000	ml/g
Vp :	1.1823e1	ml
Mp :	1.4744e5	g/mol
FI :	3.009e-3	ml*V
< 12998	0.00	
w% :	100.00	
> 1711465	0.00	

Figure 3.10 GPC analysis of **P0** (M_n = 90.000 g mol^{-1}, M_w = 175.000 g mol^{-1}, *PDI* = 1.9).

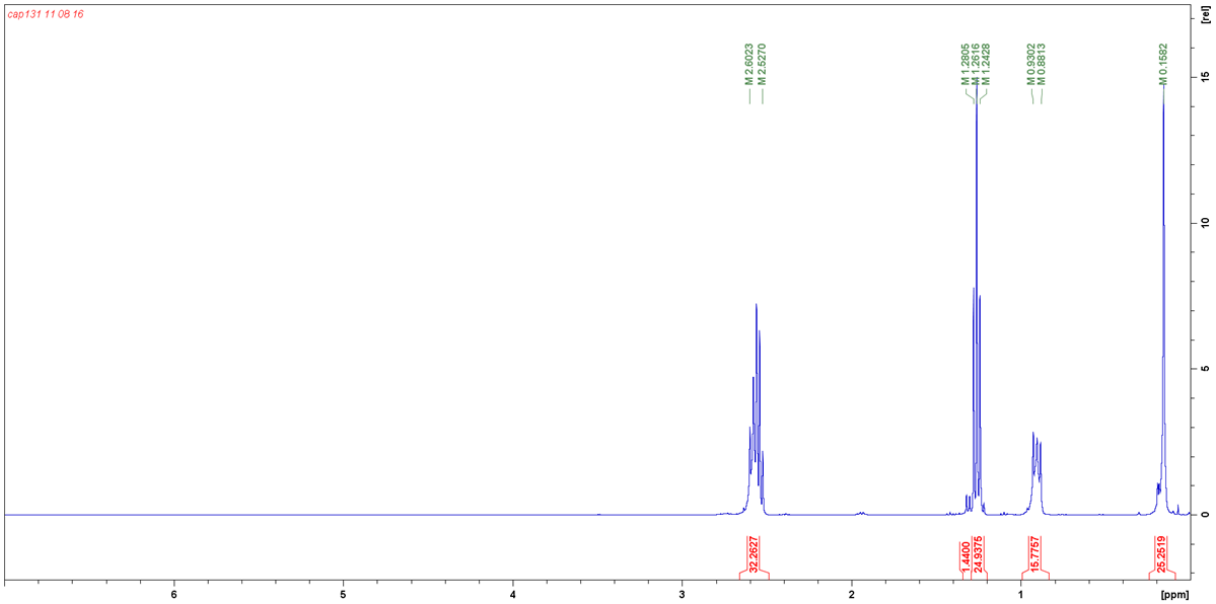

Figure 3.11 ^{1}H NMR spectrum of **P2**.

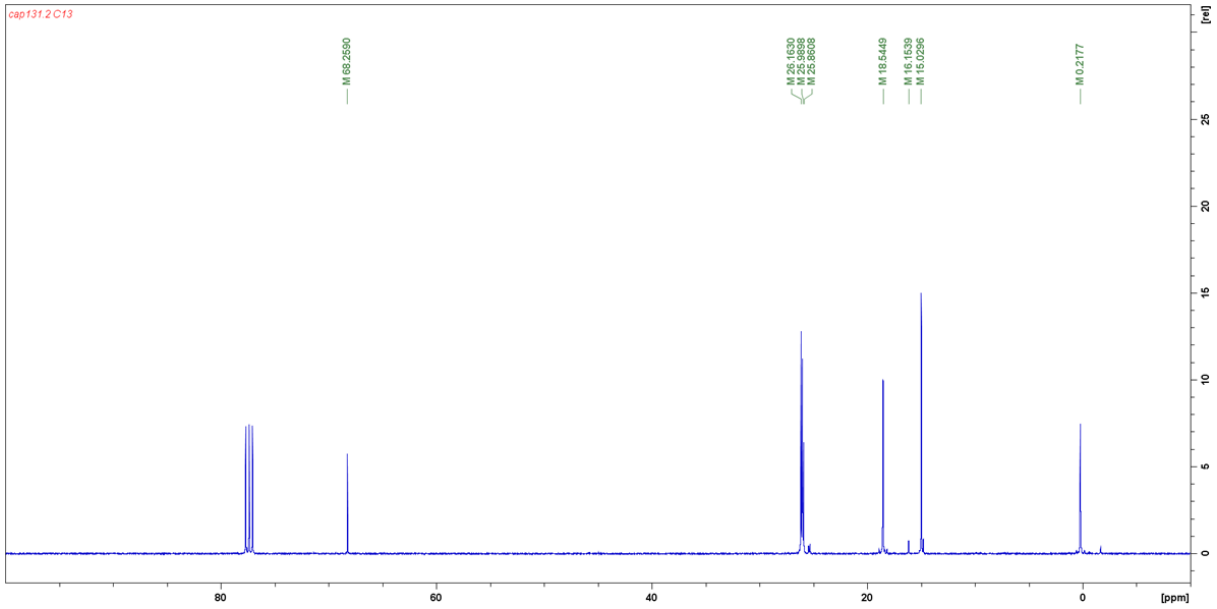

Figure 3.12 13C NMR spectrum of **P2**.

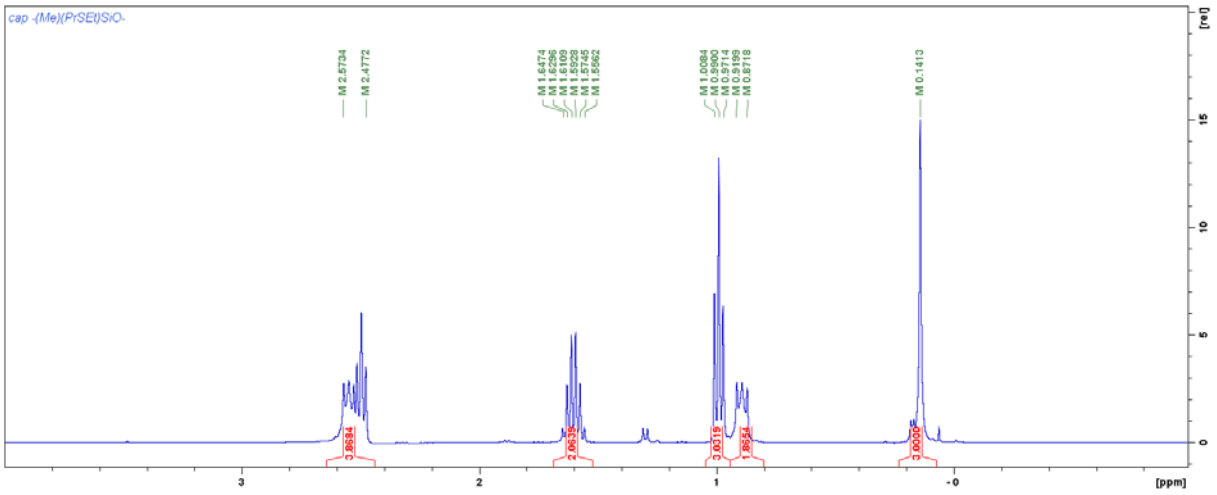

Figure 3.13 ^{1}H NMR spectrum of **P3**.

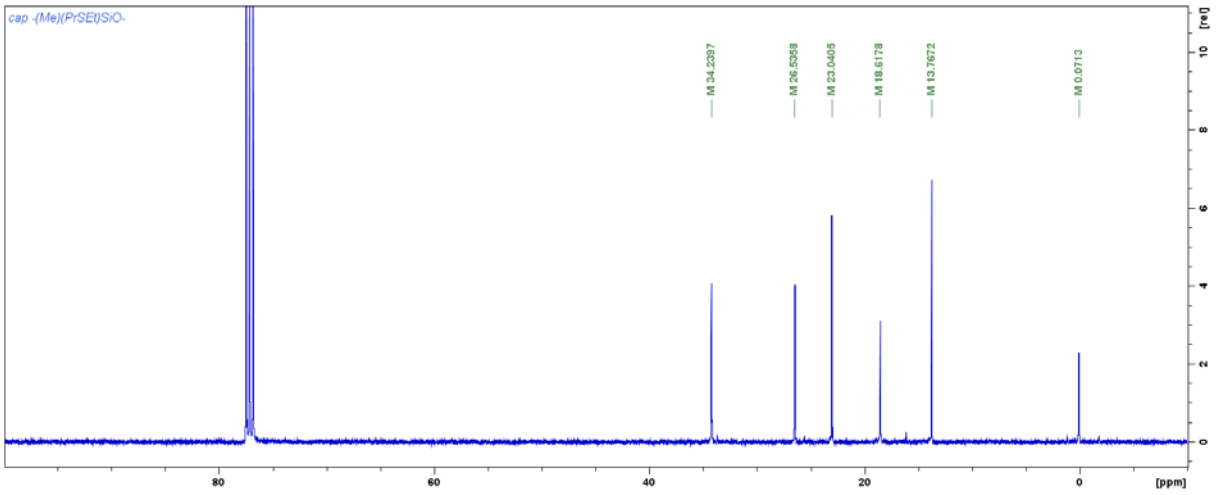

Figure 3.14 ^{13}C NMR spectrum of **P3**.

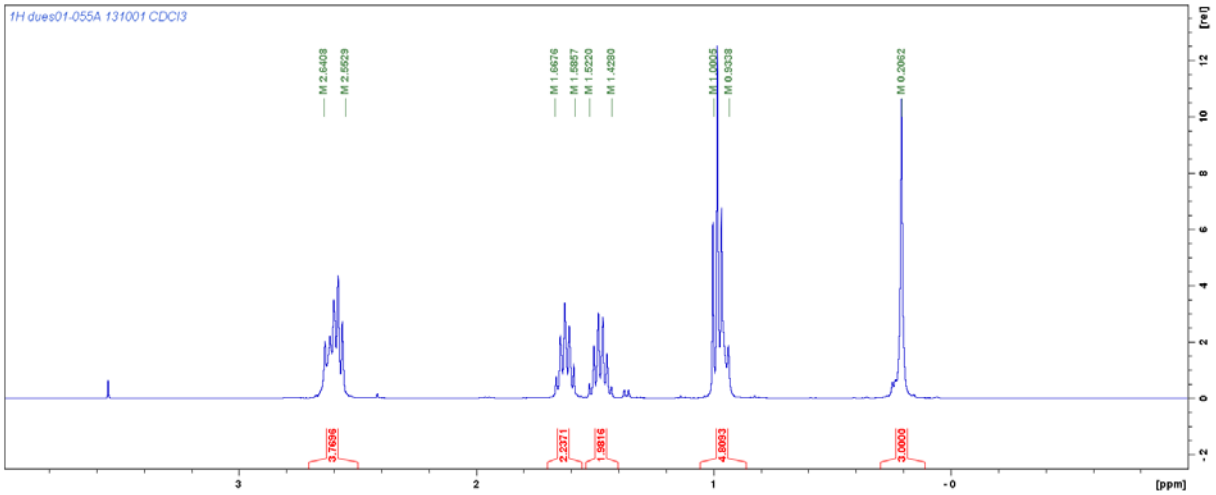

Figure 3.15[1]H NMR spectrum of **P4**.

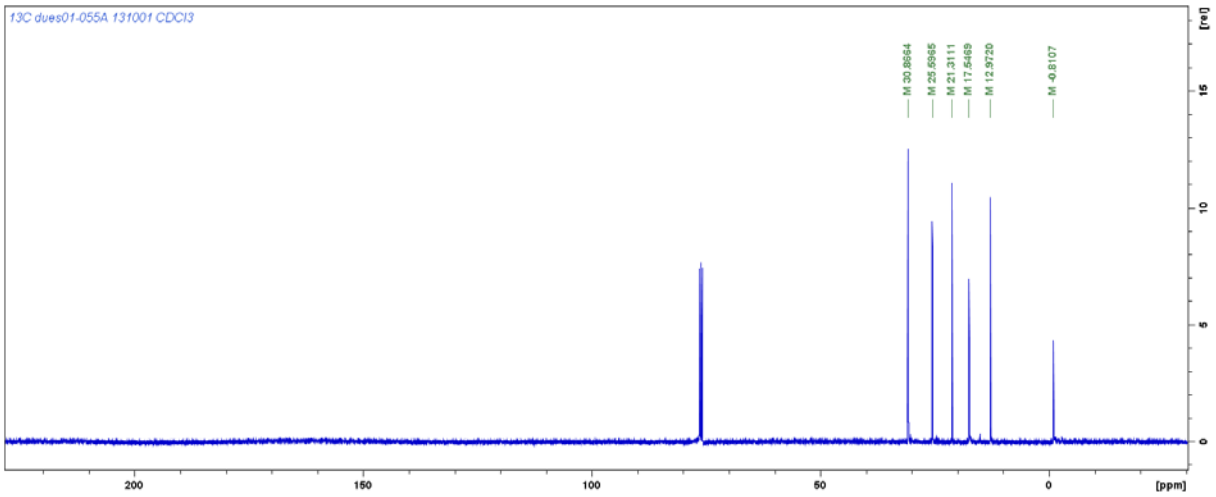

Figure 3.16**.** [13]C NMR spectrum of **P4**.

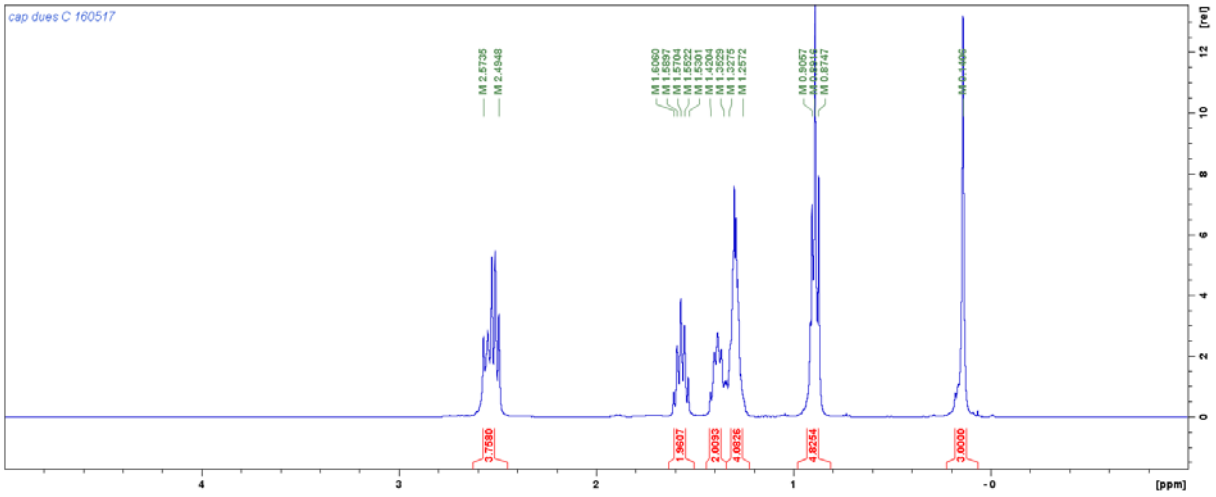

Figure 3.17 [1]H NMR spectrum of **P6**.

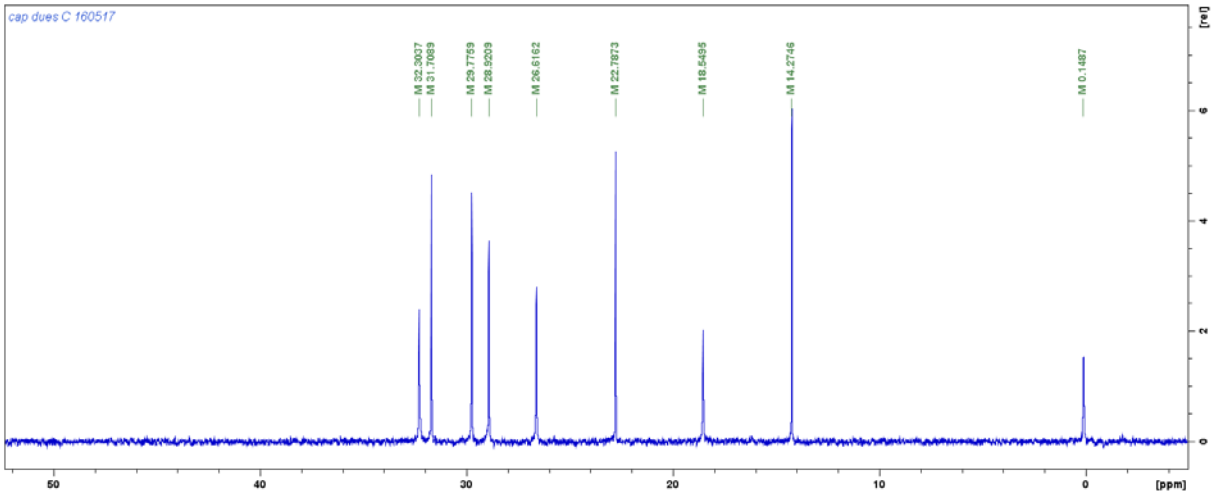

Figure 3.18 ^{13}C NMR spectrum of **P6**.

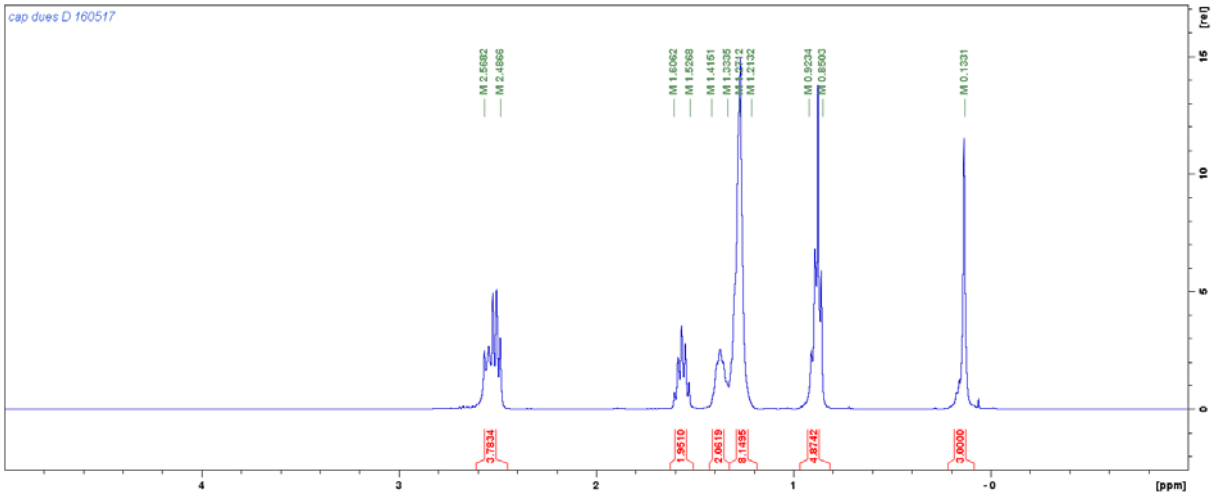

Figure 3.19 ^{1}H NMR spectrum of **P8**.

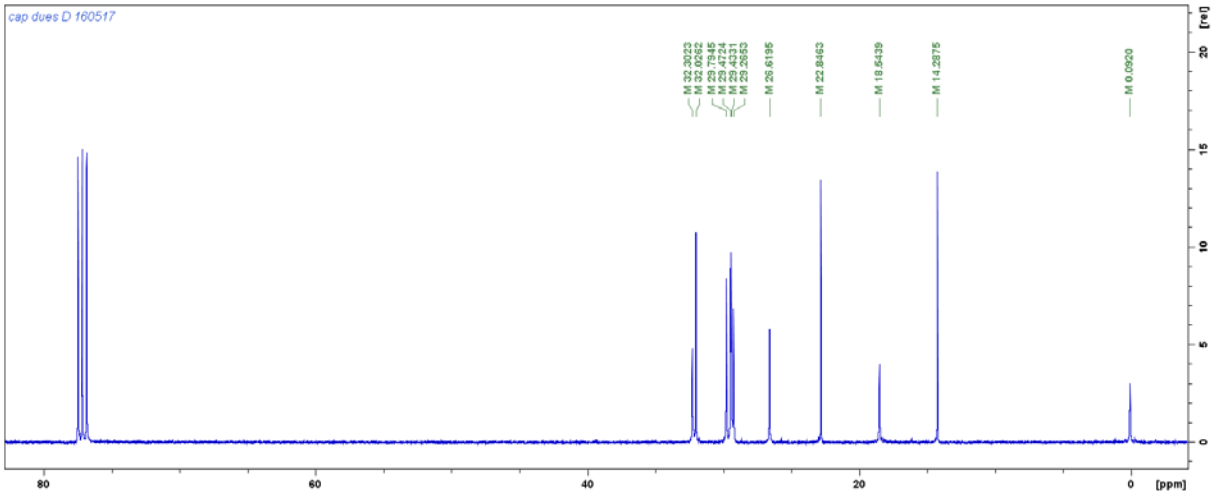

Figure 3.20 ^{13}C NMR spectrum of **P8**.

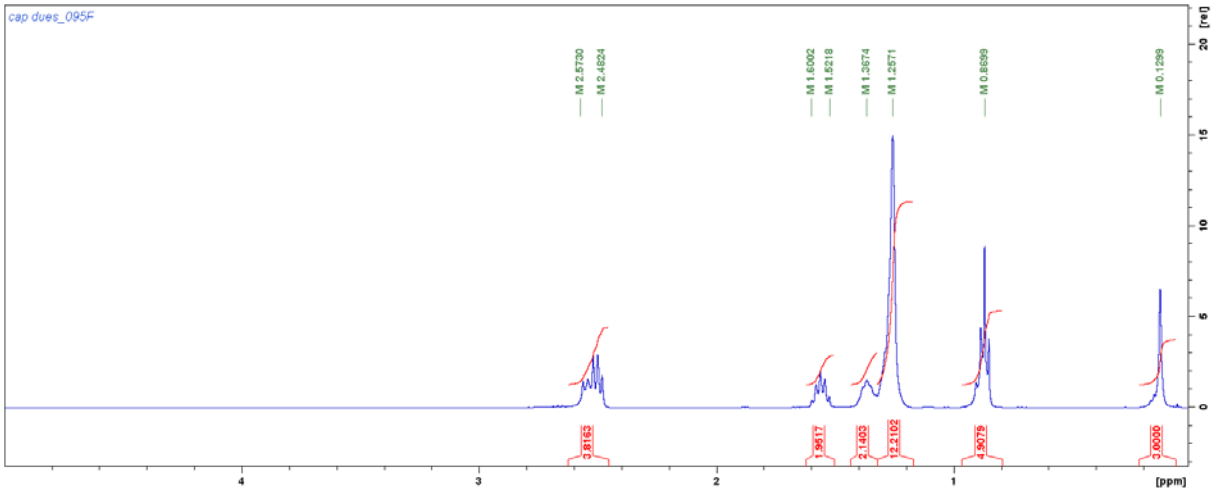

Figure 3.21 ^{1}H NMR spectrum of **P10**.

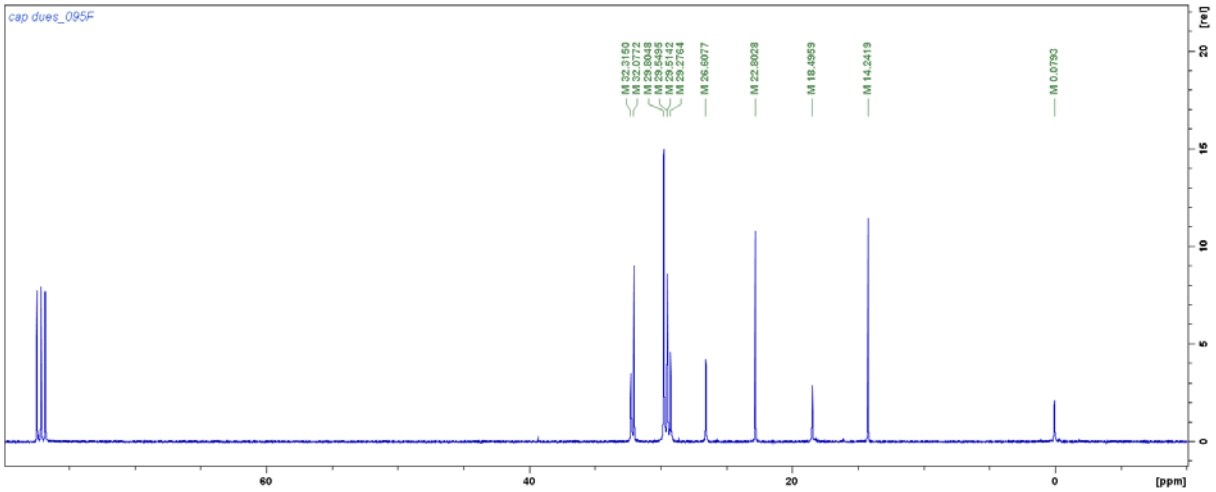

Figure 3.22 ^{13}C NMR spectrum of **P10**.

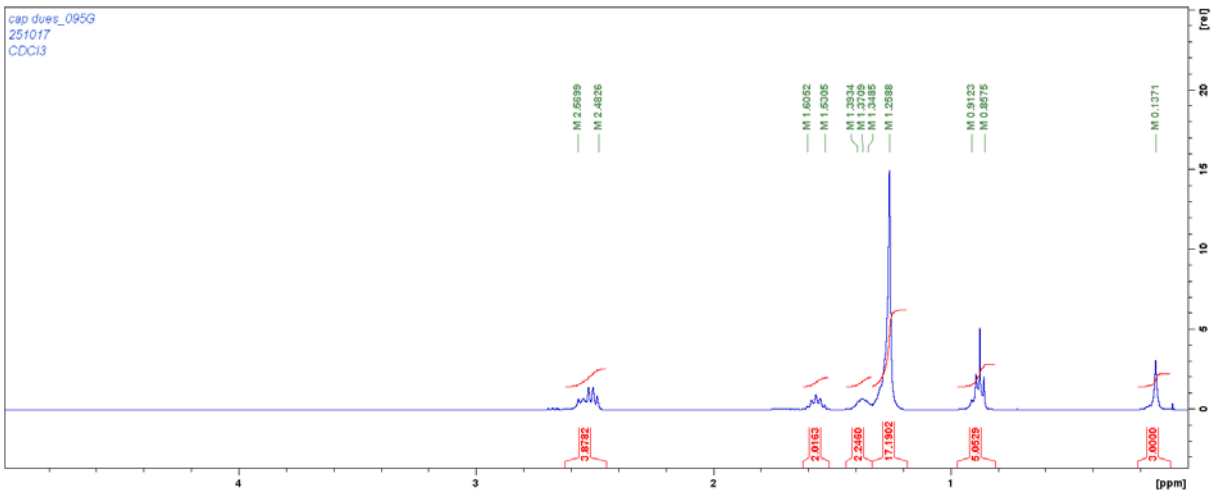

Figure 3.23 ^{1}H NMR spectrum of **P12**.

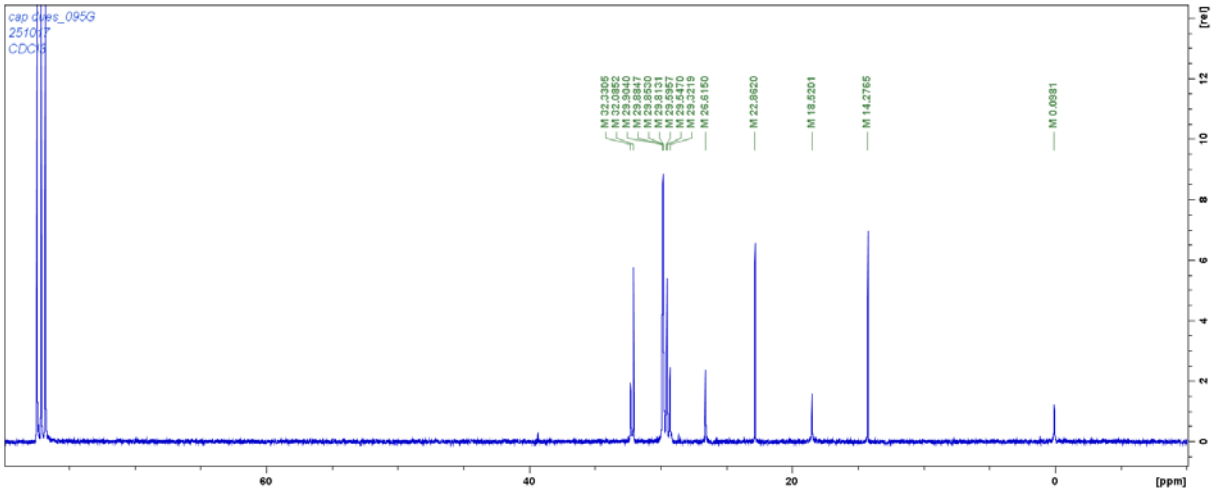

Figure 3.24 ^{13}C NMR spectrum of **P12.**

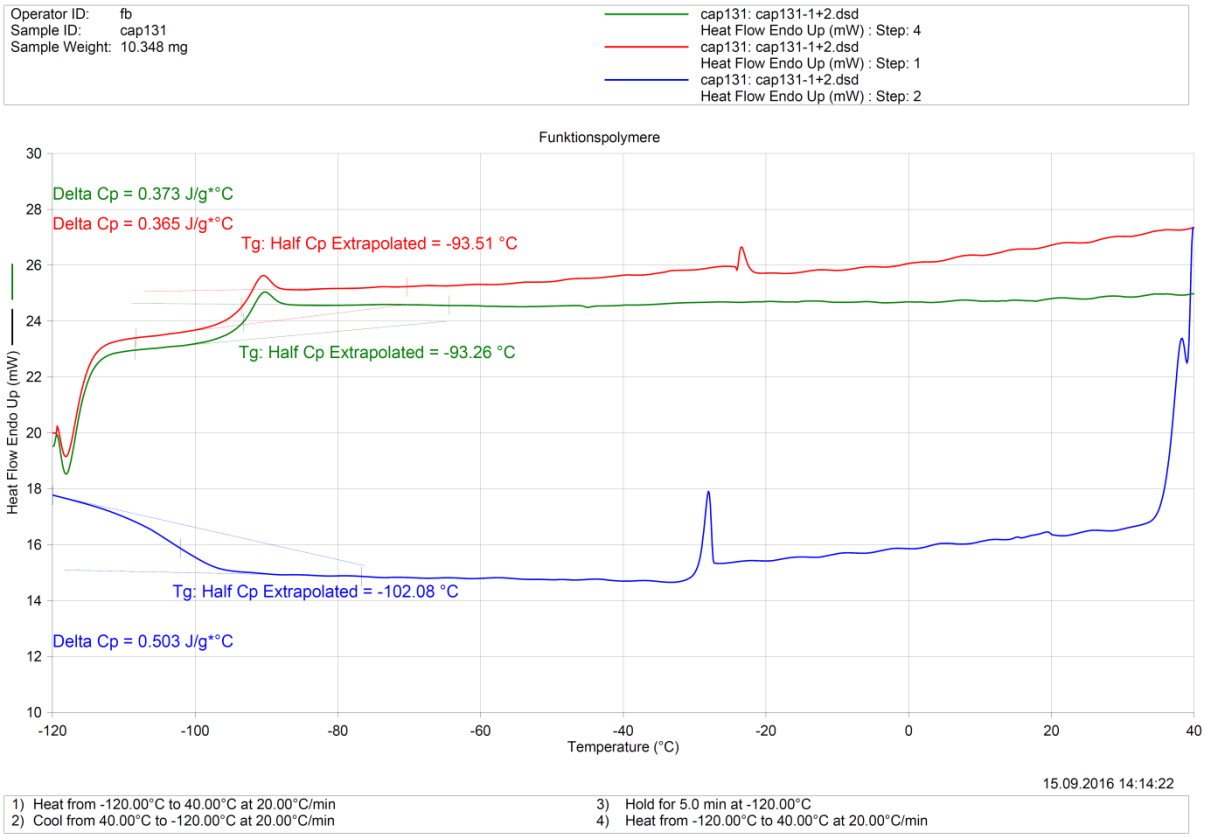

Figure 3.25 DSC curves of **P2**.

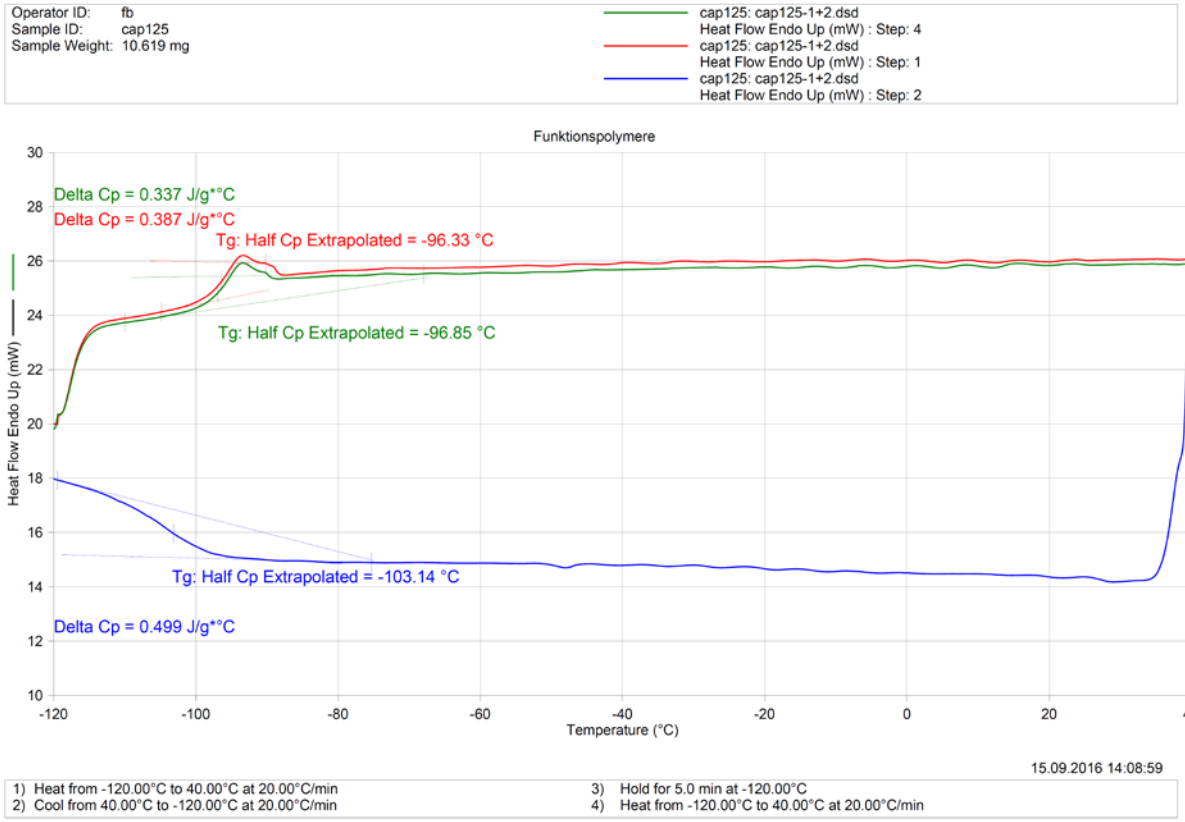

Figure 3.26 DSC curves of **P3**.

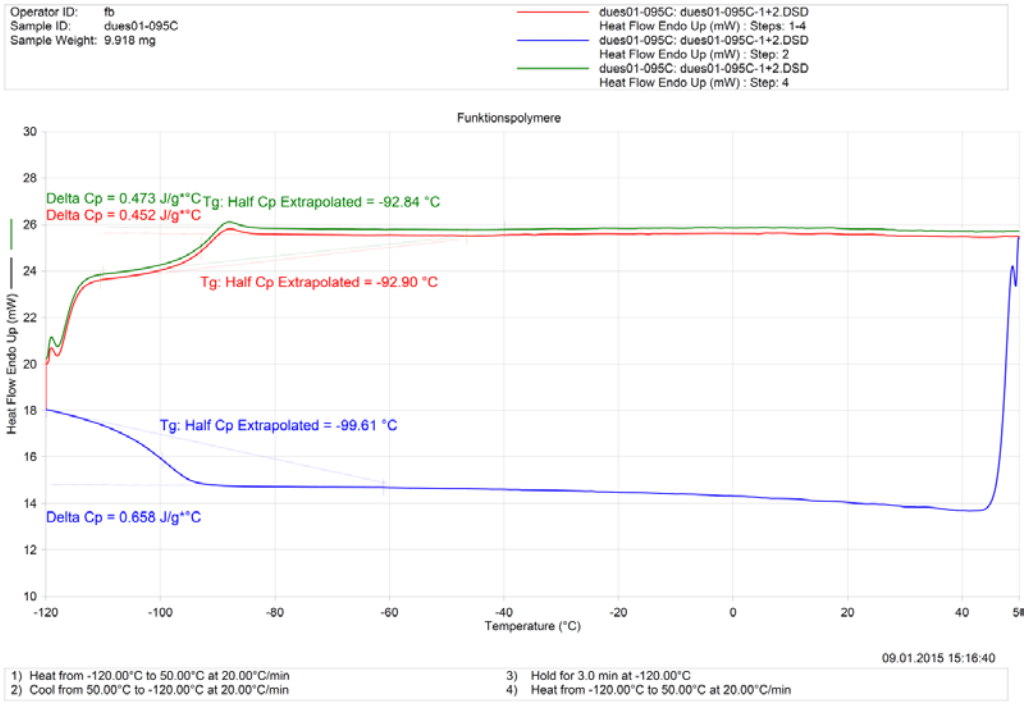

Figure 3.27 DSC curves of **P6**.

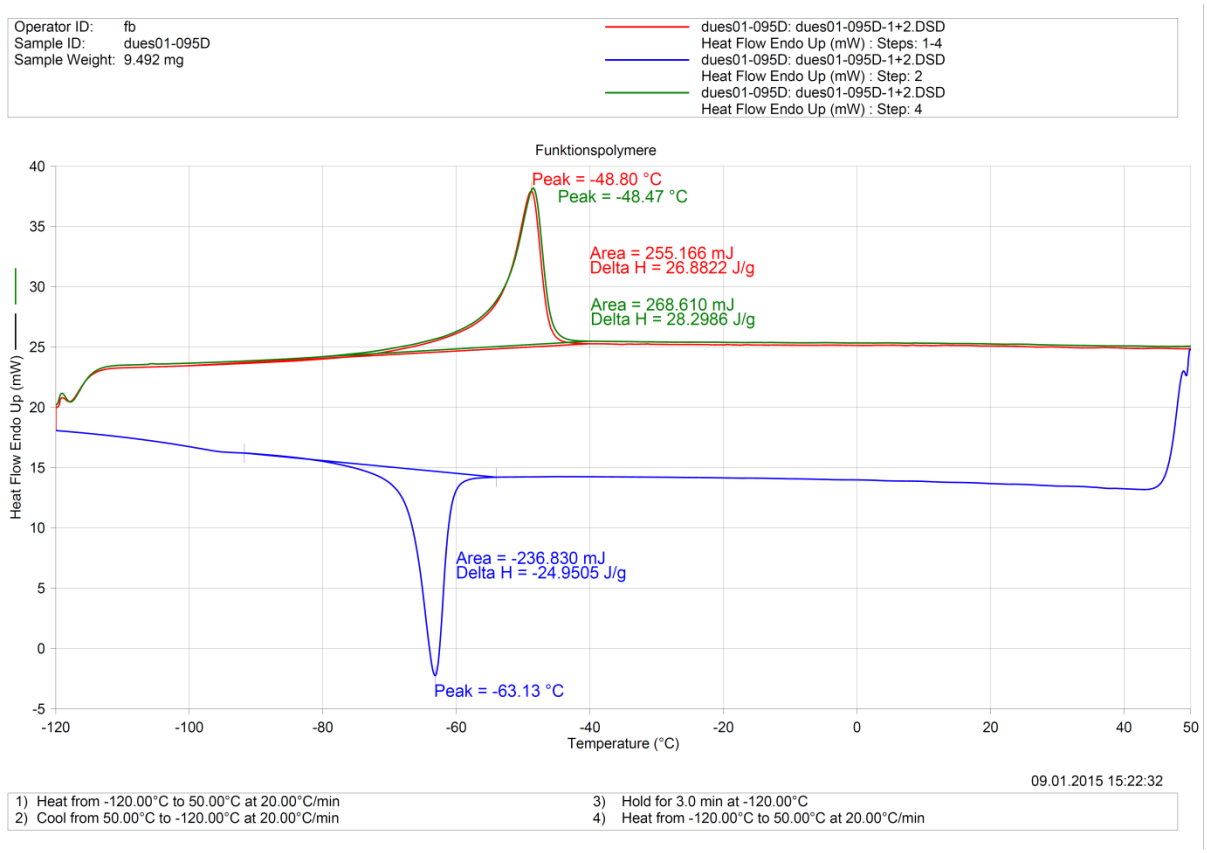

Figure 3.28 DSC curves of **P8**.

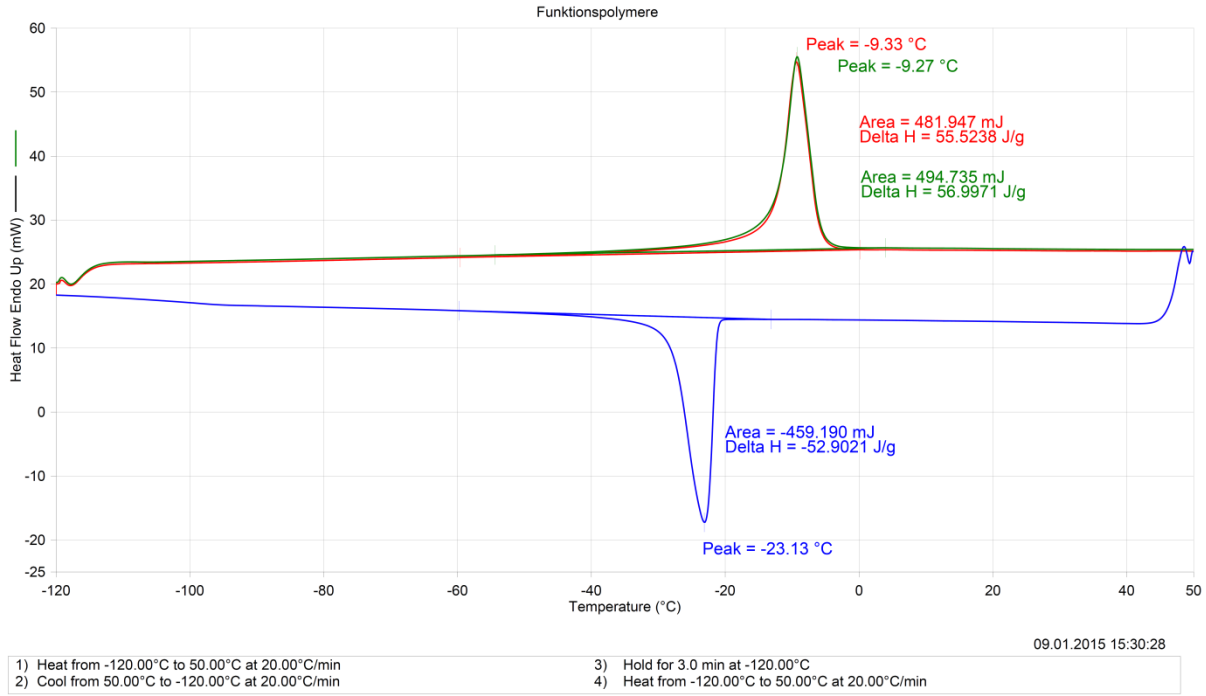

Figure 3.29 DSC curves of **P10**.

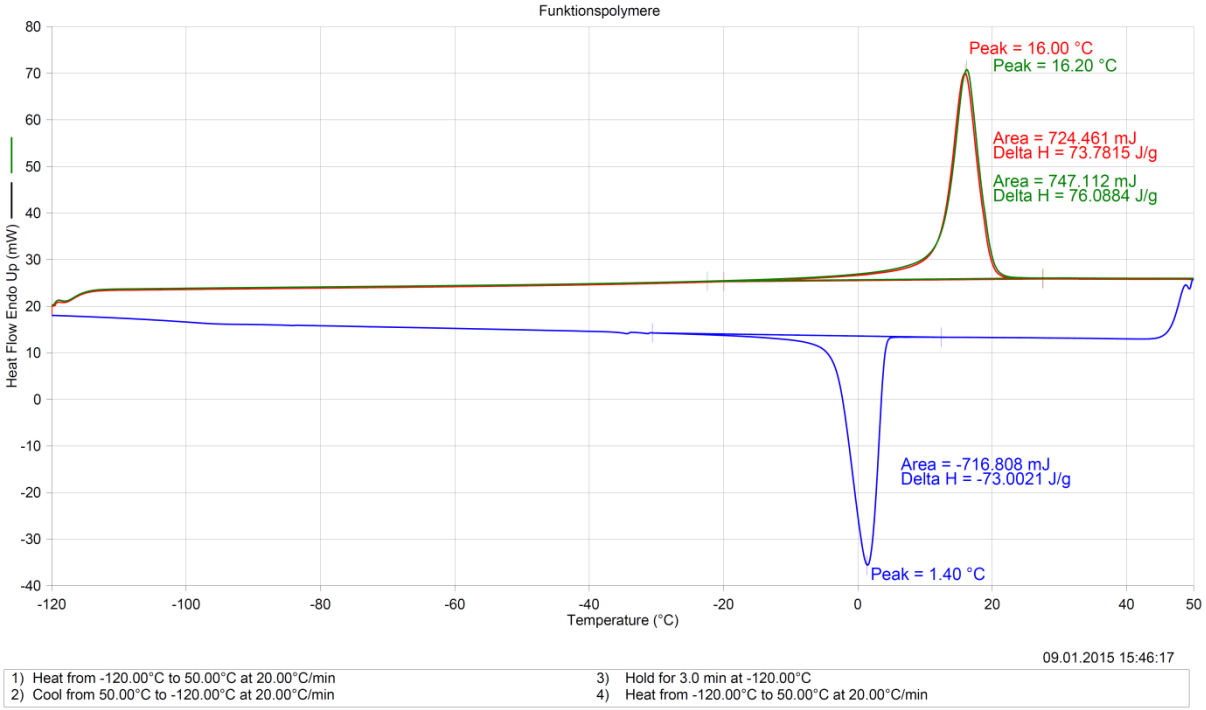

Figure 3.30 DSC curves of **P12**.

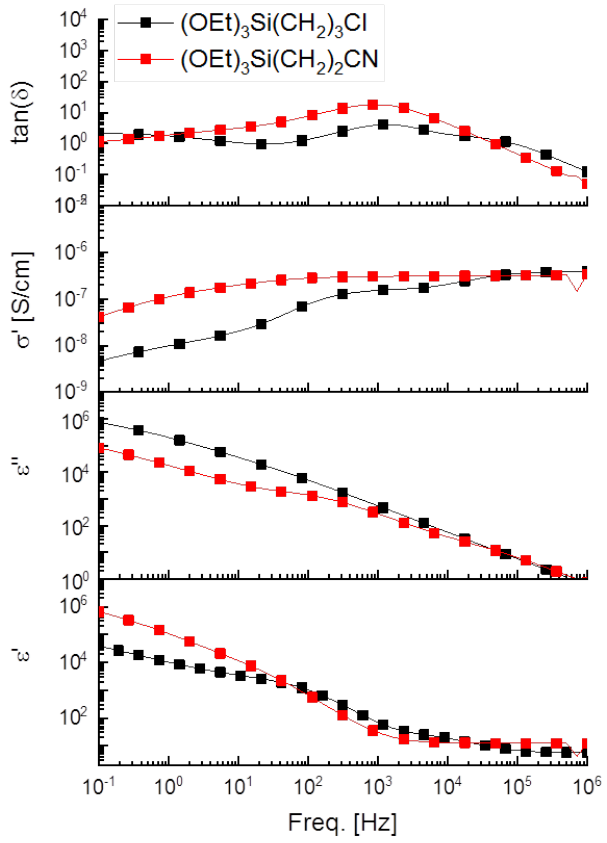

Figure 3.31 Dielectric properties of **Cl-CL** and **CN-CL**. Dielectric permittivity ε' was taken at 10^6 Hz where the contribution of ions can be neglected.

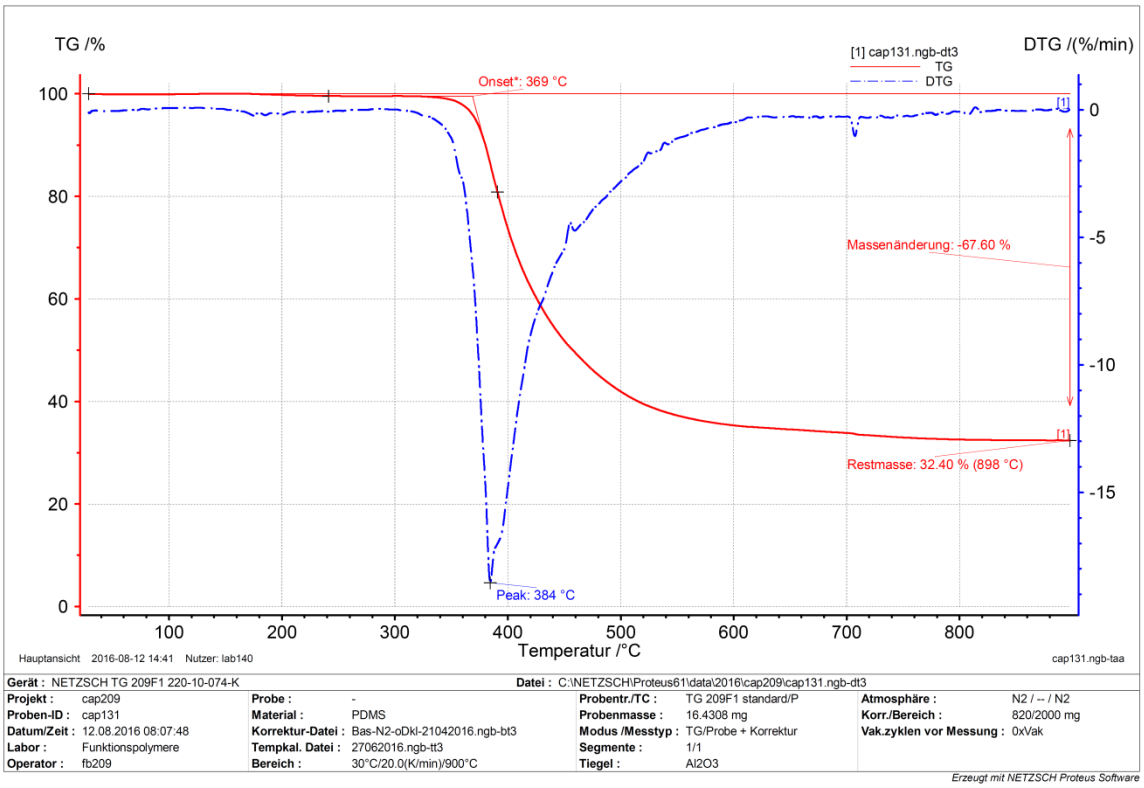

Figure 3.32 TGA curve of **P2.**

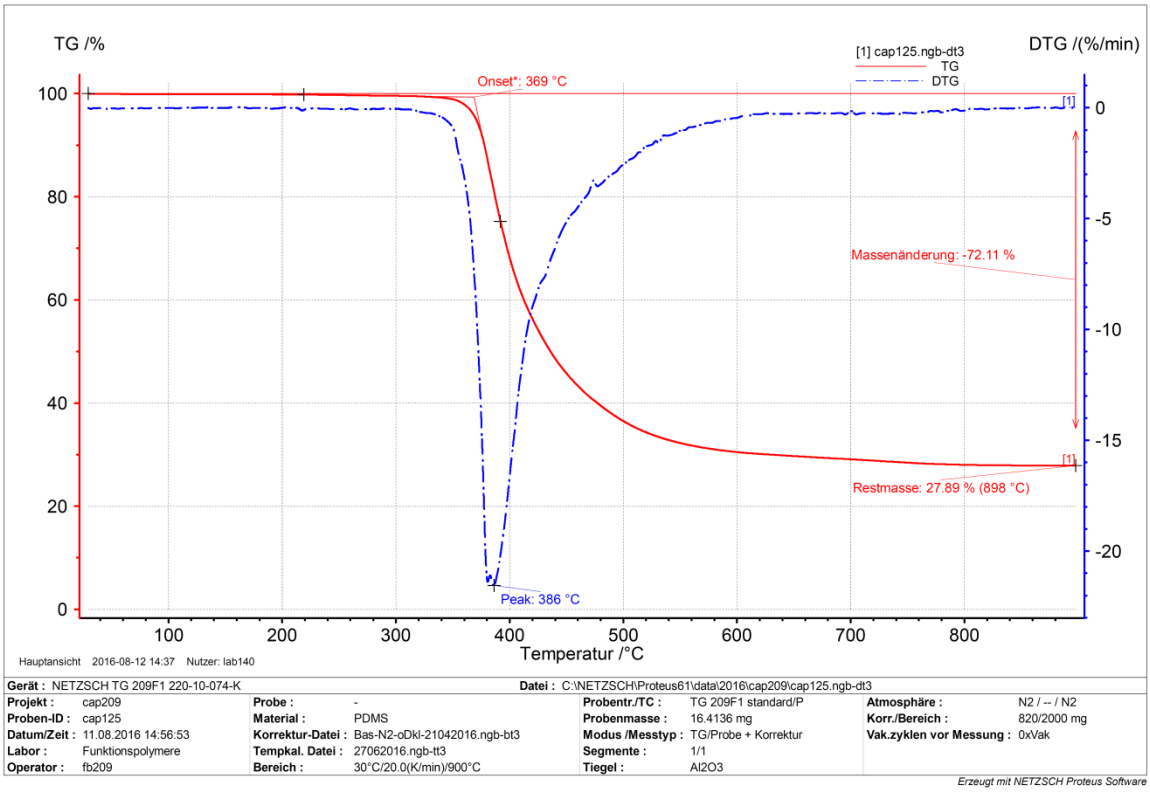

Figure 3.33 TGA curve of **P3**.

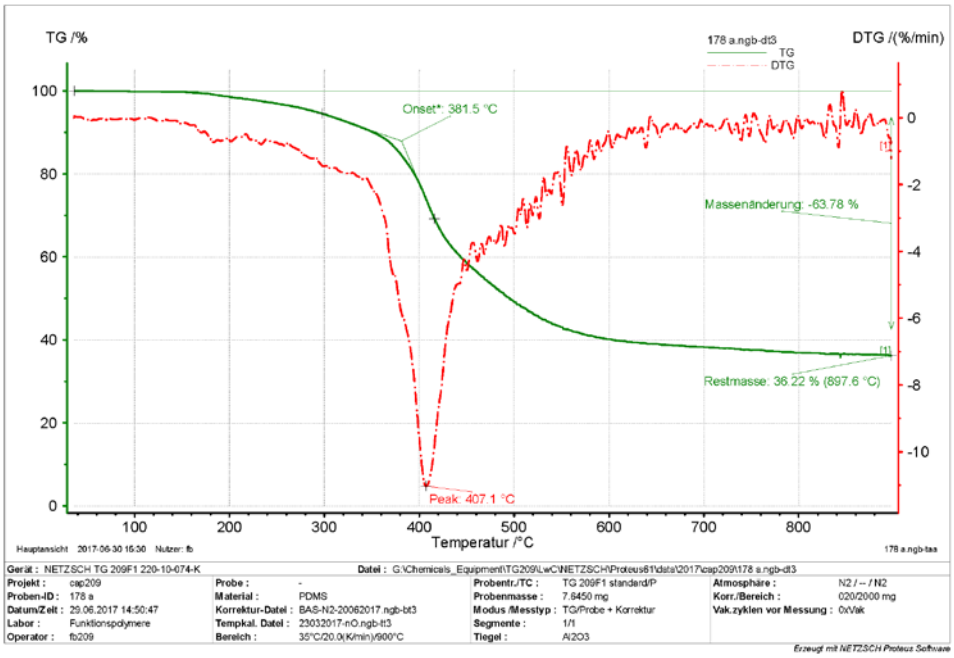

Figure 3.34 TGA curve of **E2-Cl-33**.

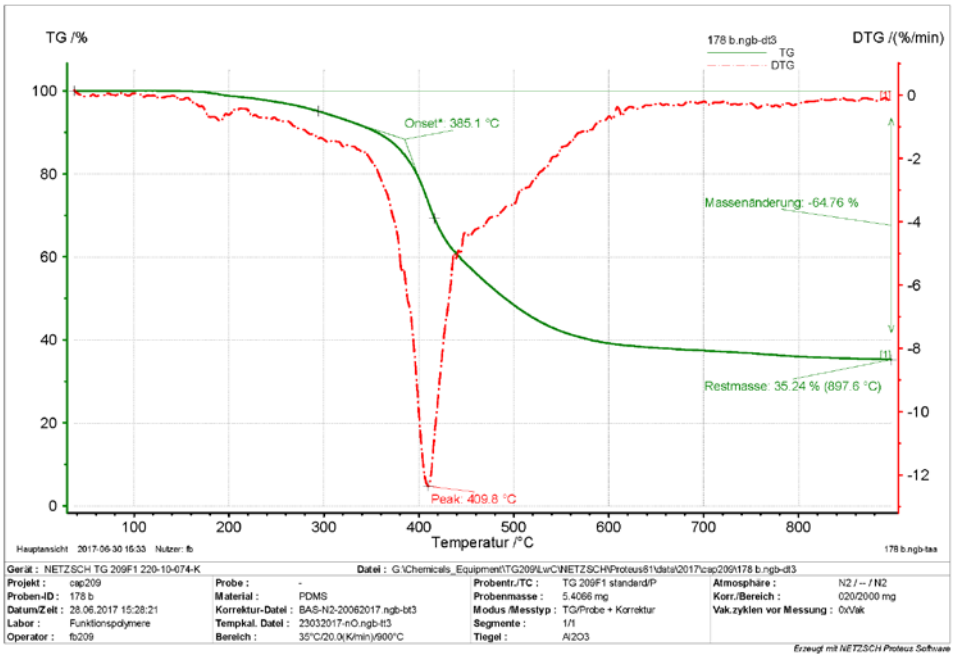

Figure 3.35 TGA curve of **E2-Cl-20**.

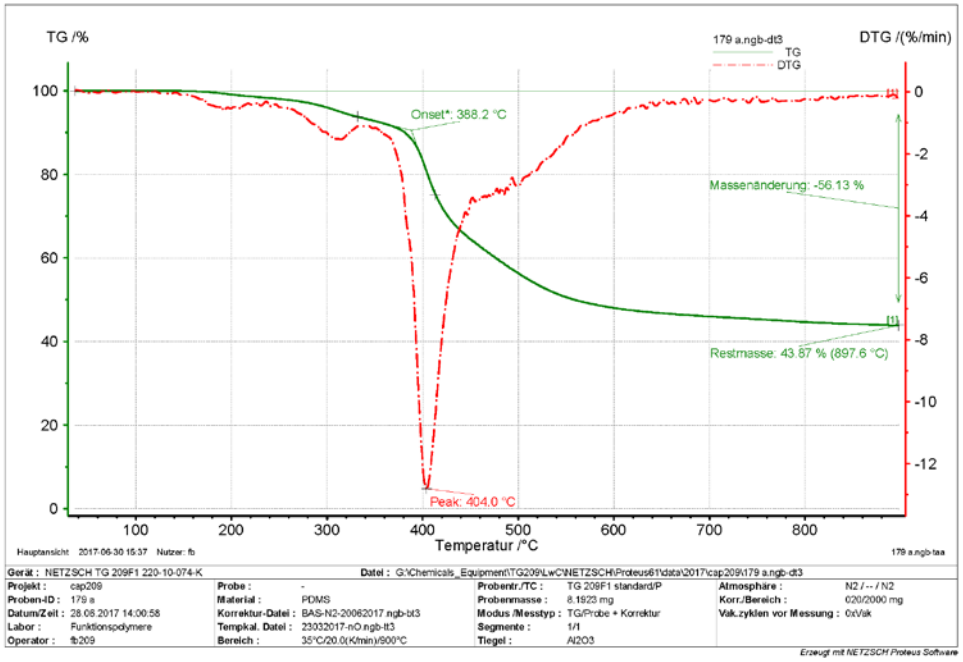

Figure 3.36 TGA curve of **E2-CN-33**.

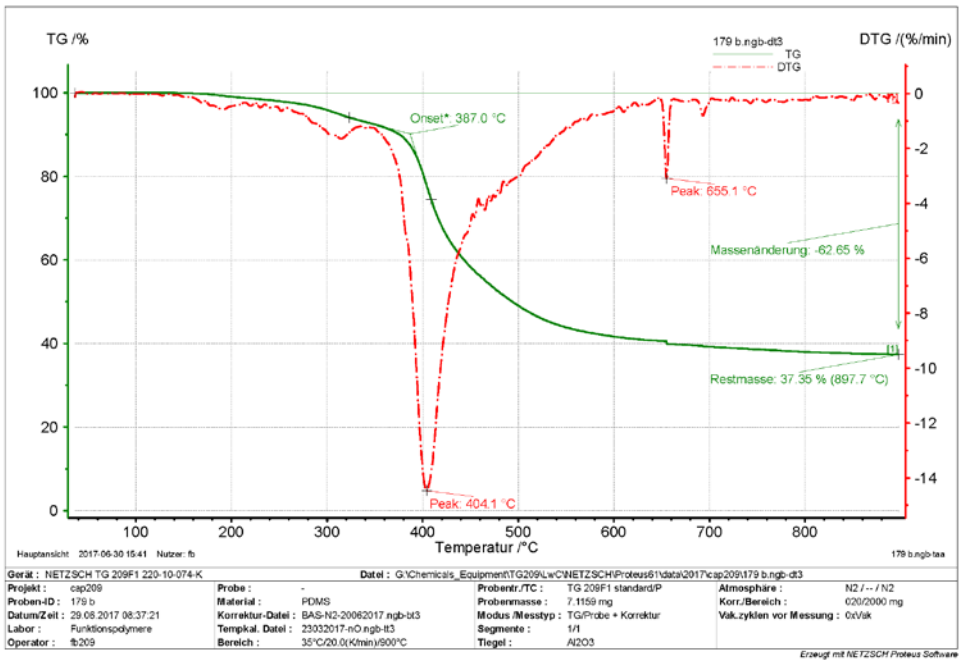

Figure 3.37 TGA curve of **E2-CN-20**.

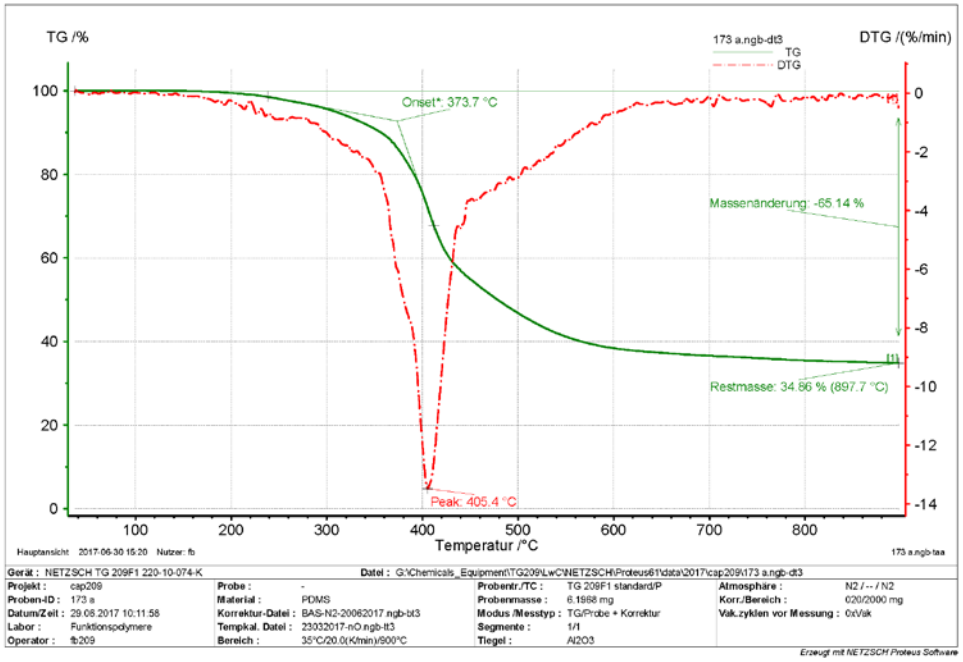

Figure 3.38 TGA curve of **E3-Cl-33**.

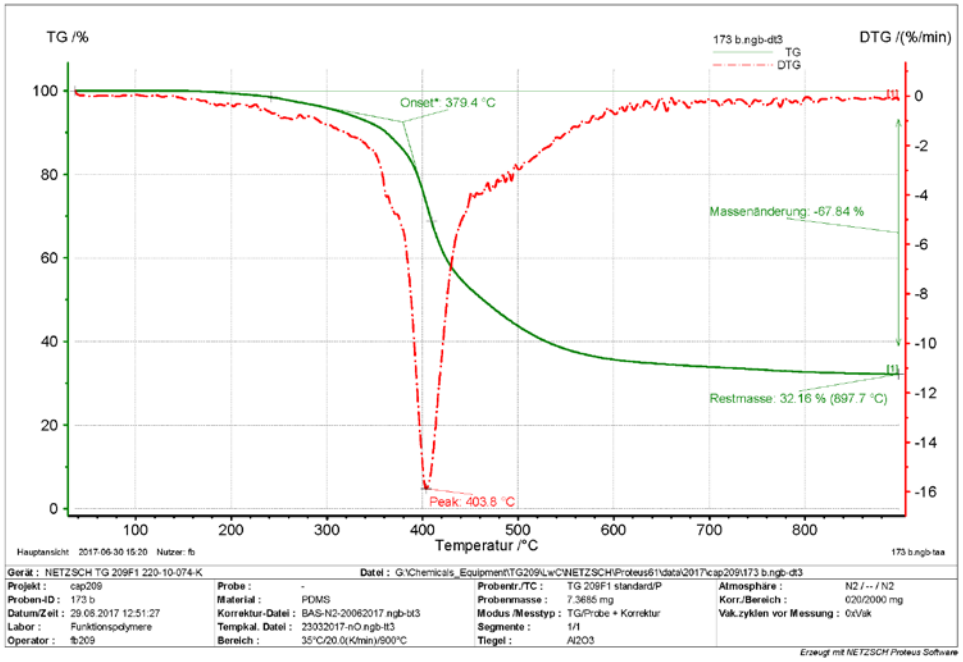

Figure 3.39 TGA curve of **E3-Cl-20**.

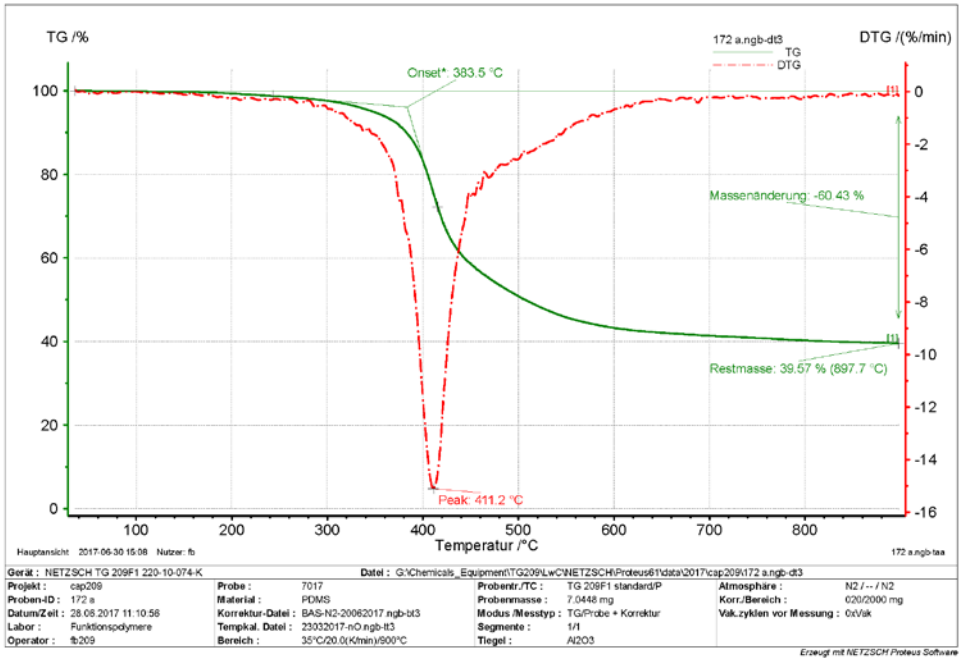

Figure 3.40 TGA curve of **E2-Cl-33**.

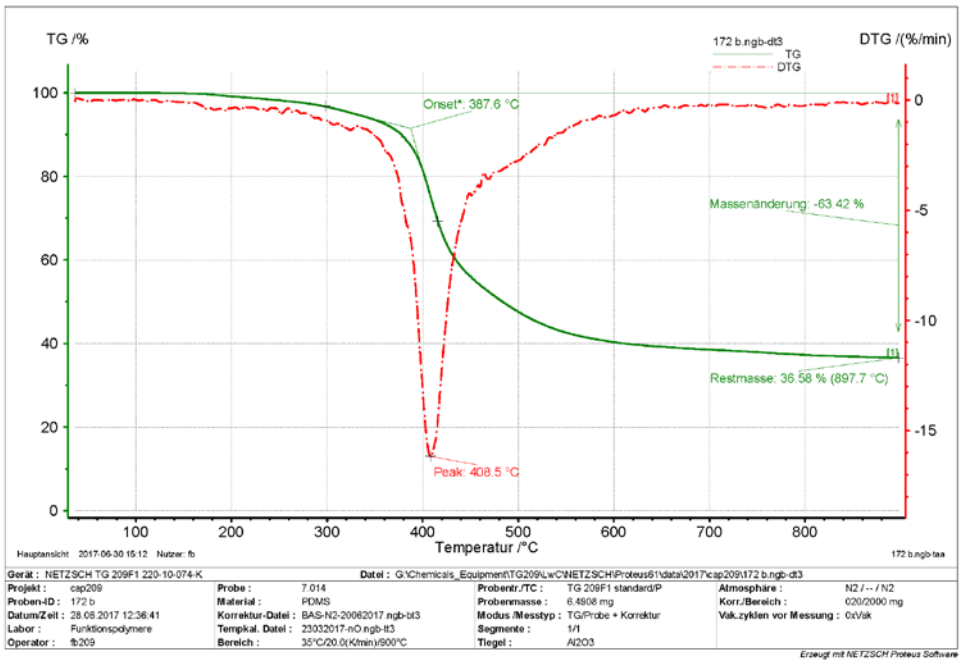

Figure 3.41 TGA curve of **E2-Cl-20**.

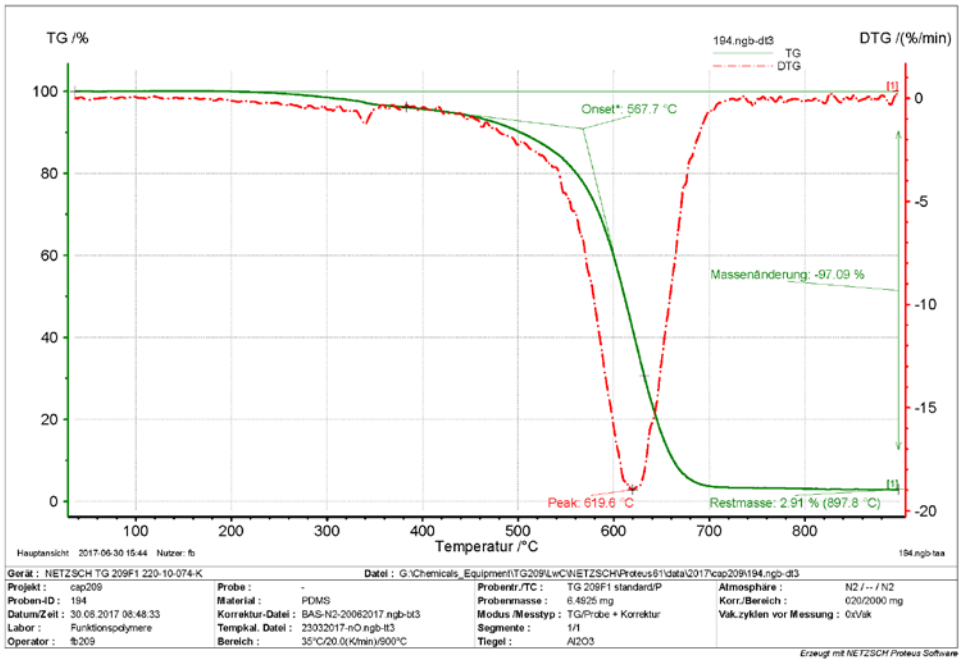

Figure 3.42 TGA curve of **Er-Cl-33**.

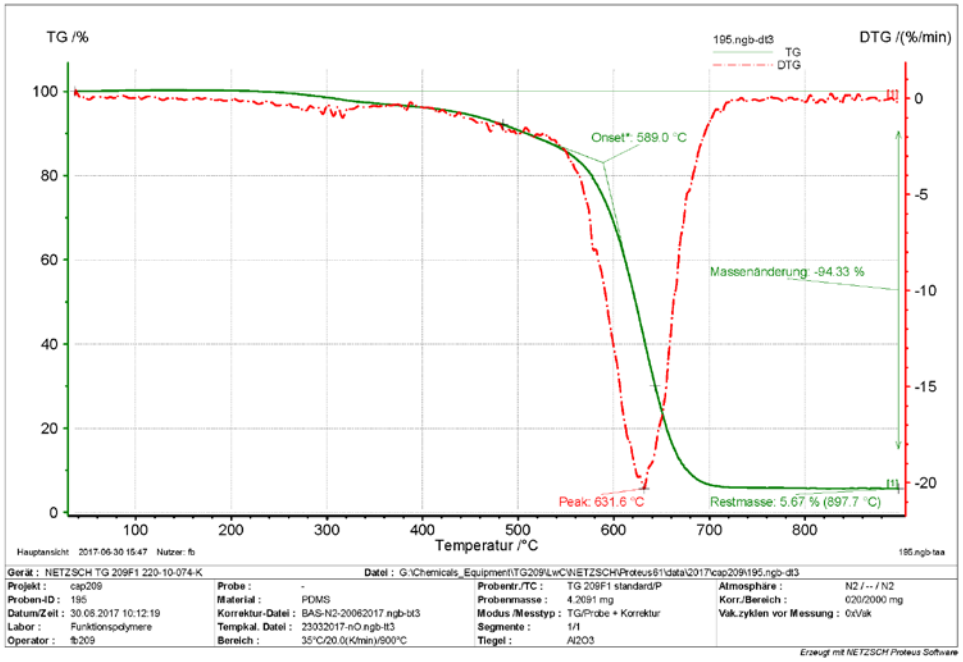

Figure 3.43 TGA curve of **Er-Cl-20**.

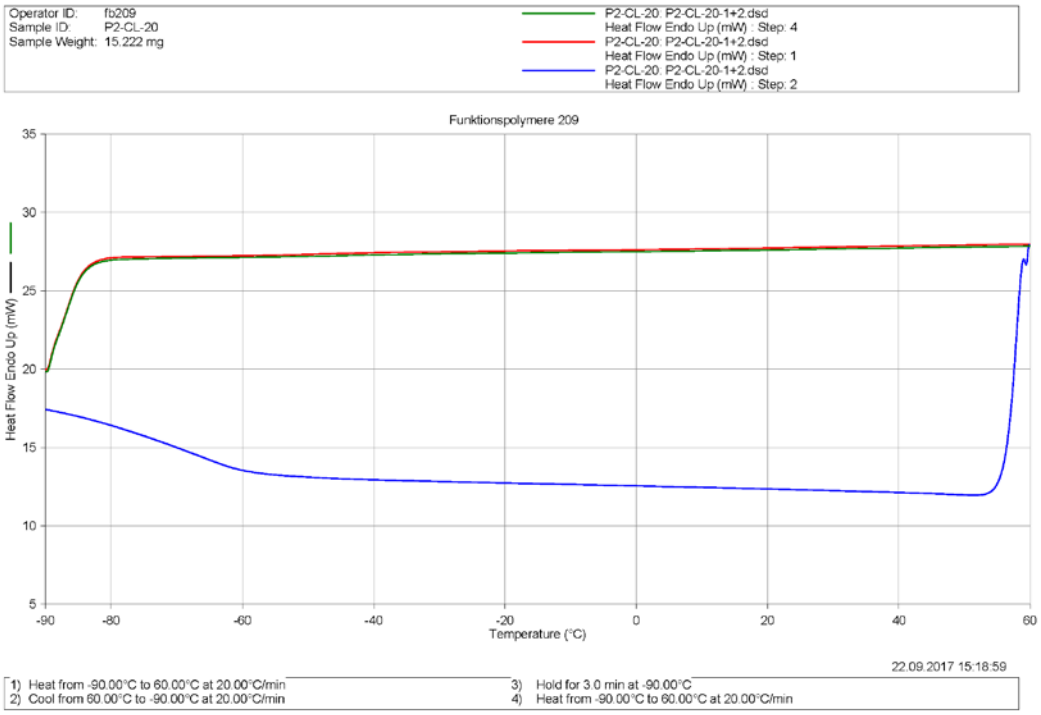

Figure 3.44 DSC curves of **P2-Cl-20**.

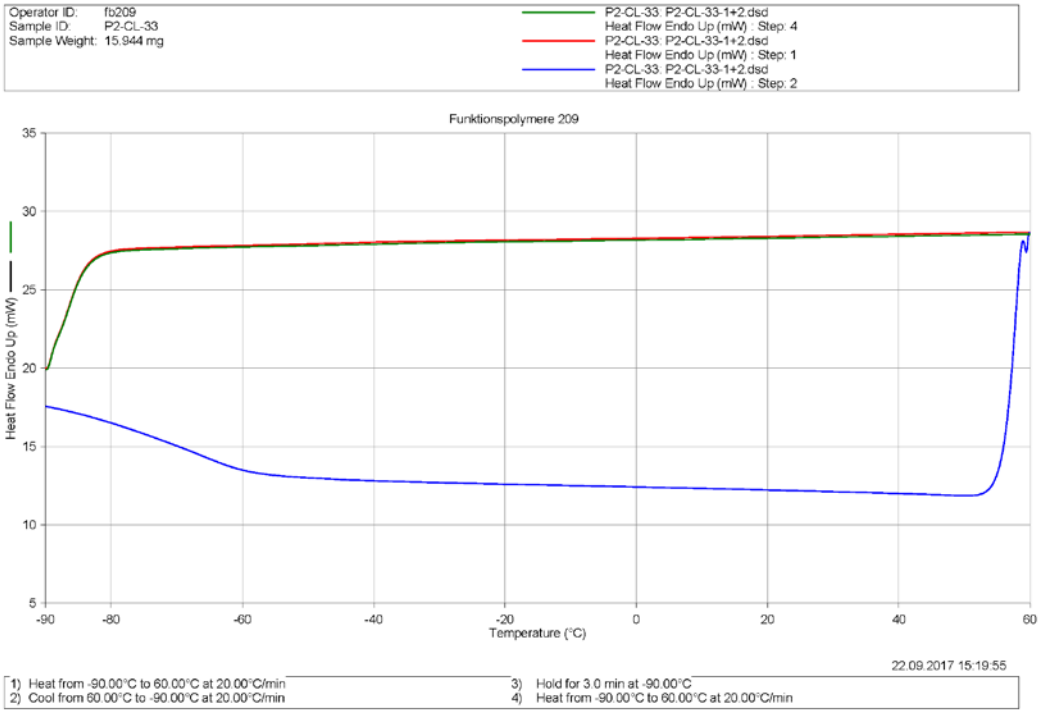

Figure 3.45 DSC curves of **P2-Cl-33**.

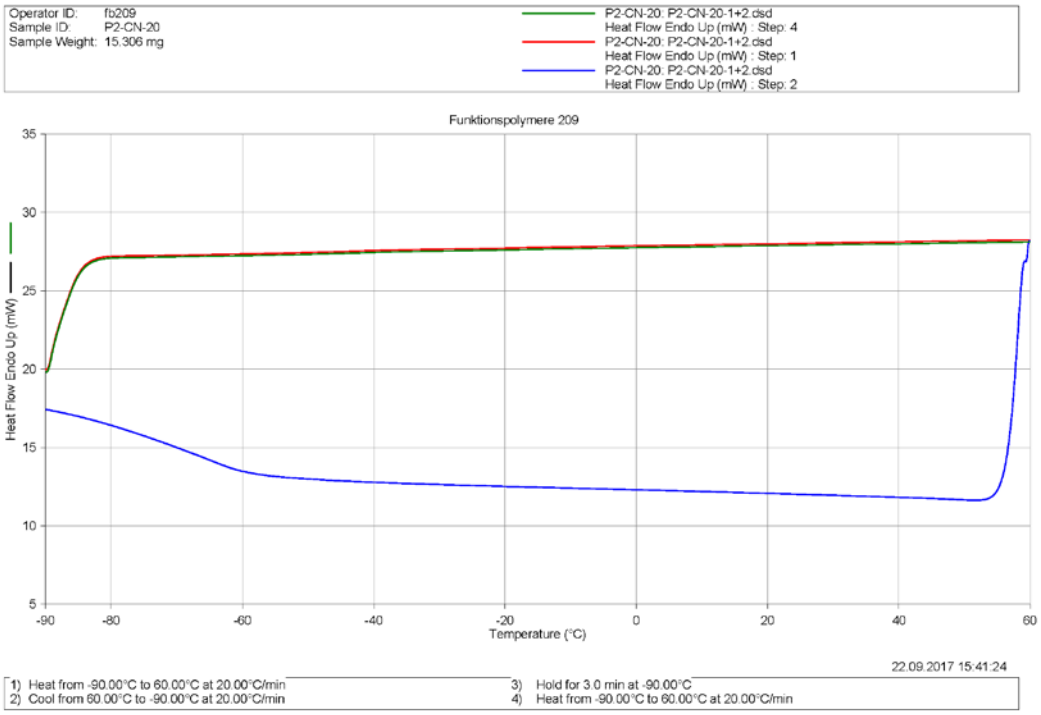

Figure 3.46 DSC curves of **P2-CN-20**.

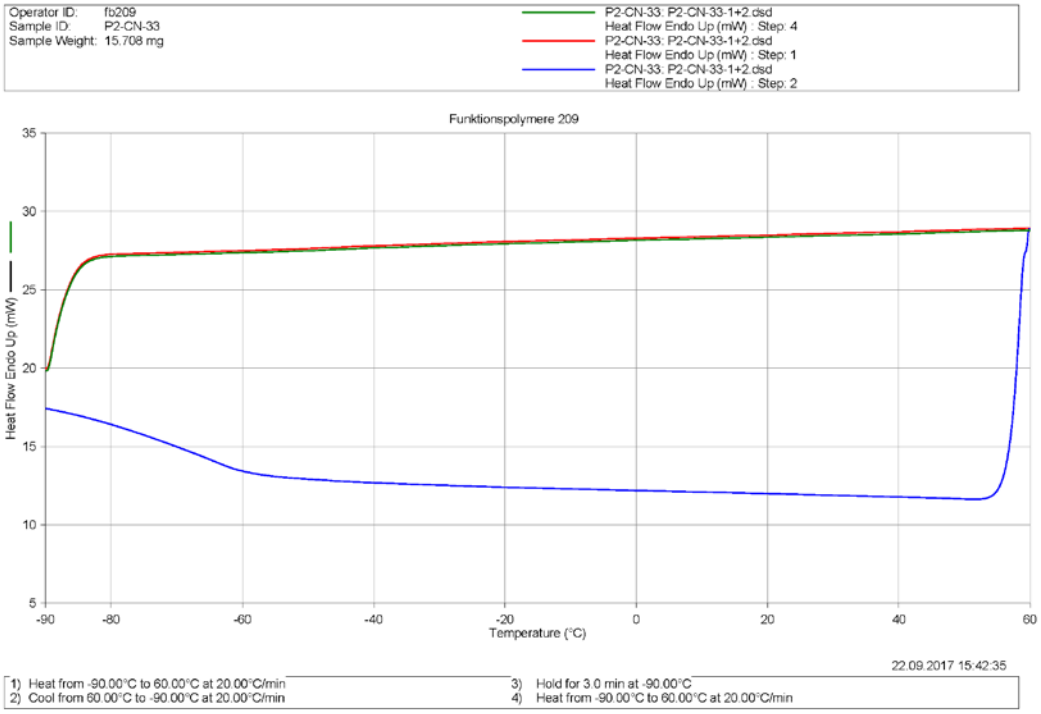

Figure 3.47 DSC curves of **P2-CN-33**.

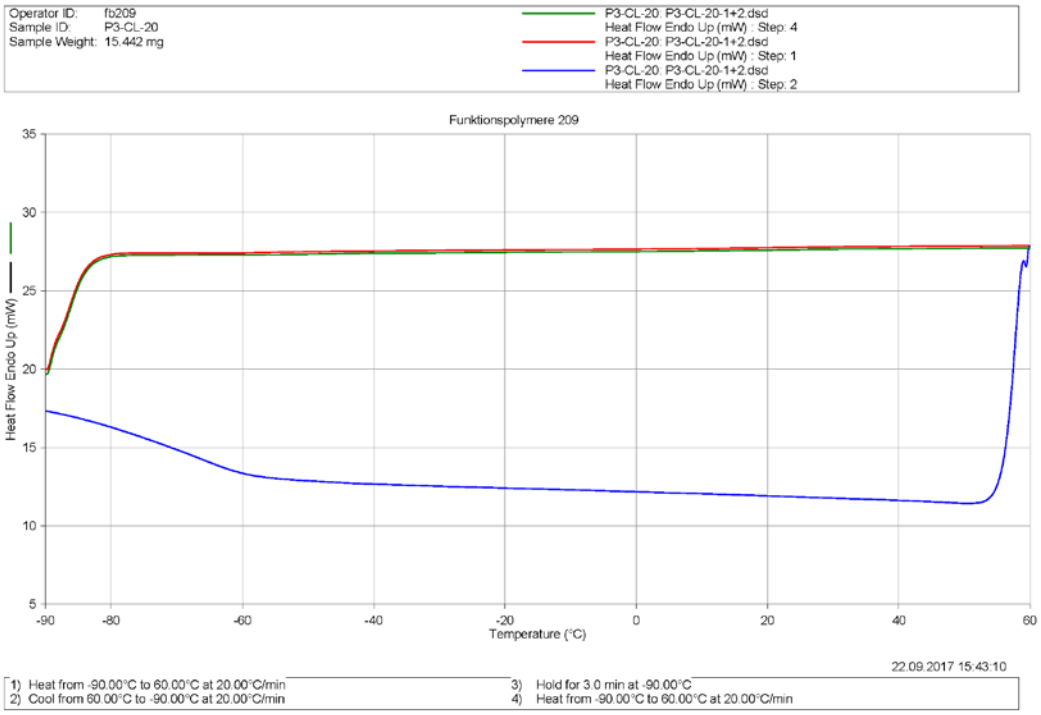

Figure 3.48 DSC curves of **P3-Cl-20**.

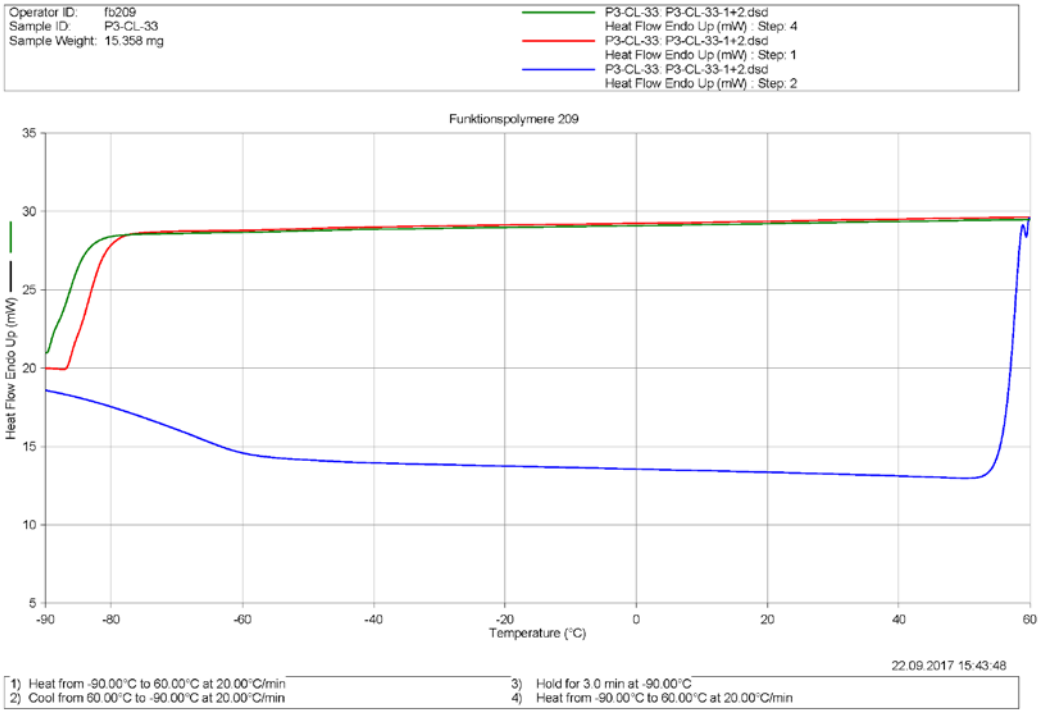

Figure 3.49 DSC curves of **P3-Cl-33**.

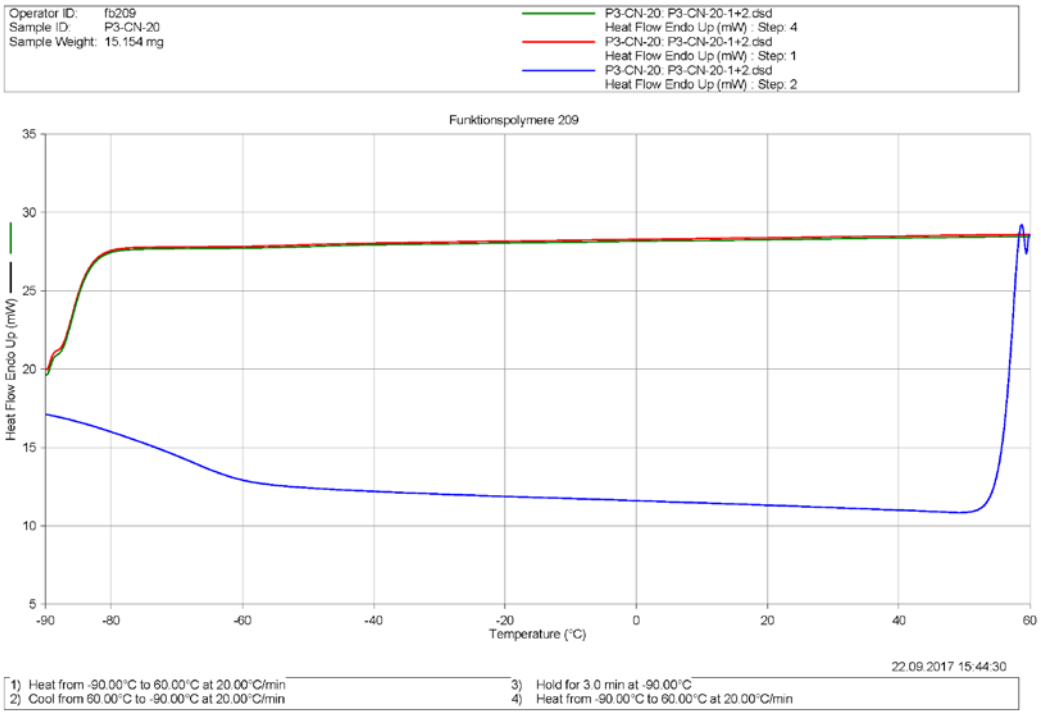

Figure 3.50 DSC curves of **P3-CN-20**.

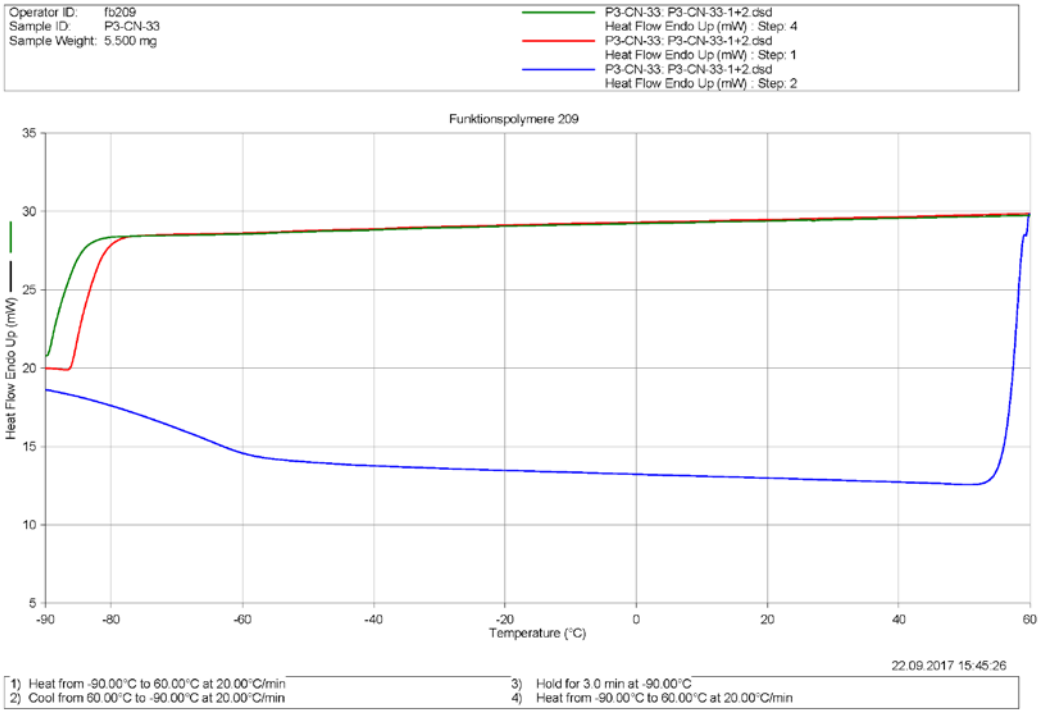

Figure 3.51 DSC curves of **P3-CN-33**.

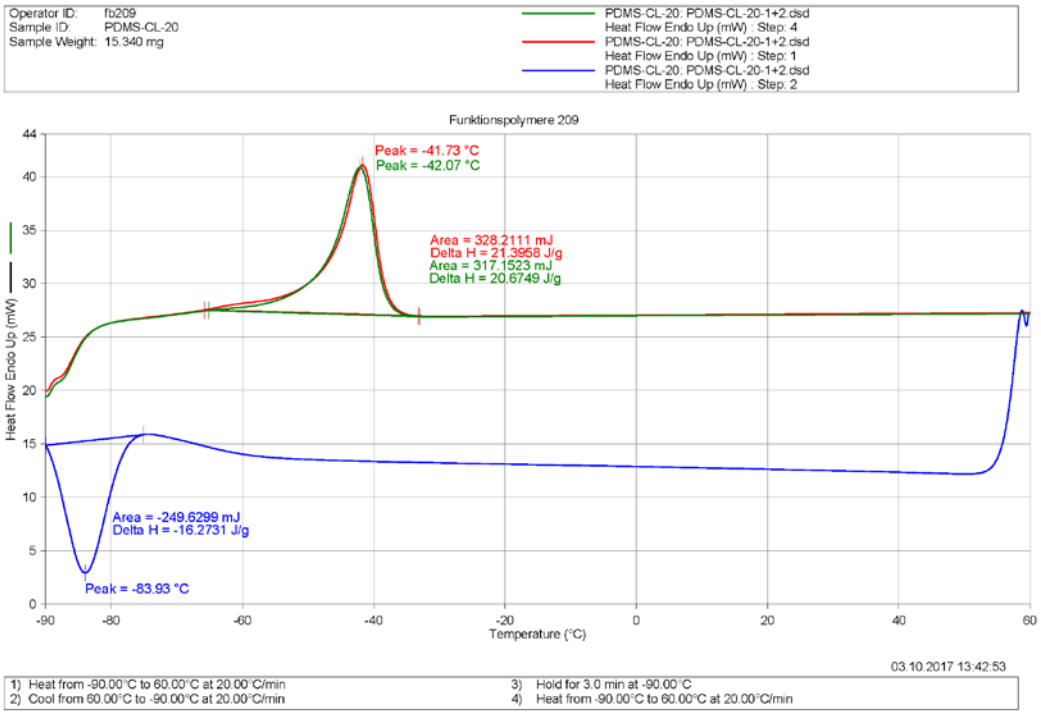

Figure 3.52 TGA curves of **Er-Cl-20**.

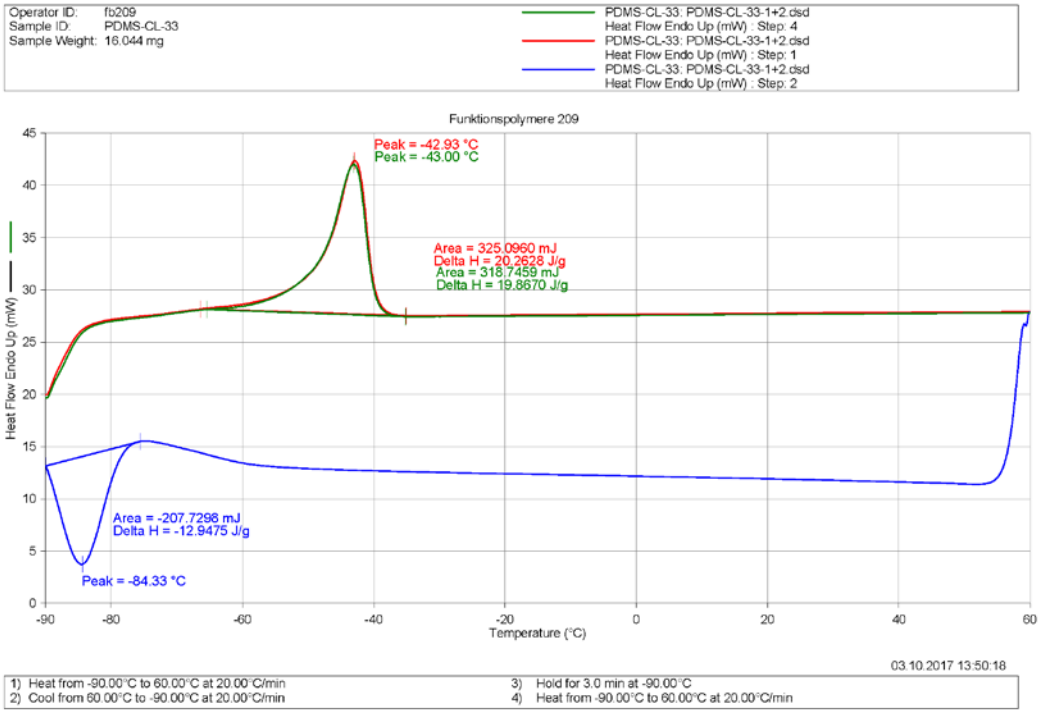

Figure 3.53 TGA curves of **Er-Cl-33**.

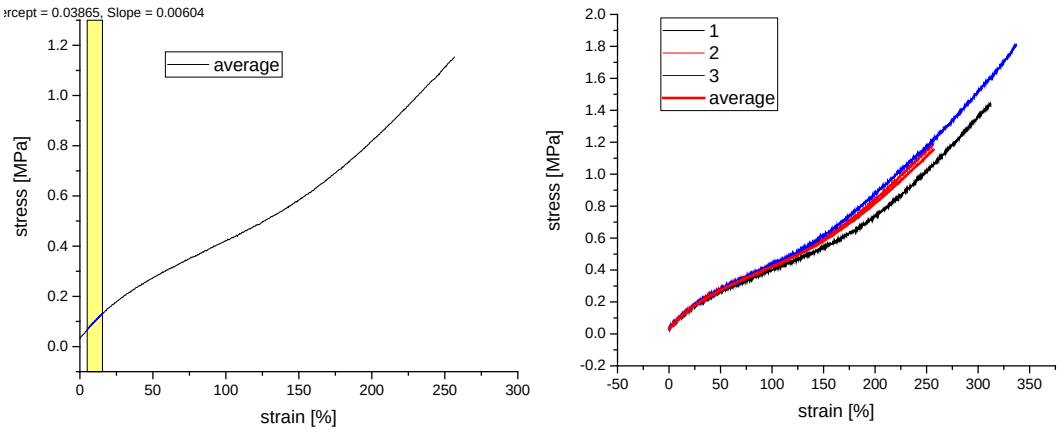

Figure 3.54 Tensile tests of **Er**. Three independent tests were performed.

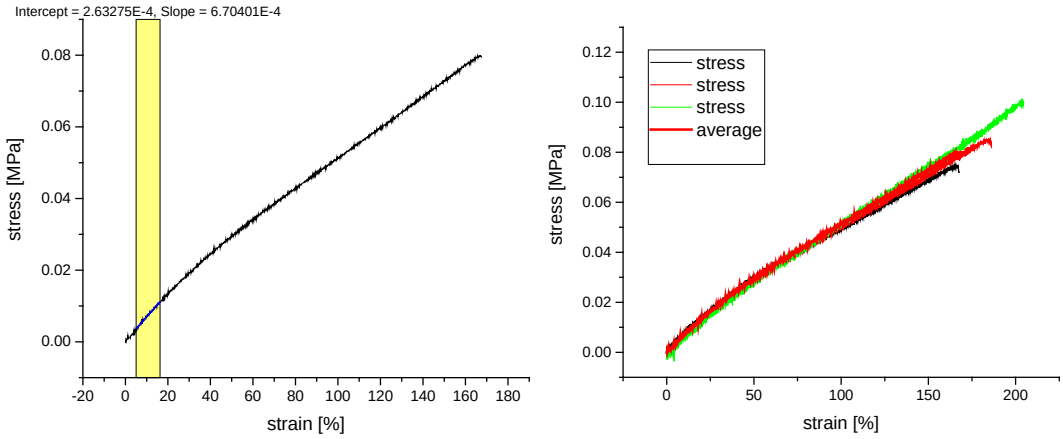

Figure 3.55 Tensile tests of **E2**. Three independent tests were performed.

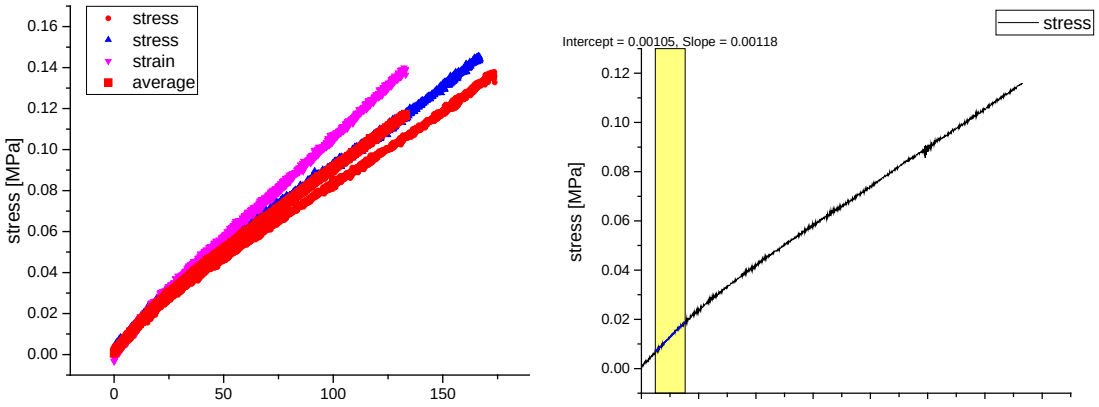

straiFigure 3.56 Tensile tests of **E3**. Three independent tests were performed.

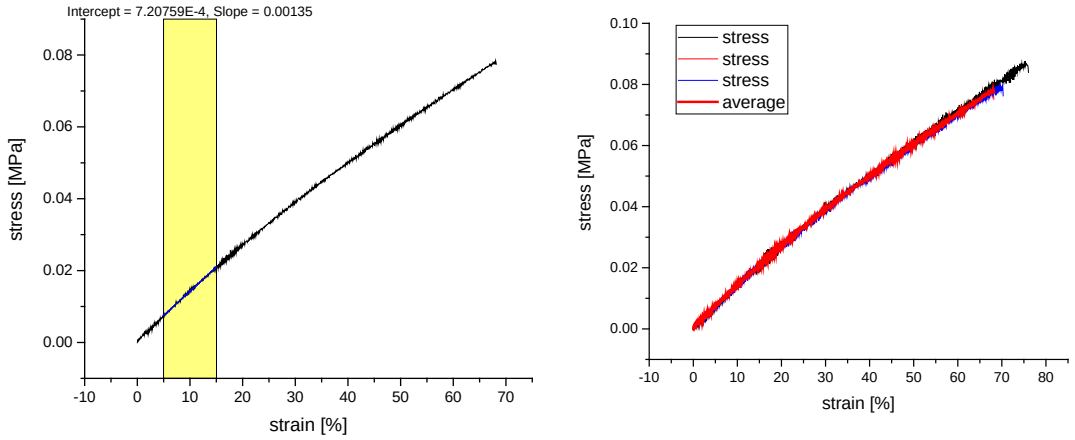

Figure 3.57 Tensile tests of **E4**. Three independent tests were performed.

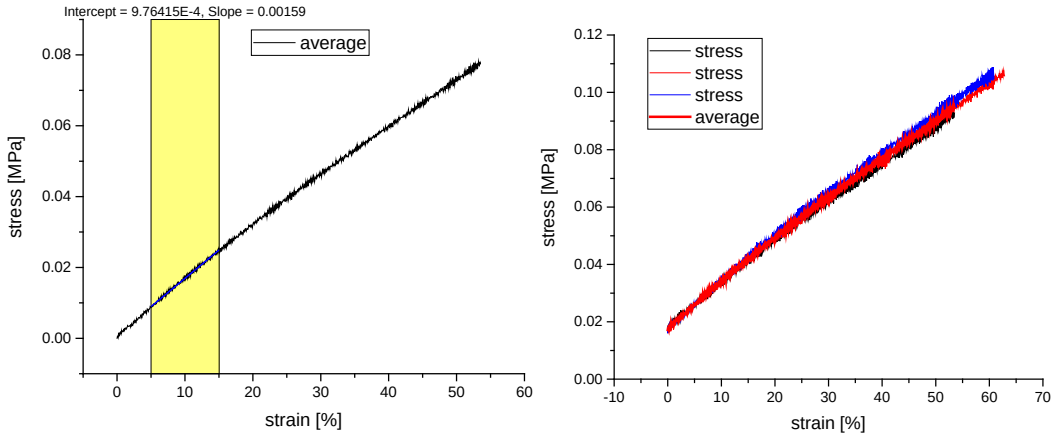

Figure 3.58 Tensile tests of **E6**. Three independent tests were performed.

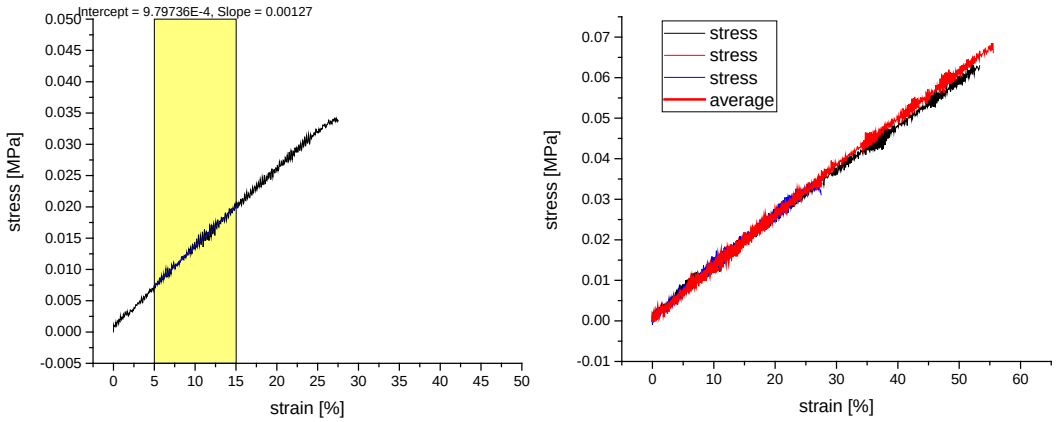

Figure 3.59 Tensile tests of **E8**. Three independent tests were performed.

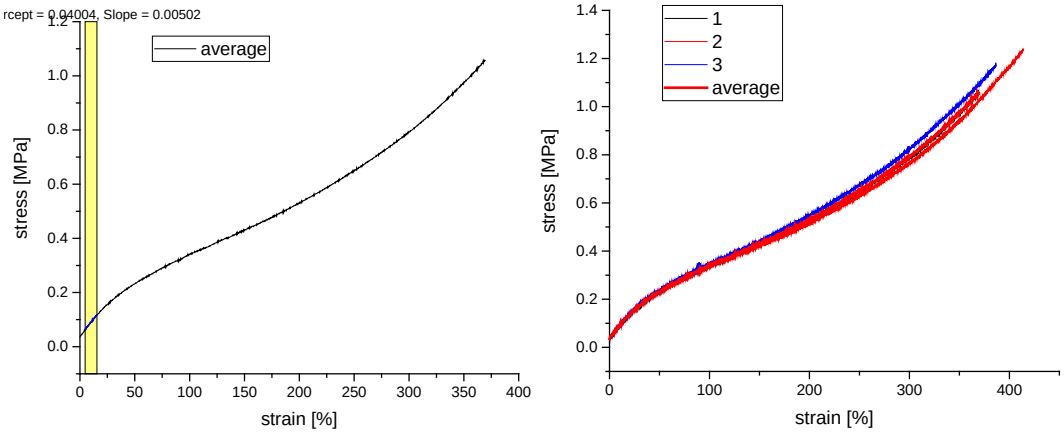

Figure 3.60 Tensile tests of **Er-Cl-20**. Three independent tests were performed.

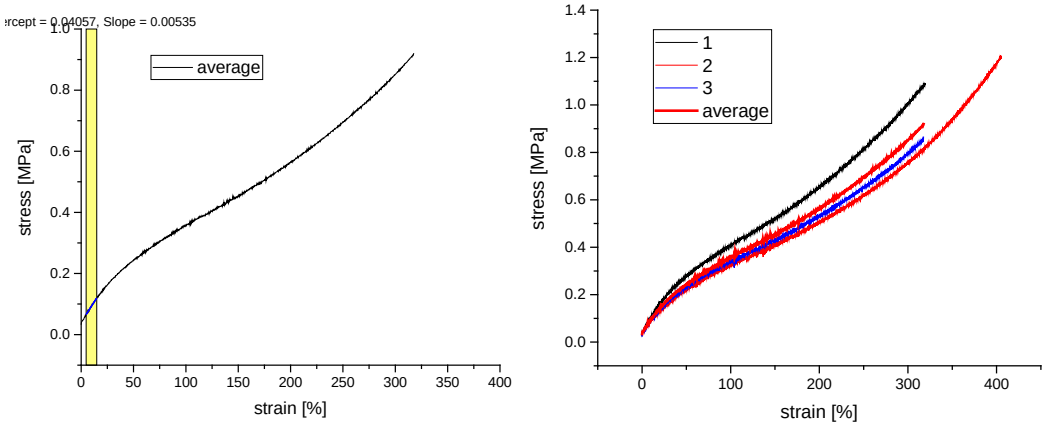

Figure 3.61 Tensile tests of **Er-Cl-33**. Three independent tests were performed.

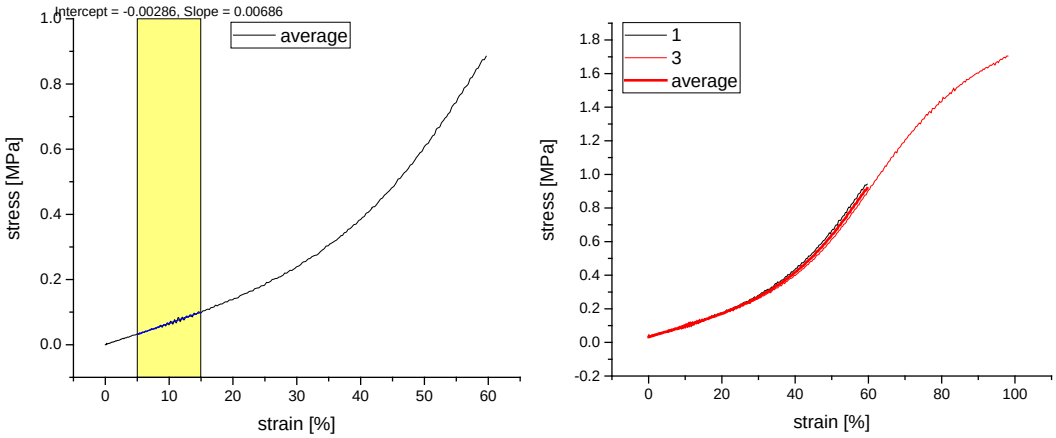

Figure S52. Tensile tests of **E2-Cl-33**. Two independent tests were performed.

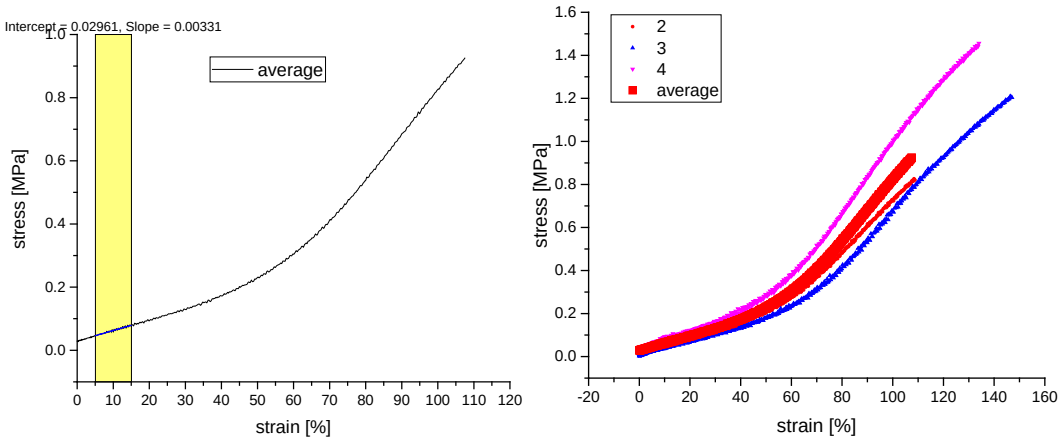

Figure 3.62 Tensile tests of **E2-Cl-20**. Three independent tests were performed.

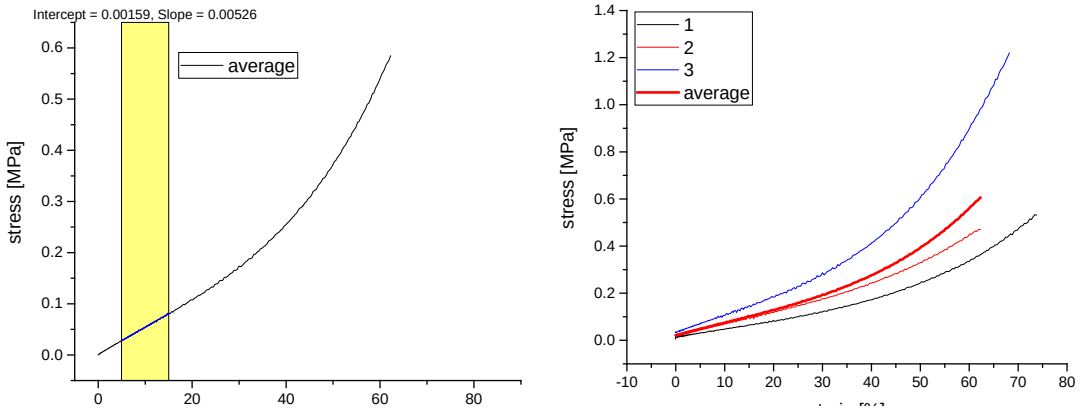

Figure 3.63 Tensile tests of **E3-Cl-33**. Three independent tests were performed.

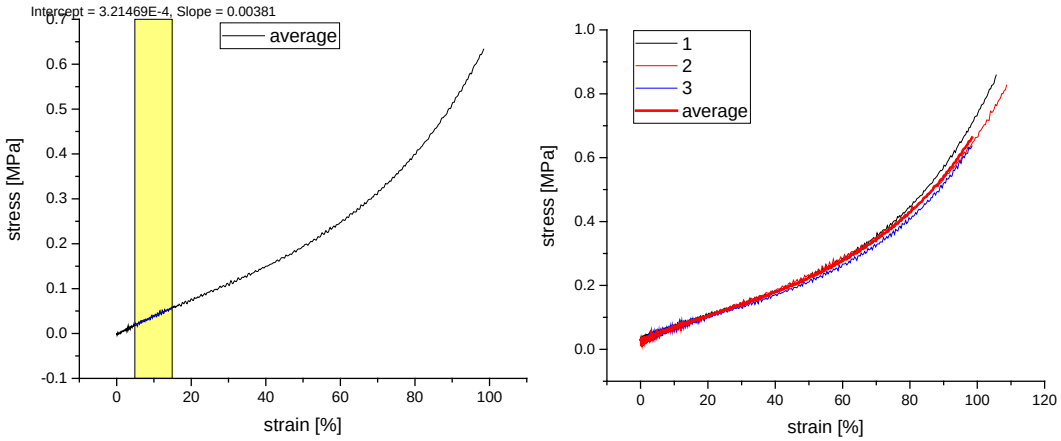

Figure 3.64 Tensile tests of **E3-Cl-20**. Three independent tests were performed.

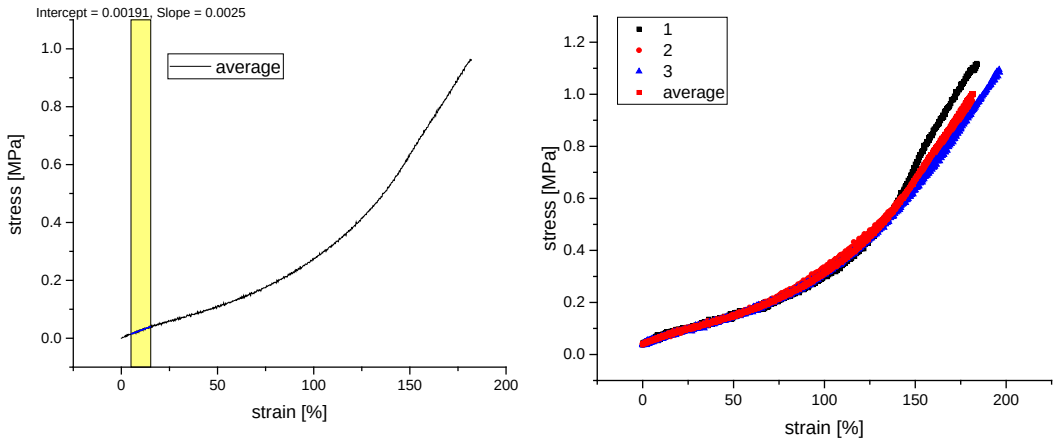

Figure 3.65 Tensile tests of **E2-CN-33**. Three independent tests were performed.

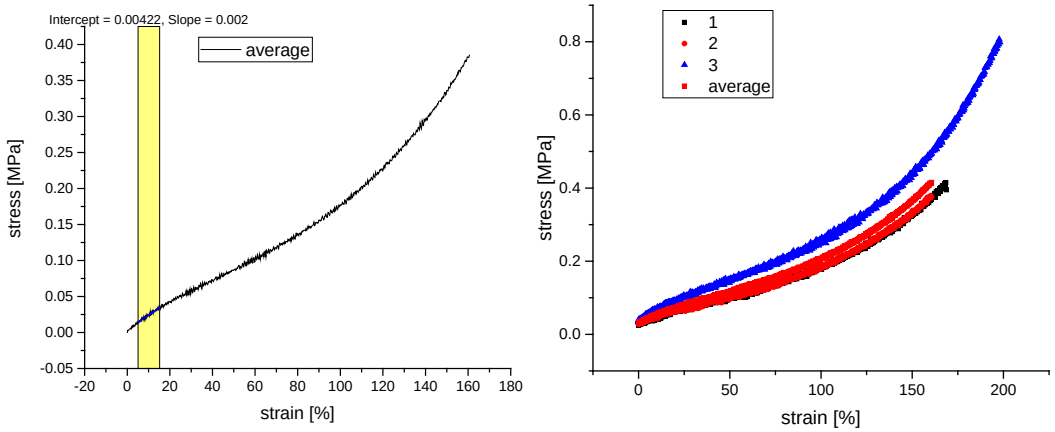

Figure 3.66 Tensile tests of **E2-CN-20**. Three independent tests were performed.

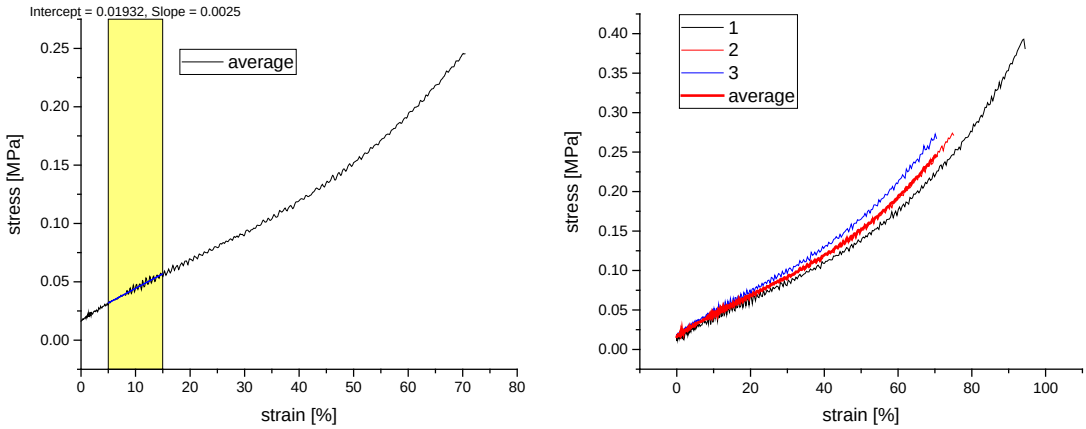

Figure 3.67 Tensile tests of **E3-CN-33**. Three independent tests were performed.

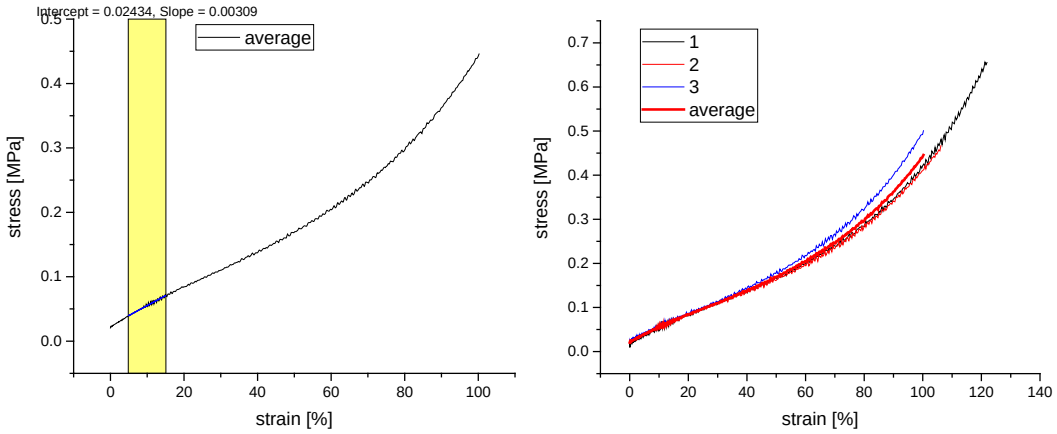

Figure 3.68 Tensile tests of **E3-CN-20**. Three independent tests were performed.

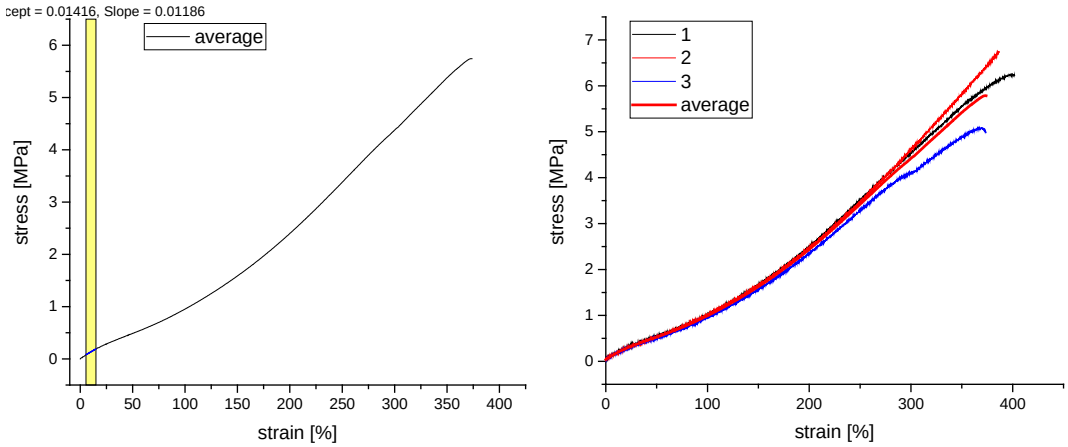

Figure 3.69 Tensile tests of **Elastosil®Film**. Three independent tests were performed.

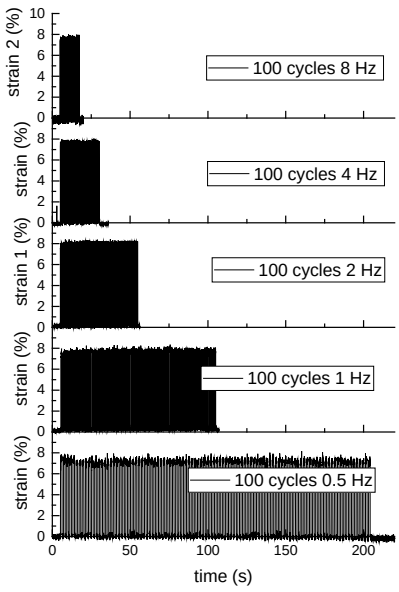

Figure 3.70 Lateral actuation strain of Elastosil®Film 30% prestrained measured at various frequencies (0.5-8 Hz) and an electric field of 90 V μm^{-1}.

Figure 3.71 Photos showing that the actuator inflates in both directions.

Chapter 4 Electrical Energy Generated by Silicone Elastomers Filled with Nano-Spring Carbon-Nanotubes

This chapter is based on the paper

Electrical energy generated by silicone elastomers filled with nano-spring carbon-nanotubes

by

Yun Jae Lee,[1,2] Philip Caspari,[3,4] Dorina M. Opris,[4] Frank A. Nüesch,[3,4] Sora Ham,[1,5] Jung-Hyuk Kim,[1,2] Sung-Ryong Kim,[6] Byeong-Kwon Ju,[2] and Won Kook Choi[1,5]

[1]Center for Opto-Electronic Materials and Devices, Post-Silicon Semiconductor Institute, Korea Institute of Science and Technology, Hwarangro 14 gil 5, Sungbuk Gu, Seoul 02792, Korea. wkchoi@kist.re.kr

[2]Department of Electronic, Electrical, and Computer Engineering, College of Engineering, Korea University, 145 Anam-ro, Seongbuk-gu, Seoul 02841, Korea.

[3]Laboratory for functional polymers, Empa, Swiss Federal Laboratories for Materials Science and Technology, Überlandstrasse 129, 8600 Dübendorf. Switzerland. dorina.opris@empa.ch

[4]École Polytechnique Fédérale de Lausanne (EPFL), Institut des matériaux, Station 12, CH 1015, Lausanne, Switzerland.

[5]Department of Nanomaterials and Nano Science, Korea University of Science and Technology (KUST), 217 Gajeong-ro Yuseong-gu, Daejeon 34113, Korea.

[6]Department of Polymer Engineering, Korea National University of Transportation, 50 Daehak-ro, Chungjusi, Chungbuk 27469, Korea.

Y.J.Lee and P. Caspari contributed equally to this work.

Adapted from

J. Mater. Chem. C **2019**, *7*, 3535

DOI: 10.1039/c8tc06460a

with permission from the Royal Society of Chemistry

Author Contributions:

P. Caspari performed the preparation of the silicone elastomers and devices as well as their characterization and contributed to the manuscript.

4.1 Abstract

Dielectric elastomer generators (DEGs) are flexible capacitors that convert mechanical into electrical energy. They rely on an external voltage source to charge the capacitor during each operation cycle. An alternative to this is an autonomous DEG which operates with an electret as integrated voltage source. To increase the amount of energy generated per cycle, elastomers with increased permittivity, low viscoelastic losses and high strain at break are of advantage. Here, we report the synthesis of elastic materials with increased permittivity by blending different silicone matrices with nanospring carbon-nanotubes (NS-CNTs) particles and their performance as dielectric in electret DEGs. The best material developed has a dielectric permittivity of $\varepsilon' = 4.6$, a mechanical loss factor of 0.03 and a strain at break of 270%. The output voltage of the DEG constructed using this composite increases from 8.8 V to 14.5 V, when the strain increases from 33% to 66%, respectively. Additionally, the output voltage increases with the rise in permittivity, from 9.3 V for a regular polydimethylsiloxane elastomer ($\varepsilon' = 2.9$) to 14.5 for the best composite ($\varepsilon' = 4.6$).

4.2 Introduction

The search for new functional materials and devices that produce reliable energy from green sources has increased significantly in the last years. Nature offers a number of sources of unlimited energy such as ocean waves, wind, and flow energy from rivers.[1] Dielectric elastomer generators (DEGs) are stretchable capacitors capable of converting mechanical into electrical energy.[2–4] They consist of a thin elastic dielectric film, on whose surface two compliant electrodes are deposited. The DEG changes its capacitance during stretching. When the elastic capacitor is stretched and charged at a certain voltage, and then let relax by the elastic restoring forces, a change in voltage is observed. This allows converting mechanical energy into electrical energy.[5–10] The maximal energy converted by DEG is limited by the dielectric breakdown, dielectric permittivity and mechanical properties such as viscoelastic losses and strain at break of the dielectric elastomer used.[8,11,12] Several DEG prototypes that harvest energy from waves and river's flow,[13–16] or human body motion were developed and showed promising performance.[17–19]

Polyurethanes,[7,20] natural rubber,[21] polyacrylates,[19,22–25] and PDMS elastomers[14,26–30] are among the most intensely studied dielectric elastomers for DEG applications. PDMS dielectric elastomers show superior mechanical stability,[31] chemical inertness and fast response speed[32] combined with excellent insulating properties.[33,34] However, the permittivity of PDMS elastomers is about 3, which is lower than that of polyurethane or polyacrylate elastomers. Chemical modification of polysiloxanes with polar groups and blending polysiloxanes with conductive fillers like Ag nanoparticles, polyaniline, polythiophene, and CNT have been used to increase the permittivity of polysiloxanes. For some of these materials it was predicted that the amount of energy harvested is increasing with the permittivity.[35–37] Despite the abundant literature on high permittivity elastomers[38–42] and composites,[43–46] reports regarding the use of such materials in generators are rare. To the best of our knowledge only one report by Wang *et al.* exists, in which materials with increased permittivity were evaluated as dielectric for DEG.[7] The limited literature on high permittivity elastomers for DEG applications may be due to the complex setup used for the energy harvesting cycle which poses safety issues, because of the high voltage and current involved. A solution to this may be the use of electret DEGs introduced by Sylvestre *et al.*[27,47–49] Electret DEGs use as a voltage source an electret which polarizes the dielectric.

It was the aim of this work to develop novel silicone based elastomers with increased permittivity and to evaluate their potential as dielectric to harvest energy from mechanical motion using an electret DEG setup. To achieve this, a nanospring carbon nanotubes filler (**NS-CNTs**) recently developed at KIST was used as filler to increase the dielectric permittivity of either a PDMS or a poly(ethylthiopropyl methyl)siloxane matrix. The composites were cross-linked with polar triethoxysilane cross-linkers via a condensation reaction catalyzed by tin. Composites containing 10 wt% **NS-CNTs** filler were prepared and the influence of the filler on the mechanical properties of the silicone composites was investigated by tensile tests and dynamic-mechanical analysis (DMA). The homogeneity of the filler dispersion in the composites was proven by scanning electron microscopy. The dielectric properties were evaluated by impedance spectroscopy. Finally, the performance of the prepared materials as dielectric in electret DEGs was also evaluated.

4.3 Results and discussion

Scheme 4.1 shows an overview of all materials synthesized. A hydroxyl terminated polydimethylsiloxane and a poly(methyl propylthioethyl)siloxane **P3**, prepared in our lab, were cross-linked with either 2-cyano-triethoxysilane or 3-chloropropyltriethoxysilane, respectively via a condensation reaction catalyzed by dibutyltin dilaurate to form materials **PDMS-CN** and **P3-Cl**.[50] For both matrices, an excess of triethoxysilane reagents was used. As a result, both matrices contain silsesquioxane structures, which are generated *in-situ* during cross-linking.[51] To increase the dielectric permittivity of **PDMS-CN** and **P3-Cl** matrices, **NS-CNTs** filler was used. This filler is known and was prepared according to the literature.[52] Shortly, its synthesis started from functionalized single-wall CNTs and zinc acetate at elevated temperatures, where ZnO nanoparticles coated with **NS-CNTs** are formed.[52] The formed particles are thereafter treated with HCl to release the **NS-CNTs**. The formed **NS-CNTs** filler has a nanometer size and has been successfully used to enhance the dielectric permittivity of poly(vinylidenefluoride-*co*-trifluoroethylene).[52] It is well dispersible in dimethylformamide , however it cannot be dispersed in common solvents used for processing polysiloxanes, like tetrahydrofuran. Therefore, the first challenge to overcome was to increase the compatibility of the filler with the silicone matrices. This was achieved by a surface treatment of **NS-CNTs** with 2-cyanoethyl(triethoxy)silane as described in the experimental part. For the composites, 10 wt% of **NS-CNTs** filler was used in either **PDMS-CN** or **P3-Cl** with formation of materials **PDMS-CN-CNT** and **P3-Cl-CNT**. The homogeneity of the filler dispersion in the composites was proven by scanning electron microscopy (Fig. 4.8, Section 4.7). The particles are evenly distributed in the matrix and no agglomerates can be observed.

As reference materials the commercial silicone **Elastosil®Film** and **PDMS** prepared from a hydroxyl terminated polydimethylsiloxane cross-linked with poly(methylhydrosiloxane-*co*-dimethylsiloxane) cross-linker with a thickness of 200 µm were used. The impact of **NS-CNTs** filler on different materials properties was evaluated and the obtained results were compared with the reference materials, **PDMS-CN**, and **P3-Cl**.

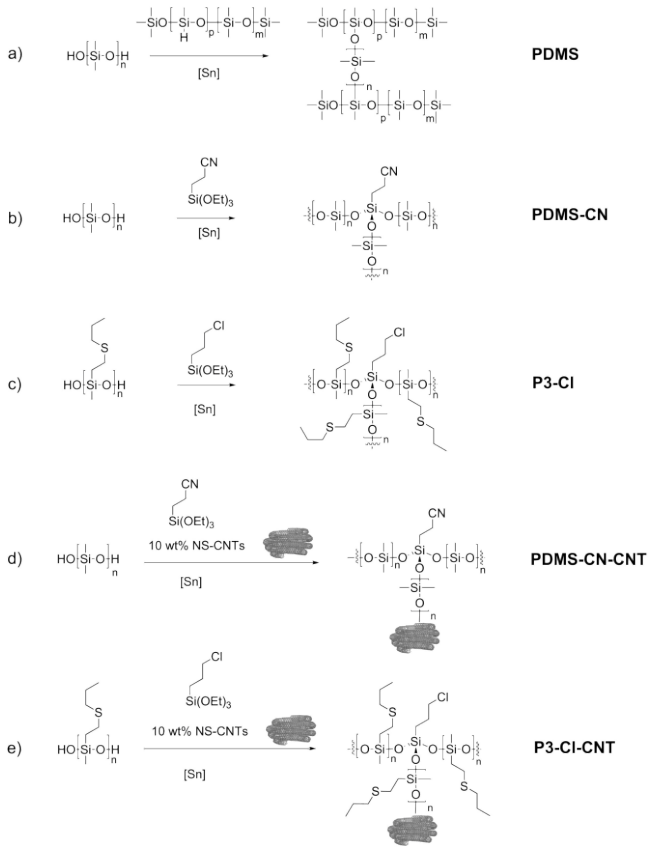

Scheme 4.1 Overview of all synthesized materials using dibutyltin dilaurate catalyst and: a hydroxyl terminated PDMS matrix and poly(methylhydrosiloxane-*co*-dimethylsiloxane) cross-liker (a), a hydroxyl terminated PDMS matrix and (2-cyanoethyl)triethoxysilane cross-linker (b), a hydroxyl terminated poly(methylpropylthioethyl)-siloxane (**P3**) and (3-chloropropyl)triethoxysilane cross-linker (c), a hydroxyl terminated PDMS matrix, (2-cyanoethyl)triethoxysilane cross-linker

and 10 wt% functionalized NS-CNTs (d) and a **P3**, (3-chloropropyl)triethoxysilane cross-linker and 10 wt% functionalized **NS-CNTs** (e).

The mechanical properties of the films were evaluated in tensile tests (Fig. 4.1). The stress–strain curves were averaged from three independent measurements (Fig. 4.9-4.14). The **PDMS** reference material had an average strain at break of 372% and an elastic modulus $Y_{10\%}$ = 0.6 MPa, whereas **Elastosil®Film** had an average strain at break of 485% and an elastic modulus $Y_{10\%}$ = 1.2 MPa. For **PDMS-CN** the $Y_{10\%}$ was about 1.28 MPa and for **PDMS-CN-CNT** the $Y_{10\%}$ was slightly lower of about 1.0 MPa, due to the lower amount of 2-cyanoethyl-(triethoxy)silane used in **PDMS-CN-CNT**. The average strain at break was 213% for **PDMS-CN** and 270% for **PDMS-CN-CNT**. The materials prepared starting from **P3** showed rather low strain at break, e.g., **P3-Cl** and **P3-Cl-CNT** had an average strain at break of 114% and of 95%, and an $Y_{10\%}$ of 0.2 MPa and 0.3 MPa, respectively.

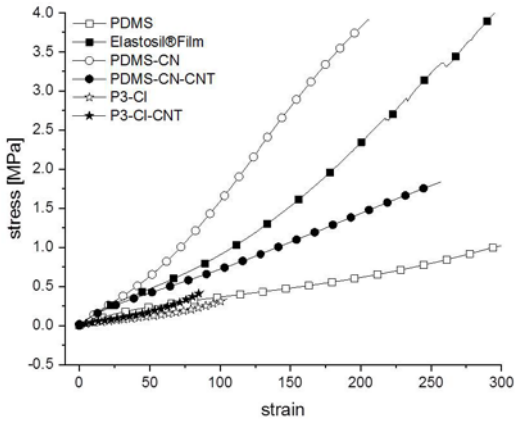

Figure 4.1 Stress–strain curves of all materials. They are the average from three independent measurements. The strain at break is the the minimum value obtained from the three tests. In text the avarage of the strain at break from three independent measurements is given.

Dynamic mechanical analysis (DMA) was used to characterize the viscoelastic behavior of all materials (Fig. 4.2).

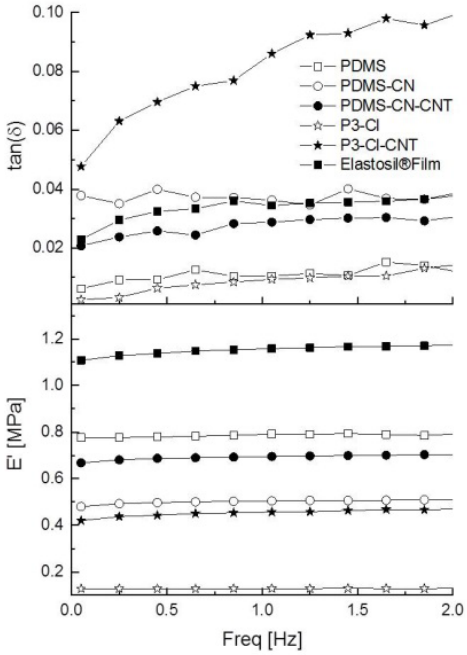

Figure 4.2 Dynamic mechanical analysis of all materials at 2% strain and at a frequency range between 0.05 to 2 Hz.

All thin film elastomers were 2% strained and tested at a frequency range of 0.05 Hz to 2 Hz at 25°C. We consider 1-2 Hz as realistic frequency range for DEG applications, *i.e.* wave energy and human motion harvesters. **PDMS** and **P3-Cl** showed the lowest mechanical loss factor *tan(δ)* which was around 0.01. The mechanical loss factor *tan(δ)* of **Elastosil®Film**, **PDMS-CN**, **PDMS-CN-CNT** was also very low around 0.03. **P3-Cl-CNT** showed a considerable increase of mechanical losses *tan(δ)* to about 0.08 at 1 Hz, which may be an indication of a sluggish cross-linking reaction of **P3** in presence of **NS-CNTs** filler.

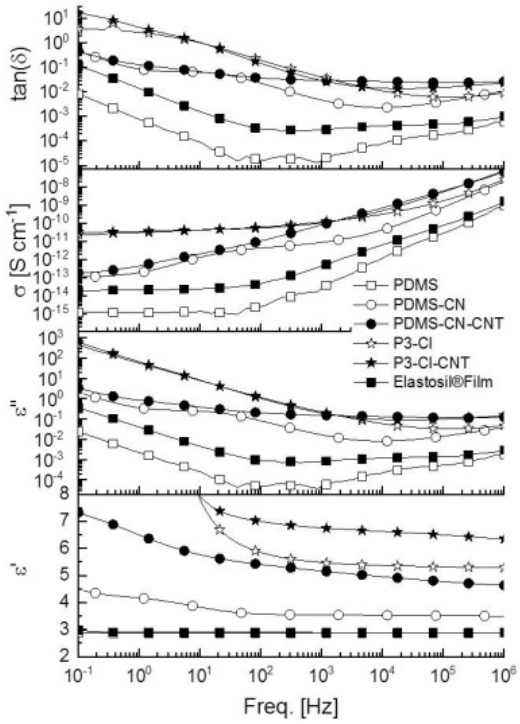

Figure 4.3 Dielectric properties of all materials in the frequency range of 10^{-1} to 10^{6} Hz.

The dielectric properties were measured in a frequency range from 10^{-1} Hz to 10^{6} Hz at ambient temperature (Fig. 4.3, Table 4.1). **PDMS** and **Elastosil®Film** had a permittivity ε' of 2.9, while **PDMS-CN** had a permittivity ε' of 3.5, which is similar to the value previously reported.[50,53] The permittivity of the composites at frequencies above 10^{3} Hz was constant and reached values of 4.6, 5.3, and 6.3 for **PDMS-CN-CNT**, **P3-Cl**, and **P3-Cl-CNT**, respectively. A strong increase in ε' for **P3-Cl** and **P3-Cl-CNT** at low frequencies was observed, which is caused by electrode polarization due to ionic conductivity.[54] Contrary to CNT/PDMS composites previously reported where a rather low amount of filler is needed to reach the percolation threshold, our composites showed excellent dielectric properties at 10 wt% filler.[44] The reason for this is the nano size of the **NS-CNTs** filler used and the increased compatibility of the filler with the matrices used which prevents agglomeration. The highest conductivity of 2.5×10^{-11} S cm^{-1} and 3.4×10^{-11} S cm^{-1} was measured for **P3-Cl** and **P3-Cl-CNT**, respectively, while all the other materials showed a conductivity which was below 2×10^{-13} S cm^{-1}. For materials **PDMS-CN** and **PDMS-CN-CNT** the conductivity was 1.2×10^{-13} S cm^{-1} and 1.9×10^{-13} S cm^{-1}. The lowest conductivity was measured for the silicone films. The conductivity of **PDMS** was 1.3×10^{-15} S cm^{-1} and of **Elastosil®Film** was 1.9×10^{-14} S cm^{-1}. The dielectric breakdown experiments were conducted by placing the dielectric films between two rigid electrodes of 0.25 mm^2 area.[45] For each material ten samples were measured and the average is given in Table 4.1. The highest dielectric breakdown was measured for **Elastosil®Film** and **PDMS**. The dielectric breakdown decreased for the materials modified with polar groups. For example, the dielectric breakdown was 52 V/µm for **P3-Cl** and 59 V/µm for **PDMS-CN**, respectively. The incorporation of **NS-CNTs** resulted in a further reduction of the dielectric breakdown to 48 V/µm for **P3-Cl-CNT** and 41 V/µm for **PDMS-CN-CNT**, respectively. The dielectric breakdown field is a critical material parameter for the DEG, where the amount of energy is increasing with the applied voltage. For the electret DEG the dielectric breakdown is less critical, since the electric fields involved in these devices are far below the dielectric breakdown field. Additionally, the dielectric exposure time to maximum electric field is rather short, contrary to DEG where the dielectric is subjected for longer periods of time to rather strong electric fields. Therefore the probability of dielectric failure in electret DEG is significantly lower as compared to regular DEG.

Table 4.1 Dielectric properties of different materials investigated.

Entry	ε'^{a}	ε''^{a}	$tan(\delta)^{a}$	σ [S cm^{-1}]^{b}	$E_{max}{}^{c}$[V/µm]
PDMS	2.9	2×10^{-3}	6×10^{-4}	1.3×10^{-15}	> 71
Elastosil®Film	2.9	3×10^{-3}	1×10^{-3}	1.9×10^{-14}	82±6[d]
PDMS-CN	3.5	4×10^{-2}	1×10^{-2}	1.2×10^{-13}	59±8
PDMS-CN-CNT	4.6	1×10^{-1}	3×10^{-2}	1.9×10^{-13}	41±5
P3-Cl	5.3	5×10^{-2}	9×10^{-3}	2.5×10^{-11}	52±6
P3-Cl-CNT	6.3	2×10^{-2}	2×10^{-2}	3.4×10^{-11}	48±10

[a]Permittivity ε', dielectric loss ε'', loss tangent $tan(\delta)=\varepsilon''/\varepsilon'$ are given at 10^{6} Hz. [b]Conductivity is given at 10^{-1} Hz. [c]E_{max} was determined by placing the dielectric film between rigid electrodes of 0.25 mm^{2} area. The average of ten measurements is given. [d]Average film thickness of 100 µm.

Finally, experiments to evaluate the potential of all materials as dielectric to harvest energy from mechanical motion were conducted using a home-made electret DEG test device similar to that reported by Jean-Mistral *et al.*,[49] but with some simplifications (Fig. 4.4, Fig. 4.7). We used an electret as a voltage source consisting of a Teflon film charged by corona discharge at an initial surface potential of 1000 V. Because most electret materials reported to date are rigid, they cannot be reversible stretched. To be nevertheless able to stretch them, the electret was shaped in an accordion like structure (Fig. 4.4).[47,49]

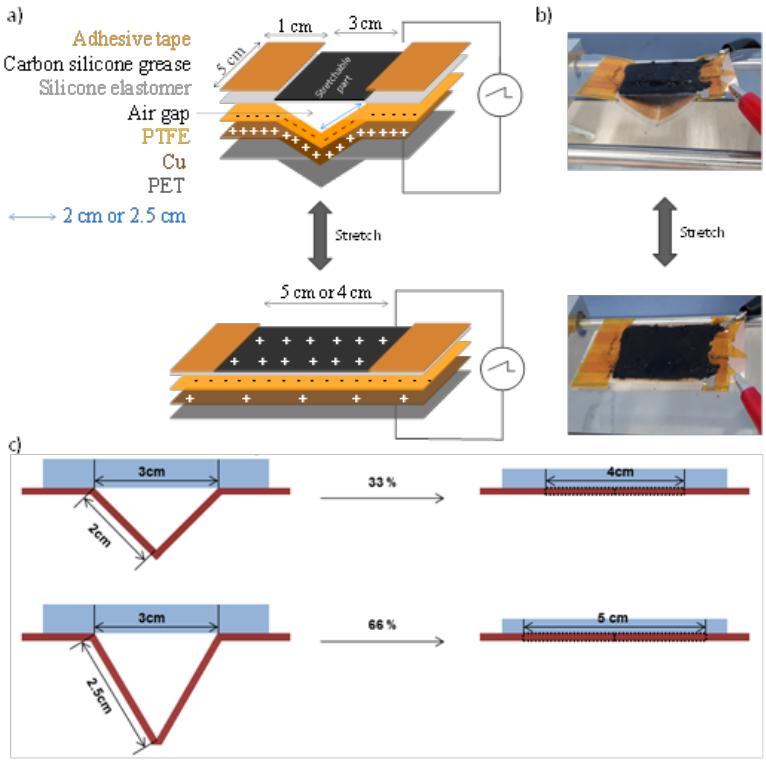

Figure 4.4 Construction and working principle of electret-DEG (a). Photos of the custom-made electret DEG in the relaxed (top) or stretched state (bottom) (b). Simplified representation of how the air gap and the maximum stretch of 33% (from 3 cm to 4 cm) (top) and 66% (from 3 cm to 5 cm) (right). The rigid frame unfolded during stretching and folded back during relaxing of the DE.

The electret DEG consisted of rigid and elastic materials. The rigid part, on which one electrode and the charged electret were fixed, had an accordion like structure which allowed unfolding and expansion. The elastic film, on top of which the second stretchable electrode was applied, was fixed on the accordion structure. In the relaxed form, a large air gap between the electret and elastomer existed. Therefore, almost all compensation charge is located on the bottom electrode close to the electret (Fig. 4.4a top). When the device was stretched, the accordion like structure deformed. This defor-

mation is followed by the elastomeric part which was elongated. The air gap distance between electret and elastomer was significantly decreased, and in an ideal case eliminated (Fig. 4.4a bottom). The electret polarizes the dielectric elastomer and charges appeared on the top electrode. At the same time the capacitance of the dielectric elastomer changes. In the relaxed state, the capacitance is smaller as compared to the capacitance in the strained state:

$$C = \varepsilon' \varepsilon'_0 \, A/d \qquad \text{Eq. 4.1}$$

where ε' is the permittivity of the elastomer, ε_0' is the permittivity of air, A is the surface area of the flexible electrode and d is the thickness of the dielectric elastomer. Rearrangement of charges between the two electrodes through a load due to variations in the capacitance generates an alternative current. The capacitance of the electret DEG is inversely proportional to the dielectric thickness.[47] A higher DEG output voltage is expected for thinner films. Because, materials **P3-Cl** and **P3-Cl-CNT** showed a rather low strain at break of 100% only, thin films constructed from them were difficult to handle and to use in electret DEG construction. To be nevertheless able to compare the properties of different materials, films with a thickness of 200 μm were tested. These films were easier to handle.

The active part of the dielectric elastomer of the device has an area of 3 cm × 5 cm. The total weight of the electret DEG was merely 8 g. As DEGs are studied with regard to wearable electronics, the device weight is considered an essential aspect. The rigid frame unfolded during stretching and folded back during relaxing of the DE and defined the maximum elongation of the active part of the dielectric elastomer (Fig. 4.4). The maximum amount of strain applied to the dielectric elastomer is given by the length of the flexible (not elastic) electret, which is 4 cm and 5 cm for the generators strain by 33% and by 66%, respectively. The minimization of the air gap was found to be crucial for the output voltage. Particularly, the high sensitivity of the DEG's output voltage against the remaining air gap between electret and DE was considered as the main experimental challenge for electret DEG measurements. On average five generators were tested for each material at each strain, except for **PDMS-CN** generator stretched by 33%, where we run out of material and measured only four generators. All generator measurements are shown in Section 4.7 (Fig. 4.15-4.23). The voltage generated by different materials at two different strains of 33% and 66% and at a frequency of 1 Hz was measured using a Tektronix 'TDS 2024B' oscilloscope with a resistance of 1 MΩ. Not all generators performed equally well, mainly due to the difficulty in precisely controlling the air left gap during stretching. We consider, however, that the best generator performance indicates material performance and not the artifacts from electret DEG sample construction/operation.

A typical response is shown in Fig. 4.5 for a DEG constructed with **PDMS-CN-CNT** at 66% strain.

Table 4.2 summarizes the maximum output voltage (best performing generator) and the average of output voltage of different materials tested in DEG at two different strains, as well as the permittivity ε' and the maximum tensile strain of the DE. The voltage peaks occurred only when the dielectric membrane was in close contact to the electret during stretching and relaxation. It was noted that the voltage signal registered during stretching and relaxation was in many cases not symmetrical, and the signal measured during relaxation was smaller and wider. We attribute this feature to the adhesion of the dielectric elastomer on the electret layer which slows down the separation process when the DEG is relaxing.

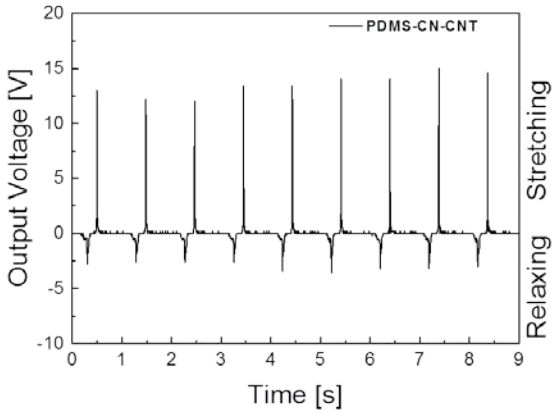

Figure 4.5 The output voltage versus time of a DEG constructed with **PDMS-CN-CNT** as dielectric elastomer which was strained 66% at 1 Hz.

The potential of the materials in DEGs using our electret setup can hardly be evaluated, since it does not allow exploring the full range of strains. The theoretical electrical energy ΔE released during one stretching cycle can be calculated according to (see section 4.7):

$$\Delta E = \frac{1}{2} V_0^2 \cdot \frac{C_1 C_2}{C_1 + C_2}$$ Eq. 4.2

where $V_0 = 1000\ V$ is the surface potential induced by the initial discharge on the Teflon electret, C_2 and C_1 is the capacitance of the electret and stretched DE film, respectively. Note that the reduction in film thickness upon straining was taken into account in the calculation of C_1. Taking the maximum strain values in Figure 4.1 and the relative permittivities in Table 4.2, we obtain increasing values ΔE of $3.1 \cdot 10^{-4}$ J, $3.4 \cdot 10^{-4}$ J, $3.9 \cdot 10^{-4}$ J and $5.0 \cdot 10^{-4}$ J for **PDMS-CN-CNT**, **PDMS-CN**, **PDMS**, and **Elastosil®Film**, respectively. If the strain is fixed to 66%, we obtain increasing values ΔE of $1.2\ 10^{-4}$ J, $1.1\ 10^{-4}$ J, and $1.0\ 10^{-4}$ J for **PDMS-CN-CNT**, **PDMS-CN**, and **PDMS**, respectively. Thus, the theoretical amount of released electrical energy at a predetermined strain is higher for **PDMS-CN-CNT**. As the electret-DEG is designed for human motion energy harvesting, strains of about 50% were considered as realistic.[49]

Table 4.2 Output voltage of the best performant DEG as well as the average of five DEGs at 33% and 66% lateral strain, the dielectric permittivity ε',the maximum tensile strain, and the calculated energy at 33%, 66% strain, and at s_{max} respectively.

Entry	V_{max} at 33%[a] [V]	V_{max} at 66%[b] [V]	$V_{average}$ at 33%[c] [V]	$V_{average}$ at 66%[d] [V]	ε'[e]	s_{max} [%]	$\Delta E_{33\%}$[f] [J]	$\Delta E_{66\%}$[f] [J]	ΔE_{max} [J]
PDMS	5.1±0.2	9.3±0.2	3±1	5±1	2.9±0.15	372	$-7.5\ 10^{-5}$	$-1.0\ 10^{-4}$	$-3.9\ 10^{-4}$
Elastosil® Film	4.5±0.1	8.6±0.1	3±1	7±1	2.9±0.15	485	$-7.5\ 10^{-5}$	$-1.0\ 10^{-4}$	$-5.0\ 10^{-4}$
PDMS-CN	5.1±0.2	6.8±0.2	4±1	7±1	3.5±0.20	313	$-8.1\ 10^{-5}$	$-1.1\ 10^{-4}$	$-3.4\ 10^{-4}$
PDMS-CN-CNT	8.8±0.3	14.5±0.3	5±1	11±2	4.6±0.25	270	$-8.9\ 10^{-5}$	$-1.2\ 10^{-4}$	$-3.1\ 10^{-4}$
P3-Cl	8.1±1	-	5±1	-	5.4±0.25	114	$-9.3\ 10^{-5}$	$-1.2\ 10^{-4}$	$-1.7\ 10^{-4}$
P3-Cl-CNT	-	-	-	-	6.3±0.3	95	$-9.8\ 10^{-5}$	$-1.3\ 10^{-4}$	$-1.6\ 10^{-4}$

[a,b] The voltage of the best performing generator at 1 Hz which is the average of nine cyclic measurements including corresponding standard deviation at a strain of [a]33% and [b]66%, respectively.[c,d] The average voltage of five generators at [c]33% and at [d]66% strain, respectively. [e]Permittivity value taken at 10^6 Hz. [f]Calculations of ΔE at 33% and 66% strain as well as at s_{max} can be found in section 4.7.

Figure 4.6 shows the output voltage of different materials as function of permittivity for 33% and 66% strain. Material **P3-Cl-CNT** has the highest permittivity of ε' = 6.3 and thus should perform best in the generator. However, it ruptured easily and therefore no DEGs could be constructed with this material. **P3-Cl** ruptured when 66% strain was used and therefore the harvested voltage could be measured only at 33% strain. Material **PDMS-CN-CNT** generated the highest average output voltage of 8.8 V and 14.5 V at 33% and 66% strain, respectively which is almost two times higher as compared to **Elastosil®Film** with 4.5 V and 8.6 V at the same strains. Most of the materials showed the expected trend, *e.g.*, an increase in the generated voltage with increasing permittivity except for material **P3-Cl** at 33% strain and **PDMS-CN** at 66% strain. While the dielectric permittivity strongly influences the voltage output, other material properties such as mechanical stability, *e.g.* the maximum achievable strain at break have a strong impact on generator performance as well.[56] The generated voltage can be increased by using materials with even higher dielectric permittivity, by reducing the thickness of the film, and by using larger stains while the air gap between the electret and the stretched elastomer should be minimized. A direct comparison of the performance of the materials developed in this work and other materials from the literature tested in DEGs cannot be done easily because of the different setup used in different laboratories.[57] It should be mention that in electret DEGs only regular silicones were investigated and we compared the performance of our materials with **Elastosil®Film**. The higher generated voltage for the composite containing **NS-CNTs** as compared to **Elastosil®Film**, clearly show the positive effect of the filler used.

Conventional DEGs require operation near dielectric breakdown and have rather complicated charge/discharge cycle. Contrary to DEGs, electret DEGs are very unlikely to suffer a breakdown and are thus more reliable. While DEGs may be superior to electret DEGs in terms of energy harvested per cycle, the safer operation of electret DEGs over the conventional DEGs

allows electret DEGs to be operated on humans. Therefore, applications of electret DEGs to recharge portable devices can be envisioned.[58]

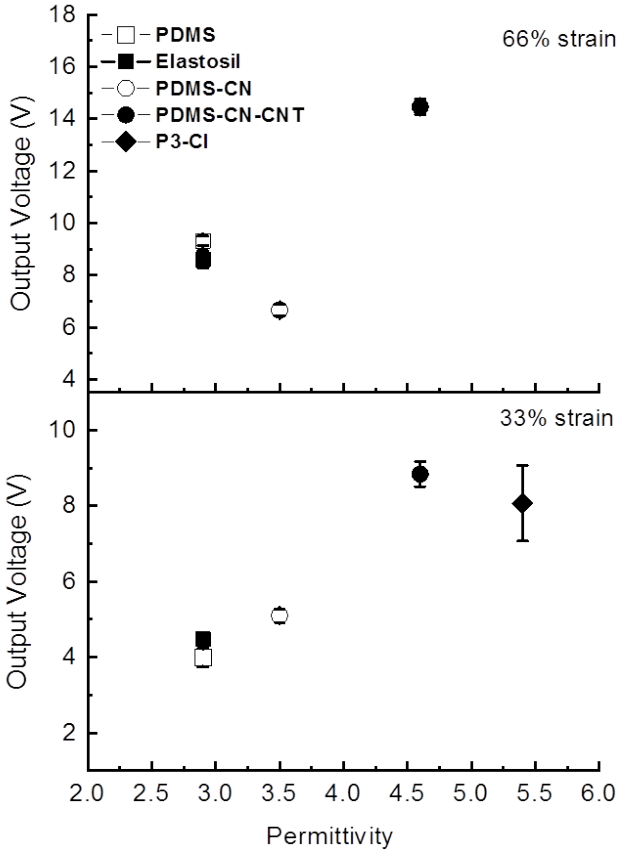

Figure 4.6 Output voltage of the best performant DEG *versus* permittivity ε' of the DE at 33% and at 66% strain

4.4 Experimental section

Unless otherwise stated, all chemicals were reagent grade and used without purification. 1,3,5,7-Tetramethyl-1,3,5,7-tetravinyl-cyclotetrasiloxane(V_4), (25–35% methylhydro-siloxane)dimethyl-siloxane (AB109380) and polydimethylsiloxane, hydroxyl terminated (AB116665, M_n = 90 000 g mol^{-1}, M_w = 130 000 g mol^{-1}) were purchased from ABCR. Tetrahydrofuran (THF) and dimethylformamide (DMF) were purchased from VWR. THF was stored over sodium under nitrogen atmosphere and distilled before use. Single-walled carbon nanotubes were purchased from Carbon Nanotech, Co., South Korea. (CNTs SP95, >95 wt%). All other chemicals were purchased from Sigma Aldrich. Poly(ethylthiopropyl methyl)siloxane P3 (M_n = 90.000 g/mol, M_w = 185.000 g/mol, *PDI* = 2.0) was synthesized according to literature.[50] Thin films of Elastosil®Film (200 µm, 100 µm, 50 µm, 20 µm) were provided from DRAWIN Vertriebs-GmbH, Riemerling while carbon black silicone grease were provided from M.G. Chemicals Ltd.

The tensile tests were performed on a Zwick Z010 tensile test machine with a crosshead speed of 50 mm min^{-1} (278% min^{-1}). Dynamic mechanical analysis was carried out on a RSA 3 DMA from TA Instruments. Stripes of 10 mm × 20 mm were measured applying 2% strain in the frequency range of 0.05–2 Hz at 25 °C. $Tan(\delta)_{DMA}$ is given as the fraction of the imaginary E'' and real elastic moduli E' at 2% strain. The microstructures of the films were measured with a SEM (FEI Inspect F) on samples prepared by freeze-breaking in liquid nitrogen and sputtered with a thin layer of Pt. Permittivity measurements were performed in the frequency range from 10^{-1} Hz to 10^6 Hz using a Novocontrol Alpha-A frequency analyzer. The V_{RMS} (root-mean-square voltage) of the probing AC electric signal applied to the samples was 1 V. Au electrodes with a thickness of 20 nm were sputtered on both sides of the film. The permittivity ε' was determined from the capacitance $C = \varepsilon'\varepsilon_0 A/d$, where A is the electrode area, d is the thickness of the film, and ε_0 is the vacuum permittivity. The thickness of the film was measured by a micrometer gauge with an uncertainty of ±5 µm. Two stainless steel discs with a diameter of 20 mm served as electrodes. The samples were annealed at 80 °C for 18 h at 10 mbar to remove any residual solvents.

For the generator, a poly(ethylene terephthalate) (PET) film (130 µm) was used as substrate on which a copper tape (75 µm) was attached, which served as bottom electrode. On the bottom electrode, the poly(tetrafluoroethylene) (PTFE) electret film (140 µm) was attached. The electret was prepared using a high frequency corona discharge generator from Electro-Technic Products Inc. (Model BD-10AS) with an output of 20 kV to 45 kV at a frequency of approximately 500 kHz. An electrostatic voltmeter (Model 347, TREK, INC) was used to measure the induced surface potential of the electret. PTFE surface potential was 1000 V ± 100 V. On top of PET/Cu/PTFE layers (rigid part), which was bended in an accordion like shape, the dielectric film (5 cm × 5 cm) coated with carbon black silicone grease top electrode (3 cm × 5 cm) was attached on the passive part of the dielectric using an adhesive tape. A large air gap between the dielectric and the electret formed (Fig. 4.4). The rigid part unfolded during stretching the elastomer and folded back due to the elastic restoring forces in the dielectric elastomer. The total length of the DEG device in the stretched form was 20 cm × 6 cm. The DEG measurement setup was equipped with a mechanical stretcher and an electrical motor (see Supporting Information). The DEGs were stretched by 33% (from 3 cm to 4 cm) or by 66% (from 3 cm to 5 cm). The output voltage was measured using Tektronix 'TDS 2024B' oscilloscope with a resistance of 1 MΩ.

4.4.1 General synthesis of the silicone elastomer thin films

A solution of hydroxyl terminated PDMS or P3, cross-linker, and catalytic amounts of dibutyltin dilaurate in THF was stirred and sonicated for 3 minutes to remove the air bubbles (Table 4.3). Thin films were made on a glass coated with PTFE or on a PET substrate by doctor blade technique. The films were stored in a closed chamber at ambient temperature of 25 °C and humidity of 30% for 48 h. They were then dried at 80 °C *in vacuo* for 12 h, left at room temperature for at least three weeks, before further testing.

Table 4.3 Amount and type of reagents used in the synthesis of different materials.

Entry[a]	Matrix [amount]	Cross-linker [amount]	NS-NTs [amount]
PDMS	AB109380 [1 g]	AB109380 [0.1 g]	-
PDMS-CN	AB109380 [0.6 g]	CN-CL[b] [0.4 g]	-
PDMS-CN-CNT	AB109380 [0.57 g]	CN-CL[b] [0.33 g]	0.1 g
P3-Cl	P3 [0.7 g]	Cl-CL[c] [0.175 g]	-
P3-Cl-CNT	P3 [0.72 g]	Cl-CL[c] [0.18 g]	0.1 g

[a] 1 g polymer and dibutyltin dilaurate (40 µl) in THF (2 ml), [b]2-cyanoethyl(triethoxy)silane, [c]3-chloropropyltriethoxysilane.

4.4.2 General synthesis of silicone composite thin films

NS-CNTs (3 g) were suspended in DMF (240 ml) and sonicated for 3 minutes with a tip sonicator at 40% power. To this suspension, 2-cyanoethyl(triethoxy)silane (6 ml) was added followed by the ammonium hydroxide aqueous solution (25 wt%, 6 ml). The reaction was stirred for 3 days. The precipitate was filtered, washed with ethanol and dispersed in THF. To this dispersion either hydroxyl terminated PDMS or **P3**, the cross-linker, and the [Sn] catalyst were added and mechanically mixed. For the amount of reagents used, see Table 4.3. The composites were subjected to three-roll milling for approximately 15 minutes. Thin films were made on PTFE coated glass or on PET substrate by doctor blade techniques and stored in a closed chamber at ambient temperature of 25 °C and humidity of 30% for 48 h. They were then dried at 80 °C *in vacuo* for 12 h before further testing.

4.5 Conclusions

Novel silicone composites consisting of **NS-CNTs** into either a PDMS or a chemically modified polysiloxane matrix were prepared. The chemical treatment of the highly polar **NS-CNTs** filler with (2-cyanoethyl)triethoxysilane increased its compatibility with the polysiloxane matrices used. The composites were homogenous and have low mechanical losses as proven by DMA measurements. Two composites, **P3-Cl-CNT** with a permittivity value of $\varepsilon' = 6.3$, but low tensile strength and a material **PDMS-CN-CNT** with a permittivity value of $\varepsilon' = 4.6$ and high tensile strength were prepared. The developed materials were investigated regarding their ability to generate a voltage in a DEG test device using an electret as polarizing source. Despite the attractively high dielectric permittivity of $\varepsilon' = 6.3$ for **P3-Cl-CNT**, no generators could be constructed with this material, because the films ruptured. An increase of the voltage generated, from 8.6 V for **Elastosil®Film** ($\varepsilon' = 3$) to 14.5 V for **PDMS-CN-CNT** ($\varepsilon' = 4.6$) was observed. While the increase in output voltage is related to the increased permittivity other materials and device related factors may also be influential.

The mechanical stability of **PDMS-CN-CNT** is not only demonstrated by the tensile tests but also by applying a 66% strain on the **PDMS-CN-CNT** thin film in the electret DEG operated at 1 Hz for 9 cycles. The safer and easy operation of electret DEGs allows their use on the humans and may be used one day for recharging portable electronic devices. Future work will be directed towards optimizing the generator setup and evaluating other high permittivity materials in electret DEGs.

4.6 References

[1] P. Brochu, W. Yuan, H. Zhang, Q. Pei, *ASME Conf. Smart Mater. Adapt. Struct. Intell. Syst. Proc.* **2009**, *1*, 197.

[2] R. D. Kornbluh, R. Pelrine, H. Prahlad, A. Wong-Foy, B. McCoy, S. Kim, J. Eckerle, T. Low, *MRS Bull.* **2012**, *37*, 246.

[3] S. Bauer, S. Bauer-Gogonea, I. Graz, M. Kaltenbrunner, C. Keplinger, R. Schwödiauer, *Adv. Mater.* **2014**, *26*, 149.

[4] R. Kaltseis, C. Keplinger, R. Baumgartner, M. Kaltenbrunner, T. Li, P. Mächler, R. Schwdiauer, Z. Suo, S. Bauer, *Appl. Phys. Lett.* **2011**, *99*, 10.

[5] R. Pelrine, R. D. Kornbluh, J. Eckerle, P. Jeuck, S. Oh, Q. Pei, S. Stanford, *Proc. SPIE* **2001**, *4329*, 148.

[6] G. Moretti, M. Righi, R. Vertechy, M. Fontana, *Polym.* **2017**, *9*, 283.

[7] G. Yin, Y. Yang, F. Song, C. Renard, Z. M. Dang, C. Y. Shi, D. Wang, *ACS Appl. Mater. Interfaces* **2017**, *9*, 5237.

[8] S. J. A. Koh, X. Zhao, Z. Suo, *Appl. Phys. Lett.* **2009**, *94*, 262902.

[9] G. Neidlein, C. Hentschel, N. Scharmann, C. Langenstein, M. Voss, B. Hagemann, *(Robert Bosch GmbH)*, **2009**, DE 10 2009 053 393 A1.

[10] R. Van Kessel, *(Single Buoy Moorings, Inc.)*, **2013**, WO 2013/167577.

[11] S. Shian, J. Huang, S. Zhu, D. R. Clarke, *Adv. Mater.* **2014**, *26*, 6617.

[12] J. Huang, S. Shian, Z. Suo, D. R. Clarke, *Adv. Funct. Mater.* **2013**, *23*, 5056.

[13] S. Chiba, M. Waki, R. Kornbluh, R. Pelrine, *Proc. SPIE* **2008**, *6927*, 692715.

[14] P. Jean, A. Wattez, G. Ardoise, C. Melis, R. Van Kessel, A. Fourmon, E. Barrabino, J. Heemskerk, J. P. Queau, *Proc. SPIE* **2012**, *8340*, 83400C.

[15] R. Van Kessel, A. Wattez, P. Bauer, *Proc. SPIE* **2014**, *9056*, 90561D.

[16] J. Maas, C. Graf, *Smart Mater. Struct.* **2012**, *21*, 064006.

[17] R. D. Kornbluh, R. Pelrine, Q. Pei, R. Heydt, S. Stanford, S. Oh, J. Eckerle, *Proc. SPIE* **2002**, *4698*, 254.

[18] C. Jean-Mistral, S. Basrour, J. Chaillout, *Proc. SPIE* **2008**, *6927*, 692716.

[19] T. G. McKay, B. M. O'Brien, E. P. Calius, I. A. Anderson, *Appl. Phys. Lett.* **2011**, *98*, 2009.

[20] J. Biggs, K. Danielmeier, J. Hitzbleck, J. Krause, T. Kridl, S. Nowak, E. Orselli, X. Quan, D. Schapeler, W. Sutherland, J. Wagner, *Angew. Chem. Int. Ed.* **2013**, *52*, 9409.

[21] R. Kaltseis, C. Keplinger, S. J. Adrian Koh, R. Baumgartner, Y. F. Goh, W. H. Ng, A. Kogler, A. Tröls, C. C. Foo, Z. Suo, S. Bauer, *RSC Adv.* **2014**, *4*, 27905.

[22] S. E. Chen, L. Deng, Z. C. He, E. Li, G. Y. Li, *Smart Mater. Struct.* **2016**, *25*, 055017.

[23] T. McKay, B. O'Brien, E. Calius, I. Anderson, *Proc. SPIE* **2012**, *8340*, 83401Y.

[24] T. McKay, B. O'Brien, E. Calius, I. Anderson, *Appl. Phys. Lett.* **2010**, *97*, 2008.

[25] I. A. Anderson, E. P. Calius, T. Gisby, T. Mckay, I. A. Anderson, E. P. Calius, T. Gisby, T. Hale, T. Mckay, B. O. Brien, S. Walbran, *Proc. SPIE* **2009**, *7287*, 72871H.

[26] F. Foerster, H. F. Schlaak, *Proc. SPIE* **2014**, *9056*, 905637.

[27] C. Jean-Mistral, T. Vu-Cong, A. Sylvestre, *Smart Mater. Struct.* **2013**, *22*, 104017.

[28] C. Tugui, C. Ursu, L. Sacarescu, M. Asandulesa, G. Stoian, G. Ababei, M. Cazacu, *ACS Sustain. Chem. Eng.* **2017**, *5*, 7851.

[29] Y. Chiu, S. H. Wu, *J. Phys. Conf. Ser.* **2013**, *476*, 012037.

[30] P. Brochu, H. Stoyanov, R. Chang, X. Niu, W. Hu, Q. Pei, *Adv. Energy Mater.* **2014**, *4*, 1.

[31] C. Jordi, A. Schmidt, G. Kovacs, S. Michel, P. Ermanni, *Smart Mater. Struct.* **2011**, *20*, 075003.

[32] L. Maffli, S. Rosset, M. Ghilardi, F. Carpi, H. Shea, *Adv. Funct. Mater.* **2015**, *25*, 1656.

[33] D. M. Opris, *Adv. Mater.* **2018**, *30*, 1703678.

[34] F. B. Madsen, A. E. Daugaard, S. Hvilsted, A. L. Skov, *Macromol. Rapid Commun.* **2016**, *37*, 378.

[35] E. Bortot, R. Springhetti, M. Gei, *J. Eur. Ceram. Soc.* **2014**, *34*, 2623.

[36] G. Boccalero, C. Jean-Mistral, M. Castellano, C. Boragno, *Compos. Part B Eng.* **2018**, *146*, 13.

[37] W. Hu, S. N. Zhang, X. Niu, C. Liu, Q. Pei, *J. Mater. Chem. C* **2014**, *2*, 1658.

[38] H. Böse, D. Uhl, R. Rabindranath, *Proc. SPIE* **2012**, *8340*, 83402E.

[39] B. Kussmaul, S. Risse, G. Kofod, R. Waché, M. Wegener, D. N. McCarthy, H. Krüger, R. Gerhard, *Adv. Funct. Mater.* **2011**, *21*, 4589.

[40] C. Racles, M. Alexandru, A. Bele, V. E. Musteata, M. Cazacu, D. M. Opris, *RSC Adv.* **2014**, *4*, 37620.

[41] S. J. Duenki, Y. S. Ko, F. A. Nueesch, D. M. Opris, *Adv. Funct. Mater.* **2015**, *25*, 2467.

[42] M. Stepp, F. Achenbach, A. Koellenbacher, *(Wacker Chemie AG)*, **2015**, WO 2015/121261 A1.

[43] M. Molberg, D. Crespy, P. Rupper, F. Nüesch, J. A. E. Manson, C. Löwe, D. M. Opris, *Adv. Funct. Mater.* **2010**, *20*, 3280.

[44] J. E. Q. Quinsaat, F. a. Nüesch, H. Hofmann, D. M. Opris, *RSC Adv.* **2013**, *3*, 6964.

[45] F. Carpi, G. Gallone, F. Galantini, D. De Rossi, *Adv. Funct. Mater.* **2008**, *18*, 235.

[46] H. Stoyanov, P. Brochu, X. Niu, E. Della Gaspera, Q. Pei, *Appl. Phys. Lett.* **2012**, *100*, 262902.

[47] T. Vu-Cong, C. Jean-Mistral, A. Sylvestre, *Proc. SPIE* **2013**, *8687*, 86870H.

[48] C. Jean-Mistral, T. Porter, T. Vu-Cong, S. Chesné, A. Sylvestre, *IEEE/ASME* **2014**, 1430.

[49] C. Jean-Mistral, T. Vu Cong, A. Sylvestre, *Appl. Phys. Lett.* **2012**, *101*, 162901.

[50] P. Caspari, S. J. Dünki, F. Nueesch, D. Opris, *J. Mater. Chem. C* **2018**, *6*, 2043.

[51] A. Bele, M. Dascalu, C. Tugui, M. Iacob, C. Racles, L. Sacarescu, M. Cazacu, *Mater. Des.* **2016**, *106*, 454.

[52] Y. J. Lee, S. R. Ham, J. H. Kim, T. H. Yoo, S. R. Kim, Y. T. Lee, D. K. Hwang, B. Angadi, W. S. Seo, B. K. Ju, W. K. Choi, *Sci. Rep.* **2018**, *8*, 4851.

[53] S. J. Dünki, M. Dascalu, F. A. Nüesch, D. M. Opris, *Proc. SPIE* **2016**, *9798*, 97982K.

[54] S. J. Dünki, E. Cuervo-Reyes, D. M. Opris, *Polym. Chem.* **2017**, *8*, 715.

[55] S. J. A. Koh, C. Keplinger, T. Li, S. Bauer, Z. Suo, *IEEE/ASME Trans. Mechatronics* **2011**, *16*, 33.

4.7 Supporting information

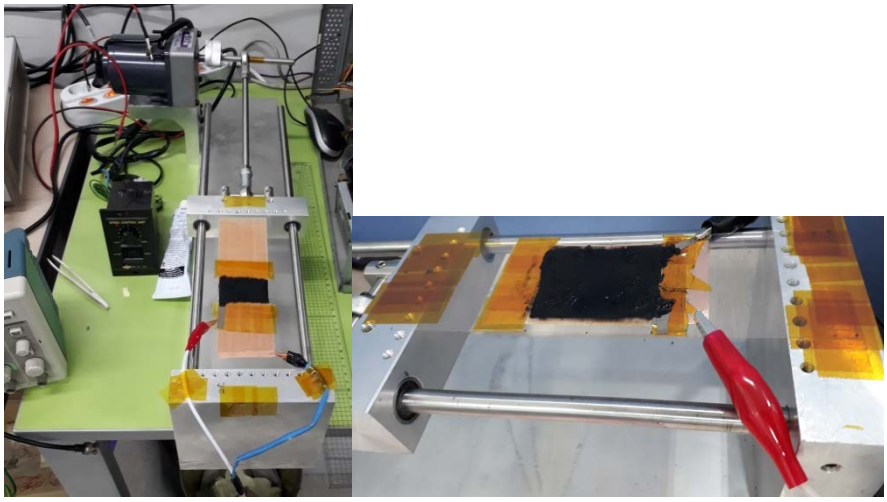

Figure 4.7 Photo of the DEG setup used.

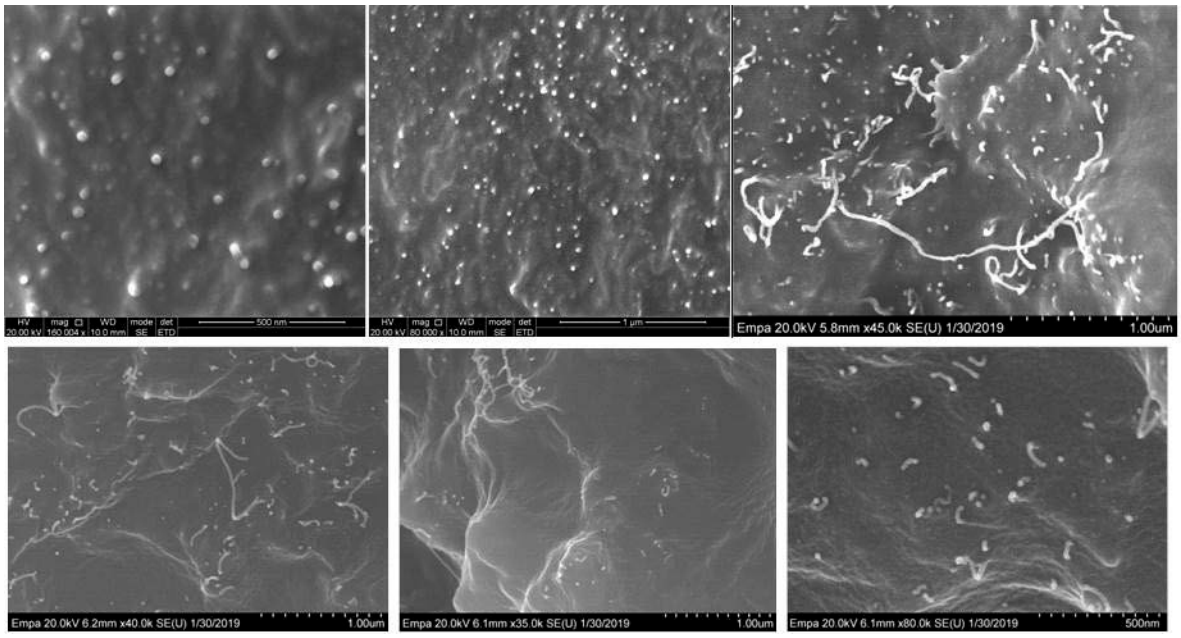

Figure 4.8 SEM image of a cross-section of **PDMS-CN-CNT**.

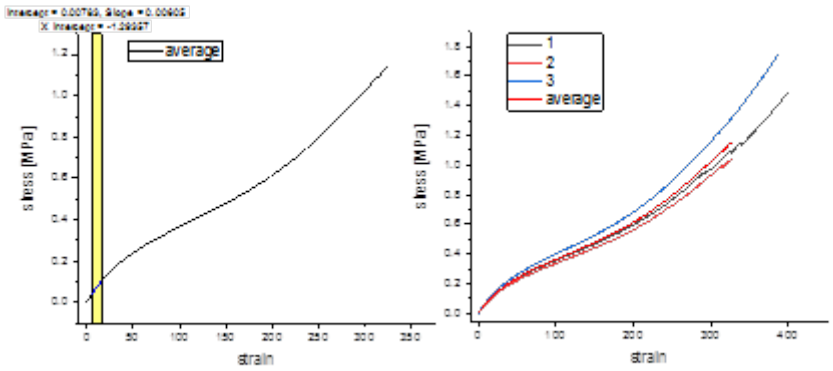

Figure 4.9 Tensile tests of **PDMS**. Three independent tests were performed.

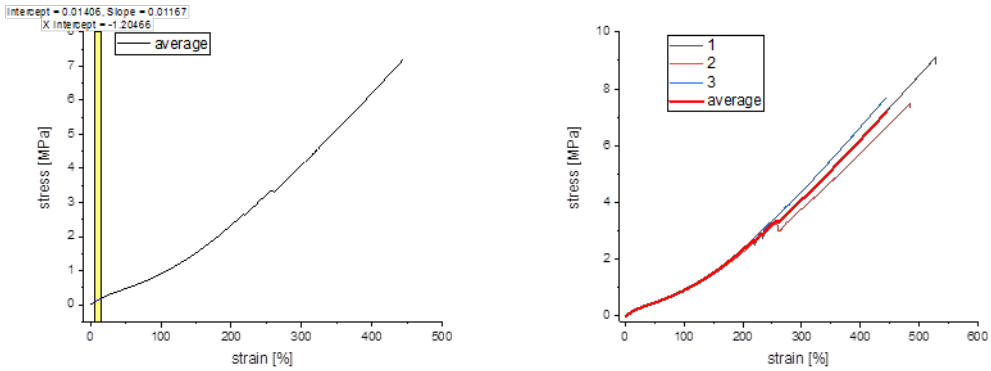

Figure 4.10 Tensile tests of **Elastosil®Film**. Three independent tests were performed.

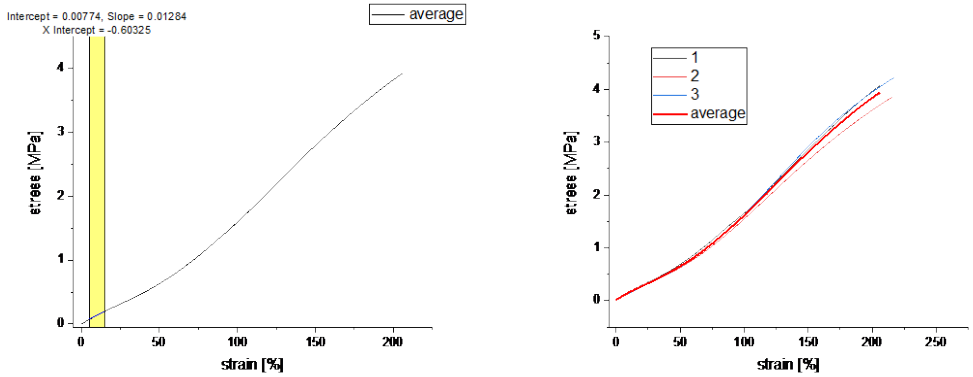

Figure 4.11 Tensile tests of **PDMS-CN**. Three independent tests were performed.

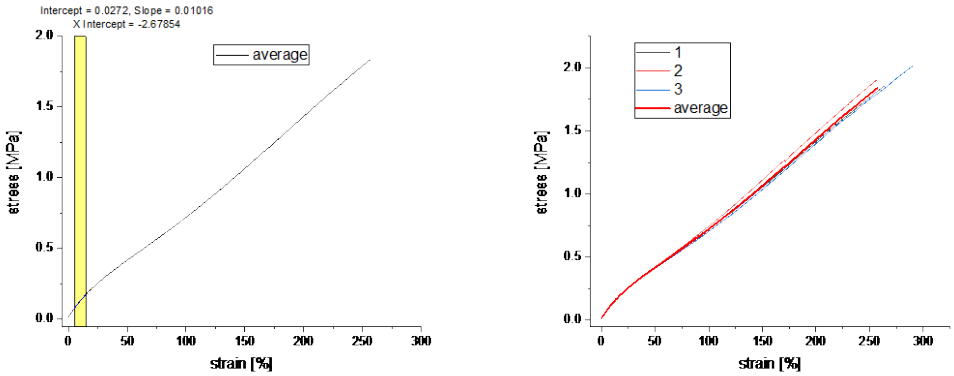

Figure 4.12 Tensile tests of **PDMS-CN-CNT**. Three independent tests were performed.

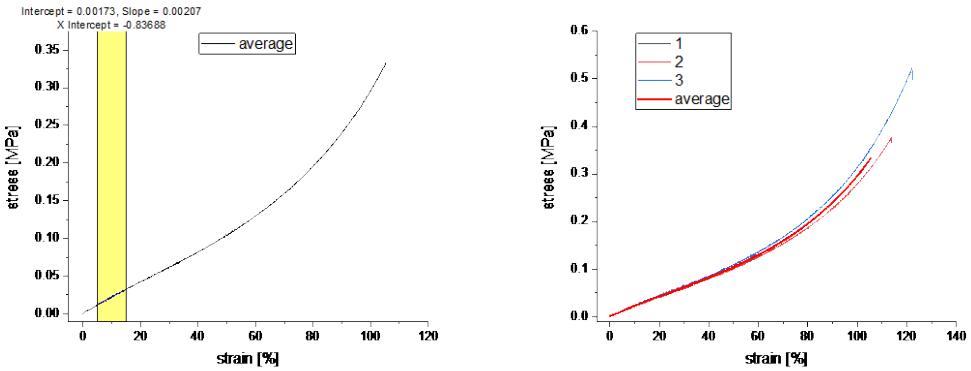

Figure 4.13 Tensile tests of **P3-Cl**. Three independent tests were performed.

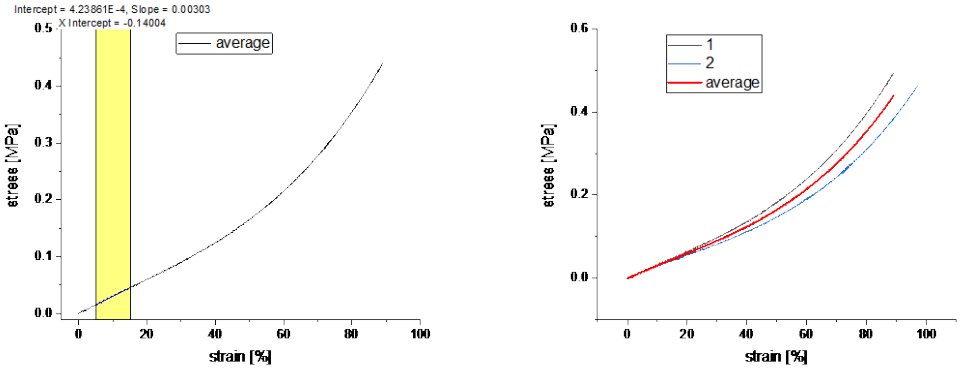

Figure 4.14 Tensile tests of **P3-Cl-CNT**. Two independent tests were performed.

4.7.1 DEG measurements at 33% strain

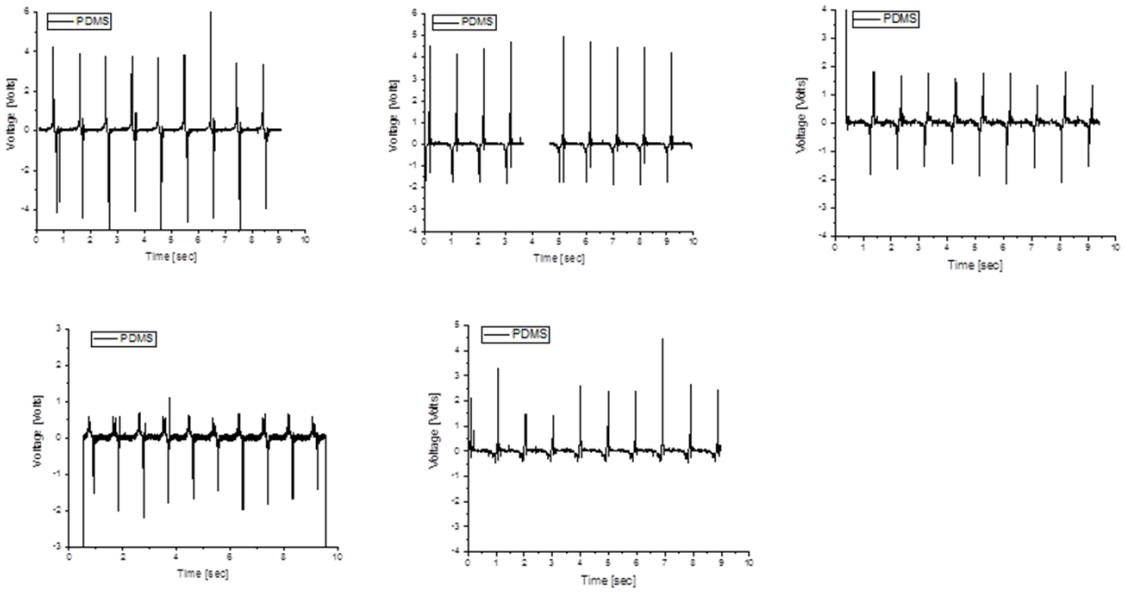

Figure 4.15 Output voltage of **PDMS** electret DEGs at 33% strain. Five independent tests were performed.

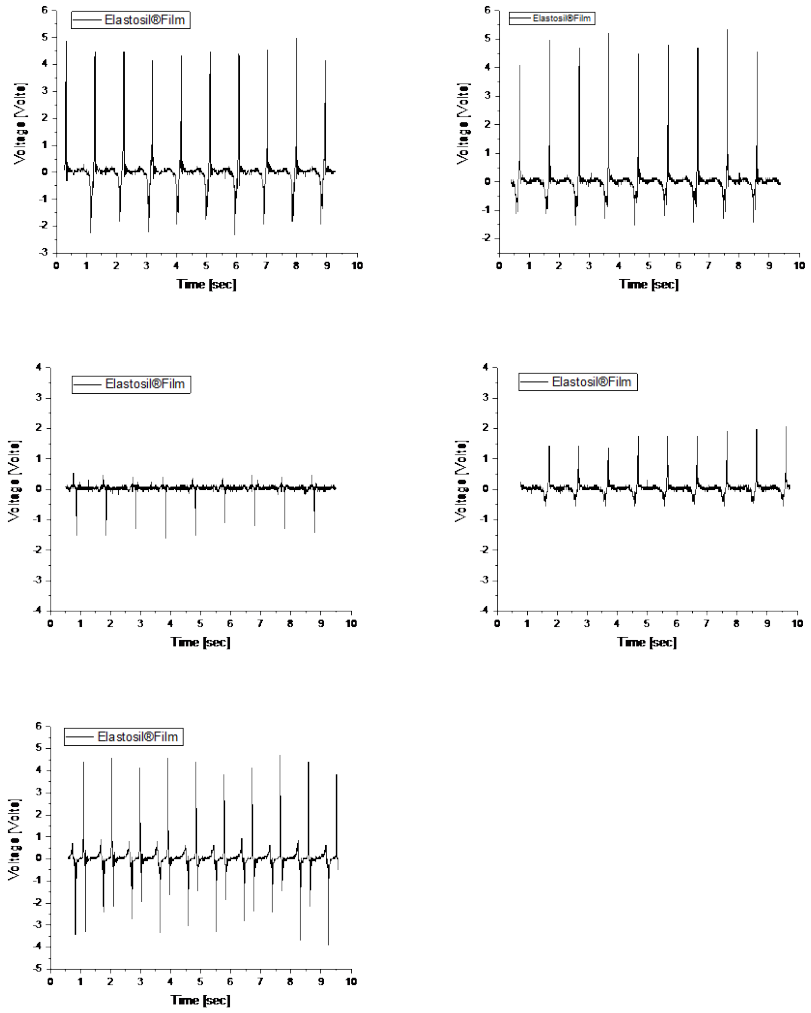

Figure 4.16 Output voltage of **Elastosil®Film** electret DEGs at 33% strain. Five independent tests were performed.

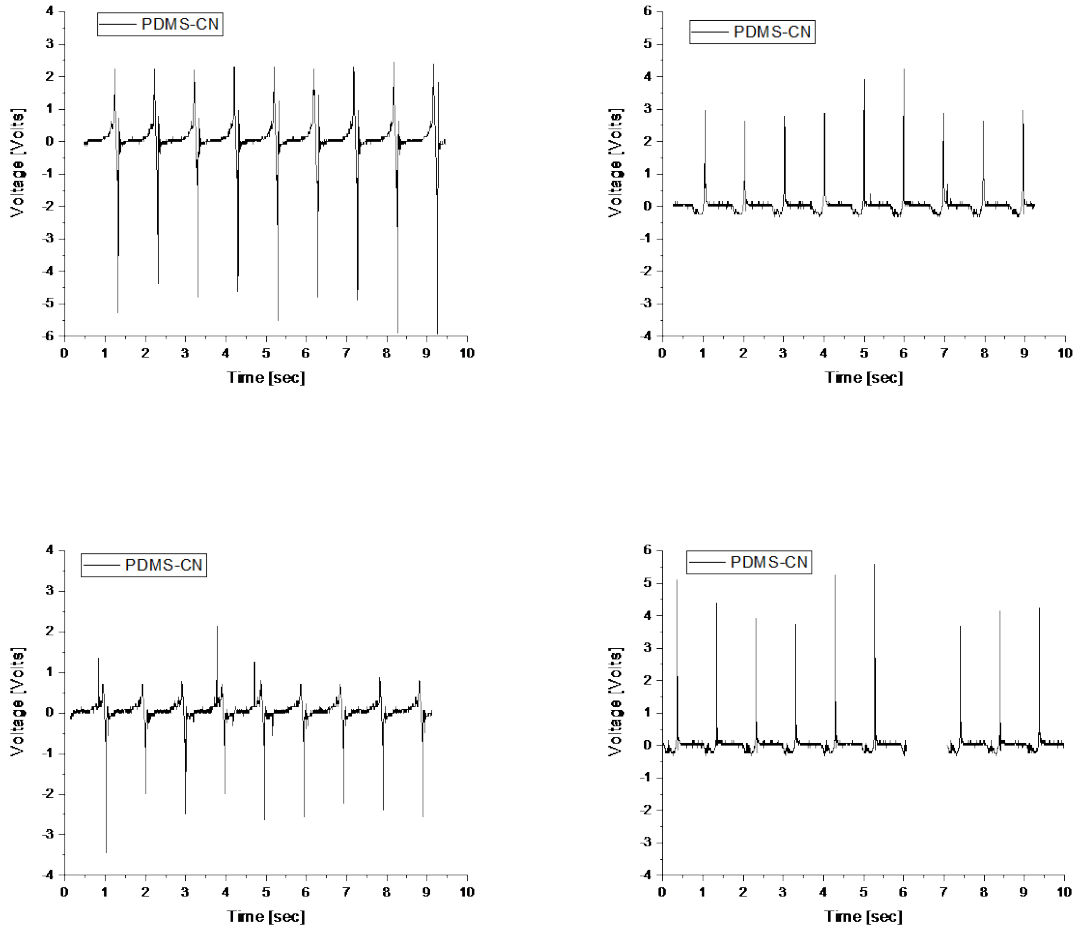

Figure 4.17 Output voltage of **PDMS-CN** electret DEGs at 33% strain. Four independent tests were performed.

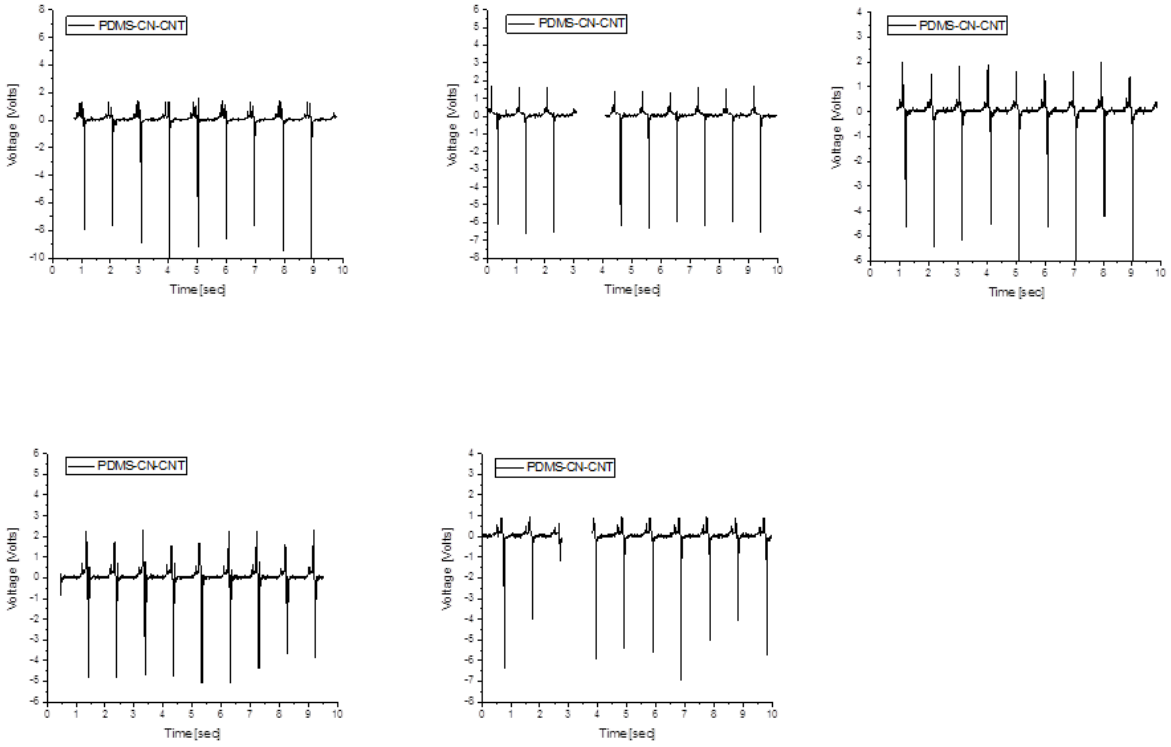

Figure 4.18 Output voltage of **PDMS-CN-CNT** electret DEGs at 33% strain.

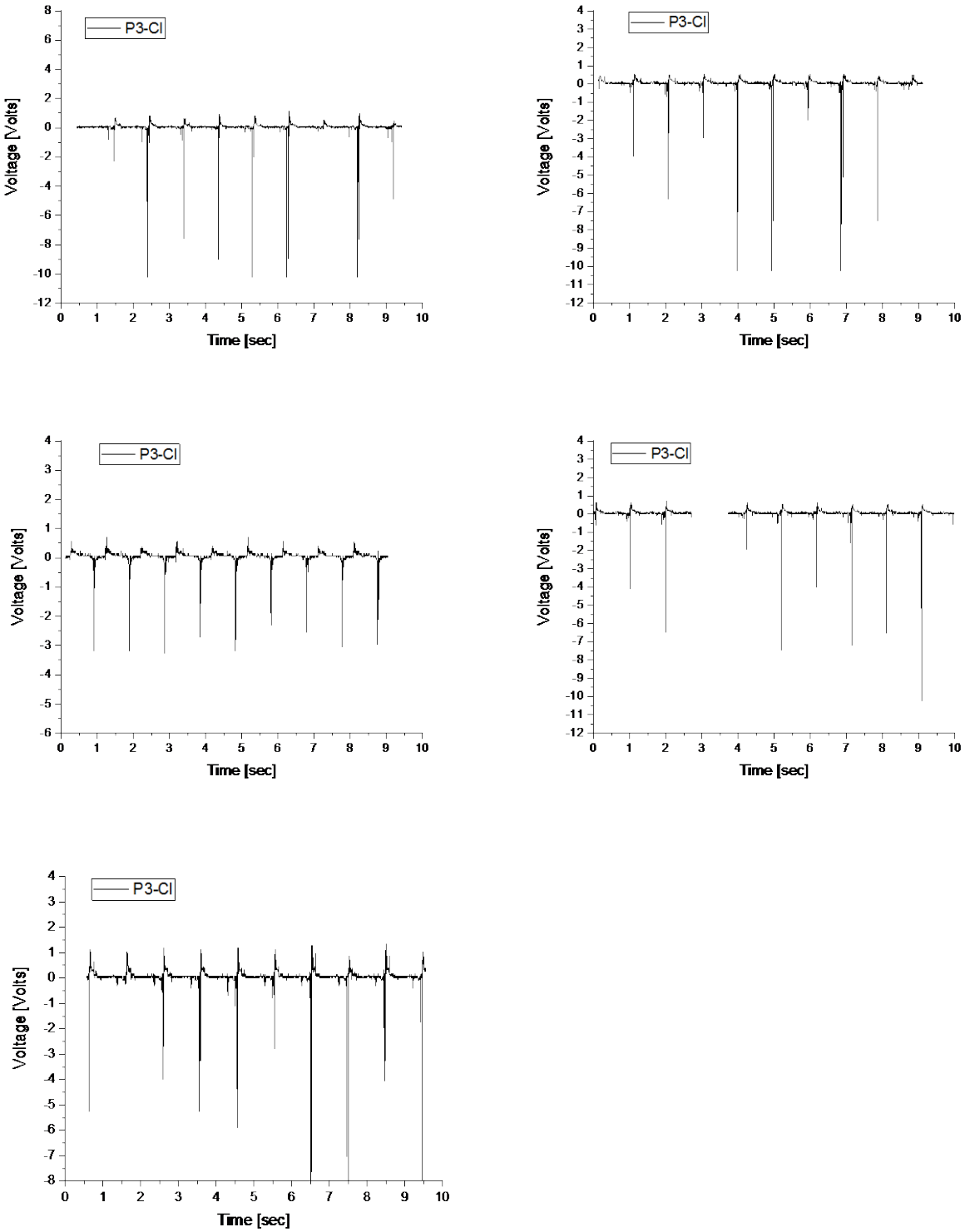

Figure 4.19 Output voltage of **P3-Cl** electret DEGs at 33% strain.

4.7.2 DEG measurements at 66% strain

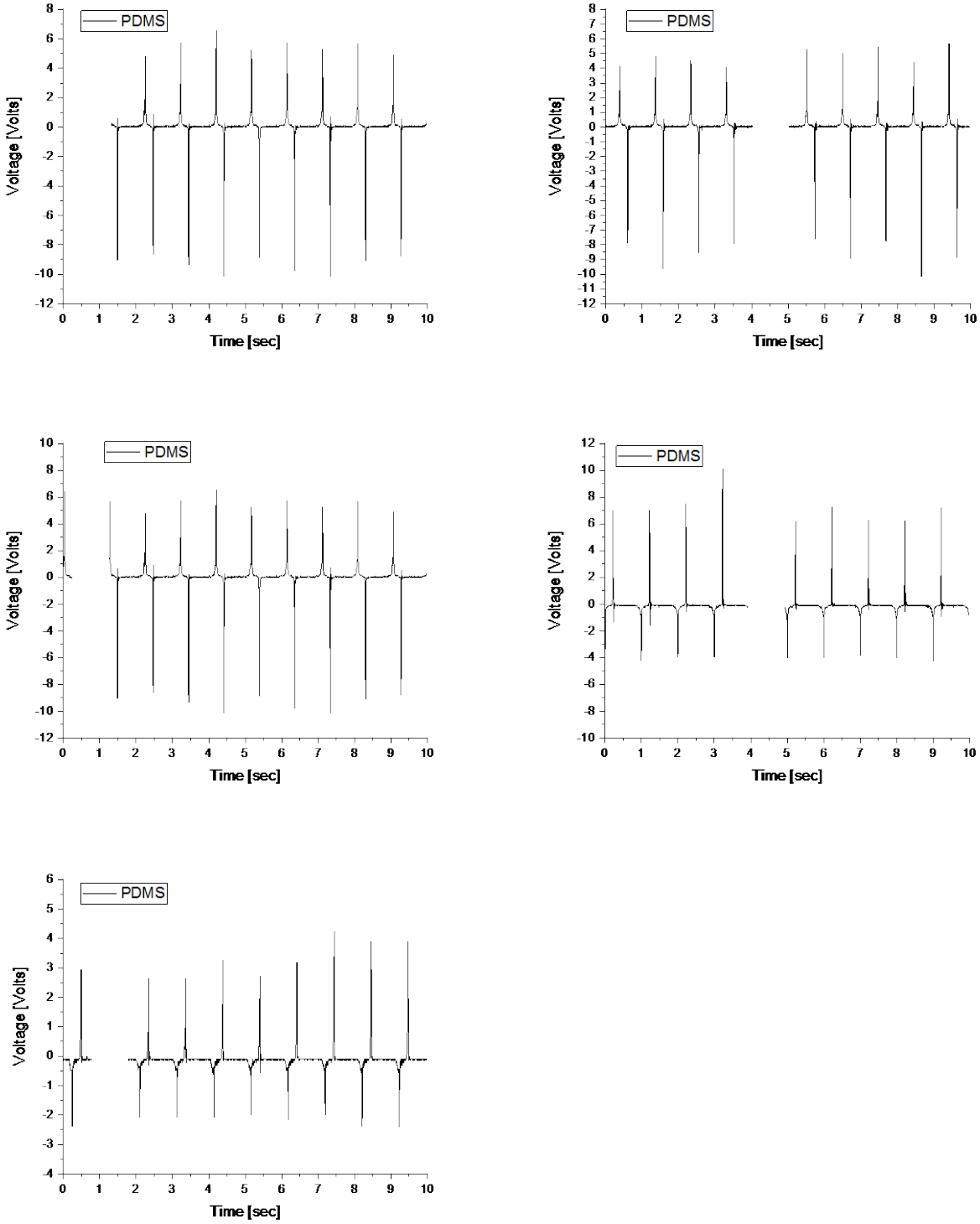

Figure 4.20 Output voltage of **PDMS** electret DEGs at 66% strai*n*.

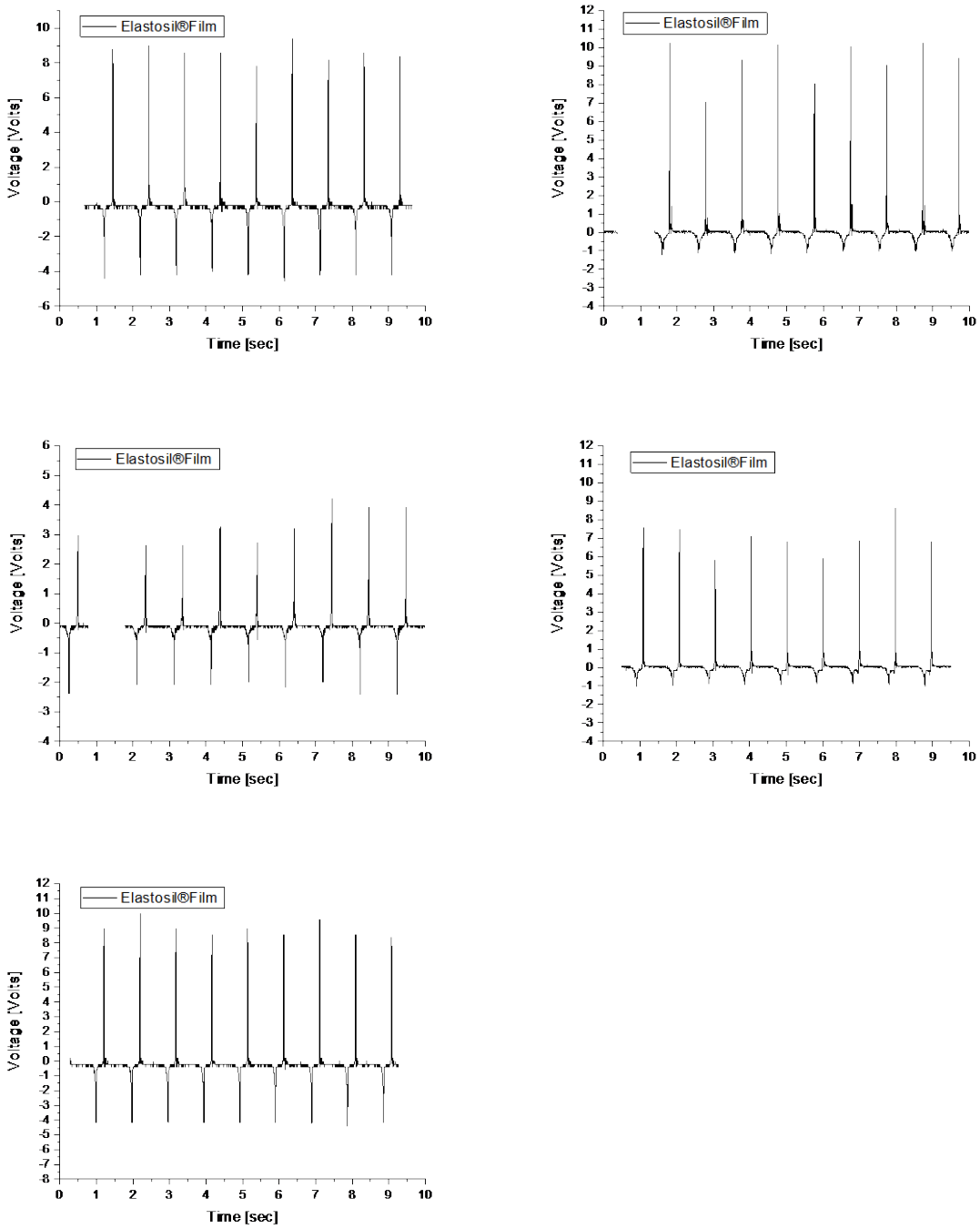

Figure 4.21 Output voltage of **Elastosil®Film** electret DEGs at 66% strain.

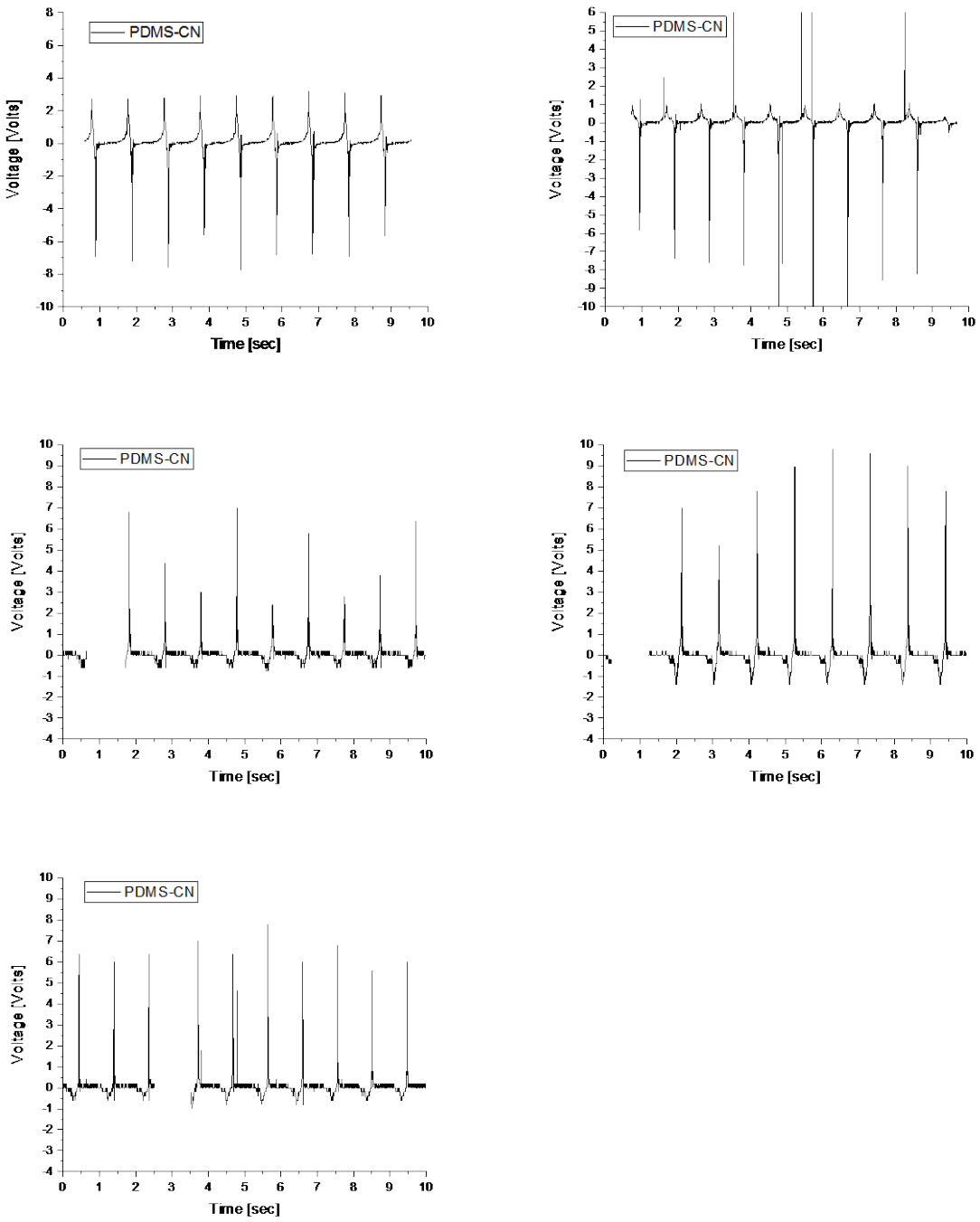

Figure 4.22 Output voltage of **PDMS-CN** electret-DEGs at 66% strain.

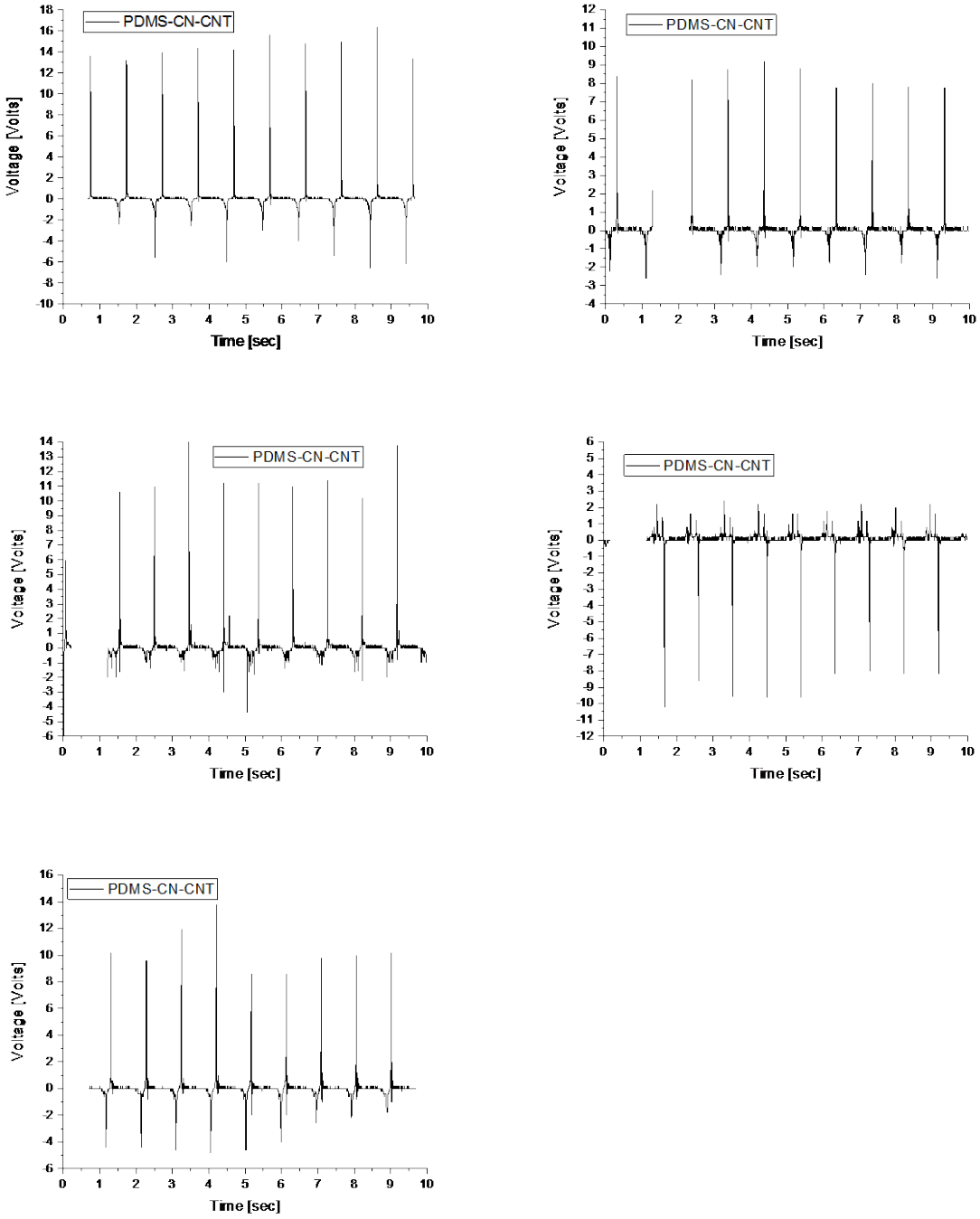

Figure 4.23 Output voltage of **PDMS-CN-CNT** electret DEGs at 66% strain.

4.7.2 Electret DEG energy considerations

DEG in the relaxed state

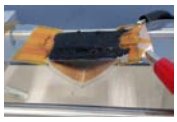

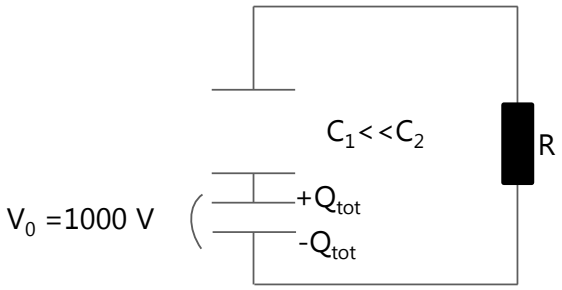

DEG in the stretched state

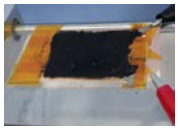

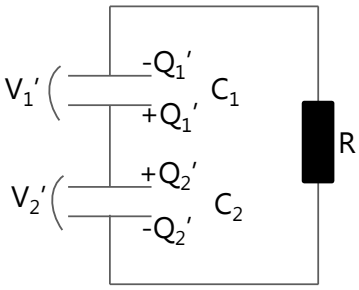

$$C_2 = \frac{\epsilon_0 A \varepsilon_{Teflon}}{d_{Teflon}}$$

$$C_1 = \frac{\epsilon_0 A \varepsilon_{DE}}{d_{DE}}$$

$V_0 = 1000\,V\ (Electret\ surface\ potential)$

$C_1 = \varepsilon_0 \varepsilon' \frac{A}{d}$ capacity of the DE when stratched

$V'_1 = V'_2\ (Equilibrium\ of\ electric\ potential\ in\ the\ stretched\ state)$

$Q_{total} = C_2\, V_0 (Total\ amount\ of\ charges\ on\ the\ electret\ surface)$

$Q_{total} = Q'_1 + Q'_2$

$V'_1 = \frac{Q'_1}{C_1}$

$Q'_1 = \frac{Q_{tot}\, C_1}{C_1 + C_2}$

$E_{stretched} = \frac{1}{2} C_1 {V'_1}^2 + \frac{1}{2} C_2 V'^2_2 = \frac{1}{2} V'^2_1 (C_1 + C_2)$

$E_{open} = \frac{1}{2} C_2 V_0^2$

$\Delta E = E_{stretched} - E_{open} = \frac{1}{2} \left(((C_1 + C_2) V'^2_1) - (C_2 V_0^2)\right) = -\frac{1}{2} V_0^2 \frac{C_1 C_2}{C_1 + C_2}$

Table 4.4 Theoretical values of ΔE for an electret device where the DE is strained at maximum.

Entry	ε'	s_{max} [%]	A[a]	d[b]	C_1 [nF]	Q'_1 [μC]	V'_1 [V]	ΔE [J]	E [V/μm]
PDMS	2.9	372	5cm × 14.2cm 0.0071 m^2	42.4	4.3	0.77	179.5	-3.86 10^{-4}	4.2
Elastosil	2.9	485	5cm × 17.6cm 0.0088 m^2	34.2	6.6	0.99	150.3	-4.95 10^{-4}	4.4
PDMS-CN	3.5	313	5cm × 12.4cm 0.0062 m^2	48.4	4.0	0.68	171.9	-3.41 10^{-4}	3.6
PDMS-CN-CNT	4.6	270	5cm × 11.1cm 0.0056 m^2	54.1	4.2	0.62	149.9	-3.13 10^{-4}	2.8
P3-Cl	5.3	114	5cm × 6.4cm 0.0032 m^2	93.5	1.6	0.34	209.2	-1.69 10^{-4}	2.2
P3-Cl-CNT	6.3	95	5cm × 5.85cm 0.0029 m^2	102.6	1.6	0.31	196.3	-1.56 10^{-4}	1.9

[a]the theoretical surface area of DE films (initial size of 5 cm × 3 cm) that were uniaxially stretched by s_{max}, [b]$d= d_0/ (1+ s_{max})$, where d represents the DE thickness after being stretched by s_{max}, C_1 represents the capacitance of the DE in the stretched state, Q'_1 is the charge on the stretched DE. $\square E$ represents the theoretical amount of energy harvested if the material was stretched at maximum. E represents the theoretical electric field in the DE calculated using V1' and d.

$$C_2 = \varepsilon_0 \varepsilon' \frac{A}{d} \; (\epsilon' = 2.1, d_{Teflon} = 140\ \mu m, A\ depends\ on\ the\ area\ of\ the\ DE)$$

$$V_2 = \frac{(Q_{total} - Q'_1)}{C_2}$$

Table 4.5 Theoretical values of the electret at maximum strain.

Electret	Electret Area[a] [m^2]	C_2 [nF]	Q_{total} [μC]	V_2 [V]
PDMS	0.0071	0.94	0.94	179.8
Elastosil	0.0088	1.17	1.17	150.3
PDMS-CN	0.0062	0.82	0.82	171.9
PDMS-CN-CNT	0.0056	0.74	0.74	149.9
P3-Cl	0.0032	0.43	0.43	209.2
P3-Cl-CNT	0.0029	0.39	0.39	196.3

[a]To be able to calculate the maximum energy when the DE materials is stretched at maximum, electrets with different surface area has to be used.

Table 4.6 Theoretical values of ΔE when the DE is stretched by 33%.

Entry	ε'	A[a]	d[b] [μm]	C_1 [nF]	Q'_1 [μC]	V'_1 [V]	ΔE [J]	E [V/μm]
PDMS	2.9	5cm × 4 cm 0.002 m^2	150.4	0.34	0.15	437.5	-7.48 10^{-5}	2.9
Elastosil	2.9	0.002 m^2	150.4	0.34	0.14	437.5	-7.48 10^{-5}	2.9
PDMS-CN	3.5	0.002 m^2	150.4	0.41	0.16	391.9	-8.08 10^{-5}	2.6
PDMS-CN-CNT	4.6	0.002 m^2	150.4	0.54	0.18	329.0	-8.92 10^{-5}	2.2
P3-Cl	5.3	0.002 m^2	150.4	0.62	0.19	298.5	-9.32 10^{-5}	2.0
P3-Cl-CNT	6.3	0.002 m^2	150.4	0.74	0.20	263.6	-9.79 10^{-5}	1.8

[a]the surface area of the electret used and of the DE films (5 cm × 3 cm) that were uniaxially stretched by 33%.

$$V_2 = \frac{(Q_{total} - Q'_1)}{C_2}$$

Table 4.7 Theoretical values of the electret when the DE is stretched by 33%.

Electret	C_2 [nF]	Q_{total} [μC]	V_2 [V]
PDMS	0.27	0.27	437.5
Elastosil	0.27	0.27	437.5
PDMS-CN	0.27	0.27	391.9
PDMS-CN-CNT	0.27	0.27	329.0
P3-Cl	0.27	0.27	298.5
P3-Cl-CNT	0.27	0.27	263.6

Table 4.8 Theoretical values at 66% DEG strain.

Entry	ε'	A[a]	d[b] [μm]	C_1 [nF]	Q'_1 [μC]	V'_1 [V]	ΔE [J]	E [V/μm]
PDMS	2.9	5cm × 5 cm 0.0025 m^2	120.5	0.53	0.20	383.9 V	-1.02 10^{-4}	3.2
Elastosil	2.9	0.0025 m^2	120.5	0.53	0.20	383.9 V	-1.02 10^{-4}	3.2
PDMS-CN	3.5	0.0025 m^2	120.5	0.64	0.22	340.5 V	-1.10 10^{-4}	2.8
PDMS-CN-CNT	4.6	0.0025 m^2	120.5	0.84	0.24	282.1 V	-1.19 10^{-4}	2.3
P3-Cl	5.3	0.0025 m^2	120.5	0.97	0.25	254.3 V	-1.24 10^{-4}	2.1
P3-Cl-CNT	6.3	0.0025 m^2	120.5	1.15	0.26	222.9 V	-1.29 10^{-4}	1.9

[a]the surface area of the electret used and of the DE films (5 cm × 3 cm) that were uniaxially stretched by 66%.

$$V_2 = \frac{(Q_{total} - Q'_1)}{C_2}$$

Table 4.9 Theoretical values of the electret when the DE is stretched by 66%.

Electret	C_2 [nF]	Q_{total} [μC]	V_2 [V]
PDMS	0.33	0.33	383.9
Elastosil	0.33	0.33	383.9
PDMS-CN	0.33	0.33	340.5
PDMS-CN-CNT	0.33	0.33	282.1
P3-Cl	0.33	0.33	254.3
P3-Cl-CNT	0.33	0.33	222.9

Chapter 5 Fast and Solvent-free Film Casting of High Permittivity Silicone Dielectric Elastomers

by

Philip Caspari,[1,2] Frank A. Nüesch,[1,2] Dorina M. Opris[1]

[1]Laboratory for functional polymers, Empa, Swiss Federal Laboratories for Materials Science and Technology, Überlandstrasse 129, 8600 Dübendorf. Switzerland. dorina.opris@empa.ch

[2]École Polytechnique Fédérale de Lausanne (EPFL), Institut des matériaux, Station 12, CH 1015, Lausanne, Switzerland.

Author Contributions:

P. Caspari performed the preparation of the materials and devices as well as their characterization and contributed to the manuscript.

5.1 Abstract

Dielectric elastomers are an emerging transducer technology, but high operation voltages limit their scope of application. Up to date, several reports have been published on high permittivity elastomers that can be operated at lower electric fields. However, there are no reports that address reliability and processability of high permittivity dielectric elastomers. In Chapter 5, the UV-induced cross-linking of low-molecular weight polar siloxanes as a novel approach for high permittivity silicone elastomers is presented. The permittivity values of the prepared elastomers are between 5.5 and 6. The low viscosity of the low molecular weight polar siloxane facilitates solvent-free formation of thin films within several minutes which highlights the technological relevance of this process. In addition, the use of dithiol as chain-prolongation-agent enables the fine-tuning of the elastic modulus between 0.4 to 1.2 MPa. The viscoelastic behavior is comparable to commercial silicone elastomer thin films. These polar silicone elastomers allow to operate dielectric elastomer actuators at reduced driving voltages in the range of 1-8 Hz without any mechanical prestrain of the dielectric elastomer. Finally, we demonstrate the reliability of the polar silicone elastomers by 180.000 cycles in a dielectric elastomer actuator. This is unprecedented for high permittivity silicone elastomers.

5.2 Introduction

Dielectric elastomer transducers (DETs) are elastic capacitors that consist of dielectric elastomer (DE) thin films which are placed between two compliant electrodes.[1] DETs can be used as actuators (DEAs), generators (DEGs) and sensors (DESs). When the capacitor is charged, the electrostatic forces generate a mechanical pressure on the incompressible DE. This results in mechanical elongation of the DE until a balance of elastic and electrostatic pressure is reached. Electrical energy is converted into mechanical work. On the contrary, DEGs convert mechanical work into electrical energy.[2] In DESs, a mechanical stress deforms the elastic capacitors and the change in capacitance is measured.[3] As yet, a few DEA devices have already been developed for commercial markets.[4,5]

Up to date, poly(dimethylsiloxane) (PDMS) elastomers (*silicone elastomers*) are the most frequently tested DE materials[6] beside natural rubber,[7] acrylates[8] and polyurethanes.[9] PDMS elastomers have a low conductivity and the elastic modulus can be tuned by the cross-link density. Additionally, well-established cross-linking techniques allow the formation of DEs with high mechanical stability.[10] Therefore, PDMS outperforms alternative DE materials in response speed[11,12] and lifetime,[13] but not in dielectric breakdown strength,[14] maximum mechanical elongation[15] and maximum actuation strain.[12] PDMS is a cross-linked elastomer that might not be as easily processed as polyurethane formulations.[16] However, the Platinum-catalyzed hydrosilylation cross-linking process is fast and clean.[17] Most commercial formulations use the Platinum-catalyzed hydrosilylation reaction to cross-link PDMS to an elastomer. PDMS formulations have a low viscosity and can be processed into thin films without solvent. Silicone elastomers are non-polar and hydrophobic which makes them less sensitive towards water uptake.[18] In contrast, the non-polar character of PDMS goes along with a low permittivity. Hence, high electric fields are required for PDMS-based DEAs. Eq. 5.1 shows the relation between actuation strain *s* and pressure *p* with the DE's parameter dielectric permittvitiy ε', elastic modulus *Y* as well as the applied electric field *U/d*.[19]

$$s = \frac{p}{Y} = \frac{\varepsilon' \varepsilon_0 \left(\frac{U}{d}\right)^2}{Y} \qquad \text{Eq. 5.1}$$

The need of a high voltage power supply is the main disadvantage of PDMS-based DEAs compared to ionic EAPs[20] or piezoelectric devices.[21] High operation voltages raise questions regarding safety for humans in direct contact to DETs.[22] Furthermore, the need of high voltage converters complicates the construction of the devices and increases costs.[23]

Therefore, over the last decade manifold research activities have been initiated to lower the driving voltage of DEAs by reducing the elastic modulus,[24] and thickness of the silicone elastomer[25,26] as well as by increasing the permittivity.[27] A low elastic modulus of the DE leads to a decrease in driving voltage but also low output pressure of the DEA (Eq. 5.1). In addition, a simultaneous reduction of electric breakdown strength (E_{max}) might pose a challenge with respect to reliability and lifetime of the device.[28] Thinning down the DE film can be a very promising approach, particularly in combination with mul-

ti-layer devices.[29] However, there is also a lower limit as low-cost processing of ultra-thin high-quality elastomers is rather challenging.[26] Therefore, the relative permittivity as an intrinsic material parameter is of highest interest in low-voltage DEA applications.

High permittivity additives such as $BaTiO_3$,[30] $Pb(Mg_{1/3}Nb_{2/3})O_3$ /$PbTiO_3$,[31] glycerol,[32] and CNTs[33] were mixed with PDMS and cross-linked. Although some silicone composites showed a remarkable rise in permittivity, reliability and lifetime tests were only rarely reported.[34] In addition, the film formation process of silicone composites relied on the use of solvent.

Chemical modification of polysiloxanes with organic dipoles is an alternative to heterogeneous additives. The integration of organic dipoles was either realized by polar cross-linkers or by polysiloxanes that carry polar side groups.[22,35–39] A drastic increase in permittivity of up to 22 was reported.[40] Lateral actuation strains of 10% at 10 V/µm were realized.[41] However, the modification of siloxane often leads to interferences with well-established siloxane cross-linking reactions. To the best of our knowledge, only two examples of solvent-free Pt-catalyzed thin-film processing of polar silicones have been reported.[22,39] In both cases, chloroalkyl polysiloxane side groups were integrated into the elastomeric network. It remains unclear to what extent the chloroalkyl moiety influences the cross-linking process with respect to conversion and reaction rate. An overall film formation time of about 30 minutes was reported, which is rather high for large scale applications.[22] However, the performance and lifetime of those polar silicone elastomers have not been tested in DEAs up to date.

We have recently reported the preparation of polar silicone elastomer thin films using the tin-catalyzed condensation reaction for cross-linking.[42] Even though the obtained elastomers showed promising DEA performance, the film processing required solvent and prolonged cross-linking reaction time. In this work, we present a novel synthetic approach to an allyl-terminated polar siloxane oligomer and to a vinyl-terminated polar oligosiloxane that can be processed into thin elastomeric films within 10 minutes. We highlight the advantages of processability and the electromechanical performance but also the limitations and remaining challenges with respect to conductivity and lifetime of the polar silicone elastomers in DEA devices. By focusing on the aspect of processability we bridge the gap between a purely academic synthetic approach and a technologically relevant process.

5.3 Experimental section

Unless otherwise stated, all chemicals were reagent grade and used without purification. Poly(ethyl-2-thioethyl)(methyl)siloxane was synthesized according to literature.[42] Except for the cross-linking reaction, all chemical manipulations were carried out under argon atmosphere. 1,3,5,7-Tetramethyl-1,3,5,7-tetravinyl cyclotetrasiloxane (**V4**), 1,3-bis(3-aminopropyl)tetramethyldisiloxane, 1,3-bis(vinyldimethyl)disiloxane, α'ω-OH-PDMS (AB116665 (M_n: 139 kDa), AB109358 (M_n: 28 kDa), AB109360 (M_n: 63 kDa) and poly(3-mercaptopropyl)(methyl)siloxane (AB 113729) were purchased from ABCR. 2,2'-(ethylene-dioxy)diethanethiol $\mathbf{R^1(SH)_2}$, allyl isocyanate, $H_2SO_{4(conc)}$, 2,2-dimethoxy-2-phenylacetophenone (DMPA), ethanethiol, tetramethylammonium hydroxide 25% in H_2O (TMAH) and DuraSeal™ laboratory stretch film were purchased from Aldrich. Tetrahydrofuran (THF) was purchased from VWR. Films of Elastosil®Film (200 µm, 100 µm, 50 µm, 20 µm) were provided by DRAWIN Vertriebs-GmbH, Riemerling. Polyvinylalcohol (PVA) was purchased from Swiss Composite. Photoreactions were conducted with a UVAHAND 250 GS H1 mercury vapor UV lamp from Dr. Hoenle AG.

^{1}H and ^{13}C NMR spectra were recorded at 298 K on a Bruker Avance 400NMR spectrometer using a 5 mm broadband inverse probe at 400.13 and 100.61 MHz, respectively. Chemical shifts (δ) in ppm were calibrated to residual solvent peaks ($CDCl_3$: δ = 7.26 and 77.16 ppm). Gel permeation chromatograms were recorded using an Agilent 1100 Series HPLC (Columns: serial coupled PSS SDV 5 m, 100A and PSS SDV 5 m, 1000A, detector: DAD, 235 nm and 360 nm; refractive index), with THF as mobile phase. PDMS standards were used for calibration and toluene as an internal standard.

Differential scanning calorimetry (DSC) experiments were undertaken on a Pyris Diamond DSC (Perkin Elmer USA) instrument under a nitrogen flow (50 ml × min^{-1}) in aluminum crucibles shut with pierced lids and using about 10 mg sample mass. The viscosity η was measured between 1-10 Hz on the ARES Rheometer from TA instruments with a parallel plate setup (50 mm plate diameter, 1 mm plate distance) at 24 °C.

The tensile tests were performed on a Zwick Z010 tensile test machine with a crosshead speed of 50 mm min^{-1} (278% min^{-1}). Tensile test specimens with a gauge width of 2 mm and a gauge length of 18 mm were prepared by die cutting. The strain was determined using a longitudinal strain extensometer. The data points were averaged over 3 different samples. The

elastic modulus *Y* was determined from the slope of the stress–strain curves using a linear fit to the data points within ±5% strain. Thermal gravimetric analysis (TGA) was conducted on a Netzsch TG 209 F1 in synthetic air (20% O_2, 80% N_2).

Dynamic mechanical analysis was carried out on a RSA 3 DMA from TA Instruments. Stripes of 10 mm × 20 mm were measured under a dynamic load of 2 g at 2% strain in the frequency range of 0.05–2.05 Hz at 25 °C. The mechanical loss factor *tan(δ)* is given as the fraction of imaginary *E''* and storage modulus *E'* at 2 Hz.

Permittivity measurements were performed in the frequency range from 10^{-1} Hz to 10^{6} Hz using a Novocontrol Alpha-A frequency analyzer. The V_{RMS} (root mean square voltage) of the probing AC electric signal applied to the samples was 1 V. The permittivity ε' was determined from the capacitance $C= \varepsilon'\varepsilon_0 A/d$, where *A* is the electrode area, *d* is the thickness of the film, and ε_0 is the vacuum permittivity. The thickness of the film was measured by a micrometer gauge with an uncertainty of ±5 µm. Two stainless steel discs with a diameter of 20 mm served as electrodes which were separated by three glass fibers with a diameter of 100 µm± 5 µm. The samples were annealed at 80 °C for 18 h at 10 mbar.

Electromechanical tests were performed using circular membrane actuators at ambient temperature and humidity (24 °C/30% RH). The silicone thin films on a PVA substrate were fixed between two circular frames immersed in H_2O subsequent to drying at 80 °C *in vacuo* for 48 h and drying at air for 48h. Circular electrodes (8 mm diameter) of carbon black powder were applied to each side of the film. A FUG HCL- 35-12500 high voltage source served as power supply for actuator tests. The voltage was increased by 50 V steps every 2 s up to maximum 5.6 kV. The actuation strain was measured optically as the extension of the diameter of the electrode area *via* a digital camera, using an edge detection tool of a LabView program to detect the boundary between the black electrode area and the transparent silicone film. The maximum resolution of LabView was 30 measurements per second. Leakage current was measured up to a voltage of 5 kV.

Synthesis of **P1:** A 25 wt% aqueous solution of tetramethylammonium hydroxide (0.1 ml, 0.0003 mol , 0.01 eq.) was added to a 250 ml Schlenk flask. All volatiles were removed at 10^{-2} mbar at ambient temperature for 1 h. Freshly distilled **V4 (**72.0 g, 0.21 mol, 5 eq.) and freshly distilled 1,3-bis(3-aminopropyl)tetramethyldisiloxane (11.0 ml, 0.04 mol, 1 eq.) were added. The reaction mixture was warmed up to 75 °C and stirred overnight. The reaction temperature was increased to 145 °C at 100 mbar for 4 h. Finally, all volatiles were removed at 150 °C at 10^{-2} mbar to yield 72.2 g (88%) of **P1** as colourless liquid. ^{1}H NMR (400 MHz, $CDCl_3$) δ, ppm: 6.03-5.75 (m, 82H, Si-C*H*=C*H*$_2$), 2.66 (t, ^{3}J= 7.0 Hz, 4H, -CH_2-CH_2-NH_2), 1.91 (br s, 4H, -CH_2-N*H*$_2$), 1.49-1.41 (m, 4H, -CH_2-C*H*$_2$-CH_2-), 0.56-0.51 (m, 4H, -Si-C*H*$_2$-CH_2-), 0.14 (br s, 82 H, -Si-C*H*$_3$), 0.08 (br s, 16 H, -Si-(C*H*$_3$)$_2$-CH_2-). ^{13}C NMR (100 MHz, $CDCl_3$) δ, ppm: 137.07, 133.45, 1.385, 0.5168, -0.2274. M_n(^{1}H NMR): 2500 g/mol. The molar mass could not be determined by GPC.

Synthesis of **P2** and **P3**: **P1 (**43 g, 0.5 mol repeat units, 1 eq.**)** was added to a solution of ethanethiol 200 ml (2.7 mol, 5.4 eq.) ethanethiol and DMPA (1.3 g, 0.005 mol, 0.01 eq.) in 600 ml THF in a 1l Schlenk-flask. The mixture was cooled down to 0 °C by an ice bath and irradiated for 3 min with UV light. Afterwards, all volatiles were removed at 10 mbar at ambient temperature. **P2** was obtained as a yellowish liquid. Allyl isocyanate (10 ml, 0.11 mol, 0.22 eq.) was added to **P2** and the reaction mixture was stirred at ambient temperature overnight. Afterwards all volatiles were removed at 10^{-2} mbar and 120 °C. The residue was dissolved in THF and filtered (PTFE syringe filter, pore size 0.2 µm). Finally, all volatiles were removed at 10^{-2} mbar and 120 °C overnight. **P3** (65 g, 85%) was obtained as a slightly yellowish liquid.

^{1}H NMR (400 MHz, $CDCl_3$) δ, ppm: 5.90-5.80 (m, 2H, -C*H*=CH_2), 5.21-5.09 (m, 4H, -CH=C*H*$_2$), 3.81-3.79 (m, 4H, C*H*$_2$-CH=CH_2), 3.18-3.14 (m, 4H, -C*H*$_2$-NH-), 2.58-2.52 (m, 84H, -C*H*$_2$-S-C*H*$_2$-), 1.24 2(t, ^{3}J= 7.4 Hz, 70H, -CH_2-C*H*$_3$), 0.91-0.87 (m, 41H, Si-C*H*$_2$-CH_2-), 0.14 (br s, 62H, Si-C*H*$_3$), 0.09 (br s, 15H, -Si-(C*H*$_3$)$_2$). ^{13}C NMR (100 MHz, $CDCl_3$) δ, ppm: 43.63, 26.20, 26.09, 18.59, 16.21, 15.64, 15.038, 14.85, 1.37, 0.58, 0.29. M_n of **P3** (^{1}H NMR): 3500 g/mol. M_n of **P3** (GPC): 3000 g/mol. M_w of **P3** (GPC): 7000 g/mol. PDI: 2.4.

Synthesis of **P2+**: High molecular weight poly(ethyl-2-thioethyl)(methyl)siloxane[42] (5 g, 0.03 mmol, 1 eq.) and 1,3-bis(vinyldimethyl)disiloxane(5 g, 28 mmol, 930 eq.) were mixed in a 50 ml Schlenk-flask at ambient temperature. Concentrated sulfuric acid (96%) (0.010 g, 0.1 mmol, 3 eq.) was added and the mixture was stirred overnight at ambient temperatures. All volatiles were removed at 130 °C *in vacuo* for 2 h. The residue was dissolved in 20 ml THF and 2 g activated charcoal was added. After filtration the suspension was filtered and all volatiles were removed at 130 °C at 10^{-2} mbar for 1h. **P2+** (3.9 g, 76%) was obtained as a pale yellowish liquid.

^{1}H NMR (400 MHz, $CDCl_3$) δ, ppm: 6.16-5.70 (m, 6H, -C*H*=C*H*$_2$), 2.58-2.50 (m, 173H, -C*H*$_2$-S-C*H*$_2$-), 1.24 2(t, ^{3}J= 7.3 Hz, 142H, -CH_2-C*H*$_3$), 0.91-0.87 (m, 85H, Si-C*H*$_2$-CH_2-), 0.15 (br s, 147H, Si-C*H*$_3$). ^{13}C NMR (100 MHz, $CDCl_3$) δ, ppm: 26.15, 26.02, 18.52, 18.24, 18.05, 14.95, 0.23, -0.23. M_n of **P2+** (^{1}H NMR): 8000 g/mol. M_n of **P2+** (GPC): 8500 g/mol. M_w of **P2+** (GPC): 20000 g/mol. PDI: 2.4.

Synthesis of **R(SH)$_3$:** Freshly distilled **V4 (**5.0 g, 0.015 mol, 1 eq.)**,** 2,2'-(ethylene-dioxy)diethanethiol (80.0 ml, 0.5 mol, 33 eq.) and DMPA (0.08 g, 0.3 mmol, 0.02 eq.) were dissolved in 150 ml THF. The reaction mixture was cooled down to 0 °C and irradiated for 3 min with UV light. Afterwards, all volatiles were removed at 100 mbar/80 °C and at 10^{-2} mbar/135 °C overnight. **R(SH)$_3$** (13.7 g, 88%) was obtained as a colourless liquid. ^{1}H NMR (400 MHz, $CDCl_3$) δ, ppm: 3.66-3.60 (m, 8H, C$\underline{H_2}$-O-(C$\underline{H_2}$)$_2$-O-C$\underline{H_2}$), 2.74-2.67 (m, 4H, S-C$\underline{H_2}$-CH$_2$-O, C$\underline{H_2}$-SH), 2.61-2.57 (m, 2H, Si-CH$_2$-C$\underline{H_2}$-), 1.58 (t, ^{3}J= 8.3 Hz, 4H, -CH$_2$-CH$_2$-NH$_2$), 0.94-0.88 (m, 2H, Si-C$\underline{H_2}$-CH$_2$-), 0.1246 (m, 3H, Si-C$\underline{H_3}$).^{13}C NMR (100 MHz, $CDCl_3$) δ, ppm: 73.34, 71.27, 70.68, 31.77, 27.28, 24.68, 18.36, 1.42, 0.00. GPC elution curves **of R(SH)$_3$** are shown in Fig. 5.18.

General synthesis of **E3-Y** and **E2+**: **P3/P2+** was mixed with DMPA, cross-linker **R(SH)$_3$**/AB113729 and chain-prologation reagent **R^1(SH)$_2$** (for the amount used, see Table 5.1) and sonicated for 10 minutes at 70 °C. The reaction mixture was directly casted by doctor-blade technique (blade thickness adjusted to 100 µm) on a PVA/glass substrate. The substrate was placed on a heating plate at 80 °C for 5 min subsequent to UV-irradiation of 3 min at ambient temperature. The silicone elastomer with the PVA layer was removed from the glass substrate and placed with the top surface on DuraSeal™ laboratory stretch film. The PVA was dissolved in H_2O and the silicone elastomer thin film was dried in vacuo for 12h at 80 °C.

Table 5.1 The amount of reagents used for the synthesis of **E3-Y**[a] (entry 1-4) and **E2+**[b] (entry 5).

Entry	**P3**[c] **/ P2+**[d] [g] / [mol]	**R(SH)$_3$**[e] [g] / [mol]	**R^1(SH)$_2$**[f] [g] / [mol]	**DMPA**[g] [g] / [mol]
1	1.5 / 4.3 10^{-4}	0.276 / 2.6 10^{-4}	-----	0.03 / 1.0 10^{-4}
2	1.5 / 4.3 10^{-4}	0.165 / 1.5 10^{-4}	0.030 / 1.6 10^{-4}	0.03
3	1.5 / 4.3 10^{-4}	0.108 / 1.0 10^{-4}	0.045 / 2.5 10^{-4}	0.03
4	1.5 / 4.3 10^{-4}	0.090 / 0.8 10^{-4}	0.060 / 3.3 10^{-4}	0.03
5	1.5/ 1.9 10^{-4}	0.045[h]/ 3.4 10^{-4}	-----	0.03

[a]**E3** indicates that the reaction products are elastomers made of **P3** and **Y** refers to entry in Table 5.1. [b] The name **E2+** indicates that the reaction product is a elastomer made of **P2+**. [c] 3500g/mol. [d] 8000 g/mol. [e] 1072 g/mol (**R(SH)$_3$**). [f] 182 g/mol. [g] 256 g/mol. [h] *AB 113729*: 134 g/mol (repeat unit).

5.4 Results and discussion

Scheme 5.1 describes the synthetic approach to the polar oligosiloxane **P3** which carries allyl end-groups and polar ethyl-thioethyl side groups. The terminal allyl groups will be subsequently used for cross-linking or for both, chain prolongation and cross-linking, into thin films. The synthesis starts from **V4**, which was polymerized by ring opening in presence of TMAH to give polymer **P1**, which carries a vinyl group at every siloxy unit. To control the molecular weight of **P1,** the amino-functional end-capping agent 1,3-bis(3-aminopropyl)tetramethyldisiloxane was used. The number average molar mass was determined according to the ^{1}H-NMR end-group signals. In the second step, the vinyl groups were converted to thioethers by UV-induced thiol-ene addition of ethanethiol mediated by 2,2-dimethoxy-1,2-diphenylethan-1-one (DMPA) under mild conditions *i.e.* 3 minutes UV-irradiation at 0°C in THF. It is important to mention that the amino end-groups were selected because they do not interfere with the thiol-ene reaction and could be used subsequently in an efficient cross-linking reaction into thin films. After the removal of volatiles, the amino end-groups of **P2** were reacted *in situ* with allyl isocyanate to afford a low viscosity polymer **P3** that carries allyl end-groups. The synthesis of **P3** was conducted on 60 g scale. The allyl group was linked to the siloxane by an urea functionality similar to urethane links in polyurethane DEs.[16]

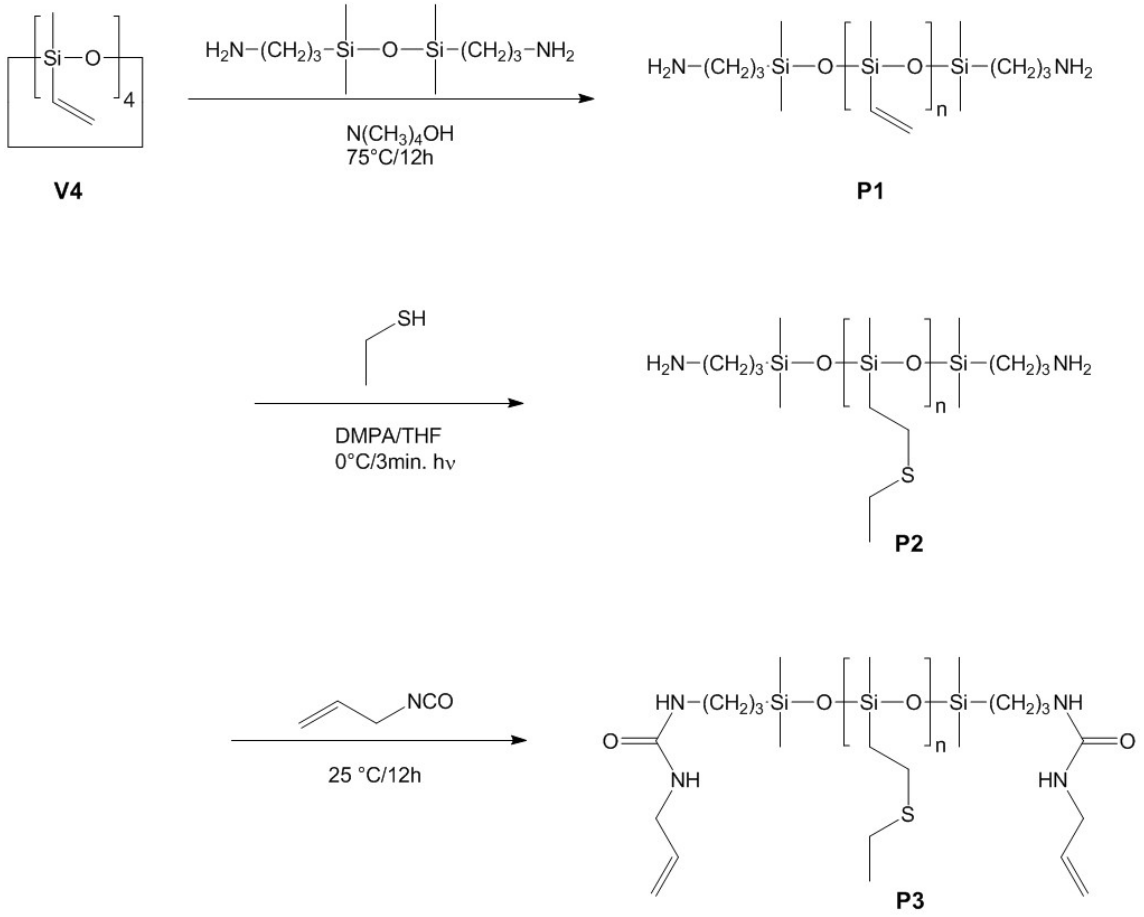

Scheme 5.1 Synthetic route from **V4** to **P3**, which was isolated with 77% overall yield.

An alternative end-capping strategy based on the addition of α,ω-OH-poly-(ethyl-thioethyl)methylsiloxane on vinyldimethyldisiloxane under basic conditions led to depolymerization of the polar polysiloxanes. However, the addition of high molecular weight α,ω-OH-poly-(ethyl-2-thioethyl)methylsiloxane to 1,3-bis(vinyldimethyl)disiloxane under acidic conditions gave vinyl-terminated oligo(ethyl-2-thioethyl)methylsiloxane with an isolated yield of 76% (Scheme 5.2). The GPC spectra revealed approximately 5% of low-molecular weight side products, most likely cyclic siloxanes.

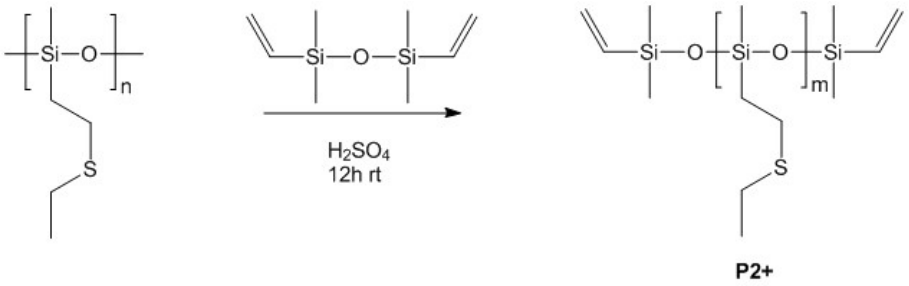

Scheme 5.2 Synthetic route from poly(ethyl-2-thioethyl)(methyl)siloxane to **P2+**, isolated with 76% yield.

The synthesis of **P3** and **P2+** was analyzed by ^{1}H NMR, ^{13}C NMR and GPC. Figure 5.1 compares the ^{1}H NMR spectra of **P1**, **P3** and **P2+**. The presence of the thioether and allyl groups of **P3** are clear indications that the reaction was well controlled. In the ^{1}H NMR spectrum of **P2+** (Fig 5.1, bottom) the terminal vinyl group signals are very pronounced at 6 ppm.

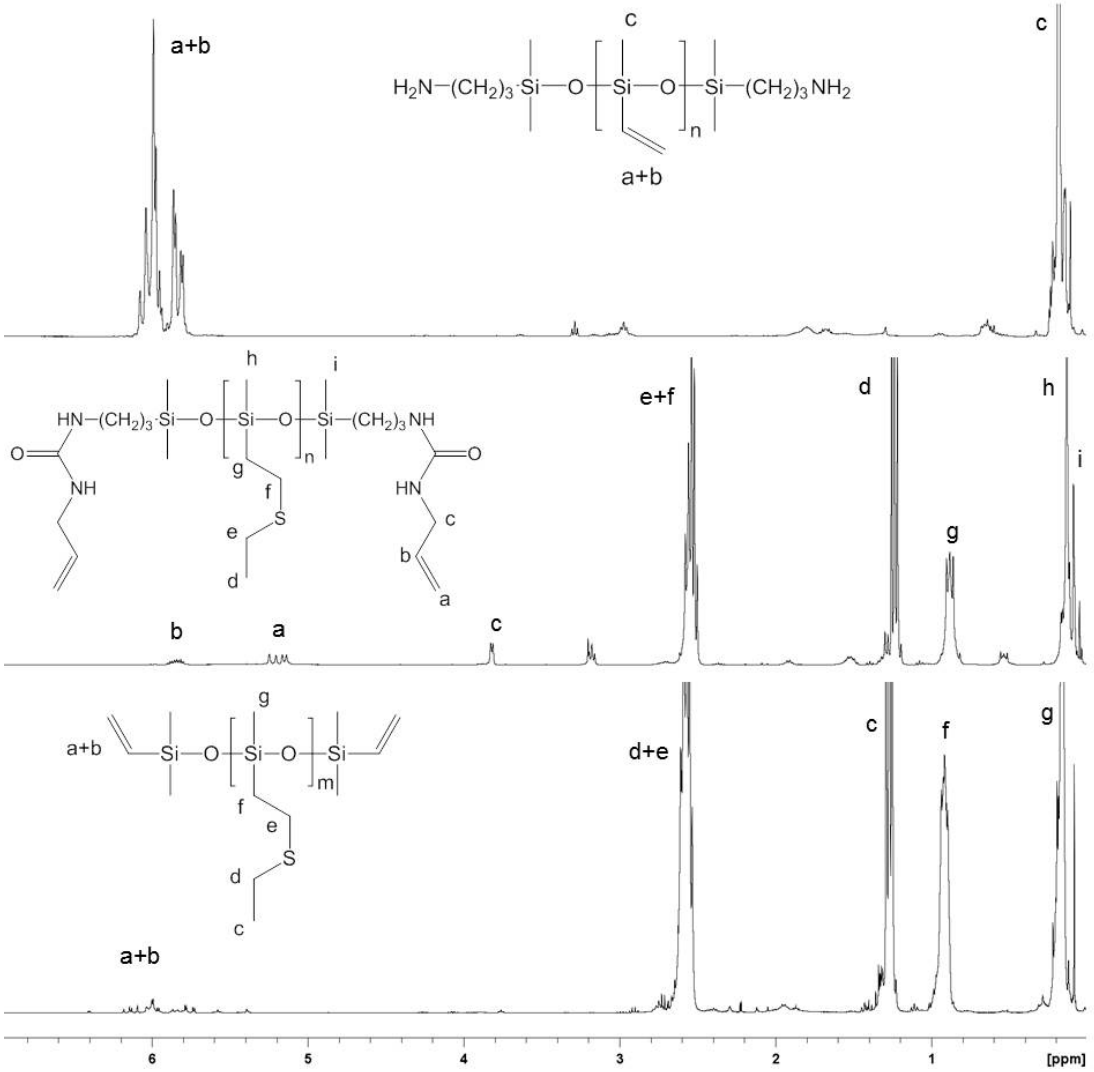

Figure 5.1 ^{1}H NMR spectra of **P1** (top) and **P3** (middle) and **P2+**(bottom).

The number average molar mass was determined by comparing the integrals of the ^{1}H signals from the end-groups to those of the side groups. For **P2+** a M_n = 8000 g/mol, for **P1** a M_n = 2500 g/mol and for for **P3** a M_n = 3500 g/mol was determined. By decreasing the amount of end-blocker in the synthesis of **P1**, the molecular weight of the corresponding **P3.2** was determined to M_n = 10.000.

The only side products observed were high molecular weight siloxanes which were most likely formed by intermolecular vinyl-vinyl-coupling during thiol-ene addition.[36] A lower concentration of **P1** in THF and of UV-irradiation time to 3 minutes eliminated this side reaction (Fig. 5.16). Organosulfur functionalities were observed to interfere with platinum- and tin-catalyzed cross-linking reactions.[17] Hence, cross-linking by thiol-ene addition on the allyl-terminated siloxanes **P3** was tested.[43–45] Initially, some commercially available multifunctional thiols were tested, *e.g.* pentaerythritol tetrakis(3-mercaptopropionate), trimethylolpropane tris(3-mercapto-propionate), and poly(3-mercaptopropyl)methylsiloxane. However, they were poorly miscible with **P3** without any additional solvent. To overcome this problem, a custom-made oligomeric cross-linker **R(SH)$_3$** was prepared in a one-step synthesis described in Scheme 5.3. Shortly, **R(SH)$_3$** is a mixture of mercapto-functionalized cyclosiloxanes (Fig. 5.14-5.15, Fig. 5.18). After removal of volatiles it was used without additional purification steps. The isolated yield was 88%. For **P2+** the commercially available poly(3-mercaptopropyl)methylsiloxane (*AB 113729,* Fig. 5.19-5.20*)* could be used as cross-linking agent.

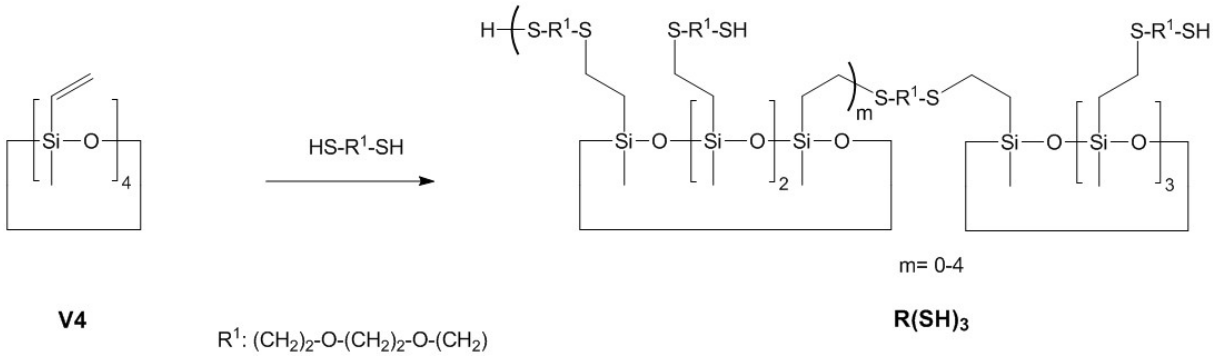

Scheme 5.3 Synthetic route from **V4** to mercapto-functionalized (oligo)cyclosiloxanes **R(SH)$_3$** by thiol-ene addition of 2,2'-(ethylene-dioxy)diethanethiol **R^1(SH)$_2$** on methylvinylcyclotetrasiloxane.

As mentioned above, the solvent-free cross-linking of silicone elastomers is a prime advantage in the thin film processing of DEs. In order to be able to process the polar silicones into thin films, their viscosity should be low. The viscosity of **P3** with a molecular weight of 3.5 kDa and **P3.2** with a molecular weight of 10 kDa (Fig. 5.21) as well as mixtures of **P3** with **R(SH)$_3$** and **R^1(SH)$_2$** were measured between 1 and 10 Hz (Fig. 5.22-5.32). Furthermore, the viscosity of **P2+** and the cross-linkable mixture (**P2+5**) of **P2+** and poly(3-mercaptopropyl)methylsiloxane (see entry 5 in Table 5.1) was determined at ambient temperature. Table 5.2 summarizes the values of viscosity η at 2 Hz with respect to α'ω-hydroxy-terminated PDMS as internal reference.

Table 5.2 Viscosity η at 2 Hz of α'ω-hydroxy-terminated PDMS, the oligomers **P3**/**P3.2** and the cross-linkable mixtures of **P3-Y** with different weight amounts of **R(SH)$_3$** and **R^1(SH)$_2$** as well as the corresponding molecular weight of the siloxane in kilodalton [kDa]. **P2+5** is the mixture of **P2+** and *AB 113729.*

Entry	η [Pa s] at 2 Hz/24 °C	M_n of the siloxane[a] [kDa]
P3.2	4.6	10
P3	2.7	3.5
P3-1	2.3	3.5
P3-2	1.9	3.5
P3-3	1.7	3.5
P3-4	1.6	3.5
P2+	2.3	8
P2+5	1.9	8
α'ω-OH-PDMS	87.8	139
α'ω-OH-PDMS	7.7	63
α'ω-OH-PDMS	0.8	28

[a] As determined by ^{1}H NMR.

P3 and **P2+** as well as the corresponding reaction mixtures **P3-Y** and **P2+5** exhibited values in the range of 1.6 to 2.7 Pa s which was comparable to α'ω-OH-PDMS with a molecular weight between 28 and 63 kDa. The addition of the oligomeric cross-linker **R(SH)$_3$** and **R^1(SH)$_2$** led to a further decrease in viscosity (η (**P3-4**) > η (**P3-3**) > η (**P3-2**) > η (**P3-1**)).

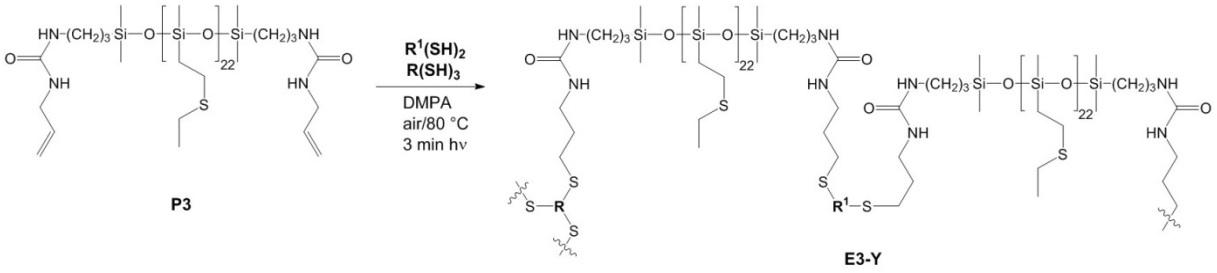

Scheme 5.4 UV-induced cross-linking reaction of **P3** with **R(SH)$_3$** and **R^1(SH)$_2$** initiated by DMPA in air.

A low viscosity value was important for the solvent free casting process of thin films. The fast formation of a defect-free film surface prior to UV-irradiation strongly relied on the low viscosity of the silicone formulation. Elevated temperature supported the fast formation of a smooth surface of the 100 µm thin coated reaction mixture. However, cross-linkable mixtures of **P3.2** did not form a smooth surface by doctor-blade techniques within 10 minutes at 80 °C. In contrast, **P3-1/2/3/4** formed cross-linked films with smooth surfaces after casting and heating at 80 °C for 5 min followed by 3 min UV irradiation (Scheme 5.4). The downside of cross-linking low molecular weight siloxanes is the high cross-link density which results in stiff silicone elastomers and low mechanical elongations.[46] Thus, **R^1(SH)$_2$** was added to **P3** (**P3-2**/**P3-3**/**P3-4**) as chain-prolongation-reagent which reduced the elastic moduli and enhanced the strain at break.

Formation of thin films without defects is a challenging task and needs careful selection of the substrate on which the film is casted. Four substrates were tested: poly(tetrafluoro)ethylene, stainless steel, polyethylene terephthalate, and a poly(vinyl alcohol) (PVA) film coated on a glass substrate. Poly(tetrafluoro)ethylene substrates, that work nicely with other silicones, did not work in the present, *i.e.* the coated film dewetted. **P3-Y** casted on a stainless steel and a polyethylene terephthalate substrate gave smooth elastomeric films. However, the peeling off the film from the substrate by hand was challenging. To avoid peeling, a sacrificial layer of poly(vinyl alcohol) (PVA) was used. First attempts to process our formulations on PVA were not successful because the casted films did not have a uniform surface. This problem was overcome by heating the casted film to 80 °C for 5 min. Also the cross-linkable mixture of **P2+** was casted on PVA and heated for 5 min to 80 °C subsequent to 3 min UV irradiation as illustrated in Scheme 5.5.

After UV irradiation, smooth films formed. A DuraSeal™ laboratory stretch film was placed on the silicone films and the PVA substrate was peeled from the glass substrate. Any mechanical stress on the silicone thin films was avoided. Thereafter, PVA was dissolved in H_2O. For DEA measurements, the silicone film on PVA was fixed between two rigid frames of the actuator device. This ensemble was immersed in H_2O and subsequently dried at 80 °C *in vacuo*.

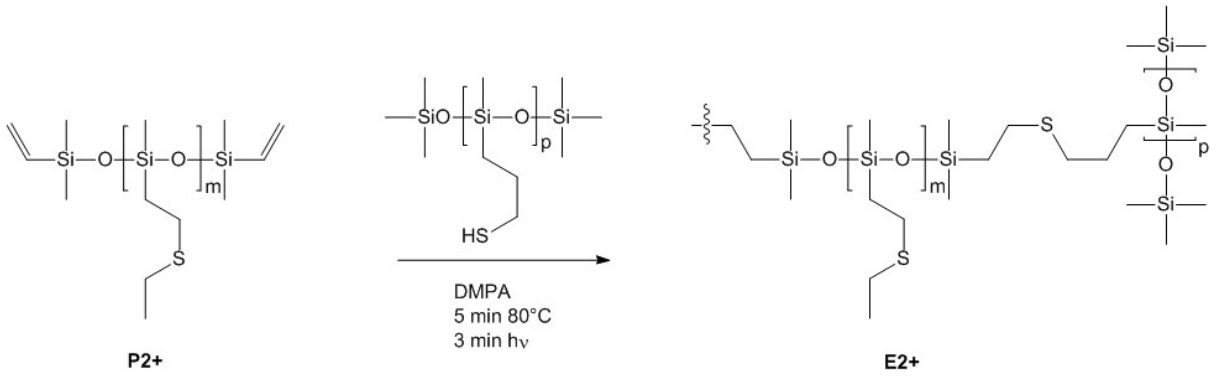

Scheme 5.5 UV-induced cross-linking reaction of **P2+** with poly(3-mercaptopropyl)(methyl)siloxane initiated by DMPA in air.

The thermal stability of **E3-Y** and **E2+** as well as of the precursors **P2+**, **P3, R(SH)$_3$** and *AB113729* were characterized by thermal gravimetric analysis (Fig. 5.33-5.41) which showed that all elastomers were stable until 150 °C in air. Above 300 °C

all materials lost considerable amount of mass. Thermal stability in air is not only relevant for the lifetime stability but also in the processing of the DEA devices at elevated temperatures.

To optimize the properties of the elastomers **E3-Y** (see Table 5.1), the amount of cross-linker **R(SH)$_3$** and of chain prolongation reagent **R^1(SH)$_2$** was varied in the cross-linking reaction of **P3**. The viscoelastic behavior of elastomers **E3-Y** and of **E2+** was characterized by dynamic mechanical analysis (DMA). The commercially available PDMS thin film **Elastosil®Film** was used as reference.[47] Three independent samples were prepared and analyzed (Fig. 5.42-5.48). The average values of elastic modulus *E'* and mechanical loss factor *tan(δ)* are depicted in Figure 5.2. The reproducibility of the cross-linking reactions (Scheme 5.4, 5.5) was studied by performing three cross-linking reactions for each elastomer with the same batch of **P3** and **P2+**.

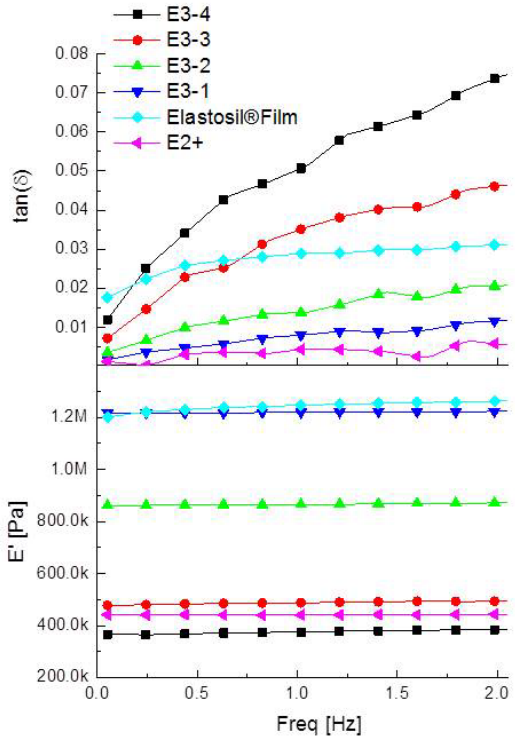

Figure 5.2 Dynamic mechanical analysis of **E3-Y, E2+** and **Elastosil®Film** ranging from 0.05 Hz to 2 Hz at a strain of 2%.

E3-1, for which no chain prolongator was used, **E3-2** and **E3-3** showed a viscoelastic behavior similar to **Elastosil®Film.** At 2 Hz the mechanical loss factor *tan(δ)* of **E3-1** was 0.01 and of **E3-2** was 0.02 in comparison to 0.03 for **Elastosil®Film**. For **E3-3** and **E3-4** which contained higher amounts of **R^1(SH)$_2$** the mechanical loss factor *tan(δ)* was 0.05 and 0.07.

As expected, there was a clear softening of **E3-Y** trend with the addition of **R^1(SH)$_2$**. The storage modulus *E'* of all materials remained constant over the investigated frequency range (0-2 Hz). It decreased from 1.22 MPa for **E3-1**, to 0.5 MPa for **E3-3**, and to 0.39 MPa for **E3-4**. **E2+** had already a low elastic modulus of 0.45 MPa without any addition of **R^1(SH)$_2$**. This might be explained by the high molecular weight of **P2+** or a plasticizing effect of uncrosslinked liquid siloxanes. The viscoelastic behavior of **E2+** was very unusual as soft silicone elastomers commonly do not possess a mechanical loss factor tan(δ) below 0.01. The elastic behavior of **E2+** did not deteriorated with time (Fig. 5.47).

Figure 5.3 depicts the unilateral stress-strain-curve of all elastomers. Three independent tests were performed (Fig. 5.49-5.54). According to the tensile tests, the strain at break s_{max} increases with decreasing elastic modulus $Y_{10\%}$ *i.e.* with the amount of **R^1(SH)$_2$**. As expected the cross-linking of low molecular weight siloxanes resulted in elastomers with relatively low strain at break compared to **Elastosil®Film** (Table 5.3). For example, the stiffest material **E3-1** has a strain at break of 47%, while the softest material prepared **E3-4** has a strain at break of 109%. **E2+** showed an unusual behavior with a low strain at break of only 46% and a low Young's modulus of only 0.41 MPa.

While these values are not impressive for elastomers in general, s_{max} is not considered as a limiting factor in silicone DEAs.[10] This is particularly the case in low-voltage DEA operations for which **E3-Y** and **E2+** are designed for. There are several reports on an improved s_{max} for polar silicone elastomers by the addition of fillers.[48] However, fillers increase the viscosity of the silicone mixtures[22] and complicate the processing into thin film elastomers.

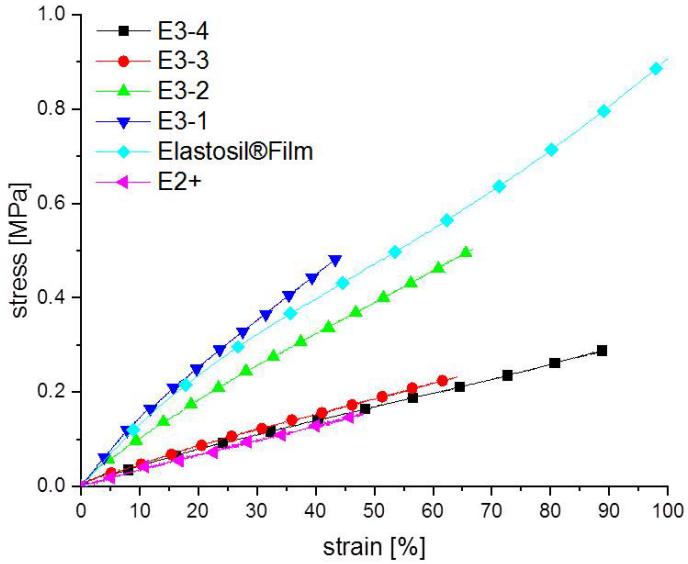

Figure 5.3 Stress-strain curves of **E3-Y**, **E2+** and **Elastosil®Film.** Three independent tests were performed. The curve of the sample with the median value of s_{max} is depicted.

The quality of the elastomeric network was further studied by swelling-extraction experiments in THF. The swelling experiments were in agreement with the DMA data. The lowest amount of extractables was found for **E3-1** which also showed the lowest *tan(δ)*. In general, the weight amount of extractables $wt\%_{ext}$ was higher compared to Pt-catalyzed cross-linked silicone elastomers. The degradation products of DMPA used in the thiol-ene functionalization of **P1** and cross-linking reaction of **P3** were non-volatile and thus contributed significantly to the amount of extractables. In addition, the softer elastomers **E3-4** and **E2+** with the lower cross-link density showed the highest amount of extractable species of all elastomers. In case of **E2+**, the low molecular weight side products in the synthesis of **P2+** might contribute to the amount of extractables considerably. For **E3-4**, **R(SH)$_3$** and **R^1(SH)$_2$** competed simultaneously for the allyl-end groups. Therefore, the ability to decrease the cross-link density by **R^1(SH)$_2$** was limited. In case of **E3-4,** the 3.5 wt% of **R^1(SH)$_2$** used for the synthesis corresponds to a molar ratio of thiol to vinyl of about 2/3. Higher ratios thiol/vinyl might further decrease the cross-link density and the elastic modulus but also increase the amount of non-bonded species and thus the viscoelastic losses. As low mechanical losses were reported as an advantage of silicone elastomers over alternative materials in the application of DEAs,[15] a well-balanced trade-off between mechanical losses *tan(δ)* and elastic modulus *E'* as well as maximum strain at break s_{max} had to be found.

Table 5.3 Elastic modulus *E'*, mechanical loss factor *tan(δ)* at 2 Hz, the amount of extractables $wt\%_{ext}$, the Young's modulus at 10% strain $Y_{10\%}$ and strain at break s_{max} of **E3-Y**, **E2+** and **Elastosil®Film**, as well as the molar ratio of chain-prolongation-reagent **R^1(SH)$_2$** to **P3**.

Entry	*E'* [MPa]	*tan(δ)*	$wt\%_{ext}$ [%]	$Y_{10\%}$ [MPa]	s_{max} [%]	Molar ratio **R^1(SH)$_2$ / P3**
E3-1	1.22 ± 0.02	$1.2\ 10^{-2} \pm 1\ 10^{-3}$	6.3	1.19	47	0
E3-2	0.87 ± 0.09	$2.2\ 10^{-2} \pm 9\ 10^{-3}$	13.6	0.86	79	1 / 3
E3-3	0.50 ± 0.03	$4.6\ 10^{-2} \pm 7\ 10^{-3}$	15.2	0.42	92	1 / 2
E3-4	0.39 ± 0.03	$7.7\ 10^{-2} \pm 3\ 10^{-3}$	19.8	0.41	109	2 / 3
E2+	0.45 ± 0.02	$6\ 10^{-3} \pm 1\ 10^{-3}$	17.6	0.41	46	-----
Elastosil®Film	1.26 ± 0.01	$3.1\ 10^{-2} \pm 1\ 10^{3}$	3.8	1.17	486	-----

Differential scanning calorimetry (DSC) was conducted to investigate the influence of the thioether side group and the urea linker on both glass transition temperature and melting temperature. **E3-Y** and **E2+** did not possess any transitions down to -80 °C, except **E3-1**, which showed a transition peak at -61 °C (Fig. 5.55-5.59).

The dielectric properties were characterized by broad band impedance spectroscopy. Relative permittivity ε', dielectric losses ε'', the real part of the frequency dependent conductivity ($\sigma' = 2\pi\nu\varepsilon''$) and the dielectric loss-tangent $tan(\delta)_{el} = \varepsilon''/\varepsilon'$ are shown in Figure 5.4. The dielectric properties of the cross-linked elastomers **E3-Y** and **E2+**, the liquid oligomer **P3** and cross-linking reagent **R(SH)$_3$** are summarized in Table 5.4. The dielectric behavior within the **E3-Y** series was very similar in the range of 10^{-1} to 10^{6} Hz. At 10^{6} Hz **E3-Y** elastomers showed values for ε' between 5.7 (**E3-4**) and 6.2 (**E3-1**). The sharp increase in permittivity at a frequency below 10^{1} Hz is due to electrode polarization. Mobile ions were able to accumulate at the electrodes under the influence of the electric field. Thus, a common feature of **E3-Y** is the presence of ionic conductivity. This resulted in overall conductivity values in the order of 10^{-10} S/cm for **E3-Y** and in the order of 10^{-12} S/cm for **E2+**, whereas **Elastosil®Film** possessed a value of 10^{-15} S/cm.

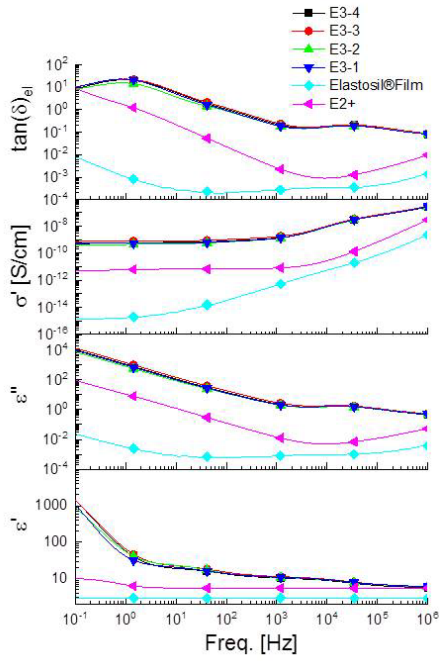

Figure 5.4 Dielectric properties of **E3-Y**, **E2+** and **Elastosil®Film**.

Both, **P3** and **R(SH)$_3$**, contain thioether functionalities but the viscosity of **P3** was higher than the viscosity of **R(SH)$_3$**. Impedance spectroscopy of the liquid precursor materials, *i.e.* **P3** and **R(SH)$_3$** revealed an ionic conductivity of 2.6 10^{-9} S/cm and 1.7 10^{-10} S/cm, respectively. In case of **P3**, a strong electrode polarization in the range of 10^{0}-10^{1} Hz was observed (Fig. 5.60). The thioether substituted polysiloxanes presented in Chapter 3 did not show such a strong polarization.[49] **P2+** showed a very weak electrode polarization.

Thus, the increased conductivity at higher frequencies must be either attributed to the urea-functionality (-NH-(C=O)-NH-) of **P3** or to unknown side products that contribute to ionic conductivity. In addition, absorbed water can contribute to the ionic conductivity as the impedance spectroscopy was performed at ambient humidity.

Table 5.4 Relative permittivity ε' at 10^{6} and 10^{-1} Hz, dielectric loss factor $tan(\delta)_{el}$ at 10^{-1} Hz and conductivity σ' at 10^{-1} Hz measured at 1 V for the cross-linking reagent **R(SH)$_3$**, siloxane **P3**, the elastomers **E3-Y**, **E2+** and **Elastosil®Film**.

Entry	ε' at 10^{6} Hz	ε' at 10^{-1} Hz	$\tan(\delta)_{el}$ at 10^{-1} Hz	σ' at 10^{-1} Hz [S/cm]
R(SH)$_3$	8.3	1.9 10^{2}	1.6 10^{1}	1.7 10^{-10}
P3	5.9	1.2 10^{4}	3.8 10^{0}	2.6 10^{-9}
E3-1	6.2	6.6 10^{2}	1.2 10^{1}	3.6 10^{-10}
E3-2	6,1	9.2 10^{2}	8.1 10^{0}	4.0 10^{-10}
E3-3	6.0	1.4 10^{3}	1.0 10^{1}	7.3 10^{-10}
E3-4	5.7	1.5 10^{3}	6.8 10^{0}	5.4 10^{-10}
E2+	5.5	1.0 10^{1}	8.9 10^{0}	5.1 10^{-12}

Elastosil®Film	2.9	$2.9\ 10^{0}$	$7.9\ 10^{-3}$	$1.3\ 10^{-15}$

Elevated conductivity values of organo-sulfur functionalized silicone elastomers have already been observed before.[42] In the operation of DEAs, the elevated conductivity led to an increase of leakage current at high electric fields, which hindered the operation range of the DEA above 30 V/µm. Therefore, these polar silicone elastomers are exclusively designed for low voltage DEA applications.

The dielectric breakdown strength E_{max} was determined in two different configurations. Free-standing elastomeric thin films with either compliant electrodes (area of 50 mm^2) or with rigid metal electrodes (area of 0.025 mm^2) were used. The rigid metal electrodes were embedded in an epoxy which prevented the electromechanical response of the dielectric elastomer (see Table 5.5). The voltage was increased in steps of 100 V up to electrical breakdown.

Table 5.5 The mean and median value with standard deviation of the dielectric breakdown strength E_{max} measured from 10 samples and the corresponding film thickness *d*. The area of the rigid electrodes was 0.025 mm^2.

Entry	Median E_{max} [V/µm]	Mean E_{max} [V/µm]	thickness *d* [µm]
E3-1	33 ± 3	34 ± 3	71 ± 9
E3-2	40 ± 6	40 ± 6	72 ± 6
E3-3	28 ± 3	27 ± 3	74 ± 10
E3-4	28 ± 1	28 ± 2	71 ± 9
E2+	60 ± 11	60 ± 11	94 ± 5
Elastosil®Film	72 ± 15	72 ± 15	50 ± 0

In contrast to the mechanical properties, the dielectric breakdown strength E_{max} measured in the unstrained state of the elastomers was only slightly affected by the cross-link density. As expected, E_{max} was lower for the polar silicone elastomers **E3-Y** compared to **Elastosil®Film** which is consistent with the elevated conductivity values found with impedance spectroscopy. In case of **E2+** the dielectric breakdown strength in the unstrained state was surprisingly high.

In order to detect realistic E_{max} values the use of any mechanical prestrain was avoided or any other mechanical manipulation of the DE samples. The positive effect of mechanical prestrain on the electromechanical performance of DEs has already been extensively described in literature.[50,51] However, mechanical prestrain always implies an additional working step and is not compatible with the production of multi-layer DEA.[52–54] Interestingly, the measured dielectric breakdown strength E_{max} of the DEA device with carbon black powder as compliant electrodes with an area of 0.5 cm^2 (diameter = 8 mm) indicated a dependence of E_{max} on the elastic modulus of **E3-Y**. Table 5.6 summarizes the E_{max} values of DEAs constructed from **E3-Y, E2+** and **Elastosil®Film** as DE and carbon black powder as compliant electrodes (see Fig. 5.7, right side).

Table 5.6 Dielectric breakdown strength E_{max}, maximum lateral actuation strain s_{max} and the lateral actuation strain s_{act} at 20 V/µm of three DEA devices (area: 0.5 cm^2) given as mean value with standard deviation. The area of the compliant electrodes was 0.5 cm^2.

Entry	E_{max} [V/µm]	s_{max} [%]	s_{act} @ 20 V/µm [%]
E3-1	44 ± 4	10 ± 3	2 ± 1
E3-2	31 ± 3	8 ± 2	4 ± 2
E3-3	26 ± 2	4 ± 1	2 ± 1
E3-4	24 ± 4	5 ± 1	4 ± 1
E2+	30 ± 4	7 ± 3	2 ± 1
Elastosil®Film	95 ± 3	4 ± 1	0 ± 0

The DEs were fixed between two circular plastic frames (inside diameter = 25 mm). Carbon black powder was considered as the best electrode material for electromechanical testing as the powder did not penetrate into the DE and thus not affected the properties of the DE. However, the carbon black powder did not adhere sufficiently to the surface of the silicone elastomers. The carbon black was distributed over the surface of the DE and a clear edge of the black electrode area and the colourless passive area was difficult to measure by optical detection.

The values of E_{max} were calculated with respect to the initial film thickness *d* of the DE. The voltage was increased in steps of 50 V. The difference between **E3-1** with a E_{max} = 44 ± 4 V/µm and **E3-4** with a E_{max} = 24 ± 4 V/µm was considerable. As both elastomers have a rather similar chemical composition the reason for this reduction is attributed to the difference in cross-link density and elastic modulus. **E2+** and **E3-2** showed similar electric breakdown strengths of about 30 V/µm. **Elastosil®Film** showed a very high dielectric strength of about 95 V/µm.

In Figure 5.5 the corresponding actuation strains are depicted. The curve is based on the average lateral strain in x- and y-direction of the median DEA performance of 3 independent DEA devices (Fig. 5.61-5-66). The deviations in DEA the strain measurements were considerable (s_{max} in Table 5.6). Nonetheless, the effect of high permittivity and a low elastic modulus can be clearly seen. In case of **E3-1** the high actuation strain at low electric fields is rather unexpected as the elastic modulus measured by DMA and tensile tests was in the same range as **Elastosil®Film**. For example, at 30 V/µm an actuation strain of 6% was measured for **E3-1**, and of 7% for **E2+**, whereas **Elastosil®Film** gave a significantly lower actuation of only 0.5%. Thus, the high strains at low electric fields must be related to the high permittivity of **E3-1** and **E2+**. Additionally, the internal stress in **E3-1** caused during cross-linking reaction, which is preserved in the DEA device might also play a role.

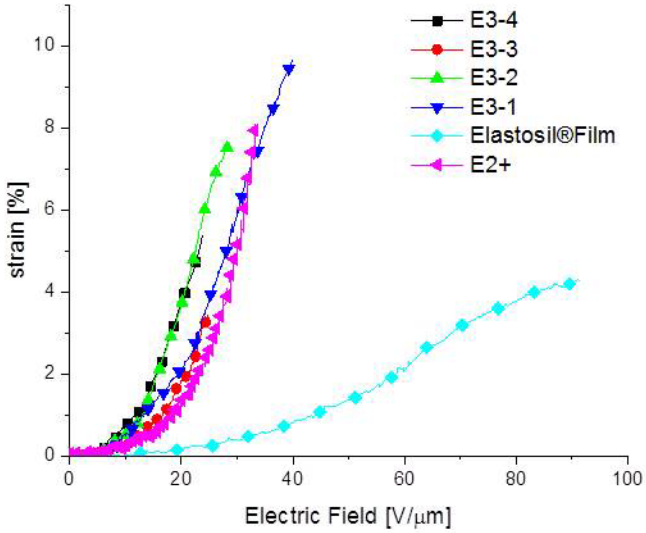

Figure 5.5 Lateral actuation strain of **E3-Y, E2+** and **Elastosil®Film** as a function of the applied electric field *U/d*.

The electromechanical response speed and reliability of the polar silicone elastomers were characterized by cyclic DEA measurements in the range of 1 to 8 Hz. For each frequency, 100 cycles were conducted. The electric field was adapted to the measured E_{max} values. **E3-1** was operated at 30 V/µm, **E3-2/3** and **E2+** at 25 V/µm, **E3-4** at 20 V/µm and **Elastosil®Film** at 80 V/µm. At electric fields below 30 V/µm the actuation strain of **Elastosil®Film** was too small to be measured. Three DEA devices were constructed and characterized for each elastomer. Figure 5.6 illustrates the cyclic behavior of the median DEA performance between 8 and 1 Hz. Again, the out-of-plane actuation was considerable as no mechanical prestrain was applied. Nonetheless, the tests are conclusive with respect to response speed and reliability of the DEA device. Many high permittivity silicone elastomers presented in the literature have shown a considerable time delay in the electromechanical response.[37,55] For **E3-Y** and **E2+** up to 8 Hz no significant dependences of actuation strain on frequency were observed (Fig. 5.67-5.70). The actuation strain of all samples was similar but the applied electric fields could be reduced to values of 30 V/µm (**E3-1**) and 20 V/µm (**E3-4**). The lateral strain was about 2-4% for **E3-2/3/4,** and **Elastosil®Film.** For **E3-1** and **E2+** it was about 4-6%.

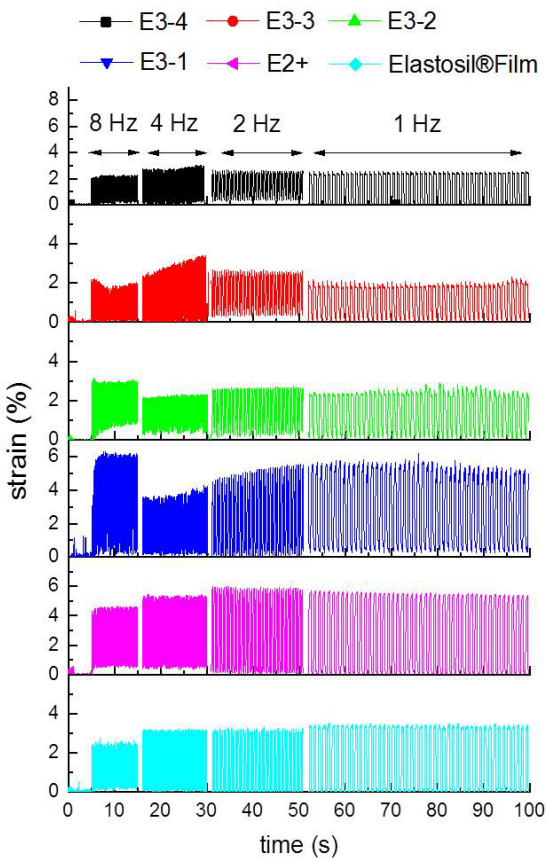

Figure 5.6 100 actuation cycles at 1–8 Hz at an electric field of 80 V/µm for **Elastosil®Film**, 30 V/µm for **E3-1,** 25 V/µm for **E3-2/E3-3** and **E2+,** and 20 Vµm for **E3-4**.

Notably, one DEA constructed from **E3-4** and **E3-2** and two DEAs of **E3-3** suffered electric breakdown during the cyclic tests. In case of **E3-4** and **E3-3** the mechanical stability of the elastomeric thin films characterized by DMA might have been too low. In addition, the applied electric fields might have been too close to the measured dielectric breakdown strengths E_{max} of the materials. The defective DE samples showed clear signs of morphological changes on the entire electrode surface. This is unusual for silicone elastomers. In case of **Elastosil®Film** the electric breakdown could be exactly located on the surface of the elastic film. The elevated conductivities of **E3-Y** have already been noticed with broadband impedance spectroscopy at 1 V. Thus, the DC leakage current i_{leak} of the DEA device was measured. The values are summarized in Table 5.7. The leakage current led to dissipation of electrical energy in the DEA. This might be an important aspect to explain the electrical breakdown of the polar silicone elastomers. The dissipated electrical power is proportional to the leakage current and the applied voltage. This implies a dependence of the dissipated electrical power on the thickness *d* of the DE.

Table 5.7 Leakage current i_{leak} (DC) of the DEA test devices at a given electric field *U/d* with the corresponding dissipated electrical power.

Entry	i_{leak} [µA][a]	*U/d* [V/µm]	Dissipated power[b] [mW]
E3-1	10	10	7.5[c]
E3-2	8	10	6.8[d]
E3-3	10	10	9.0[e]
E3-4	10	10	10.0[f]
E2+	< 3	25	< 6.2[g]
Elastosil®Film	< 1	80	< 3.6[h]

[a] Carbon black electrode area of 0.5 cm^2. [b] Dissipated power = $i_{leak} \frac{U}{d} d$. [c] *d*: 75 µm. [d] *d*: 85 µm. [e] *d*: 90 µm. [f] *d*: 100 µm. [g] *d*: 95 µm. [h] *d*: 46 µm.

In case of **E3-Y** elastomers the leakage current was remarkably high at low electric fields. **E2+** did not suffer from leakage current below 20 V/µm. At 24 V/µm a leakage current of about 3 µA was detected for **E2+**. We have recently reported a thioether functionalized polar silicone elastomer that did not show any leakage current until an electric field of 27 V/µm.[42] The polar siloxane was a α,ω-OH-poly(propylthioethyl)methylsiloxane cross-linked in a tin-catalyzed condensation reaction with $(EtO)_3Si(CH_2)_3Cl$. The **$R(SH)_3$** cross-linker used in the thiol-ene cross-linking (Scheme 5.3) did not exhibited significant differences in its dielectric properties compared to $(EtO)_3Si(CH_2)_3Cl$.[42] Therefore, the microscopic reason for the increased leakage current must be either attributed to the different polar groups at the cross-links or to unidentified side products of the cross-linking reaction. As increased ionic conductivity has already been observed for **P3**, it is very likely that the urea functionality that links the oligosiloxane with the terminal allyl groups is responsible for the increased leakage current of **E3-Y**. With respect to the urea functionality the structural similarity to the urethane group (-O-(C=O)-NH-) might lead to the question whether polyurethane elastomers in general might suffer from elevated conductivity as well. However, until today none of the reported polyurethane DEs were tested for leakage current in electromechanical devices.[16]

Finally, the maximum lifetime of **E3-Y** and **E2+** in DEAs was determined by cyclic measurements at low electric fields (Fig. 5.71-5.75). The applied electric field with a frequency of 8 Hz was further reduced in order to prevent premature electric breakdown due to excessive heat. No mechanical prestrain was applied and carbon black powder was used as electrode material which was renewed every 10.000 cycles. Carbon black powder was considered as the best electrode material for DEA testing as the powder did not penetrate into the dielectric elastomer and thus did not affect the properties of the DE. However, the carbon black powder is not long-term persistent itself. Due to the out-of-plane deformation of the DE the carbon black was distributed over the surface of the DE in the lifetime measurements. This made accurate measurements of the actuation strain based on a digital camera system challenging. Interestingly, it was observed that the adhesion of the carbon black powder onto the surface of the DE was better for **E3-4/E3-3** than for **E3-1** which could be rationalized by the rather viscous behavior of **E3-4** and **E3-3**. Good adhesion of the carbon black powder allowed continuous actuation cycles of up to 30.000 without new carbon black powder in case of **E3-3**.

In summary, **E2+** showed the best DEA lifetime performance with 180.000 actuation cycles at 25 V/µm (2 x 50.000 cycles and 2x 40.000 cycles at 8 Hz). Again, an exact measurement of the actuation strain was rather challenging due to out-of-plane deformation and the non-persistent carbon black powder electrode. The DEA lifetime performance of **E3-1** was unexpectedly high with 100.000 cycles at 25 V/µm (10 x 10.000 cycles at 8 Hz). This was not anticipated due to the high leakage current of **E3-1**. Figure 7 shows an image section of 50 seconds of the first (Fig.5.7, left) and the last operation run (Fig. 5.7, middle). In case of **E3-1** neither mechanical fatigue nor excessive heat could limit the DEA lifetime. The lateral strain was about 2-3%. However, the carbon black powder was distributed with time on the surface of the DE and rendered exact strain measurements impossible (Fig 5.7, right side). For **E3-2** and **E3-3** the DEA lifetime was 70.000 and 90.000 cycles at 29 V/µm and 25 V/µm. **E3-4** could only be operated for 10.000 cycles at 15 V/µm. The actuation strain was not constant though. Signs of excessive heat and material fatigue of the free-standing elastomeric film in the DEA device were obvious. This can be attributed to both, the high mechanical loss factor, observed by DMA, in combination with the high leakage current.

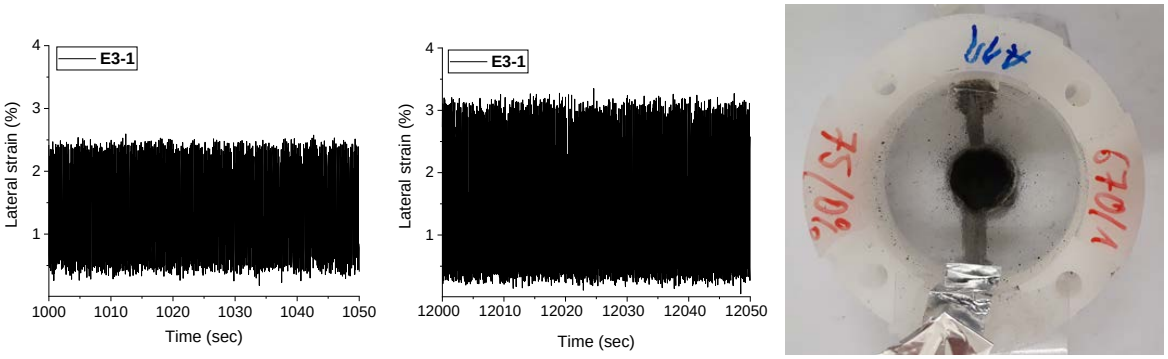

Figure 5.7 DEA constructed from 75 µm-thin film of **E3-1** driven by an electric field of 25 V/µm at 8 Hz for 100.000 cycles. Left: 400 cycles/50 seconds of the first operation sweep of 10.000 repetitions. A lateral strain of about 2.5 % was observed. Middle: 400 cycles/50 seconds of the last operation sweep of 10.000 repetitions. A lateral strain of about 3% was observed. The difference in strain could be rationalized by the error range of the optical detection system. Right: Photo of the DEA constructed from **E3-1** after 100.000 cycles.

5.5 Conclusion

A simple and cost-efficient synthesis of low-viscosity high permittivity siloxanes was developed which can be processed solvent-free and cross-linked within few minutes by exposure to the UV-light. The dielectric and mechanical properties of the DE thin films were compared with that of **Elastosil®Film**. The permittivity of the elastomers developed here was enhanced by a factor of about 2, but the strain at break was considerably lower. However, this property did not affect the DEA performance of the dielectric elastomers. Due to the increased permittivity and low elastic modulus, an enhanced DEA performance at electric fields of only 20-30 V/µm were realized. A reduction of the elastic modulus by chain-prolongation was possible, but the mechanical losses increased and the lifetime of the DEAs was reduced. In addition, the effect of the urea functionality on the increased conductivity of the silicone elastomers was discussed in detail. Nonetheless, a lifetime of 100.000 actuation cycles demonstrated the mechanical stability of the polar silicone elastomer **E3-1** in the unprestrained DEA operated at 25 V/µm. In contrast to **E3-Y**, the high permittivity silicone elastomer **E2+** did not suffer from leakage current until 20 V/µm. The permittivity was about 5.5 and the DEA device reached a lifetime of 180.000 actuation cycles at 25 V/µm. The simplicity of this synthetic approach addressed all major issues that limit the technological relevance of high permittivity silicone elastomers for DEAs.

5.6 References

[1] R. D. Kornbluh, R. Pelrine, Q. Pei, R. Heydt, S. Stanford, S. Oh, J. Eckerle, *Proc. SPIE* **2002**, *4698*, 254.

[2] R. Pelrine, R. D. Kornbluh, J. Eckerle, P. Jeuck, S. Oh, Q. Pei, S. Stanford, *Proc. SPIE* **2001**, *4329*, 148.

[3] B. O'Brien, T. Gisby, I. A. Anderson, *Proc. SPIE* **2014**, *9056*, 905618.

[4] M. Aschwanden, D. Niederer, A. Stemmer, *Proc. SPIE* **2008**, *6927*, 69271R.

[5] G. Kovacs, L. Düring, *Proc. SPIE* **2009**, *7287*, 72870A.

[6] C. Ellingford, C. Bowen, T. McNally, C. Wan, *Macromol. Rapid Commun.* **2018**, *39*, 1800340.

[7] R. Kaltseis, C. Keplinger, S. J. Adrian Koh, R. Baumgartner, Y. F. Goh, W. H. Ng, A. Kogler, A. Tröls, C. C. Foo, Z. Suo, S. Bauer, *RSC Adv.* **2014**, *4*, 27905.

[8] C. Jean-Mistral, A. Sylvestre, S. Basrour, J. J. Chaillout, *Smart Mater. Struct.* **2010**, *19*, 075019.

[9] R. Pelrine, R. Kornbluh, J. Joseph, R. Heydt, Q. Pei, S. Chiba, *Mater. Sci. Eng. C* **2000**, *11*, 89.

[10] F. B. Madsen, A. E. Daugaard, S. Hvilsted, A. L. Skov, *Macromol. Rapid Commun.* **2016**, *37*, 378.

[11] L. Maffli, S. Rosset, M. Ghilardi, F. Carpi, H. Shea, *Adv. Funct. Mater.* **2015**, *25*, 1656.

[12] C. Jordi, A. Schmidt, G. Kovacs, S. Michel, P. Ermanni, *Smart Mater. Struct.* **2011**, *20*, 075003.

[13] P. Lotz, M. Matysek, H. F. Schlaak, *Proc. SPIE* **2011**, *7976*, 79760P.

[14] P. Brochu, Q. Pei, *Macromol. Rapid Commun.* **2010**, *31*, 10.

[15] S. Michel, X. Q. Zhang, M. Wissler, C. Löwe, G. Kovacs, *Polym. Int.* **2010**, *59*, 391.

[16] J. Biggs, K. Danielmeier, J. Hitzbleck, J. Krause, T. Kridl, S. Nowak, E. Orselli, X. Quan, D. Schapeler, W. Sutherland, J. Wagner, *Angew. Chem. Int. Ed.* **2013**, *52*, 9409.

[17] D. Troegel, J. Stohrer, *Coord. Chem. Rev.* **2011**, *255*, 1440.

[18] P. Jean, A. Wattez, G. Ardoise, C. Melis, R. Van Kessel, A. Fourmon, E. Barrabino, J. Heemskerk, J. P. Queau, *Proc. SPIE* **2012**, *8340*, 83400C.

[19] R. Pelrine, R. Kornbluh, Q. Pei, J. Joseph, *Science (80-.).* **2000**, *287*, 836.

[20] L. Bay, K. West, P. Sommer-Larsen, S. Skaarup, M. Benslimane, *Adv. Mater.* **2003**, *15*, 310.

[21] L. X. Zhang, W. Chen, X. Ren, *Appl. Phys. Lett.* **2004**, *85*, 5658.

[22] M. Stepp, F. Achenbach, A. Koellenbacher, *(Wacker Chemie AG)*, **2015**, WO 2015/121261 A1.

[23] T. Hoffstadt, J. Maas, *Proc. SPIE* **2015**, *943007*, 943007.

[24] F. Galantini, F. Carpi, G. Gallone, *Smart Mater. Struct.* **2013**, *22*, 104020.

[25] D. McCoul, S. Rosset, S. Schlatter, H. Shea, *Smart Mater. Struct.* **2017**, *26*, 125022.

[26] F. M. Weiss, F. B. Madsen, T. Töpper, B. Osmani, V. Leung, B. Müller, *Mater. Des.* **2016**, *105*, 106.

[27] H. Krüger, B. Kussmaul, G. Kofod, S. Risse, *(Fraunhofer-Gesellschaft E. V.)*, **2012**, WO 2012/038093 A1.

[28] D. M. Opris, J. E. Q. Quinsaat, S. Dünki, Y. S. Ko, M. Alexandru, C. Racles, F. A. Nüesch, *Proc. SPIE* **2015**, *9430*, 94300A.

[29] G. Kovacs, L. Duering, S. Michel, G. Terrasi, *Sensors Actuators, A Phys.* **2009**, *155*, 299.

[30] J. P. Szabo, J. A. Hiltz, C. G. Cameron, R. S. Underhill, J. Massey, B. White, J. Leidner, *Proc. SPIE* **2003**, *5051*, 180.

[31] G. Gallone, F. Carpi, D. De Rossi, G. Levita, A. Marchetti, *Mater. Sci. Eng. C* **2007**, *27*, 110.

[32] P. Mazurek, S. Hvilsted, A. L. Skov, *Polymer.* **2016**, *87*, 1.

[33] S. K. Yadav, I. J. Kim, H. J. Kim, J. Kim, S. M. Hong, C. M. Koo, *J. Mater. Chem. C* **2013**, *1*, 5463.

[34] D. M. Opris, M. Molberg, C. Walder, Y. S. Ko, B. Fischer, F. A. Nüesch, *Adv. Funct. Mater.* **2011**, *21*, 3531.

[35] C. Racles, V. Cozan, A. Bele, M. Dascalu, *Des. Monomers Polym.* **2016**, *5551*, 1.

[36] S. J. Duenki, Y. S. Ko, F. A. Nueesch, D. M. Opris, *Adv. Funct. Mater.* **2015**, *25*, 2467.

[37] D. Opris, M. Dascalu, S. Dünki, J. E. Quinsaat, Y. S. Ko, *RSC Adv.* **2015**, *5*, 104516.

[38] B. Kussmaul, S. Risse, G. Kofod, R. Waché, M. Wegener, D. N. McCarthy, H. Krüger, R. Gerhard, *Adv. Funct. Mater.* **2011**, *21*, 4589.

[39] F. B. Madsen, L. Yu, A. E. Daugaard, S. Hvilsted, A. L. Skov, *RSC Adv.* **2015**, *5*, 10254.

[40] S. J. Dünki, E. Cuervo-Reyes, D. M. Opris, *Polym. Chem.* **2017**, *8*, 715.

[41] D. Opris, S. Dünki, F. Nueesch, *J. Mater. Chem. C* **2016**, 10545.

[42] P. Caspari, S. J. Dünki, F. Nueesch, D. Opris, *J. Mater. Chem. C* **2018**, *6*, 2043.

[43] L. Xue, Y. Zhang, Y. Zuo, S. Diao, J. Zhang, S. Feng, *Mater. Lett.* **2013**, *106*, 425.

[44] K. Goswami, A. L. Skov, A. E. Daugaard, *Chem. Eur. J.* **2014**, *20*, 9230.

[45] Y. Zuo, H. Lu, L. Xue, X. Wang, L. Ning, S. Feng, *J. Mater. Chem. C* **2014**, *2*, 2724.

[46] A. L. Larsen, P. Sommer-Larsen, O. Hassager, *Proc. SPIE* **2004**, *5385*, 108.

[47] F. Förster-Zuegel, T. Grotepaß, H. F. Schlaak, *SPIE Proc.* **2015**, *9430*, 94300D.

[48] A. Bele, M. Dascalu, C. Tugui, M. Iacob, C. Racles, L. Sacarescu, M. Cazacu, *Mater. Des.* **2016**, *106*, 454.

[49] S. J. Dünki, M. Tress, F. Kremer, S. Y. Ko, F. A. Nüesch, C.-D. Varganici, C. Racles, D. M. Opris, *RSC Adv.* **2015**, *5*, 50054.

[50] A. Tröls, A. Kogler, R. Baumgartner, R. Kaltseis, C. Keplinger, R. Schwödiauer, I. Graz, S. Bauer, *Smart Mater. Struct.* **2013**, *22*, 104012.

[51] F. Carpi, I. Anderson, S. Bauer, G. Frediani, G. Gallone, M. Gei, C. Graaf, C. Jean-Mistral, W. Kaal, G. Kofod, M. Kollosche, R. Kornbluh, B. Lassen, M. Matysek, S. Michel, S. Nowak, B. O'Brien, Q. Pei, R. Pelrine, B. Rechenbach, S. Rosset, H. Shea, *Smart Mater. Struct.* **2015**, *24*, 105025.

[52] M. Matysek, P. Lotz, K. Flittner, H. F. Schlaak, *Proc. SPIE* **2008**, *6927*, 692722.

[53] L. Düring, G. Kovacs, *(EMPA)*, **2009**, WO 2009/135328 A2.

[54] M. Duduta, R. J. Wood, D. R. Clarke, *Adv. Mater.* **2016**, *28*, 8058.

[55] C. Racles, M. Cazacu, B. Fischer, D. M. Opris, *Smart Mater. Struct.* **2013**, *22*, 10.

5.7 Supporting information

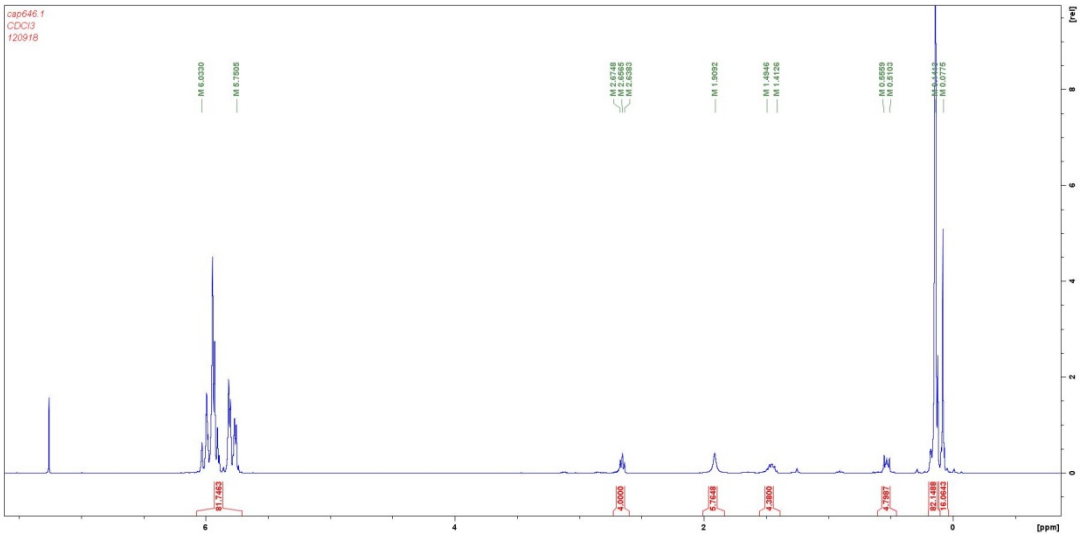

Figure 5.8 ^{1}H NMR spectrum of **P1** in $CDCl_3$.

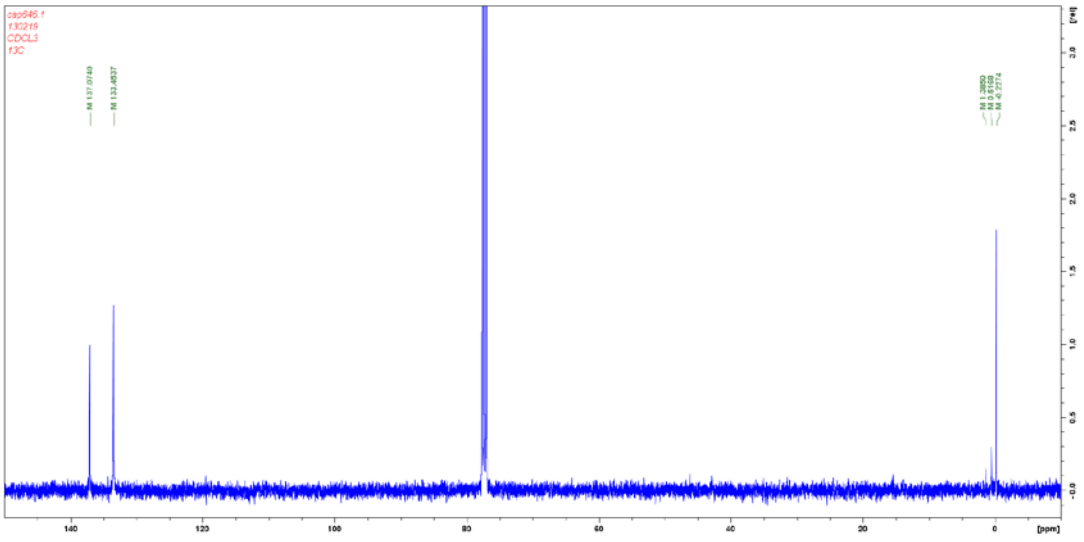

Figure 5.9 ^{13}C NMR spectrum of **P1** in $CDCl_3$.

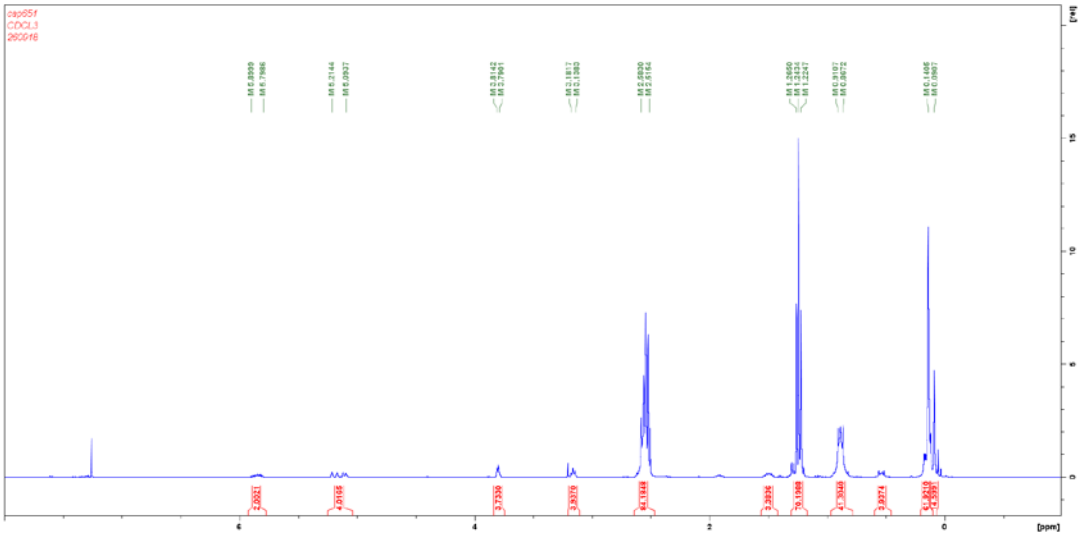

Figure 5.10 ^{1}H NMR spectrum of **P3** in $CDCl_3$.

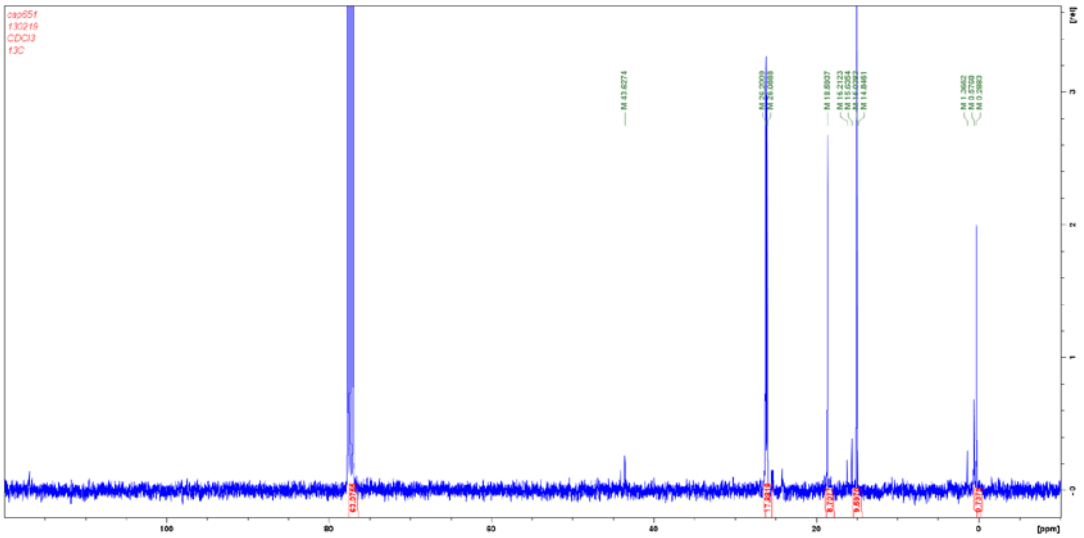

Figure 5.11 ^{13}C NMR spectrum of **P3** in $CDCl_3$.

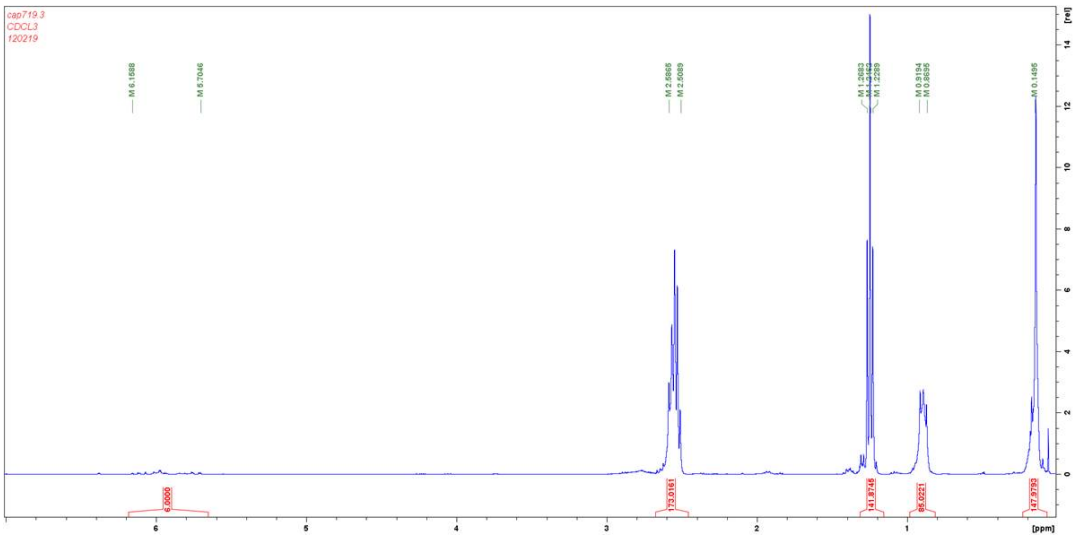

Figure 5.12 ^{1}H NMR spectrum of **P2+** in $CDCl_3$.

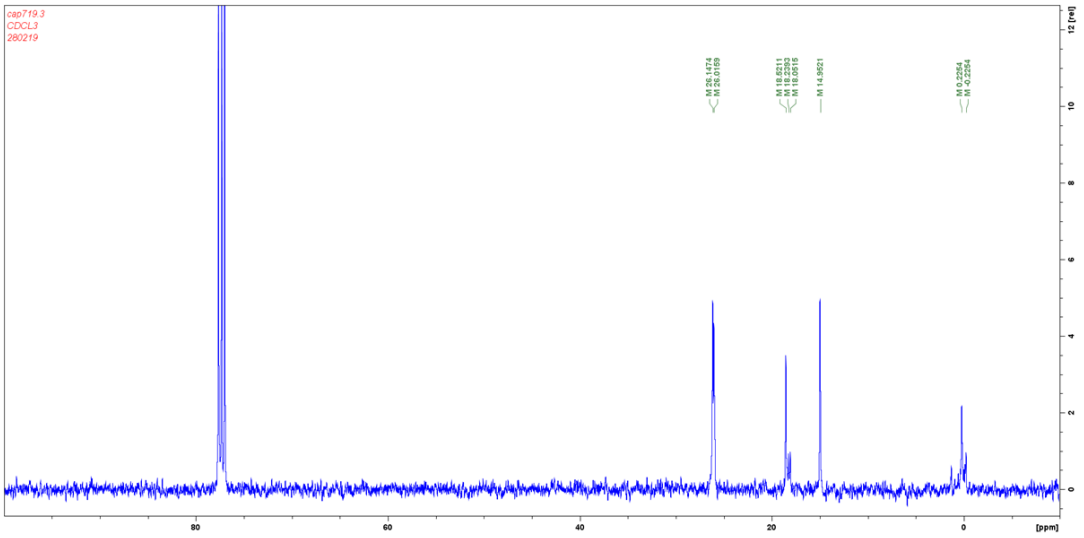

Figure 5.13 ^{13}C NMR spectrum of **P2+** in $CDCl_3$.

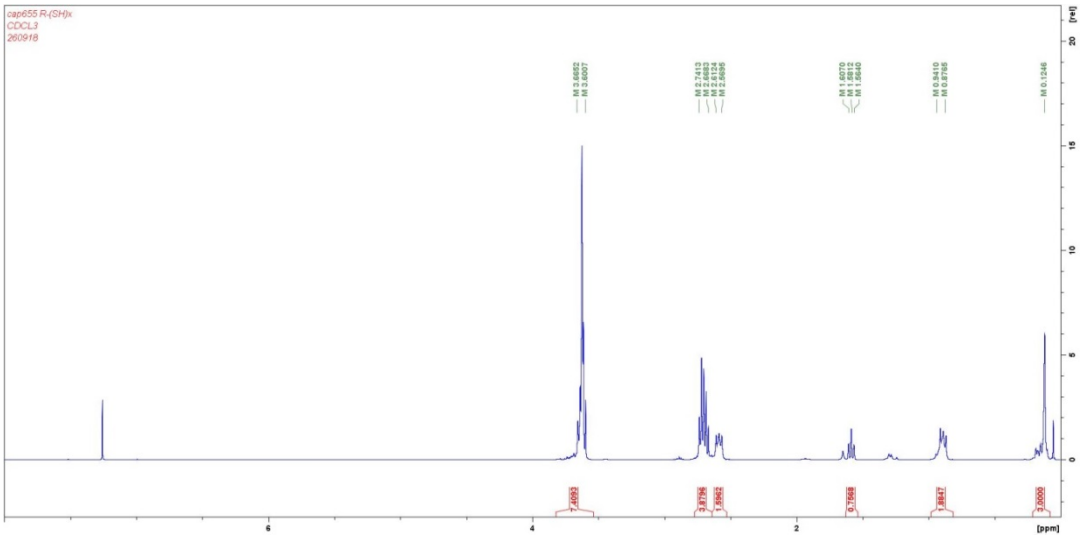

Figure 5.14 ^{1}H NMR spectrum of **R(SH)$_3$** in $CDCl_3$.

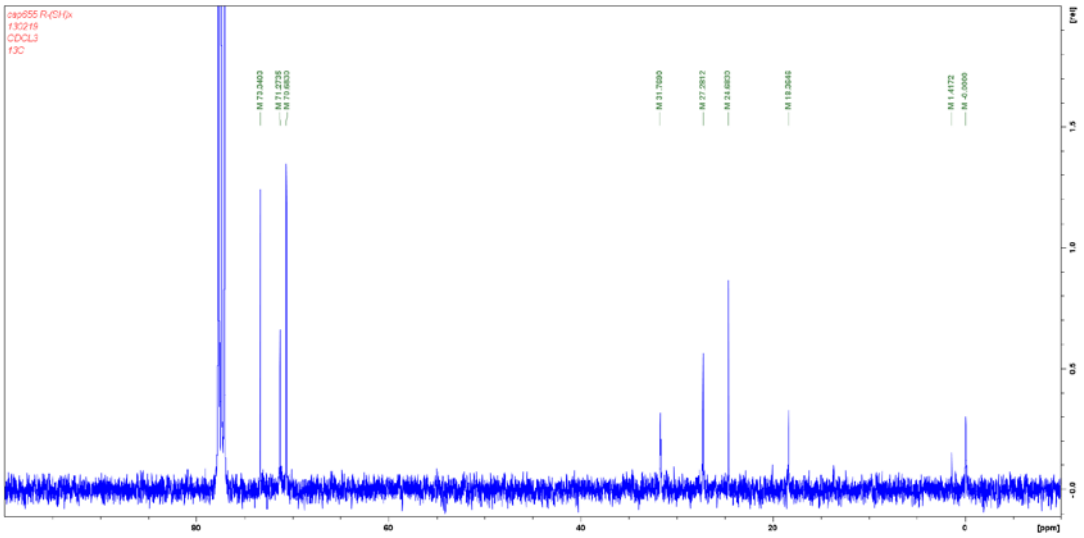

Figure 5.15 ^{13}C NMR spectrum of **R(SH)$_3$** in CDCl3.

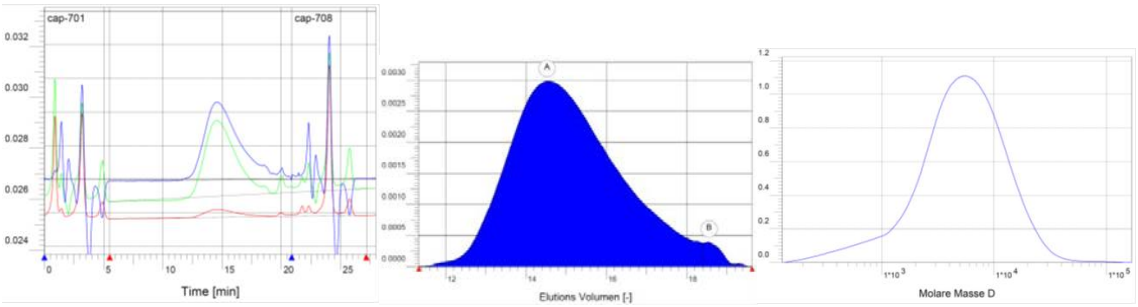

Figure 5.16 GPC elution curves of **P3**. M_n: 3000 M_w: 7000 PDI: 2.4.

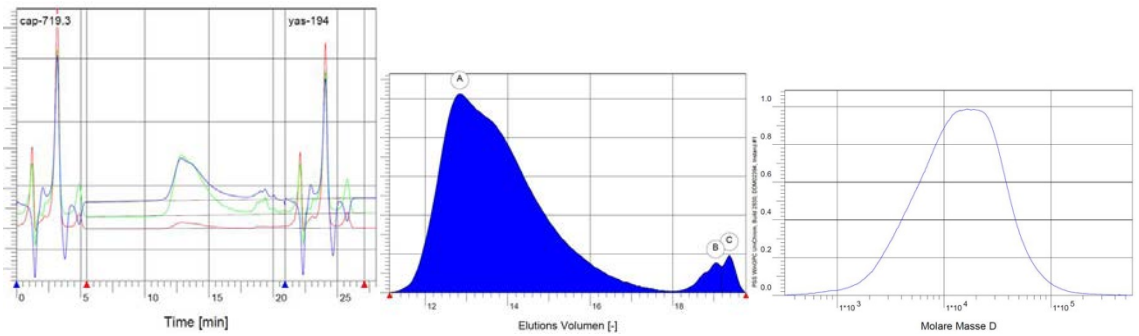

Figure 5.17 GPC elution curves of **P2+**. M_n: 8500. M_w: 20000. PDI: 2.4.

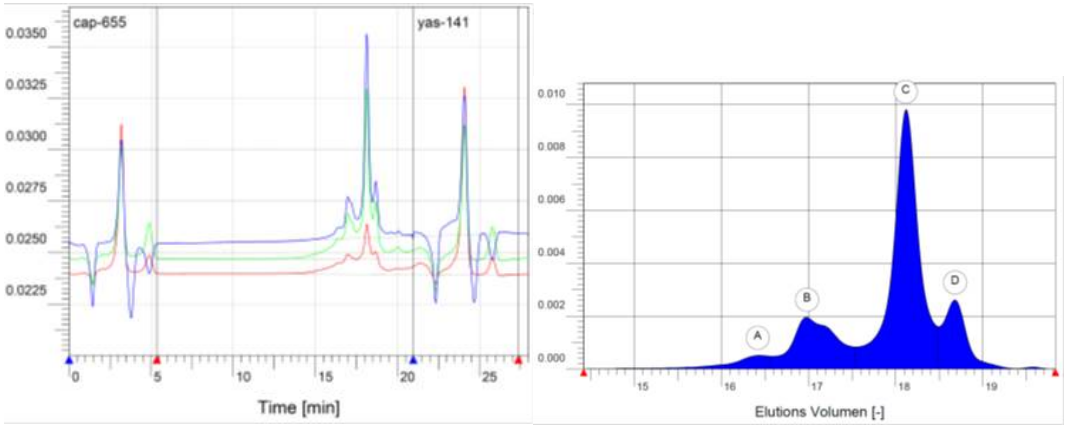

Figure 5.18 GPC elution curves of **$R(SH)_3$**.

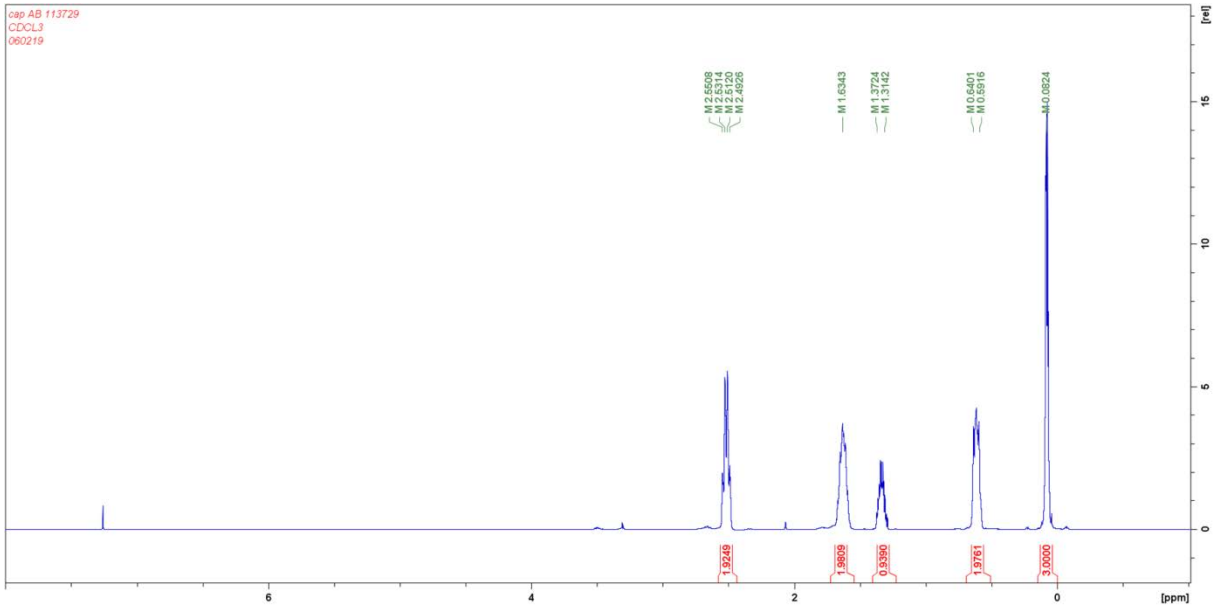

Figure 5.19 ^{1}H NMR spectrum of *AB 113729* in $CDCl_3$.

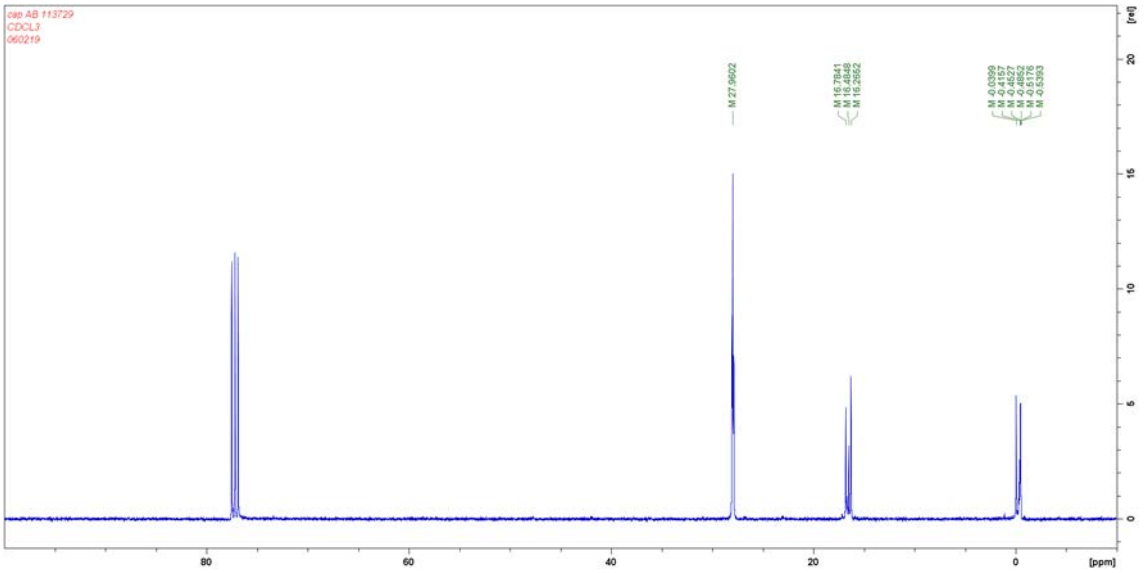

Figure 5.20 ^{13}C NMR spectrum of *AB 113729* in $CDCl_3$.

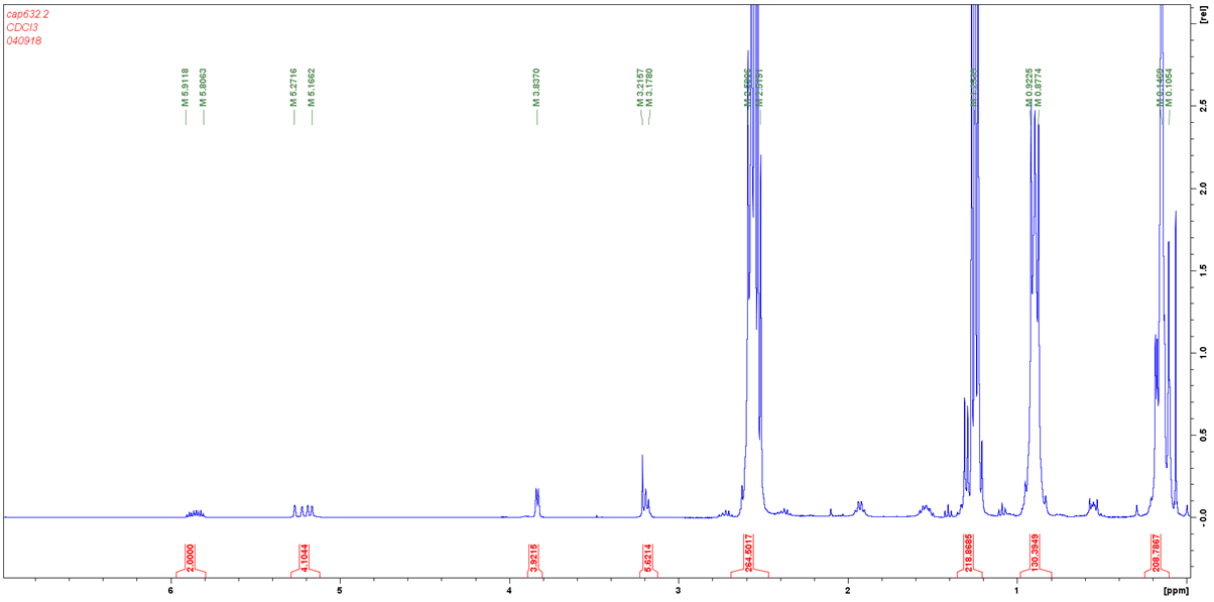

Figure 5.21 1H NMR spectrum of **P3.2**. M_n: 10.000

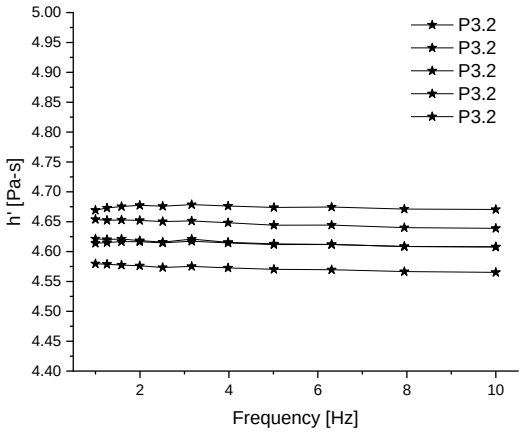

Figure 5.22 Viscosity of **P3.2** measured in the frequency range of 1-10 Hz. Five measurements were performed.

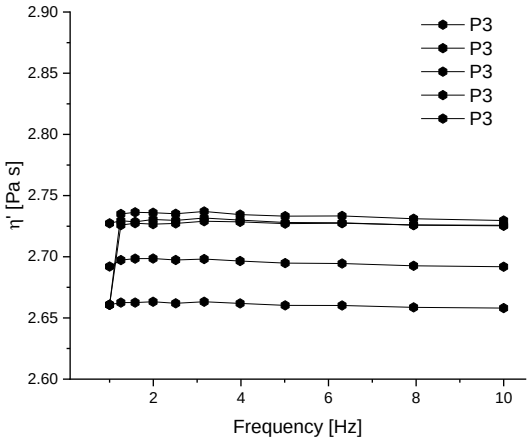

Figure 5.23 Viscosity of **P3** measured in the frequency range of 1-10 Hz. Five measurements were performed.

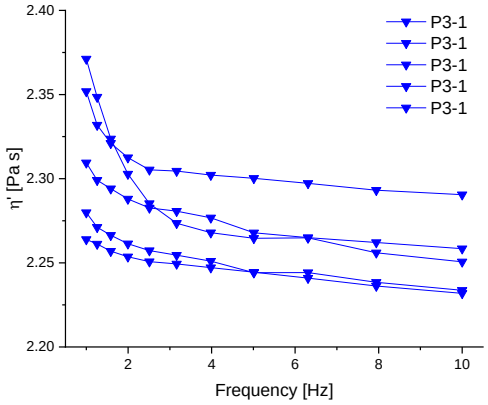

Figure 5.24 Viscosity of **P3-1** measured in the frequency range of 1-10 Hz. Five measurements were performed.

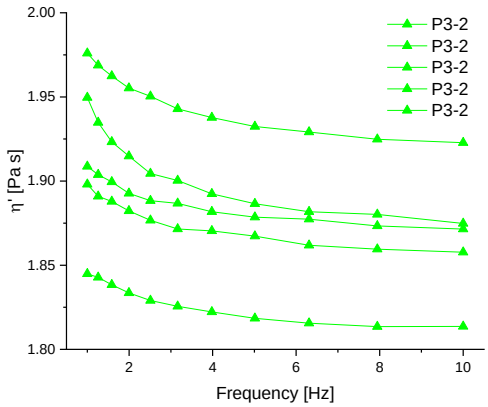

Figure 5.25 Viscosity of **P3-2** measured in the frequency range of 1-10 Hz. Five measurements were performed.

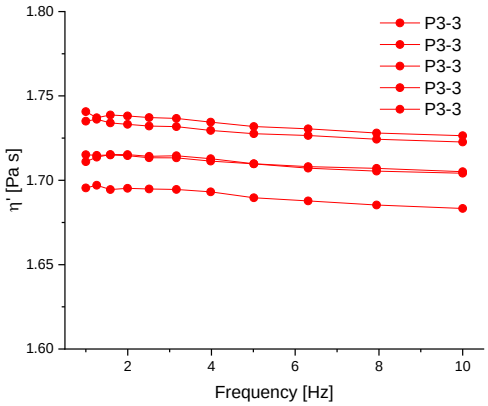

Figure 5.26 Viscosity of **P3-3** measured in the frequency range of 1-10 Hz. Five measurements were performed.

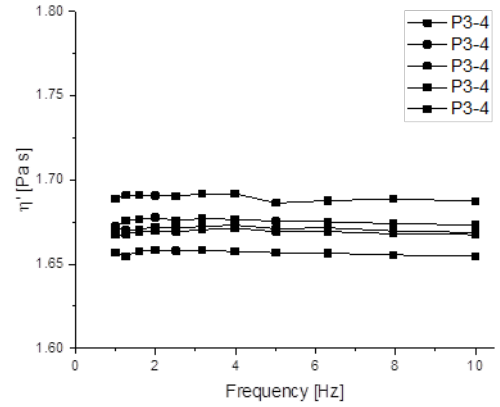

Figure 5.27 Viscosity of **P3-4** measured in the frequency range of 1-10 Hz. Five measurements were performed.

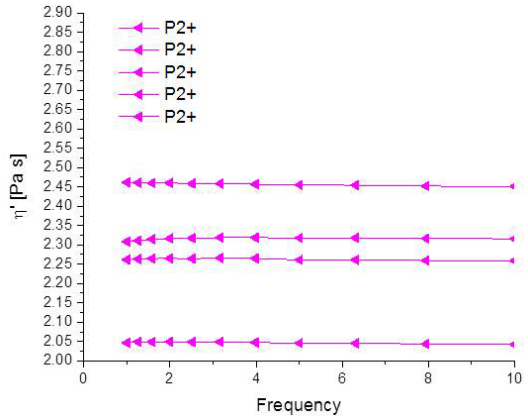

Figure 5.28 Viscosity of **P2+** measured in the frequency range of 1-10 Hz. Five measurements were performed.

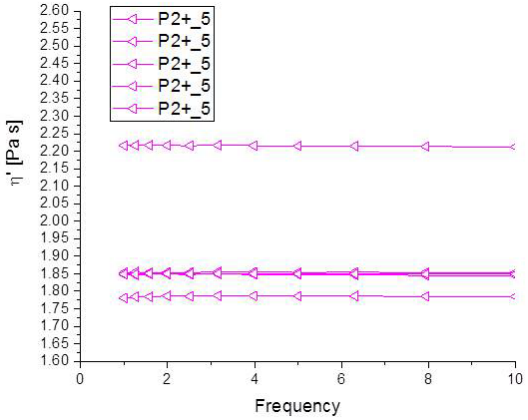

Figure 5.29 Viscosity of **P2+5** measured in the frequency range of 1-10 Hz. Five measurements were performed.

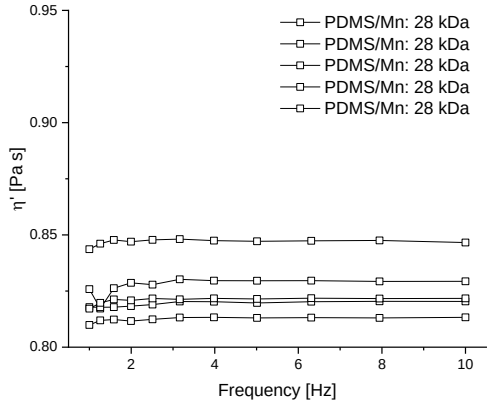

Figure 5.30 Viscosity of α'ω-OH-PDMS (M_n: 28 kDa) measured in the frequency range of 1-10 Hz. Five measurements were performed.

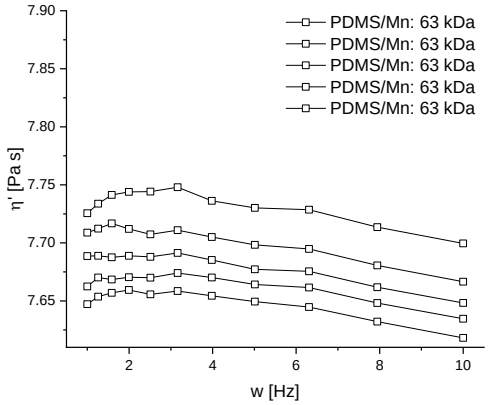

Figure 5.31 Viscosity of α'ω-OH-PDMS (M_n: 28 kDa) measured in the frequency range of 1-10 Hz. Five measurements were performed.

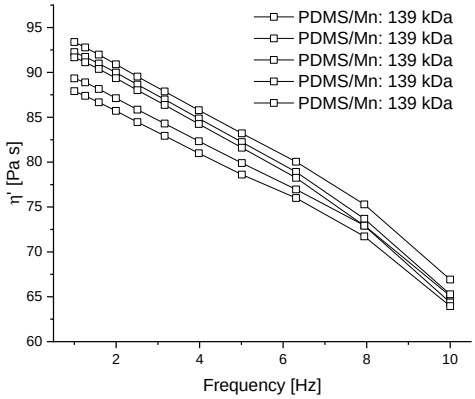

Figure 5.32 Viscosity of α'ω-OH-PDMS (M_n: 28 kDa) measured in the frequency range of 1-10 Hz. Five measurements were performed.

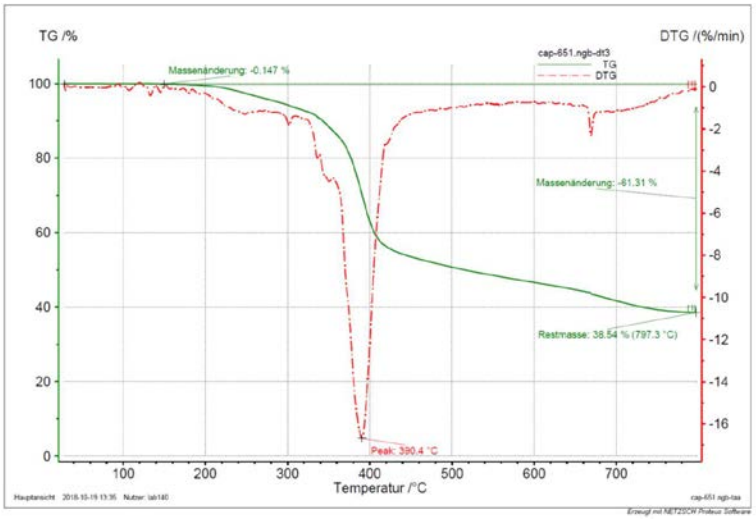

Figure 5.33 TGA curve of **P3** at air.

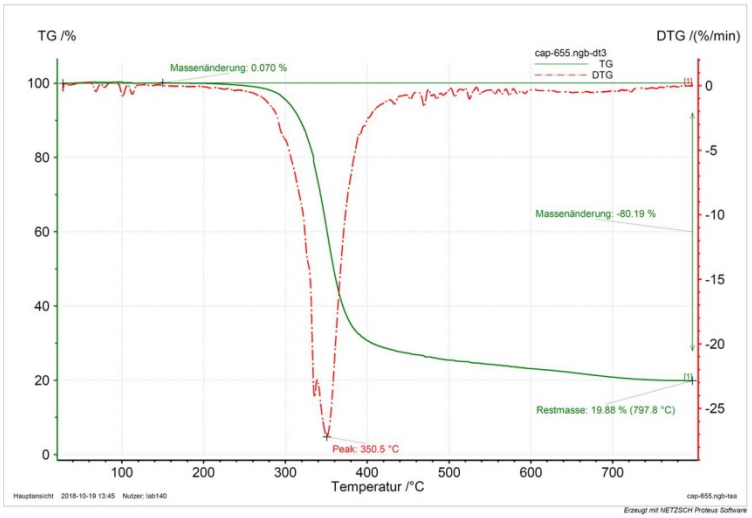

Figure 5.34 TGA curve of **R(SH)$_3$** at air.

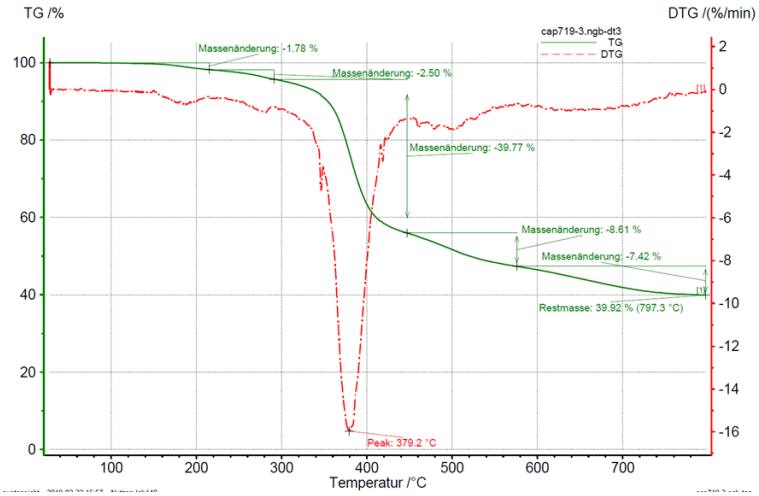

Figure 5.35 TGA curve of **P2+** at air.

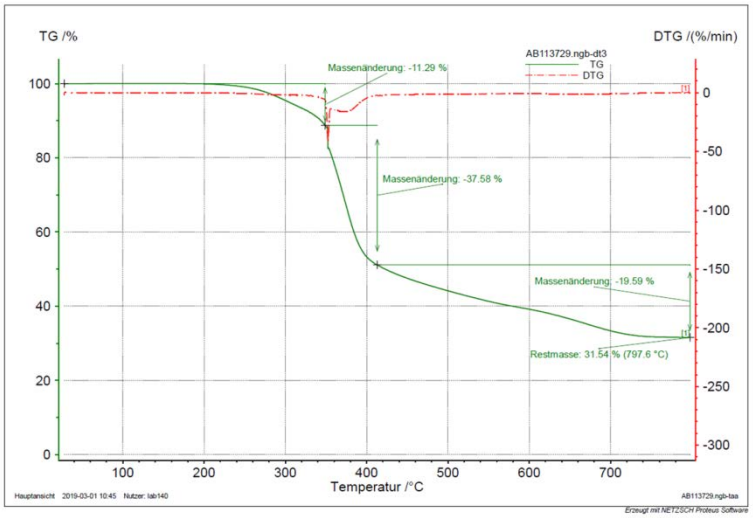

Figure 5.36 TGA curve of *AB113729* at air.

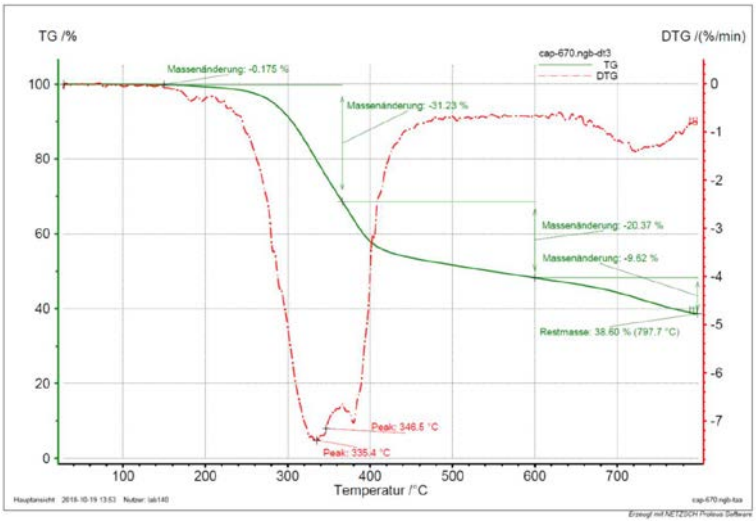

Figure 5.37 TGA curve of **E3-1** at air.

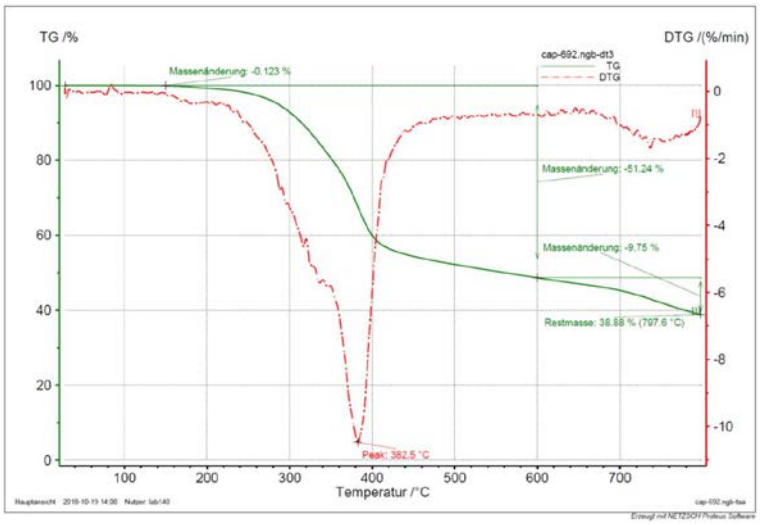

Figure 5.38 TGA curve of **E3-2** at air.

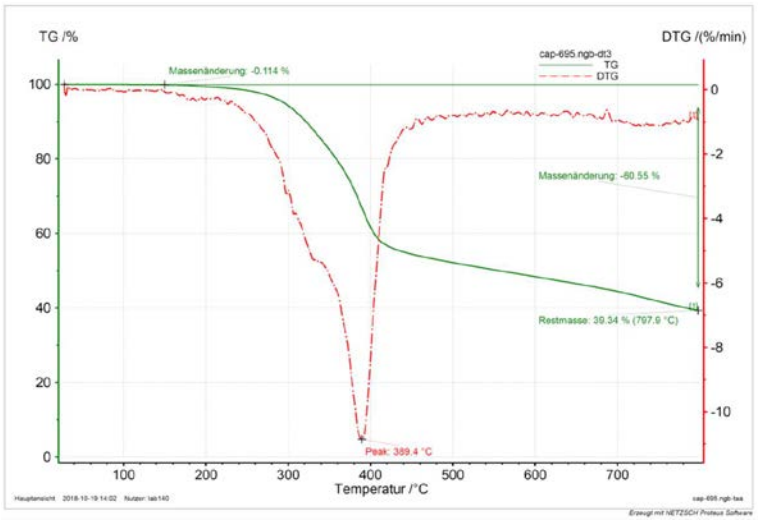

Figure 5.39 TGA curve of **E3-3** at air.

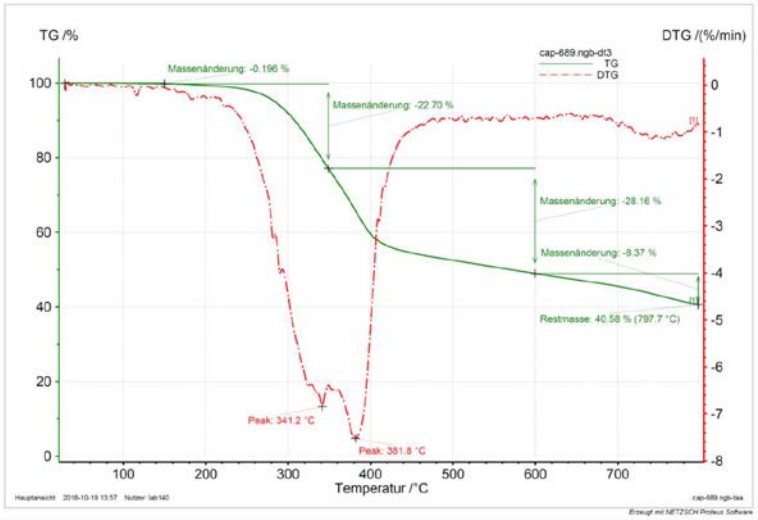

Figure 5.40 TGA curve of **E3-4** at air.

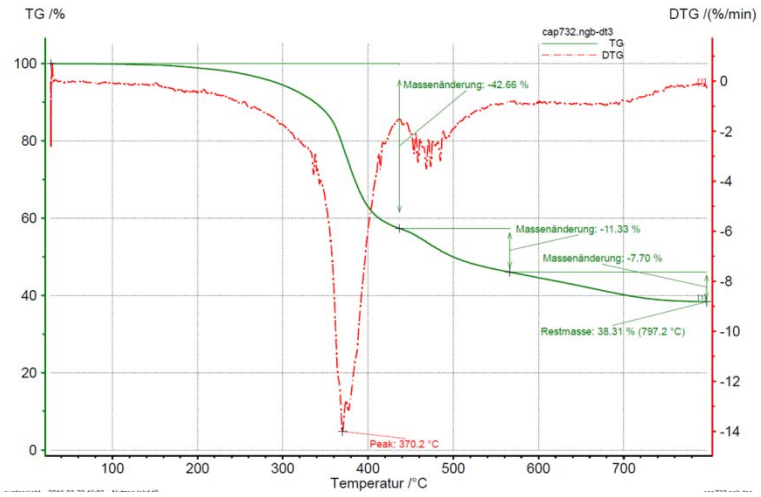

Figure 5.41 TGA curve of **E2+** at air.

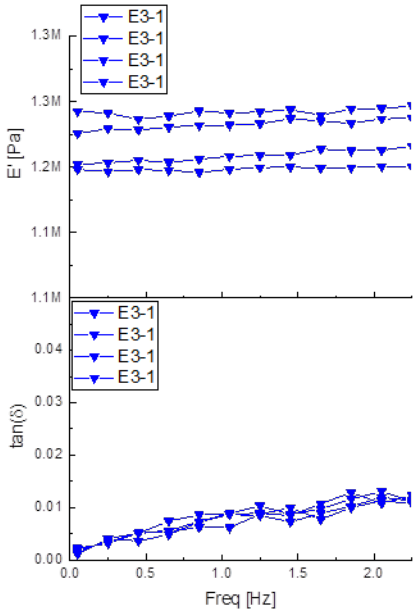

Figure 5.42 DMA of **E3-1**. Four samples were measured.

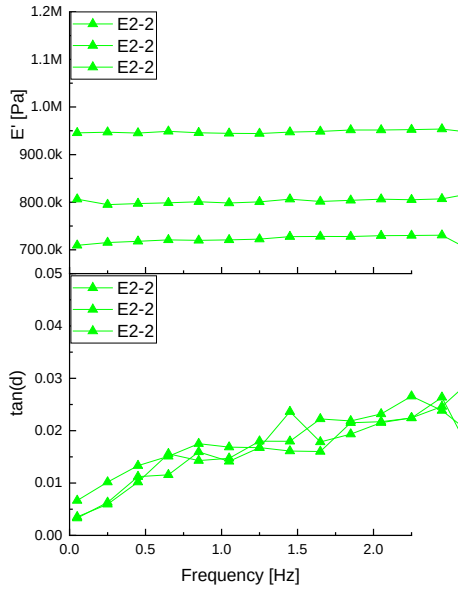

Figure 5.43 DMA of **E3-2**. Three samples were measured.

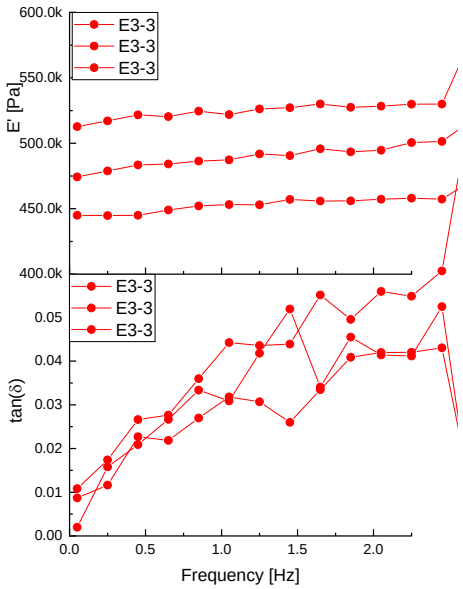

Figure 5.44 DMA of **E3-3**. Three samples were measured.

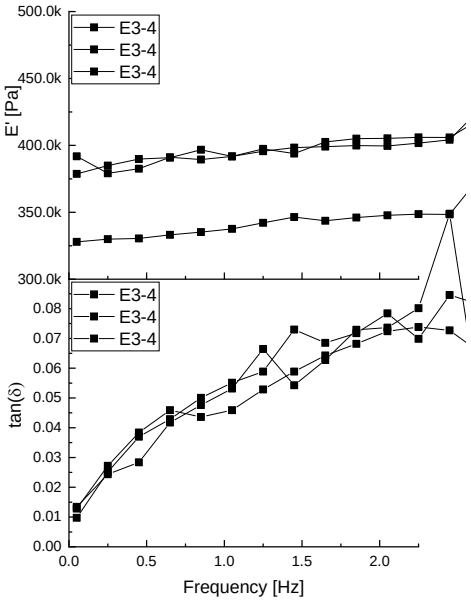

Figure 5.45 DMA of **E3-4**. Three samples were measured.

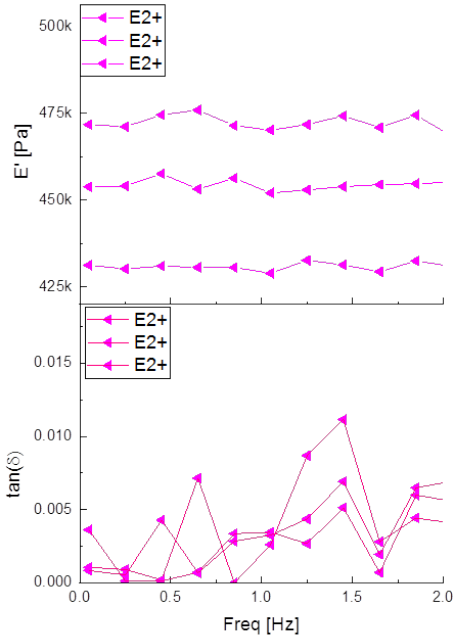

Figure 5.46 DMA of **E2+**. Three samples were measured.

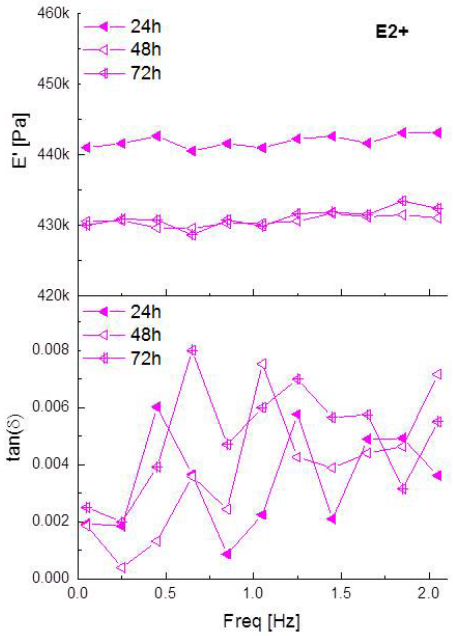

Figure 5.47 DMA of **E2+** measured 24h/48h/72h after synthesis. The average curve of 3 measurements is given. The identical sample was measured.

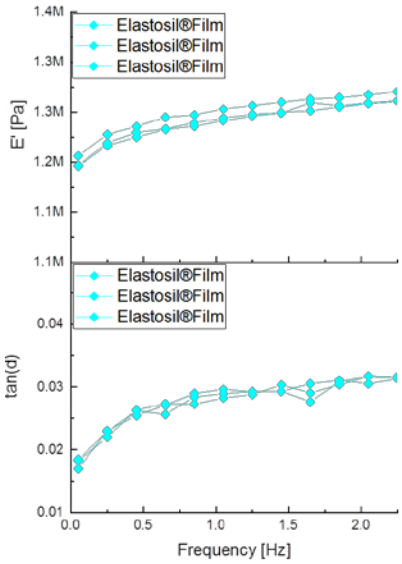

Figure 5.48 DMA of **Elastosil®Film**. Three samples were measured.

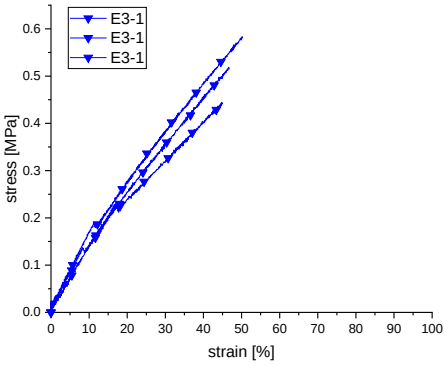

Figure 5.49 Tensile tests of **E3-1**. Three independent tests were performed.

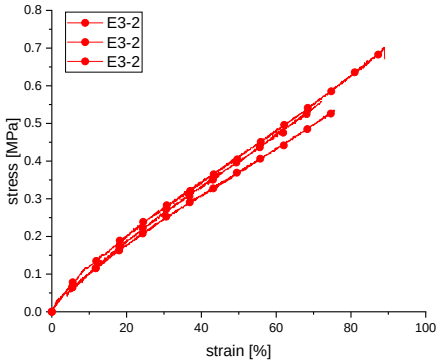

Figure 5.50 Tensile tests of **E3-2**. Three independent tests were performed.

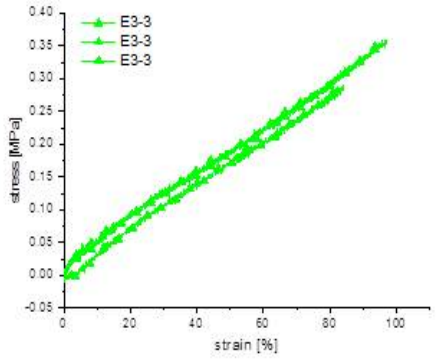

Figure 5.51 Tensile tests of **E3-3**. Three independent tests were performed.

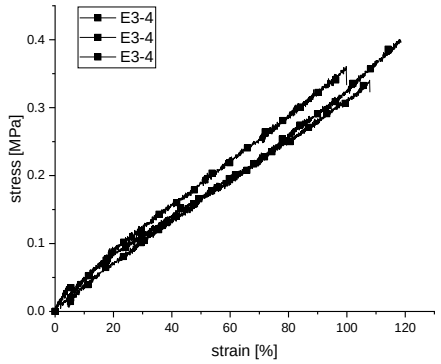

Figure 5.52 Tensile tests of **E3-4**. Three independent tests were performed.

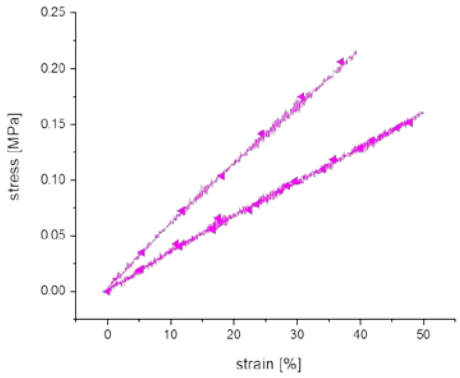

Figure 5.53 Tensile tests of **E2+**. Three independent tests were performed.

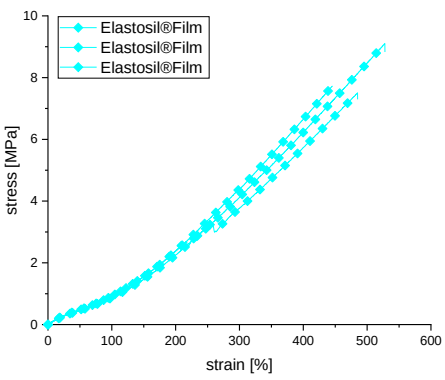

Figure 5.54 Tensile tests of **Elastosil®Film**. Three independent tests were performed.

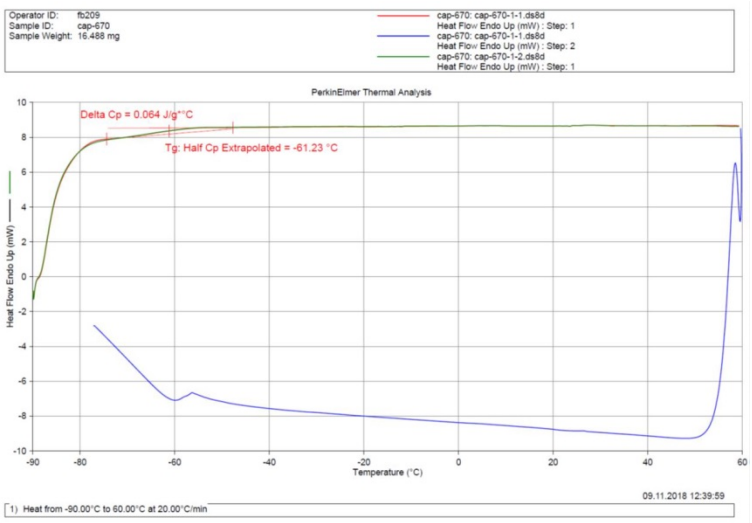

Figure 5.55 DSC curves of **E3-1**.

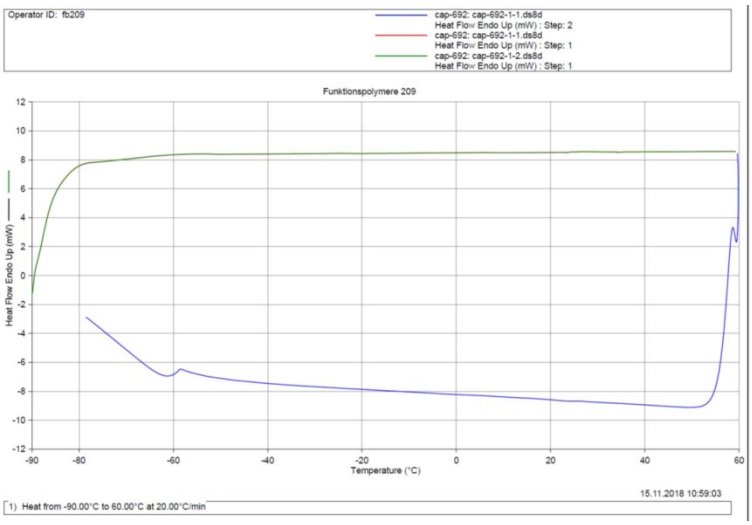

Figure 5.56 DSC curves of **E3-2**.

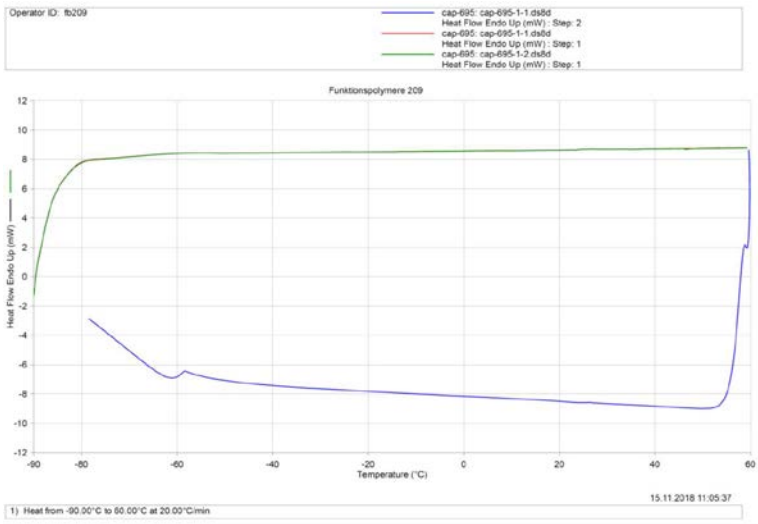

Figure 5.57 DSC curves of **E3-3**.

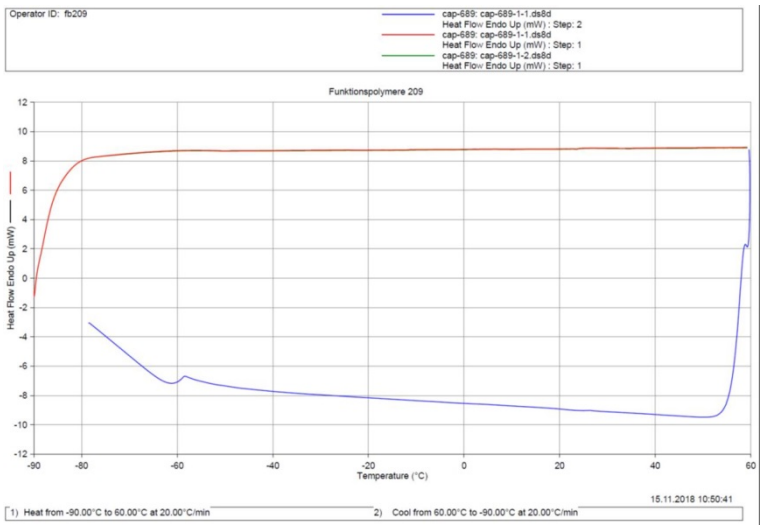

Figure 5.58 DSC curves of **E3-4**.

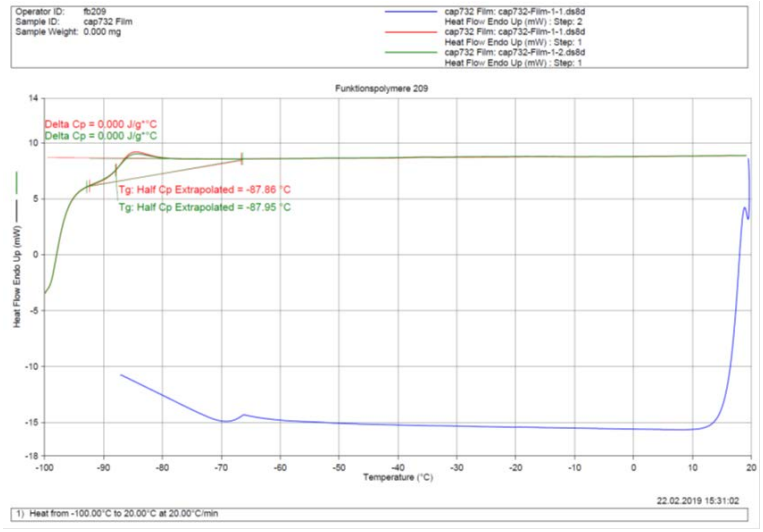

Figure 5.59 DSC curves of **E2+**.

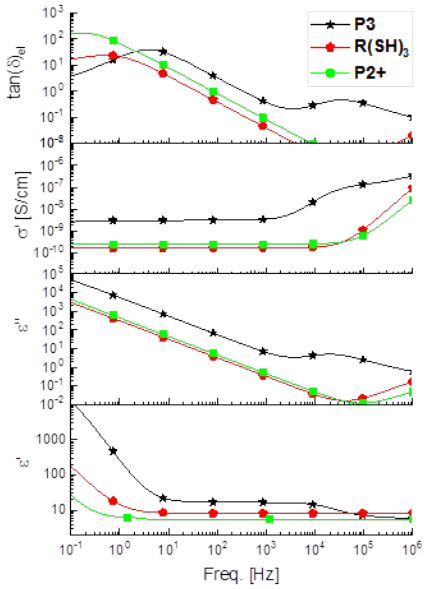

Figure 5.60 Dielectric properties of **P3, P2+** and **R(SH)$_3$**.

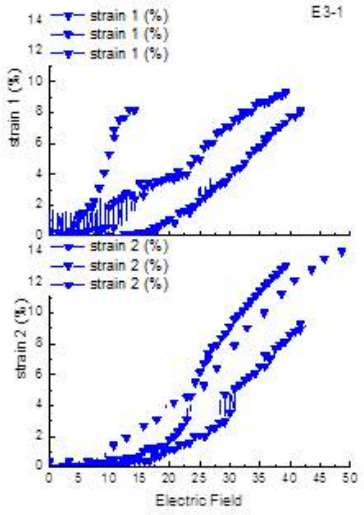

Figure 5.61 Lateral strain in x-and y-direction (strain 1 and strain 2) of **E3-1** as a function of the applied electric field.

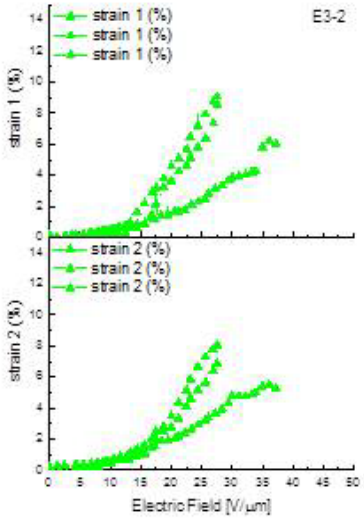

Figure 5.62 Lateral strain in x-and y-direction (strain 1 and strain 2) of **E3-2** as a function of the applied electric field.

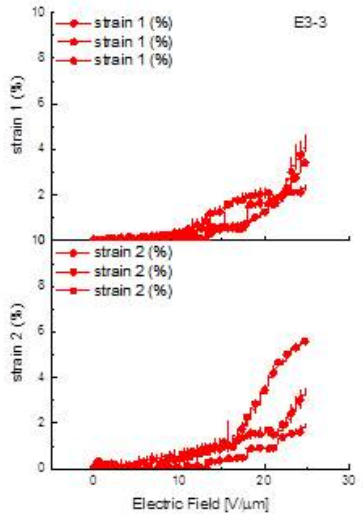

Figure 5.63 Lateral strain in x-and y-direction (strain 1 and strain 2) of **E3-3** as a function of the applied electric field.

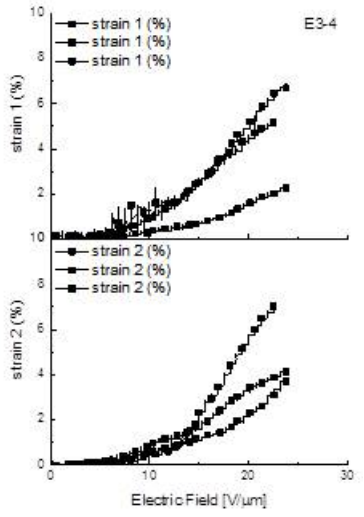

Figure 5.64 Lateral strain in x-and y-direction (strain 1 and strain 2) of **E3-4** as a function of the applied electric field.

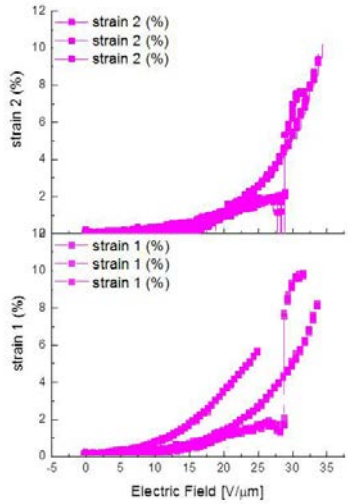

Figure 5.65 Lateral strain in x-and y-direction (strain 1 and strain 2) of **E2+** as a function of the applied electric field.

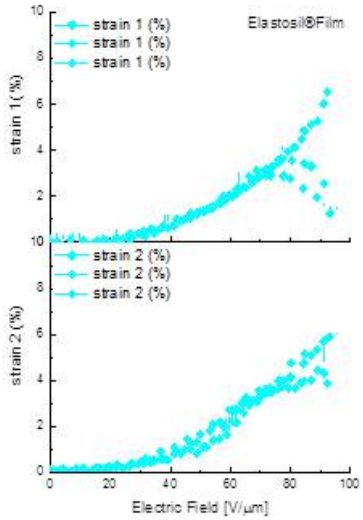

Figure 5.66 Lateral strain in x-and y-direction (strain 1 and strain 2) of **Elastosil®Film** as a function of the applied electric field.

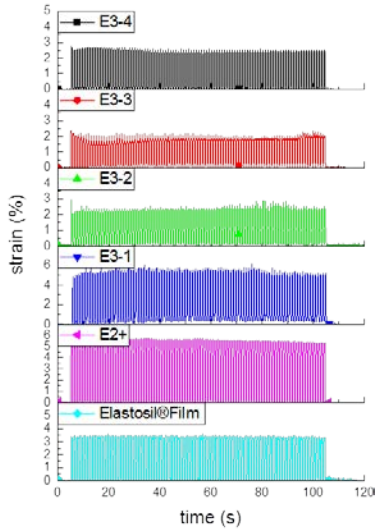

Figure 5.67 Average lateral strain of **E3-Y**, **E2+** and **Elastosil®Film** as a function of the applied electric field (DC) operated at 1 Hz . The electric field was 80 V/µm for **Elastosil®Film**, 30 V/µm for **E3-1**, 25 V/µm for **E3-2/E3-3** and **E2+**, and 20 Vµm for **E3-4**.

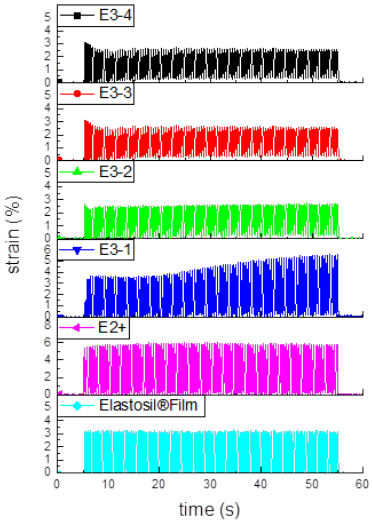

Figure 5.68 Average lateral strain of **E3-Y**, **E2+** and **Elastosil®Film** as a function of the applied electric field (DC) operated at 2 Hz. The electric field was 80 V/µm for **Elastosil®Film**, 30 V/µm for **E3-1**, 25 V/µm for **E3-2/E3-3** and **E2+**, and 20 Vµm for **E3-4.**

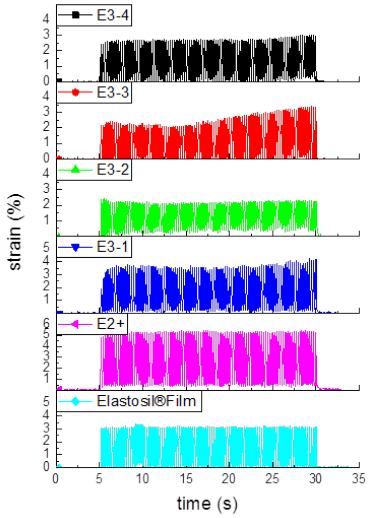

Figure 5.69 Average lateral strain of **E3-Y** and **Elastosil®Film** as a function of the applied electric field (DC) operated at 4 Hz. The electric field was 80 V/µm for **Elastosil®Film**, 30 V/µm for **E3-1**, 25 V/µm for **E3-2/E3-3** and **E2+**, and 20 Vµm for **E3-4.**

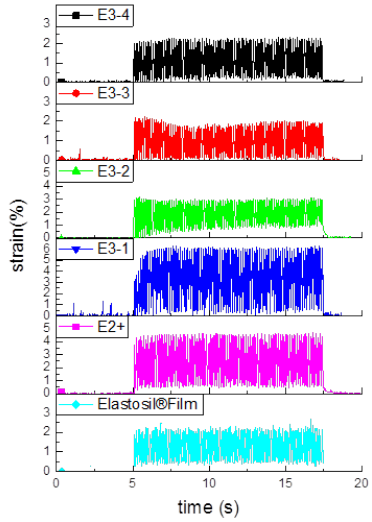

Figure 5.70 Average lateral strain of **E3-Y** and **Elastosil®Film** as a function of the applied electric field (DC) operated at 8 Hz. The electric field was 80 V/µm for **Elastosil®Film**, 30 V/µm for **E3-1**, 25 V/µm for **E3-2/E3-3** and **E2+**, and 20 Vµm for **E3-4.**

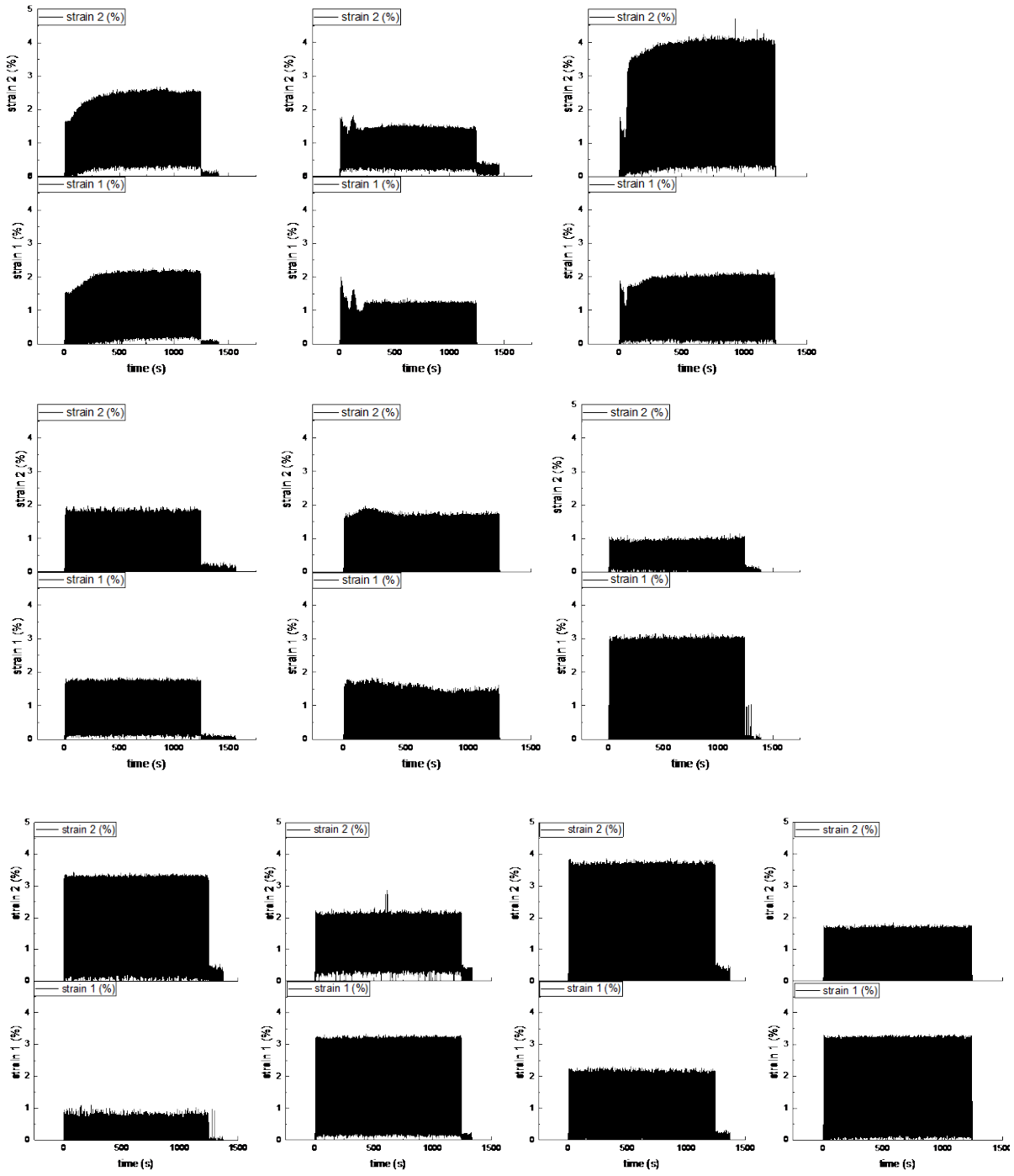

Figure 5.71 10 x 10.000 operation cycles at 8 Hz at 25 V/µm of a circular DEA test device constructed from a 75 µm-thin film of **E3-1** with an area diameter of 8 mm. Strain 1 is defined as the lateral strain in x-direction. Strain 2 is defined as the lateral strain in y-direction.

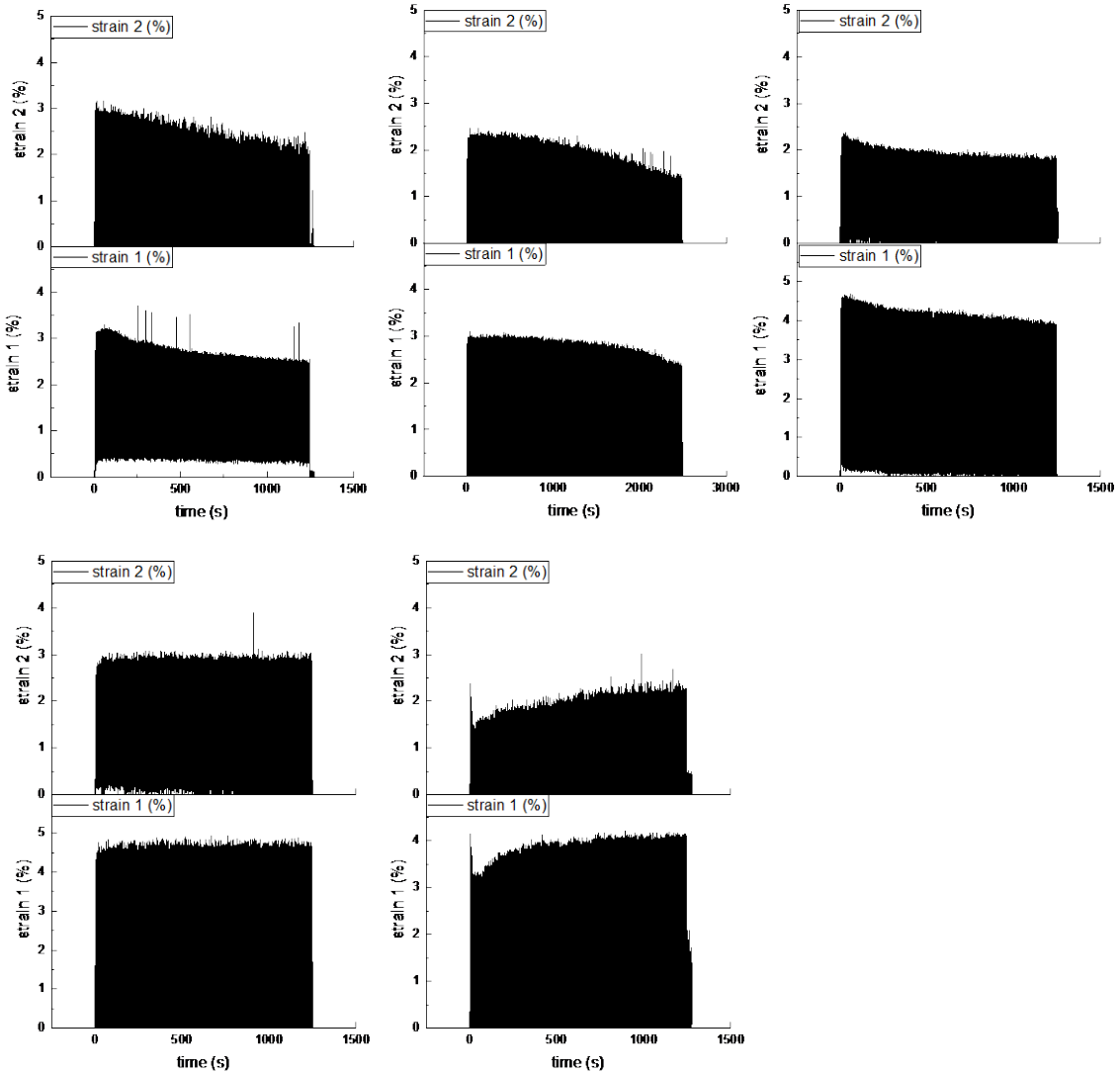

Figure 5.72 5 x 10.000 operation cycles + 1 x 20.0000 at 8 Hz at 29 V/µm of a circular DEA test device constructed from a 85 µm-thin film of **E3-2** with an area diameter of 8 mm. Strain 1 is defined as the lateral strain in x-direction. Strain 2 is defined as the lateral strain in y-direction.

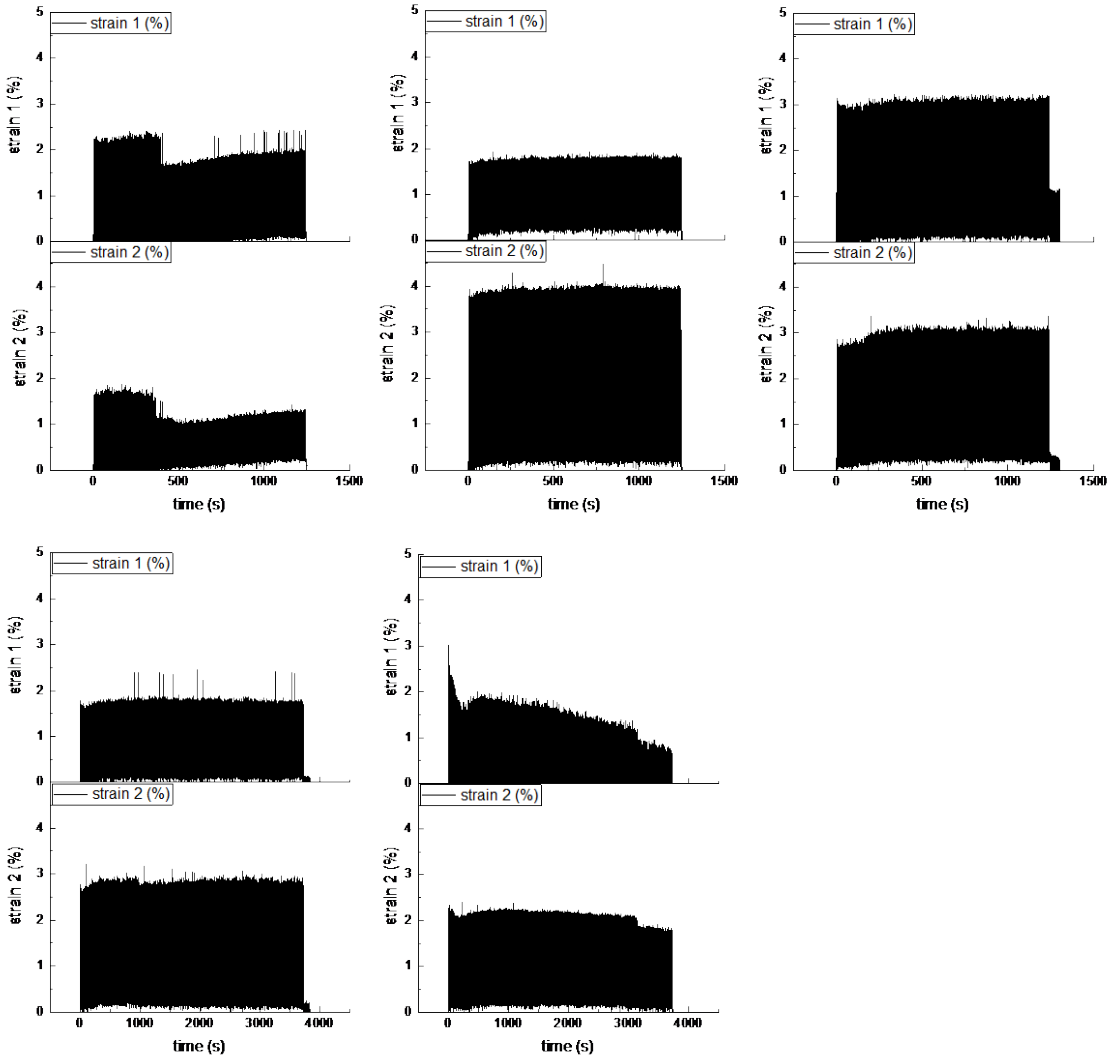

Figure 5.73 3 x 10.000 + 2 x 30.0000 DEA operation cycles at 8 Hz at 25 V/µm of a circular DEA test device constructed from a 90 µm-thin film of **E3-3** with an area diameter of 8 mm. Strain 1 is defined as the lateral strain in x-direction. Strain 2 is defined as the lateral strain in y-direction.

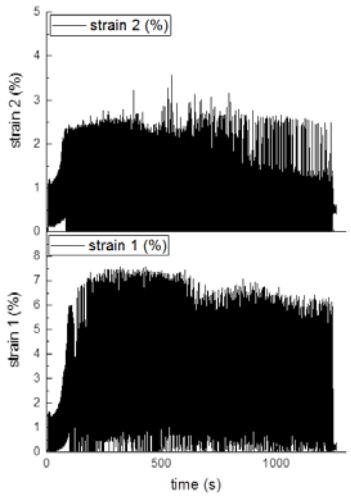

Figure 5.74 10.000 DEA operation cycles at 8 Hz at 15 V/µm of a circular DEA test device constructed from a 100 µm-thin film of **E3-4** with an area diameter of 8 mm. Strain 1 is defined as the lateral strain in x-direction. Strain 2 is defined as the lateral strain in y-direction.

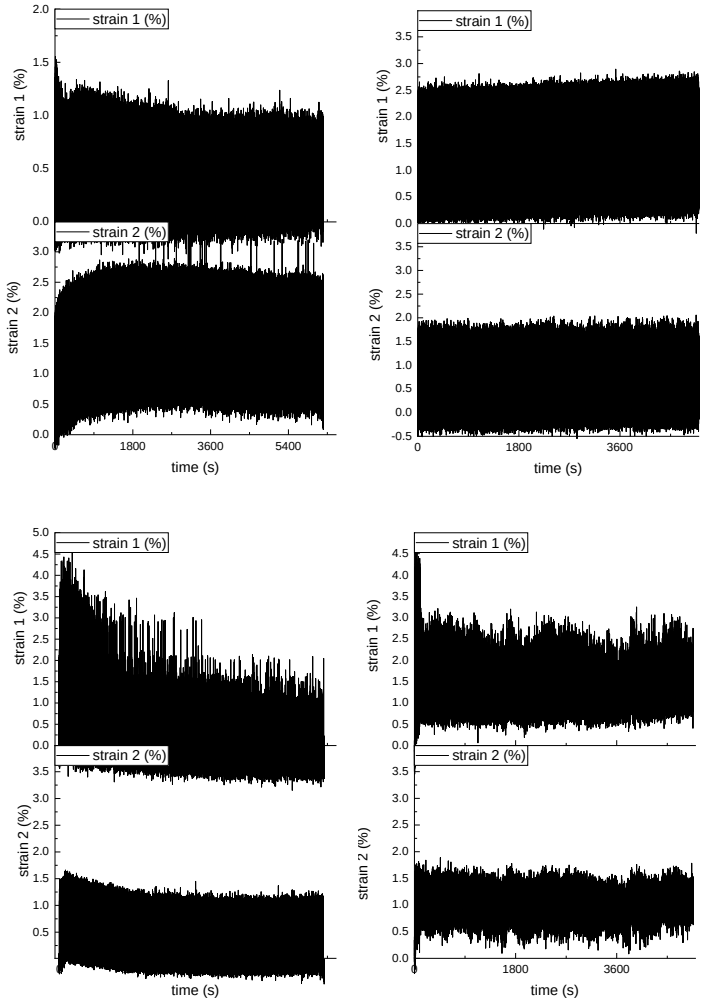

Figure 5.75 2 x 50.000 and 2 x 40.000 DEA operation cycles at 8 Hz at 25 V/µm of a circular DEA test device constructed from a 85 µm-thin film of **E2+** with an area diameter of 8 mm. Strain 1 is defined as the lateral strain in x-direction. Strain 2 is defined as the lateral strain in y-direction.

Chapter 6 Conclusion and Outlook

It was the goal of this thesis to develop a high permittivity siloxane elastomer that is of technological relevance for DET applications. Thus, the chemical design of high permittivity siloxane elastomers and their performance as dielectric elastomers in dielectric elastomer transducers were studied. All relevant aspects were taken into consideration in the evaluation of the technological potential of the polar siloxane elastomers. This included the synthesis of polar siloxanes that can be casted into thin films and cross-linked to silicone elastomers. Eventually, dielectric elastomer transducers were constructed and the performance of the high permittivity siloxane elastomers was analyzed.

Figure 6.1 illustrates each step in the development of dielectric elastomers for the fabrication of thin film-transducers.

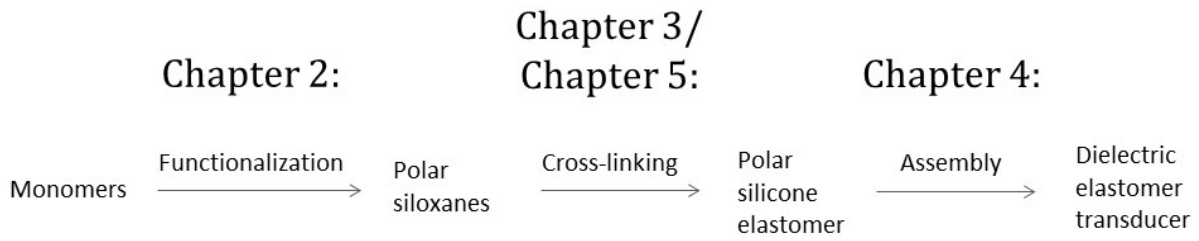

Figure 6.1 Development of dielectric elastomer generators and actuators.

In Chapter 2, the synthesis of polar thiols was described as the first step in the functionalization of siloxanes. The thiol-ene addition of mercaptonitriles to poly(vinylmethylsiloxane) had already been reported before as a powerful tool in the synthesis of high permittivity polysiloxanes due to the mild reaction conditions and quantitative conversion. Thus, various mercaptonitriles were tested as precursor for the functionalization of polysiloxanes. Finally, only one precursor, the 4-((2-mercaptoethyl)thio)butanenitrile, was found to be a promising candidate due to the strong nucleophilicity of thiols towards the electrophilic cyano group. This polar cyano thiol was successfully grafted onto the polysiloxane by thiol-ene addition. Even though an increased permittvitiy of about 10 was found for the corresponding poly(3-cyanopropyl-2-thioethyl-2-thioethyl)methylsiloxane, it was decided to simplify the molecular structure of the polar side group to enhance its chemical stability in the cross-linking reaction.

Hence, the focus of this research was on the thioether substituted siloxanes which were synthesized by the addition of alkylthiols to vinyl-substituted siloxanes. The polar siloxanes were cross-linked by the well-established tin-catalyzed silanol alkoxysilane condensation reaction reported in Chapter 3 or cross-linked by the UV-induced thiol-ene addition discussed in Chapter 5, respectively. In addition, the tin-catalyzed condensation cross-linking reaction was employed in the preparation of silicone composites and polar silicone elastomers. These materials were used for the assembly of dielectric elastomer generators described in Chapter 4.

The polar silicone elastomers presented in Chapter 3 showed an unprecedented high actuation strain for silicone elastomers in dielectric elastomer actuator test devices. Up to 21% lateral strain was measured for **P3-Cl-20** at 40 V/µm without any mechanical prestrain of the dielectric elastomer. The effect of an increased permittivity could be clearly demonstrated. Most importantly, the enhancement of permittivity was not accompanied by an increase in electric leakage current of the DEA up to 27 V/µm. **P3-Cl-20** is the first high permittivity silicone elastomer that has proven a high lifetime of the DEA by 50.000 actuation cycles at 10% lateral strain. However, the tin-catalyzed condensation reaction required the use of solvent and prolonged reaction times of about 48 hours. This severely compromises the technological relevance of the tin-catalyzed condensation reaction for thioether functionalized silicone elastomers.

Apart from their application in thin film actuators, the polar silicone elastomers were tested for their performance in dielectric elastomer generators. In cooperation with the Korea Institute of Science and Technology, electret-DEGs were constructed with PDMS elastomers, polar silicone elastomers and silicone composites. This project highlighted the necessity of high mechanical strain at break and very low viscous losses of any dielectric elastomer used for this application. Even

though the construction of the test device still leaves room for improvement, we could demonstrate the effect of high permittivity silicone elastomers on the output voltage of the electret-DEG.

Chapter 5 summarized the synthetic routes to polar silicone elastomers that are fast and easily processable. The thiol-ene cross-linking of vinyl-terminated PDMS has already been published. However, it is impossible to selectively functionalize the vinyl side-groups by thiol-ene addition, while leaving the terminal vinyl groups unreacted. Therefore, a functional end-group that could be converted into the vinyl-functionality had to be found. The amino end-groups were stable in the thiol-ene addition of ethanethiol to the vinyl side-groups and reacted very smoothly with allyl isocyanate which gave an allyl-terminated thioether substituted siloxane. Accordingly, the allyl end groups were linked by the urea moieties to the siloxane. A custom-made thiol cross-linker showed acceptable miscibility with the allyl-terminated thioether-substituted siloxane. The solvent-free formulation could be casted in thin films and solidified after 3 minutes UV-irradiation.

As expected, the cross-linking of oligomers led to highly cross-linked elastomers with a low strain at break that are exclusively attractive for DEAs operated at low voltages. The viscoelastic losses of the thioether-substituted silicone elastomers were comparable to PDMS elastomers. This corresponded to high lifetimes of DEA devices *i.e.* 100.000 actuation cycles at 3% lateral strain were measured at an electric field of 25 V/µm without any mechanical manipulation of the sample. However, the elevated conductivity led to an increase in leakage current of the DEA.

Therefore, an alternative synthetic route to a vinyl-terminated thioether-substituted siloxane was developed which eliminated the need of the urea linker between the terminal vinyl group and the siloxane (Scheme 6.1). **E2+** was processed solvent-free into a thin film elastomer (90 µm) by well-established doctor-blade techniques within a few minutes. The elastic modulus was below 0.5 MPa. The low strain at break of 40% leaves room for improvement though. **E2+** possessed a slightly lower permittivity of about 5.5 but did not show an increased leakage current of the DEA up to an electric field of 20 V/µm. The mechanical loss factor tan(δ) was below 0.01 at 2 Hz. On average, the DEA suffered dielectric breakdown at 30 V/µm and 7% lateral strain. At 25 V/µm, **E2+** reached a lifetime of 180.000 actuation cycles.

E2+ is the first polar silicone elastomer that unites electromechanical long-term stability in DEAs with technological relevant processability.

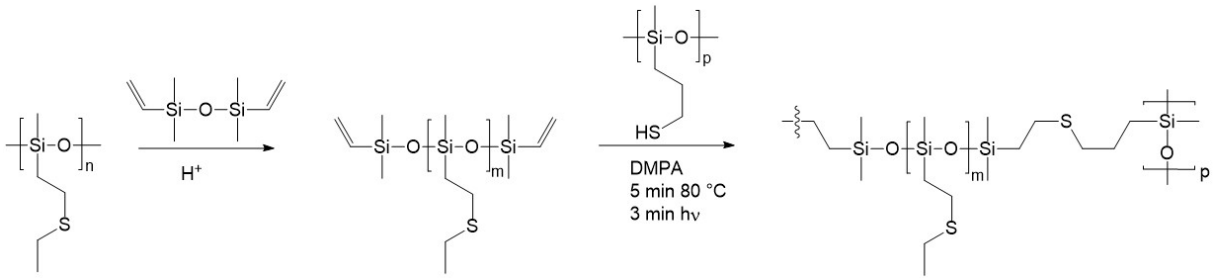

Scheme 6.1 Synthetic route to the high permittivity silicone elastomer **E2+**.

Future research projects will either study **E2+** with respect to its performance in various DET devices or further optimize the functionalization and the cross-linking process. In particular, the solvent-free process of **E2+** is highly attractive for the fabrication of multi-layer DEA devices.

Regarding the siloxane functionalization, there have already been several polar siloxanes developed with a permittivity as high as 22. It will be interesting to study the compatibility of those polar siloxanes with the newly developed cross-linking strategy. Particularly, polar functionalities that are stable under acidic conditions are of interest.

The synthetic strategy to **E2+** could still be further optimized. In particular, the solvent-free processing into films with a thickness comparable to commercial silicone elastomer thin films (20 µm) is an attractive task. Moreover, the possibility of simultaneous chain-prolongation and cross-linking deserves attraction. So far, the low strain at break of **E2+** severely limits its potential for DEGs.

Curriculum Vitae

Personal Details

Name	Philip Horst Caspari
Date of birth	03th of May 1989
Nationality	German
Address	Überlandstrasse 228, 8600 Dübendorf, Switzerland
Email	phca35@gmail.com
Phone	+41 76 804 74 66

Education

06/2015-present	PhD Student in Material Science and Engineering at Swiss Federal Institute for Science and Technology (Empa) and École Polytechnique Fédéral de Lausanne (EPFL), Switzerland
09/2012-12/2024	Master of Science ETH in Chemistry, ETH Zurich, Switzerland Master thesis: Nickel olefin complexes in the hydrosilylation reaction of nitriles and the dehydrogenative heterocoupling reaction of silanes with amines
04/2009-08/2012	Bachelor of Science in Chemistry, Goethe University Frankfurt am Main, Germany Bachelor thesis: Synthesis of quinazoline-ligands for TAR-RNA of HIV-1

Working Experience

09/2013-04/2014	Intern at BASF Schweiz AG, Basel, Switzerland

Language Skills

German	Native speaker
English	Fluent

Grants

2018	Korean-Swiss Young Researchers Exchange Program

Patents

2016	R. Oehrlein, P. Caspari, K. Dietliker, N. Kukaleva, D. Niederer, (*BASF SE, Germany*), **2016** WO 2016046292 A1.

Publications

2019 Y. J. Lee, P. Caspari, D. M. Opris, F. A. Nüesch, S. Nam, J.-H. Kim, S.-R. Kim, B-K. Ju, W. K. Choi, *J. Mater Chem C* **2019**, 10.1039/c8tc06460a.

2018 Philip Caspari, Simon J. Dünki, Frank A. Nüesch, Dorina M. Opris, *J. Mater. Chem. C* **2018**, *6*, 2043

2016 Philip Caspari, Frank A. Nüesch, Antonia Neels, Dorina M. Opris, *RSC Adv.* **2016**, *6*, 98059.

**Ce document a été imprimé au Centre d'impression EPFL,
imprimerie climatiquement neutre, certifiée myClimate.**